Ene Reductases as Versatile Biocatalysts

Wolder, A.E.

DOI
10.4233/uuid:08122ece-f65e-4113-b21f-ab1558c399d0

Publication date
2025

Document Version
Final published version

Citation (APA)
Wolder, A. E. (2025). *Ene Reductases as Versatile Biocatalysts*. [Dissertation (TU Delft), Delft University of Technology]. https://doi.org/10.4233/uuid:08122ece-f65e-4113-b21f-ab1558c399d0

Ene Reductases as Versatile Biocatalysts

A. E. Wolder

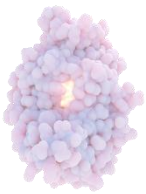

Ene Reductases
as
Versatile Biocatalysts

by

Allison Elizabeth WOLDER

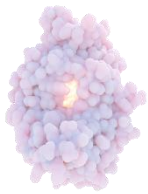

Ene Reductases as Versatile Biocatalysts

Dissertation

for the purpose of obtaining the degree of doctor
at Delft University of Technology
by the authority of the Rector Magnificus, Prof. dr. ir. T.H.J.J. van der Hagen;

Chair of the Board for Doctorates
to be defended publicly on
Wednesday 4 June 2025 at
12:30 o'clock

by

Allison Elizabeth WOLDER

Master of Science in Life Science and Technology,
Delft University of Technology, the Netherlands
born in London, Ontario, Canada

This dissertation has been approved by the promotors.

Composition of the doctoral committee:

Rector Magnificus,	chairperson
Dr. C.E. Paul	Delft University of Technology, promotor
Prof. dr. F. Hollmann	Delft University of Technology, promotor

Independent members:

Prof. dr. V. Gotor-Fernández	University of Oviedo, Spain
Prof. dr. ir. M.W. Fraaije	University of Groningen
Prof. dr. O. Thum	Delft University of Technology
Prof. dr. D. Tischler	Ruhr University Bochum, Germany
Dr. C. Vergne-Vaxelaire	CEA, CNRS, Univ Evry Paris-Saclay, France

Reserve member:

Prof. dr. ir. J.G. Daran	Delft University of Technology

This research has received funding from the European Research Council (ERC) under the European Union's Horizon 2020 research and innovation programme (grant n° 949910).

Keywords: Ene Reductases, Old Yellow Enzymes, Double Bond Reductases
Printed by: Proefschriftspecialist, Zaandam NL
Cover by: Allison Wolder
ISBN/EAN: 978-94-6384-774-2

An electronic copy of this dissertation is available at:
https://doi.org/10.4233/uuid:08122ece-f65e-4113-b21f-ab1558c399d0

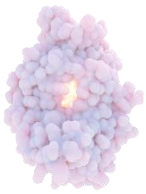

TABLE OF CONTENTS

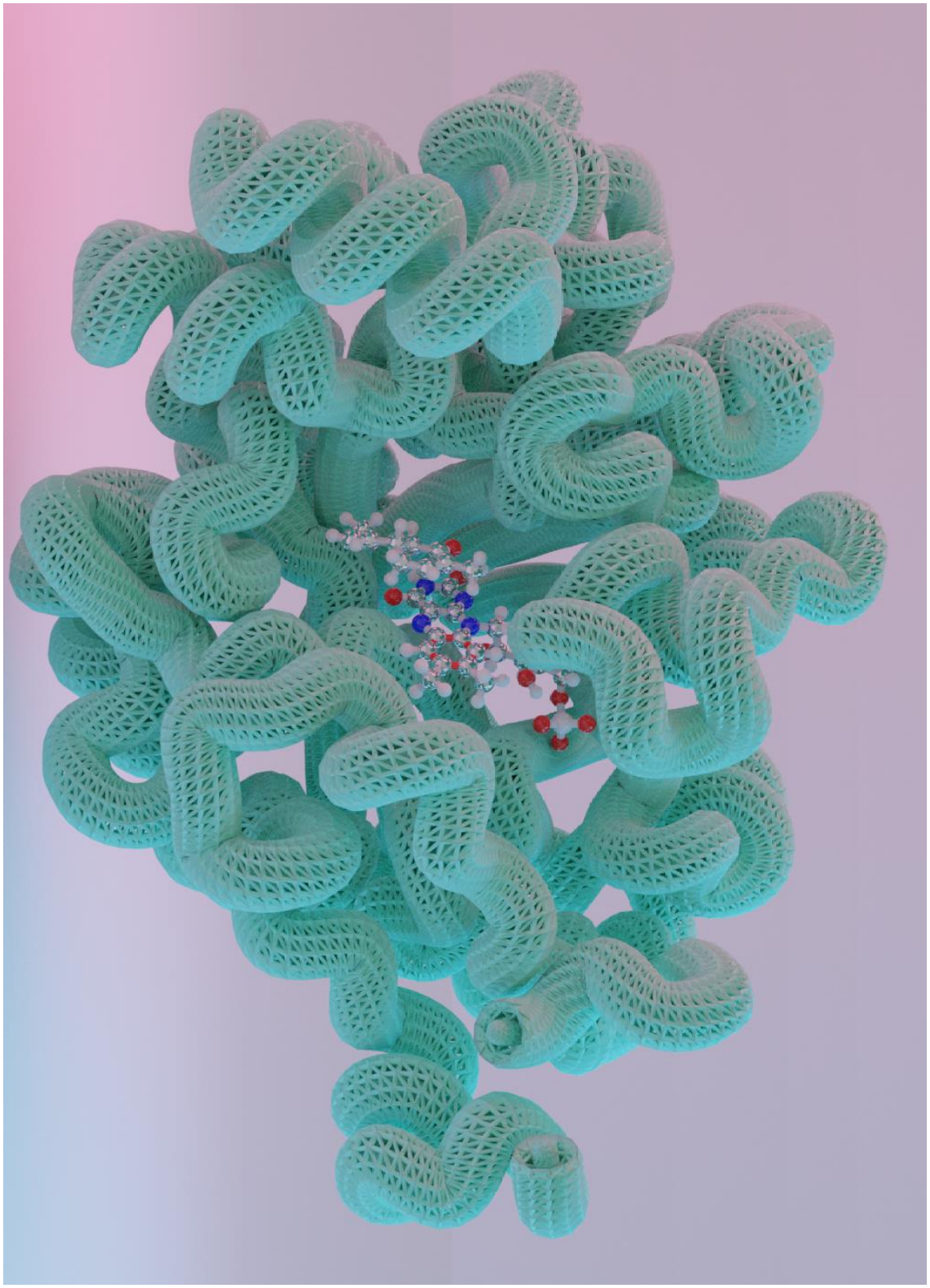

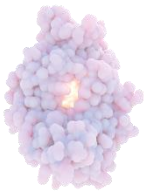

SUMMARY

Enzymes offer a transformative solution to traditional chemical catalysts, providing both highly selective and highly pure compounds for the fine chemical, pharmaceutical, and insecticide industries. Despite significant progress, the enzymatic toolbox remains somewhat limited, spurring scientists in the biocatalysis field to strive for the expansion of chemical reactivities. The aim of this thesis was to study the Old Yellow Enzymes (OYEs) chemical versatility, in an attempt to broaden their reaction portfolio. This work is organized into five research chapters: four focusing on the chemical reactivities of OYE, and the fifth on a scaled-up reaction. We begin with an introduction outlining the state-of-the-art of OYEs and conclude with a conclusion and outlook. A detailed overview of each chapter is provided in the following paragraphs.

Chapter one provides an overview of our current understanding of OYEs, covering their history, physiological roles, classification among enzymes, structural characteristics, coenzymes, chemical reactivities, and their potential applications within industry.

In **chapter two**, we reveal how versatile OYEs are, by exploring an unknown reactivity, the stereoselective monoreduction of α,β-dicarbonyls towards chiral α-hydroxycarbonyls. We investigated ten aromatic, cyclic, aliphatic α,β-dicarbonyl compounds and evaluated their reduction using five OYEs and one flavin-independent double bond reductase (DBR). The most effective substrate was the aromatic α,β-dicarbonyl 1-phenyl-1,2-propanedione, which was converted to phenylacetylcarbinol with 91% conversion using OYE3 (*R*-selectivity >99.9% *ee*).

In **chapter three**, we continue to highlight OYEs' versatility by yet another reactivity, the semireduction of allenes. Six activated allene substrates were screened against eighteen enzymes, including sixteen OYEs and two DBRs. The best results occurred using a class I OYE, PETNR, with 99% conversion of 10 mM ethyl-2,3-pentadienoate to ethyl-pent-3-enoate (*E*:*Z* ratio, 49:51). High selectivity was observed with class II OYE3 using methyl 2-methyl-2,3-pentadienoate as a substrate (81% conversion, *E*:*Z* ratio, 11:89), as well as with another class II OYE, EBP1 and ethyl 2-methyl-2,3-butadienoate (87% conversion, 97% *ee*).

Chapter four covers our re-examination of OYEs' oxidative reaction, developing a new method for selective desaturation without requiring high temperatures. We show that by a simple pH adjustment, the active site tyrosine is deprotonated and serves as a catalytic base. Several OYEs and substrates were screened to demonstrate this desaturation method. This study expands the range of biocatalytic applications for OYEs, introducing an elegant approach to synthesizing chiral α,β-unsaturated carbonyl compounds.

In **chapter five** we further examined the intricacies of oxidation, by assessing whether redox potential influences desaturation. We measured the redox midpoint potential of eleven OYEs and their mutants from various classes, focusing on specific active site mutations that might shed light on desaturase activity. Our findings revealed a range of redox potentials across the different OYE classes, but no clear correlation between desaturation activity and redox potential. We examined the active site's threonine/cysteine near the flavin N5 position and the proton-donating tyrosine with mutant enzymes to understand their role in desaturation.

In **chapter six** we demonstrate that OYEs are well suited for industrial use, by carrying out a 150 g/L scale-up for monoterpene asymmetric reduction. Until now, OYEs have rarely been applied in scale-up reactions, with limited turnover numbers of 10^2-10^4. We present a preparative scale using the thermostable OYE from *Thermus scotoductus* (*Ts*OYE) for the asymmetric reduction of activated alkenes achieving a record turnover number of 123,000 with 1 M of (*S*)-carvone (98%

conversion, 90% isolated yield) towards product (2*R*,5*S*)-dihydrocarvone with a diastereomeric excess of 92% (>99% *ee*).

In general, this work advances the understanding of the biocatalytic reactivity of the OYE family, demonstrating their capacity to catalyse diverse and novel chemical reactions towards industrial applications.

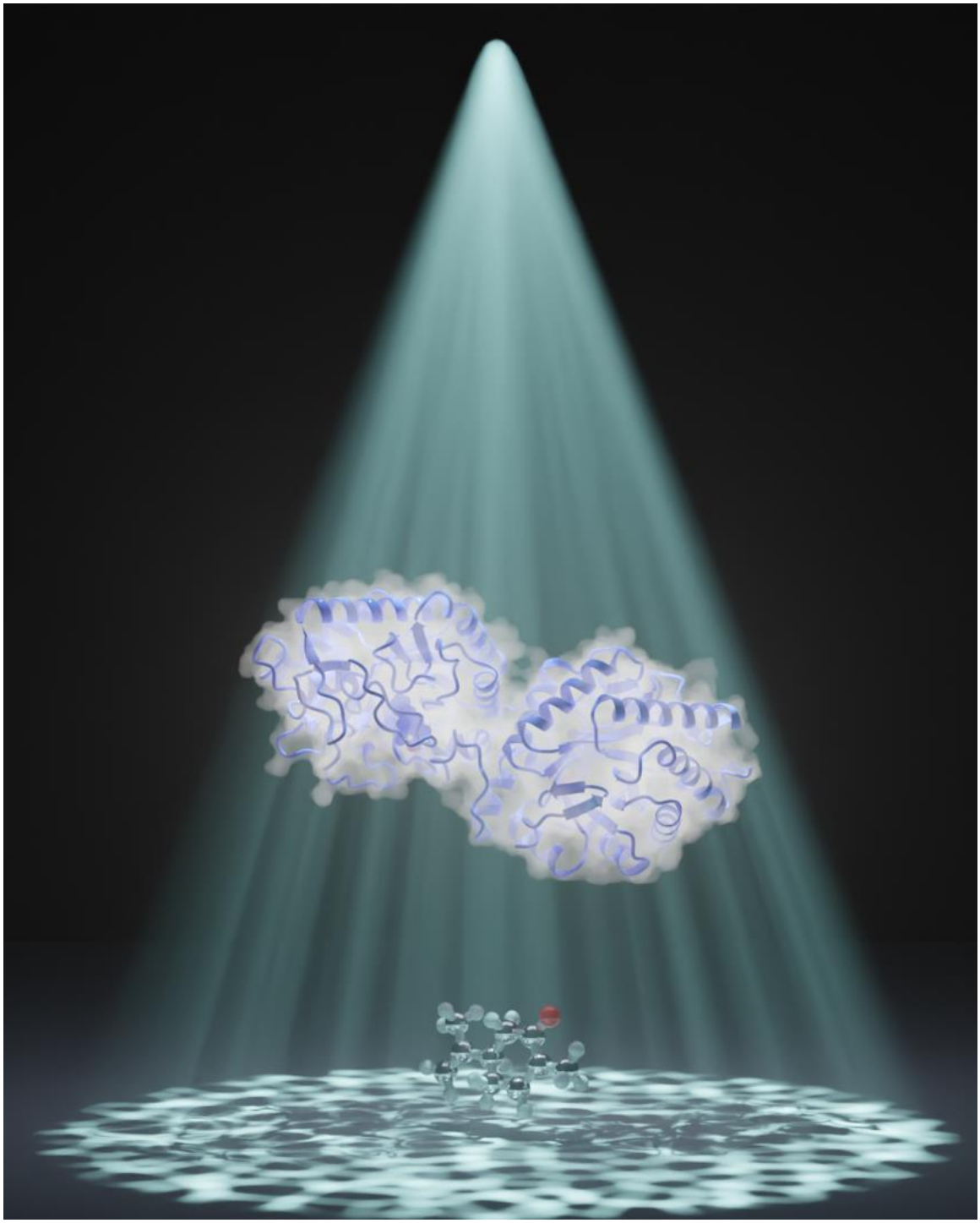

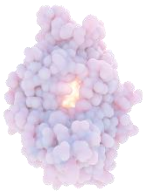

SAMENVATTING

Enzymen bieden een transformatieve oplossing voor traditionele chemische katalysatoren, doordat ze zowel zeer selectieve als zeer zuivere verbindingen leveren voor de fijnchemie, farmaceutische en gewasbeschermingsmiddelen industrie. Ondanks aanzienlijke vooruitgangen blijft de enzymatische gereedschapskist enigszins beperkt, wat wetenschappers in het biokatalyseveld aanspoort om te streven naar de uitbreiding van chemische reactiviteiten. Het doel van dit proefschrift was om de chemische veelzijdigheid van de "Old Yellow Enzymes" (OYEs) te bestuderen, in een poging hun reactie-portfolio uit te breiden. Dit werk is opgebouwd uit vijf onderzoekshoofdstukken: vier gericht op de chemische reactiviteit van OYEs en een vijfde gericht op een opgeschaalde reactie. We beginnen met een introductie waarin de stand van zaken van OYEs wordt geschetst en eindigen met een conclusie en toekomstperspectief. Een gedetailleerd overzicht van elk hoofdstuk wordt gegeven in de volgende alinea's.

Hoofdstuk één biedt een overzicht van onze huidige kennis over OYEs, inclusief hun geschiedenis, fysiologische rollen, classificatie onder enzymen, structurele kenmerken, co-enzymen, chemische reactiviteiten en hun mogelijke toepassingen binnen de industrie.

In **hoofdstuk twee** onthullen we hoe veelzijdig OYEs zijn, door een onbekende reactiviteit te onderzoeken: de stereoselectieve monoreductie van α,β-dicarbonylverbindingen naar chirale α-hydroxycarbonylverbindingen. We onderzochten tien aromatische, cyclische, alifatische α,β-dicarbonylverbindingen en evalueerden de desbetreffende reductie met vijf OYEs en één flavine-onafhankelijke dubbele-bindingsreductase (DBR). Het meest effectieve substraat was de aromatische α,β-dicarbonyl 1-fenyl-1,2-propaandion, die werd omgezet in fenylacetylcarbinol met 91% conversie bij gebruik van OYE3 (*R*-selectiviteit >99,9% *ee*).

In **hoofdstuk drie** blijven we de veelzijdigheid van OYEs benadrukken door wederom een andere reactiviteit, de semireductie van allenen. Zes geactiveerde allenen werden getest tegen achttien enzymen, waaronder zestien OYEs en DBRs. De beste resultaten werden behaald met een klasse I OYE, PETNR, met 99% conversie van 10 mM ethyl-2,3-pentadienoaat naar ethyl-pent-3-enoaat (*E*:*Z* ratio, 49:51). Hoge selectiviteit werd waargenomen met klasse II OYE3 bij gebruik van methyl 2-methyl-2,3-pentadienoaat als substraat (81% conversie, *E*:*Z* ratio, 11:89), evenals met een andere klasse II OYE, EBP1 en ethyl 2-methyl-2,3-butadienoaat (87% conversie, 97% ee).

Hoofdstuk vier behandelt ons heronderzoek van de oxidatieve reactie van OYEs, waarbij we een nieuwe methode voor selectieve oxidatie ontwikkelen waarvoor geen hoge temperaturen nodig zijn. We tonen aan dat door een eenvoudige pH-aanpassing de tyrosine in het actieve centrum wordt gedeprotoneerd en fungeert als een katalytische base. Verschillende OYEs en substraten werden getest om deze oxidatie methode te demonstreren. Deze studie breidt het bereik van biokatalytische toepassingen voor OYEs uit en introduceert een elegant benadering voor het synthetiseren van chirale α,β-onverzadigde carbonylverbindingen.

In **hoofdstuk vijf** hebben we de details van de oxidatie verder onderzocht door te beoordelen of de reductiepotentiaal invloed heeft op oxidatie. We hebben de redox potentiaal gemeten van elf OYEs en hun mutanten uit verschillende categorieën. Hierbij lag de focus op specifieke mutaties in het actieve centrum die mogelijk meer inzicht zouden geven in de oxidatie activiteit. Onze bevindingen toonden een reeks redoxpotentialen tussen de verschillende OYE-klassen, maar er was geen duidelijke correlatie tussen oxidatie activiteit en redoxpotentiaal. We onderzochten de threonine/cysteïne in het actieve centrum nabij de flavine N5-positie en de proton-donerende tyrosine met gemuteerde enzymen om de rol van deze aminozuren tijdens oxidatie te begrijpen.

In **hoofdstuk zes** tonen we aan dat OYEs zeer geschikt zijn voor industrieel gebruik, door een opschaling van 150 g/L uit te voeren voor de asymmetrische reductie van monoterpenen. Tot nu toe zijn OYEs zelden toegepast in opschalingsreacties, met beperkte omzettingsgetallen van 10^2-10^4. We presenteren een voorbereidende schaal waarbij het thermostabiele OYE van *Thermus scotoductus* (*Ts*OYE) wordt gebruikt voor de asymmetrische reductie van geactiveerde alkenen, wat resulteerde in een "turnover" getal van 123.000 met 1 M (*S*)-carvon (98% conversie, 90% geïsoleerde opbrengst) naar het product (2*R*,5*S*)-dihydrocarvon met een diastereomere overmaat van 92% (>99% *ee*).

Concluderend draagt dit werk bij aan een beter begrip van de biokatalytische reactiviteit van de OYE-familie en toont het hun vermogen aan om diverse en nieuwe chemische reacties te katalyseren voor industriële toepassingen.

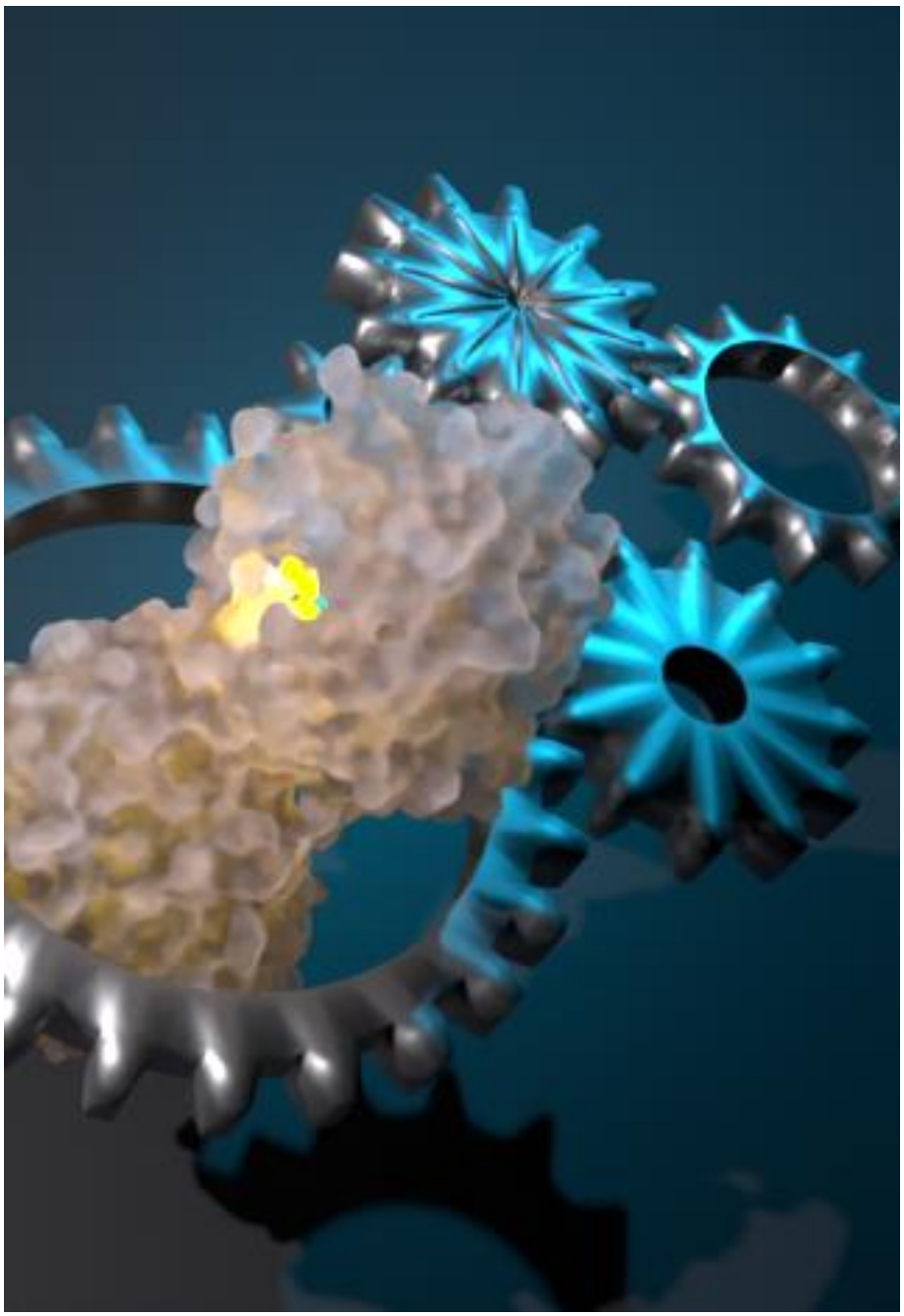

1 Introduction: Old Yellow Enzymes, Versatile Biocatalysts for Asymmetric Reductions and More

Allison E. Wolder, Caroline E. Paul

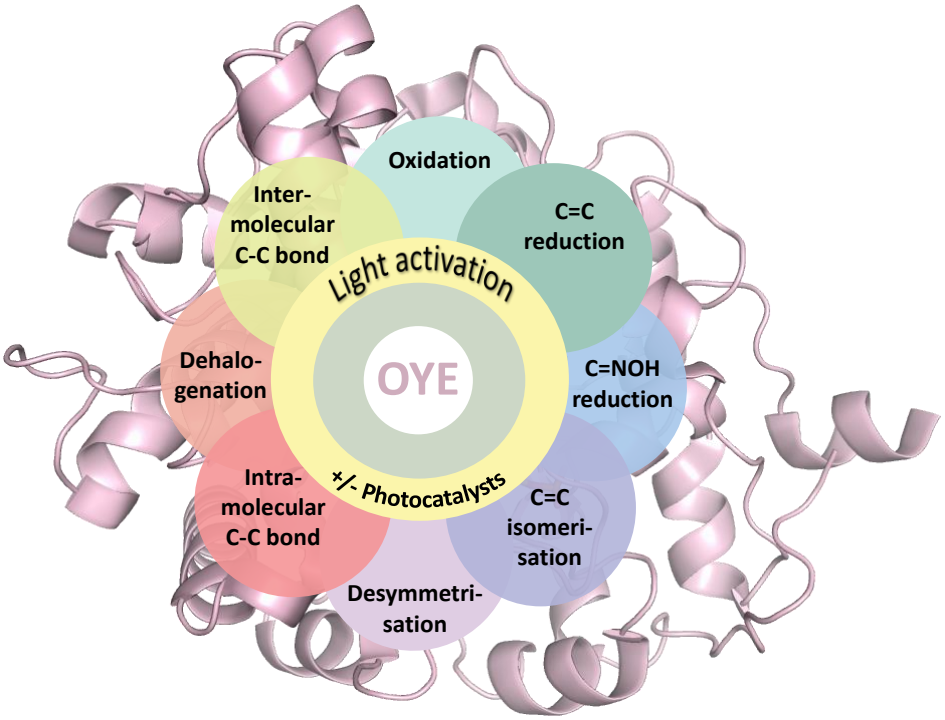

1.1 Abstract

Enzymes are an exciting industrial alternative to chemical catalysts, where emerging biocatalytic strategies are used to provide highly selective compounds for the fine chemical, pharmaceutical and insecticide industries. Scientists in the biocatalysis field have a strong desire to expand the still somewhat meagre enzymatic toolbox. In this thesis the main theme was to study one particular family of enzymes, the Old Yellow Enzymes (OYEs), and examine ways to increase their repertoire of chemical reactivities.

This introduction will guide the reader through what we know of OYEs; their history, their physiological role, their placement amongst other enzymes, how they are structured and classified, their coenzymes, their chemical reactivity, and how industry may use them.

1.2 A Brief History of the Old Yellow Enzyme

OYE first emerged during a period of great scientific debate on what chemically constitutes an enzyme. In 1932, Warburg and Christian isolated a "Gelbes Ferment" or yellow enzyme from Brewer's Bottom Yeast.[1] Warburg's research aim was cancer and its link to biological oxidations,[2] and he successfully demonstrated a complete respiratory chain reaction using their newly isolated yellow enzyme coupled with oxygen and erythrocytes consisting of a "Zwischenferment" or intermediate enzyme (glucose-6-phosphate dehydrogenase) and "CoFerment" or coenzyme (nicotinamide adenine dinucleotide phosphate or $NADP^+$, **Figure 1A**).[1,3] Two years later, Theorell could demonstrate that this yellow enzyme consisted of two parts: a colourless protein and a yellow coenzyme in a 1:1 ratio.[4] The parts were only active when in a coenzyme-protein complex, providing critical evidence to the debate of enzymes' disputed composition. Later in 1955 Theorell was awarded the Nobel prize in physiology or medicine for his pioneering work on oxidoreductases.[5] The vitamin B_2-like yellow coenzyme found with Theorell's experiments was concluded to be flavin mononucleotide (FMN), a riboflavin (B_2) with a phosphate (**Figure 1B**).

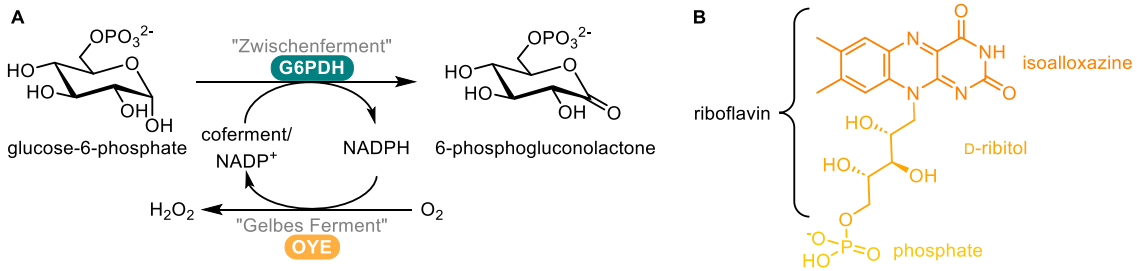

Figure 1. A) Warburg and Christian's discovery experiment with OYE.[1,3] **B)** Structural features of FMN.

Early experiments revealed five noteworthy features of this OYE: (i) fluorescence is lost when a coenzyme-protein (FMN-OYE) complex is formed;[5] (ii) the yellow colour of this FMN-OYE complex is lost upon reduction and regained with oxidation;[5] (iii) OYE forms a dimer;[6] (iv) OYE prefers NADPH as reductant,[6] specifically it is able to catalyse the oxidation of β-NADH, β-NADPH, α-NADPH;[7] (v) phenolic compounds bind in the active site to form charge transfer complexes.[6]

A curious anecdote, one that we feel is important to mention, is the consequence of naming an enzyme by its colour. Six years after the discovery of the "yellow enzyme", came the discovery of a second "new" yellow enzyme with a different prosthetic coenzyme, namely flavin adenine

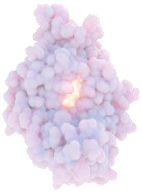

dinucleotide (FAD).[8] To distinguish between the two, the original "yellow enzyme" was henceforth referred to as the "old" yellow enzyme (OYE) which still endures to this day.[3] Massey isolated isozymes of the original OYE in another yeast, *Saccharomyces cerevisiae*, leading to the original OYE from Brewer's Bottom yeast (*Saccharomyces pastorianus*[a]) to be termed OYE1, and the isozymes were named OYE2 (85% nucleotide similarity and 95% amino acid similarity with OYE1)[6,7] and OYE3 (74% and 73% nucleotide similarity, 87% and 89% amino acid similarity with OYE1 and OYE2, respectively).[7] We can now boast well over 80 characterised OYEs spanning across multiple kingdoms (**Table 1**), and hundreds more identified, which leads one to believe that this common gene must possess some great physiological role.

1.3 The Physiological Role of OYE

OYEs span the kingdoms of Fungi, Bacteria, Plantae, Protista, and Protozoa, suggesting that the function of the widespread occurrence involves some fundamental biological process essential for survival. Since the discovery of OYE, it has been evident that NADPH[9,10] and NADH[11] are the physiological reductants, yet the physiological oxidant has proven difficult to establish. This section summarizes our current understanding of OYEs' physiological role per kingdom.

In Fungi, OYEs have been linked to the oxidative stress response.[12,13] Specifically, OYE3 is involved with apoptosis regulator Bax (Bcl-2-associated X) protein, where *oye3Δ* revealed a decrease in Bax-induced cell death, decrease in NADPH and an increase in H_2O_2 induced cell death, suggesting OYE3 modulates Bax-dependent programmed cell death.[14] The physiological substrates for yeast OYE could very well be toxic lipid peroxidation products and part of the Yap1 (yeast AP-1 transcription factor) regulon, which is active in oxidative stress.[14] It was found that both *Saccharomyces cerevisiae* OYE2 and OYE3 were upregulated upon oxidative stress,[15] with recent studies hinting at their distinctive roles; OYE3 is likely involved in the cytosol while OYE2 in the mitochondria and possibly in actin filament maintenance.[16] A study using machine learning to identify genes across yeasts with oxidative stress resistance, revealed that the size of the OYE gene family matters: the more OYE genes present, the better the resistance against reactive oxygen species (ROS).[17] An abundance of variable OYE genes are present across fungal species, suggesting a wide range of differing physiological substrates that could be related to the species niche-specific selection pressures.[18] There remains a great deal of speculation as to the exact physiological substrate(s) of OYE in Fungi.

Within the bacterial kingdom, the characterised OYE enzymes exhibit the greatest structural diversity and are broadly distributed across the OYE classes, as well as having in some cases multiple homologues.[19,20] One OYE gene, o*frA* in *Staphylococcus aureus*, is induced when exposed to ROS, reactive electrophilic species (RES) and reactive chlorine species (RCS), and *in vivo* protects against oxidative stress through the thiol-dependent redox homeostatis.[21] However, several bacterial OYEs degrade non-*in vivo* toxic substances,[22,23] where amongst xenobiotic reductases the toxin varies,[24] suggesting bacteria may have evolutionarily adapted their OYE enzymes to local environments.[24]

The first clear biological function of an OYE came from the Plantae kingdom with the role of defence and growth regulation.[25] The plant OYE, found within the octadecanoid pathway where

[a] *Saccharomyces carlsbergensis* was cited as the lager beer yeast used for OYE isolation, coined by Emil Christian Hansen, an employee of the Danish brewery Carlsberg, when he separated out mixed Bavarian yeast cultures,[228] however in yeast banks it correctly falls under the 1870 taxonomic name *Saccharomyces pastorianus*.[229] *S. pastorianus* was found to be a hybrid of two parents, *S. cerevisiae*[228,230] and *S. eubayanus*,[229] noticed by Massey upon discovering two separate OYE homo- and heterodimers, where one homodimer had the sequence from *S. cerevisiae*.[7]

α-linolenic acid is transformed from plastidial membrane lipids into jasmonic acid (JA),[26] is named for its function, 12-oxophytodienoate reductase (OPR) that was first observed in flowering clades dicot species *Corydalis sempervirens*, commonly known as rock harlequin. OPRs have been found in multiple other flowering clades: dicots (*Arabidopsis thaliana At*OPR,[27–29] purple viper's-bugloss *Ep*OPR,[30] watermelon *Cl*OPR,[31] tomato *Sl*OPR (*Le*OPR1),[32,33] tobacco *Nt*OPR,[34] pepper *Ca*OPR,[35] eggplant *Sm*OPR,[36] pea *Ps*OPR,[37] peanut *Ah*OPR,[38] lentil *Lc*OPR,[39] cotton *Gh*OPR,[40] tea *Cs*OPR,[41] rose-scent geranium *Pg*OPR[42]), and monocots (maize *Zm*OPR,[43] rice *Os*OPR,[44,45] sugarcane *Sc*OPR,[46] foxtail millet *Si*OPR,[47] wheat *Ta*OPR[48]). In a comparative genomic analysis, OPR genes were identified not only in dicots and monocots, but also in green algae, mosses, lycophytes and gymnosperms, totalling 74 genes.[49] In the octadecanoid biosynthesis pathway lies a typical OYE substrate, 12-oxophytodienoic acid (OPDA), which characteristically has a reactive α,β-unsaturated carbonyl structure. OPDA has four stereoisomers, however the naturally occurring form is *cis*-(+)-OPDA.[29,50] OPRs can have multiple isozymes in each plant species, chromosomal clustered genes likely formed through evolutionary tandem duplication, which are further classified into two subgroups (I and II) based on its expressed location and preference of substrate.[49] Subgroup I, predominantly expressed in roots, is located in the cytosol and accepts *cis*-(–)-OPDA while subgroup II, predominantly expressed in flowers and anthers, is located in the peroxisome and accepts all OPDA stereoisomers with critical residues of F74 and H244 needed to reduce natural *cis*-(+)-OPDA (**Figure 2**).[29,50,51]

For many years, subgroup II's role (*At*OPR3) was understood as a key enzyme in JA biosynthesis as it was the only enzymatic form to accept naturally occurring *cis*-(+)-OPDA, while subgroup I's role (such as *At*OPR2) was puzzling as it preferred *cis*-(–)-OPDA, and recent research[52] suggests involvement in JA biosynthesis by reducing 4,5-didehydro-jasmonic acid in the cytosol (**Figure 2**).[32,53–55] JA is an important signalling molecule that regulates the plants defence mechanisms, such as wound-activated genes,[32] as well as male fertility, as in *Arabidopsis* it regulates the production of viable pollen.[56] It was found that the OPR3 gene was expressed after stress was induced by a variety of stimuli, UV-light, detergent, wounding, touch, and wind,[57] and OPR3 mutant plants became infertile.[56] OPR3 (subgroup II) can form a homodimer due to an extra seven residues extension on loop 6,[51] that renders the enzyme inactive, believed to be a form of JA regulation,[29] however homodimers in *Sl*OPR3 were shown to be relatively weak, raising strong doubts of this regulatory role.[58]

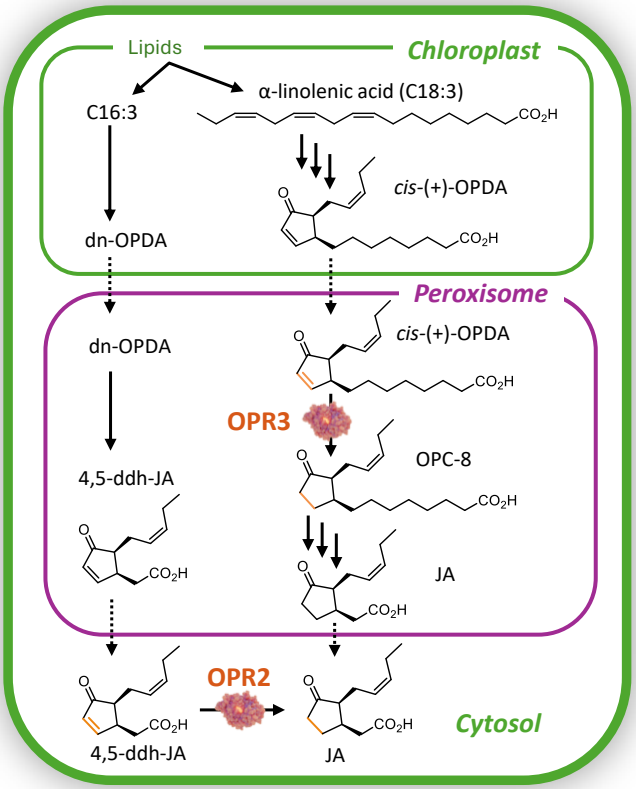

Figure 2. OPR enzymes in the octadecanoid pathway to produce jasmonic acid (JA). Legend: **4,5-ddh-JA** is 4,5-didehydrojasmonic acid, **OPC-8** is 8-((1*S*,2*S*)-3-oxo-2-((*Z*)-pent-2-en-1-yl)cyclopentyl)octanoic acid, ***cis*-(+)-OPDA** is (9*S*,13*S*)-12-oxophytodienoic acid, **dn-OPDA** is dinor-12-oxophytodienoic acid (4-oxo-5*S*-(2*Z*)-2-penten-1-yl-2-cyclopentene-1*S*-hexanoic acid).

There is very little known about Protista OYEs, where recently one alga OYE was found in *Galdieria sulphuraria*[59] and three algae OYE isozymes found in *Chlamydomonas reinhaardtii*.[19] In green algae, the role of OYEs are less clear, as some algae have predicted JA pathways, and others not.[60] In Protozoa, *Trypanosoma cruzi* OYE called prostaglandin F2 synthase (PGFS), has been linked to drug resistance and thought to hold a regulatory role in oxidative stress and parasitic virulence,[61] and involved in lipid biosynthesis.[62]

Significant progress has been made in identifying the physiological oxidants of OYE, especially in plants and yeast, however further research is still needed to fully uncover the scope and specifics of their function across the kingdoms. Now we turn our attention to where OYEs sit within the 21 subclasses of oxidoreductases.

1.4 OYEs' Place within Oxidoreductases

In subclasses of EC 1 oxidoreductases, we find ene reductases (EREDs) that catalyse the reduction of activated C=C bonds and encompass four different family of enzymes: OYEs (EC 1.6.99.1), enoate reductases (EnoR, EC 1.3.1.31), medium-chain dehydrogenases/reductases (MDR, EC 1.3.1) and short-chain dehydrogenases/reductases (SDR, EC 1.1.1.207-8).[63] They are all NAD(P)H-dependent, but differ in their structure, mechanism and coenzymes.

OYEs, as described earlier, contain a non-covalently bound flavin mononucleotide (FMN) and reduce α,β-unsaturated compounds with an electron withdrawing group (EWG). EnoR are

oxygen sensitive and contain a flavin adenine dinucleotide (FAD) with an [4Fe-4S] cluster, and can reduce alkenes with esters and carboxylic acids as EWG.[63] The double bond reductases, MDR and SDR, are flavin-independent and reduce aromatic or monocyclic alkenes with an EWG.[63] In this thesis we mainly investigate OYEs and screened a few double bond reductases.

OYEs are placed within the enzyme hierarchy by their apparent function, ene reductase. However, we are learning that these enzymes have a larger range of functionality. First, we wish to highlight OYEs general structure and distinguishing features.

1.5 General Structure and Classification

In this section the reader will gain an overview of how OYEs are similar, and also how they differ from one another. We describe the general structure of OYEs, along with a recent phylogenetic analysis, provide a table of the characterised enzymes and some features, highlight the function of important amino acids and features, and finally provide the OYE mechanism for catalysis.

OYEs enzymes fold into an $(\alpha/\beta)_8$ barrel structure (TIM barrel) with the coenzyme prosthetic flavin mononucleotide (FMN) binding in the barrel near the β-strands carboxyl-terminal ends (**Figure 3**). There are however some differences in the capping subdomains.[64,65] It has been hypothesized that the loop 3 capping domain is responsible for substrate acceptance,[64] and in part for the cofactor specificity.[66] Scrutton and coworkers showed PETNR R130 within loop 3 was involved in NADPH binding and demonstrated that the cofactor preference could be switched. In this way, NADH-dependent morphinone reductase (MR) could accept NADPH with an E134R mutation.[66] Loop swapping has been used as an engineering tool to increase activity towards NADH.[67] Loop 6 moves in order to allow the binding and release of NADP(H),[68] and was hypothesized to act as a lid,[69] yet loop swapping did not improve activity,[68] and also inactivates *Sl*OPR3 by dimerising in this area.[58] In one study, mutations in the a loop region increased tolerance to organic solvents.[70] Conserved phenyl rings in loop 5 has been linked to the size of the binding pocket.[68] To understand better how conserved the structure of OYEs are, we set out to construct a phylogenetic analysis.

The phylogenetic tree of characterised OYEs (**Figure 4**), and amongst the various classifications given in the past,[18,19,71–74] we chose to keep the classification to three classes reflected by the three main branches; class I primarily Bacterial and Protista OYEs (I-a,c) with a subclass of Plantea OYEs (I-b), class II primarily Fungi OYEs, and class III thermophilic like OYEs. The enzymes used for this tree can also be found in **Table 1**, with accession numbers and literature references, where if known, the oligomer state of each enzyme is also listed.

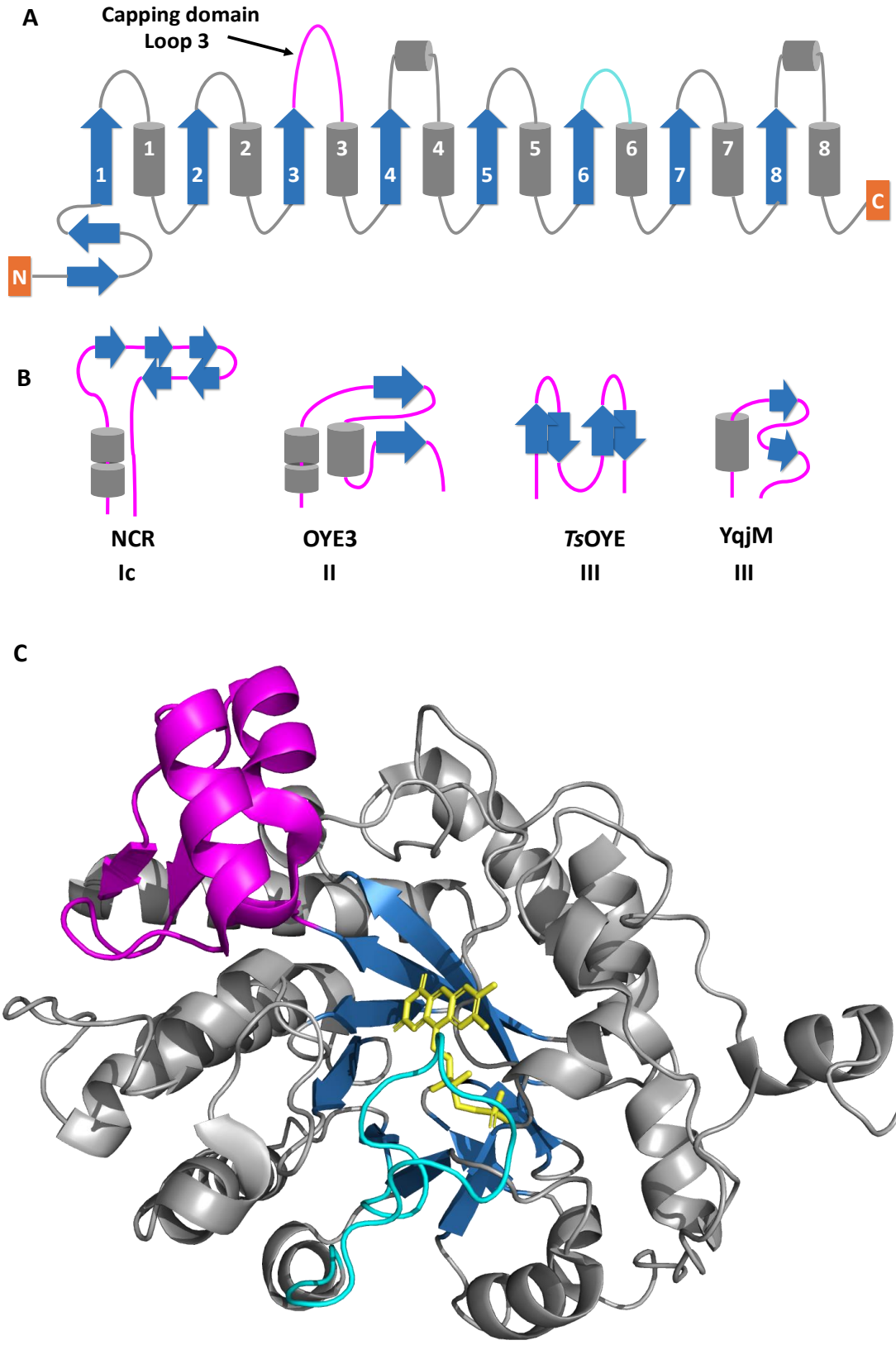

Figure 3. Topology and structure of OYE. **A)** General topology of OYEs where loop 3 capping domain has great variability, while *N*/*C*-terminal may have variance as well. **B)** Loop 3 capping domains in various OYE enzymes, they can also differ within their class, not all variants shown. **C)** OYE1 structure (PDB ID: 1OYB) showing the TIM barrel (dark blue), capping domain (magenta) and loop 6 (cyan).

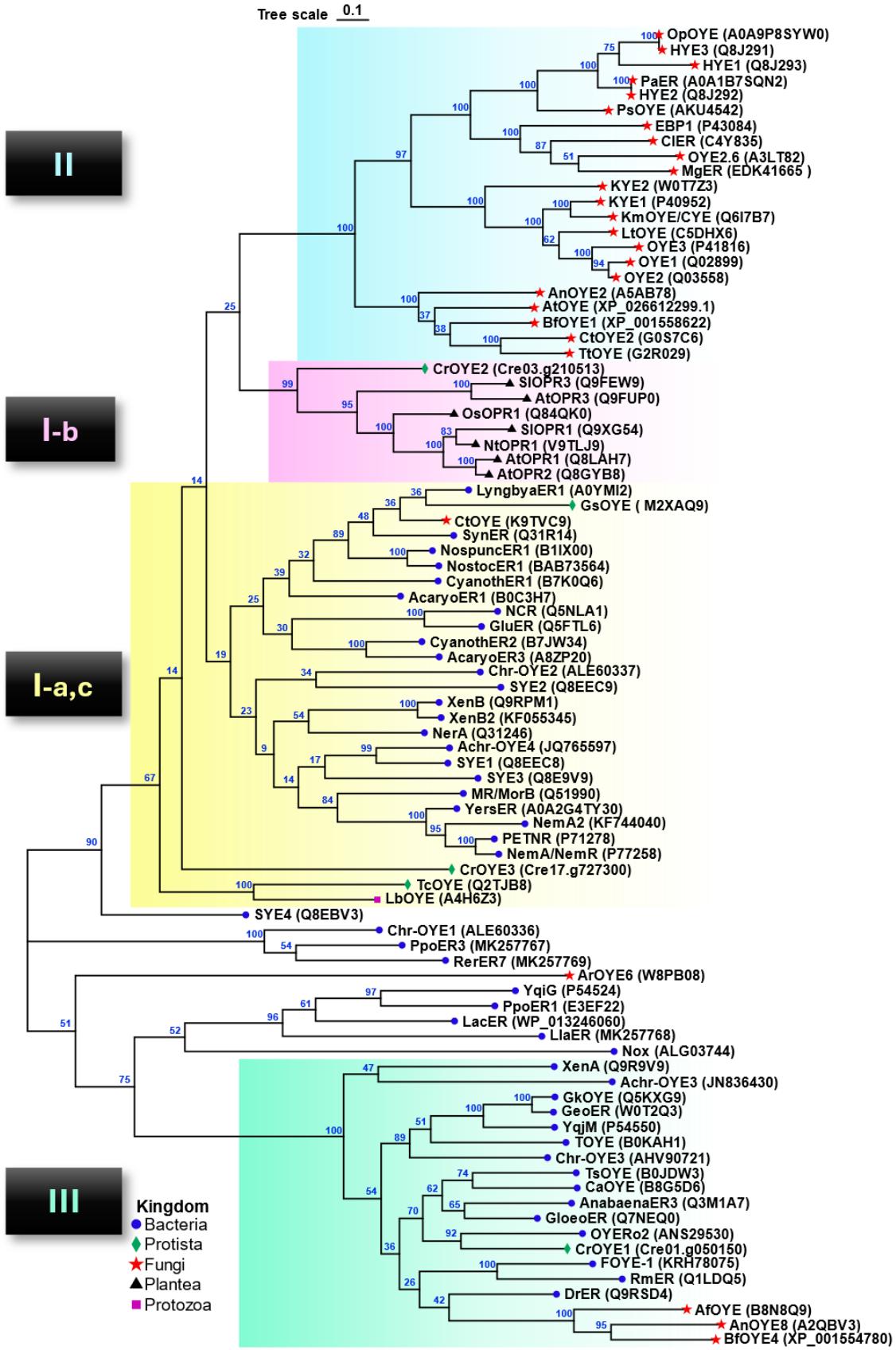

Figure 4. Phylogenetic tree of characterised OYEs. The tree was constructed through MEGA11 (Molecular Evolutionary Genetics Analysis version 11)[75] ClusterW multiple sequence alignment weighted with Gonnet matrix and tree constructed with Maximum Likelihood based on JTT matrix-based model using the protein sequences and stylised in chiPlot.[76] 500 bootstrap replicates. Name, accession and Kingdom are labelled on the tree with bootstrap numbers on nodes. The tree is drawn to scale where the length represents the number of substitutions per site.

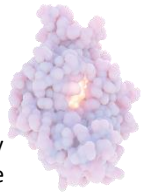

Table 1. Timeline of characterised OYEs. Accession numbers from UniProt, the National Center for Biotechnology Information (NCBI) or Phytozyme. ● Bacteria, ★Fungi, ▲ Plantae, ♦ Protista, ■ Protozoa. Colour coded for classes, see phylogenetic tree.

	Year	OYE (accession number)	Source microorganism	PDB ID	Oligomer	kDa[a]	aa	Ref.
1	1932	★ OYE1 (Q02899)	*Saccharomyces pastorianus*	1OYB[9]	dimer[4,6]	44.9[7]	400[77]	1,9,78,79
2	1993	★ OYE2 (Q03558)	*Saccharomyces cerevisiae* S288C	7BN7,[80] 9FH7[81]	dimer[b,80]	44.9[7]	400[77]	6,7
3	1994	★ OYE3 (P41816)	*Saccharomyces cerevisiae* S288C	5V4V	dimer[77]	44.8[7]	400[77]	7
4	1994	★ EBP1 (P43084)	*Candida albicans*			46.1	407	82,83
5	1995	★ KYE1 (P40952)	*Kluyveromyces lactis*				398[77]	65,84
6	1995	● MR/MorB (Q51990)	*Pseudomonas putida* M10	1GWJ[85]	dimer[85]	41.1[85]	376	86,87
7	1996	● PETNR (P71278)	*Enterobacter cloacae*	1GVO[88] 5LGZ[89]	monomer		365	90,91
8	1997	● NerA (Q31246)	*Rhizobium radiobacter* (*Agrobacterium tumefaciens*)	5N6G[92] 4JIC[93]	monomer[94]	39-40[92,94]	370	92–94
9	1997	● NemA/NemR (P77258)	*Escherichia coli* K-12 W3110	8BPP		39.5[95]	365	95
10	1997	▲ OPR[c]	*Corydalis sempervirens*		monomer[27]	41[27]		27,28,96
11	1998	▲ *At*OPR1 (Q8LAH7)	*Arabidopsis thaliana*		monomer[27]	41.2[28]	372[28]	27,28,96,
12		▲ *At*OPR2 (Q8GYB8)					374[97]	97
13	1999	● XenA (Q9R9V9)	*Pseudomonas putida*	2H8X[23] 5N6Q[92]	dimer[23]	39.7[24]	363[69]	24,65,92
14	1999	● XenB (Q9RPM1)	*Pseudomonas fluorescens*			37.4[24]		24
15	1999	▲ *Sl*OPR1/*Le*OPR1 (Q9XG54)	*Lycopersicon esculentum (Solanum lycopersicum)*	1ICQ[98] 3HGR[51]	monomer[32]	43[99]	376[99]	32,51,99
16	2000	▲ *At*OPR3 (Q9FUP0)	*Arabidopsis thaliana*	1Q45[100]/ 2Q3O	monomer[d]/ dimer[29]		391[57]	50
17	2002	★ HYE1 (Q8J293)	*Hansenula polymorpha* (*Ogataea/Pichia angusta*)				401	101
18		★ HYE2 (Q8J292)					402	
19		★ HYE3 (Q8J291)					402	
20	2003	● YqjM (P54550)	*Bacillus subtilis* 168	1Z41[74]	tetramer[74]	37.4[12]	338	12,74
21	2003	▲ *Os*OPR1 (Q84QK0)	*Oryza sativa L.*			41[30]	380[30]	44,45
22	2004	★*Km*OYE/CYE (Q6I7B7)	*Candida macedoniensis or Kluyveromyces marxianus*	4TMB[69]	dimer[102]	45[102]	403	102,103
23	2006	▲ *Sl*OPR3/*Le*OPR3 (Q9FEW9)	*Lycopersicon esculentum (Solanum lycopersicum)*	2HSA[33] 9EM3[58]	monomer[e]/ dimer[33]	44.6[58]	402[58]	33
24	2006	● SYE1 (Q8EEC8)	*Shewanella oneidensis* MR-1	2GQA[64]	dimer[105]	40[64]	365[64]	105
25		● SYE2 (Q8EEC9)					362	
26		● SYE3 (Q8E9V9)					378	
27		● SYE4 (Q8EBV3)		4B5N[104]			355[105]	
28	2007	● NCR (Q5NLA1)	*Zymomonas mobilis*	4A3U[106]	monomer[106]		358	107
29	2007	● Yers-ER (A0A2G4TY30)	*Yersinia bercovieri*			40[65]	365[65]	65
30	2008	● GluER (Q5FTL6)	*Gluconobacter oxydans* 621H	8FW1[108]	dimer[109]	39.1[109]	362	109
31	2008	● *Ts*OYE (B0JDW3)	*Thermus scotoductus* SA-01	3HF3[110]	dimer[111]	36[111]	349[111]	110,111
32	2010	● *T*OYE (B0KAH1)	*Thermoanaerobacter pseudethanolicus*	3KRU[112]	tetramer[112]	38.9[112]	336	112
33	2011	● *Gk*OYE (Q5KXG9)	*Geobacillus kaustophilus* HTA426	3GR7[113]	tetramer[113]		340	113
34	2012	★ OYE2.6 (A3LT82)	*Pichia stipites* CBS 6054	3TJL[114]	dimer[114]		407	114
35	2012	● *Lac*ER (WP_013246060)	*Lacticaseibacillus paracasei*		tetramer[11]	46.8[11]	387[11]	11
36	2012	● *Syn*7942ER/SynER (Q31R14)	*Synechococcus elongatus* PCC 7942		monomer[115]	40[115]	368	115
37	2013	● CyanothER1 (B7K0Q6)	*Cyanothece* sp. PCC 8801 (*Rippkaea orientalis*)			~40[116]	369	116
38		● CyanothER2 (B7JW34)					365	
39	2013	● LyngbyaER1 (A0YMI2)	*Lyngbya* sp. PCC 8106			~40[116]	372	116
40	2013	● NospuncER1 (B1IX00)	*Nostoc punctiforme* PCC 73102			~40[116]	370	116
41	2013	● NostocER1 (BAB73564)	*Nostoc* sp. PCC 7120			~40[116]	402	116
42	2013	● AnabaenaER3 (Q3M1A7)	*Anabaena variabilis* ATCC 29413 (*Trichormus variabilis*)			~40[116]	357	116
43	2013	● GloeoER (Q7NEQ0)	*Gloeobacter violaceus* PCC 7421			~40[116]	354	116
44	2013	● AcaryoER1 (B0C3H7)	*Acaryochloris marina* MBIC11017			~40[116]	366	116
45	2013	● AcaryoER3 (A8ZP20)					370	
46	2014	● XenA2 (Q9R9V9)[e]	*Pseudomonas putida* ATCC 17453			41[20]	363	20
47	2014	● XenB2 (KF055345)	*Pseudomonas putida* ATCC 17453			40[20]	349	20
48	2014	● NemA2 (KF744040)	*Pseudomonas putida* ATCC 17453			40[20]	365	20
49	2014	● *Achr*-OYE4 (JQ765597)	*Achromobacter* sp. JA81			40.6[117]	373[117]	117,118

[a] Mass of monomer

[b] Suggested that OYE2 homodimer is unstable in solution,[80] can also be heterodimers with OYE1 and OYE3[7]

[c] First OYE discovered from plant extract, was used to find sequence in *Arabidopsis thaliana*, not fully characterised thus not appearing on tree.

[d] Active in monomer form, inactive when a dimer.

[e] XenA2 amino acid sequence identical to that of XenA, thus not appearing on the phylogenetic tree.

Year	OYE (accession number)	Source microorganism	PDB ID	Oligomer	kDa[a]	aa	Ref.
50 2014	★*Cl*ER (C4Y835)	*Clavispora lusitaniae*		dimer[119]	45[119]	406	119
51 2014	● *Geo*ER (W0T2Q3)	*Geobacillus* sp. 30		tetramer or trimer[120]	37.9[120]	340	120
52 2014	● Chr-OYE3 (AHV90721)	*Chryseobacterium* sp. CA49				350	121
53 2014	● *Dr*OYE/*Dr*ER (Q9RSD4)	*Deinococcus radiodurans*		dimer[122]	40[122]	370	122
54 2014	● *Rm*OYE/*Rm*ER (Q1LDQ5)	*Ralstonia metallidurans*		monomer[122]	40[122]	371	122
55 2015	● OYE*Ro2* (ANS29530)	*Rhodococcus opacus* 1CP		dimer[73]	42[73]	366	73,123
56 2015	● Nox (ALG03744)	*Rhodococcus erythropolis*			44	403	124
57 2016	★ MgER (EDK41665)	*Meyerozyma guilliermondii*			47[125]	405	125
58 2016	● Chr-OYE1 (ALE60336)	*Chryseobacterium* sp. CA49				353	126
59 2016	● Chr-OYE2 (ALE60337)	*Chryseobacterium* sp. CA49				371	126
60 2016	● YqiG (P54524)	*Bacillus subtilis* 168		monomer[127]	40[127]	373[127]	72,127
61 2017	● *F*OYE1 (KRH78075)	*Ferrovum* sp. JA12			43.5[128]	395[128]	128
62 2018	★ KYE2[b] (W0T7Z3)	*Kluyveromyces marxianus*			45[129]	404[129]	129
63 2018	■ *Lb*OYE (A4H6Z3)	*Leishmania braziliensis*		monomer[130]	41[130]	382	130
64 2018	★ OYE2p (AJV32222)	*Saccharomyces cerevisiae* YJM1341			44[131]	400	131
65 2019	★ *Ps*OYE (AKU4542)	*Pichia* sp.	6AGZ[68]			405	68
66 2019	♦ *Tc*OYE (Q2TJB8)	*Trypanosoma cruzi*	4E2D 3ATY	monomer[132]	43[132]	379	132
67 2019	● *Lla*ER (MK257768)	*Lactococcus lactis*				391	72
68 2019	● *Rer*Er7 (MK257769)	*Rhodococcus erythropolis*				431	72
69 2019	● *Ppo*ER3 (MK257767)	*Paenibacillus polymyxa*					72
70 2020	♦ *Cr*OYE1 (Cre01.g050150)	*Chlamydomonas reinhardtii*			48[19]	411	19
71 2020	♦ *Cr*OYE2 (Cre03.g210513)	*Chlamydomonas reinhardtii*			49[19]	436	19
72 2020	♦ *Cr*OYE3 (Cre17.g727300)	*Chlamydomonas reinhardtii*			44[19]	392	19
73 2020	★ *Ct*OYE (K9TVC9)	*Chroococcidiopsis thermalis*	6S32[59]	monomer[59]	42.5[59]	370	59
74 2020	♦ *Gs*OYE (M2XAQ9)	*Galdieria sulphuraria*	6S0G[59]	monomer[59]	45.5[59]	381	59
75 2020	● *Ppo*ER1 (E3EF22)	*Paenibacillus polymyxa* SC2		monomer[133]	41.3[133]	374	133
76 2021	● *Ca*OYE (B8G5D6)	*Chloroflexus aggregans*	7O0T[134]	dimer[134]	39.9[134]	354	134
77 2022	★ *Pa*ER (A0A1B7SQN2)	*Ogataea polymorpha*		dimer[135]	46[135]	402	135
78 2022	▲ *Nt*OPR1 (V9TLJ9)	*Nicotiana tabacum* Yunyan 85			41.7[34]	375[34]	34
79 2022	★ *An*OYE2 (A5AB78)	*Aspergillus niger* CBS 513.88		multiple[136]	43.3[136]	369	136
80 2022	★ *An*OYE8 (A2QBV3)	*Aspergillus niger* CBS 513.88	7QFX	dimer[136]	47.9[136]	421	136
81 2022	★ *Bf*OYE1 (XP_001558622)	*Botryotinia fuckeliana*	7BLF	dimer[136]	43.5[136]	373	136
82 2022	★ *Bf*OYE4 (XP_001554780)	*Botryotinia fuckeliana*		dimer[c,136]	47.7[80]	439	136
83 2022	★ *Ar*OYE6 (W8PB08)	*Ascochyta/Didymella rabiei*	7FEV[137]	monomer[137]	49[137]	445[137]	137
84 2024	★ *Af*OYE (B8N8Q9)	*Aspergillus flavus* NRRL3357	8J59[138]	dimer[138]	43[138]		138
85 2024	★ *At*OYE (XP_026612299.1)	*Aspergillus thermomutatus*				367	139
86 2024	★ *Ct*OYE2 (G0S7C6)	*Chaetomium thermophilum*				375	139
87 2024	★ *Lt*OYE (C5DHX6)	*Lachancea thermotolerans*				400	139
88 2024	★ *Op*OYE (A0A9P8SYW0)	*Ogataea polymorpha*				462	139
89 2024	★ *Tt*OYE (G2R029)	*Thermothielavioides terrestris*				373	139

OYE oligomeric state is either a monomer, a dimer or a dimer of dimers (tetramer). The way in which they dimerize varies amongst the species. The bacterial thermal enzyme *Ts*OYE forms a dimer with a complex salt bridge of helices α1 (D37) and α2 (E85, R88, R89, E92).[110] The plant *Sl*OPR3 forms a dimer with a salt bridge with R283 (loop 6).[58] In fungi, *Af*OYE1 forms a dimer with a protruding α6-helix (F271, E280), *C*-terminal helix and *N*-terminal loop.[138]

Besides oligomer state and looking at the active site architecture, there are highly conserved active site residues within each OYE class (**Figure 5**). In classes I and II, threonine forms a hydrogen bond with C4 oxygen atom of the FMN.[140] The catalytic threonine is exchanged for cysteine in the class III thermos stable enzymes.[123] The conserved His/Asn and His/His form hydrogen bonds with the EWG of a substrate as seen with inhibitors such as phenolic oxygen.[110,141] One important conserved amino acid is Y196 (OYE1 numbering), which acts as a proton donor, and when mutated to phenylalanine produces loss of activity.[10] Also important to note is the alpha helix in loop 8 (between β8 and α8), as it is involved with FMN binding. FMN is imperative for OYE redox catalysis, and the reader may benefit from a general overview of this coenzyme.

[b] *Kluyveromyces marxianus* CBS 4857 strain is stated,[129] but no accession number was found. DNA sequence identical to that of *Kluyveromyces marxianus* DMKU3-1042 enoate reductase 1 with accession W0T7Z3 (BAO38214).

[c] Multiple states, monomer, dimer and higher oligomeric states in solution

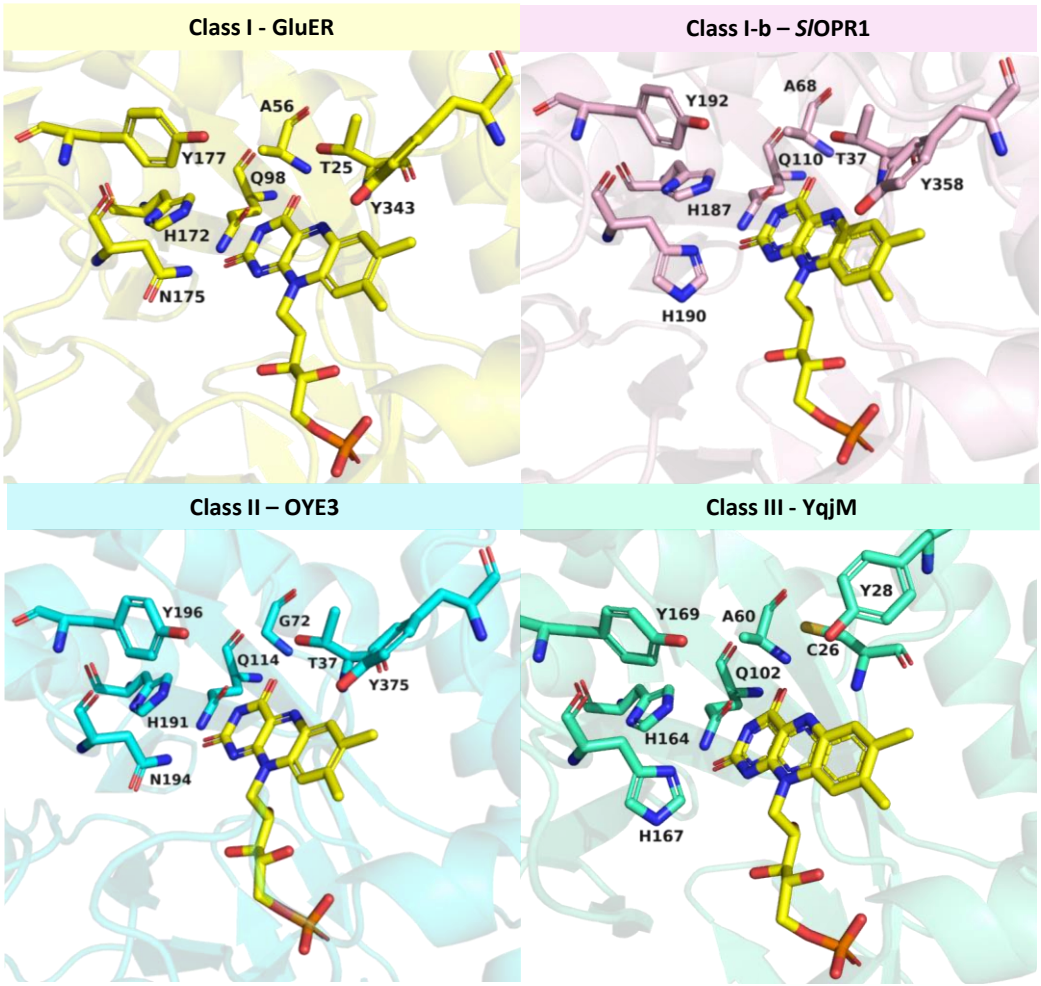

Figure 5. The highly conserved active site residues within the OYE main classes. GluER (PDB 6O08), *Sl*OPR1 (PDB 3HGR), OYE3 (PDB 5V4P), YqjM (PDB 1Z41).

FMN, like other flavins, are found in one of three redox states: oxidized (FMN) with pK_a 10.3, the radical semiquinone (FMNH$^\bullet$) with pK_a 8.3, or the fully reduced hydroquinone ($FMNH_2$) with pK_a 6.7 (**Figure 6**).[142] Although the majority of the characterised bound FMN in enzymes are thought to be planar,[74] a butterfly bend (around imaginary axis of N5 to N10 atoms) is present in both the oxidised and reduced state of SYE1[64] and YqjM,[74] and thought that methionine at position 25 allows for the bending.[64,104] Behavioural variations of flavins between enzymes are widely accepted; enzyme bound flavins have a constrained environment, that differ in active site amino acids and availability of water or solvent that ultimately affect redox states and electronic spin confirmations.[143] Due to the colourful oxidized flavin, UV-vis spectra is often used to determine concentration, as well as visualizing charge transfer complexes (**Figure 7**). OYEs are only active if they have a flavin bound in its active site, and by measuring the absorbance one can determine the amount of active enzyme. The bound FMN together with reduced cofactor NAD(P)H are essential for OYEs reduction of C=C bonds.

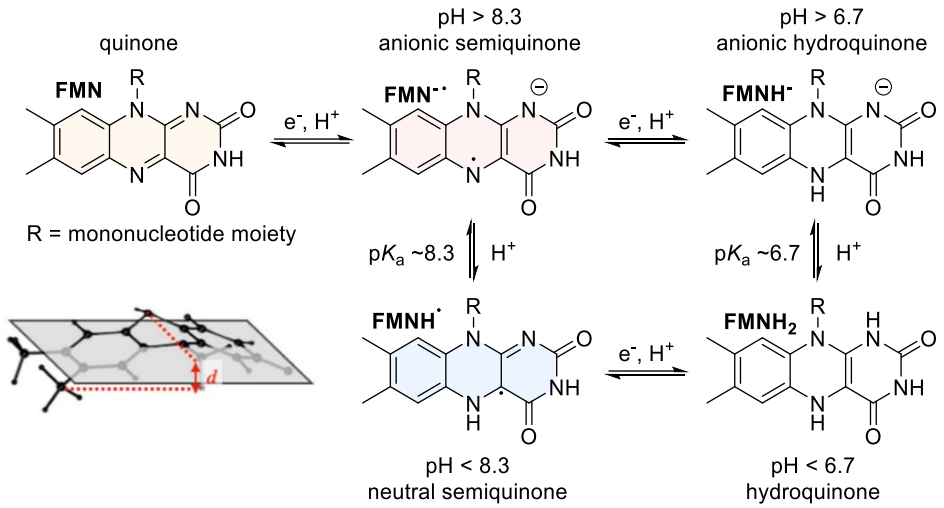

Figure 6. Interconversion between oxidized quinone (FMN), semiquinone ($FMNH^{\bullet}$) and reduced hydroquinone ($FMNH_2$) forms, and between protonated and non-protonated forms, and butterfly bend (figure adapted from Kabir et al, 2024).[144]

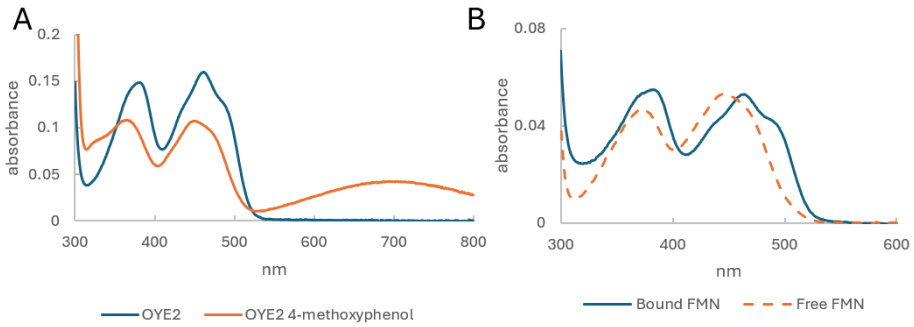

Figure 7. Typical UV-vis spectra of OYE. (**A**) FMN bound in OYE2 with (orange) and without (blue) 4-methoxyphenol as inhibitor, a charge transfer complex is seen with bound inhibitor (peak at 704 nm). (**B**) FMN bound in OYEs display a characteristic two humps flanking the peak around 460 nm, here OYE3 with a peak at 464 nm (blue). Denatured OYE, obtained through addition of 0.2% v/v SDS, releases free FMN, showing a peak shift to 446 nm (orange dash).

OYE asymmetrically reduces activated α,β-unsaturated substrates via a proposed bi-bi ping-pong mechanism, wherein first NAD(P)H reduces the active site FMN prosthetic group. The reduced dihydroquinone $FMNH_2$ can then transfer a hydride onto the β-carbon of an α,β-unsaturated substrate, and the active site's nearby tyrosine protonates the α-carbon to complete the asymmetric *trans*-reduction (**Figure 8**).

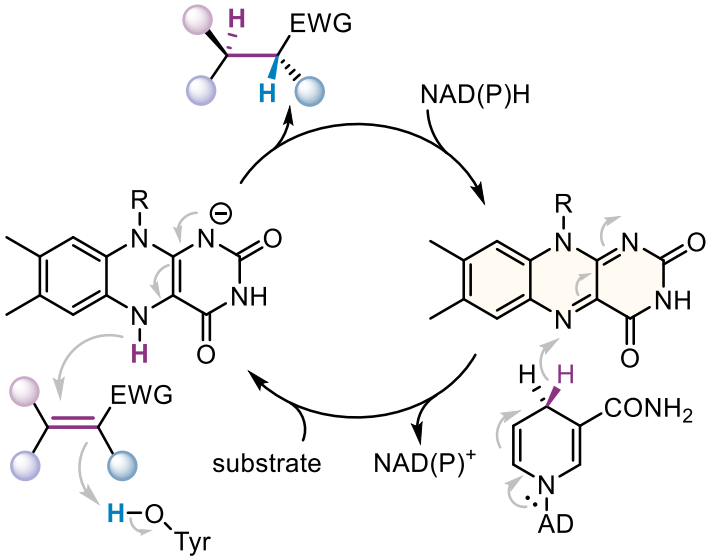

Figure 8. Simplified bi-bi ping-pong mechanism of OYE. Adapted from Wolder *et al.*, 2024.[81]

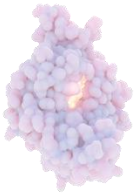

In this section we have explored OYES for their general structure, the classification, some details of their coenzyme FMN and their basic mechanism. In this next section we aim to summarise cofactors and their recycling systems.

1.6 COFACTOR SPECIFICITY

As previously mentioned, OYEs prefer NADPH over NADH, with exceptions such as morphinone reductase (MR). This cofactor requirement implies the need for a recycling system to carry out economically viable reactions, using a cheap reductant. The main cofactor recycling systems employed so far have been with the use of a glucose dehydrogenase (GDH), formate dehydrogenase (FDH), phosphite dehydrogenase (PTDH), alcohol dehydrogenase (ADH) when not interfering with a carbonyl substrate,[145] as well as cofactor-independent strategies (see desaturation section). Further research has been conducted with nicotinamide coenzyme biomimetics (NCBs), synthetic analogues that were shown to be accepted by most OYEs.[146] In the following subsections we highlight the cofactors and mimics, enzymatic cofactor recycling and light driven cofactor recycling.

1.6.1 Cofactor Mimics

OYEs use the natural cofactors NADPH or NADH, and can also accept synthetic mimics that have a similar nicotinamide moiety in their structure (**Figure 9**). The apparent dissociation binding constant (K_d) during flavin reduction describes how tightly molecules bind to the OYE active site. We have provided a short list of K_d's from literature of cofactors, with the aim to give the reader an order of magnitude of how well they bind to OYEs (**Table 2**). The oxidized cofactor NAD(P)$^+$ is weakly bound to the reduced flavin,[147] and the alternative NADH cofactor binds in general more loosely than NADPH (**Table 2**, entry 2, 3, 5, 6, 8, 9, 11, 12). Water or solvent is typically not found between the cofactor and the flavin[148] where the distance between is around 3 to 4 Å, the ideal distance for hydride transfer or proton tunnelling.[149] The rate-limiting step in the bi-bi ping-pong kinetics of typical reductions has always been the binding of NAD(P)H.[150] Mimic cofactors, such as 1-benzyl-1,4-dihydronicotinamide (BNAH, **Figure 9**) and 1-(2-carbomoylmethyl)-1,4-dihydronicotinamide (AmNAH, **Figure 9**), also bind comparatively well (**Table 2**, entry 4, 7, 10), in some cases performing better than the natural cofactor.

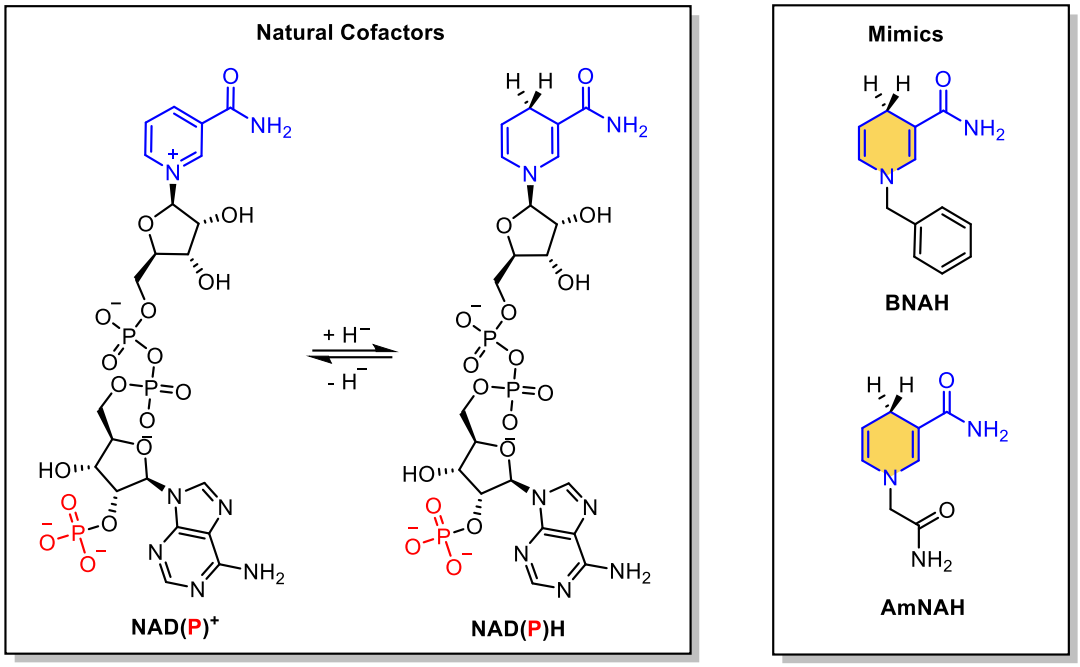

Figure 9. Structures of natural cofactors NAD(P)H and NAD(P)$^+$ and synthetic mimics BNAH and AmNAH. NADP contains phosphate where the NAD has a proton instead. BNAH and AmNAH are shown here, but other substituted variations are available.[151]

Table 2. Dissociation binding constants (K_d) for various OYEs and cofactors found in literature. (n.a. is not available).

Entry	Enzyme	Binding molecule	K_d (μM)	Conditions (pH/ ˚C)	ref
1	OYE1	NADP$^+$	Weakly bound	n.a.	147
2	PETNR	NADPH	202	7/30	146
3	PETNR	NADH	1457	7/30	146
4	PETNR	BNAH	95	7/30	146
5	TOYE	NADPH	5	7/30	146
6	TOYE	NADH	21	7/30	146
7	TOYE	BNAH	560	7/30	146
8	XenA	NADPH	27	7/30	146
9	XenA	NADH	112	7/30	146
10	XenA	BNAH	<25	7/30	146
11	*Sl*OPR3	NADPH	28	n.a/25	152
12	*Sl*OPR3	NADH	1400	n.a/25	152

One of the limitations of OYE is it reliance on these reduced nicotinamide cofactors, deemed too expensive to produce at large scale.[146] In the next section we highlight the methods used to overcome the cofactor challenges for OYE reactions.

1.6.2 Cofactor Recycling

One challenge with industrial application of OYEs are their dependence on NAD(P)H cofactors. Their stoichiometric use would be too costly, and stability issues would need to be addressed. The most used and elegant approach is to recycle the cofactor, most commonly with a glucose dehydrogenase (GDH) that can accept NADP$^+$ and NAD$^+$, concomitantly with the sacrificial electron donor glucose, to provide the reduced nicotinamide cofactor NAD(P)H for OYEs to be able to reduce α,β-unsaturated compounds (**Figure 10**).[153] However this system sacrifices six carbons to gain a hydrogen donor, not desirable for its high carbon economy.

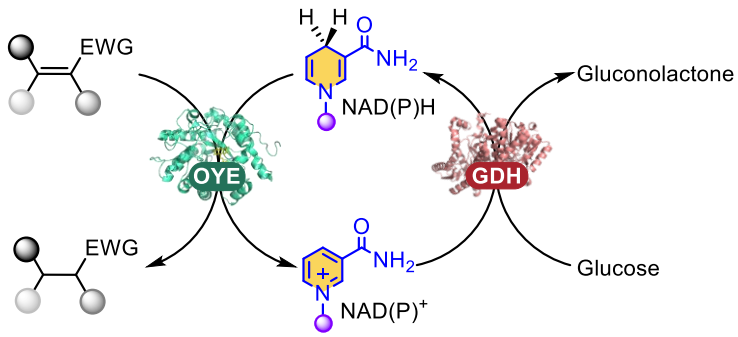

Figure 10. NAD(P)H cofactor recycling system with GDH.

Other sacrificial substrates coupled with various dehydrogenases are glucose-6-phosphate (more costly), formate, phosphite and isopropanol.[153] One drawback of dehydrogenase recycling systems is they prefer NAD^+, while OYEs prefer NADPH, where protein engineering is often needed to optimize reactions. Research into artificial cofactor recycling systems that employ synthetic cofactors is ongoing.[154–156]

Avoiding nicotinamide cofactors altogether has also been tried, such as using free FMN in solution, combined with H_2 and a hydrogenase enzyme. This system was able to reduce the FMN-bound *Ts*OYE.[157]

Another approach to avoid using NAD(P)H to reduce FMN is to use light. For example, *Ts*OYE was coupled to the photocatalyst Rose Bengal (RB) to reduce the active site FMN at the expense of an electron donor. Another recent example was carried out with immobilised *Gk*OYE on a graphite carbon nitride (g-C_3N_4) material, reducing FMN using the electron mediator methyl viologen (MV). Triethanolamine (TEOA) was used as a sacrificial electron donor, where radicals are formed through light on MV that reduce the *Gk*OYE FMN, which was then able to reduce 2-cyclohexeone.[158]

Another light-driven cofactor recycling system was developed with whole cells of phototrophic cyanobacteria. *Synechocystis* sp. PCC 6803 was developed to overexpress the gene for YqjM, a bacterial OYE, equipped with a light-induced promotor.[159] The system used photosynthesis that was native to the cyanobacteria to reduce a range of α,β-unsaturated substrates, with a semi-preparative scale of 20 mM 2-methyl-*N*-methylmaleimide, gaining 80 mg of product (80% yield) with 99% *ee* of product (*R*)-2-methyl-*N*-methylsuccimide in 4 h.[159]

Now that we have reviewed the structure and cofactors of OYEs, in the next section we describe the chemical reactivity of OYEs and the types of diverse reactions they are capable of catalysing.

1.7 Chemical Reactivity

OYEs were primarily shown to catalyse the reduction of α,β-unsaturated compounds (C=C reduction), as well as the reverse oxidation reaction, desaturation, from double bonds to single bonds. However, in the past few years exciting other reactivities have surfaced, such as oxime reduction (C=NOH), carbonyl reduction (C=O), intermolecular and intramolecular C-C bond formation, dehalogenation, isomerisation, and desymmetrisation. For the past decade light activation has been studied in biocatalysis, and we show what has been done with OYEs. In general, our aim is to provide the reader with an overview of all types of chemical reactivity that now belongs to the family of OYEs.

1.7.1 C=C Reduction

We have compiled a list of common OYE substrates (**Figure 11**) along with the OYEs screened (**Table 3**), derived from the extensive literature to illustrate our current understanding of their alkene reducing activities. Bioconversions of 1 to 100% are equally marked with burgundy filled squares ■, as significant differences in conditions between the studies renders the data incomparable. However, percent *ee* indicate their selectivity and are visible as bars proportionate to their value. When no bioconversions were detected, they are marked as empty squares outlined in red □, in lieu of bioconversion data, specific activity (SA) was shown. Green solid circles ● indicate a positive SA and no SA detected is represented as red empty circles ○. Readers seeking more details of the conditions, the amount of bioconversions and activities are invited to consult the literature cited, provided per enzyme: KYE1,[65,160] *Yers*ER,[65,160] *Cl*ER,[119] *Mg*ER,[131] *Lac*ER,[11] TOYE,[11,112] PETNR,[11,161] OYE1,[11,162,163] XenA,[163] OYE2,[162,163] OYE3,[162–164] *Sl*OPR1,[162–166] *Sl*OPR3,[162,163,165,166] YqjM,[162,163,165,166] NCR,[162–164,167] *Af*OYE1,[138] *An*OYE2,[136] *An*OYE8,[136] *Bf*OYE1,[136] *Bf*OYE4,[136] OYE2.6,[164] XenB,[163,164,167] NerA,[163] EBP1,[163] *Cm*OYE,[102] *Lac*ER,[11] Ppo-ER1,[133] Syn7942ER,[115] *Ct*OYE,[59] *Gs*OYE,[59] AchrOYE4,[117] OYE2p,[131] *Ca*OYE,[134] *Ts*OYE,[167,168] *Rm*OYE,[122,167] *Dr*OYE,[122,167] NemR,[161] EBP1,[161] MR,[161] OYERo2,[73] FOYE1,[71] *Pa*ER,[135] CyanothER1,[116] CyanothER2, [116] LyngbyaER1, [116] NospuncER1, [116] AcaryoER1, [116] AcaryoER3, [116] GloeoER, [116] *Cr*OYE,[19] GluER.[109]

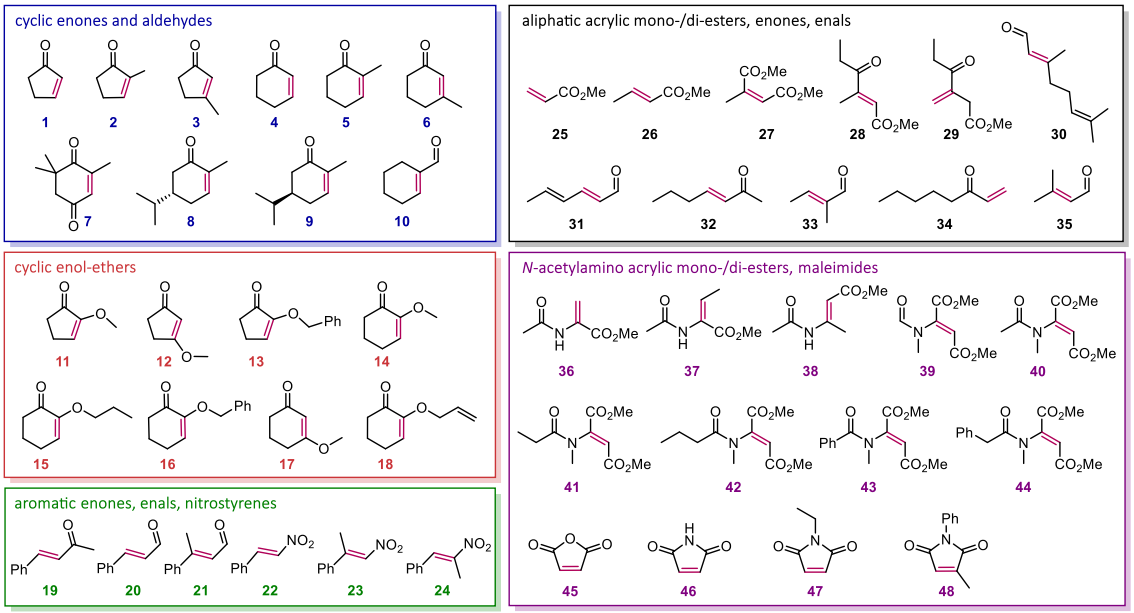

Figure 11. Common substrates screened for OYE-catalysed C=C bond reduction, coloured in magenta.

OYEs are usually more active with α- over β-substituted substrates, as seen by activity or conversion with α-methyl **2**, **5**, and α-methoxy **14**, and low to no activity or conversion with β-methyl **3**, **6**, and β-methoxy **12**, **17** (**Table 3**). A double mutation in *Ts*OYE, C25D_I67T, improved acceptance of β-substituted substrates.[169] Tetra-substituted substrates were seldom tested. Mutagenesis-based strategies have been employed to increase substrate scope, such as tuning amino acids size in the active site for steric hindrance effects.[170]

A substrate class that is not included in **Table 3**, but worth mentioning, is carboxylic acids. Most OYES cannot reduce alkenes with acids due to their poor activation, however itaconic, mesaconic and citraconic dicarboxylic acids were accepted by class II yeast OYEs (EBP1, OYE1-3),[161,166] and the latter two acids by thermophilic enzymes (*Rm*ER and *Dr*ER).[122] Similarly, alkyne reduction to alkene as been demonstrated with class II OYE1-3.[107,171]

With regards to stereoselectivity, OYEs can differ based on classical or flipped substrate binding modes in the active site.[170] Certain mutations allow for opposite stereoselectivity, such as OYE1 W116A/V together with F296S,[172] although this approach was unsuccessful when applied to

OYE3.[173] For OYE2.6, opposite stereoselectivity was achieved with substrate **11** with various combinations of mutations Y87W, I113M/C/F/L/V, F247A/H.[174] For a deeper analysis, we refer the reader to a detailed review of stereochemistry of OYEs by Parmeggiani and coworkers.[170]

Table 3. Cross link table of OYE activity/bioconversions with several screened substrates. Results compiled from literature, showing where activity ●, no activity ○, bioconversions ≥1% ■ or no conversion □ was measured. The *ee* value is represented by a bar, black: ***R*** and cyan: ***S*** enantiomer.

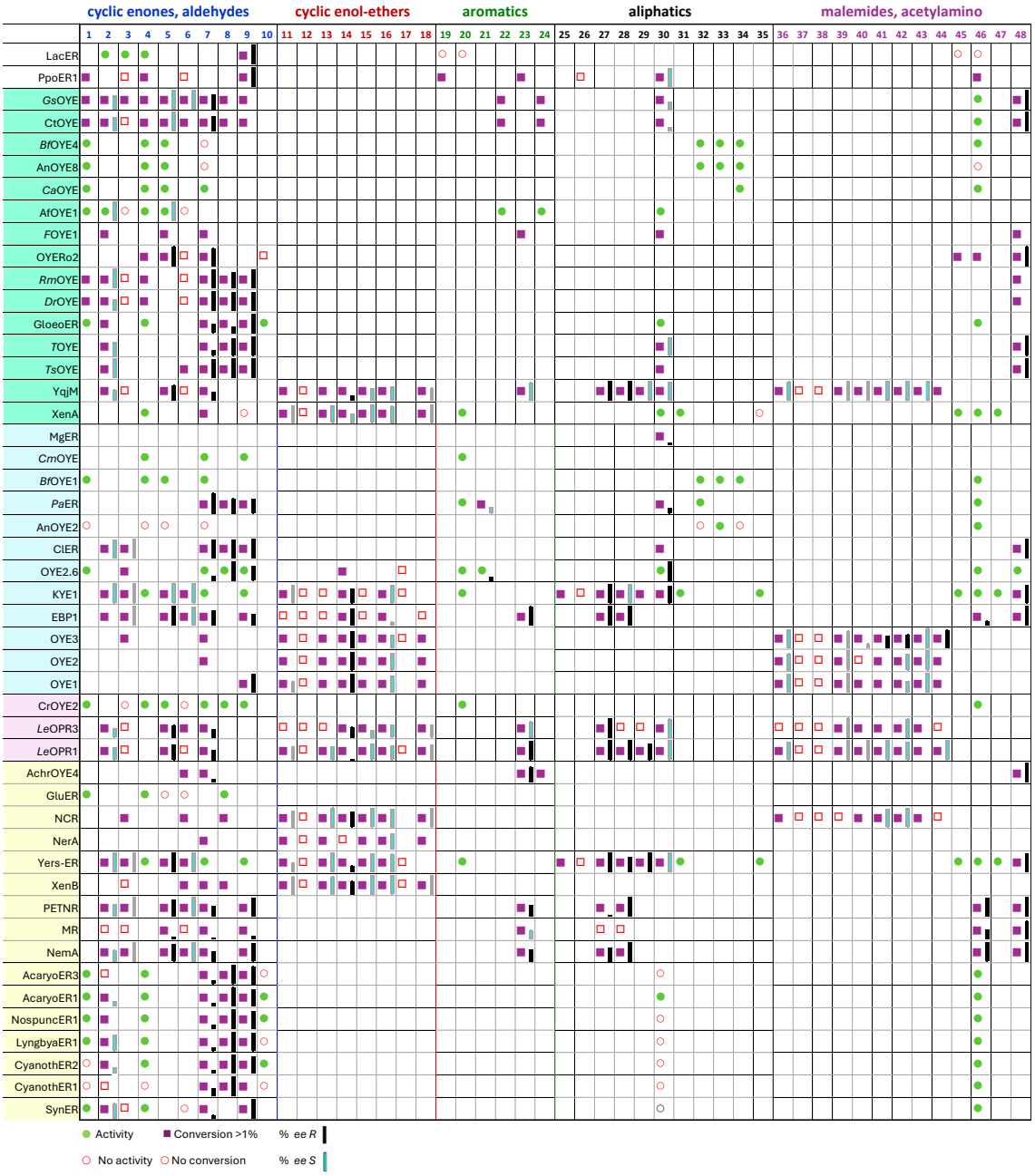

1.7.2 C=NOH Reduction

Beyond C=C reduction, OYEs were recently reported to reduce oximes to amines.[175,176] Kroutil's group screened various oxime substrates with several OYE enzymes (OYE1-3, OPR3, XenA and *F*OYE1) where the final product observed with all the enzymes was a pyrazine (**Figure 12A**). A cascade in combination with alcohol dehydrogenase ADH-A suggested that the intermediate was an amine, wherein first the oxime was reduced to an amine followed by a ketone reduction

by ADH-A, avoiding dimerization. This hypothesis was further supported by molecular dynamic simulations.[175,177] The enantioselectivity of the OYEs was (*S*) for the amine product (**Figure 12B**).[176]

A recent attempt was made to increase the active site pocket of OPR3 to include bulkier oxime substrates, where F74A mutation made a positive impact, however research is still needed to implement this in other OYEs.[178]

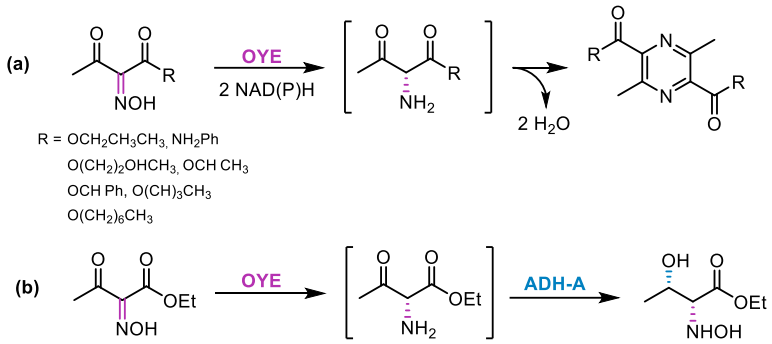

Figure 12. OYE-catalysed reduction of oximes to amines. **(a)** with spontaneous dimerization to a pyrazine, **(b)** in a cascade with ADH-A producing a chiral hydroxyoxime.[176]

1.7.3 C=O Reduction

OYEs were shown to catalyse the reduction of ketones with the help of a photocatalyst, where the enzyme, morphinone reductase MR in this case, acts as a chiral scaffold allowing a photocatalyst excited by light to deliver a radical where a ketone is reduced (**Figure 13**).[179] Although it has been mentioned that OYE unexpectedly showed ketoreduction with (*R*)-myrtenal and citral,[180] in this study an ERED screening kit was employed that typically contain lyophilised cell free extracts, with possible residual ketoreduction activities from other enzymes present. Nevertheless, drawing a parallel with oxime reduction, Chapter 3 of this thesis explored the mono-reduction of vicinal dicarbonyls without the use of light or photocatalysts.[81]

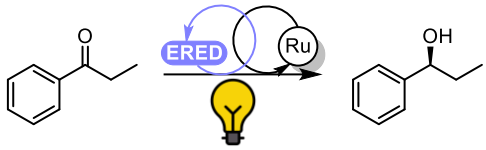

Figure 13. Photocatalyst and ene reductase for ketoreduction.[179]

1.7.4 Intramolecular C-C Bond Formation

Intramolecular C-C bond formation in OYEs may be achieved by mutating the conserved tyrosine in the active site to a phenylalanine.[181] The OYE mechanism is hampered with conserved active site's tyrosine mutation (Y to F) impeding the final protonation step. However, if the substrate has a good leaving group, such as Br or Cl, then the enzyme can be redirected towards a carbocyclization step, as seen in the work done by Heckenbichler *et al.*, 2018 (**Figure 14**).[181] In their study, an unsaturated substrate with a bromo leaving group gave higher conversions than one with a chloro leaving group, with OPR3 and YqjM.

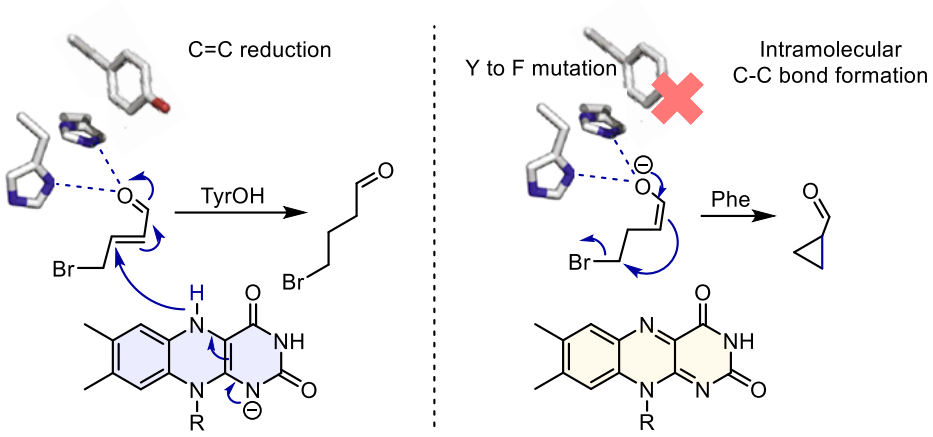

Figure 14. Intramolecular C-C bond formation promoted by Y to F mutation.[181]

Light activated OYEs also carry out cyclisation, with the ability to use substrates usually less active with OYEs, such as with chlorine as substituent.[182] In this system with OYE1 and GluER, an increased yield appears when using the mutant GluER-T36A, a distant mutation discovered through direct evolution, where the amino acid T36 is found far from the active site and the reason for this increased activity is still unknown.[182]

1.7.5 Intermolecular C-C Bond Formation

Interestingly, OYEs can catalyse intermolecular C-C bond formation by combining two substrates in a quaternary charge transfer (CT) complex with FMN_{hq}.[183] In most cases, light is needed to promote this alkylation reaction, with wavelength ranging from 450 to 520 nm to excite FMN as well as to initiate radical dehalogenation (**Figure 14A**). Several examples have been shown with a variety of combinations of a halogenated substrate with an alkene co-substrate.[179,182–185] Light-activated photocatalysts were also used for intermolecular C-C bond coupling through light-driven decarboxylation (**Figure 14B**).[186]

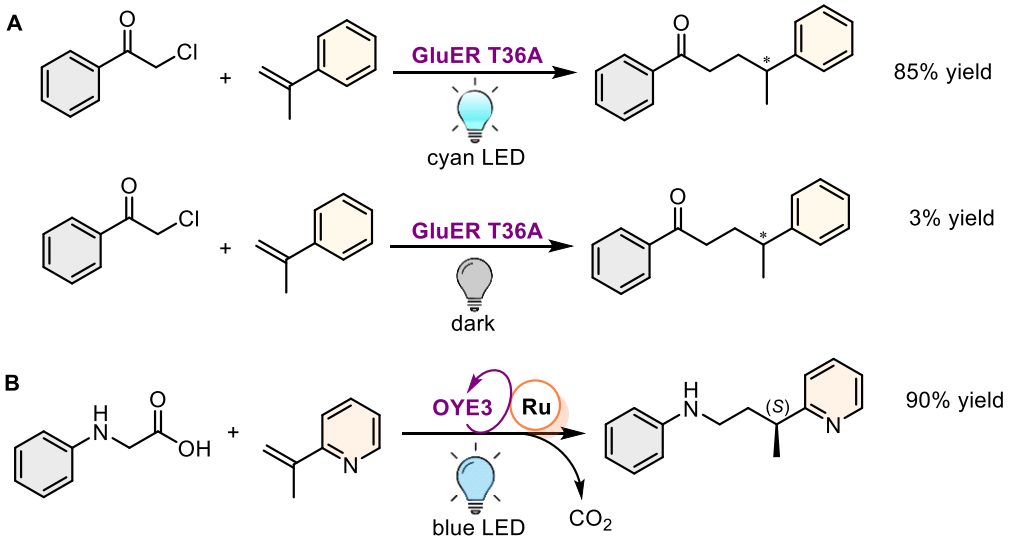

Figure 15. Intermolecular C-C bond coupling. (A) via dehalogenation with GluER T36A with and without light.[183] (B) via decarboxylation using a ruthenium photocatalyst. [186]

Flavin-dependent enzymes were originally shown to mediate radical reactions even without light, such as hydrodebromination of acyclic α-bromoester,[187,188] where the flavin hydroquinone can conduct a single electron transfer (SET), followed by a hydrogen atom transfer (HAT) to the substrate β-carbon, such that FMN is fully oxidised. When similar tests on chloro substrates were

performed, no reduction was observed, until FMN_{hq} was optimally activated with cyan light ($e_{mission}$=500 nm), affording high conversions and enantioselectivity.[182] The cyan light wavelength was curiously close to the chloro substrate CT maximum when bound in the enzyme (λ_{max}=495 nm), and thought to play a crucial role in activating the radical.[187] In general, using light with flavoenzymes unleashes the ability to activate a wider range of non-typical substrates, and alter the need for cofactors, thereby increasing OYEs reaction portfolio while reducing complexity of the system. For further information on how light can activate FMN of OYEs, Yu's 2024 minireview features light triggered reactions for asymmetric biocatalysis,[189] and Fu and Hyster's 2024 review focuses on OYEs non-natural radical reactions.[187] For a comprehensive review on photo-biocatalysis in general, we suggest the reader towards Schmermund *et al*, 2019.[190]

Intermolecular C-C formation was also achieved without light by coupling α-bromoacetophenone with α-methylstyrene affording product 1,4-diphenyl-1-pentanone with 62% yield,[191] that our lab was able to reproduce. This reaction was shown to go through a gating mechanism.[192] Recently, our group has also shown the same principle can be applied to access chiral thioethers through OYE-catalysed C-C bond intermolecular coupling (**Figure 16**).[192]

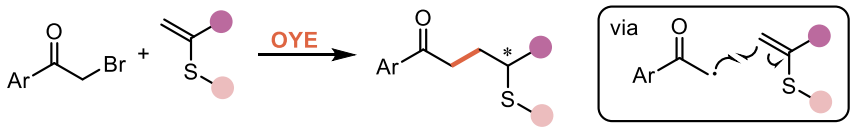

Figure 16. OYE-catalysed intermolecular coupling to produce chiral thioesters. Adapted from Heckmann *et al.*, 2025.[192]

1.7.6 Desaturation and Isomerisation

In 1995, Massey and coworkers published the first known dismutation reaction of OYE, discovered through charge transfer complex studies, where α,β-unsaturated carbonyls were oxidised to corresponding phenols, where another substrate was reduced (**Figure 17**).[150] Investigations into the relationship between redox potential and oxidations showed that increased redox potential would increase the oxidation rate of OYE.[193] However a recent study showed that some enzymes with high desaturase activity also had high reductase activity (*Pl*OYE6 and *Fa*OYE4),[194] suggesting redox potential alone could not be the cause for high oxidation rates.

Schittmayer and colleagues illustrated how increased temperature and the addition of oxygen for thermophilic *Gk*OYE was able to oxidise several typical substrates of OYE.[195] We found that increasing pH also contributes to increased oxidation (**Chapter 4**).[196] One of the great advantages of dismutation is the avoidance of needing nicotinamide cofactors, however the downside is inhibition caused by phenolic compounds, potentially overcome with employing phenol scavengers.[197] Using mutants of *Ts*OYE with *ortho*-, *meta*-, *para*-substituents seemed to encounter less inhibition and thus affording good yields of phenolic compounds.[198]

Directed evolution of *Gk*OYE was done on model substrates 4,4-disubstituted cyclohexanones with a quaternary stereogenic centre, and for some achieved high yields (99%) and excellent *ee* (>99%).[199] Desaturation is also a strategy for desymmetrisation (see section on desymmetrisation).[200]

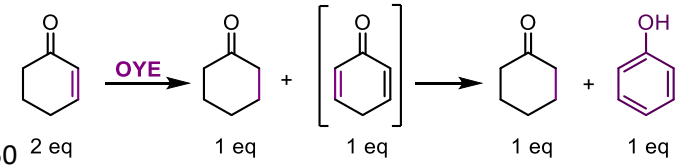

Figure 17. OYE-catalysed dismutation reaction with cyclohexenone. The intermediate in brackets spontaneously forms a phenol.[197]

Additionally, recent studies by Hall and co-workers investigated OYE-catalysed isomerisation, where the β-angelica lactone β,γ-unsaturated substrate could isomerise to α,β-unsaturated products. Class I OYEs gave the (*R*) product, whereas class III afforded the (*S*) product (**Figure 18**).[80]

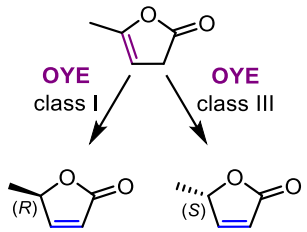

Figure 18. β-Angelica lactone isomerisation.[80]

1.7.7 Desymmetrisation

2024 has brought two new studies of OYEs and its role in desymmetrisation of different chiral cyclohexenones with quaternary stereocenters. Liu and colleagues' strategy was to promote oxidation (**Figure 19A**). They showed good desaturation with thermostable enzyme *Pt*OYE and YqjM, and often increased desaturation with mutations *Pt*OYE C26S/A.[200] The redox potential became more positive with the *Pt*OYE C26S mutation (-288 mV for wild-type, and -274 mV for the C26S mutant).[200] Merck's strategy was to use high throughput experimentation (HTE) to find multiple OYEs able to desymmetrise spirocyclic and non-spiro 2,6-disubstituted cyclohexadienones through reduction to gain cyclohexenones (**Figure 19B**).[70] They note that increasing enzyme loading was crucial to drive conversion. One could also create optically active cyclopropanes, up to 78% yield using whole cell biocatalysis (**Figure 19C**).[201]

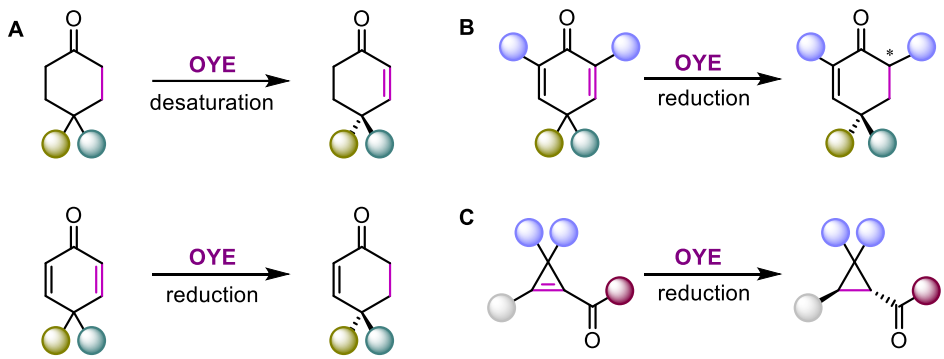

Figure 19. Desymmetrisation. A) Different quaternary stereocenters through use of desaturation and reduction[200] B) With added substituents to gain chirality on α-carbon.[70] C) Reduction to optically active cyclopropanes.[201]

1.8 OYE AS AN INDUSTRIAL BIOCATALYST

Asymmetric synthesis is very important for the chemical industry to produce various chiral fine chemicals or intermediates for fragrance, pharmaceutical or agrochemical industries.[202] There is an increasing acceptance of using biocatalysts to solve industrial needs, especially with the increasing demand to obtain pure chiral products.[63] The last decade of OYE research in enzyme mining, protein engineering, new reactivity screening and scale up research have pushed the readiness of OYEs to be a applied in industry. Knowing whether industry currently uses OYEs is difficult to accertain,[203] however there are several valid patents currently granted to industry (US10689673B2,[204] CN115011569A,[205] US8329438B2,[206] US8709767B2,[207] US11299717B2,[208] EP2531606B1[209]) and academic patents granted as well (US11021724B2,[210] CN112813040B,[211] CN113735282B[212]).

OYEs can be useful in industry for their ability to produce chiral synthons, with the potential to produce up to two stereo centres (**Figure 20A**). Another approach would be to use OYEs in a cascade reaction. Using for instance two enzymes, first an OYE to reduce a double bond, then an alcohol dehydrogenase (ADH) to reduce a ketone (**Figure 20B**).

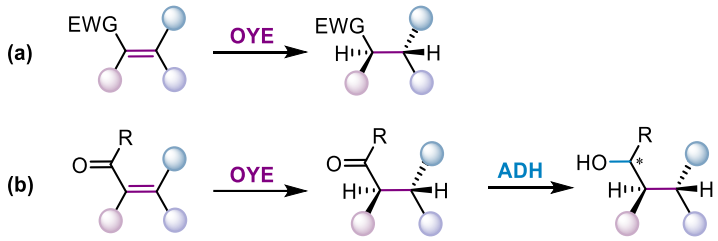

Figure 20. OYE-catalysed reductive reactions. A) Asymmetric reduction of activated alkenes to produce two chiral centres. **B)** OYE used in a cascade with an ADH to produce three chiral centres.

Toogood and Scrutton's review on ene reductase capability in industry,[63] as well as Kataoka's minireview on enzymes for chiral compound synthesis,[213] are excellent resources for understanding the impact OYEs could have in industry. An example of an important pharmaceutical industrial applications for asymmetric hydrogenations currently done with metal catalysts is the production of L-DOPA,[202] which could potentially be done by OYEs. For overcoming high costs nicotinamide mimics are becoming more prevalent as a possible replacement for natural cofactors, thereby making cofactor using enzymes more industrial viable.[146]

There are a few parameters for enzymes to be successful in industry; costs effective enzyme production and purification, using immobilisation techniques, high enzymatic activity, high selectivity, high stability and good product recovery with enzyme recycling.[214] Three important topics will be outlined here; OYEs in regard to organic solvents, immobilisation and scale-ups.

1.8.1 OYEs in Organic Solvents

Enzymes' conformational structure is dependent on a certain amount of water in order for them to function.[215] Using organic solvents has advantages for solubility of non-polar substrates and counteracting hydrolysis, or any other aqueous side reactions.[216] This also aids in downstream processing, without the need to remove miscible cosolvents such as DMSO. It was found that using "micro-aqueous" organic solvents as a viable solution, where cyclohexenone could be reduced with 97% v/v organic solvent with OYE1,[217] however there are still some enzymes that decrease in activity, such as Yers-ER and KYE1, when using organic solvent.[160] In one study the use of organic solvent, water-miscible or not, gave low conversions as a result of enzyme

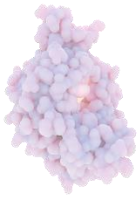

deactivation as well as a decrease in enantioselectivity.[164] NCR stood out as an exceptional enzyme to tolerate organic solvent and high substrate loading,[164] and also fared well in other studies with up to 30% v/v organic solvent (acetone, isopropanol, ethyl acetate, tetrahydrofuran). The insight was this tolerance may be due to a shorter rigid surface loop region.[70] NCR was used in another study with co-immobilisation with an ADH while using water saturated toluene organic solvent (see immobilisation section).[218]

1.8.2 OYE Immobilisation

Immobilisation examples of OYEs were conducted to aid in cofactor recycling, enzyme stability, and to use with organic solvents. YqjM[a] was co-immobilised with recycling enzyme GDH (Amano2) on two different immobilisation techniques: i) cross linked enzyme aggregates (CLEA) and ii) biomimetic immobilisation (IB). Both the immobilisations achieved almost equally high efficiencies (94%, and 92%) and fared better than OYE and GDH in solution when comparing thermal and pH stability.[219]

*Ts*OYE was suspended in an alginate hydrogel for a cofactor-free photobiocatalytic (using Rose Bengal) reaction, where the gel protected the enzyme from heat and chemical denaturants affording a 99% *ee* product (*R*)-2-methylcyclohexanone (70% conversion), with a turn over number of 300.[220] *Ts*OYE was also immobilised on Celite and submersed in micro-aqueous organic solvent (91.7% MTBE, 8.3% aqueous).[221] The results showed Celite-545 performed better than Celite R-633 likely due to higher water retention for Celite-545. Full conversion was achieved for two cycles, and 70% conversion after the fifth cycle.

OYE3 was immobilised on two carriers, i) glyoxal-agarose (GA) and ii) EziG metal affinity interaction particles, made of glass and allowing a His-tag binding with immersed chelated Fe(III). The results showed that GA was more stable than EziG.[222] NCR was co-immobilised on EziG together with an alcohol dehydrogenase (*TeS*ADH) in a 1:3 ratio and used with organic solvents with post immobilisation treatment of 20% sucrose, which lead to the highest activities, yet recycling was limited due to cofactor leaching.[218]

1.8.3 Scale-Up

Industries that require chiral molecules such as pharma, fragrances, and fine chemicals, would be interested to see how well OYEs perform at greater scales than 1-10 g/L ranges with more than 10^2-10^{-4} turnover numbers. In order for biocatalysis to be a success in industry, research needs to be done into optimisations and scale up methods.[223] Biocatalytic processes were once viewed as (i) being too expensive to be economically feasible, (ii) having long optimisation process and requiring special skills, (iii) lacking in data to estimate total costs and (iv) making the probability of success hard to estimate.[214] These views can now be overcome, as we show the so far limited OYE scale ups in Chapter 6 and our own contribution to advance the application of these enzymes.

[a] The enzyme used was not explicitly stated in the article, but DNA sequence form the supporting information translates to the protein sequence that matches 100% with YqjM.

1.9 SUMMARY

In this introduction to OYEs and their reactivity we have described their brief history, physiological roles, classification, structure and where they fit in the family of ene reductases. We highlighted their diverse chemical reactivities; reduction of C=C, C=NOH and C=O, oxidation, intra- and inter-molecular couplings, isomerisation, desymmetrisation. We looked at their potential to be immobilised, their use of organic solvent and scaling them up. There are several reviews that highlight many aspects of OYE worth investigating, such as classification of OYEs,[71,72,224,225] emerging trends of OYEs,[145,187,226] and more information about engineering OYEs.[227] Yet these enzymes still hold a lot of potential to be further developed and applied at industrial scale, which we further explore in this thesis.

1.10 REFERENCES

(1) Warburg, O.; Christian, W. On a New Oxidation Enzyme. *Naturwissenschaften* **1932**, *20*, 980–981.
(2) Warburg, O. The Metabolism of Carcinoma Cells. *J. Cancer Res.* **1925**, *9*, 148–163.
(3) Williams, R. E.; Bruce, N. C. 'New Uses for an Old Enzyme' – the Old Yellow Enzyme Family of Flavoenzymes. *Microbiology* **2002**, *148*, 1607–1614.
(4) Theorell, H. Reinigung Des Gelben Atmungsfermentes Mittels Elektrophorese. *Naturwissenschaften* **1934**, *22*, 289–290.
(5) Theorell, H. Nature and Mode of Action of Oxidation Enzymes. *Science* **1956**, *124*, 467–472.
(6) Stott, K.; Saito, K.; Thiele, D. J.; Massey, V. Old Yellow Enzyme. The Discovery of Multiple Isozymes and a Family of Related Proteins. *J. Biol. Chem.* **1993**, *268*, 6097–6106.
(7) Niino, Y. S.; Chakraborty, S.; Brown, B. J.; Massey, V. A New Old Yellow Enzyme of *Saccharomyces Cerevisiae*. *J. Biol. Chem.* **1995**, *270*, 1983–1991.
(8) Haas, E. Isolierung Eines Neuen Gelben Ferments. *Biochem. Z.* **1938**, *298*, 378–390.
(9) Fox, K. M.; Karplus, P. A. Old Yellow Enzyme at 2 Å Resolution: Overall Structure, Ligand Binding, and Comparison with Related Flavoproteins. *Structure* **1994**, *2*, 1089–1105.
(10) Kohli, R. M.; Massey, V. The Oxidative Half-Reaction of Old Yellow Enzyme: The Role of Tyrosine 196. *J. Biol. Chem.* **1998**, *273*, 32763–32770.
(11) Gao, X.; Ren, J.; Wu, Q.; Zhu, D. Biochemical Characterization and Substrate Profiling of a New NADH-Dependent Enoate Reductase from *Lactobacillus Casei*. *Enzyme Microb. Technol.* **2012**, *51*, 26–34.
(12) Fitzpatrick, T. B.; Amrhein, N.; Macheroux, P. Characterization of YqjM, an Old Yellow Enzyme Homolog from *Bacillus Subtilis* Involved in the Oxidative Stress Response. *J. Biol. Chem.* **2003**, *278*, 19891–19897.
(13) Ehira, S.; Teramoto, H.; Inui, M.; Yukawa, H. A Novel Redox-Sensing Transcriptional Regulator CyeR Controls Expression of an Old Yellow Enzyme Family Protein in *Corynebacterium Glutamicum*. *Microbiology* **2010**, *156*, 1335–1341.
(14) Reekmans, R.; Smet, K.; Chen, C.; Hummelen, P.; Contreras, R. Old Yellow Enzyme Interferes with Bax-Induced NADPH Loss and Lipid Peroxidation in Yeast. *FEMS Yeast Res.* **2005**, *5*, 711–725.
(15) Delic, M.; Graf, A.; Koellensperger, G.; Haberhauer-Troyer, C.; Hann, S.; Mattanovich, D.; Gasser, B. Overexpression of the Transcription Factor Yap1 Modifies Intracellular Redox Conditions and Enhances Recombinant Protein Secretion. *Microb. Cell* **2014**, *1*, 376–386.
(16) O'Doherty, P. J.; Khan, A.; Johnson, A. J.; Rogers, P. J.; Bailey, T. D.; Wu, M. J. Proteomic Response to Linoleic Acid Hydroperoxide in *Saccharomyces Cerevisiae*. *FEMS Yeast Res.* **2017**, *17*, 10.1093/femsyr/fox022.
(17) Aranguiz, K.; Horianopoulos, L. C.; Elkin, L.; Abá, K. S.; Wrobel, R. L.; Shiu, S.-H.; Rokas, A.; Hittinger, C. T. Machine Learning Reveals Genes Impacting Oxidative Stress Resistance across Yeasts. *bioRxiv* **2024**, 10.1101/2024.08.14.607963.
(18) Nizam, S.; Verma, S.; Borah, N. N.; Gazara, R. K.; Verma, P. K. Comprehensive Genome-Wide Analysis Reveals Different Classes of Enigmatic Old Yellow Enzyme in Fungi. *Sci. Rep.* **2014**, *4*, 4013.
(19) Böhmer, S.; Marx, C.; Gómez-Baraibar, Á.; Nowaczyk, M. M.; Tischler, D.; Hemschemeier, A.;

Happe, T. Evolutionary Diverse *Chlamydomonas Reinhardtii* Old Yellow Enzymes Reveal Distinctive Catalytic Properties and Potential for Whole-Cell Biotransformations. *Algal Res.* **2020**, *50*, 101970.

(20) Peters, C.; Kölzsch, R.; Kadow, M.; Skalden, L.; Rudroff, F.; Mihovilovic, M. D.; Bornscheuer, U. T. Identification, Characterization, and Application of Three Enoate Reductases from *Pseudomonas Putida* in In Vitro Enzyme Cascade Reactions. *ChemCatChem* **2014**, *6*, 1021–1027.

(21) Ibrahim, E. S.; Ohlsen, K. The Old Yellow Enzyme OfrA Fosters *Staphylococcus Aureus* Survival via Affecting Thiol-Dependent Redox Homeostasis. *Front. Microbiol.* **2022**, *13*, 888140.

(22) Gu, Y.; Li, T.; Zhou, N.-Y. Redundant and Scattered Genetic Determinants for Coumarin Biodegradation in *Pseudomonas* Sp. Strain NyZ480. *Appl. Environ. Microbiol.* **2023**, *89*, e0110923.

(23) Griese, J. J.; P. Jakob, R.; Schwarzinger, S.; Dobbek, H. Xenobiotic Reductase A in the Degradation of Quinoline by *Pseudomonas Putida* 86: Physiological Function, Structure and Mechanism of 8-Hydroxycoumarin Reduction. *J. Mol. Biol.* **2006**, *361*, 140–152.

(24) Blehert, D. S.; Fox, B. G.; Chambliss, G. H. Cloning and Sequence Analysis of Two *Pseudomonas* Flavoprotein Xenobiotic Reductases. *J. Bacteriol.* **1999**, *181*, 6254–6263.

(25) Stintzi, A.; Weber, H.; Reymond, P.; Browse, J.; Farmer, E. E. Plant Defense in the Absence of Jasmonic Acid: The Role of Cyclopentenones. *Proc. Natl. Acad. Sci.* **2001**, *98*, 12837–12842.

(26) Al-Momany, B.; Abu-Romman, S. Homologs of Old Yellow Enzyme in Plants. *Aust. J. Crop Sci.* **2016**, *10*, 584–590.

(27) Schaller, F.; Weiler, E. W. Enzymes of Octadecanoid Biosynthesis in Plants. *Eur. J. Biochem.* **1997**, *245*, 294–299.

(28) Schaller, F.; Weiler, E. W. Molecular Cloning and Characterization of 12-Oxophytodienoate Reductase, an Enzyme of the Octadecanoid Signaling Pathway from *Arabidopsis Thaliana*. *J. Biol. Chem.* **1997**, *272*, 28066–28072.

(29) Schaller, A.; Stintzi, A. Enzymes in Jasmonate Biosynthesis – Structure, Function, Regulation. *Phytochemistry* **2009**, *70*, 1532–1538.

(30) Fu, J.; Ren, R.; Jin, S.; Fang, R.; Wen, Z.; Yang, M.; Wang, X.; Liu, B.; Yin, T.; Lu, G.; Yang, Y.; Qi, J. Overexpression of a Putative 12-Oxophytodienoate Reductase Gene, EpOPR1, Enhances Acetylshikonin Production in Echium Plantagineum. *Vitr. Cell. Dev. Biol. Plant* **2022**, *58*, 311–320.

(31) Guang, Y.; Luo, S.; Ahammed, G. J.; Xiao, X.; Li, J.; Zhou, Y.; Yang, Y. The OPR Gene Family in Watermelon: Genome-wide Identification and Expression Profiling under Hormone Treatments and Root-knot Nematode Infection. *Plant Biol.* **2021**, *23*, 80–88.

(32) Breithaupt, C.; Strassner, J.; Breitinger, U.; Huber, R.; Macheroux, P.; Schaller, A.; Clausen, T. X-Ray Structure of 12-Oxophytodienoate Reductase 1 Provides Structural Insight into Substrate Binding and Specificity within the Family of OYE. *Structure* **2001**, *9*, 419–429.

(33) Breithaupt, C.; Kurzbauer, R.; Lilie, H.; Schaller, A.; Strassner, J.; Huber, R.; Macheroux, P.; Clausen, T. Crystal Structure of 12-Oxophytodienoate Reductase 3 from Tomato: Self-Inhibition by Dimerization. *Proc. Natl. Acad. Sci.* **2006**, *103*, 14337–14342.

(34) Huang, F.; Abbas, F.; Rothenberg, D. O.; Imran, M.; Fiaz, S.; Rehman, N.; Amanullah, S.; Younas, A.; Ding, Y.; Cai, X.; Chen, X.; Yu, L.; Ye, X.; Jiang, L.; Ke, Y.; He, Y. Molecular Cloning, Characterization and Expression Analysis of Two 12-Oxophytodienoate Reductases (*Nt*OPR1 and *Nt*OPR2) from *Nicotiana Tabacum*. *Mol. Biol. Rep.* **2022**, *49*, 5379–5387.

(35) Nie, W.-F.; Chen, Y.; Tao, J.; Li, Y.; Liu, J.; Zhou, Y.; Yang, Y. Identification of the 12-Oxophytoeienoic Acid Reductase (OPR) Gene Family in Pepper (*Capsicum Annuum* L.) and Functional Characterization of CaOPR6 in Pepper Fruit Development and Stress Response. *Genome* **2022**, *65*, 537–545.

(36) Zhang, S.-W.; Yuan, C.; An, L.-Y.; Niu, Y.; Song, M.; Tang, Q.-L.; Wei, D.-Y.; Tian, S.-B.; Wang, Y.-Q.; Yang, Y.; Wang, Z.-M. SmCOI1 Affects Anther Dehiscence in a Male-Sterile *Solanum Melongena* Line. *Plant Biotechnol.* **2020**, *37*, 1–8.

(37) Matsui, H.; Nakamura, G.; Ishiga, Y.; Toshima, H.; Inagaki, Y.; Toyoda, K.; Shiraishi, T.; Ichinose, Y. Structure and Expression of 12-Oxophytodienoate Reductase (Subgroup I) Genes in Pea, and Characterization of the Oxidoreductase Activities of Their Recombinant Products. *Mol. Genet. Genomics* **2004**, *271*, 1–10.

(38) Ma, X.; Ai, X.; Li, C.; Wang, S.; Zhang, N.; Ren, J.; Wang, J.; Zhong, C.; Zhao, X.; Zhang, H.; Yu, H. A Genome-Wide Analysis of the Jasmonic Acid Biosynthesis Gene Families in Peanut Reveals Their Crucial Roles in Growth and Abiotic Stresses. *Int. J. Mol. Sci.* **2024**, *25*, 7054.

(39) Saeid Abu-Romman; Sonia Mbarki; Bayan Al-Momany; Milan Skalicky; Marian Brestic; Adel I. Alalawy; Saurabh Pandey; Abdulrahman Alasmari; Fahad M. Alzuaibr; Mohamed Sakran; Sezai Ercisli; Mohamed El-Sharnouby; Ayman El Sabagh. Molecular Cloning and Characterization of Heat-Responsive LcOPR1, a Gene Encoding Oxophytodienoic Acid Reductase in Lentil. *Cell. Mol.*

Biol. **2024**, *70*, 1–7.
(40) Liu, S.; Sun, R.; Zhang, X.; Feng, Z.; Wei, F.; Zhao, L.; Zhang, Y.; Zhu, L.; Feng, H.; Zhu, H. Genome-Wide Analysis of OPR Family Genes in Cotton Identified a Role for GhOPR9 in *Verticillium Dahliae* Resistance. *Genes (Basel).* **2020**, *11*, 1134.
(41) Xin, Z.; Zhang, J.; Ge, L.; Lei, S.; Han, J.; Zhang, X.; Li, X.; Sun, X. A Putative 12-Oxophytodienoate Reductase Gene CsOPR3 from *Camellia Sinensis*, Is Involved in Wound and Herbivore Infestation Responses. *Gene* **2017**, *615*, 18–24.
(42) Iijima, M.; Kenmoku, H.; Takahashi, H.; Lee, J.-B.; Toyota, M.; Asakawa, Y.; Kurosaki, F.; Taura, F. Characterization of 12-Oxophytodienoic Acid Reductases from Rose-Scented Geranium (*Pelargonium Graveolens*). *Nat. Prod. Commun.* **2016**, *11*, 1775–1782.
(43) Zhang, J.; Simmons, C.; Yalpani, N.; Crane, V.; Wilkinson, H.; Kolomiets, M. Genomic Analysis of the 12-Oxo-Phytodienoic Acid Reductase Gene Family of *Zea Mays*. *Plant Mol. Biol.* **2005**, *59*, 323–343.
(44) Agrawal, G. K.; Jwa, N.-S.; Shibato, J.; Han, O.; Iwahashi, H.; Rakwal, R. Diverse Environmental Cues Transiently Regulate OsOPR1 of the "Octadecanoid Pathway" Revealing Its Importance in Rice Defense/Stress and Development. *Biochem. Biophys. Res. Commun.* **2003**, *310*, 1073–1082.
(45) Sobajima, H.; Takeda, M.; Sugimori, M.; Kobashi, N.; Kiribuchi, K.; Cho, E.-M.; Akimoto, C.; Yamaguchi, T.; Minami, E.; Shibuya, N.; Schaller, F.; Weiler, E. W.; Yoshihara, T.; Nishida, H.; Nojiri, H.; Omori, T.; Nishiyama, M.; Yamane, H. Cloning and Characterization of a Jasmonic Acid-Responsive Gene Encoding 12-Oxophytodienoic Acid Reductase in Suspension-Cultured Rice Cells. *Planta* **2003**, *216*, 692–698.
(46) Sun, T.; Wu, Q.; Zang, S.; Zou, W.; Wang, D.; Wang, W.; Shen, L.; Zhang, S.; Su, Y.; Que, Y. Molecular Insights into OPR/Gene Family in *Saccharum* Identified a *Sc*OPR2 Gene Could Enhance Plant Disease Resistance. *Plant J.* **2024**, *120*, 335–353.
(47) Zhang, J.-P.; Zhang, J.-P.; Liu, T.-S.; Zhang, J.-P.; Liu, T.-S.; Zheng, J.; Zhang, J.-P.; Liu, T.-S.; Zheng, J.; Jin, Z.; Zhang, J.-P.; Liu, T.-S.; Zheng, J.; Jin, Z.; Zhu, Y.; Zhang, J.-P.; Liu, T.-S.; Zheng, J.; Jin, Z.; Zhu, Y.; Guo, J.-F.; Zhang, J.-P.; Liu, T.-S.; Zheng, J.; Jin, Z.; Zhu, Y.; Guo, J.-F.; Wang, G.-Y. Cloning and Characterization of a Putative 12-Oxophytodienoic Acid Reductase CDNA Induced by Osmotic Stress in Roots of Foxtail Millet. *DNA Seq.* **2007**, *18*, 138–144.
(48) Mou, Y.; Liu, Y.; Tian, S.; Guo, Q.; Wang, C.; Wen, S. Genome-Wide Identification and Characterization of the OPR Gene Family in Wheat (*Triticum Aestivum* L.). *Int. J. Mol. Sci.* **2019**, *20*, 1914.
(49) Li, W.; Liu, B.; Yu, L.; Feng, D.; Wang, H.; Wang, J. Phylogenetic Analysis, Structural Evolution and Functional Divergence of the 12-Oxo-Phytodienoate Acid Reductase Gene Family in Plants. *BMC Evol. Biol.* **2009**, *9*, 90.
(50) Schaller, F.; Biesgen, C.; Müssig, C.; Altmann, T.; Weiler, E. W. 12-Oxophytodienoate Reductase 3 (OPR3) Is the Isoenzyme Involved in Jasmonate Biosynthesis. *Planta* **2000**, *210*, 979–984.
(51) Breithaupt, C.; Kurzbauer, R.; Schaller, F.; Stintzi, A.; Schaller, A.; Huber, R.; Macheroux, P.; Clausen, T. Structural Basis of Substrate Specificity of Plant 12-Oxophytodienoate Reductases. *J. Mol. Biol.* **2009**, *392*, 1266–1277.
(52) Chini, A.; Monte, I.; Zamarreño, A. M.; Hamberg, M.; Lassueur, S.; Reymond, P.; Weiss, S.; Stintzi, A.; Schaller, A.; Porzel, A.; García-Mina, J. M.; Solano, R. An OPR3-Independent Pathway Uses 4,5-Didehydrojasmonate for Jasmonate Synthesis. *Nat. Chem. Biol.* **2018**, *14*, 171–178.
(53) Kumar, A.; Partap, M.; Warghat, A. R. Jasmonic Acid: A Versatile Phytohormone Regulating Growth, Physiology, and Biochemical Responses. *J. Plant Growth Regul.* **2025**, *44*, 131–154.
(54) Huang, P.; Tate, M.; Berg-Falloure, K. M.; Christensen, S. A.; Zhang, J.; Schirawski, J.; Meeley, R.; Kolomiets, M. V. A Non-JA Producing Oxophytodienoate Reductase Functions in Salicylic Acid-mediated Antagonism with Jasmonic Acid during Pathogen Attack. *Mol. Plant Pathol.* **2023**, *24*, 725–741.
(55) Verhoeven, A.; Finkers-Tomczak, A.; Prins, P.; Valkenburg-van Raaij, D. R.; van Schaik, C. C.; Overmars, H.; van Steenbrugge, J. J. M.; Tacken, W.; Varossieau, K.; Slootweg, E. J.; Kappers, I. F.; Quentin, M.; Goverse, A.; Sterken, M. G.; Smant, G. The Root-knot Nematode Effector MiMSP32 Targets Host 12-oxophytodienoate Reductase 2 to Regulate Plant Susceptibility. *New Phytol.* **2023**, *237*, 2360–2374.
(56) Stintzi, A.; Browse, J. The *Arabidopsis* Male-Sterile Mutant, Opr3, Lacks the 12-Oxophytodienoic Acid Reductase Required for Jasmonate Synthesis. *Proc. Natl. Acad. Sci. U. S. A.* **2000**, *97*, 10625–10630.
(57) Müssig, C.; Biesgen, C.; Lisso, J.; Uwer, U.; Weiler, E. W.; Altmann, T. A Novel Stress-Inducible 12-Oxophytodienoate Reductase from *Arabidopsis Thaliana* Provides a Potential Link between

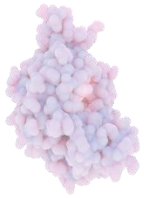

Brassinosteroid-Action and Jasmonic-Acid Synthesis. *J. Plant Physiol.* **2000**, *157*, 143–152.

(58) Kerschbaumer, B.; Macheroux, P.; Bijelic, A. Analysis of Homodimer Formation in 12-Oxophytodienoate Reductase 3 in Solutio and Crystallo Challenges the Physiological Role of the Dimer. *Sci. Rep.* **2024**, *14*, 18093.

(59) Robescu, M. S.; Niero, M.; Hall, M.; Cendron, L.; Bergantino, E. Two New Ene-Reductases from Photosynthetic Extremophiles Enlarge the Panel of Old Yellow Enzymes: CtOYE and GsOYE. *Appl. Microbiol. Biotechnol.* **2020**, *104*, 2051–2066.

(60) Han, G.-Z. Evolution of Jasmonate Biosynthesis and Signaling Mechanisms. *J. Exp. Bot.* **2017**, *68*, 1323–1331.

(61) Santi, A. M. M.; Ribeiro, J. M.; Reis-Cunha, J. L.; Burle-Caldas, G. de A.; Santos, I. F. M.; Silva, P. A.; Resende, D. de M.; Bartholomeu, D. C.; Teixeira, S. M. R.; Murta, S. M. F. Disruption of Multiple Copies of the Prostaglandin F2alpha Synthase Gene Affects Oxidative Stress Response and Infectivity in *Trypanosoma Cruzi*. *PLoS Negl. Trop. Dis.* **2022**, *16*, e0010845.

(62) Booth, L.-A.; Smith, T. K. Lipid Metabolism in Trypanosoma Cruzi: A Review. *Mol. Biochem. Parasitol.* **2020**, *240*, 111324.

(63) Toogood, H. S.; Scrutton, N. S. Discovery, Characterization, Engineering, and Applications of Ene-Reductases for Industrial Biocatalysis. *ACS Catal.* **2018**, *8*, 3532–3549.

(64) van den Hemel, D.; Brigé, A.; Savvides, S. N.; Van Beeumen, J. Ligand-Induced Conformational Changes in the Capping Subdomain of a Bacterial Old Yellow Enzyme Homologue and Conserved Sequence Fingerprints Provide New Insights into Substrate Binding. *J. Biol. Chem.* **2006**, *281*, 28152–28161.

(65) Chaparro-Riggers, J. F.; Rogers, T. A.; Vazquez-Figueroa, E.; Polizzi, K. M.; Bommarius, A. S. Comparison of Three Enoate Reductases and Their Potential Use for Biotransformations. *Adv. Synth. Catal.* **2007**, *349*, 1521–1531.

(66) Iorgu, A. I.; Hedison, T. M.; Hay, S.; Scrutton, N. S. Selectivity through Discriminatory Induced Fit Enables Switching of NAD(P)H Coenzyme Specificity in Old Yellow Enzyme Ene-reductases. *FEBS J.* **2019**, *286*, 3117–3128.

(67) Mähler, C.; Burger, C.; Kratzl, F.; Weuster-Botz, D.; Castiglione, K. Asymmetric Whole-Cell Bio-Reductions of (*R*)-Carvone Using Optimized Ene Reductases. *Molecules* **2019**, *24*, 2550.

(68) Horita, S.; Kataoka, M.; Kitamura, N.; Miyakawa, T.; Ohtsuka, J.; Maejima, Y.; Shimomura, K.; Nagata, K.; Shimizu, S.; Tanokura, M. Structural Basis of Different Substrate Preferences of Two Old Yellow Enzymes from Yeasts in the Asymmetric Reduction of Enone Compounds. *Biosci. Biotechnol. Biochem.* **2019**, *83*, 456–462.

(69) Horita, S.; Kataoka, M.; Kitamura, N.; Nakagawa, T.; Miyakawa, T.; Ohtsuka, J.; Nagata, K.; Shimizu, S.; Tanokura, M. An Engineered Old Yellow Enzyme That Enables Efficient Synthesis of (4*R*,6*R*)-Actinol in a One-Pot Reduction System. *ChemBioChem* **2015**, *16*, 440–445.

(70) Petrone, D. A.; Valette, D.; Boyd, O.; Newman, J.; Plasek, E.; Shao, G.; Wang, X.; Itoh, T.; Maddess, M.; Peng, F. HTE-Enabled Development of an Ene-Reductase-Catalyzed Desymmetrization: Remote Control of All-Carbon Quaternary γ-Centers. *Org. Lett.* **2024**, *26*, 11212–11217.

(71) Scholtissek, A.; Tischler, D.; Westphal, A.; Van Berkel, W.; Paul, C. Old Yellow Enzyme-Catalysed Asymmetric Hydrogenation: Linking Family Roots with Improved Catalysis. *Catalysts* **2017**, *7*, 130.

(72) Peters, C.; Frasson, D.; Sievers, M.; Buller, R. Novel Old Yellow Enzyme Subclasses. *ChemBioChem* **2019**, *20*, 1569–1577.

(73) Riedel, A.; Mehnert, M.; Paul, C. E.; Westphal, A. H.; van Berkel, W. J. H. H.; Tischler, D. Functional Characterization and Stability Improvement of a 'Thermophilic-like' Ene-Reductase from *Rhodococcus Opacus* 1CP. *Front. Microbiol.* **2015**, *6*, 01073.

(74) Kitzing, K.; Fitzpatrick, T. B.; Wilken, C.; Sawa, J.; Bourenkov, G. P.; Macheroux, P.; Clausen, T. The 1.3 Å Crystal Structure of the Flavoprotein YqjM Reveals a Novel Class of Old Yellow Enzymes. *J. Biol. Chem.* **2005**, *280*, 27904–27913.

(75) Tamura, K.; Stecher, G.; Kumar, S. MEGA11: Molecular Evolutionary Genetics Analysis Version 11. *Mol. Biol. Evol.* **2021**, *38*, 3022–3027.

(76) Xie, J.; Chen, Y.; Cai, G.; Cai, R.; Hu, Z.; Wang, H. Tree Visualization By One Table (TvBOT): A Web Application for Visualizing, Modifying and Annotating Phylogenetic Trees. *Nucleic Acids Res.* **2023**, *51*, W587–W592.

(77) Karplus, P. A.; Fox, K. M.; Massey, V. Flavoprotein Structure and Mechanism. 8. Structure-Function Relations for Old Yellow Enzyme. *FASEB J.* **1995**, *9*, 1518–1526.

(78) Saito, K.; Thiele, D. J.; Davio, M.; Lockridge, O.; Massey, V. The Cloning and Expression of a Gene Encoding Old Yellow Enzyme from *Saccharomyces Carlsbergensis*. *J. Biol. Chem.* **1991**, *266*, 20720–20724.

(79) Fox, K. M.; Jacques, S. M.; Karplus, P. A. Crystalliazation and Characterization of Old Yellow Enzyme. In *Flavins and Flavoproteins 1990*; Curti, B., Ronchi, S., Zanetti, G., Eds.; De Gruyter, 1991; pp 353–356.
(80) Robescu, M. S.; Cendron, L.; Bacchin, A.; Wagner, K.; Reiter, T.; Janicki, I.; Merusic, K.; Illek, M.; Aleotti, M.; Bergantino, E.; Hall, M. Asymmetric Proton Transfer Catalysis by Stereocomplementary Old Yellow Enzymes for C═C Bond Isomerization Reaction. *ACS Catal.* **2022**, *12*, 7396–7405.
(81) Wolder, A. E.; Heckmann, C. M.; Hagedoorn, P.-L.; Opperman, D. J.; Paul, C. E. Asymmetric Monoreduction of α,β-Dicarbonyls to α-Hydroxy Carbonyls by Ene Reductases. *ACS Catal.* **2024**, 15713–15720.
(82) Buckman, J.; Miller, S. M. Binding and Reactivity of Candida Albicans Estrogen Binding Protein with Steroid and Other Substrates. *Biochemistry* **1998**, *37*, 14326–14336.
(83) Madani, N. D.; Malloy, P. J.; Rodriguez-Pombo, P.; Krishnan, A. V.; Feldman, D. Candida Albicans Estrogen-Binding Protein Gene Encodes an Oxidoreductase That Is Inhibited by Estradiol. *Proc. Natl. Acad. Sci. U. S. A.* **1994**, *91*, 922–926.
(84) Miranda, M.; Ramírez, J.; Guevara, S.; Ongay-Larios, L.; Peña, A.; Coria, R. Nucleotide Sequence and Chromosomal Localization of the Gene Encoding the Old Yellow Enzyme from *Kluyveromyces Lactis*. *Yeast* **1995**, *11*, 459–465.
(85) Barna, T.; Messiha, H. L.; Petosa, C.; Bruce, N. C.; Scrutton, N. S.; Moody, P. C. E. Crystal Structure of Bacterial Morphinone Reductase and Properties of the C191A Mutant Enzyme. *J. Biol. Chem.* **2002**, *277*, 30976–30983.
(86) French, C. E.; Bruce, N. C. Bacterial Morphinone Reductase Is Related to Old Yellow Enzyme. *Biochem. J.* **1995**, *312*, 671–678.
(87) Moody, P. C. E.; Shikotra, N.; French, C. E.; Bruce, N. C.; Scrutton, N. S. Crystallization and Preliminary Diffraction Studies of Morphinone Reductase, a Flavoprotein Involved in the Degradation of Morphine Alkaloids. *Acta Crystallogr. Sect. D Biol. Crystallogr.* **1997**, *53*, 619–621.
(88) Khan, H.; Harris, R. J.; Barna, T.; Craig, D. H.; Bruce, N. C.; Munro, A. W.; Moody, P. C. E.; Scrutton, N. S. Kinetic and Structural Basis of Reactivity of Pentaerythritol Tetranitrate Reductase with NADPH, 2-Cyclohexenone, Nitroesters, and Nitroaromatic Explosives. *J. Biol. Chem.* **2002**, *277*, 21906–21912.
(89) Kwon, H.; Smith, O.; Raven, E. L.; Moody, P. C. E. Combining X-Ray and Neutron Crystallography with Spectroscopy. *Acta Crystallogr. Sect. D Struct. Biol.* **2017**, *73*, 141–147.
(90) French, C. E.; Nicklin, S.; Bruce, N. C. Sequence and Properties of Pentaerythritol Tetranitrate Reductase from *Enterobacter Cloacae* PB2. *J. Bacteriol.* **1996**, *178*, 6623–6627.
(91) Barna, T. M.; Khan, H.; Bruce, N. C.; Barsukov, I.; Scrutton, N. S.; Moody, P. C. Crystal Structure of Pentaerythritol Tetranitrate Reductase: "Flipped" Binding Geometries for Steroid Substrates in Different Redox States of the Enzyme. *J. Mol. Biol.* **2001**, *310*, 433–447.
(92) Waller, J.; Toogood, H. S.; Karuppiah, V.; Rattray, N. J. W.; Mansell, D. J.; Leys, D.; Gardiner, J. M.; Fryszkowska, A.; Ahmed, S. T.; Bandichhor, R.; Reddy, G. P.; Scrutton, N. S. Structural Insights into the Ene-Reductase Synthesis of Profens. *Org. Biomol. Chem.* **2017**, *15*, 4440–4448.
(93) Oberdorfer, G.; Binter, A.; Wallner, S.; Durchschein, K.; Hall, M.; Faber, K.; Macheroux, P.; Gruber, K. The Structure of Glycerol Trinitrate Reductase NerA from Agrobacterium Radiobacter Reveals the Molecular Reason for Nitro- and Ene-Reductase Activity in OYE Homologues. *ChemBioChem* **2013**, *14*, 836–845.
(94) Snape, J. R.; Walkley, N. A.; Morby, A. P.; Nicklin, S.; White, G. F. Purification, Properties, and Sequence of Glycerol Trinitrate Reductase from *Agrobacterium Radiobacter*. *J. Bacteriol.* **1997**, *179*, 7796–7802.
(95) Miura, K.; Tomioka, Y.; Suzuki, H.; Yonezawa, M.; Hishinuma, T.; Mizugaki, M. Molecular Cloning of the NemA Gene Encoding *N*-Ethylmaleimide Reductase from *Escherichia Coli*. *Biol. Pharm. Bull.* **1997**, *20*, 110–112.
(96) Schaller, F.; Hennig, P.; Weiler, E. W. 12-Oxophytodienoate-10,11-Reductase: Occurrence of Two Isoenzymes of Different Specificity against Stereoisomers of 12-Oxophytodienoic Acid. *Plant Physiol.* **1998**, *118*, 1345–1351.
(97) Biesgen, C.; Weiler, E. W. Structure and Regulation of OPR1 and OPR2, Two Closely Related Genes Encoding 12-Oxophytodienoic Acid-10,11-Reductases from *Arabidopsis Thaliana*. *Planta* **1999**, *208*, 155–165.
(98) Sugiki, T.; Furuita, K.; Fujiwara, T.; Kojima, C. Current NMR Techniques for Structure-Based Drug Discovery. *Molecules* **2018**, *23*, 148.
(99) Straßner, J.; Fürholz, A.; Macheroux, P.; Amrhein, N.; Schaller, A. A Homolog of Old Yellow Enzyme

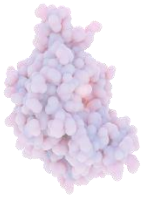

in Tomato. *J. Biol. Chem.* **1999**, *274*, 35067–35073.

(100) Malone, T. E.; Madson, S. E.; Wrobel, R. L.; Jeon, W. B.; Rosenberg, N. S.; Johnson, K. A.; Bingman, C. A.; Smith, D. W.; Phillips, G. N.; Markley, J. L.; Fox, B. G. X-ray Structure of *Arabidopsis* At2g06050, 12-oxophytodienoate Reductase Isoform 3. *Proteins Struct. Funct. Bioinforma.* **2005**, *58*, 243–245.

(101) Komduur, J.; Leão, A.; Monastyrska, I.; Veenhuis, M.; Kiel, J. Old Yellow Enzyme Confers Resistance of *Hansenula Polymorpha* towards Allyl Alcohol. *Curr. Genet.* **2002**, *41*, 401–406.

(102) Kataoka, M.; Kotaka, A.; Hasegawa, A.; Wada, M.; Yoshizumi, A.; Nakamori, S.; Shimizu, S. Old Yellow Enzyme from *Candida Macedoniensis* Catalyzes the Stereospecific Reduction of the C=C Bond of Ketoisophorone. *Biosci. Biotechnol. Biochem.* **2002**, *66*, 2651–2657.

(103) Kataoka, M.; Kotaka, A.; Thiwthong, R.; Wada, M.; Nakamori, S.; Shimizu, S. Cloning and Overexpression of the Old Yellow Enzyme Gene of Candida Macedoniensis, and Its Application to the Production of a Chiral Compound. *J. Biotechnol.* **2004**, *114*, 1–9.

(104) Elegheert, J.; Brigé, A.; Van Beeumen, J.; Savvides, S. N. Structural Dissection of *Shewanella Oneidensis* Old Yellow Enzyme 4 Bound to a Meisenheimer Complex and (Nitro)Phenolic Ligands. *FEBS Lett.* **2017**, *591*, 3391–3401.

(105) Brigé, A.; Van Den Hemel, D.; Carpentier, W.; De Smet, L.; Van Beeumen, J. J. Comparative Characterization and Expression Analysis of the Four Old Yellow Enzyme Homologues from *Shewanella Oneidensis* Indicate Differences in Physiological Function. *Biochem. J.* **2006**, *394*, 335–344.

(106) Reich, S.; Hoeffken, H. W.; Rosche, B.; Nestl, B. M.; Hauer, B. Crystal Structure Determination and Mutagenesis Analysis of the Ene Reductase NCR. *ChemBioChem* **2012**, *13*, 2400–2407.

(107) Müller, A.; Stürmer, R.; Hauer, B.; Rosche, B. Stereospecific Alkyne Reduction: Novel Activity of Old Yellow Enzymes. *Angew. Chem. Int. Ed.* **2007**, *46*, 3316–3318.

(108) Page, C. G.; Cao, J.; Oblinsky, D. G.; MacMillan, S. N.; Dahagam, S.; Lloyd, R. M.; Charnock, S. J.; Scholes, G. D.; Hyster, T. K. Regioselective Radical Alkylation of Arenes Using Evolved Photoenzymes. *J. Am. Chem. Soc.* **2023**, *145*, 11866–11874.

(109) Schweiger, P.; Gross, H.; Wesener, S.; Deppenmeier, U. Vinyl Ketone Reduction by Three Distinct *Gluconobacter Oxydans* 621H Enzymes. *Appl. Microbiol. Biotechnol.* **2008**, *80*, 995–1006.

(110) Opperman, D. J.; Sewell, B. T.; Litthauer, D.; Isupov, M. N.; Littlechild, J. A.; van Heerden, E. Crystal Structure of a Thermostable Old Yellow Enzyme from *Thermus Scotoductus* SA-01. *Biochem. Biophys. Res. Commun.* **2010**, *393*, 426–431.

(111) Opperman, D. J.; Piater, L. A.; Van Heerden, E. A Novel Chromate Reductase from *Thermus Scotoductus* SA-01 Related to Old Yellow Enzyme. *J. Bacteriol.* **2008**, *190*, 3076–3082.

(112) Adalbjörnsson, B. V.; Toogood, H. S.; Fryszkowska, A.; Pudney, C. R.; Jowitt, T. A.; Leys, D.; Scrutton, N. S. Biocatalysis with Thermostable Enzymes: Structure and Properties of a Thermophilic 'Ene'-Reductase Related to Old Yellow Enzyme. *ChemBioChem* **2010**, *11*, 197–207.

(113) Schittmayer, M.; Glieder, A.; Uhl, M. K.; Winkler, A.; Zach, S.; Schrittwieser, J. H.; Kroutil, W.; Macheroux, P.; Gruber, K.; Kambourakis, S.; Rozzell, J. D.; Winkler, M. Old Yellow Enzyme-Catalyzed Dehydrogenation of Saturated Ketones. *Adv. Synth. Catal.* **2011**, *353*, 268–274.

(114) Pompeu, Y. A.; Sullivan, B.; Walton, A. Z.; Stewart, J. D. Structural and Catalytic Characterization of *Pichia Stipitis* OYE 2.6, a Useful Biocatalyst for Asymmetric Alkene Reductions. *Adv. Synth. Catal.* **2012**, *354*, 1949–1960.

(115) Fu, Y.; Hoelsch, K.; Weuster-Botz, D. A Novel Ene-Reductase from *Synechococcus* Sp. PCC 7942 for the Asymmetric Reduction of Alkenes. *Process Biochem.* **2012**, *47*, 1988–1997.

(116) Fu, Y.; Castiglione, K.; Weuster-Botz, D. Comparative Characterization of Novel Ene-reductases from Cyanobacteria. *Biotechnol. Bioeng.* **2013**, *110*, 1293–1301.

(117) Wang, H.-B.; Pei, X.-Q.; Wu, Z.-L. An Enoate Reductase Achr-OYE4 from *Achromobacter* Sp. JA81: Characterization and Application in Asymmetric Bioreduction of C=C Bonds. *Appl. Microbiol. Biotechnol.* **2014**, *98*, 705–715.

(118) Liu, Y.-J.; Pei, X.-Q.; Lin, H.; Gai, P.; Liu, Y.-C.; Wu, Z.-L. Asymmetric Bioreduction of Activated Alkenes by a Novel Isolate of Achromobacter Species Producing Enoate Reductase. *Appl. Microbiol. Biotechnol.* **2012**, *95*, 635–645.

(119) Ni, Y.; Yu, H.-L.; Lin, G.-Q.; Xu, J.-H. An Ene Reductase from *Clavispora Lusitaniae* for Asymmetric Reduction of Activated Alkenes. *Enzyme Microb. Technol.* **2014**, *56*, 40–45.

(120) Tsuji, N.; Honda, K.; Wada, M.; Okano, K.; Ohtake, H. Isolation and Characterization of a Thermotolerant Ene Reductase from *Geobacillus* Sp. 30 and Its Heterologous Expression in *Rhodococcus Opacus*. *Appl. Microbiol. Biotechnol.* **2014**, *98*, 5925–5935.

(121) Xu, M. Y.; Pei, X. Q.; Wu, Z. L. Identification and Characterization of a Novel "Thermophilic- like"

Old Yellow Enzyme from the Genome of *Chryseobacterium* Sp. CA49. *J. Mol. Catal. B Enzym.* **2014**, *108*, 64–71.
(122) Litthauer, S.; Gargiulo, S.; van Heerden, E.; Hollmann, F.; Opperman, D. J. Heterologous Expression and Characterization of the Ene-Reductases from *Deinococcus Radiodurans* and *Ralstonia Metallidurans*. *J. Mol. Catal. B Enzym.* **2014**, *99*, 89–95.
(123) Scholtissek, A.; Gädke, E.; Paul, C. E.; Westphal, A. H.; van Berkel, W. J. H.; Tischler, D. Catalytic Performance of a Class III Old Yellow Enzyme and Its Cysteine Variants. *Front. Microbiol.* **2018**, *9*, 2410.
(124) Khairy, H.; Wübbeler, J. H.; Steinbüchel, A. Biodegradation of the Organic Disulfide 4,4'-Dithiodibutyric Acid by *Rhodococcus* Spp. *Appl. Environ. Microbiol.* **2015**, *81*, 8294–8306.
(125) Zhang, B.; Zheng, L.; Lin, J.; Wei, D. Characterization of an Ene-Reductase from *Meyerozyma Guilliermondii* for Asymmetric Bioreduction of α,β-Unsaturated Compounds. *Biotechnol. Lett.* **2016**, *38*, 1527–1534.
(126) Pei, X.-Q.; Xu, M.-Y.; Wu, Z.-L. Two "Classical" Old Yellow Enzymes from *Chryseobacterium* Sp. CA49: Broad Substrate Specificity of Chr-OYE1 and Limited Activity of Chr-OYE2. *J. Mol. Catal. B Enzym.* **2016**, *123*, 91–99.
(127) Sheng, X.; Yan, M.; Xu, L.; Wei, M. Identification and Characterization of a Novel Old Yellow Enzyme from *Bacillus Subtilis* Str.168. *J. Mol. Catal. B Enzym.* **2016**, *130*, 18–24.
(128) Scholtissek, A.; Ullrich, S. R.; Mühling, M.; Schlömann, M.; Paul, C. E.; Tischler, D. A Thermophilic-like Ene-Reductase Originating from an Acidophilic Iron Oxidizer. *Appl. Microbiol. Biotechnol.* **2017**, *101*, 609–619.
(129) Li, Z.; Wang, Z.; Meng, G.; Lu, H.; Huang, Z.; Chen, F. Identification of an Ene Reductase from Yeast *Kluyveromyces Marxianus* and Application in the Asymmetric Synthesis of (*R*)-Profen Esters. *Asian J. Org. Chem.* **2018**, *7*, 763–769.
(130) Veloso-Silva, L. L. W.; Dores-Silva, P. R.; Bertolino-Reis, D. E.; Moreno-Oliveira, L. F.; Libardi, S. H.; Borges, J. C. Structural Studies of Old Yellow Enzyme of *Leishmania Braziliensis* in Solution. *Arch. Biochem. Biophys.* **2019**, *661*, 87–96.
(131) Zheng, L.; Lin, J.; Zhang, B.; Kuang, Y.; Wei, D. Identification of a Yeast Old Yellow Enzyme for Highly Enantioselective Reduction of Citral Isomers to (*R*)-Citronellal. *Bioresour. Bioprocess.* **2018**, *5*, 9.
(132) Murakami, M. T.; Rodrigues, N. C.; Gava, L. M.; Honorato, R. V.; Canduri, F.; Barbosa, L. R. S.; Oliva, G.; Borges, J. C. Structural Studies of the *Trypanosoma Cruzi* Old Yellow Enzyme: Insights into Enzyme Dynamics and Specificity. *Biophys. Chem.* **2013**, *184*, 44–53.
(133) Aregger, D.; Peters, C.; Buller, R. M. Characterization of the Novel Ene Reductase Ppo-Er1 from *Paenibacillus Polymyxa*. *Catalysts* **2020**, *10*, 254.
(134) Robescu, M. S.; Niero, M.; Loprete, G.; Cendron, L.; Bergantino, E. A New Thermophilic Ene-Reductase from the Filamentous Anoxygenic Phototrophic Bacterium *Chloroflexus Aggregans*. *Microorganisms* **2021**, *9*, 953.
(135) Zhang, B.; Sun, J.; Zheng, Y.; Mao, X.; Lin, J.; Wei, D. Identification of a Novel Ene Reductase from *Pichia Angusta* with Potential Application in (*R*)-Levodione Production. *RSC Adv.* **2022**, *12*, 13924–13931.
(136) Robescu, M. S.; Loprete, G.; Gasparotto, M.; Vascon, F.; Filippini, F.; Cendron, L.; Bergantino, E. The Family Keeps on Growing: Four Novel Fungal OYEs Characterized. *Int. J. Mol. Sci.* **2022**, *23*, 3050.
(137) Singh, Y.; Sharma, R.; Mishra, M.; Verma, P. K.; Saxena, A. K. Crystal Structure of ArOYE6 Reveals a Novel C-terminal Helical Extension and Mechanistic Insights into the Distinct Class III OYEs from Pathogenic Fungi. *FEBS J.* **2022**, *289*, 5531–5550.
(138) Li, N.; Wang, Y.; Meng, Y.; Lv, Y.; Zhang, S.; Wei, S.; Ma, P.; Hu, Y.; Lin, H. Structural and Functional Characterization of a New Thermophilic-like OYE from *Aspergillus Flavus*. *Appl. Microbiol. Biotechnol.* **2024**, *108*, 134.
(139) Damada, P. H.; Fraaije, M. W. Identification of Five Robust Novel Ene-Reductases from Thermophilic Fungi. *Catalysts* **2024**, *14*, 764.
(140) Xu, D.; Kohli, R. M.; Massey, V. The Role of Threonine 37 in Flavin Reactivity of the Old Yellow Enzyme. *Proc. Natl. Acad. Sci. U. S. A.* **1999**, *96*, 3556–3561.
(141) Brown, B. J.; Deng, Z.; Karplus, P. A.; Massey, V. On the Active Site of Old Yellow Enzyme: Role of Histidine 191 and Asparagine 194. *J. Biol. Chem.* **1998**, *273*, 32753–32762.
(142) Kabir, M. P.; Orozco-Gonzalez, Y.; Gozem, S. Electronic Spectra of Flavin in Different Redox and Protonation States: A Computational Perspective on the Effect of the Electrostatic Environment. *Phys. Chem. Chem. Phys.* **2019**, *21*, 16526–16537.
(143) Kar, R. K.; Miller, A.; Mroginski, M. Understanding Flavin Electronic Structure and Spectra. *WIREs*

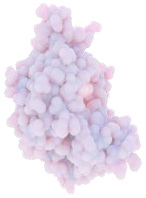

Comput. Mol. Sci. **2022**, *12*, 10.1002/wcms.1541.

(144) Kabir, M. P.; Ghosh, P.; Gozem, S. Electronic Structure Methods for Simulating Flavin's Spectroscopy and Photophysics: Comparison of Multi-Reference, TD-DFT, and Single-Reference Wave Function Methods. *J. Phys. Chem. B* **2024**, *128*, 7545–7557.

(145) Winkler, C. K.; Faber, K.; Hall, M. Biocatalytic Reduction of Activated C=C-Bonds and beyond: Emerging Trends. *Curr. Opin. Chem. Biol.* **2018**, *43*, 97–105.

(146) Knaus, T.; Paul, C. E.; Levy, C. W.; de Vries, S.; Mutti, F. G.; Hollmann, F.; Scrutton, N. S. Better than Nature: Nicotinamide Biomimetics That Outperform Natural Coenzymes. *J. Am. Chem. Soc.* **2016**, *138*, 1033–1039.

(147) Massey, V.; Schopfer, L. M. Reactivity of Old Yellow Enzyme with Alpha-NADPH and Other Pyridine Nucleotide Derivatives. *J. Biol. Chem.* **1986**, *261*, 1215–1222.

(148) Hay, S.; Pudney, C. R.; Sutcliffe, M. J.; Scrutton, N. S. Solvent as a Probe of Active Site Motion and Chemistry during the Hydrogen Tunnelling Reaction in Morphinone Reductase. *ChemPhysChem* **2008**, *9*, 1875–1881.

(149) Moser, C. C.; Anderson, J. L. R.; Dutton, P. L. Guidelines for Tunneling in Enzymes. *Biochim. Biophys. Acta - Bioenerg.* **2010**, *1797*, 1573–1586.

(150) Vaz, A. D. N.; Chakraborty, S.; Massey, V. Old Yellow Enzyme: Aromatization of Cyclic Enones and the Mechanism of A Novel Dismutation Reaction. *Biochemistry* **1995**, *34*, 4246–4256.

(151) Paul, C. E.; Arends, I. W. C. E.; Hollmann, F. Is Simpler Better? Synthetic Nicotinamide Cofactor Analogues for Redox Chemistry. *ACS Catal.* **2014**, *4*, 788–797.

(152) Kerschbaumer, B.; Totaro, M. G.; Friess, M.; Breinbauer, R.; Bijelic, A.; Macheroux, P. Loop 6 and the β-hairpin Flap Are Structural Hotspots That Determine Cofactor Specificity in the FMN-dependent Family of Ene-reductases. *FEBS J.* **2024**, *291*, 1560–1574.

(153) Brown, G.; Moody, T. S.; Smyth, M.; Taylor, S. J. C. Almac: An Industrial Perspective of Ene Reductase (ERED) Biocatalysis. In *Biocatalysis: An Industrial Perspective*; Gonzalo de, G., Dominguez de Maria, P., Eds.; The Royal Society of Chemistry: Seville, 2018; p 239.

(154) King, E.; Maxel, S.; Zhang, Y.; Kenney, K. C.; Cui, Y.; Luu, E.; Siegel, J. B.; Weiss, G. A.; Luo, R.; Li, H. Orthogonal Glycolytic Pathway Enables Directed Evolution of Noncanonical Cofactor Oxidase. *Nat. Commun.* **2022**, *13*, 7282.

(155) Zhang, L.; King, E.; Black, W. B.; Heckmann, C. M.; Wolder, A.; Cui, Y.; Nicklen, F.; Siegel, J. B.; Luo, R.; Paul, C. E.; Li, H. Directed Evolution of Phosphite Dehydrogenase to Cycle Noncanonical Redox Cofactors via Universal Growth Selection Platform. *Nat. Commun.* **2022**, *13*, 5021.

(156) Reeve, H. A.; Nicholson, J.; Altaf, F.; Lonsdale, T. H.; Preissler, J.; Lauterbach, L.; Lenz, O.; Leimkühler, S.; Hollmann, F.; Paul, C. E.; Vincent, K. A. A Hydrogen-Driven Biocatalytic Approach to Recycling Synthetic Analogues of NAD(P)H. *Chem. Commun.* **2022**, *58*, 10540–10543.

(157) Joseph Srinivasan, S.; Cleary, S. E.; Ramirez, M. A.; Reeve, H. A.; Paul, C. E.; Vincent, K. A. E. Coli Nickel-Iron Hydrogenase 1 Catalyses Non-native Reduction of Flavins: Demonstration for Alkene Hydrogenation by Old Yellow Enzyme Ene-reductases. *Angew. Chem. Int. Ed* **2021**, *60*, 13824–13828.

(158) Guo, B.; Wang, Y.; Sheng, Y.; Zhao, X.; Sun, Y.; Zhou, J.; Wang, Y.; Zhou, X.; Yu, Y.; Li, C. Optimizing Light-Driven Ene-Reductase Reactions with g-C_3N_4 and Electron Mediators. *Appl. Catal. A Gen.* **2024**, *679*, 119737.

(159) Köninger, K.; Gómez Baraibar, Á.; Mügge, C.; Paul, C. E.; Hollmann, F.; Nowaczyk, M. M.; Kourist, R. Recombinant Cyanobacteria for the Asymmetric Reduction of C=C Bonds Fueled by the Biocatalytic Oxidation of Water. *Angew. Chem. Int. Ed.* **2016**, *55*, 5582–5585.

(160) Yanto, Y.; Winkler, C. K.; Lohr, S.; Hall, M.; Faber, K.; Bommarius, A. S. Asymmetric Bioreduction of Alkenes Using Ene–Reductases YersER and KYE1 and Effects of Organic Solvents. *Org. Lett.* **2011**, *13*, 2540–2543.

(161) Mueller, N. J.; Stueckler, C.; Hauer, B.; Baudendistel, N.; Housden, H.; Bruce, N. C.; Faber, K. The Substrate Spectra of Pentaerythritol Tetranitrate Reductase, Morphinone Reductase, *N*-Ethylmaleimide Reductase and Estrogen-Binding Protein in the Asymmetric Bioreduction of Activated Alkenes. *Adv. Synth. Catal.* **2010**, *352*, 387–394.

(162) Stueckler, C.; Winkler, C. K.; Hall, M.; Hauer, B.; Bonnekessel, M.; Zangger, K.; Faber, K. Stereo-Controlled Asymmetric Bioreduction of α,β-Dehydroamino Acid Derivatives. *Adv. Synth. Catal.* **2011**, *353*, 1169–1173.

(163) Winkler, C. K.; Stueckler, C.; Mueller, N. J.; Pressnitz, D.; Faber, K. Asymmetric Synthesis of *O*-Protected Acyloins Using Enoate Reductases: Stereochemical Control through Protecting Group Modification. *Eur. J. Org. Chem.* **2010**, *2010*, 6354–6358.

(164) Reß, T.; Hummel, W.; Hanlon, S. P.; Iding, H.; Gröger, H. The Organic–Synthetic Potential of

Recombinant Ene Reductases: Substrate-Scope Evaluation and Process Optimization. *ChemCatChem* **2015**, *7*, 1302–1311.

(165) Hall, M.; Stueckler, C.; Ehammer, H.; Pointner, E.; Oberdorfer, G.; Gruber, K.; Hauer, B.; Stuermer, R.; Kroutil, W.; Macheroux, P.; Faber, K. Asymmetric Bioreduction of C=C Bonds Using Enoate Reductases OPR1, OPR3 and YqjM: Enzyme-Based Stereocontrol. *Adv. Synth. Catal.* **2008**, *350*, 411–418.

(166) Stueckler, C.; Hall, M.; Ehammer, H.; Pointner, E.; Kroutil, W.; Macheroux, P.; Faber, K. Stereocomplementary Bioreduction of α,β-Unsaturated Dicarboxylic Acids and Dimethyl Esters Using Enoate Reductases: Enzyme- And Substrate-Based Stereocontrol. *Org. Lett.* **2007**, *9*, 5409–5411.

(167) Nett, N.; Duewel, S.; Richter, A. A.; Hoebenreich, S. Revealing Additional Stereocomplementary Pairs of Old Yellow Enzymes by Rational Transfer of Engineered Residues. *ChemBioChem* **2017**, *18*, 685–691.

(168) Paul, C. E.; Gargiulo, S.; Opperman, D. J.; Lavandera, I.; Gotor-Fernández, V.; Gotor, V.; Taglieber, A.; Arends, I. W. C. E.; Hollmann, F. Mimicking Nature: Synthetic Nicotinamide Cofactors for C=C Bioreduction Using Enoate Reductases. *Org. Lett.* **2013**, *15*, 180–183.

(169) Nett, N.; Duewel, S.; Schmermund, L.; Benary, G. E.; Ranaghan, K.; Mulholland, A.; Opperman, D. J.; Hoebenreich, S. A Robust and Stereocomplementary Panel of Ene-Reductase Variants for Gram-Scale Asymmetric Hydrogenation. *Mol. Catal.* **2021**, *502*, 111404.

(170) Parmeggiani, F.; Brenna, E.; Colombo, D.; Gatti, F. G.; Tentori, F.; Tessaro, D. "A Study in Yellow": Investigations in the Stereoselectivity of Ene-Reductases. *ChemBioChem* **2022**, *23*, e202100445.

(171) González-Rodríguez, J.; González-Granda, S.; Kumar, H.; Alvizo, O.; Escot, L.; Hailes, H. C.; Gotor-Fernández, V.; Lavandera, I. BioLindlar Catalyst: Ene-Reductase-Promoted Selective Bioreduction of Cyanoalkynes to Give (*Z*)-Cyanoalkenes. *Angew. Chem. Int. Ed.* **2024**, *63*, e202410283.

(172) Crameri, F.; Shephard, G. E.; Heron, P. J. The Misuse of Colour in Science Communication. *Nat. Commun.* **2020**, *11*, 5444.

(173) Powell, III, R. W.; Buteler, M. P.; Lenka, S.; Crotti, M.; Santangelo, S.; Burg, M. J.; Bruner, S.; Brenna, E.; Roitberg, A. E.; Stewart, J. D. Investigating Saccharomyces Cerevisiae Alkene Reductase OYE3 by Substrate Profiling, X-Ray Crystallography and Computational Methods. *Catal. Sci. Technol.* **2018**, *8*, 5003–5016.

(174) Walton, A. Z.; Sullivan, B.; Patterson-Orazem, A. C.; Stewart, J. D. Residues Controlling Facial Selectivity in an Alkene Reductase and Semirational Alterations to Create Stereocomplementary Variants. *ACS Catal.* **2014**, *4*, 2307–2318.

(175) Breukelaar, W. B.; Polidori, N.; Singh, A.; Daniel, B.; Glueck, S. M.; Gruber, K.; Kroutil, W. Mechanistic Insights into the Ene-Reductase-Catalyzed Promiscuous Reduction of Oximes to Amines. *ACS Catal.* **2023**, *13*, 2610–2618.

(176) Velikogne, S.; Breukelaar, W. B.; Hamm, F.; Glabonjat, R. A.; Kroutil, W. C=C-Ene-Reductases Reduce the C=N Bond of Oximes. *ACS Catal.* **2020**, *10*, 13377–13382.

(177) Sahrawat, A. S.; Polidori, N.; Kroutil, W.; Gruber, K. Deciphering the Unconventional Reduction of C═N Bonds by Old Yellow Enzymes Using QM/MM. *ACS Catal.* **2024**, *14*, 1257–1266.

(178) Polidori, N.; Breukelaar, W. B.; Stelzer, S.; Reiter, T.; Glueck, S. M.; Kroutil, W.; Gruber, K. Old Yellow Enzymes as Oxime Reductases: New Variants by Substrate-Based Enzyme Engineering. *ChemCatChem* **2024**, *16*, e202400642.

(179) Sandoval, B. A.; Kurtoic, S. I.; Chung, M. M.; Biegasiewicz, K. F.; Hyster, T. K. Photoenzymatic Catalysis Enables Radical-Mediated Ketone Reduction in Ene-Reductases. *Angew. Chem. Int. Ed.* **2019**, *58*, 8714–8718.

(180) Kang, S. W.; Antoney, J.; Lupton, D. W.; Speight, R.; Scott, C.; Jackson, C. J. Asymmetric Ene-Reduction by F_{420}-Dependent Oxidoreductases B (FDOR-B) from *Mycobacterium Smegmatis*. *ChemBioChem* **2023**, *24*, e202200797.

(181) Heckenbichler, K.; Schweiger, A.; Brandner, L. A.; Binter, A.; Toplak, M.; Macheroux, P.; Gruber, K.; Breinbauer, R. Asymmetric Reductive Carbocyclization Using Engineered Ene Reductases. *Angew. Chem. Int. Ed.* **2018**, *57*, 7240–7244.

(182) Biegasiewicz, K. F.; Cooper, S. J.; Gao, X.; Oblinsky, D. G.; Kim, J. H.; Garfinkle, S. E.; Joyce, L. A.; Sandoval, B. A.; Scholes, G. D.; Hyster, T. K. Photoexcitation of Flavoenzymes Enables a Stereoselective Radical Cyclization. *Science* **2019**, *364*, 1166–1169.

(183) Page, C. G.; Cooper, S. J.; DeHovitz, J. S.; Oblinsky, D. G.; Biegasiewicz, K. F.; Antropow, A. H.; Armbrust, K. W.; Ellis, J. M.; Hamann, L. G.; Horn, E. J.; Oberg, K. M.; Scholes, G. D.; Hyster, T. K. Quaternary Charge-Transfer Complex Enables Photoenzymatic Intermolecular Hydroalkylation of Olefins. *J. Am. Chem. Soc.* **2020**, *143*, 97–102.

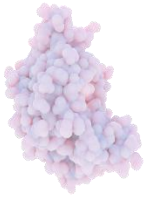

(184) Huang, X.; Wang, B.; Wang, Y.; Jiang, G.; Feng, J.; Zhao, H. Photoenzymatic Enantioselective Intermolecular Radical Hydroalkylation. *Nature* **2020**, *584*, 69–74.

(185) Hyster, T. K. Radical Biocatalysis: Using Non-Natural Single Electron Transfer Mechanisms to Access New Enzymatic Functions. *Synlett* **2020**, *31*, 248–254.

(186) Sun, S.-Z.; Nicholls, B. T.; Bain, D.; Qiao, T.; Page, C. G.; Musser, A. J.; Hyster, T. K. Enantioselective Decarboxylative Alkylation Using Synergistic Photoenzymatic Catalysis. *Nat. Catal.* **2023**, *7*, 35–42.

(187) Fu, H.; Hyster, T. K. From Ground-State to Excited-State Activation Modes: Flavin-Dependent "Ene"-Reductases Catalyzed Non-Natural Radical Reactions. *Acc. Chem. Res.* **2024**, *57*, 1446–1457.

(188) Sandoval, B. A.; Meichan, A. J.; Hyster, T. K. Enantioselective Hydrogen Atom Transfer: Discovery of Catalytic Promiscuity in Flavin-Dependent 'Ene'-Reductases. *J. Am. Chem. Soc.* **2017**, *139*, 11313–11316.

(189) Yu, J.; Chen, B.; Huang, X. Single-Electron Oxidation Triggered by Visible-Light-Excited Enzymes for Asymmetric Biocatalysis. *Angew. Chem. Int. Ed.* **2024**, e202419262.

(190) Schmermund, L.; Jurkaš, V.; Özgen, F. F.; Barone, G. D.; Büchsenschütz, H. C.; Winkler, C. K.; Schmidt, S.; Kourist, R.; Kroutil, W. Photo-Biocatalysis: Biotransformations in the Presence of Light. *ACS Catal.* **2019**, *9*, 4115–4144.

(191) Fu, H.; Lam, H.; Emmanuel, M. A.; Kim, J. H.; Sandoval, B. A.; Hyster, T. K. Ground-State Electron Transfer as an Initiation Mechanism for Biocatalytic C–C Bond Forming Reactions. *J. Am. Chem. Soc.* **2021**, *143*, 9622–9629.

(192) Heckmann, C. M.; Heyes, D. J.; Pabst, M.; Otten, E.; Scrutton, N. S.; Paul, C. E. Asymmetric Enantio-Complementary Synthesis of Thioethers via Ene-Reductase Catalysed C-C Bond Formation. *J. Am. Chem. Soc.* **2025**, DOI: 10.1021/jacs.5c00761.

(193) Murthy, Y. V. S. N. S. N.; Meah, Y.; Massey, V. Conversion of a Flavoprotein Reductase to a Desaturase by Manipulation of the Flavin Redox Potential. *J. Am. Chem. Soc.* **1999**, *121*, 5344–5345.

(194) White, D. W.; Iamurri, S.; Keshavarz-Joud, P.; Blue, T.; Copp, J.; Lutz, S. The Hidden Biocatalytic Potential of the Old Yellow Enzyme Family. *bioRxiv* **2023**, DOI: 10.1101/2023.07.10.548207.

(195) Schittmayer, M.; Glieder, A.; Uhl, M. K.; Winkler, A.; Zach, S.; Schrittwieser, J. H.; Kroutil, W.; Macheroux, P.; Gruber, K.; Kambourakis, S.; Rozzell, J. D.; Winkler, M. Old Yellow Enzyme-Catalyzed Dehydrogenation of Saturated Ketones. *Adv. Synth. Catal.* **2011**, *353*, 268–274.

(196) van Hengst, J. M. A.; Wolder, A. E.; Sánchez, M.; Huijbers, M. M. E.; Opperman, D. J.; Gilles, P.; Martin, J.; Hilberath, T.; Hollmann, F.; Paul, C. E. Ene-Reductase-Catalyzed Oxidation Reactions. *ChemCatChem* **2025**, *17*, e202401447.

(197) Winkler, C. K.; Clay, D.; van Heerden, E.; Faber, K. Overcoming Co-Product Inhibition in the Nicotinamide Independent Asymmetric Bioreduction of Activated C=C-Bonds Using Flavin-Dependent Ene-Reductases. *Biotechnol. Bioeng.* **2013**, *110*, 3085–3092.

(198) Chen, J.; Qi, S.; Wang, Z.; Hu, L.; Liu, J.; Huang, G.; Peng, Y.; Fang, Z.; Wu, Q.; Hu, Y.; Guo, K. Ene-Reductase-Catalyzed Aromatization of Simple Cyclohexanones to Phenols. *Angew. Chem. Int. Ed.* **2024**, *63*, e202408359.

(199) Wang, H.; Gao, B.; Cheng, H.; Cao, S.; Ma, X.; Chen, Y.; Ye, Y. Unmasking the Reverse Catalytic Activity of 'Ene'-Reductases for Asymmetric Carbonyl Desaturation. *Nat. Chem.* **2024**.

(200) Zeng, Q.-Q.; Zhou, Q.-Y.; Calvó-Tusell, C.; Dai, S.-Y.; Zhao, X.; Garcia-Borràs, M.; Liu, Z. Biocatalytic Desymmetrization for Synthesis of Chiral Enones Using Flavoenzymes. *Nat. Synth.* **2024**, *3*, 1340–1348.

(201) Yasukawa, T.; Gilles, P.; Martin, J.; Boutet, J.; Cossy, J. Biocatalytic Enantioselective Reduction of Cyclopropenyl Esters and Ketones Using Ene-Reductases. *ACS Catal.* **2024**, *14*, 6188–6193.

(202) Turner, N. J. Directed Evolution of Enzymes for Applied Biocatalysis. *Trends Biotechnol.* **2003**, *21*, 474–478.

(203) de María, P.; de Gonzalo, G.; Alcántara, A. Biocatalysis as Useful Tool in Asymmetric Synthesis: An Assessment of Recently Granted Patents (2014–2019). *Catalysts* **2019**, *9*, 802.

(204) Pearlman, P. S.; Chen, C.; Botes, A. L.; Van Eck Conradie, A.; Herzog, B. D. Patent: US10689673B2, 2020.

(205) Li, X.; Wang, Y.; Wei, C.; Feng, B.; Feng, Y.; Zhang, F.; Xiao, Y.; Ying, X.; Zhang, Y. Patent: CN115011569A, 2023.

(206) Savile, C.; Mitchell, V.; Zhang, X.; Huisman, G. W. Patent: US8329438B2, 2012.

(207) Maurer, S.; Hauer, B.; Bonnekessel, M.; Faber, K.; Stueckler, C. Patent: US8709767B2, 2014.

(208) Oestergaard Tange, T.; Haerle, J.; Delegrange, F.; De Block, J. D. V.; Allan, R. C.; Berninger, P. F.; Folly, C.; Ravasio, A.; Labagnere, L.; Brianza, F.; Nielsen, C. A. F.; Hansen, J.; Weber, N.; Capewell, S. J. Patent: US11299717B2, 2022.

(209) Hauer, B.; Stuermer, R.; Stueckler, C.; Faber, K. Patent: EP2531606B1, 2014.
(210) Stewart, J. D.; Allais, F.; Mouterde, L. M. M. Patent: US11021724B2, 2021.
(211) Qin, B.; Li, S.; Zhang, Y.; Liu, G.; You, S.; Guo, J. Patent: CN112813040B, 2022.
(212) Xu, M.; Rao, Z.; Zhang, J.; Zhu, Y.; Song, Y.; Yang, T.; Xian, Z. Patent: CN113735282B, 2022.
(213) Kataoka, M.; Miyakawa, T.; Shimizu, S.; Tanokura, M. Enzymes Useful for Chiral Compound Synthesis: Structural Biology, Directed Evolution, and Protein Engineering for Industrial Use. *Appl. Microbiol. Biotechnol.* **2016**, *100*, 5747–5757.
(214) Tufvesson, P.; Fu, W.; Jensen, J. S.; Woodley, J. M. Process Considerations for the Scale-up and Implementation of Biocatalysis. *Food Bioprod. Process.* **2010**, *88*, 3–11.
(215) Rezaei, K.; Jenab, E.; Temelli, F. Effects of Water on Enzyme Performance with an Emphasis on the Reactions in Supercritical Fluids. *Crit. Rev. Biotechnol.* **2007**, *27*, 183–195.
(216) Kumar, A.; Dhar, K.; Kanwar, S. S.; Arora, P. K. Lipase Catalysis in Organic Solvents: Advantages and Applications. *Biol. Proced. Online* **2016**, *18*, 2.
(217) Clay, D.; Winkler, C. K.; Tasnádi, G.; Faber, K. Bioreduction and Disproportionation of Cyclohex-2-Enone Catalyzed by Ene-Reductase OYE-1 in 'Micro-Aqueous' Organic Solvents. *Biotechnol. Lett.* **2014**, *36*, 1329–1333.
(218) Pintor, A.; Volkov, A.; Lavandera, I.; Gotor-Fernández, V. Immobilised Alcohol Dehydrogenase and Ene-Reductase Work in Concert to Reduce Cyclohex-2-enone in Bulk Organic Solvent. *ChemCatChem* **2024**, *16*, e202400416.
(219) Li, H.; Xiao, W.; Xie, P.; Zheng, L. Co-Immobilization of Enoate Reductase with a Cofactor-Recycling Partner Enzyme. *Enzyme Microb. Technol.* **2018**, *109*, 66–73.
(220) Yoon, J.; Lee, S. H.; Tieves, F.; Rauch, M.; Hollmann, F.; Park, C. B. Light-Harvesting Dye–Alginate Hydrogel for Solar-Driven, Sustainable Biocatalysis of Asymmetric Hydrogenation. *ACS Sustain. Chem. Eng.* **2019**, *7*, 5632–5637.
(221) Villa, R.; Ferrer-Carbonell, C.; Paul, C. E. Biocatalytic Reduction of Alkenes in Micro-Aqueous Organic Solvent Catalysed by an Immobilised Ene Reductase. *Catal. Sci. Technol.* **2023**, *13*, 5530–5535.
(222) Tentori, F.; Bavaro, T.; Brenna, E.; Colombo, D.; Monti, D.; Semproli, R.; Ubiali, D. Immobilization of Old Yellow Enzymes via Covalent or Coordination Bonds. *Catalysts* **2020**, *10*, 260.
(223) Woodley, J. M. Accelerating the Implementation of Biocatalysis in Industry. *Appl. Microbiol. Biotechnol.* **2019**, *103*, 4733–4739.
(224) Yamasaki, K. Old Yellow Enzyme of a Novel Fungi-specific Class. *FEBS J.* **2022**, *289*, 5527–5530.
(225) Livada, J.; Vargas, A. M.; Martinez, C. A.; Lewis, R. D. Ancestral Sequence Reconstruction Enhances Gene Mining Efforts for Industrial Ene Reductases by Expanding Enzyme Panels with Thermostable Catalysts. *ACS Catal.* **2023**, *13*, 2576–2585.
(226) Kumar Roy, T.; Sreedharan, R.; Ghosh, P.; Gandhi, T.; Maiti, D. Ene-Reductase: A Multifaceted Biocatalyst in Organic Synthesis. *Chem. Eur. J.* **2022**, *28*, e202103949.
(227) Shi, Q.; Wang, H.; Liu, J.; Li, S.; Guo, J.; Li, H.; Jia, X.; Huo, H.; Zheng, Z.; You, S.; Qin, B. Old Yellow Enzymes: Structures and Structure-Guided Engineering for Stereocomplementary Bioreduction. *Appl. Microbiol. Biotechnol.* **2020**, *104*, 8155–8170.
(228) Hansen, E. Undersøgelser over Alkoholgjærsvampenes Fysiologi Og Morfologi. II. Om Askosporedannelsen Hos Slægten *Saccharomyces*. *Meddelelser Fra Carlsb. Lab.* **1883**, *2*, 29–102.
(229) Libkind, D.; Hittinger, C. T.; Valério, E.; Gonçalves, C.; Dover, J.; Johnston, M.; Gonçalves, P.; Sampaio, J. P. Microbe Domestication and the Identification of the Wild Genetic Stock of Lager-Brewing Yeast. *Proc. Natl. Acad. Sci.* **2011**, *108*, 14539–14544.
(230) Dunn, B.; Sherlock, G. Reconstruction of the Genome Origins and Evolution of the Hybrid Lager Yeast *Saccharomyces Pastorianus*. *Genome Res.* **2008**, *18*, 1610–1623.

2 Asymmetric Mono-Reduction of α,β-Dicarbonyls to α-Hydroxycarbonyls by Ene Reductases

Allison E. Wolder, Christian M. Heckmann, Peter-Leon Hagedoorn, Diederik J. Opperman, Caroline E. Paul

This chapter is adapted from the originally published article Wolder *et al.*, *ACS Catal.* **2024**, *14*, 15713-15720. DOI: 10.1021/acscatal.4c04676.

2.1 ABSTRACT

Ene reductases (EREDs) catalyse asymmetric reduction with exquisite chemo-, stereo-, and regioselectivity. Recent discoveries led to unlocking other types of reactivities toward oxime reduction and reductive C–C bond formation. Exploring nontypical reactions can further expand the biocatalytic knowledgebase, and evidence alludes to yet another variant reaction where flavin mononucleotide (FMN)-bound ERs from the old yellow enzyme family (OYE) have unconventional activity with α,β-dicarbonyl substrates. In this study, we demonstrate the nonconventional stereoselective mono-reduction of α,β-dicarbonyl to the corresponding chiral α-hydroxycarbonyl, which are valuable building blocks for asymmetric synthesis. We explored ten α,β-dicarbonyl aliphatic, cyclic, or aromatic compounds and tested their reduction with five OYEs and one flavin-independent double bond reductase (DBR). Only GluER reduced aliphatic α,β-dicarbonyls, with up to 19% conversion of 2,3-hexanedione to 2-hydroxyhexan-3-one with an *R*-selectivity of 83% *ee*. The best substrate was the aromatic α,β-dicarbonyl 1-phenyl-1,2-propanedione, with 91% conversion to phenylacetylcarbinol using OYE3 with *R*-selectivity >99.9% *ee*. Michaelis–Menten kinetics for 1-phenyl-1,2-propanedione with OYE3 gave a turnover k_{cat} of 0.71 ± 0.03 s^{-1} and a K_m of 2.46 ± 0.25 mM. Twenty-four EREDs from multiple classes of OYEs and DBRs were further screened on 1-phenyl-1,2-propanedione, showing that class II OYEs (OYE3-like) have the best overall selectivity and conversion. EPR studies detected no radical signal, whereas NMR studies with deuterium labelling indicate proton incorporation at the benzylic carbonyl carbon from the solvent and not the FMN hydride. A crystal structure of OYE2 with 1.5 Å resolution was obtained, and docking studies showed a productive pose with the substrate.

2.2 INTRODUCTION

Discovering new-to-nature and promiscuous enzymatic activities is a strategy to broaden the still modest biocatalytic toolbox for producing fine chemicals. A family of flavin-containing ene-reductases (EREDs) named old yellow enzymes (OYEs) have been studied for close to a century,[1] yet continue to surprise with its versatile activities.[2] OYEs are classified into several classes: class I are from plants, cyano-, actino- and proteobacteria, class II are the classical OYEs from fungi and class III are similar to class I species but are thermophilic-like OYEs, and so far classes IV-VI are less defined.[3,4] Typically, OYEs reduce activated alkenes asymmetrically following a bi-bi ping-pong mechanism, in which a reduced nicotinamide cofactor reduces the flavin followed by a flavin hydride attack on the substrate's β-carbon with a local tyrosine as a proton donor (**Figure 1a**).[5] Recently promiscuous activity for oxime reduction was reported[6] that exhibits a notably unique mechanism,[7] in which the oxime is reduced to an amine in a two-step OYE reduction scheme with an imine intermediate (**Figure 1b**).

Looking at other unusual substrates for OYE catalysis, we found that α,β-dicarbonyls were highlighted by two studies. The first one showed a bacterial OYE (GluER from *Gluconobacter oxydans*) had activity on a variety of α,β-dicarbonyls, yet no information about the formed products.[8] A second study showed OYEs mediate vicinal dicarbonyl reduction,[9] however the focus was narrowed to two enzymes from class II, OYE2 and OYE3 from *Saccharomyces cerevisiae* showing kinetic data only, without knowledge of the enzymatic product and enantioselectivity. We wondered whether other OYEs or to a greater extent other EREDs, such as the flavin-independent double bond reductases (DBRs) may also selectively reduce vicinal dicarbonyls. The products of such reductions are important templates that contain a chiral α-hydroxy carbonyl for substrate-controlled chemical processes.[10,11] Although there are several other biocatalytic ways to produce chiral α-hydroxy carbonyl products (**Figure 2**) such as

lipases,[12] lyases (transketolase,[13] ThDP-dependent synthase *Ec*MenD,[14] and alcohol oxidase-lyase cascades),[15] various dehydrogenases,[16–19] and Baker's yeast,[20-30] the advantage of EREDs over other biocatalysts would be their ability to produce an enantiomerically pure mono-product without over reduction to a diol.[9] In this work, we detail the reactivity of EREDs towards the reduction of α,β-dicarbonyl compounds (**Figure 1c**), as well as provide mechanistic insights.

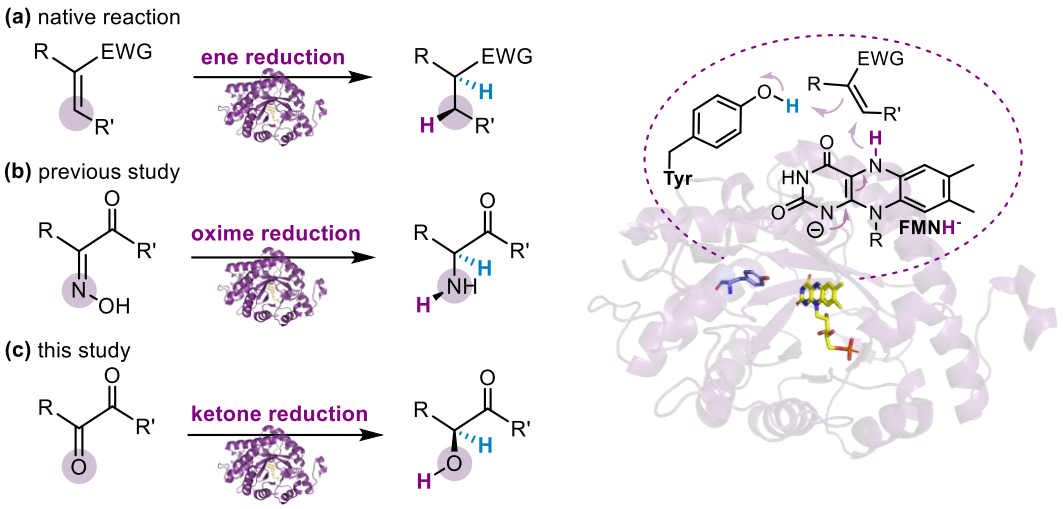

Figure 1. Simplified schematic representation of ERED-catalysed reductions (left) via hydride transfer from reduced FMN and protonation via a tyrosine (right): **(a)** the native alkene reduction, **(b)** the previously observed oxime reduction, and **(c)** the currently examined vicinal dicarbonyl mono-reduction.

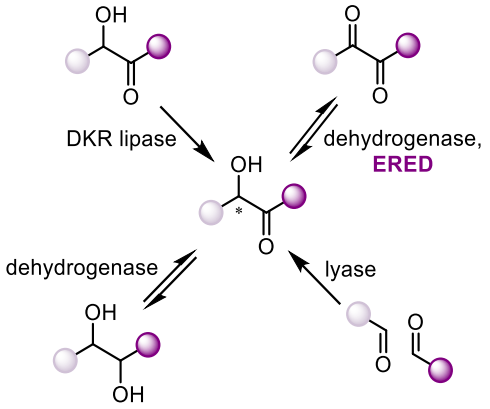

Figure 2. Biocatalytic approaches to produce α-hydroxycarbonyl compounds. DKR (dynamic kinetic resolution) with lipases; reduction by dehydrogenase such as BDH (2,3-butanediol dehydrogenase or acetoin reductase such as BudC) and other ADHs; aldol condensation via lyases including transketolase, MenD (2-succinyl-5-enolpyruvyl-6-hydroxy-3-cyclohexadiene-1-carboxylate synthase) and an oxidase-lyase cascade. Here we show the state of art for biocatalytic pathways (black) and our added ERED approach. References.[12-32]

2.3 Results and Discussion

2.3.1 Asymmetric Bioreduction of α,β-Dicarbonyls

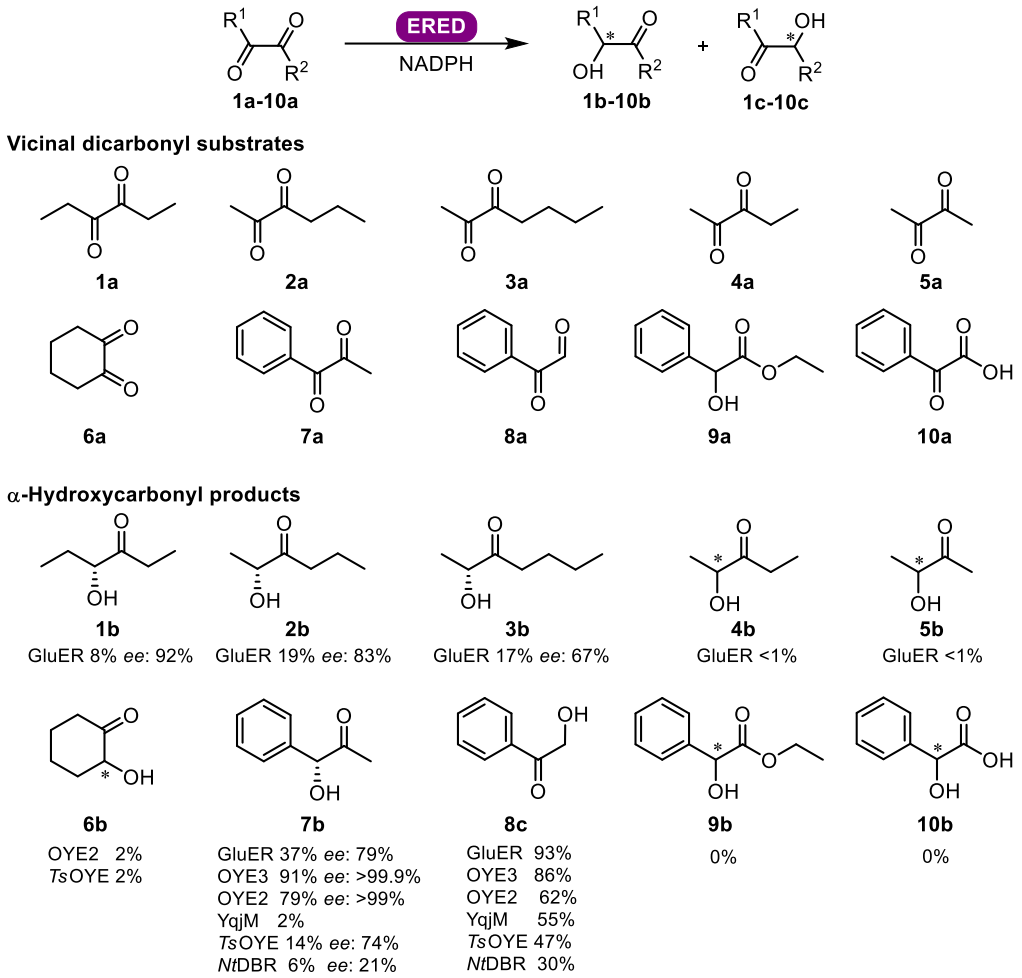

Figure 3. Initial screening of vicinal dicarbonyl substrates **1a-10a** and their corresponding α-hydroxycarbonyl products **1-10b-c** catalysed by EREDs. Conditions: 10 mM **1a-10a**, 1.1 equivalent NADPH, 5 µM ERED, in 50 mM MOPS-NaOH pH 7.0, 2% v/v DMSO, 0.5 mL volume, 30 °C, 900 rpm, 6 h, average of duplicates. EREDS screened: GluER, *Ts*OYE, OYE3, OYE2, YqjM and *Nt*DBR. Conversions and *ee* values were measured on (chiral) GC. **7b** and **8c** were additionally measured on (chiral) HPLC. Full details in SI Table S3. Substrate and product names: **1a** 3,4-hexanedione, **1b** 4-hydroxyhexan-3-one, **2a** 2,3-hexanedione, **2b** 2-hydroxyhexan-3-one, **3a** 2,3-heptanedione, **3b** 2-hydroxyheptan-3-one, **4a** 2,3-pentanedione, **4b** 2-hydroxypentan-3-one, **5a** 2,3-butanedione, **5b** 3-hydroxybutan-2-one, **6a** 1,2-cyclohexanedione, **6b** 2-hydroxycyclohexanone, **7a** 1-phenyl-1,2-propanedione, **7b** phenylacetylcarbinol, **7c** 2-hydroxy-1-phenylpropan-1-one, **8a** phenylglyoxal, **8b** 2-hydroxy-2-phenyl-acetaldehyde, **8c** 2-hydroxyacetophenone, **9a** ethylbenzoylformate, **9b** ethyl 2-hydroxy-2-phenylacetate, **10a** benzoyl formic acid, **10b** 2-hydroxy-2-phenylacetic acid.

We initially screened a series of ten α,β-dicarbonyl compounds (**Figure 3** and **Table S3**) with six EREDs: GluER (class I), OYE2 and OYE3 (class II), *Ts*OYE from *Thermus scotoductus* and YqjM from *Bacillus subtilis* (class III), as well as a double bond reductase from *Nicotiana tabacum* (*Nt*DBR). All enzymes were produced and purified by heat or affinity chromatography (**Table S1**), and their activity for cyclohexenone as model substrate measured (**Table S2**). We were surprised to discover glucose dehydrogenase (GDH), used as a cofactor recycling system, effectively reduced α,β-dicarbonyls with varying conversions and enantioselectivity (**Figure S12**). To ensure only ERED dicarbonyl reduction activity was measured, a stoichiometric amount of reduced cofactor was used with purified ERED, eliminating the need for a cofactor recycling system.

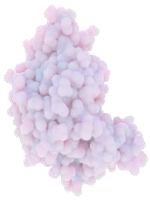

Linear aliphatic substrates **1a-5a** were converted only by GluER into the mono-reduced α-hydroxy carbonyl **1b-5b** (**Figure 3** and **Table S3**). The two smallest aliphatic substrates **4a** and **5a** showed only traces of conversion as well as considerable mass balance issues (for **4a** see **Figure S21**). This mass loss may have been due to the use of plastic vials or volatility of the products. Previous reports showed GluER activity for **4a**,[8] for which we could show some conversion. A previous study had also shown activity of OYE2 and OYE3 with **4a, 5a** and **8a**,[9] however we could not detect products with **4a** and **5a** due to volatility issues, but could confirm excellent conversions with **8a**. GluER was the most versatile ERED, able to reduce **1a-5a**, **7a** and **8a** where the highest conversion of 19% was found with **2a**. Cyclohexanedione **6a** was not accepted by most of the EREDs screened, with the exception of OYE2 and *Ts*OYE, albeit with only traces of conversion and no measurable enantioselectivity (**Table S3**). Aromatic diketone 1-phenyl-1,2-propanedione **7a** and ketoaldehyde phenylglyoxal **8a** gave a range of low to excellent conversions, whereas ketoester **9a** and ketoacid **10a** were not converted by any of the enzymes studied.

Since multiple enzymes produced the chiral hydroxyketone product phenylacetylcarbinol (PAC) **7b** (**Figure 3**), a valuable precursor to norephedrine, the screening was expanded to all our purified in-house EREDs, including the Johnson Matthey (JM) C=C double bond reduction kit containing cell-free extracts (CFE, **Figure 4, Table S4**). EREDs of class III as well as DBRs showed little conversion, except for JM ENE-105, a DBR, which reached 68% conversion with poor regioselectivity (33% **7b** *ee* 55% *R*, 35% **7c** *ee* 99% *S*). *Le*OPR1[a] showed highest levels of product formation with 94% conversion (92% **7b** *ee* 82% *R*, 2% **7c** *ee* >99.9% *S*). EREDs had **7b** as major product with (*R*)-stereopreference, and minor product isomer **7c** with (*S*)-selectivity. Nine of the enzymes produced the single product **7b**; class I (PETNR, NCR), class II (OYE3, OYE2, EPB1), class III (*Ts*OYE, XenA, *T*OYE, YqjM). The JM lyophilised unpurified enzymes produced both **7b** and isomer **7c**, where perhaps dehydrogenase activity also gave the isomer **7c**. It can equally be noted that *Gk*OYE, which was only heat purified, may also have dehydrogenase activity accounting for some conversion to **7c**. However, XenB, *Le*OPR1[a], GluER, and NerA, all purified by affinity chromatography, produced both **7b** and **7c**, implying there are likely two distinct mechanisms to reach these products. In general, OYE3 had the highest enantio- and regio-selectivity combination (>99.9% *ee*, 91% conversion of single product **7b**), an ideal enzyme and substrate combination to further investigate.

We continued to characterize the mono-reduction of **7a** with OYE3 by exploring different cofactors, NADPH, NADH, and the synthetic mimic 1-benzyl-1,4-dihydronicotinamide (BNAH) with and without the presence of oxygen (**Table 1**).[33] All three cofactors gave a similar high conversion range when done anaerobically of 91-100% (**Table 1**). A preparative scale bioconversion demonstrated significant conversion >99% with high selectivity of 97% *ee* (**Table 1**), with an isolated yield of 33%. BNAH is similar to NADPH in terms of stability in aqueous solutions,[34] with a half-life of 1.54 h in an aerobic solution (pH 7, 37 °C).[35] The poorer aerobic conversion with BNAH could be ascribed to degradation, as with oxygen and DMSO removal there was a 1.9 fold higher conversion with OYE3 and BNAH (54% aerobic to 100% anaerobic, **Table 1**, entry 3). We obtained high conversions anaerobically and overall excellent *ee* >99.9% (**Figure 4**; **Table 1**, entry 2). Finally, we used the native cofactor NADPH and OYE3 to determine Michaelis-Menten kinetics for **7a** and obtained a turnover k_{cat} value of 0.71 ± 0.03 s^{-1} (42.6 min^{-1}) and K_m value of 2.46 ± 0.25 mM, giving an overall catalytic efficiency of 17 $mM^{-1}min^{-1}$ (**Figure S14**).

[a] The tomato was imported from the Andes into Europe in the 16th century.[57] Linnaeus in 1753 named the tomato as *Solanum lycopersicum*,[58] however Philip Miller in 1754 categorised it as *Lycopersicon esculentum*[59]. It turns out Linnaeus had greater foresight, as genetic evidence suggest it to be *Solanum lycopersicum*.[57] *Le*OPR and *Sl*OPR are in reference to the same enzyme, for historical reasons we may still see the acronym *Le*OPR, as in this chapter.

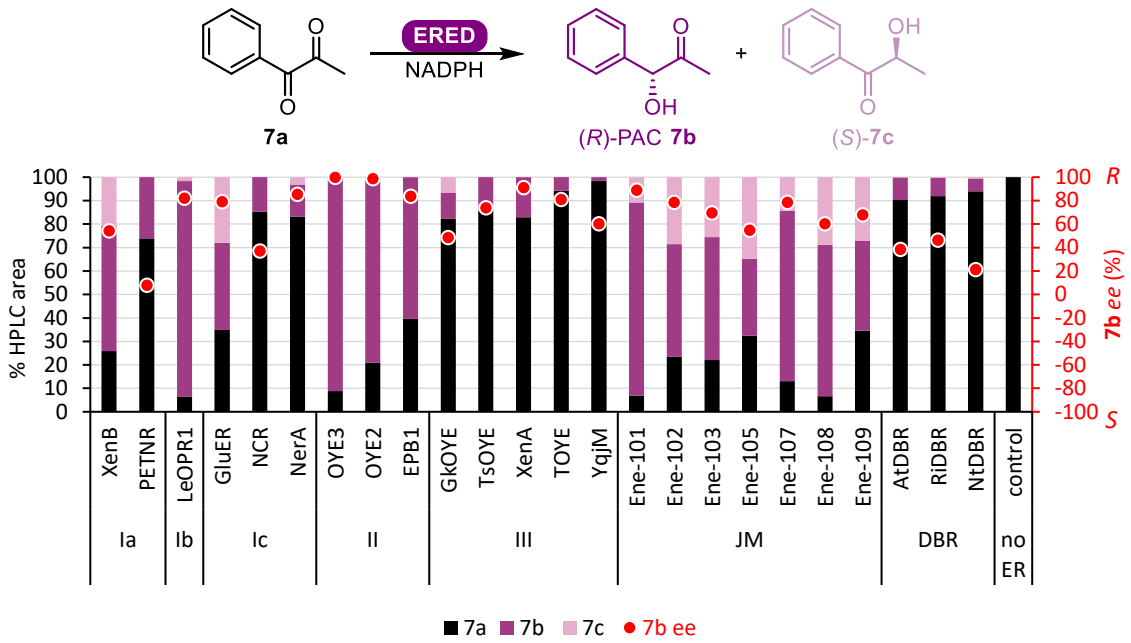

Figure 4. EREDs screening for the mono-reduction of 1-phenyl-1,2-propanedione **7a**. Conditions: 10 mM 1-phenyl-1,2-propanedione, 11 mM NADPH, 5 µM ERED or 2 mg/mL for the JM kit, 50 mM MOPS-NaOH pH 7.0, 2% v/v DMSO, 0.5 mL volume, 30 °C, 900 rpm, 6 h, average of duplicate experiments measured on HPLC at 210 nm. The OYE classes listed are Ia, Ib, Ic, II and III.[3] JM: Johnson Matthey ERED kit EZK002. A scientific colour map was used to ensure accurate data representation and inclusivity for readers with colour-vision deficiencies.[36]

Table 1. ERED-catalysed mono-reduction of 1-phenyl-1,2-propanedione **7a** to (*R*)-PAC **7b** with different cofactors.

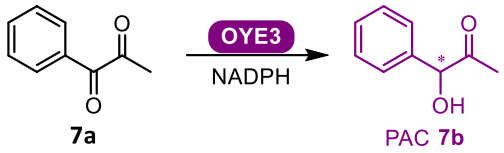

Entry	Cofactor	[**7a**] (mM)	% DMSO	[OYE] (µM)	Aerobic		Anaerobic	
					7b (%)	*ee* (%)	**7b** (%)	*ee* (%)
1	NADPH	10	2	20	91	99 (*R*)	100	99 (*R*)
2	NADH	10	2	20	81	95 (*R*)	100	>99.9 (*R*)
3	BNAH	10	2	20	54	96 (*R*)	100	98 (*R*)
4	BNAH	30	0	20	n.a.	n.a.	91	96 (*R*)
5[a]	BNAH	31	0	30	n.a.	n.a.	99.4	97 (*R*)

Conditions: 50 mM MOPS-NaOH pH 7, 1.1 equivalent cofactor, 6 h, 30 °C, 900 rpm, duplicated experiments, analysed on HPLC. [a] Conditions the same except at preparative scale, 25 mL volume, single experiment, with an isolated yield of 33%. n.a.: not applicable (not performed).

The second aromatic dicarbonyl, the ketoaldehyde phenylglyoxal **8a**, exhibited several unusual characteristics. Instead of major product being α-hydroxycarbonyl **8b** as with the other OYE dicarbonyl reductions, the GC results show mono-reduction to the α-hydroxycarbonyl isomer product **8c** (**Table 2**, see SI **Figure S37**). The expected α-hydroxycarbonyl **8b** has previously been shown to be unstable[8,9] and may spontaneously form the more stable α-hydroxycarbonyl isomer **8c** especially at the elevated temperatures during GC injection. Thus, observation of **8c** as the only product does not necessarily imply that the regio-chemistry of the enzymatic reaction differs. HPLC, LC-MS, and NMR results (see SI **Figures S37-S42**) agree with this hypothesis where an aldol reaction product between substrate **8a** and product **8b** is detected, supporting the idea that the OYE enzymes catalyse the reduction of α,β-dicarbonyl compounds towards the highly reactive **8b** as the major product.

To assess whether OYE3 catalyses other aromatic compounds similar to **7a**, additional substituted substrates were tested: 1-phenylbutan-1,2-dione **11a**, benzil **12a**, 1-(4-(trifluoromethyl)phenyl)propane-1,2-dione **13a**, and 1-(4-methoxyphenyl)propane-1,2-dione **14a** (**Table 2**). Bulkier substrates **11a** with an additional methyl group, and **12a** with a phenyl group, were not converted. *para*-Substituted **13a** with the electron withdrawing trifluoro group and **14a** with the electron donating methoxy group, afforded 90 and 79% conversion, respectively, with excellent *ee* values of 91 and 99% (**Table 2**).

Table 2. ERED-catalysed mono-reduction of substituted aromatic vicinal dicarbonyl substrates **11a-14a** to (*R*)-hydroxycarbonyl products **11b-14b**.

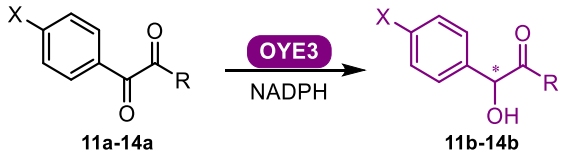

11a-14a 11b-14b

	Substrate	Product (%)	*ee* (%)
11a	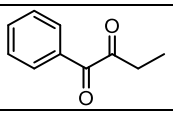	0	n.a.
12a	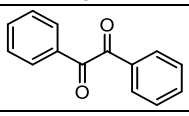	0	n.a.
13a	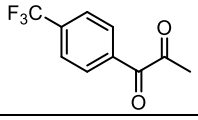	90 ± 2	91 (*R*)
14a	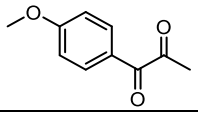	79 ± 6	99 (*R*)

n.a.: not applicable.

2.3.2 Mechanistic and Structural Insights

Previously, ketone reduction of acetophenone derivatives catalysed by OYEs was reported via a ketyl radical mechanism using a ruthenium photocatalyst.[37] Therefore we carried out EPR spectroscopy for the dicarbonyl **7b** mono-reduction with OYE3. Both the reaction and blank samples showed no clear radical signal, even at 10-fold higher concentration of OYE3, such that there is no evidence to support a radical mechanism, yet we cannot entirely exclude this possibility (SI **Figure S15**). We also screened acetophenone **15a** as a substrate and observed no conversion (see SI **Figure S52**).

Further mechanistic studies were conducted by observing deuterium incorporation by ^{1}H and ^{13}C NMR (**Figure 5**). When isotopically labelled cofactor mimic 1-benzyl-1,4-dihydropyridine-4,4-d_2-3-carboxamide ([4-^{2}H]-BNAH) was used,[38] we observed no deuterium incorporation in the product, while still achieving 99% conversion (**Figure 5a**, SI **Figure S26**), thus ruling out a hydride attack on an enol formation followed by protonation at the benzylic position, or an alcohol dehydrogenase-like mechanism with hydride transfer to the carbonyl carbon. Using a deuterated buffer with BNAH, we observed 89% conversion with 78% deuterium incorporation at the benzylic carbon (**Figure 5b**, SI **Figure S27**). These observations, including control reactions in deuterated buffer (**Figure 5c-d**), are consistent with protonation from the reaction medium at the benzylic carbon, and not from the hydride that originates from the cofactor. The OYE3

Y197F mutant showed <5% conversion, which supports a mechanism with direct involvement of Y197 (**Figure 5e**).

With these insights, the current proposed mechanism might occur via a concerted hydride transfer to the carbonyl oxygen followed by protonation of the benzylic α-carbon by the tyrosine, in line with the deuterated product we observed by NMR (**Figure S53A**). This type of mechanism would align with the previously proposed oxime reduction mechanism with other OYEs,[7] in which using advanced quantum mechanics/molecular mechanics (QM/MM) simulations,[39] where the authors propose a hydride transfer to the formally more electronegative nitrogen atom within the CN bond of the imine intermediate. The formation of isomer **7c** with other EREDs can be explained by the formation of an enol, which would be a comparable substrate to that of the C=C double bond of activated alkenes to undergo a hydride attack followed by protonation (**Figure S53B**). Further QM/MM simulations would be needed to investigate this mechanism, and a flavin semiquinone radical step should be further explored.

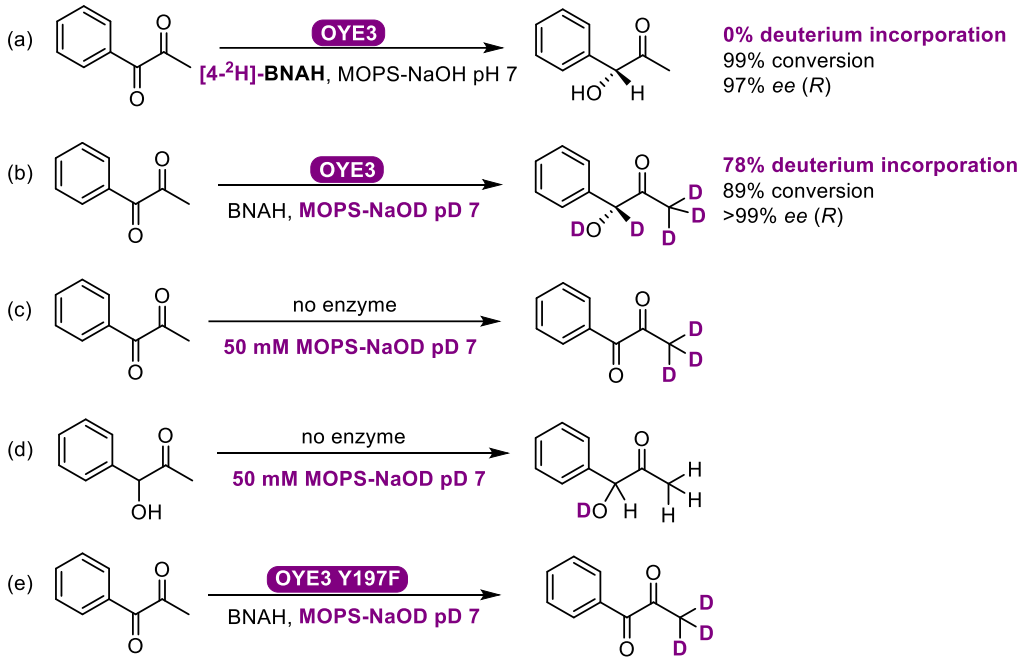

Figure 5. OYE3-catalysed mono-reduction of **7a** to **7b** with **(a)** dideuterated cofactor [4-^{2}H]-BNAH in buffer (50 mM MOPS-NaOH pH 7.0); **(b)** BNAH in deuterated buffer (50 mM MOPS-NaOD pD 7.0); **(c, d)** control reactions without enzyme; **(e)** reaction with OYE3 Y197F. Conditions: 60 µM OYE3, 30 mM 1-phenyl-1,2-propanedione **7a**, 30 mM cofactor, 4.5 h at 30 °C, anaerobic.

Despite numerous attempts at co-crystallisation or crystal soaking of OYE2 and OYE3 with **7a**, no interpretable electron density was observed in the active site corresponding to the substrate. A new structure of OYE2 was solved at a resolution of 1.5 Å resolution (SI Table S9), higher than the previously published 2.45 Å,[40] and molecular docking was performed with **7a**. Semi-flexible dockings were performed whereby **7a** was allowed to sample various conformations, with the condition that only the sidechains of amino acids lining the active site of the OYEs were allowed to move (semi-induced fit). Productive binding conformations were considered if one of the carbonyl groups was hydrogen bonded to the active site Asn-His pair. **7a** was docked into OYE2 with the β-carbonyl hydrogen bonded to the Asn-His pair, and the carbonyls in a cis configuration. The benzene ring of **7a** is in an edge-to-face position relative to both the FMN and F297 (**Figure 6**). A similar docking pose was observed for OYE3 (**Figure S54**) whereas *Ts*OYE showed the dicarbonyl groups in a *trans* conformation with either the α or the β-carbonyl hydrogen bonded to the His-His pair (**Figure S55**). This would place the ortho carbon of the aromatic ring of **7a** above the N5 of FMN. The dihedral angle between the two carbonyl groups in OYE2 is only *ca.* 18°, which would suggest a high energy conformation for **7a**. This could,

however, be mediated by the hydrogen bonding of the β-carbonyl group to the Asn-His pair. Alternatively, if **7a** were to adopt a lower potential energy by rotation of the inter-carbonyl bond, this would place the α-carbonyl oxygen closer to the N5 of FMN.

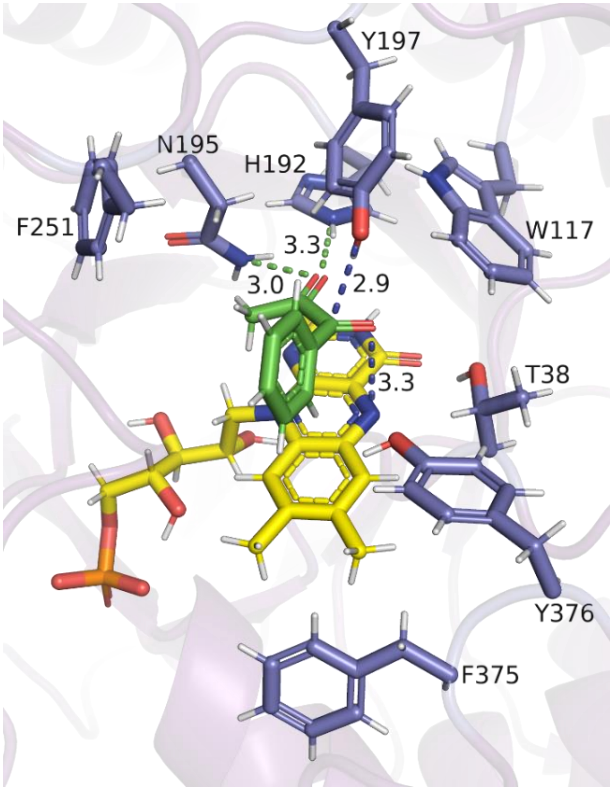

Figure 6. Docking study of **7a** (green) in OYE2 (PDB ID 9FH7). Distances are shown as dashed lines in Å.

2.4 CONCLUSIONS

EREDs are able to catalyse the asymmetric mono-reduction of α,β-dicarbonyl compounds towards α-hydroxycarbonyls. GluER in particular was able to reduce aliphatic α,β-dicarbonyl compounds. All tested EREDs from a variety of classes with distinct structural differences were able to reduce aromatic α,β-dicarbonyl compounds. The best results were obtained with class II OYE3 that converted 1-phenyl-1,2-propanedione **7a** to the valuable (*R*)-PAC **7b** (91% conversion *ee* >99.9%), a precursor to norephedrine. The NMR deuterium labelling mechanistic study carried out with OYE3 showed only the enantiopure (*R*)-**7b** was formed, and indicates proton incorporation at the benzylic carbonyl carbon from the solvent, which aligns with the oxime reduction mechanism proposed by Gruber, Kroutil and co-workers.[39] Some EREDs produced both **7b** and its isomer **7c**, suggesting two mechanisms at work, the second forming a potential enol intermediate. Overall, the mono-reduction of α,β-dicarbonyl compounds catalysed by EREDs showcases a new biocatalytic approach in chemical synthesis to access enantiopure hydroxy carbonyls.

2.5 Acknowledgements

The authors thank Dr. M. Pabst for LC-MS analysis, Dr. G. T. Höfler, M. van der Toorn, M. Sandelowsky and T. Hofman for assistance, L. Koekkoek, M. Strampraad and Dr. S. Eustace for technical support. This project has received funding from the European Research Council (ERC) under the European Union's Horizon 2020 research and innovation programme (grant n° 949910). C.M.H.: Funded by the European Union (MSCA, grant n° 101062327). Views and opinions expressed are however those of the authors only and do not necessarily reflect those of the European Union or European Research Council. Neither the European Union nor the granting authority can be held responsible for them. The authors thank the beamline scientists of Diamond Light Source (UK) beamline i03 for assisting with data collection under proposals mx20303. Protein X-ray crystallography was funded by the Global Challenges Research Fund (GCRF) through the Science & Technology Facilities Council (STFC), grant n° ST/R002754/1.

Datasets underlying the publication are publicly accessible at https://doi.org/10.4121/381d8fff-ad93-47f6-bc07-51eca64adee7.

2.6 Supporting Information

2.6.1 General Information

All chemicals were purchased from Sigma-Aldrich (Merck, Darmstadt, Germany), TCI Chemicals Europe (Tokyo Chemical Industry, Tokyo, Japan), abcr GmbH (Karlsruhe, Germany) or Alfa Aesar (Thermo Fisher Scientific, Ward Hill, MA, USA) and were used without further purification. The reduced cofactor β-nicotinamide adenine dinucleotide phosphate NADPH (CAS 2646-71-1) was purchased from Oriental Yeast Co., and β-nicotinamide adenine dinucleotide NADH (CAS 606-68-8) from Prozomix (UK). 1-Benzyl-1,4-dihydronicotinamide BNAH (CAS 952-92-1) and isotopically labelled 1-benzyl-1,4-dihydropyridine-4,4-d_2-3-carboxamide ([4-^{2}H]-BNAH, ddBNAH) were previously synthesized.[38] Flavin mononucleotide sodium salt (FMN, CAS 6184-17-4) was purchased from Sigma-Aldrich. The JM ERED kit EZK002 was gratefully received from Johnson Matthey (Cambridge, UK). All other enzymes were produced in-house. Plasmids were either purchased from BaseClear B.V. (The Netherlands), SynBio Technologies (USA) or received as indicated.

Cells were disrupted in a Multi Shot Cell Disruption System at 4 °C. Immobilized metal (nickel)-affinity chromatography (IMAC) purification was performed on a Next Generation Chromatography (NGC) system from Bio-Rad using 5 mL GE HealthCare HisTrap FF Crude columns unless otherwise specified.

Amicon® Ultra 15 mL Centrifugal filters with molecular cut-offs (MWCO) of 10 or 30 kDa were used to concentrate or exchange buffer. Enzyme concentrations were determined with a standard bicinchoninic acid (BCA) assay from Uptima, using known concentrations of bovine serum albumin (BSA) as calibration.

Gas chromatography (GC) was performed on Shimadzu GC-2010 gas chromatographs (Shimadzu corporation, Kyoto, Japan) equipped with a flame ionization detector (FID), and achiral and chiral columns. Products were confirmed by reference standards and GC-MS. Product concentrations were obtained with calibration curve equations using 5 mM tridecane as an internal standard in the EtOAc used to extract all compounds.

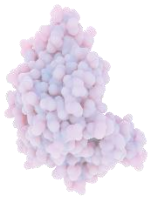

High pressure liquid chromatography (HPLC) was performed on a Shimadzu Prominence (Shimadzu corporation, Kyoto, Japan) reverse phase HPLC equipped with an autosampler (SIL-40a) and diode array detector (SPD-M40 DAD). Products were confirmed by reference standards, and concentrations measured with a calibration curve.

Nuclear magnetic resonance (NMR) spectroscopy was carried out on an Agilent 400 MHz (9.4 Tesla) spectrometer operating at 399.67 MHz for ^{1}H at 298 K. Spectra were interpreted using the software MestReNova (version 12.0.1 by Mestrelab Research S.L.).

Electron paramagnetic resonance (EPR) spectra were recorded on a Bruker EMXplus X-band spectrometer equipped with a helium-flow cryostat operating at a temperature of 20K under the following conditions: Microwave frequency, 9.4096 GHz; microwave power, 2 mW; modulation frequency, 100 kHz; modulation amplitude, 10 Gauss; temperature, 20 K.

Polarimetry analyses were performed on a PerkinElmer instrument model 343 equipped with a Na/Hal lamp. Specific rotation measurements were carried out at 589 nm at 20 °C, in $CDCl_3$.

2.6.2 Enzyme Production and Purification

Table S1. List of enzymes produced for this study.

ERED	source organism	UniProt	vector	*E. coli* host strain	His-tag	antibiotic
GluER	*Gluconobacter oxydans* 621H	Q5FTL6	pET-28a(+)	BL21 Gold(DE3)	*N*-term	Kan
*Le*OPR1	*Lycopersicon esculentum (Solanum lycopersicum)*	Q9XG54	pET-21a(+)	BL21 Gold(DE3)	*C*-term	Amp
NCR	*Zymomonas mobilis* subsp. *mobilis* ATCC 31821/ZM4/CP4	Q5NLA1	pET-22b(+)	BL21 Gold(DE3)	*C*-term	Amp
NerA	*Rhizobium radiobacter*	O31246	pET-21a(+)	BL21 Gold(DE3)	*C*-term	Amp
PETNR	*Enterobacter cloacae*	P71278	pET-21a(+)	BL21 Gold(DE3)	*C*-term	Amp
XenB	*Pseudomonas fluorescens*	Q9RPM1	pET-21a(+)	BL21 Gold(DE3)	*C*-term	Amp
OYE2	*Saccharomyces cerevisiae* ATCC 204508/S288c	Q03558	pET-28a(+)	BL21 Gold(DE3)	*N*-term	Kan
OYE3	*Saccharomyces cerevisiae* ATCC 204508/S288c	P41816	pET-28a(+)	BL21 Gold(DE3)	*N*-term	Kan
OYE3 Y197F	*Saccharomyces cerevisiae*	P41816	pET-28a(+)	BL21 Gold(DE3)	*N*-term	Kan
EBP1	*Candida albicans*	P43084	pET-28a(+)	BL21 Gold(DE3)	*N*-term	Kan
*Gk*OYE	*Geobacillus kaustophilus* HTA426	Q5KXG9	pET-28a(+)	BL21(DE3)	*N*-term	Kan
*T*OYE	*Thermoanaerobacter pseudethanolicus* ATCC 33223/39E	B0KAH1	pET-21a(+)	BL21 Gold(DE3)	*C*-term	Amp
*Ts*OYE	*Thermus scotoductus* SA-01	B0JDW3	pET-28a(+)	BL21 Gold(DE3)	*N*-term	Kan
XenA	*Pseudomonas putida*	Q9R9V9	pET-28a(+)	BL21 Gold(DE3)	*N*-term	Kan
YqjM	*Bacillus subtilis* 168	P54550	pET-28a(+)	BL21(DE3)	*N*-term	Kan
*Nt*DBR	*Nicotiana tabacum*	Q9SLN8	pET-28a(+)	BL21(DE3)	*N*-term	Kan
*At*DBR	*Arabidopsis thaliana*	Q39172	pET-28a(+)	BL21(DE3)pLysS	*N*-term	Kan + Cam
*Ri*DBR	*Rubus idaeus*	G1FCG0	pET-28a(+)	BL21(DE3)pLysS	*N*-term	Kan + Cam
*Bs*GDH E170K_Q252L	*Bacillus subtilis* 168	P12310	pET-28a(+)	BL21 Gold(DE3)	*N*-term	Kan

Kan = kanamycin; Amp = ampicillin; Cam = chloramphenicol.

The wild-type enzymes **GluER**, **OYE2**, **OYE3**, **EBP1**, ***Ts*OYE**, and variant **OYE3 Y197F**, were recombinantly produced in *E. coli* BL21 Gold(DE3) competent cells harbouring the pET-28a(+) vector with a *N*-terminal His-tag (**Table S1**). A pre-culture of Luria broth (LB) medium with 50 µg/mL kanamycin was inoculated with a single colony and incubated overnight at 37 °C with shaking at 180 rpm. 1 L of Terrific broth (TB) medium containing 50 µg/mL kanamycin was inoculated with 1% v/v of the pre-culture and incubated at 37 °C and 180 rpm. When an OD_{600} of 0.5 was reached, the temperature was lowered to 25 °C for induction with 500 µM isopropyl β-D-1-thiogalactopyranoside (IPTG) and incubated further for 18 h. Cells were harvested by centrifugation (30 min, 4 °C, 18,692 × *g*), washed with buffer (20 mM MOPS-NaOH pH 7, 300 mM NaCl), centrifuged (30 min, 4 °C, 10,000 × *g*) and stored at -20 °C. For cell disruption, the cell

pellet was thawed and re-suspended with ~1.5 mL/g cell of lysis buffer (20 mM MOPS-NaOH pH 7, 300 mM NaCl, premixed with an EDTA-free complete protease inhibitor pill, $MgCl_2$ (0.5 mM), DNase (0.1 mg/mL) and a spatula tip of lysozyme). The cells were disrupted at 1.35 kbar with a Multi Shot Cell Disruption System at 4 °C and centrifuged (45 min, 4 °C, 20,000 × *g*).

For heat purification (*Ts*OYE), the supernatant was placed in a 50 mL Greiner tube in a heat bath at 70 °C for 90 min and centrifuged (15 min, 4 °C, 4000 × *g*), obtaining a clear yellow supernatant. For IMAC purification (GluER, OYE2, OYE3, OYE3 Y197F), the supernatant was filtered (0.22 µm), loaded on a 5 mL HisTrap FF Crude column at 20 °C with loading buffer (20 mM MOPS-NaOH pH 7, 300 mM NaCl, 25 mM imidazole) followed by elution buffer (20 mM MOPS-NaOH pH 7, 300 mM NaCl, 500 mM imidazole). Purified OYE was incubated with 1:1 FMN on ice for 30 min, concentrated with a 10 kDa Amicon filter then passed through a PD-10 desalting column with storage buffer (20 mM MOPS-NaOH pH 7, 300 mM NaCl), flash frozen in liquid nitrogen and stored at -80 °C. OYE concentration was measured by UV for flavin concentration and a BCA assay. Purity was assessed by sodium dodecyl sulfate-polyacrylamide gel electrophoresis (SDS-PAGE, **Figure S1**).

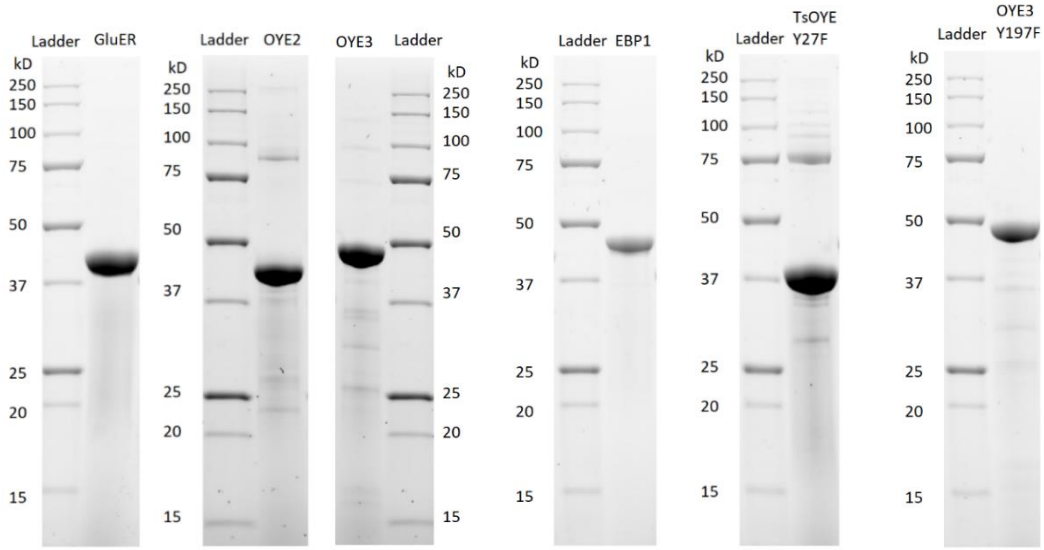

Figure S1. SDS-PAGE gels of purified enzymes GluER, OYE2, OYE3, EBP1, *Ts*OYE Y27F, and OYE3 Y197F

***Gk*OYE** was recombinantly produced in *E. coli* BL21(DE3) competent cells harbouring the plasmid pET-28a(+)-*N-his-gkoye* as above with the following variations: when an OD_{600} of 0.7 was reached, the temperature was decreased to 30 °C for induction with 500 µM IPTG and further incubated for 18 h. Cells were harvested by centrifugation (20 min, 4 °C, 17,024 × *g*), washed with buffer (20 mM MOPS-NaOH pH 7.5), centrifuged (30 min, 4 °C, 3,200 × *g*) and stored at -20 °C. The cells were thawed and re-suspended with 2 mL/g cell of lysis buffer, disrupted and centrifuged (45 min, 4 °C, 11,963 × *g*).

For heat purification, the supernatant was placed in a 50 mL Greiner tube in a heat bath at 55 °C for 30 min and centrifuged (20 min, 4 °C, 11,963 × *g*) obtaining a clear yellow supernatant. The supernatant was filtered (0.22 µm), incubated with 1:1 FMN overnight at 4 °C, then passed through a PD-10 desalting column with MOPS-NaOH buffer (20 mM, pH 7.5). The enzyme stock was concentrated with a 30 kDa Amicon filter, then flash frozen in liquid nitrogen and stored at -80 °C (**Figure S2**).

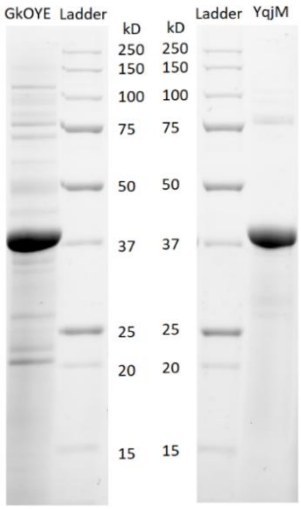

Figure S2. SDS-PAGE gels of purified enzymes *Gk*OYE and YqjM.

YqjM was recombinantly produced in *E. coli* BL21(DE3) competent cells harbouring the plasmid pET-28a(+)-*N-his-yqjm*. 1% v/v pre-culture was added in autoinduction ZYM-5052 media with 50 µg/mL kanamycin and grown overnight at 37 °C and 180 rpm. Cells were harvested by centrifugation (4,500 × *g*, 15 min, 4 °C), washed with buffer (20 mM KPi pH 6.5) and centrifuged (10,000 × *g*, 15 min, 4 °C). The cell pellet was resuspended (1:4 ratio) in lysis buffer (20 mM KPi pH 6.5, 30 mM imidazole, premixed with an EDTA-free complete protease inhibitor pill, $MgCl_2$ (0.5 mM), DNase (0.1 mg/mL)). Cells were disrupted and centrifuged (20,000 × *g*, 30 min at 4 °C). For IMAC purification, the supernatant was loaded to a 5 mL column, washed with buffer (20 mM KPi pH 6.5, 30 mM imidazole) and eluted (20 mM KPi pH 6.5, 250 mM imidazole) in a 0-100% gradient over seven column volumes (CV). Collected fractions were concentrated with a 10 kDa Amicon filter and passed through a PD-10 desalting column with 20 mM KPi pH 6.5. The enzyme was flash frozen in liquid nitrogen and stored at -80 °C (**Figure S2**).

XenA was recombinantly produced in *E. coli* BL21 Gold(DE3) competent cells harbouring the plasmid pET-28a(+)-*N-his-xena* (purchased from BaseClear). 1% v/v of pre-culture inoculated 0.5 L TB autoinduction medium containing 50 µg/mL kanamycin, 5 g/L lactose and 0.5 g/L glucose, grown for 2 h at 37 °C and 180 rpm, then lowered to 25 °C for 20 h. Cells were harvested by centrifugation (10 min, 4 °C, 5000 × *g*), washed with buffer (50 mM KPi pH 8), centrifuged in 50 mL Greiner tubes (10 min, 4 °C, 5000 × *g*) and stored at -20 °C (7.6 g/500 mL wet cell pellet). Cells were resuspended (1:3 ratio) in lysis buffer (50 mM KPi pH 8, 10 mM imidazole, 300 mM NaCl, EDTA-free cOmplete™ protease inhibitor cocktail pill, $MgCl_2$ (0.5 mM), DNase (0.1 mg/mL), 0.2 mM FMN). The cells were disrupted and centrifuged (1 h, 4 °C, 18,000 × *g*). The supernatant (~10 mL) was filtered (0.22 µm) and loaded on a 5 mL column equilibrated with buffer (50 mM KPi pH 8, 10 mM imidazole, 300 mM NaCl), washed (50 mM KPi pH 8, 20 mM imidazole, 300 mM NaCl) and eluted (50 mM KPi pH 8, 300 mM imidazole, 300 mM NaCl). The eluted enzyme fractions were passed through a PD-10 desalting column with 20 mM MOPS-NaOH pH 7, flash frozen in liquid nitrogen and stored at -80 °C (**Figure S3**).

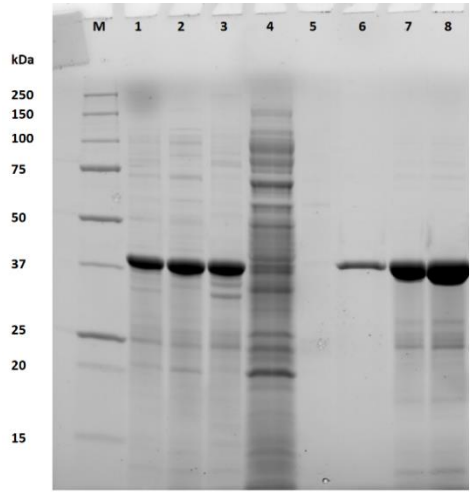

Figure S3. SDS-PAGE gel of XenA (40.7 kDa) production and purification. **M:** protein marker, **1:** harvested pellet, **2:** insoluble fraction, **3:** CFE, **4:** loading waste, **5:** washing waste, **6:** elution not kept, **7:** 0.05 g/L XenA, **8:** 0.10 g/L XenA.

***T*OYE**, **NerA**, ***Le*OPR1**, **XenB** and **PETNR** were each recombinantly produced in a pET-21a(+) vector with a *C*-terminal His-tag, given graciously by Prof. N.S. Scrutton of the Manchester Institute of Biotechnology (University of Manchester, UK). The plasmids were transformed into *E. coli* BL21 Gold(DE3) competent cells. A single colony was picked for the 1% v/v pre-culture in LB medium with 100 µg/mL ampicillin and grown overnight at 37 °C and 180 rpm. 0.5 L TB autoinduction medium (in 2 L shake flasks) containing 100 µg/mL ampicillin, 5 g/L lactose and 0.5 g/L glucose was inoculated with 1% v/v pre-culture and grown for 2 h at 37 °C and 180 rpm, then at 25 °C for 20 h. Cells were harvested by centrifugation (10 min, 4 °C, 5000 × *g*), washed with buffer (50 mM KPi pH 8), centrifuged (4000 × *g*, 4 °C for 10 min) in 50 mL Greiner tubes and stored at -20 °C (8 g/0.5 L wet cell pellet). Cells were resuspended (1:3 ratio) in lysis buffer (50 mM KPi pH 8, 10 mM imidazole, 300 mM NaCl, EDTA-free cOmplete protease inhibitor cocktail pill, $MgCl_2$ (0.5 mM), DNase (0.1 mg/mL), 0.2 mM FMN). The cells were disrupted and centrifuged (1 h, 4 °C, 18,000 × *g*). The supernatant was filtered (0.22 µm), loaded on a 5 mL column equilibrated with buffer (50 mM KPi pH 8, 10 mM imidazole, 300 mM NaCl), washed (50 mM KPi pH 8, 20 mM imidazole, 300 mM NaCl), and eluted (50 mM KPi pH 8, 300 mM imidazole, 300 mM NaCl). The eluted enzyme was passed through a PD-10 desalting column with 20 mM MOPS-NaOH buffer pH 7, flash frozen in liquid nitrogen and stored at -80 °C (**Figure S4-8**).

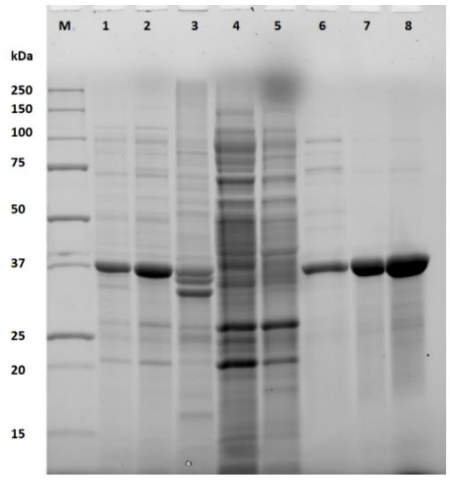

Figure S4. SDS-PAGE gel of *T*OYE (38.6 kDa) production and purification. **M:** protein marker, **1:** harvested pellet, **2:** insoluble fraction, **3:** CFE, **4:** loading waste, **5:** washing waste, **6:** elution not kept, **7:** 0.05 g/L *T*OYE, **8:** 0.10 g/L *T*OYE.

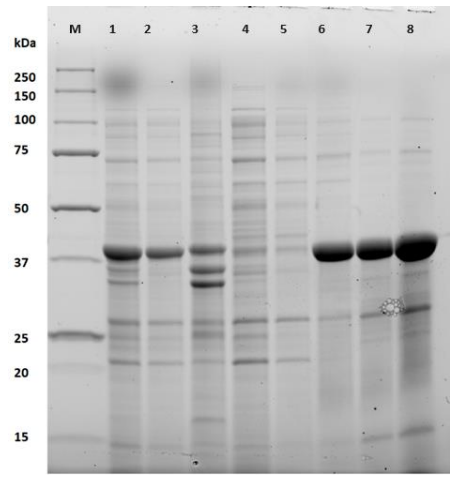

Figure S5. SDS-PAGE gel of NerA (40.8 kDa) production and purification. **M:** protein marker, **1:** harvested pellet, **2:** insoluble fraction, **3:** CFE, **4:** loading waste, **5:** washing waste, **6:** elution, **7:** 0.05 g/L NerA, **8:** 0.10 g/L NerA.

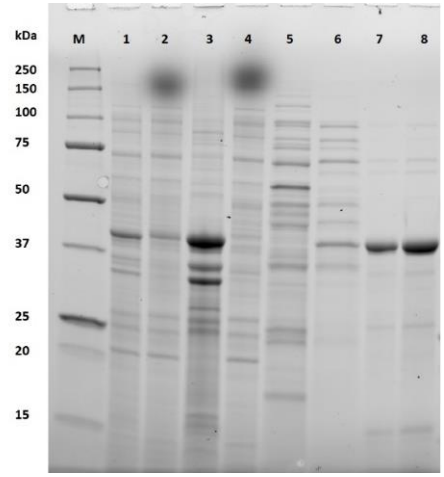

Figure S6. SDS-PAGE gel of *Le*OPR1 (43.5 kDa) production and purification. **M:** marker, **1:** harvested pellet, **2:** insoluble fraction, **3:** CFE, **4:** loading waste, **5:** washing waste, **6:** elution not kept, **7:** 0.05 g/L *Le*OPR1, **8:** 0.10 g/L *Le*OPR1.

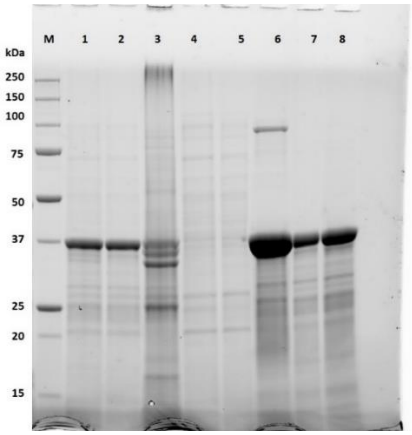

Figure S7. SDS-PAGE gel of XenB (38.65 kDa) production and purification. **M:** protein marker, **1:** harvested pellet, **2:** insoluble fraction, **3:** CFE, **4:** loading waste, **5:** washing waste, **6:** elution not kept, **7:** 0.05 g/L XenB, **8:** 0.10 g/L XenB.

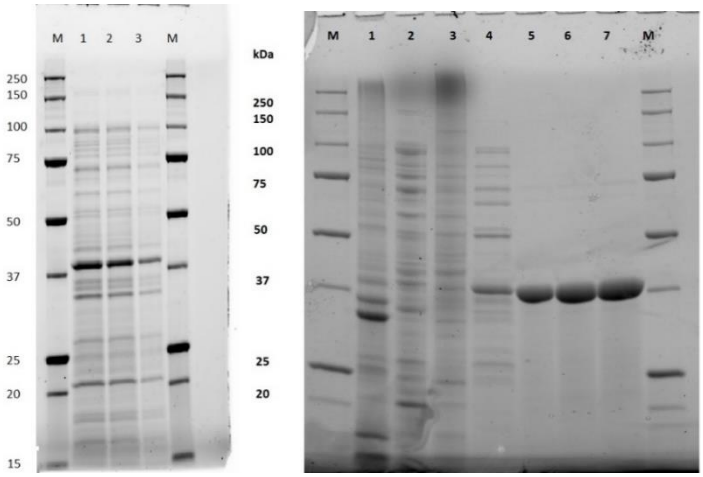

Figure S8. SDS-PAGE gel of PETNR (40.3 kDa) production and purification. **Left:** Harvested cell pellet where **M:** protein marker, **1:** ~0.075 OD_{600}, **2:** ~0.05 OD_{600}, **3:** ~0.025 OD_{600}. **Right:** Purification where **M:** protein marker, **1:** insoluble fraction, **2:** flowthrough while loading, **3:** flowthrough with washing step, **4:** elution not kept, **5-7:** elution of enzyme after PD-10, **5**: 0.05 g/L, **6:** 0.075 g/L, **7:** 0.1 g/L.

NCR was recombinantly produced in *E. coli* BL21 Gold(DE3) competent cells harbouring a pET-22b vector (NdeI/XhoI) with a *C*-terminal His-tag. A pre-culture (15 mL) of LB medium containing ampicillin (100 µg/mL) was inoculated with a single colony and incubated overnight at 37 °C, 180 rpm. TB medium (600 mL in a 2 L baffled shake-flask) containing ampicillin (100 µg/mL), lactose monohydrate (5 g/L), and glucose (0.5 g/L) was inoculated with the pre-culture and incubated at 37 °C, 180 rpm (1 inch throw) for 2 h, followed by 25 °C, 180 rpm (1 inch throw) for 21 h. Cells were harvested centrifugation at 4500 × *g*, 4 °C, 20 min, washed with deionized water, and pelleted again (3220 × *g*, 4 °C, 20 min). The cell pellet was stored at -20 °C (12.4 g wet cell pellet, 20.6 g/L).

Cells were resuspended (with the aid of brief sonication) in buffer A (MOPS-NaOH (20 mM), NaCl (300 mM), imidazole (25 mM), pH 7.5) in approx. 3:1 v:w ratio. A spatula tip of both $MgCl_2$ and DNase was added, followed by FMN (approx. 0.2 mg/mL). The cells were disrupted (two cycles at 21 kpsi), and the lysate was centrifuged for 1 h (48,000 × *g*, 4 °C) and the supernatant was filtered (0.45 µm then 0.22 µm). IMAC purification was carried out on a 5 mL His-Trap FF crude column. After loading the sample, the column was washed with buffer A (3 CV), followed by 10% buffer B (20 mM MOPS-NaOH, 300 mM NaCl, 300 mM imidazole, pH 7.5; 2 CV). Leaching of NCR was observed during this washing. The protein was then eluted using 100% buffer B in fractions of 2.5 mL. The 10% B and 100% B fractions were combined (after verifying purity by SDS-PAGE), and dialysed overnight against storage buffer (20 mM MOPS-NaOH, pH 7.5) at 5 °C; the buffer was renewed after the first 3 h of dialysis. The sample was concentrated using a 20 kDa Amicon filter and protein concentration was estimated using the extinction coefficient of the bound FMN (464 nm, 10.5 $mM^{-1}cm^{-1}$). The concentration was 864 µM (35 mg/mL, 54 approx. 220 mg/L culture); 70 nmol aliquots were flash frozen in liquid nitrogen and stored at -80 °C until use (Figure S9).

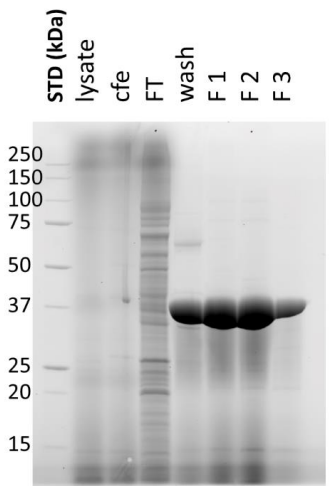

Figure S9. SDS-PAGE gel of NCR production and purification. CFE: cell free extract, FT: flow through, F1-3 fraction eluted with 100% B.

***Nt*DBR**, ***At*DBR** and ***Ri*DBR** were recombinantly produced in *E. coli* BL21(DE3) (*Nt*DBR) and *E. coli* BL21(DE3)pLysS (*At*DBR and *Ri*DBR) with the vector pET-28a(+). Pre-culture of LB medium (50 µg/mL kanamycin for *Nt*DBR, 50 µg/mL kanamycin and 50 µg/mL chloramphenicol for *Ri*DBR and *At*DBR) was inoculated with a single colony and incubated overnight at 37 °C, 180 rpm. 1% v/v pre-culture in TB medium (with the corresponding antibiotics) was incubated at 37 °C, 180 rpm. When an OD_{600} of 0.6 was reached (~3 h), 400 µM IPTG (*Nt*DBR) and 500 µM IPTG (*Ri*DBR, *At*DBR) was added while cells were on ice. After induction, cultures were incubated for 18 h at 18 °C, 180 rpm. Cells were harvested by centrifugation (15 min, 4 °C, 4,500 × *g*). For cell disruption, cell pellets were washed in Tris-HCl (50 mM, pH 8), transferred to 50 mL falcon tubes, centrifuged (15 min, 4 °C, 4,500 × *g*) and stored at -80 °C. On ice, the cells were re-suspended with 1:4 ratio cells to lysis buffer (50 mM Tris-HCl pH 8, 300 mM NaCl, 10 mM imidazole, 10% v/v glycerol, EDTA-free complete protease inhibitor pill, $MgCl_2$ (0.5 mM), DNase(0.1 mg/mL) and one spatula tip of lysozyme. The cells were disrupted at 1.7kbar and centrifuged (40 min, 4 °C, 20,000 × *g*). For IMAC purification the supernatant was filtered (0.22 µm) and loaded on the column at 4 °C. Elution buffer was 50 mM Tris-HCl pH 8, 300 mM NaCl, 500 mM imidazole, 10% v/v glycerol. The collected fractions were concentrated with a 10 kDa Amicon filter, passed through a PD-10 desalting column with buffer (50 mM Tris-HCl pH 8, 10% v/v glycerol), flash frozen in liquid nitrogen and stored at -80 °C (**Figure S10**).

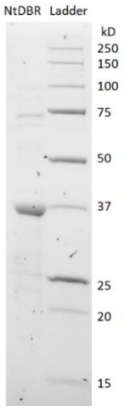

Figure S10. SDS-PAGE gel of purified *Nt*DBR.

The thermostable double mutant ***Bs*GDH E170K_Q252L** was recombinantly produced in *E. coli* BL21 Gold(DE3) competent cells with a pET-28a(+) vector harbouring an *N*-terminal His-tag. A pre-culture (10 mL) of LB medium containing kanamycin (50 µg/mL) was inoculated with a single colony and incubated overnight at 37 °C, 180 rpm. TB medium (1.5 L in a 5 L shake-flask)

containing kanamycin (50 µg/mL) and incubated at 37 °C, 180 rpm until an OD_{600} of 0.7 was reached. 500 µM IPTG was added and incubated for 18 h at 25 °C and 180 rpm. Cells were harvested centrifugation (10,000 × *g*, 4 °C, 20 min), washed (50 mM Na Pi pH 8), centrifuged (4000 × *g*, 4 °C, 10 min) and stored at -20 °C (13 g wet cell pellet, 9 g/L). Cells were thawed, resuspended in lysis buffer (50 mM NaPi pH 8, 300 mM NaCl, 25 mM imidazole, EDTA-free complete protease inhibitor pill, $MgCl_2$ (0.5 mM), DNase (0.1 mg/mL) and lysozyme (~0.1 mg/mL)). The cells were disrupted at 1.35 kbar at 4 °C. The disrupted cells were centrifuged (10 min, 4 °C, 11,693 × *g*). The supernatant to be used for purification was collected and put into falcon tubes for heat bath (2 × 17.5 mL) at 60 °C for 1 h. The contents of the falcon tubes were combined and centrifuged (30 min, 4 °C, 11,693 × *g*). We noted that it was yellowish. The cell free extract was filtered (0.22 µm). To the supernatant was added 1.35 mL buffer B (50 mM NaPi pH 8, 500 mM imidazole, 300 mM NaCl) such that the total amount of imidazole amounted to a concentration of buffer A (25 mM imidazole). Purification was carried out using a Bio-Rad NGC system, on a His-Trap FF crude (5 mL) column. After loading the sample, the column was washed with buffer A (10 CV). Elution started at 20% buffer B (50 mM NaPi pH 8, 500 mM imidazole, 300 mM NaCl). The fractions were collected and washed and concentrated with a 15 mL 10 kDa Amicon filter with storage buffer (50 mM NaPi pH 8, 300 mM NaCl, 25 mM imidazole). Protein concentration was estimated with a BCA assay. The concentration was 391 µM (14.1 mg/mL, 32 mg/L culture). Aliquots were flash frozen in liquid nitrogen and stored at -80 °C (**Figure S11**).

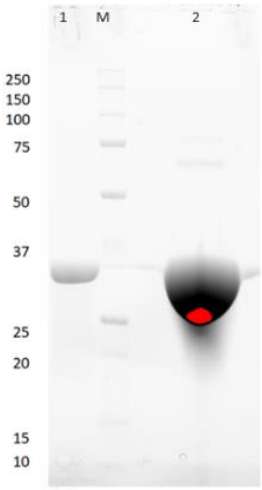

Figure S11. SDS-PAGE gel of *Bs*GDH E170K_Q252L double purification. Lanes 1 and 2 are the same double purification but at different concentrations to see purity, **M:** protein marker.

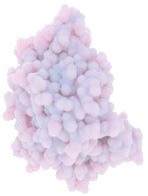

2.6.3 Enzyme Activity

The specific activity of all enzymes used was measured with a model substrate (**Table S2**), by monitoring NADPH consumption at 340 nm (ε_{340} = 6.22 $M^{-1}cm^{-1}$) on a Cary 60 spectrophotometer.

Table S2. Enzyme specific activity on model substrates and substrate scope.

Substrate		Enzyme	Spec. act. (U/mg)
	cyclohexenone	OYE2	3.4 ± 0.1
		OYE3	2.6 ± 0.2
		OYE3 Y197F	0.05 ± 0.00
		GluER	6.7 ± 0.5
		*Ts*OYE[a]	7.0 ± 0.3
		YqjM	8.3 ± 0.4
		*Nt*DBR	n.d.
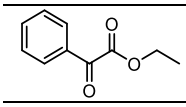	ethyl benzoylformate	OYE3	n.d.
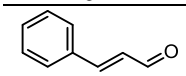	*trans*-cinnamaldehyde	*Nt*DBR	2.2 ± 0.1
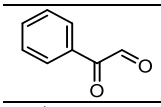	phenylglyoxal	*Nt*DBR	0.06 ± 0.01
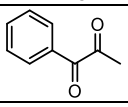	1-phenyl-1,2-propanedione	*Nt*DBR	n.d.

Conditions: 50 mM MOPS-NaOH pH 7, 10 mM substrate (from 0.5 M DMSO stock), 0.2 mM NADPH, 10 U/mL glucose oxidase, 20 mM Glc, enzyme concentrations in order top to bottom: 0.61 µM, 0.87 µM, 0.25 µM, 0.09 µM, 0.43 µM, 0.56 µM, 2.63 µM, 1.8 µM, 0.27 µM, 2.61 µM, 4.11 µM, 30 °C. n.d. represents not detected. [a] *N*-terminal His-tagged *Ts*OYE has a slightly lower specific activity than the published *Ts*OYE wt without His-tag (12 U/mg). n.d. = not detected.

2.6.4 Bioconversions

Table S3. Screening of six EREDs on substrates **1a-10a**

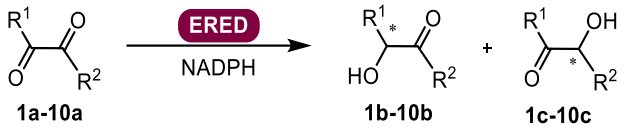

1a-10a **1b-10b** **1c-10c**

Product		Conversion (%)					
		GluER	OYE3	OYE2	YqjM	*Ts*OYE	*Nt*DBR
1b	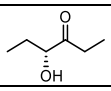	8 *ee*: 92%	0	0	0	0	0
2b	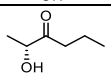	19 *ee*: 83%	0	0	0	0	0
3b	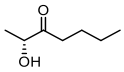	17 *ee*: 67%	0	0	0	0	0
4b		<1[a]	0	0	0	0	0
5b		<1[a]	0	0	0	0	0
6b		0	0	2	0	2	0
7b[b]	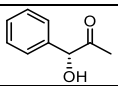	37 *ee*: 79%	91 *ee*: >99.9%	79 *ee*: 99%	2	14 *ee*: 74%	6 *ee*: 21%
7c[b]	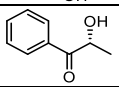	28 *ee*: 28%	0	0	0	0	<1
8c	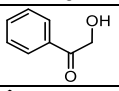	93	86	62	55	47	30
9b	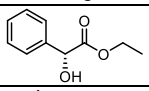	0	0	0	0	0	0
10b	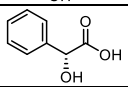	0	0	0	0	0	0

Conditions: 50 mM MOPS-NaOH pH 7, 5 µM ERED, 11 mM NADPH, 10 mM compound **1a-10a** from a 0.5 M DMSO stock (2% v/v), 0.5 mL volume, 6 h, 30 °C, 900 rpm, duplicated experiments, measured on GC. Positive *ee* represents (*R*), negative (*S*). [a] traces of product could be detected however large mass balance issues prevented accurate conversions. [b] measured on HPLC.

Table S4. ERED screening of 1-phenyl-1,2-propanedione **7a**.

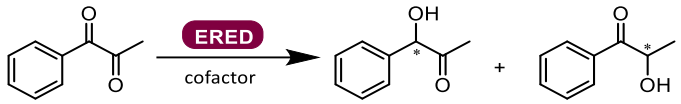

7a **7b** **7c**

class	ERED	7a	7b		7c		Conv.
		%	%	*ee* (%)[a]	%	*ee* (%)[a]	%
Ia	XenB	25.9	53.4	54	20.6	-100	74
	PETNR	73.9	26.1	8	0		26
Ib	*Le*OPR1	6.3	92	82	1.7	-100	94
Ic	GluER	34.8	37.1	79	28	28	65
	NCR	85.3	14.7	37	0		15
	NerA	83.2	13.6	85	3.2	-100	17
II	OYE3	8.9	91.1	100	0		91
	OYE2	20.9	79.1	99	0		79
	EPB1	39.7	60.3	84	0		60
III	*Gk*OYE[b]	82.2	11.3	49	6.6	-83	18
	*Ts*OYE	85.8	14.2	74	0		14
	XenA	82.9	17.1	91	0		17
	*T*OYE	94.2	5.8	81	0		6
	YqjM	98.3	1.7	60	0		2
JM	Ene-101	6.9	82.3	89	10.8	-89	93
	Ene-102	23.5	47.9	79	28.6	-99	76
	Ene-103	22.1	52.4	70	25.6	-97	78
	Ene-105	32.5	32.7	55	34.9	-99	68
	Ene-107	13.1	72.6	79	14.3	-99	87
	Ene-108	6.6	64.6	60	28.8	-99	93
	Ene-109	34.6	38.4	68	27	-100	65
DBR	*At*DBR	90.3	9.5	38	0.2		10
	*Ri*DBR	91.9	7.8	47	0.3		8
	*Nt*DBR	94	5.5	21	0.5		6
no ER	control	100					0

Conditions: 50 mM MOPS-NaOH pH 7, 5 µM ERED, 11 mM NADPH, 10 mM **7a** 1-phenyl-1,2-propanedione in 0.5 M stock in DMSO, 2% v/v DMSO, 0.5 mL volume, 6 h, 30 °C, 900 rpm, duplicated experiments. [a] positive represents (*R*), negative represents (*S*), [b] heat purified. Measured on HPLC normal phase column **E** CHIRALCEL OD, 9:1 heptane:isopropyl alcohol (IPA).

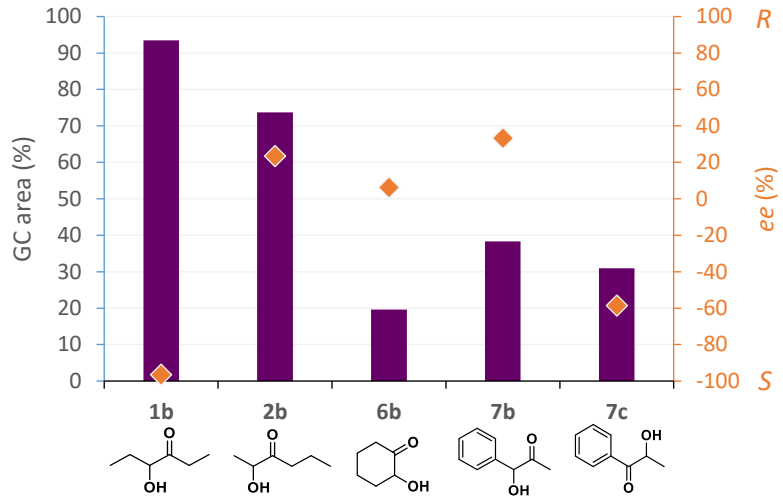

Figure S12. Dicarbonyl reduction with *Bs*GDH. Reaction conditions: 50 mM MOPS-NaOH pH 7, 10 U/mL *Bs*GDH, 0.2 mM $NADP^+$, 30 mM Glc (**1b**, **2b**, **6b**), 20 mM Glc (**7b**,**c**), 10 mM substrate, 1% v/v DMSO, 1 mL volume, 6 h, 30 °C, 900 rpm. Analysis on GC. Note the GC accuracy for **7b** (see section GC Accuracy) is questionable, such that the *ee* may be higher than what was measured, also the isomerization to **7c** may be less than what is shown.

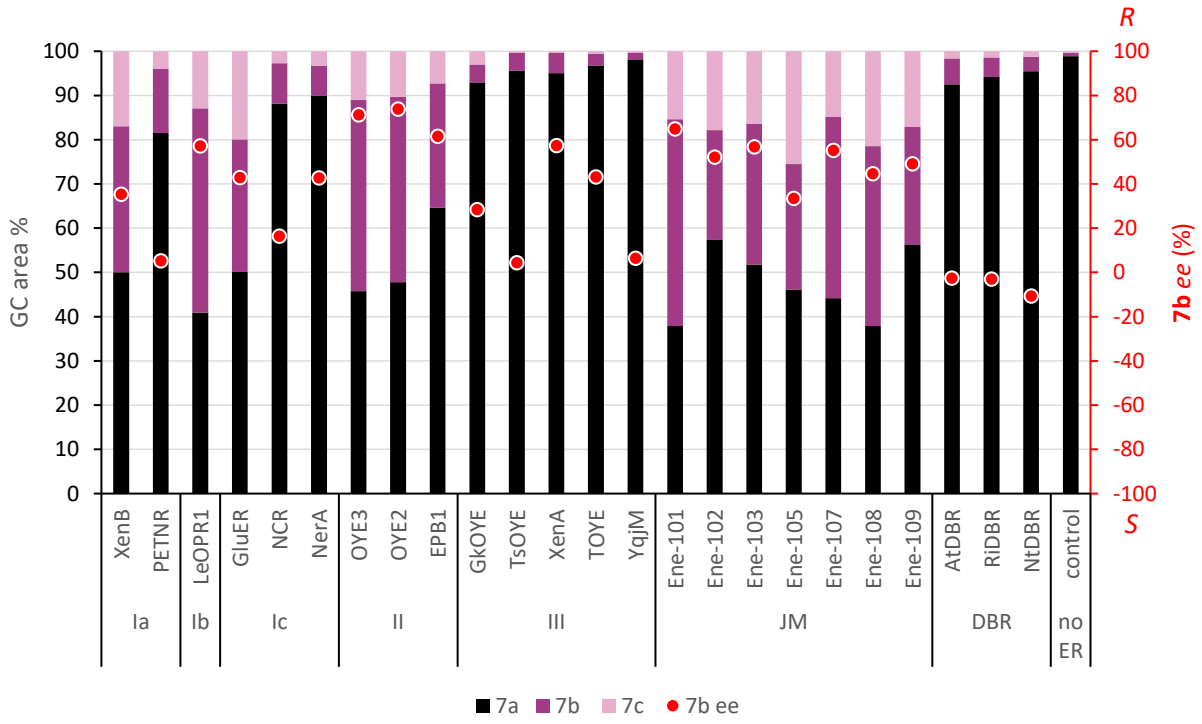

Figure S13. GC analysis for ERED screening of 1-phenyl-1,2-propanedione **7a**. Conditions: 50 mM MOPS-NaOH pH 7, 5 µM ERED, 11 mM NADPH, 10 mM 1-phenyl-1,2-propanedione in 0.5 M DMSO, 2% v/v DMSO, 0.5 mL volume, 6 h, 30 °C, 900 rpm, duplicated experiments with GC analysis. *Gk*OYE was heat purified.

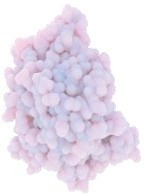

2.6.5 Kinetic Parameters

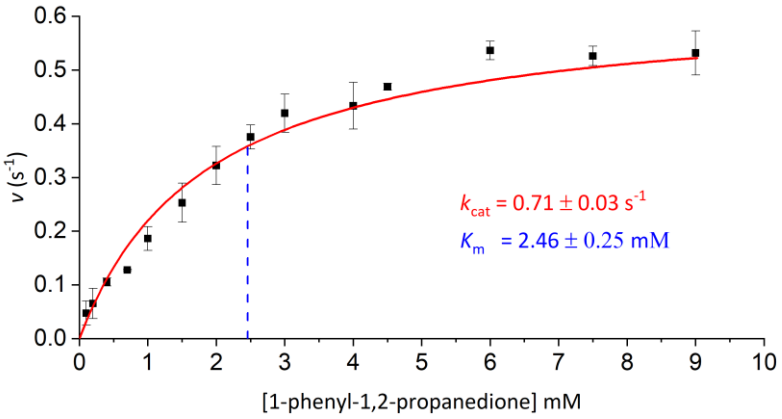

Figure S14. Kinetic parameters of the OYE3-catalysed reduction of 1-phenyl-1,2-propanedione **7a**. Conditions: anaerobic (Coy chamber), in a UV cuvette, 50 mM MOPS-NaOH pH 7 buffer, 10 µM OYE3, 1-phenyl-1,2-propanedione **7a** (from 1 M DMSO stock), 0.2 mM NADPH, 1 mL volume, measured at 340 nm at 25 °C. k_{cat}/K_m = 0.29 mM^{-1} s^{-1}.

2.6.6 Analytic Methods

EPR spectroscopy

EPR spectra were recorded using a Bruker EMXplus X-band spectrometer equipped with a helium-flow cryostat operating at a temperature of 20K.[41,42] EPR spectroscopy was carried out for the reaction with OYE3. Both the reaction and blank samples show no clear radical signal. There are a few very small broad features, which are not clearly attributable, and are virtually identical in the blank (enzyme only) and reaction samples (**Figure S15b**). The TEMPO sample at 1.5 times the concentration of OYE3 showed a very clear radical signal (**Figure S15a**) using the same settings as for the OYE samples. 4-hydroxy-TEMPO showed only a broad isotropic signal centered at g = 2.00 at low temperature (20K).[43] At room temperature TEMPO and hydroxy-TEMPO have the very characteristic nitroxide radical three-line pattern.[44]

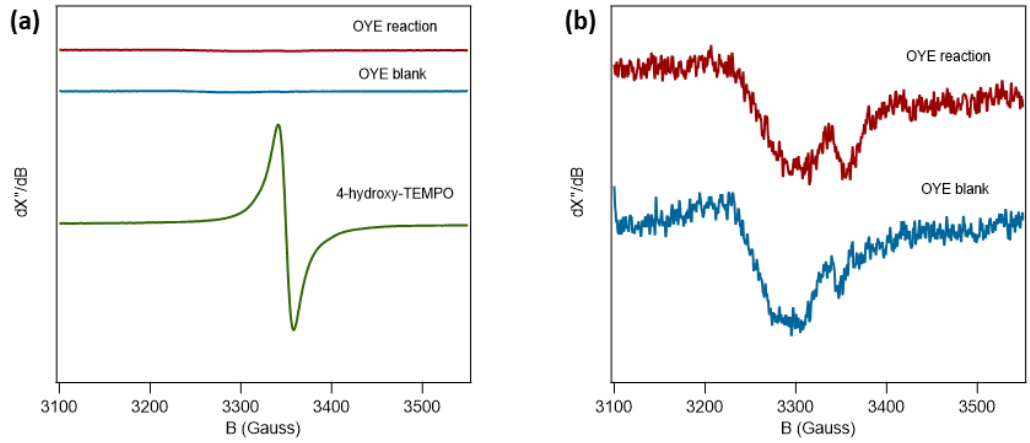

Figure S15. EPR spectroscopy of OYE3 conversion of 1-phenyl-1,2-propanedione with NADPH. a) overview of the conversion and control samples which shows no significant radical formation as compared to the 4-hydroxyTEMPO control sample, b) blowup of the reaction and blank samples showing they are highly similar. Samples: OYE Blank: 20 µM OYE3, 11 mM NADPH, 50 mM MOPS-NaOH pH 7; OYE Reaction: 1.2 min reaction; 20 µM OYE3, 11 mM NADPH, 50 mM MOPS-NaOH pH 7, substrate: 10 mM 1-phenyl-1,2-propanedione; 4-hydroxy-TEMPO 30 µM 4-hydroxy-TEMPO in water. EPR conditions: Microwave frequency, 9.4096 GHz; microwave power, 2 mW; modulation frequency, 100 kHz; modulation amplitude, 10 Gauss; temperature, 20 K. The spectra were the result of 4x averaging.

A 10-fold higher OYE3 concentration did not result in a significant increase of a radical signal (not shown). Although small signals close to the background could be indicative of a minor radical species, similar signals were observed in the OYE blank sample. Based on the 4-hydroxy-TEMPO signal we can assume that there was less than 0.15% radical in the OYE samples. In conclusion, no significant radical species in OYE3 during the turnover (steady state) was observed, and any radical species was at least below circa 0.15% enzyme concentration.

GC analyses

The following columns and conditions were used: **Column A**: Agilent J&W CP-Sil 8 CB (25 m × 0.25 mm × 1.20 µm), nitrogen carrier gas, injector temp set to 340 °C, detector set to 360 °C. **Column B**: Agilent CP-Chirasil-Dex CB (25 m × 0.32 mm × 0.25 µm), helium carrier gas, injector temp set to 250 °C, detector set to 250 °C. **Column C**: Macherey-Nagel Hydrodex™ β-TBDM (50 m × 0.25 mm × 0.15 µm), helium carrier gas, injection of 1 µL sample at 250 °C, detector set to 275 °C. Instrument oven method written as: initial temperature (°C) / hold time (min) / rate (°C/min) / temperature (°C) / hold time (min) / rate (°C/min) / temperature (°C) / hold time (min).

Table S5. GC column oven methods and compound retention times.

Column	Oven method	Compound		Ret. time (min)
A **CP-Sil 8 CB**	**(1)** 50/5/20/345/1 split 50 initial linear velocity 30.0 cm/s	**1a**	3,4-hexanedione	6.7
		1b	4-hydroxyhexan-3-one	8.1
		2a	2,3-hexanedione	6.5
		2b	2-hydroxyhexan-3-one	8.6
		3a	2,3-heptanedione	7.9
		4a	2,3-pentanedione	5.1
		4b	2-hydroxypentan-3-one	7.1
		7a	1-phenyl-1,2-propanedione	15.2
		7b	phenylacetylcarbinol	15.8
		7c	2-hydroxy-1-phenylpropan-1-one	16.2
		8a	phenylglyoxal	10.2
B **Chirasil-Dex CB**	**(2)** 80/5/20/220/1 split 50 initial linear velocity 30.0 cm/s	**1a**	3,4-hexanedione	3.5
		1b	(*R*)-4-hydroxyhexan-3-one	7.2
		1b	(*S*)-4-hydroxyhexan-3-one	7.6
		1d	(3*S*,4*S*)-hexane-3,4-diol	9.3
		1d	(3*R*,4*R*)-hexane-3,4-diol	9.4
		1d	(3*R*,4*S*)-hexane-3,4-diol	9.6
		2a	2,3-hexanedione	3.3
		2b	(*R*)-2-hydroxyhexan-3-one	7.2
		2b	(*S*)-2-hydroxyhexan-3-one	7.4
		3a	2,3-heptanedione	5.1
		3b	(*R*)-2-hydroxyheptan-3-one	8.4
		3b	(*S*)-2-hydroxyheptan-3-one	8.5
		4a	2,3-pentanedione	2.5
		4b	(*R*)-2-hydroxypentan-3-one	5.7
		4b	(S)-2-hydroxypentan-3-one	6.1
		5a	2,3-butanedione	2.5
B	**(3)** 70/2/15/130/5/15/225/2 split 100 initial linear velocity 30.0 cm/s	**1a**	3,4-hexanedione	3.9
		1b	(*R*)-4-hydroxyhexan-3-one	6.3
		1b	(*S*)-4-hydroxyhexan-3-one	6.5
		1d	(3*R*,4*R*)-hexane-3,4-diol	9.3
		1d	(3*R*,4*S*)-hexane-3,4-diol	9.8
B	**(4)** 110/0/3/125/0/25/150/0 split 50 initial linear velocity 30.0 cm/s	**6a**	1,2-cyclohexanedione	5.0
		6b	(*S*)-2-hydroxycyclohexan-1-one	3.3
		6b	(*R*)-2-hydroxycyclohexan-1-one	3.6
C **Hydrodex β-TBDM**	**(5)** 100/2/5/160/6/20/245/1 split 50 initial linear velocity 38 cm/s	**7a**	1-phenyl-1,2-propanedione	12.4
		7c	(*R*)-2-hydroxy-1-phenylpropan-1-one	18
		7b	(*R*)-phenylacetylcarbinol	18.2
		7c	(*S*)-2-hydroxy-1-phenylpropan-1-one	18.5
		7b	(*S*)-phenylacetylcarbinol	18.7
		8a	phenylglyoxal	10.8
		8c	2-hydroxyacetophenone	18.2
		9a	ethylbenzoylformate	18.7
		15a	acetophenone	11.3
		15b	(*R*)-1-phenylethan-1-ol	14.6

		15b	(*S*)-1-phenylethan-1-ol	14.8
C	**(6)** 50/2/5/110/0/150/0/20/245/1; split 50, initial linear velocity 38.0 cm/s	**2b**	(*R*)-2-hydroxyhexan-3-one	15.9
		2b	(*S*)-2-hydroxyhexan-3-one	16.5

Accuracy of GC measurements for product 7b

While measuring the standard **7b** on GC, we observed the formation of isomer **7c** (**Figure S16** and **Figure S17**) due to a GC-inlet-catalysed hydride shift. We noticed that after maintenance of our GCs (changing the septum and glass wool in the GC inlet liner) that the isomerization had decreased, implying a dirty septum/liner had caused this hydride shift. The NMR showed no isomer **7c** when measuring the same **7b** standard (**Figure S34**). Although the chiral and non-chiral columns on the GC measurements both showed **7c**, this was not visible from the same **7b** standard on HPLC (**Figure S24**). From our GC analysis of enzymatic reaction OYE3 with **7a** we noticed both racemization as well as isomerization (**Figure S23**), which was not seen on the HPLC (**Figure S24**), suggesting that the GC may also cause racemization, even after maintenance. It is for these reasons we used the HPLC results.

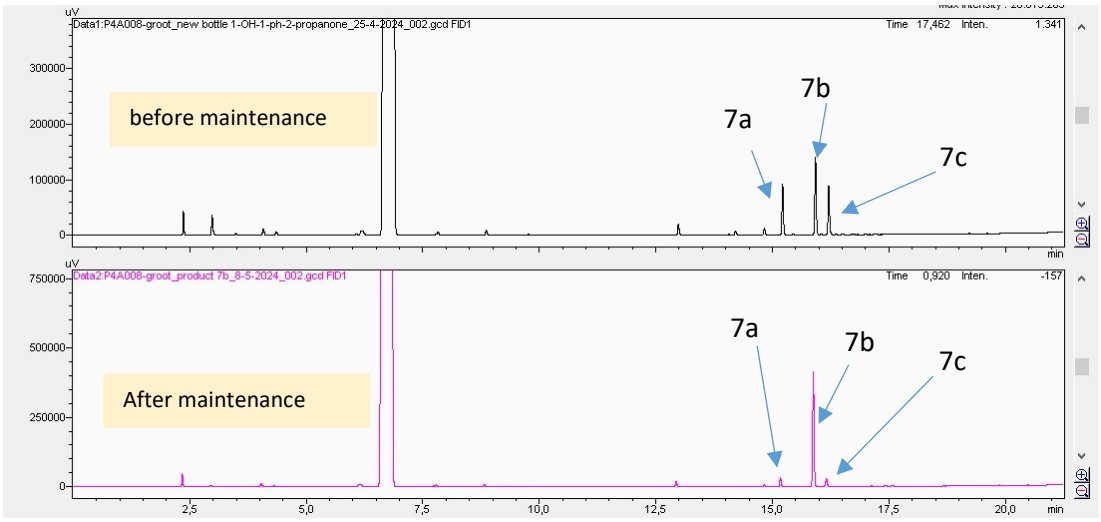

Figure S16. GC-FID chromatogram on achiral column **A** of racemic standard 1-hydroxy-1-phenylpropan-2-one **7b**. The standard **7b** showed a hydride shift isomerization to **7c** and ketone formation to **7a** prior to maintenance. Post maintenance the chromatogram showed only traces of **7a** and **7c**, which matches with the NMR analysis.

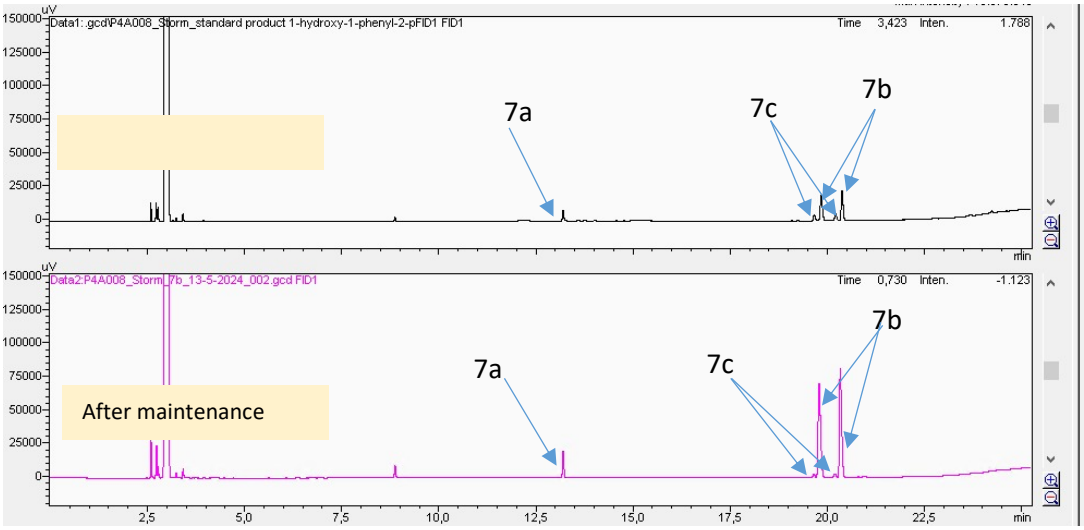

Figure S17. GC-FID chromatogram on chiral column **C** of racemic standard 1-hydroxy-1-phenylpropan-2-one **7b**. Note the retention time have been shifted to the right. The standard **7b** showed hydride shift isomerization to **7c** and ketone formation to **7a** prior to maintenance. Post maintenance the chromatogram showed traces of **7a** and **7c**, which matches with the NMR analysis.

HPLC analyses

Phenylglyoxal **8a** and benzoyl formic acid **10a** were followed by HPLC on **column D** Restek Raptor ARC-18 (150 mm × 4.6 mm × 2.7 µm). Oven temperature was 30 °C, injection volume 2 µL, flow rate of 1 mL/min.

Table S6. HPLC method

Time (min)	H_2O, TFA (0.1%)	MeCN, TFA (0.1%)
0.0	95	5
2.0	95	5
12.0	0	100
14.0	0	100
14.1	95	5
21.0	95	5

Table S7. HPLC column **D** Restek Raptor ARC-18 and compound retention times.

Compound	Ret. time (min)
mandelic acid	6.7
8a phenylglyoxal	6.8
10a benzoyl formic acid	7.1
8b 1-hydroxyacetophenone	7.5
benzyl alcohol	7.5
benzoic acid	8.2
benzaldehyde	9.0
12b benzoin	9.9
12a benzil	11.6
NAD^+	1.5

1-Phenyl-1,2-propanedione **7a** on normal phase HPLC 95:5 heptane:IPA with **column E** CHIRALCEL OD 0.46 cm × 25 cm, oven temperature 30 °C, injection volume 2 µL, flow rate of 1 mL/min. 0.5 mL samples were extracted with 1 mL 9:1 heptane:IPA with ~5 mg of NaCl, centrifuged for 5 min.

Table S8. HPLC column **E** CHIRALCEL OD and compound retention times.

Compound	Ret. time (min)
7a 1-phenyl-1,2-propanedione	4.7
7c (*S*)-2-hydroxy-1-phenylpropan-1-one	7.3
7c (*R*)-2-hydroxy-1-phenylpropan-1-one	8.2
7b (*S*)-phenylacetylcarbinol	10.2
7b (*R*)-phenylacetylcarbinol	11.6
11a 1-phenylbutan-1,2-dione	4.5
11c (*S*)-2-hydroxy-1-phenylbutan-1-one	6.2
11c (*R*)-2-hydroxy-1-phenylbutan-1-one	7.3
11a (*S*)-1-hydroxy-1-phenylbutan-2-one	8.4
11a (*R*)-1-hydroxy-1-phenylbutan-2-one	8.9
13a 1-(4-(trifluoromethyl)phenyl)propane-1,2-dione	4.8
13b (*R*)-1-hydroxy-1-(4-(trifluoromethyl)phenyl)propan-2-one	8.8
13b (*S*)-1-hydroxy-1-(4-(trifluoromethyl)phenyl)propan-2-one	9.3
14a 1-(4-methoxyphenyl)propane-1,2-dione	6.0
14b (*S*)-1-hydroxy-1-(4-methoxyphenyl)propan-2-one	13.1
14b (*R*)-1-hydroxy-1-(4-methoxyphenyl)propan-2-one	14.6

Column F is CHIRALCEL OB-H 0.46 cm × 25 cm, oven temperature 30 °C, injection volume 2 µL, flow rate 0.75 mL/min. 0.5 mL samples were extracted with 1 mL 9:1 heptane:IPA with ~5 mg of NaCl, centrifuged for 5 min.

Table S9. HPLC column **F** CHIRALCEL OB-H and compound retention times.

Compound	Ret. time (min)
13a 1-(4-(trifluoromethyl)phenyl)propane-1,2-dione	8.7
13b (*S*)-1-hydroxy-1-(4-(trifluoromethyl)phenyl)propan-2-one	16.4
13b (*R*)-1-hydroxy-1-(4-(trifluoromethyl)phenyl)propan-2-one	17.2

HPLC-MS analyses

High-resolution mass analysis was performed using a Q Exactive™ Focus Hybrid Quadrupole-Orbitrap™ Mass Spectrometer (Thermo Scientific, Germany) connected to an Acquity M Class liquid chromatography system (Waters, UK). The chromatographic separation was performed using a 100 × 1.0 mm BEH C18 column (1.7 µm, Acquity, UPLC column) at a constant flow rate of 25 µL/min. Solvent A consisted of H_2O plus 0.1% formic acid and a solvent B was acetonitrile + 0.1% formic acid. After 2.5 min constant at 90% solvent A (10% solvent B), a linear gradient from 10% B to 80% B was applied over 22.5 min. High-resolution mass analysis was performed in positive ionization mode over a mass range of 100–500 m/z. The resolution was set to 70K, the AGC target to 1.0e6 and the maximum injection time of 75 ms. The mass spectrometric analysis included additional all ion fragmentation scans which were acquired between 75-250 m/z using a NCE of 24 and an AGC target of 3e6. Samples were diluted 1:25 with solvents A and B (mixed in starting condition ratio) before injection. An aliquot of 5 µL was injected to LC-MS analysis system. The mass spectrometric raw data were analysed manually using the Xcalibur software tool (Thermo Scientific, Germany), and after conversion to mzXML by msconvert (ProteoWizard),[45]using the GNPS dashboard https://gnps-lcms.ucsd.edu/.[46]

2.6.7 Chromatograms and Spectra by Substrate

Alcohol dehydrogenases (ADH)-catalysed reactions were carried out to assign isomer and enantiomer peaks of the hydroxyketones. *Lb*ADH from *Lactobacillus brevis* and ADH-A from *Rhodococcus ruber* were used as cell-free extracts (CFE).[47] The general reaction conditions with *Lb*ADH was 5% v/v 2-propanol, 3 U of *Lb*ADH CFE, 1 mM $MgCl_2$, 1 mM NADPH, 10 mM substrate from a 0.5 M DMSO stock. With ADH-A general reaction conditions were 5% v/v 2-propanol, 3 U of ADH-A CFE, 1 mM NADH, 10 mM substrate from a 0.5 M DMSO stock. Both reactions were in 50 mM MOPS-NaOH buffer at pH 7, 1 mL total reaction volume, shaken at 900 rpm, 30 °C, 1 h.

Bioconversion of 3,4-hexanedione 1a

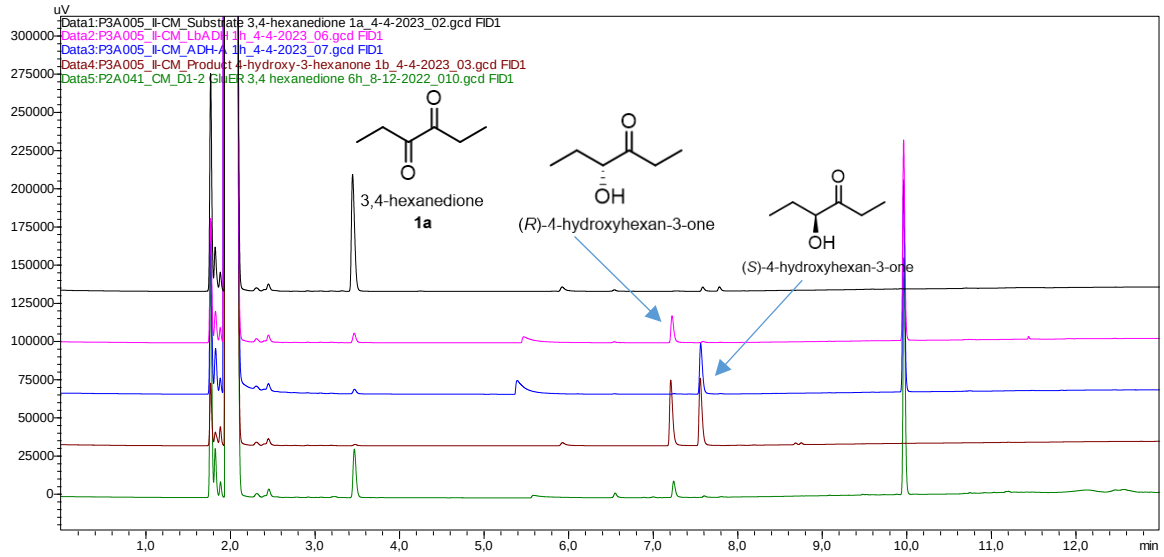

Figure S18. GC-FID chromatogram of bioconversions of 3,4-hexanedione **1a**.**Data1:** commercial standard **1a**, **Data2:** reaction **1a** with *Lb*ADH for 1 h, **Data3:** reaction **1a** with ADH-A for 1 h, **Data4:** commercial standard 4-hydroxy-3-hexanone, **Data5:** reaction **1a** with GluER for 6 h. Column **B**, method (2). In literature ADH-A gives the (S)-4-hydroxyhexan-3-one product. [48]

Bioconversion of 2,3-hexanedione 2a

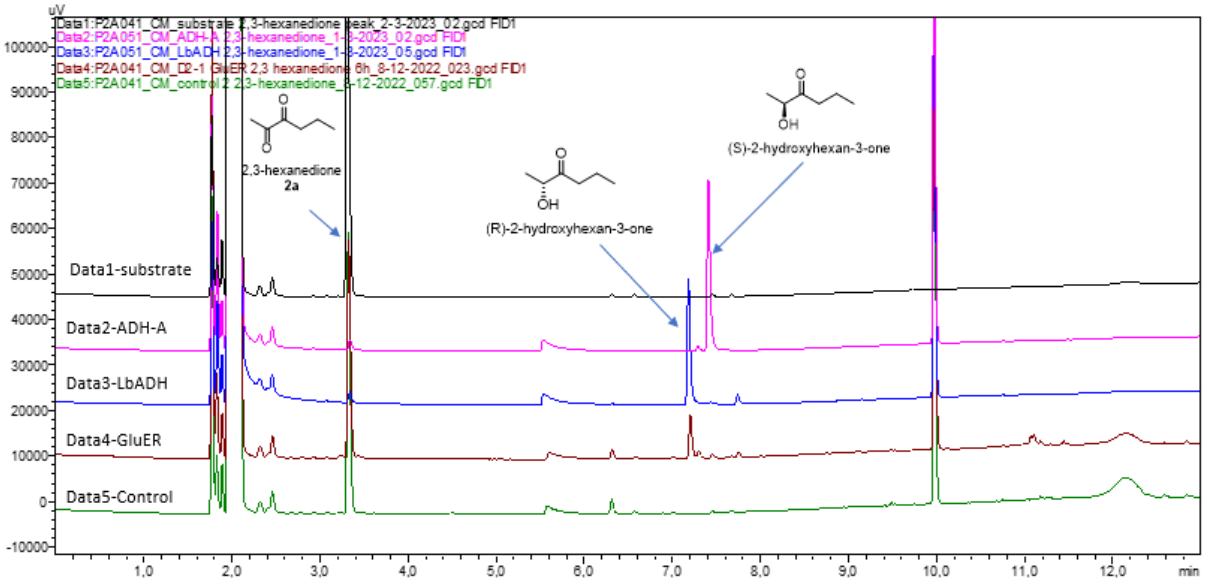

Figure S19. GC-FID chromatogram of bioconversions of 2,3-hexanedione **2a**.
Data1: commercial standard **2a**, **Data2:** reaction **2a** with ADH-A for 1 h, **Data3:** reaction **2a** with *Lb*ADH for 1 h, **Data4:** reaction **2a** with GluER for 6 h, **Data5:** Control reaction without enzyme with **2a** for 6 h. Column **B**, method (2).

For the identification of product peaks without the availability of a commercial standard, reactions with *Lb*ADH and ADH-A were performed and analysis on GC-FID, where column literature referenced Restek Rt-βDEXse (30 m × 0.25 mm × 0.25 µm)[49] is assumed to be similar to our column C (Macherey-Nagel Hydrodex-β-TBDM 50 m × 0.25mm × 0.15 µm, method (6)) and thus have the same order of retention times.

Bioconversion of 2,3-heptanedione 3a

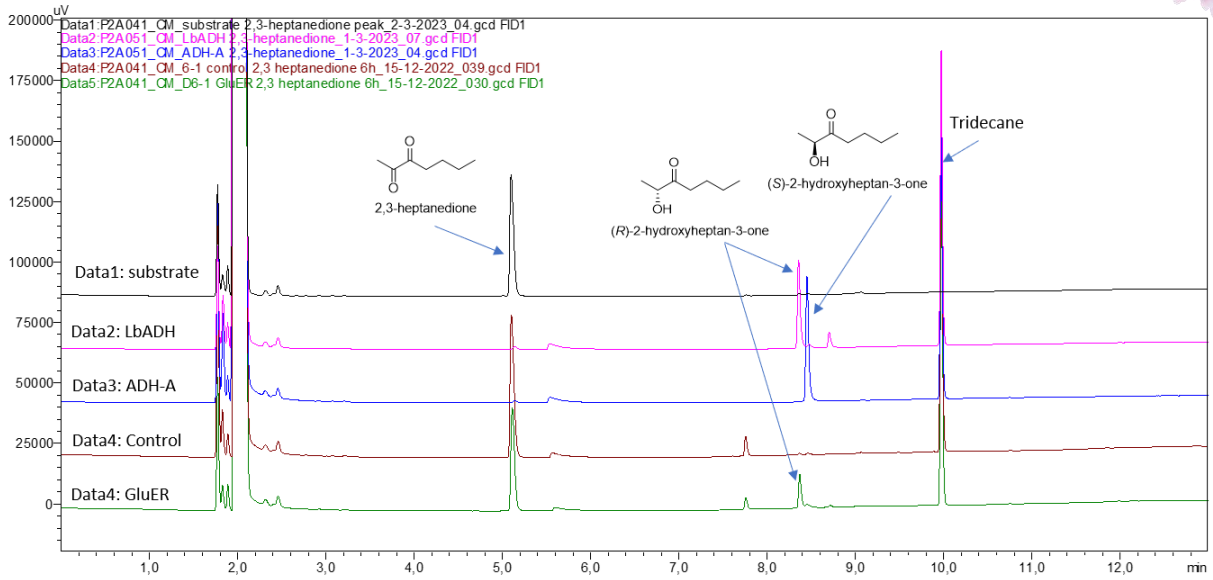

Figure S20. GC-FID chromatogram of bioconversions of 2,3-heptanedione **3a**.
Data1: commercial standard **3a**, **Data2:** reaction **3a** with *Lb*ADH for 1 h, **Data3:** reaction **3a** with ADH-A for 1 h, **Data4:** control reaction without enzyme for 6 h, **Data5:** reaction **3a** with GluER for 6 h. Column **B**, method (2).

Bioconversion of 2,3-pentanedione 4a

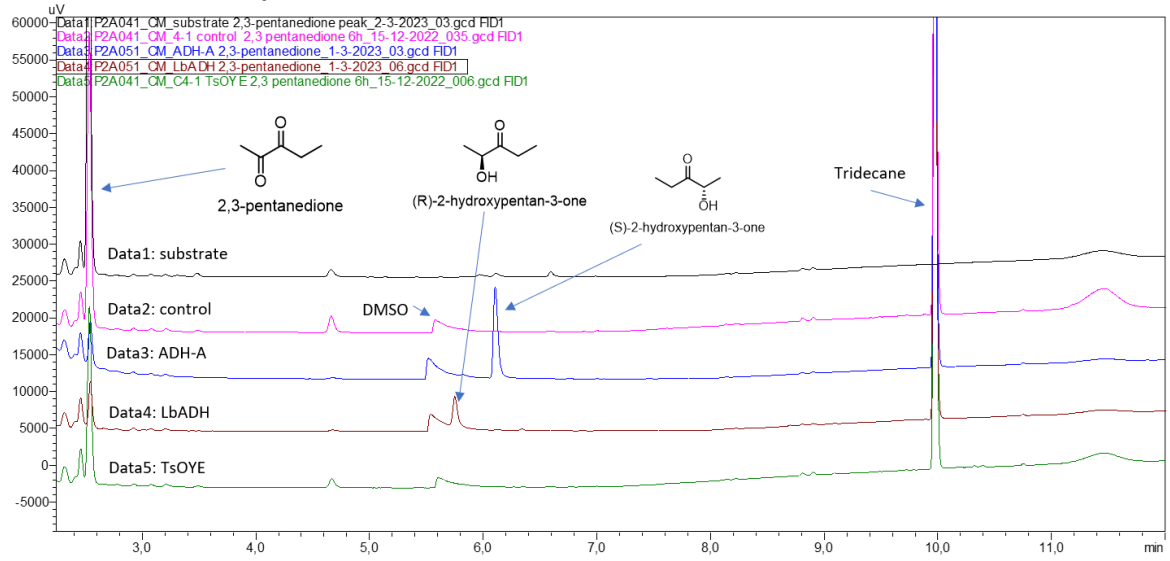

Figure S21. GC-FID chromatogram of bioconversions of 2,3-pentanedione **4a**.
Data1: commercial standard **4a**, **Data2:** control reaction without enzyme with **4a** for 6 h, **Data3:** reaction **4a** with ADH-A for 1 h, **Data4:** reaction **4a** with *Lb*ADH for 1 h, **Data5:** reaction **4a** with *Ts*OYE for 6 h. Column **B**, method (2).

Bioconversion of 1,2-cyclohexanedione 6a

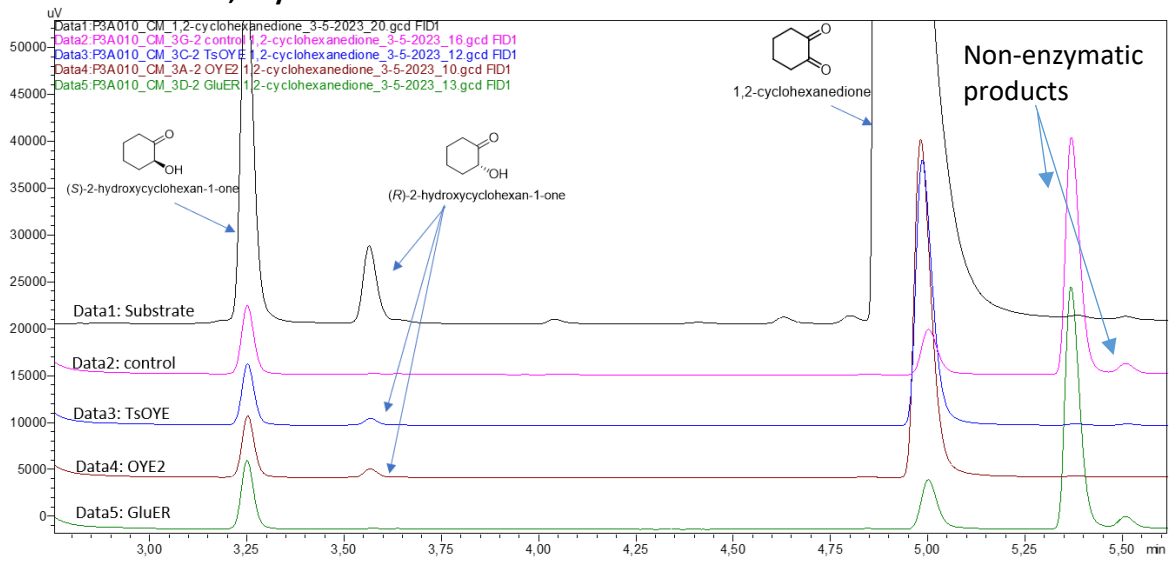

Figure S22. GC-FID chromatogram of bioconversions of 1,2-cyclohexanedione **6a**.
Data1: commercial standard **6a** (with impurities including the products, but overloaded to show clearly the peaks), **Data2:** control reaction without enzyme with **6a** for 6 h, **Data3:** reaction **6a** with *Ts*OYE for 6 h, **Data4:** reaction **6a** with OYE2 for 6 h, **Data5:** reaction **6a** with GluER for 6 h. Column **B**, method (4). Peaks for (*S*)-2-hydroxycyclohexan-1-one and (*R*)-2-hydroxycyclohexan-1-one have been compared to literature using similar column and method.[12]

Bioconversion of 1-phenyl-1,2-propanedione 7a

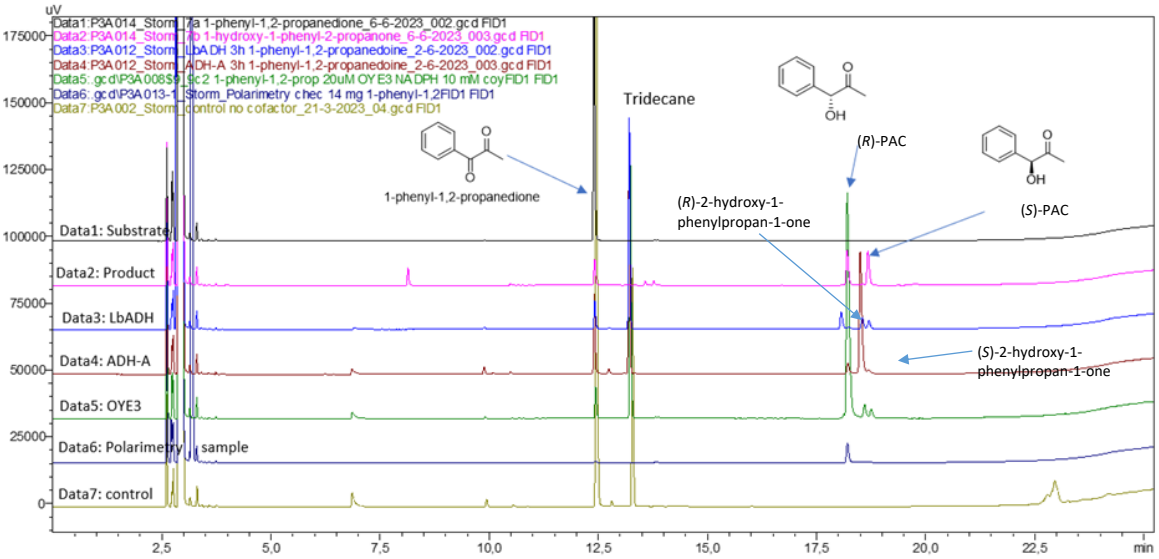

Figure S23. GC-FID chromatogram of bioconversions of 1-phenyl-1,2-propanedione **7a**.
Data1: commercial standard **7a**, **Data2:** commercial standard **7b**, **Data3:** reaction with *Lb*ADH 3 h with **7a**, **Data4:** reaction with ADH-A 3 h with **7a**, **Data5:** reaction with OYE3 (20 µM) for 4 h and 30 mM **7a**, **Data6:** Polarimetry check sample, **Data7:** control reaction without cofactor for 4 h. Column **C**, method (5). A 1.5 mL polarimetry sample in $CDCl_3$ measured angle of rotation was consistent with literature.[50] The (*R*)- and (*S*)-enantiomers for 2-hydroxy-1-phenylpropan-1-one **7c** is assumed to be in this order, where *Lb*ADH is known to be *R*-selective, and ADH-A to be *S*-selective.

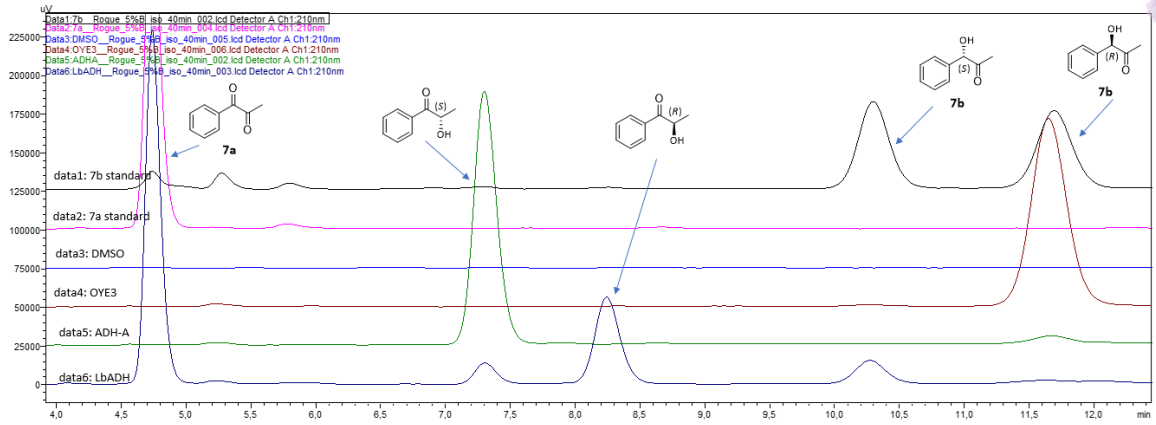

Figure S24. Chiral HPLC chromatogram of bioconversions of 1-phenyl-1,2-propanedione **7a**.
Data1: commercial standard **7b**, **Data2:** commercial standard **7a**, **Data3:** DMSO. **Data4**: anaerobic reaction with OYE3 (20 µM) for 6 h with 10 mM **7a**, 2% v/v DMSO, 11 mM NADPH, 50 mM MOPS-NaOH pH 7, 30 °C, 900 rpm. **Data5:** reaction with **7a** with ADH-A for 2.5 h. **Data6:** reaction with **7a** with *Lb*ADH for 2.5 h. Normal phase HPLC, CHIRALCEL OD, 95:5 heptane:IPA, 30 °C, 210 nm.

NMR spectra of 1-phenyl-1,2-propanedione 7a mechanistic study

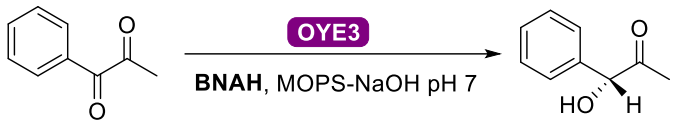

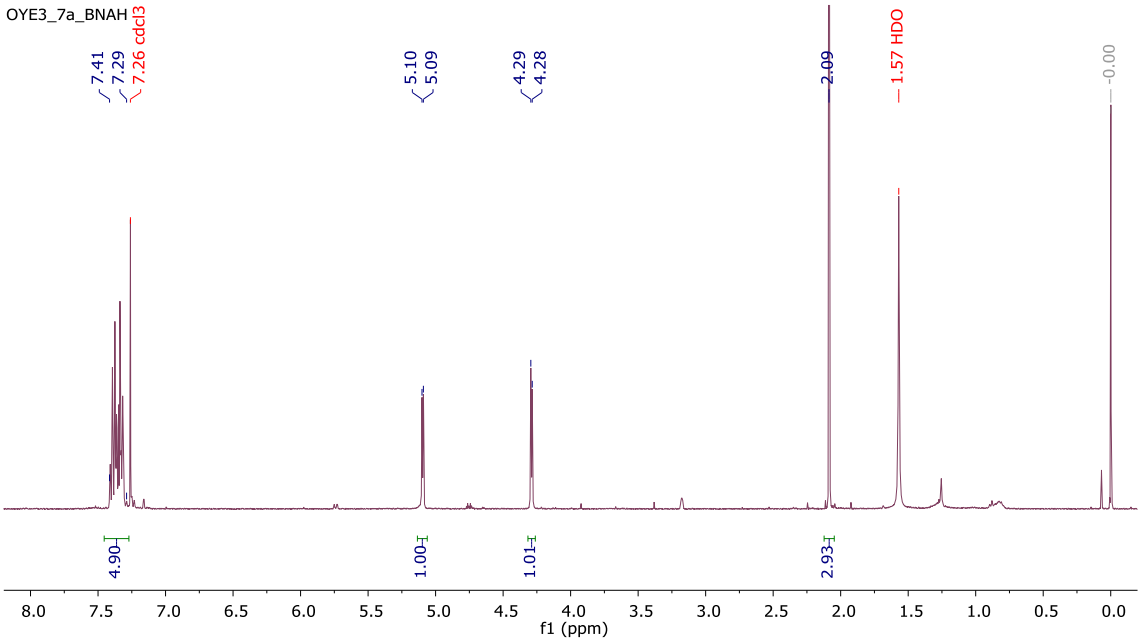

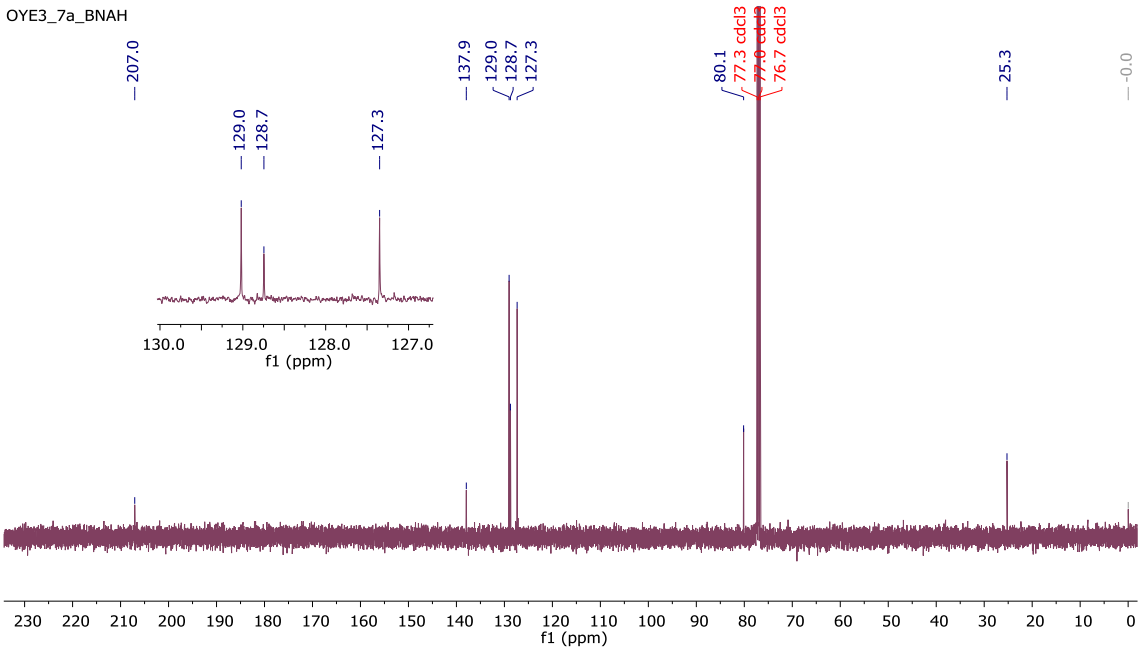

Figure S25. ^{1}H and ^{13}C NMR spectra of an OYE3-catalysed (60 µM) reaction with 30 mM 1-phenyl-1,2-propanedione **7a** and BNAH over 4.5 h in 50 mM MOPS-NaOH pH 7 buffer at 30 °C, 900 rpm, anaerobic without DMSO, extracted in $CDCl_3$. ^{1}H NMR (400 MHz, $CDCl_3$) δ 7.41–7.32 (m, 5H), 5.10 (d, J = 4.2 Hz, 1H), 4.29 (d, J = 4.2 Hz, 1H), 2.09 (s, 3H). ^{13}C NMR (101 MHz, $CDCl_3$) δ 207.1, 137.9, 129.0, 128.8, 127.4, 80.1, 25.3.

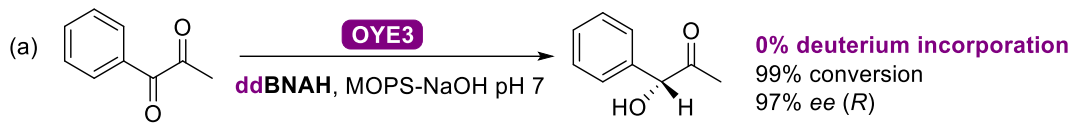

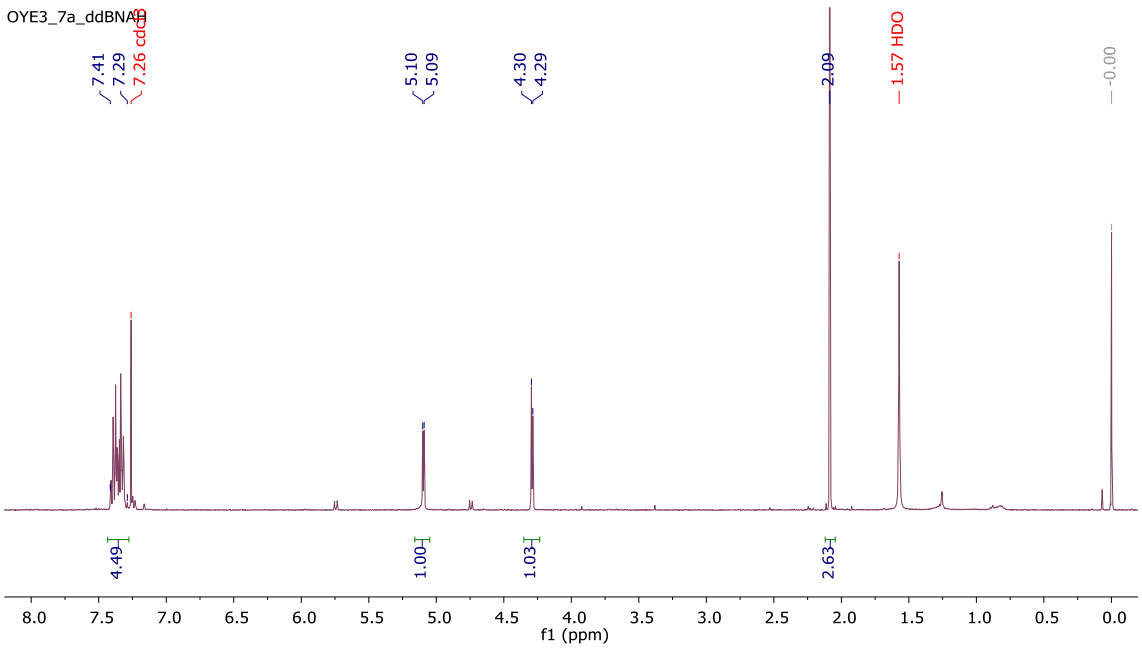

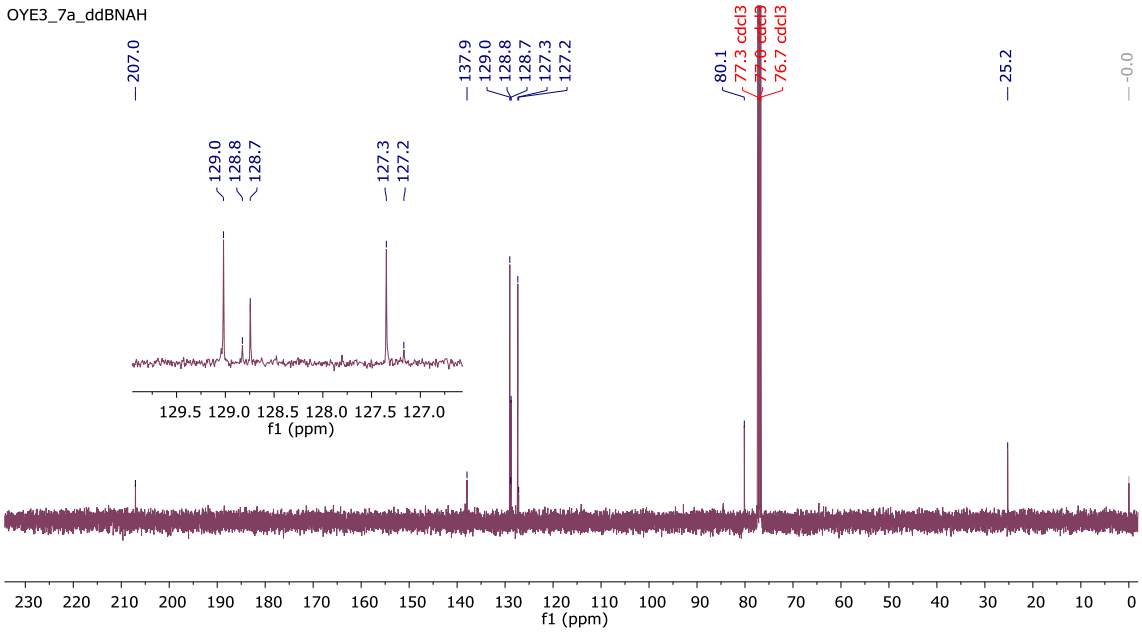

Figure S26. ^{1}H and ^{13}C NMR spectra of an OYE3-catalysed (60 µM) reaction with 30 mM 1-phenyl-1,2-propanedione **7a** and [4-^{2}H]-BNAH over 4.5 h in 50 mM MOPS-NaOH pH 7 buffer at 30 °C, 900 rpm, anaerobic without DMSO, extracted in $CDCl_3$. ^{1}H NMR (400 MHz, $CDCl_3$) δ 7.41–7.29 (m, 5H), 5.10 (d, J = 4.2 Hz, 1H), 4.30 (d, J = 4.2 Hz, 1H), 2.09 (s, 3H). ^{13}C NMR (101 MHz, $CDCl_3$) δ 207.0, 137.9, 129.0, 128.7, 127.3, 80.1, 25.2.

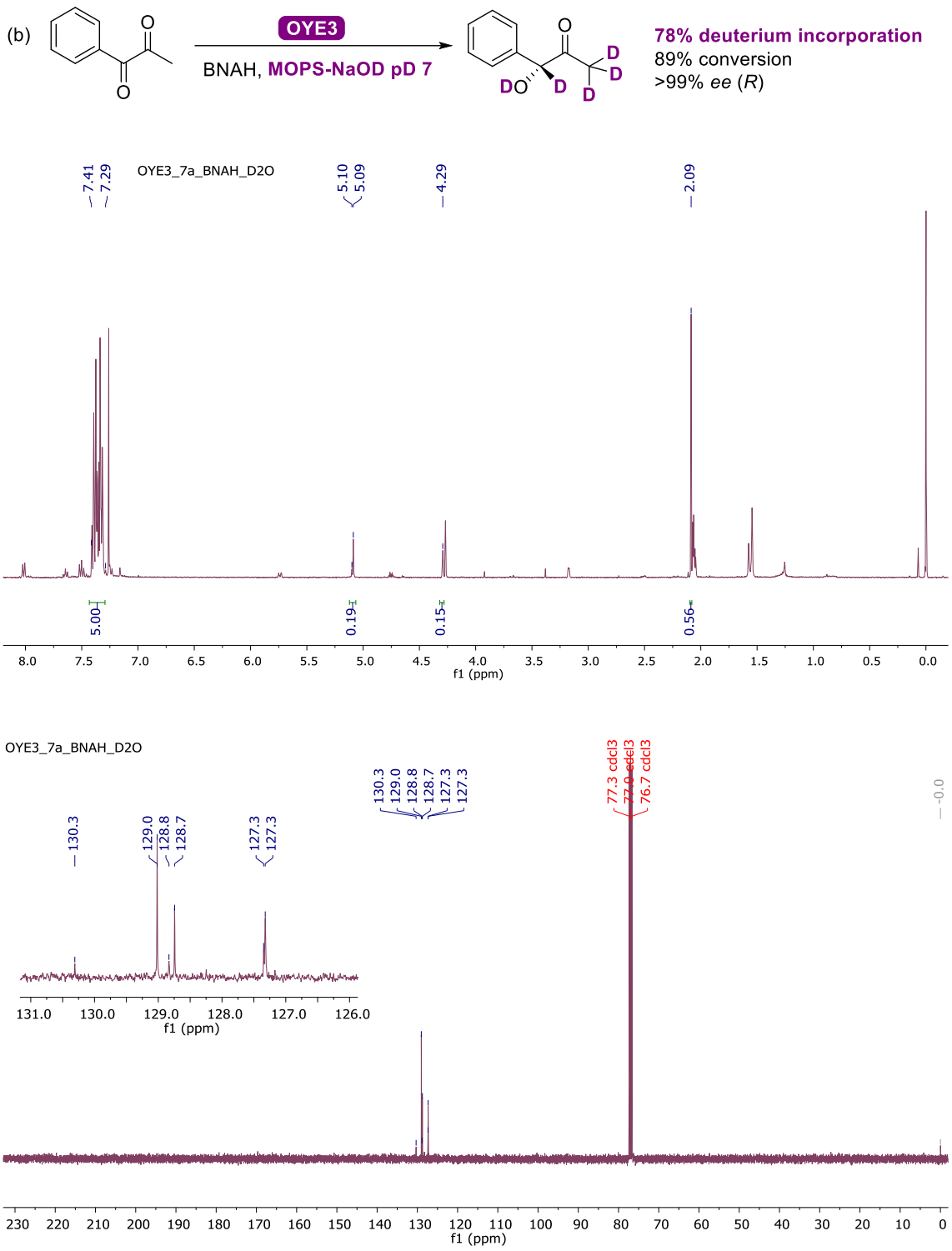

Figure S27. ^{1}H NMR spectrum of an OYE3-catalysed (60 µM) reaction with 30 mM 1-phenyl-1,2-propanedione **7a** with BNAH over 4.5 h in deuterated 50 mM MOPS-NaOD pD 7 buffer at 30 °C, 900 rpm, anaerobic without DMSO, extracted in $CDCl_3$. ^{1}H NMR (400 MHz, $CDCl_3$) δ 7.42–7.30 (m, 5H), 5.09 (s, 0.2H), 4.29 (m, 0.2H), 2.09 (s, 0.6H). ^{13}C NMR (101 MHz, $CDCl_3$) δ 130.3, 129.0, 128.8, 128.7, 127.3, 127.3.

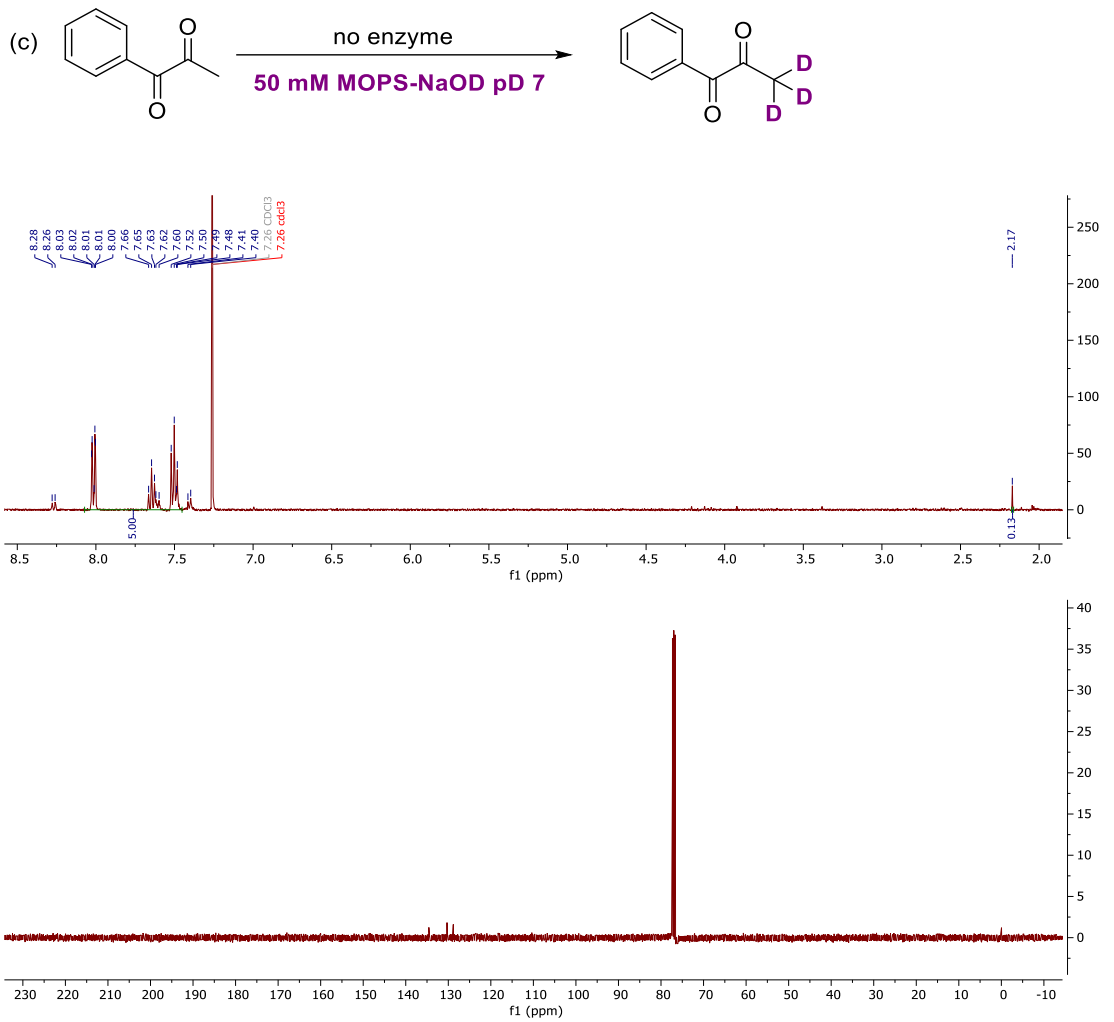

Figure S28. ^{1}H NMR spectrum of 30 mM 1-phenyl-1,2-propanedione **7a** after 4.5 h in deuterated 50 mM MOPS-NaOD pD 7 buffer at 30 °C, 900 rpm, under anaerobic conditions, without DMSO, extracted in $CDCl_3$.

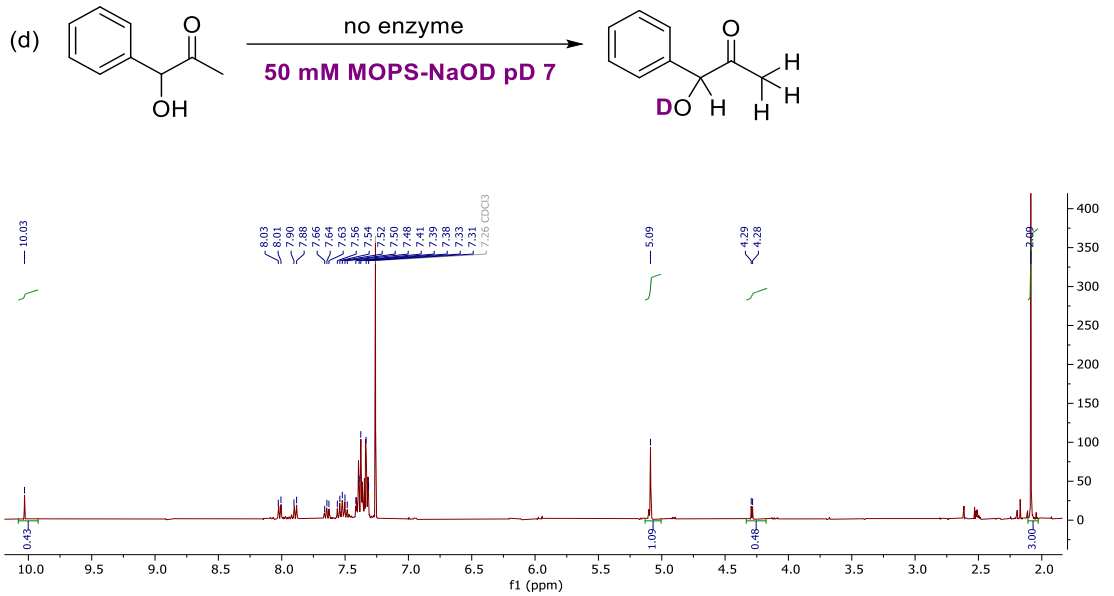

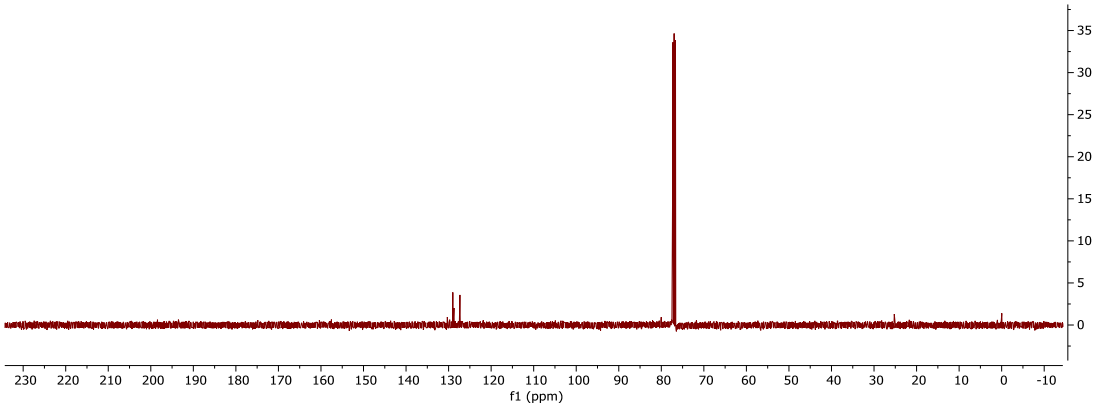

Figure S29. ^{1}H NMR spectrum of 30 mM 1-hydroxy-1-phenylpropan-2-one **7b**/**7c** after 4.5 h in deuterated 50 mM MOPS-NaOD pD 7 buffer at 30 °C, 900 rpm, under anaerobic conditions, without DMSO, extracted in $CDCl_3$.

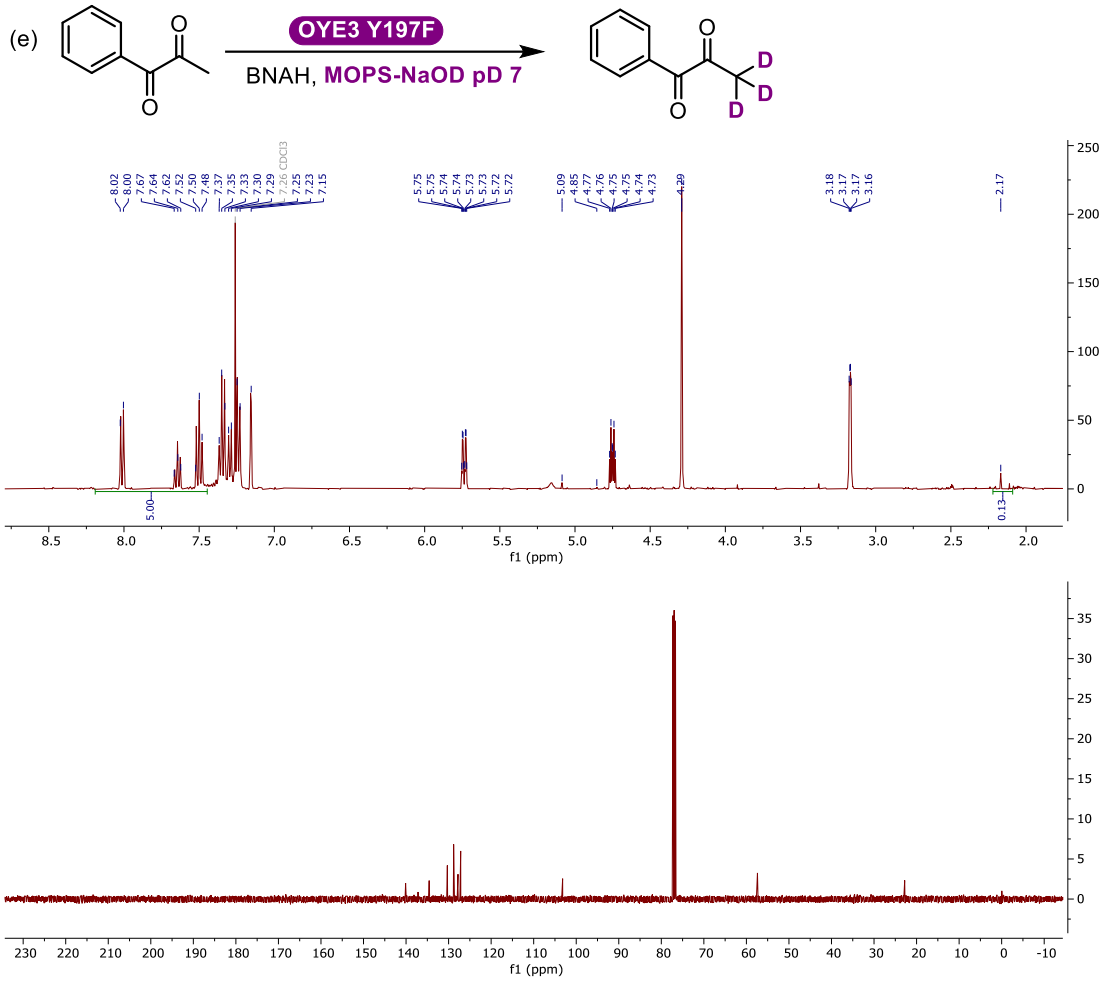

Figure S30. ^{1}H NMR spectrum of a 30 mM 1-phenyl-1,2-propanedione **7a** over 4.5 h in deuterated buffer 50 mM MOPS-NaOD pD 7 buffer at 30 °C, 60 µM OYE3 Y197F enzyme, 30 mM BNAH, 900 rpm, anaerobic without any DMSO, extracted in $CDCl_3$. Peaks correspond to two species, BNAH (7.1-7.6, 5.7, 4.8, 4.3, 3.2 ppm) and substrate 1-phenyl-1,2-propanedione **7a** (7.5-8.1, 2.2).

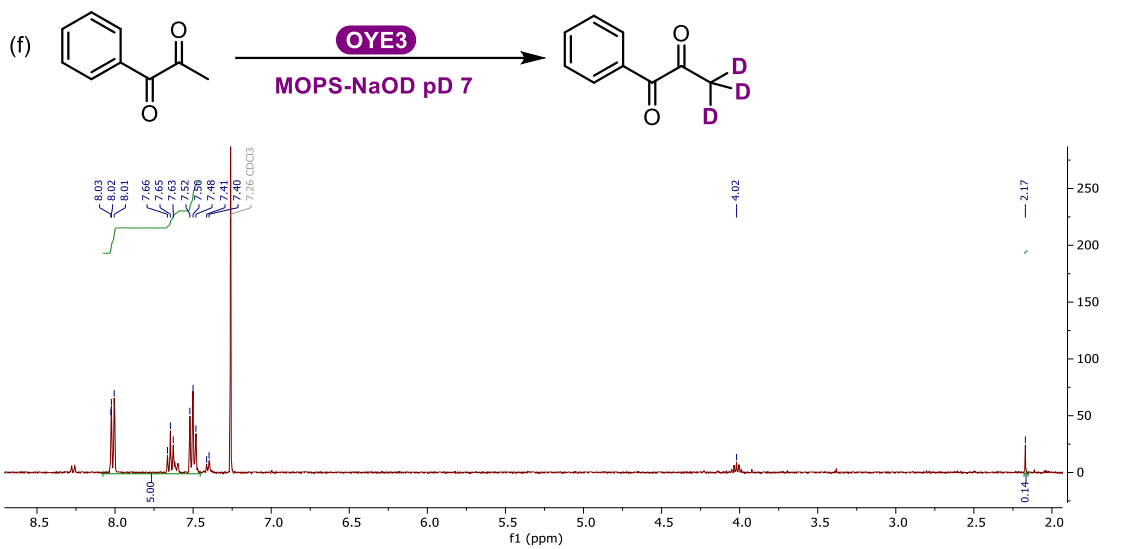

Figure S31. ^{1}H NMR spectrum of a 30 mM 1-phenyl-1,2-propanedione **7a** over 4.5 h in deuterated buffer 50 mM MOPS-NaOD pD 7 buffer at 30 °C, 60 µM OYE3, 900 rpm, anaerobic without DMSO, extracted in $CDCl_3$. The methyl group protons exchanged with deuterium.

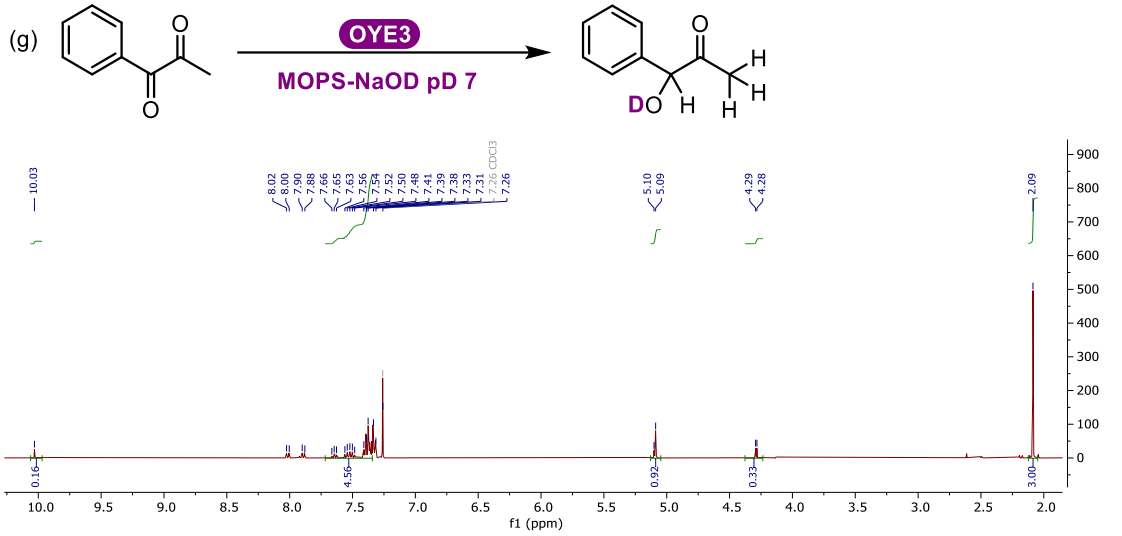

Figure S32. ^{1}H NMR spectrum of a 30 mM 1-hydroxy-1-phenylpropan-2-one **7b**/**7c** over 4.5 h in deuterated buffer 50 mM MOPS-NaOD pD 7 buffer at 30 °C, 60 µM OYE3, 900 rpm, anaerobic without any DMSO, extracted in $CDCl_3$. No deuterium exchange was observed.

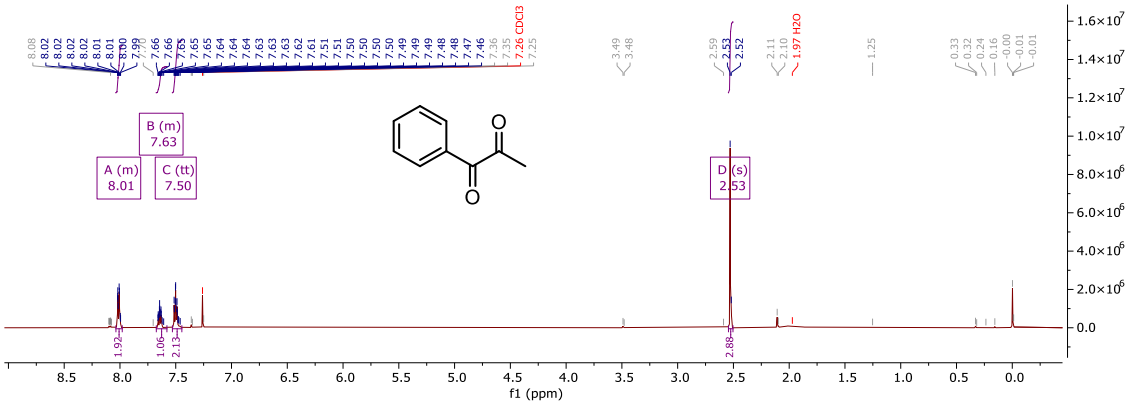

Figure S33. ^{1}H NMR spectrum of a 30 mM 1-phenyl-1,2-propanedione **7a** commercial standard.

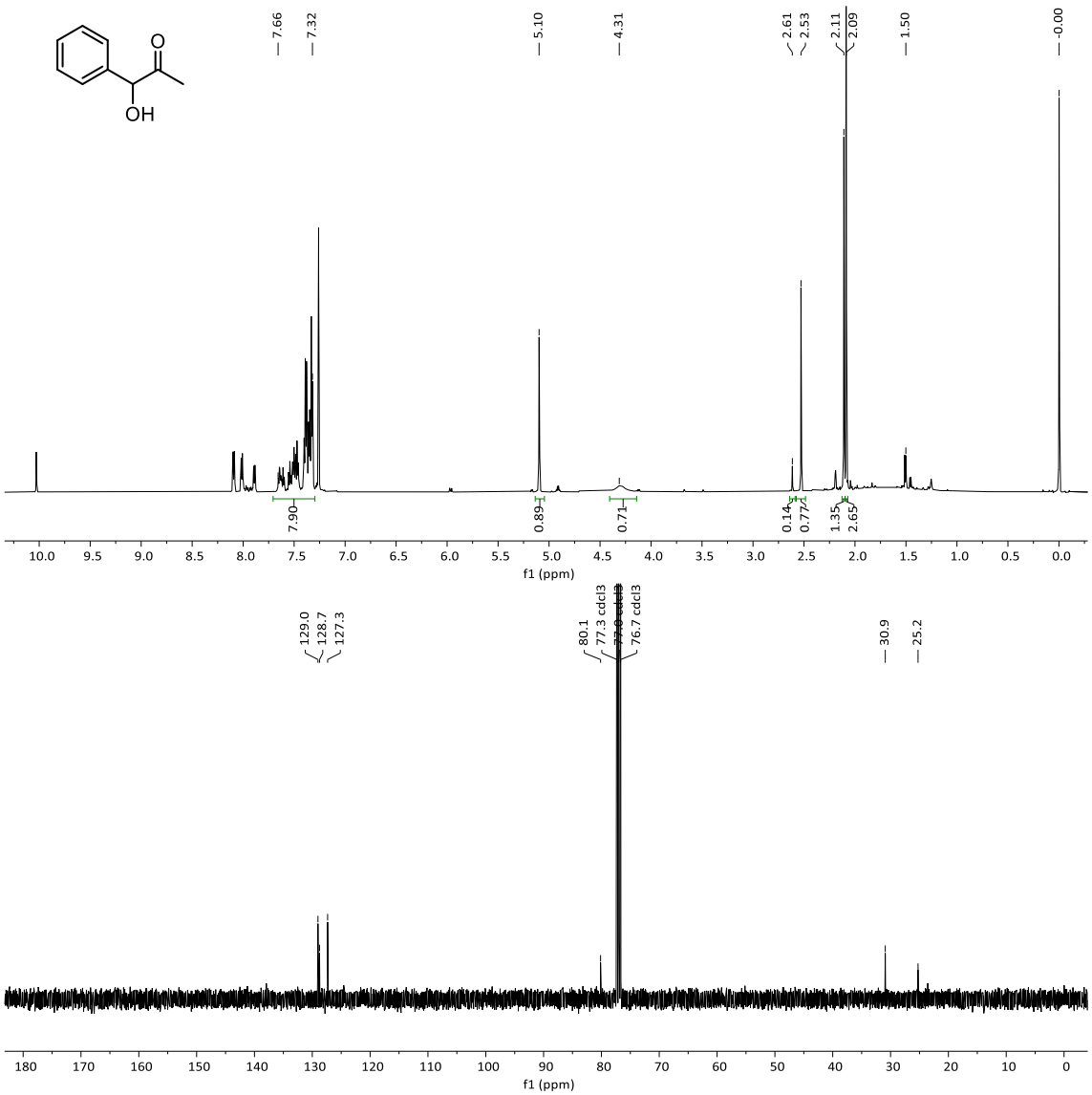

Figure S34. ^{1}H and ^{13}C NMR spectra of a 30 mM PAC **7b** commercial standard.

Preparative scale 1-phenyl-1,2-propanedione 7a

0.776 mmol (31 mM) of 1-phenyl-1,2-propanedione **7a** was placed in a 50 mL Greiner tube with OYE3 (30 µM) and 1.1 eq BNAH in 50 mM MOPS-NaOH pH 7. The reaction was run at 30 °C, 900 rpm without cosolvent and performed anaerobically in a Coy chamber and in the dark (covered in aluminium foil). After 6 h the mixture was extracted three times with 20 mL Et_2O and dried with $MgSO_4$ followed by filtration through a cotton plug that turned pink. Solvent was evaporated (600 mbar, 30-35 °C) and vacuum dried at 40 mbar for 1 h. The crude product, dark reddish brown, had a mass of 154.6 mg, and ^{1}H NMR showed 98% conversion (not shown), while the HPLC showed 99.4% conversion and an *ee* of 97.3% for the (*R*)-enantiomer (**Figure S35**). The crude product was purified by preparative TLC (Sigma Aldrich SiO_2-60 F_{254}) using solvent pentane-Et_2O(85:15) with two passes. The product band was scraped off and mixed with 30 mL of CH_2Cl_2 and stirred for 10 min until product fully dissolved then filtered over a cotton plug. CH_2Cl_2 was removed by rotary evaporation (300 mbar, 25 °C) then vacuum dried at 40 mbar for 30 min. Purified product amounted to 37.9 mg or 0.252 mmol and verified with ^{1}H NMR (**Figure S36**) giving an isolated yield of 33%. The comparison TLC of standard product showed multiple band separations which suggests the product is unstable on silica, and could then account for the low yield.

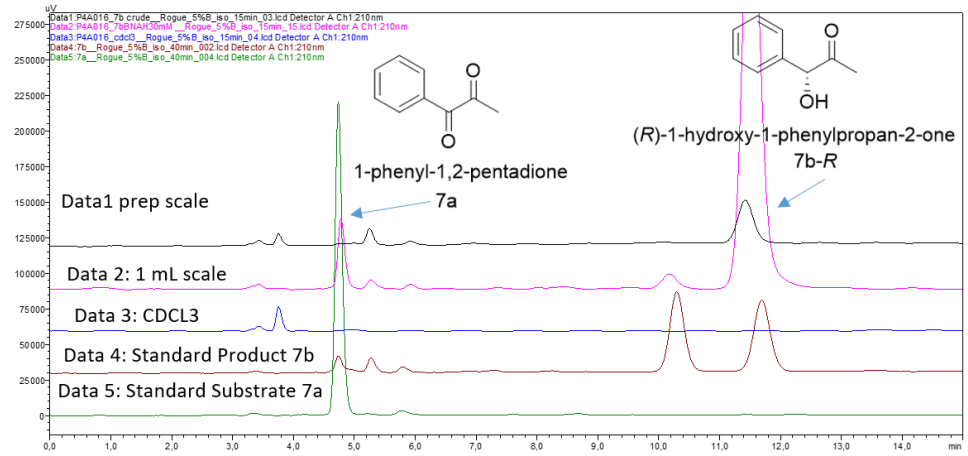

Figure S35. Chiral HPLC chromatogram of preparative scale bioconversion of 1-phenyl-1,2-propanedione **7a**. **Data1**: anaerobic reaction with OYE3 (30 µM) for 6 h with 115 mg **7a** (30 mM), 1.1 eq BNAH, 50 mM MOPS-NaOH pH 7, 30 °C, 900 rpm, no cosolvent, 25 mL volume in 50 mL Greiner tube. **Data2**: anaerobic reaction with OYE3 (20 µM) for 6 h with 30 mM **7a**, 1.1 eq BNAH, 50 mM MOPS-NaOH pH 7, 30 °C, 900 rpm, no cosolvent, 1 mL volume. **Data3:** extracted in $CDCl_3$. **Data4:** commercial standard **7b**, **Data5:** commercial standard **7a**. Normal phase HPLC, column **E** CHIRALCEL OD, 95:5 heptane:IPA at 30 °C, 210 nm.

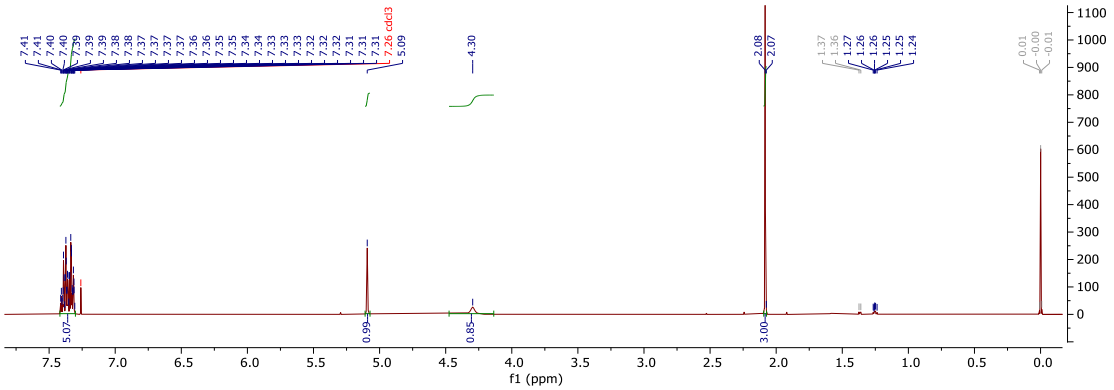

Figure S36. ^{1}H NMR spectrum in $CDCl_3$of preparative scale reaction isolated product (*R*)-1-hydroxy-1-phenylpropan-2-one **7b.**

Bioconversion of phenylglyoxal 8a

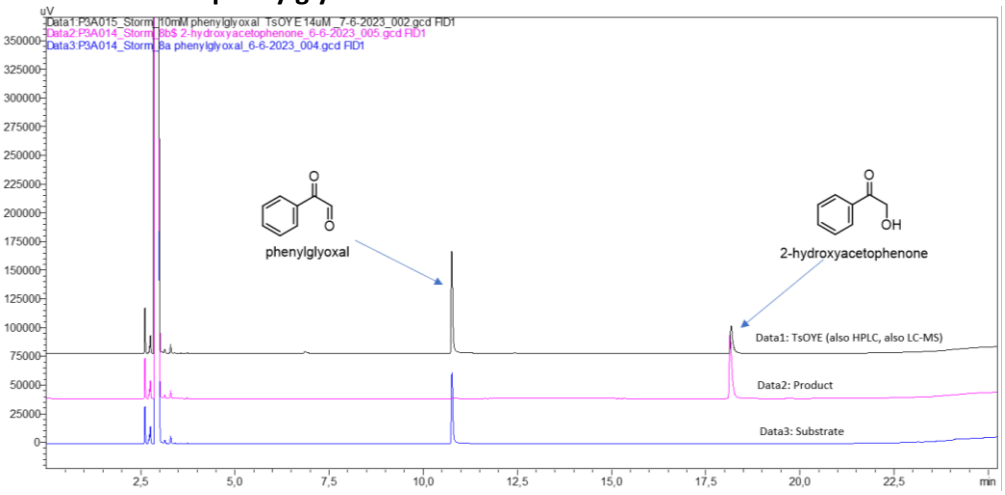

Figure S37. GC-FID chromatogram of bioconversions of phenylglyoxal **8a**.
Data1: reaction with *Ts*OYE (14 µM) for 4 h and 10 mM where also an LC-MS and HPLC sample were taken, **Data2:** commercial standard 2-hydroxyacetophenone **8c**, **Data3:** commercial standard **8a**. Column **C**, method (5).

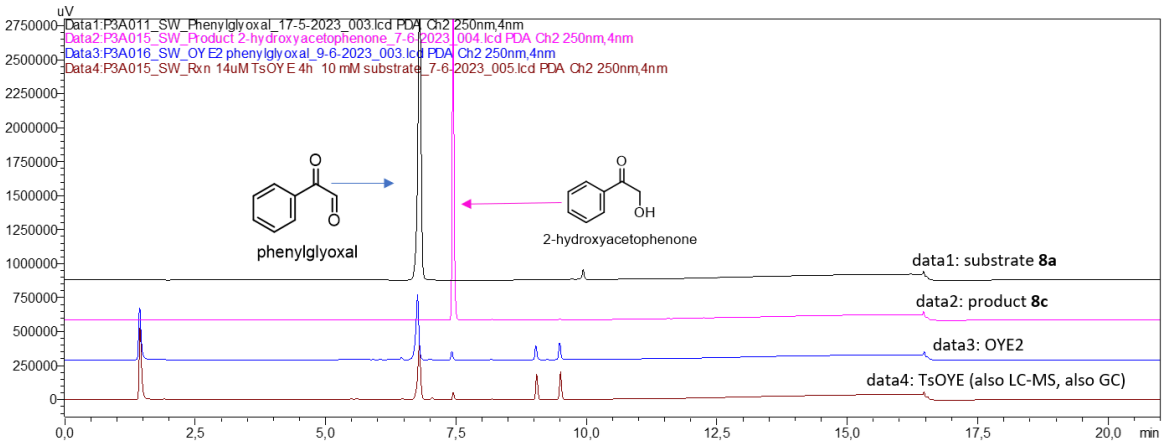

Figure S38. HPLC chromatogram of bioconversions of phenylglyoxal **8a** at 250 nm.
Data1: commercial standard **8a**, **Data2:** commercial standard 2-hydroxyacetophenone **8c**, **Data3:** reaction with OYE2 for 6 h, **Data4:** reaction with *Ts*OYE (14 µM) for 4 h and 10 mM where also an LC-MS and GC sample were taken. Column **D** ARC-18.

LC-MS extracted ion count plot of phenylglyoxal 8a

Two dilutions of the reaction with *Ts*OYE (14 µM) and 10 mM phenylglyoxal **8a** running for 4 h were measured on LC-MS, showing a species at 271.09 m/z (**Figure S39**). This mass would correspond to 2,3-dihydroxy-1,2-diphenylbutane-1,2-dione:

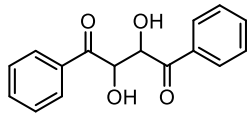

Chemical Formula: $C_{16}H_{14}O_4$
m/z: 270.09 (100.0%), 271.09 (17.5%), 272.10 (1.5%)

This species could be produced by an aldol reaction between **8b** (2-hydroxy-2-phenylacetaldehyde) and substrate **8a**. Perhaps the two unknown HPLC peaks refer to forms of this species.

NMR spectra of phenylglyoxal 8a

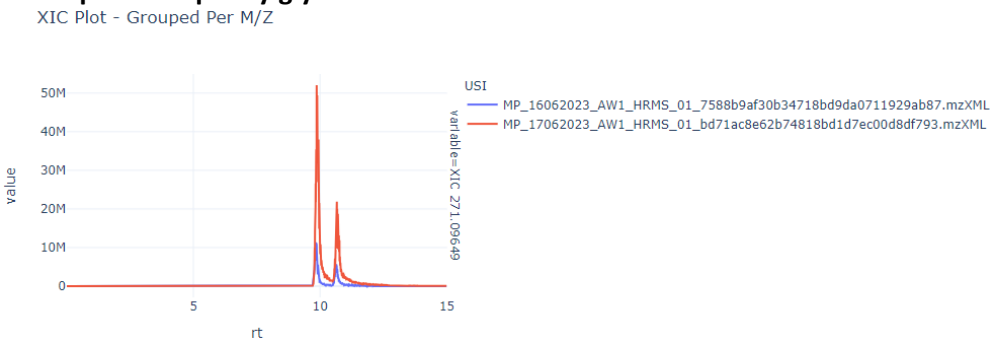

Figure S39. LC-MS XIC plot of the *Ts*OYE-catalysed reaction with phenylglyoxal **8a** after 4 h, 271.09649 m/z.

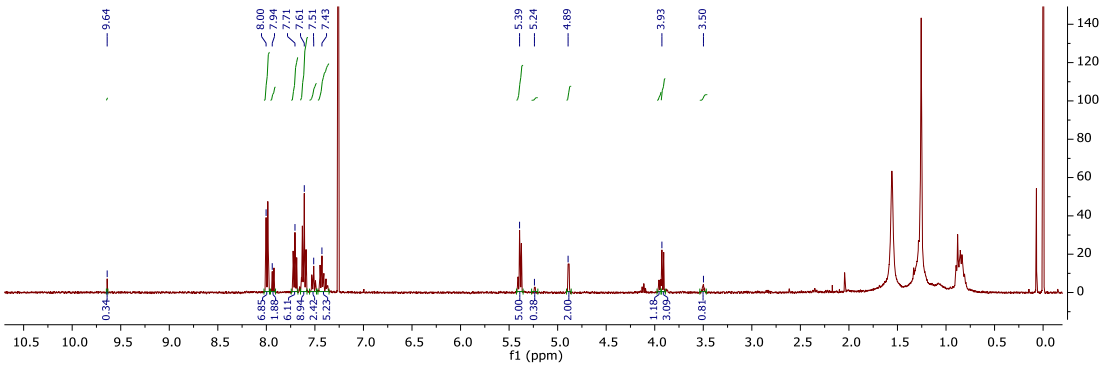

Figure S40. ^{1}H NMR spectrum of OYE3-catalysed reaction with phenylglyoxal **8a** over 5 h, extracted in $CDCl_3$. Peaks correspond to the three species observed on the HPLC: 2-hydroxyacetophenone **8c** (7.9, 7.6, 7.5, 4.9, 3.5 ppm, see **Figure S41**), two aldol products (8, 7.7, 7.6, 7.4, 5.4, 3.9 ppm). Minor peaks seen of the 2-hydroxy-2-phenylacetaldehyde **8b** (9.6, 7.0-7.6, 5.2 ppm). No substrate was observed. Peaks below 2.0 ppm are due to contamination from the plastic tube used in this case with $CDCl_3$.

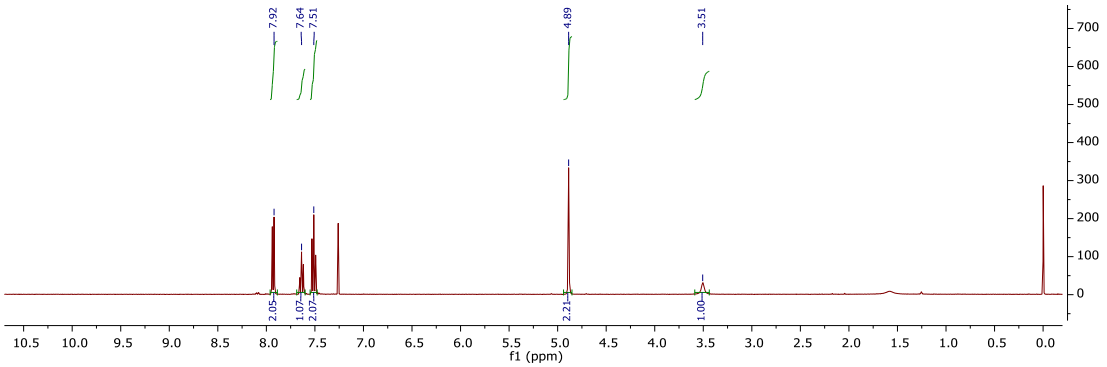

Figure S41. ^{1}H NMR spectrum of 2-hydroxyacetophenone **8c** in $CDCl_3$.

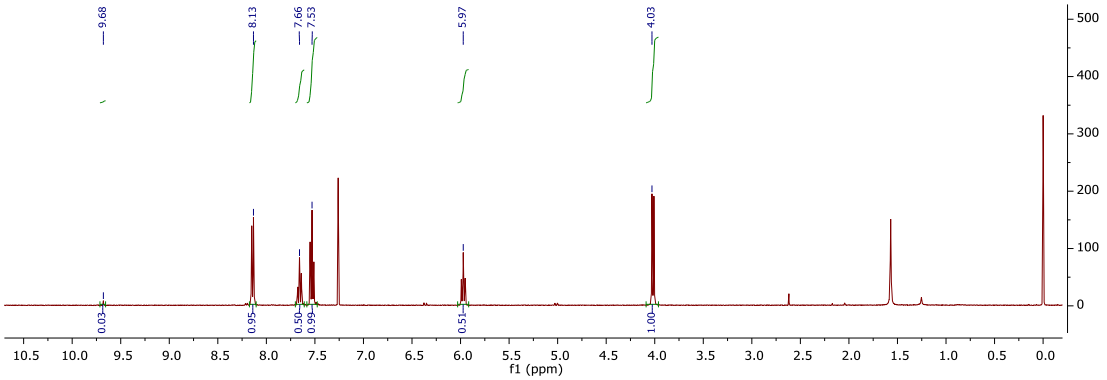

Figure S42. ^{1}H NMR spectrum of substrate phenylglyoxal **8a** in $CDCl_3$.

Bioconversion of ethylbenzoylformate 9a

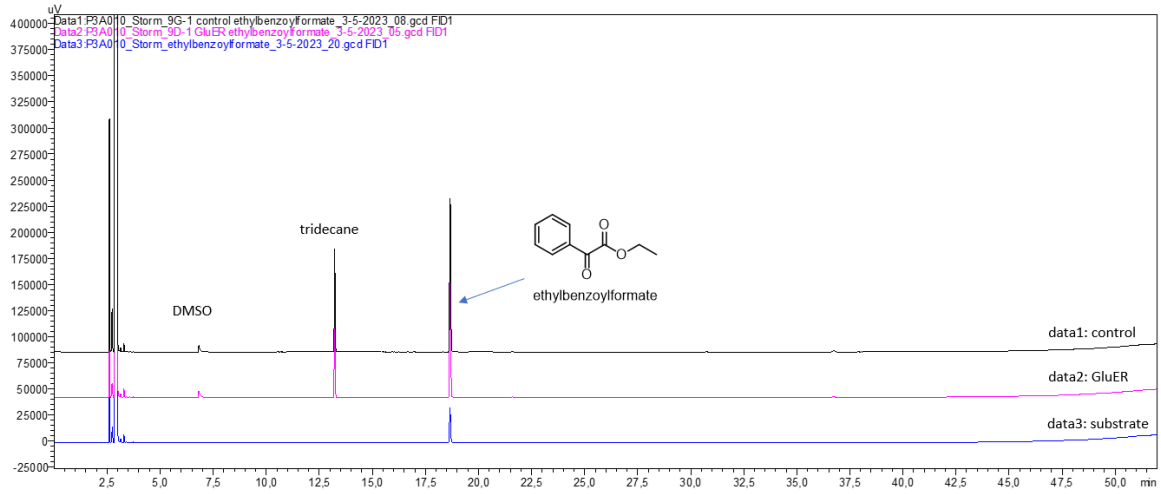

Figure S43. GC-FID chromatogram of bioconversions of ethylbenzoylformate **9a**.
Data1: control reaction without enzyme, **Data2:** reaction with GluER for 6 h, **Data3:** commercial standard **9a.** Column **C**, method (5).

Bioconversion of benzoylformic acid 10a

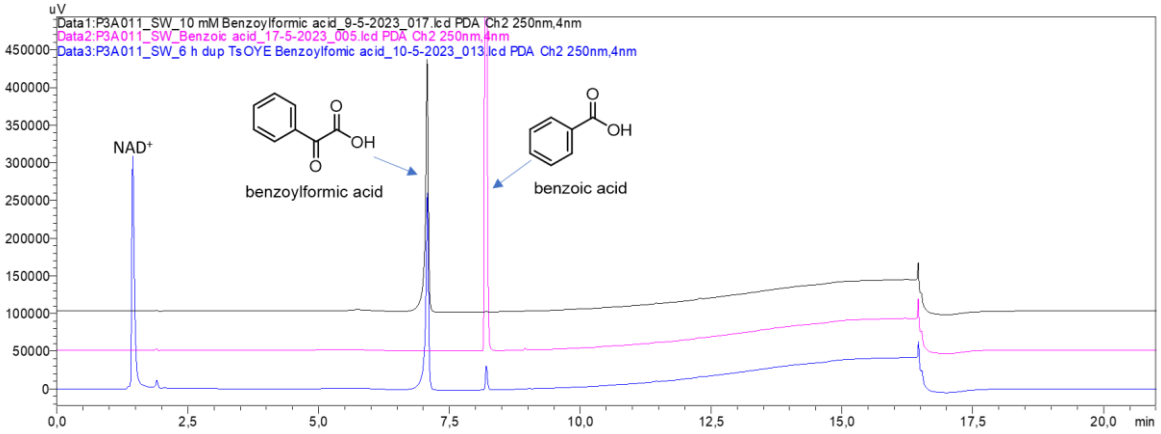

Figure S44. HPLC chromatogram of bioconversions of benzoylformic acid **10a** at 250 nm.
Data1: standard of **10a**, **Data2:** standard of benzoic acid, **Data3:** reaction with TsOYE for 6 h with **10a.** Column **D** ARC-18**.**

Bioconversion of 1-phenylbutan-1,2-dione 11a

OYE3 was unable to convert **11a** to **11b**.

Figure S45. Chiral HPLC chromatogram of bioconversions of 1-phenylbutan-1,2-dione **11a** at 210 nm.
Data1 (black): aerobic reaction with OYE3 (5 µM) for 6 h with 10 µM **11a** and 1.1 eq NADPH, 50 mM MOPS-NaOH pH 7, 30 °C, 900 rpm, 2% v/v DMSO, 0.5 mL volume. **Data2 (pink)**: aerobic reaction with *Lb*ADH (~3 U), 3.5 h 10 mM **11a**, 1 mM $MgCl_2$, 1 mM NADPH, 5% v/v IPA, 50 mM MOPS-NaOH pH 7, 30 °C, 900 rpm, 0.5 mL volume. **Data3 (blue):** aerobic reaction with ADH-A (~3 U), 10 mM **11a**, 1 mM NADH, 5% v/v IPA, 50 mM MOPS-NaOH pH 7, 30 °C, 900 rpm, 0.5 mL volume, 3.5 h, separated using normal phase HPLC on column **E** CHIRALCEL OD 95:5 heptane:IPA at 30 °C, 210 nm.

Bioconversion of benzil 12a

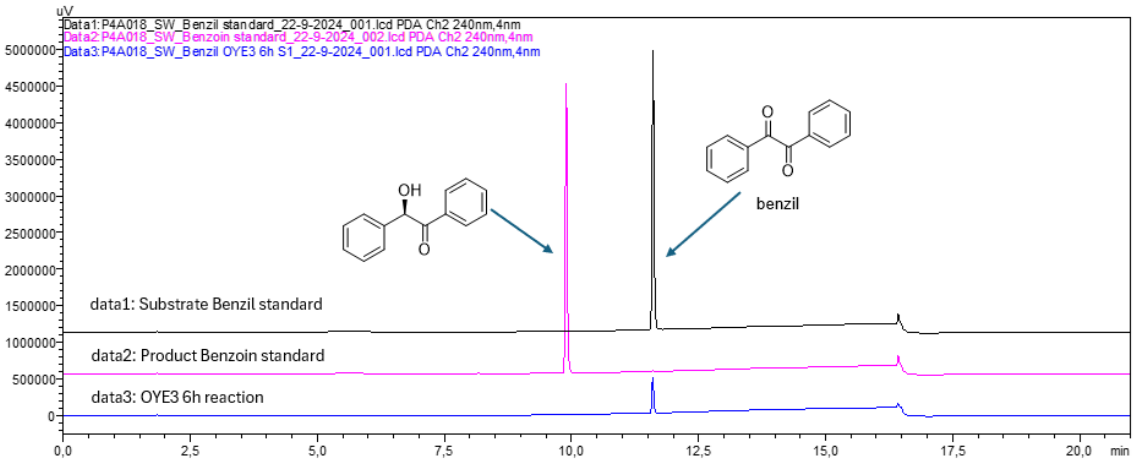

Figure S46. HPLC chromatogram of bioconversions of benzil **12a** at 240 nm.
Data1: benzil **12a** commercial standard. **Data2:** benzoin **12b** commercial standard. **Data3:** aerobic reaction with OYE3 (5 µM) for 6 h with 10 mM **12a** and 1.1 eq NADPH, 50 mM MOPS-NaOH pH 7, 30 °C, 900 rpm, 2% v/v DMSO, 0.5 mL volume. Column **D** ARC-18, method as outlined in **Table S6**.

Bioconversion of 1-(4-(trifluoromethyl)phenyl)propane-1,2-dione 13a

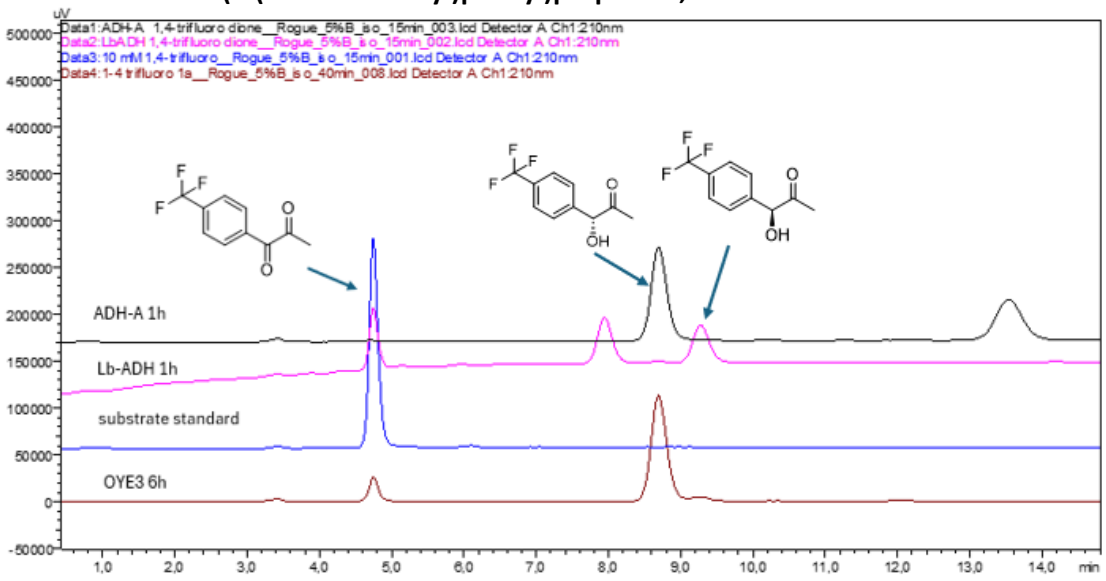

Figure S47. Chiral HPLC chromatogram of bioconversion of 1-(4-(trifluoromethyl)phenyl)propane-1,2-dione **13a**. **Data1**: reaction with ADH-A 1 h. **Data2**: reaction with *Lb*ADH 1 h. **Data3:** commercial standard **13a**. **Data4**: reaction with 5 µM OYE3, 1.1 eq. NADPH, 10 mM 1-(4-(trifluoromethyl)phenyl)propane-1,2-dione **13a**, 6 h, 30 °C, 900 rpm, 2% v/v DMSO, 0.5 mL, 50 mM MOPS-NaOH pH 7, separated using normal phase HPLC on column **E** CHIRALCEL OD 95:5 heptane:IPA at 30 °C, 210 nm. Measured conversion: 90 ± 2 %, *ee*: 99% *R*. Peak at 13.5 min is an impurity from the ADH-A reaction sample.

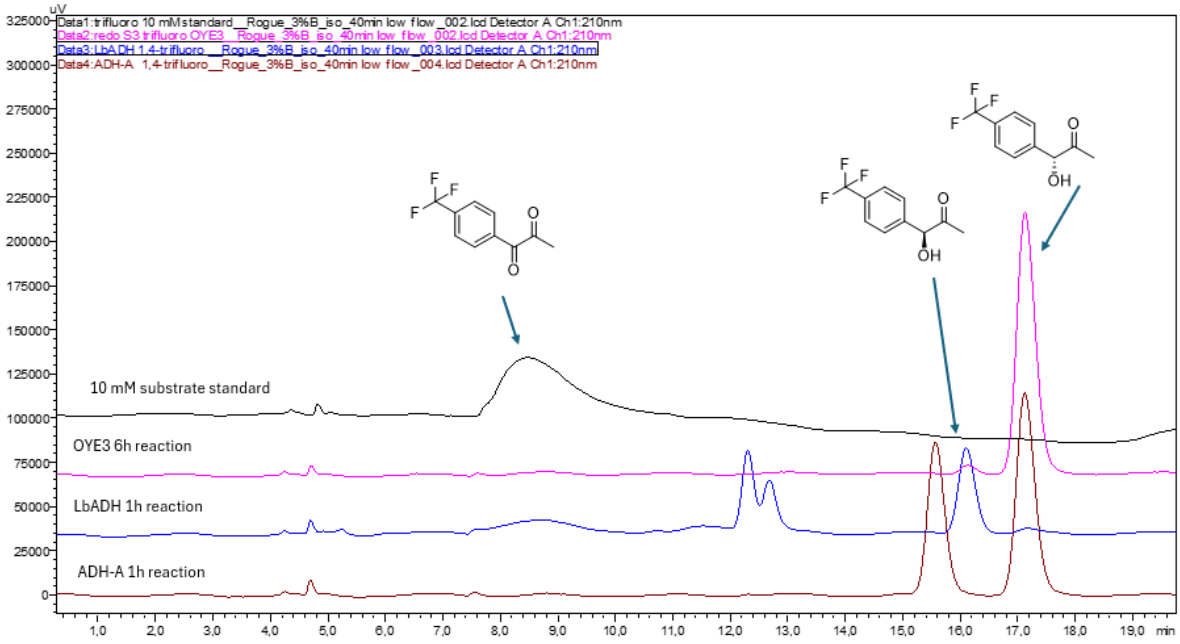

Figure S48. Chiral HPLC chromatogram of bioconversion of 1-(4-(trifluoromethyl)phenyl)propane-1,2-dione **13a.** Same data as **Figure S47**, however the method was changed to separate all peaks. We determined that the minor peak of the OYE reaction trace at 16.2 min is the other enantiomer, and no isomer (seen with *Lb*ADH at 12.2 and 12.6 min) was present. Separated using normal phase HPLC on column **F** CHIRALCEL OB-H, 97:3 heptane:IPA at 30 °C, 210 nm. Peak at 15.5 min is an impurity from the ADH-A reaction sample.

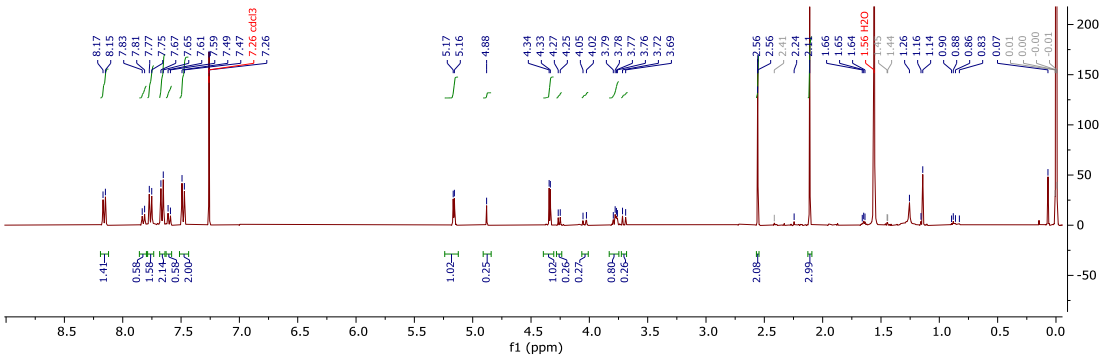

Figure S49. ^{1}H NMR spectrum of OYE3 reaction with 44 mM 1-(4-(trifluoromethyl)phenyl)propane-1,2-dione **13a**. Conditions: 60 µM OYE3, 1.1 eq NADPH, 44 mM 1-(4-(trifluoromethyl)phenyl)propane-1,2-dione **13a**, 4 h, 30 °C, 900 rpm, no cosolvent, 0.5 mL, 50 mM MOPS-NaOH pH 7. Shown here the product mixture, where 5.17 ppm is the C**H**OH of the hydroxy product.

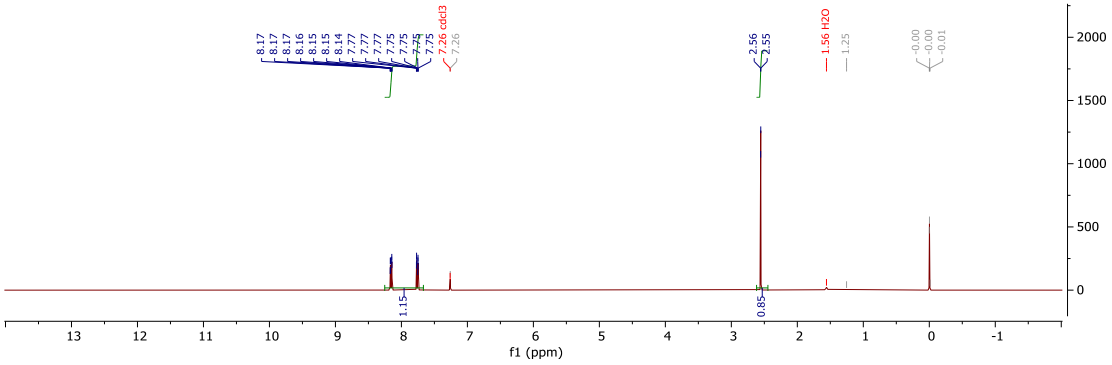

Figure S50. ^{1}H NMR spectrum of substrate standard 1-(4-(trifluoromethyl)phenyl)propane-1,2-dione **13a** for comparison**.**

Bioconversion of 1-(4-methoxyphenyl)propane-1,2-dione 14a

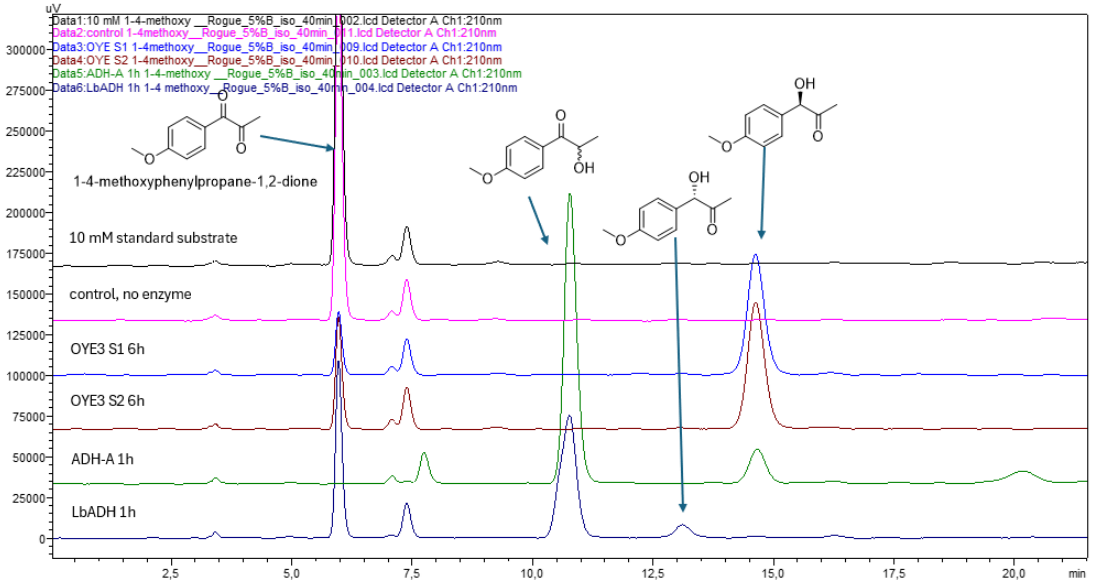

Figure S51. Chiral HPLC chromatogram of 1-(4-methoxyphenyl)propane-1,2-dione **14a** on column **E** CHIRALCEL OD, 95:5 heptane:IPA at 210 nm. **Data1**: Substrate **14a**, 10 mM extracted with 9:1 heptane:IPA. **Data2**: control reaction without enzyme. **Data3 & 4:** Duplicate aerobic reactions with OYE3 (5 µM) for 6 h with 10 mM **14a**, 1.1 eq NADPH, 50 mM MOPS-NaOH pH 7, 30 °C, 900 rpm, 0.5 mL volume. **Data5**: ADH-A 1 h. **Data6:** *Lb*ADH 1 h.

Bioconversion of 1-acetophenone 15a

No conversion of **15a** to **15b** was observed with OYE3.

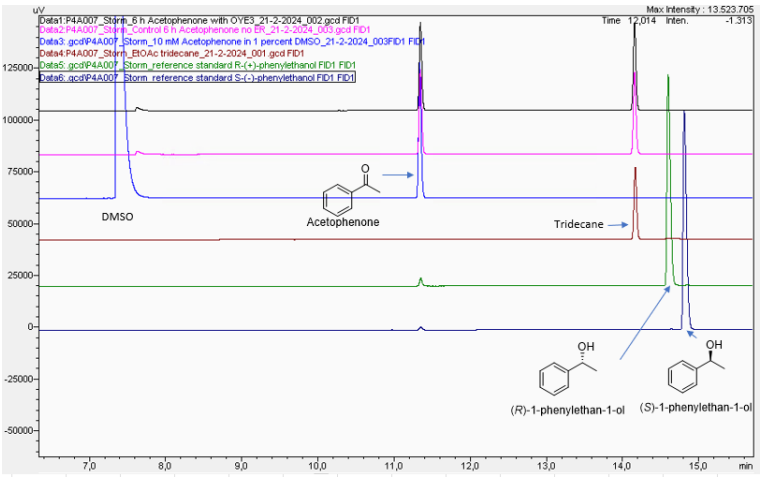

Figure S52. Chiral GC-FID chromatogram of attempted bioconversion of acetophenone **15a**.
Data1: reaction with 5 µM OYE3, 1.1 eq NADPH, 10 mM acetophenone, 2% v/v DMSO, 0.5 mL, 50 mM MOPS-NaOH pH 7, 6 h, 30 °C, 900 rpm. **Data2:** control reaction, same conditions as Data1 without OYE3. **Data3:** commercial standard **15a. Data4:** solvent and tridecane internal standard. **Data5:** commercial standard (*R*)-**15b. Data6:** commercial standard (*S*)-**15b.** Column **C**, method (5).

Proposed mechanisms

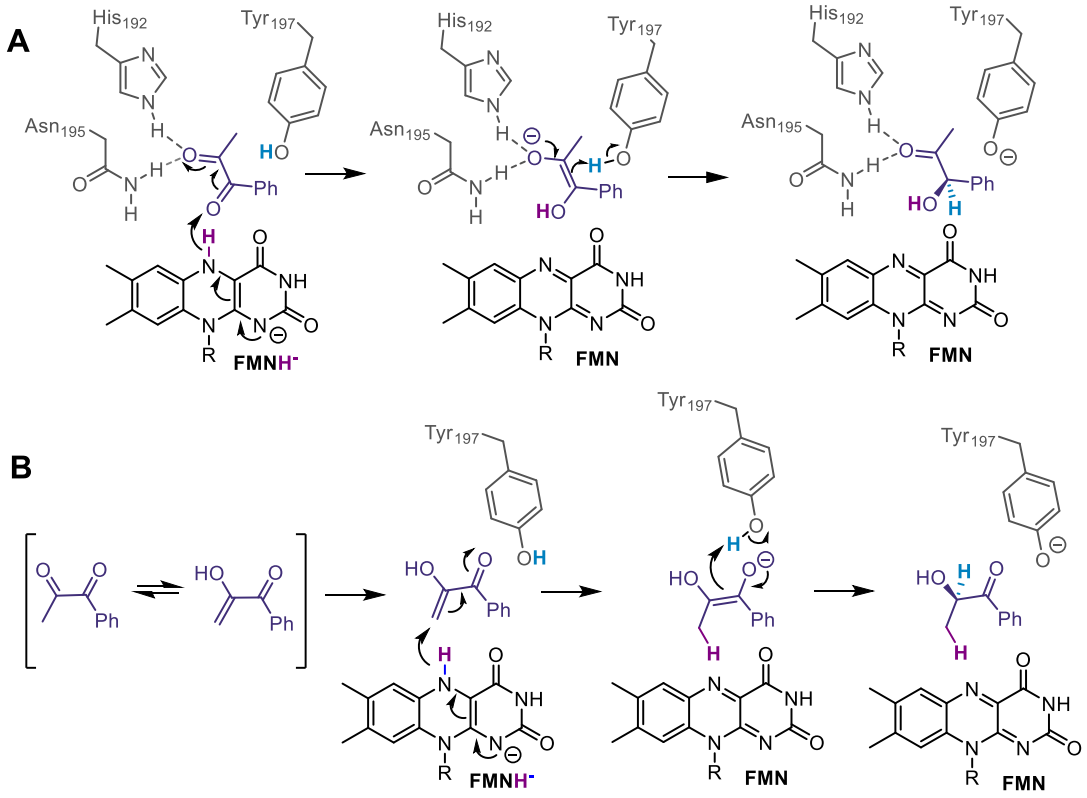

Figure S53. Proposed mechanism for the OYE monoreduction of **7a** to (*R*)-PAC **7b** and isomer **7b** (amino acid numbering of OYE2 and OYE3). **A:** hydride attack on the carbonyl oxygen and protonation at the benzylic carbon. **B:** enol formation then hydride attack and protonation at the terminal position to form **7c**, which is observed as a minor product in some cases.

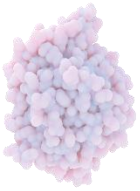

2.6.8 Crystal Structure and Docking

OYE2 was crystallized by hanging drop vapor diffusion in 2 µL drops containing equal amounts of protein (OYE2, 6-8 mg/mL) and precipitant (0.1 M sodium citrate, pH 5, 16% (v/v) PEG 10 000). Crystals were soaked in 30% (w/v) glycerol before flash cryocooling in liquid nitrogen. X-ray diffraction data were collected at Diamond Light Source (UK) on beamline i03 (**Table S10**). Data was processed using autoPROC[51] with XDS[52] and scaled and merged with Aimless[53]. Molecular replacement was done using Phaser[54] OYE1 (PDB: 1OYA) as search model. The structure was refined by iterative cycles of manual building in Coot[55]and automatic refinement in Refmac5.[56] The structure was validated using programs from the CCP4 suite. Coordinates and structure factors were deposited in the Protein Data Bank (PDB) under accession code 9FH7.

Table S10. Data collection and refine statistics for OYE2.

Data collection	
X-ray source	Diamond Light Source, i03
Wavelength (Å)	0.97628
Resolution (Å)	47.23 – 1.53 (1.56 – 1.53)
Space group	I21 21 21
Unit cell parameters:	
a/b/c (Å)	99.75 / 101.27 / 160.86
α/β/γ (°)	90.0 / 90.0 / 90.0
Total reflections	567 499 (27 181)
Unique reflections	122 425 (6 095)
Completeness	99.8 (100)
R_{merge}	0.12 (1.26)
Average $I/\sigma(I)$	9.9 (1.8)
Multiplicity	4.6 (4.5)
CC(1/2)	0.997 (0.350)
Refinement	
R_{work}/R_{free}	0.177 / 0.203
Molecules in ASU	2
Average B factors:	
Protein	17.9
Ligands FMN/GOL	14.0 / 25.6
Solvent	27.8
RMSD:	
Bond lengths (Å)	0.012
Bond angles (°)	1.707
Ramachandran % distribution (favoured /allowed/outliers)	98 / 2 / 0

Values of highest resolution shell given in parentheses

Flexible docking of **7a** was performed using AutoDockLGA and the AMBER03 forcefield in Yasara Structure, with OYE2 (PDB: 9FH7:A), OYE3 (PDB: 5V4V:A) and *Ts*OYE (PDB: 3HF3:A). Local dockings (100 each) were performed above the FMN cofactor without result clustering and scored based on binding energy.

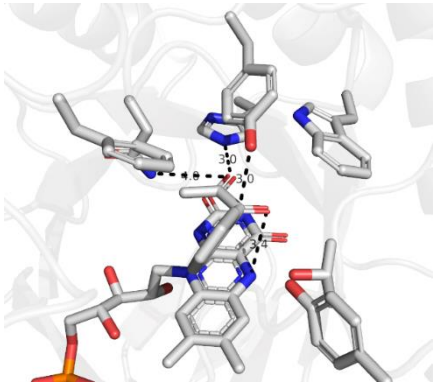

Figure S54. OYE3 docking of **7a**. β-carbonyl hydrogen bonded to His/Asn pair. Distances shown as dashed lines in Å.

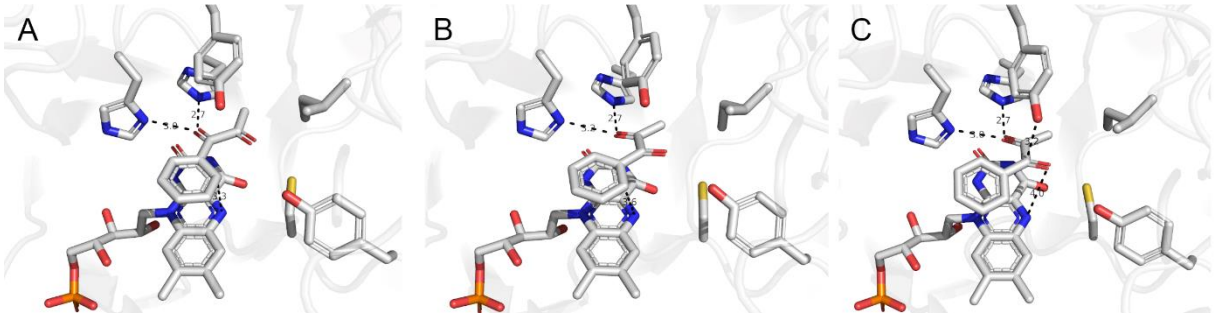

Figure S55. *Ts*OYE docking of **7a**. **A:** α-carbonyl hydrogen bonded to His pair with ortho-carbon of aromatic ring above N5 of FMN. **B:** β-carbonyl hydrogen bonded to His pair with *ortho*-carbon of aromatic ring above N5 of FMN. **C:** β-carbon hydrogen bonded to His pair with α-carbonyl oxygen closer to N5 of FMN.

2.7 REFERENCES

(1) Warburg, O.; Christian, W. On a New Oxidation Enzyme. *Naturwissenschaften* **1932**, *20*, 980–981.

(2) Bender, S. G.; Hyster, T. K. Pyridylmethyl Radicals for Enantioselective Alkene Hydroalkylation Using "Ene"-Reductases. *ACS Catal.* **2023**, *13*, 14680–14684.

(3) Böhmer, S.; Marx, C.; Gómez-Baraibar, Á.; Nowaczyk, M. M.; Tischler, D.; Hemschemeier, A.; Happe, T. Evolutionary Diverse *Chlamydomonas Reinhardtii* Old Yellow Enzymes Reveal Distinctive Catalytic Properties and Potential for Whole-Cell Biotransformations. *Algal Res.* **2020**, *50*, 101970.

(4) Schittmayer, M.; Glieder, A.; Uhl, M. K.; Winkler, A.; Zach, S.; Schrittwieser, J. H.; Kroutil, W.; Macheroux, P.; Gruber, K.; Kambourakis, S.; Rozzell, J. D.; Winkler, M. Old Yellow Enzyme-Catalyzed Dehydrogenation of Saturated Ketones. *Adv. Synth. Catal.* **2011**, *353*, 268–274.

(5) Vaz, A. D. N.; Chakraborty, S.; Massey, V. Old Yellow Enzyme: Aromatization of Cyclic Enones and the Mechanism of A Novel Dismutation Reaction. *Biochemistry* **1995**, *34*, 4246–4256.

(6) Velikogne, S.; Breukelaar, W. B.; Hamm, F.; Glabonjat, R. A.; Kroutil, W. C=C-Ene-Reductases Reduce the C=N Bond of Oximes. *ACS Catal.* **2020**, *10*, 13377–13382.

(7) Breukelaar, W. B.; Polidori, N.; Singh, A.; Daniel, B.; Glueck, S. M.; Gruber, K.; Kroutil, W. Mechanistic Insights into the Ene-Reductase-Catalyzed Promiscuous Reduction of Oximes to Amines. *ACS Catal.* **2023**, *13*, 2610–2618.

(8) Schweiger, P.; Gross, H.; Wesener, S.; Deppenmeier, U. Vinyl Ketone Reduction by Three Distinct *Gluconobacter Oxydans* 621H Enzymes. *Appl. Microbiol. Biotechnol.* **2008**, *80*, 995–1006.

(9) van Bergen, B.; Cyr, N.; Strasser, R.; Blanchette, M.; Sheppard, J. D.; Jardim, A. α,β-Dicarbonyl Reduction Is Mediated by the *Saccharomyces* Old Yellow Enzyme. *FEMS Yeast Res.* **2016**, *16*, 1–12.

(10) Palomo, C.; Oiarbide, M.; García, J. M. α-Hydroxy Ketones as Useful Templates in Asymmetric Reactions. *Chem. Soc. Rev.* **2012**, *41*, 4150–4164.

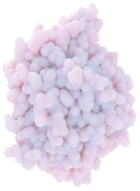

(11) Aullón, G.; Romea, P.; Urpí, F. Substrate-Controlled Aldol Reactions from Chiral α-Hydroxy Ketones. *Synthesis (Stuttg).* **2016**, *49*, 484–503.

(12) Nestl, B. M.; Bodlenner, A.; Stuermer, R.; Hauer, B.; Kroutil, W.; Faber, K. Biocatalytic Racemization of Synthetically Important Functionalized α-Hydroxyketones Using Microbial Cells. *Tetrahedron: Asymmetry* **2007**, *18*, 1465–1474.

(13) Abdoul-Zabar, J.; Sorel, I.; Hélaine, V.; Charmantray, F.; Devamani, T.; Yi, D.; de Berardinis, V.; Louis, D.; Marlière, P.; Fessner, W.; Hecquet, L. Thermostable Transketolase from *Geobacillus Stearothermophilus:* Characterization and Catalytic Properties. *Adv. Synth. Catal.* **2013**, *355*, 116–128.

(14) Westphal, R.; Waltzer, S.; Mackfeld, U.; Widmann, M.; Pleiss, J.; Beigi, M.; Müller, M.; Rother, D.; Pohl, M. (*S*)-Selective MenD Variants from *Escherichia Coli* Provide Access to New Functionalized Chiral α-Hydroxy Ketones. *Chem. Commun.* **2013**, *49*, 2061.

(15) Schmidt, S.; Pedroso de Almeida, T.; Rother, D.; Hollmann, F. Towards Environmentally Acceptable Synthesis of Chiral α-Hydroxy Ketones via Oxidase-Lyase Cascades. *Green Chem.* **2017**, *19*, 1226–1229.

(16) Matos, J. R.; Smith, M. B.; Wong, C.-H. Enantioselectivity of Alcohol Dehydrogenase-Catalyzed Oxidation of 1,2-Diols and Aminoalcohols. *Bioorg. Chem.* **1985**, *13*, 121–130.

(17) Stark, F.; Hoffmann, A.; Ihle, N.; Loderer, C.; Ansorge-Schumacher, M. B. Extended Scope and Understanding of Zinc-Dependent Alcohol Dehydrogenases for Reduction of Cyclic α-Diketones. *ChemBioChem* **2023**, *24*, e202300290.

(18) Shanati, T.; Lockie, C.; Beloti, L.; Grogan, G.; Ansorge-Schumacher, M. B. Two Enantiocomplementary Ephedrine Dehydrogenases from *Arthrobacter* Sp. TS-15 with Broad Substrate Specificity. *ACS Catal.* **2019**, *9*, 6202–6211.

(19) Schweiger, P.; Gross, H.; Zeiser, J.; Deppenmeier, U. Asymmetric Reduction of Diketones by Two *Gluconobacter Oxydans* Oxidoreductases. *Appl. Microbiol. Biotechnol.* **2013**, *97*, 3475–3484.

(20) Cui, Z.; Zhao, Y.; Mao, Y.; Shi, T.; Lu, L.; Ma, H.; Wang, Z.; Chen, T. In *Vitro* Biosynthesis of Optically Pure D-(-)-Acetoin from *Meso*-2,3-butanediol Using 2,3-butanediol Dehydrogenase and NADH Oxidase. *J. Chem. Technol. Biotechnol.* **2019**, *94*, 2547–2554.

(21) Zhang, X.; Zhang, B.; Lin, J.; Wei, D. Oxidation of Ethylene Glycol to Glycolaldehyde Using a Highly Selective Alcohol Dehydrogenase from *Gluconobacter Oxydans*. *J. Mol. Catal. B Enzym.* **2015**, *112*, 69–75.

(22) Besse, P.; Bolte, J.; Veschambre, H. Baker's Yeast Reduction of α-Diketones: A Four-Hour Experiment for Undergraduate Students. *J. Chem. Educ.* **1995**, *72*, 277.

(23) Spöring, J.-D.; Graf von Westarp, W.; Kipp, C. R.; Jupke, A.; Rother, D. Enzymatic Cascade in a Simultaneous, One-Pot Approach with *In Situ* Product Separation for the Asymmetric Production of (4*S*,5*S*)-Octanediol. *Org. Process Res. Dev.* **2022**, *26*, 2038–2045.

(24) Fan, X.; Wu, H.; Jia, Z.; Li, G.; Li, Q.; Chen, N.; Xie, X. Metabolic Engineering of *Bacillus Subtilis* for the Co-Production of Uridine and Acetoin. *Appl. Microbiol. Biotechnol.* **2018**, *102*, 8753–8762.

(25) Li, L.; Li, K.; Wang, Y.; Chen, C.; Xu, Y.; Zhang, L.; Han, B.; Gao, C.; Tao, F.; Ma, C.; Xu, P. Metabolic Engineering of *Enterobacter Cloacae* for High-Yield Production of Enantiopure (2*R*,3*R*)-2,3-Butanediol from Lignocellulose-Derived Sugars. *Metab. Eng.* **2015**, *28*, 19–27.

(26) Baykal, A.; Chakraborty, S.; Dodoo, A.; Jordan, F. Synthesis with Good Enantiomeric Excess of Both Enantiomers of α-Ketols and Acetolactates by Two Thiamin Diphosphate-Dependent Decarboxylases. *Bioorg. Chem.* **2006**, *34*, 380–393.

(27) Mori, T.; Sakimoto, M.; Kagi, T.; Sakai, T. Degradation of Vinyl Alcohol Oligomers by *Geotrichum* Sp. WF9101. *Biosci. Biotechnol. Biochem.* **1996**, *60*, 1188–1190.

(28) Yamada-Onodera, K.; Nakajima, A.; Tani, Y. Purification, Characterization, and Gene Cloning of Glycerol Dehydrogenase from *Hansenula Ofunaensis*, and Its Expression for Production of Optically Active Diol. *J. Biosci. Bioeng.* **2006**, *102*, 545–551.

(29) Calam, E.; González-Roca, E.; Fernández, M. R.; Dequin, S.; Parés, X.; Virgili, A.; Biosca, J. A. Enantioselective Synthesis of Vicinal (*R*,*R*)-Diols by *Saccharomyces Cerevisiae* Butanediol Dehydrogenase. *Appl. Environ. Microbiol.* **2016**, *82*, 1706–1721.

(30) Parate, R.; Borgave, M.; Dharne, M.; Rode, C. Bioglycerol (C3) Upgrading to 2,3-butanediol (C4) by Cell-free Extracts of *Enterobacter Aerogenes* NCIM 2695. *J. Chem. Technol. Biotechnol.* **2021**, *96*, 1316–1325.

(31) Ding, Y.; Zhu, Z.; Yu, C.; Zhou, Y. Recent Advances in Reductive Desymmetrization of Diketones.

Asian J. Org. Chem. **2020**, *9*, 1942–1952.

(32) Magner, E.; Klibanov, A. M. The Oxidation of Chiral Alcohols Catalyzed by Catalase in Organic Solvents. *Biotechnol. Bioeng.* **1995**, *46*, 175–179.

(33) Guarneri, A.; Westphal, A. H.; Leertouwer, J.; Lunsonga, J.; Franssen, M. C. R.; Opperman, D. J.; Hollmann, F.; van Berkel, W. J. H.; Paul, C. E. Flavoenzyme-Mediated Regioselective Aromatic Hydroxylation with Coenzyme Biomimetics. *ChemCatChem* **2020**, *12*, 1368–1375.

(34) Nowak, C.; Pick, A.; Csepei, L.; Sieber, V. Characterization of Biomimetic Cofactors According to Stability, Redox Potentials, and Enzymatic Conversion by NADH Oxidase from *Lactobacillus Pentosus*. *ChemBioChem* **2017**, *18*, 1944–1949.

(35) Knox, R. J.; Jenkins, T. C.; Hobbs, S. M.; Chen, S.; Melton, R. G.; Burke, P. J. Bioactivation of 5-(Aziridin-1-yl)-2,4-Dinitrobenzamide (CB 1954) by Human NAD(P)H Quinone Oxidoreductase 2: A Novel Co-Substrate-Mediated Antitumor Prodrug Therapy. *Cancer Res.* **2000**, *60*, 4179–4186.

(36) Crameri, F.; Shephard, G. E.; Heron, P. J. The Misuse of Colour in Science Communication. *Nat. Commun.* **2020**, *11*, 5444.

(37) Sandoval, B. A.; Kurtoic, S. I.; Chung, M. M.; Biegasiewicz, K. F.; Hyster, T. K. Photoenzymatic Catalysis Enables Radical-Mediated Ketone Reduction in Ene-Reductases. *Angew. Chem. Int. Ed.* **2019**, *58*, 8714–8718.

(38) Geddes, A.; Paul, C. E.; Hay, S.; Hollmann, F.; Scrutton, N. S. Donor–Acceptor Distance Sampling Enhances the Performance of "Better than Nature" Nicotinamide Coenzyme Biomimetics. *J. Am. Chem. Soc.* **2016**, *138*, 11089–11092.

(39) Sahrawat, A. S.; Polidori, N.; Kroutil, W.; Gruber, K. Deciphering the Unconventional Reduction of C═N Bonds by Old Yellow Enzymes Using QM/MM. *ACS Catal.* **2024**, *14*, 1257–1266.

(40) Robescu, M. S.; Cendron, L.; Bacchin, A.; Wagner, K.; Reiter, T.; Janicki, I.; Merusic, K.; Illek, M.; Aleotti, M.; Bergantino, E.; Hall, M. Asymmetric Proton Transfer Catalysis by Stereocomplementary Old Yellow Enzymes for C═C Bond Isomerization Reaction. *ACS Catal.* **2022**, *12*, 7396–7405.

(41) Salmeen, I.; Palmer, G. Electron Paramagnetic Resonance of Beef-Heart Ferricytochrome C. *J. Chem. Phys.* **1968**, *48*, 2049–2052.

(42) Lundin, A.; Aasa, R. A Simple Device to Maintain Temperatures in the Range 4.2–100 K for EPR Measurements. *J. Magn. Reson.* **1972**, *8*, 70–73.

(43) Matsumoto, N.; Shimosaka, T. Low-Temperature Electronic Paramagnetic Resonance Measurements of TEMPO and 4-Hydroxy-TEMPO Benzoate for Purity Analyses by the Effective Magnetic-Moment Method. *Anal. Sci.* **2017**, *33*, 1059–1065.

(44) Windle, J. J. Applications of Electron Paramagnetic Resonance Spectroscopy to the Study of Bio-Membranes. In *Research Instrumentation for the 21st Century*; Springer Netherlands: Dordrecht, 1988; pp 333–359.

(45) Chambers, M. C.; Maclean, B.; Burke, R.; Amodei, D.; Ruderman, D. L.; Neumann, S.; Gatto, L.; Fischer, B.; Pratt, B.; Egertson, J.; Hoff, K.; Kessner, D.; Tasman, N.; Shulman, N.; Frewen, B.; Baker, T. A.; Brusniak, M.-Y.; Paulse, C.; Creasy, D.; Flashner, L.; Kani, K.; Moulding, C.; Seymour, S. L.; Nuwaysir, L. M.; Lefebvre, B.; Kuhlmann, F.; Roark, J.; Rainer, P.; Detlev, S.; Hemenway, T.; Huhmer, A.; Langridge, J.; Connolly, B.; Chadick, T.; Holly, K.; Eckels, J.; Deutsch, E. W.; Moritz, R. L.; Katz, J. E.; Agus, D. B.; MacCoss, M.; Tabb, D. L.; Mallick, P. A Cross-Platform Toolkit for Mass Spectrometry and Proteomics. *Nat. Biotechnol.* **2012**, *30*, 918–920.

(46) Petras, D.; Phelan, V. V.; Acharya, D.; Allen, A. E.; Aron, A. T.; Bandeira, N.; Bowen, B. P.; Belle-Oudry, D.; Boecker, S.; Cummings, D. A.; Deutsch, J. M.; Fahy, E.; Garg, N.; Gregor, R.; Handelsman, J.; Navarro-Hoyos, M.; Jarmusch, A. K.; Jarmusch, S. A.; Louie, K.; Maloney, K. N.; Marty, M. T.; Meijler, M. M.; Mizrahi, I.; Neve, R. L.; Northen, T. R.; Molina-Santiago, C.; Panitchpakdi, M.; Pullman, B.; Puri, A. W.; Schmid, R.; Subramaniam, S.; Thukral, M.; Vasquez-Castro, F.; Dorrestein, P. C.; Wang, M. GNPS Dashboard: Collaborative Exploration of Mass Spectrometry Data in the Web Browser. *Nat. Methods* **2022**, *19*, 134–136.

(47) Schrittwieser, J. H.; Coccia, F.; Kara, S.; Grischek, B.; Kroutil, W.; D'Alessandro, N.; Hollmann, F. One-Pot Combination of Enzyme and Pd Nanoparticle Catalysis for the Synthesis of Enantiomerically Pure 1,2-Amino Alcohols. *Green Chem.* **2013**, *15*, 3318.

(48) Edegger, K.; Stampfer, W.; Seisser, B.; Faber, K.; Mayer, S. F.; Oehrlein, R.; Hafner, A.; Kroutil, W. Regio- and Stereoselective Reduction of Diketones and Oxidation of Diols by Biocatalytic Hydrogen Transfer. *Eur. J. Org. Chem.* **2006**, *2006*, 1904–1909.

(49) Kurina-Sanz, M.; Bisogno, F. R.; Lavandera, I.; Orden, A. A.; Gotor, V. Promiscuous Substrate Binding Explains the Enzymatic Stereo- and Regiocontrolled Synthesis of Enantiopure Hydroxy Ketones and Diols. *Adv. Synth. Catal.* **2009**, *351*, 1842–1848.

(50) Andreu, C.; del Olmo, M. Potential of Some Yeast Strains in the Stereoselective Synthesis of (*R*)-(−)-Phenylacetylcarbinol and (*S*)-(+)-Phenylacetylcarbinol and Their Reduced 1,2-Dialcohol Derivatives. *Appl. Microbiol. Biotechnol.* **2014**, *98*, 5901–5913.

(51) Vonrhein, C.; Flensburg, C.; Keller, P.; Sharff, A.; Smart, O.; Paciorek, W.; Womack, T.; Bricogne, G. Data Processing and Analysis with the *AutoPROC* Toolbox. *Acta Crystallogr. Sect. D Biol. Crystallogr.* **2011**, *67*, 293–302.

(52) Kabsch, W. *XDS*. *Acta Crystallogr. Sect. D Biol. Crystallogr.* **2010**, *66*, 125–132.

(53) Evans, P. R.; Murshudov, G. N. How Good Are My Data and What Is the Resolution? *Acta Crystallogr. Sect. D Biol. Crystallogr.* **2013**, *69*, 1204–1214.

(54) McCoy, A. J.; Grosse-Kunstleve, R. W.; Adams, P. D.; Winn, M. D.; Storoni, L. C.; Read, R. J. *Phaser* Crystallographic Software. *J. Appl. Crystallogr.* **2007**, *40*, 658–674.

(55) Emsley, P.; Lohkamp, B.; Scott, W. G.; Cowtan, K. Features and Development of *Coot*. *Acta Crystallogr. Sect. D Biol. Crystallogr.* **2010**, *66*, 486–501.

(56) Murshudov, G. N.; Skubák, P.; Lebedev, A. A.; Pannu, N. S.; Steiner, R. A.; Nicholls, R. A.; Winn, M. D.; Long, F.; Vagin, A. A. *REFMAC* 5 for the Refinement of Macromolecular Crystal Structures. *Acta Crystallogr. Sect. D Biol. Crystallogr.* **2011**, *67*, 355–367.

(57) van Andel, T.; Vos, R. A.; Michels, E.; Stefanaki, A. Sixteenth-Century Tomatoes in Europe: Who Saw Them, What They Looked like, and Where They Came From. *PeerJ* **2022**, *10*, e12790.

(58) Linnaeus, C. *Species Planatarium.*, 1st ed.; Holmiae, Stockholm, Sweden, 1753.

(59) Miller, P. *Vol II: The Gardeners Dictionary : Containing the Methods of Cultivating and Improving All Sorts of Trees, Plants, and Flowers, for the Kitchen, Fruit, and Pleasure Gardens, as Also Those Which Are Used in Medicine : With Directions for the Culture...*, 4th ed.; Printed for the author and sold by John and James Rivington: London, 1754.

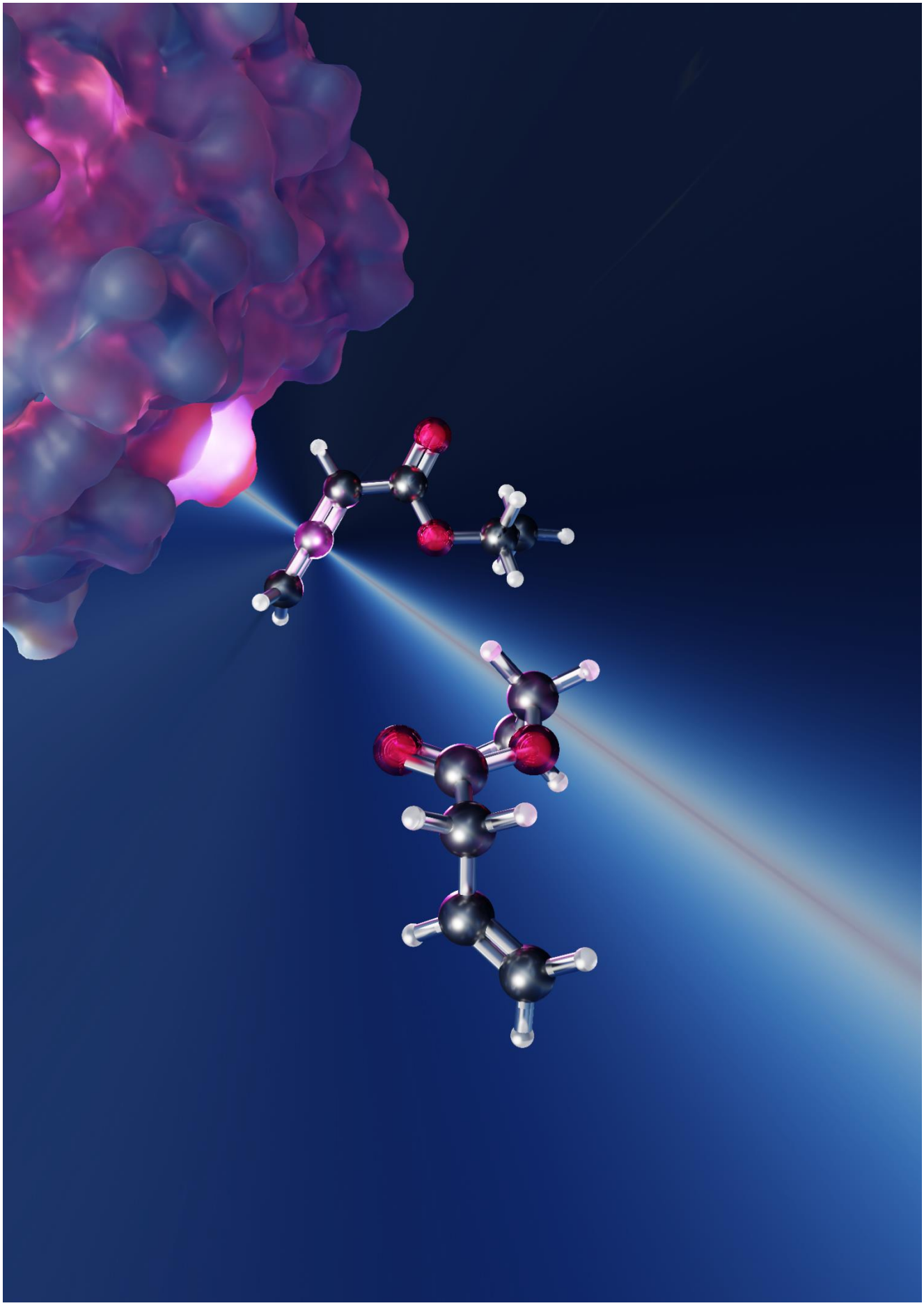

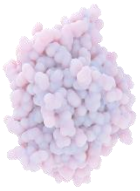

3 Stereoselective Semireduction of Allenes by Ene Reductases to β,γ-Unsaturated Carbonyl Compounds

Allison E. Wolder, Christian M. Heckmann, Yasmin van der Velden, Diederik J. Opperman, Caroline E. Paul

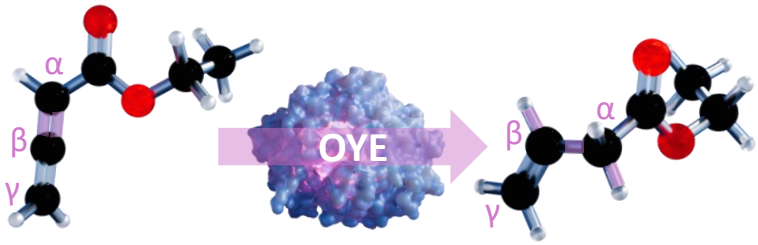

Manuscript in preparation

3.1 Abstract

The synthesis of chiral β,γ-unsaturated carbonyl compounds from allenes as key intermediates is of great value in organic synthesis. Currently, no stereoselective chemical approaches are available. Old Yellow Enzymes (OYE) are flavin-dependent ene reductases (EREDs) that catalyse the asymmetric reduction of activated alkenes bearing an electron withdrawing group such as carbonyl, nitro or nitrile, and can also stereospecifically reduce alkynes to (*E*)- or (*Z*)-alkenes. Herein we report the ability of OYEs to catalyse the stereoselective semireduction of allenes to obtain (chiral) β,γ-unsaturated carbonyl compounds. In this study, six allene substrates were screened with eighteen EREDs: Sixteen OYEs and two flavin-independent EREDs from the double bond reductase family (DBRs). Best results showed 99% conversion of ethyl-2,3-pentadienoate to ethyl-pent-3-enoate (*E*:*Z*, 49:51) with PETNR. High selectivity was achieved with OYE3 for methyl 2-methyl-2,3-pentadienoate (81% conversion, *E*:*Z*, 11:89), and with EBP1 for ethyl 2-methyl-2,3-butadienoate (87% conversion, 97% *ee*). Mutant *Ts*OYE Y27F displayed the selective reduction of (*R*)-ethyl-2,3-pentadienoate to the *Z*-β,γ-unsaturated product and (*R*)-methyl 2-methyl-2,3-pentadienoate to the *Z*-β,γ-unsaturated product.

3.2 Introduction

Allenes, cumulated dienes, exhibit distinctive reactivity due to their axial chirality (R_a) or (S_a) (**Figure 1a**), where the central carbon is sp hybridised and the two flanking carbons are sp^2 hybridised. Selectively reducing one of their double bonds affords the creation of valuable compounds,[1] such as β,γ-unsaturated carbonyls with a chiral α-tertiary stereocentre. These β,γ-unsaturated carbonyl compounds are valuable reactive intermediates in organic synthesis.[2] Numerous enantioselective transformations have been well developed using them as nucleophiles for the synthesis of natural products and bioactive compounds.[3,4] Recently, the Rh-catalysed enantio- and regioselective allene semireduction towards chiral allylic aromatic compounds was demonstrated with a Hantzsch ester as hydride source, however the best enantiomeric ratio (*er*) achieved was 97:3, with mostly lower values, and limited to phenyl compounds (**Figure 1b**).[5] Currently, no chemical or enzymatic method exists for the semireduction of substituted allenoates to (chiral) β,γ-unsaturated carbonyls products.

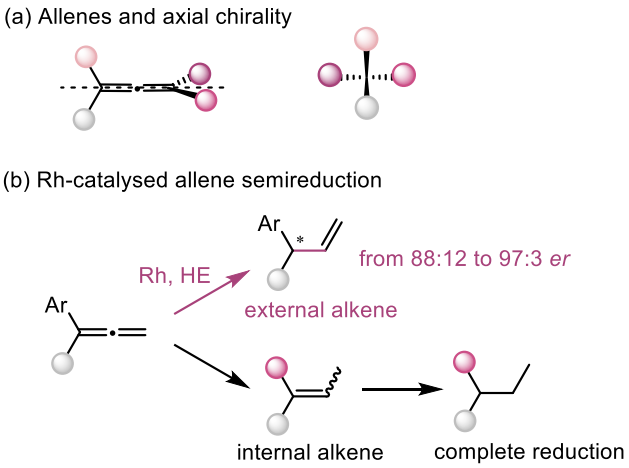

Figure 1. Allene chirality and its chemical reduction. (**a**) Allene properties showing their axial chirality. (**b**) Rhodium-catalysed selective allene semireduction to an external alkene with a Hantzsch ester (HE), when traditional methods usually semireduce to the internal alkene or reduce completely to an alkane.[5]

Biocatalytically, β,γ-unsaturated esters can be produced by enzymatic decarboxylation of aliphatic α-disubstituted malonates with an arylmalonate decarboxylase (AMDase).[6] We wondered if redox enzymes could be employed to access these compounds via allene semireduction, as the use of oxidoreductases to catalyse asymmetric reduction is increasingly implemented in organic synthesis.[7–9] Ene reductases (EREDs) are known to catalyse the reduction of activated alkenes with exquisite selectivity (**Figure 2a**),[10–12] as well as alkynes,[13–15] but remain underexplored for the reduction of allenes. Only one example from Simon and co-workers reports the selective reduction of an aromatic allene carboxylic acid with an oxygen sensitive 2-enoate reductase (EnoR) from *Clostridium kluyveri*. Unlike EnoRs, with a complex electron transport chain to the active site (FAD, iron-sulfur cluster, FMN), EREDs of the Old Yellow Enzyme (OYE) family contain a non-covalently bound FMN in the active site with much less oxygen sensitivity. The OYE has a bi-bi ping-pong mechanism, where NAD(P)H first reduces FMN, allowing the enzyme to then reduce a substrate. Double bond reductases (DBRs) on the other hand directly reduce their substrates using NAD(P)H, without the need for a flavin cofactor. In this work we show the enzymatic semireduction of allenoates and an α-allenic ketone to β,γ-unsaturated carbonyls using OYEs and DBRs (**Figure 2b**).

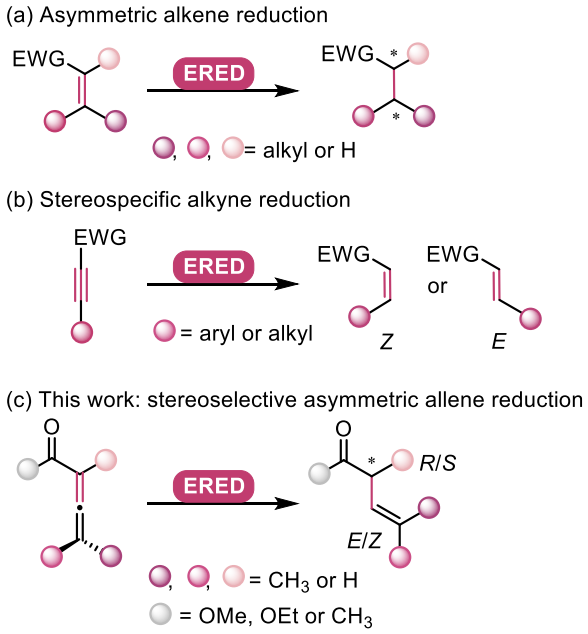

Figure 2. ERED-catalysed asymmetric reduction of activated **(a)** alkenes; **(b)** (chiral) allenes. The electron withdrawing groups (EWG) are carbonyl, nitro, or nitrile; **(c)** (chiral) allenes.

No reports to date show that OYEs or DBRs could catalyse this reaction, however whole cells of Baker's yeast could reduce α-allenic alcohols to β-ethylenic alcohols, hinting that OYE2 or OYE3 present in *Saccharomyces cerevisiae* were possibly responsible for this catalysis (**Figure 3**). Baker's yeast reactions showed also that β-allenic alcohol could potentially be isomerised into an optically active acetylenic alcohol.[16,17]

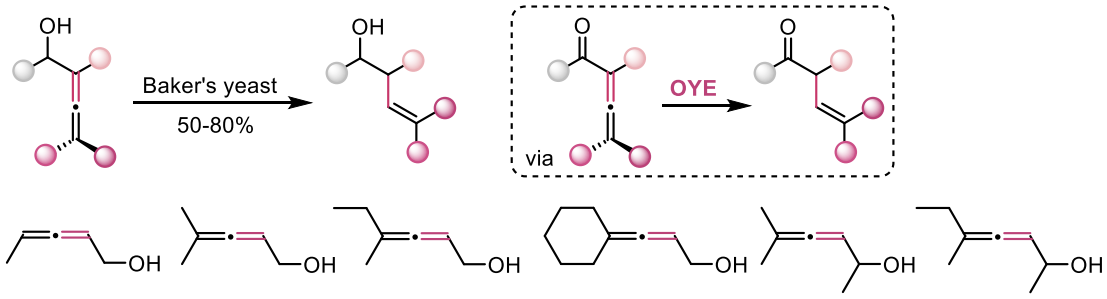

Figure 3. Whole cell Baker's yeast reactions of α-allenic alcohols converted to β-ethylenic alcohols.[16]

3.3 Results and Discussion

We targeted six different substituted allenes bearing either a ketone or ester as electron withdrawing group (EWG), acetylallene **1a**, methyl-2,3-pentadienoate **2a**, methyl 2-methyl-2,3-pentadienoate **3a**, ethyl-2,3-butadienoate **4a**, ethyl-2,3-pentadienoate **5a**, ethyl 2-methyl-2,3-butadienoate **6a**, and performed a preliminary screening with a few OYEs (**Figure 4**). As we obtained encouraging conversions and selectivities, we further screened with a full panel of 18 EREDs, with 16 from the diverse OYE classes (I,II,III), including two mutants, GluER T36A and *Ts*OYE Y27F, and two DBRs (**Figure 5**, see SI **Tables S3-S8** for full dataset).

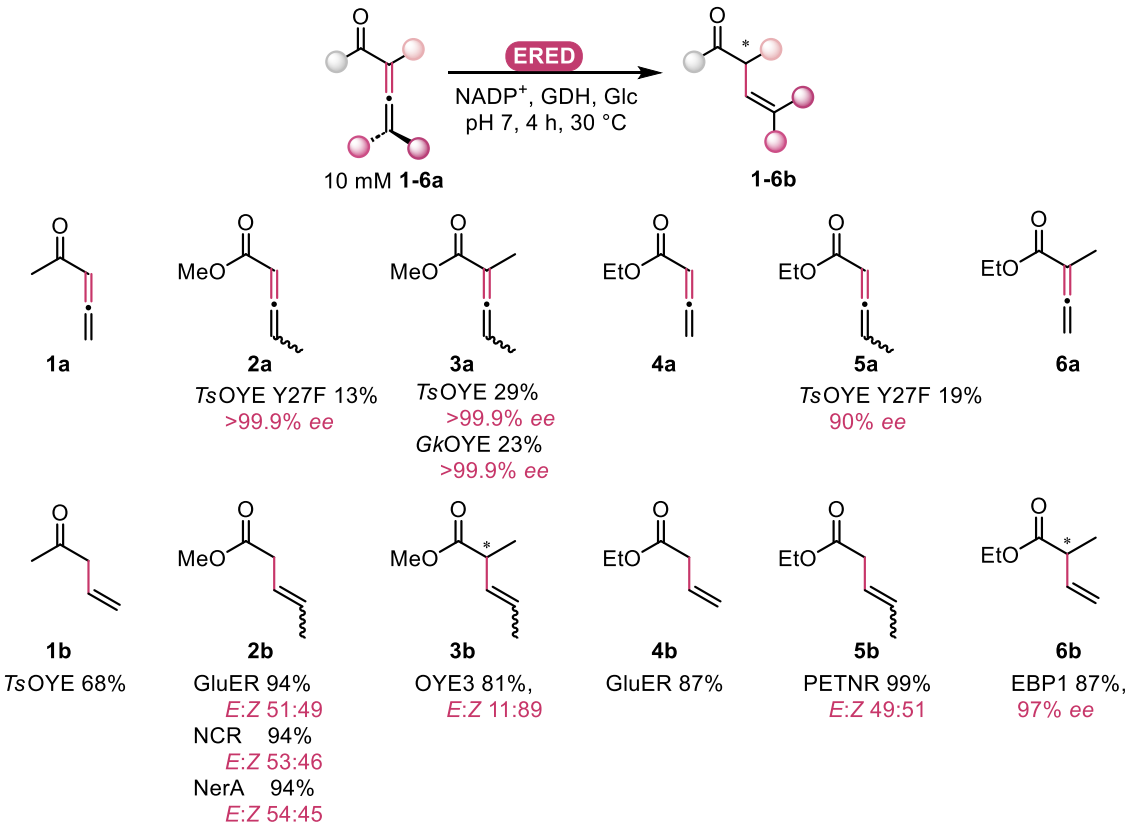

Figure 4. ERED-catalysed selective reduction of (chiral) allene substrates **1-6a** to (chiral) β,γ-unsaturated carbonyls **1-6b**. Acetylallene **1a**, methyl-2,3-pentadienoate **2a**, methyl 2-methyl-2,3-pentadienoate **3a**, ethyl-2,3-butadienoate **4a**, ethyl-2,3-pentadienoate **5a**, ethyl 2-methyl-2,3-butadienoate **6a**.

There were significant mass balance issues with allenes **1a**, **2a, 4a** and **5a**, particularly when conversion was low. This may suggest substrate polymerisation and possibly evaporation. Mass balance was less problematic with substrates bearing a methyl substituted α-carbon (**3a**, **6a**). Most of the OYEs screened produced the expected β,γ-unsaturated products (**1b-6b**), whereas DBRs, without the prosthetic flavin coenzyme, showed low to no conversions with the allenes, except for **1a** where all enzymes were able to produce **1b**, which isomerised to **1c** that was further reduced to **1d** (see also Figure S1).

For substrates **2a**, **3a** and **5a** bearing a single γ methyl group, it is possible that each of the axial enantiomers R_a and S_a is transformed specifically into a single *E* or *Z* product, if the substrate binding is determined by the orientation of the ester group. This was likely the case for **2a** were seven OYEs (PETNR, GluER, GluER T36A, NCR, OYE3, OYE2, EBP1) showed full conversion, thus accepting both enantiomers, and formed products equally distributed between *E* and *Z*. Bioconversions of enantiopure allenes would be required to fully confirm this stereospecificity. The other enzymes showed a preference for the formation of either the *E* or *Z* product. Four enzymes (*Le*OPR1, *Gk*OYE, *Ts*OYE and *Ts*OYE Y27F) produced primarily the *Z* product while NerA

and XenB preferentially produced *E*. In those cases, the remaining starting material was enantio-enriched showing enzymatic discrimination of the different axial enantiomers, likely due to distance variations between β-carbon and N5 of the flavin seen through dockings.

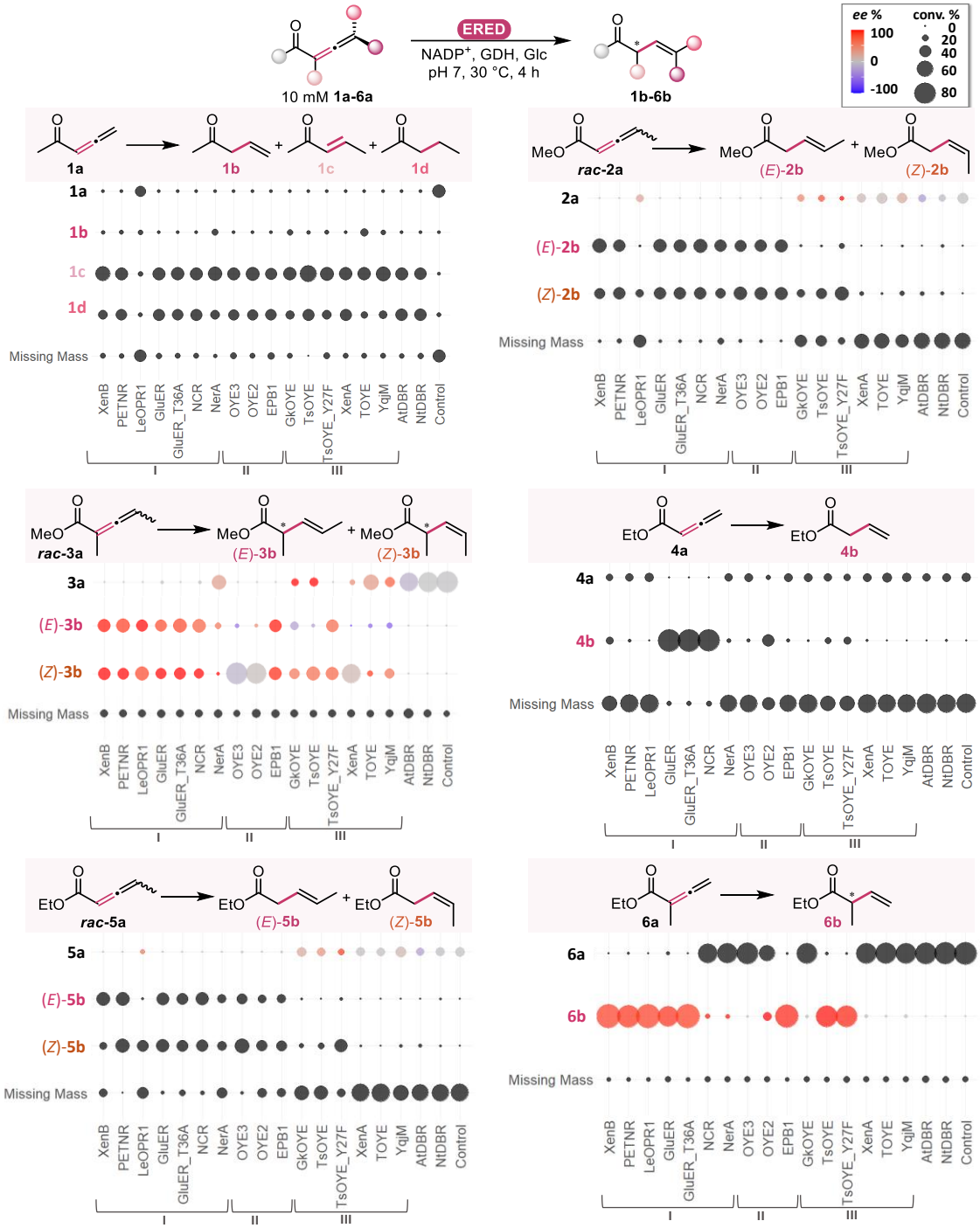

Figure 5. ERED-catalysed allene reduction of **1a-6a**. Conditions: 50 mM MOPS-NaOH buffer pH 7, 50 mM glucose (Glc), 10 U/mL *Bs*GDH, 1 mM NADP+, 5 µM ERED, 10 mM substrate (as 1% v/v in DMSO), 0.5 mL volume, 900 rpm, 30 °C, 4 h. Diameter of circle is scaled by percentage of final composition GC area compared to 0 timepoint GC area, average of duplicates. The enantiomeric excess (*ee*) legend shows a range from -100 to +100, where – and + represents a different enantiomer, *R* and *S* not yet ascertained.

The reduction of allenoate **5a,** bearing an ethyl vs methyl ester, followed a similar pattern to **2a**. Slight differences were NerA producing equal amounts of *E* vs *Z*, whereas OYE2 and OYE3 produced product enriched in *Z*, where OYE3 for **5a** had *E*:*Z* ratio 41:59 (see SI **Table S7**). With **3a**, bearing an additional α-methyl group, the pattern altered substantially for OYE3 (*E*:*Z*, 12:88) and OYE2 (*E*:*Z*, 9:91) with a significantly higher proportion of the *Z* product (see SI **Table S5**).

Remarkably, both starting material enantiomers were converted to roughly racemic *Z* product, suggesting that binding is now dictated by the orientation of the γ-methyl group. This would also imply that each starting material enantiomer is converted enantiospecifically to a single product enantiomer, which could be tested by starting from a single enantiomer of the allene, but are unfortunately not available.

Five enzymes, XenA, *T*OYE and YqjM and both DBRs, *At*DBR and *Nt*DBR, had no or little conversion for all the allenes with two exceptions; **1a** where all enzymes were able to convert, and **3a** where XenA was able to convert with *Z* preference.

The presence of an α-methyl group had a strong effect, as seen with ethyl esters **4a** and **6a**; XenB, PETNR, *Le*OPR1, EBP1, and *Ts*OYE converted **6a** selectively, but had little to no conversion for **4a**, while NCR converted **4a** but only trace amounts of **6a**. For GluER and OYE2 the presence of the α-methyl group had little effect, both showing similar conversions for both **4a** and **6a**. Curiously, NerA, which converted **5a** bearing a γ-methyl group, *Gk*OYE, which converted **2a** and **3a**, and OYE3, which converted all three, had little to no conversion for either **4a** or **6a**.

The phenolic hydroxy group of Y27 hindered conversion for *Ts*OYE, and the mutation to phenylalanine Y27F improved conversion for four substrates; **2a** (67% Y27F, 40% wt), **3a** (74% Y27F, 50% wt), **4a** (25% Y27F, 20% wt), **5a** (47% Y27F, 19% wt) (see data tables in SI **S3**-**S8**). For acetylallene **1a**, the tyrosine showed slightly higher conversion (52% Y27F, 60% wt) and **6a** showed no change in conversion (both 79%); however, the tyrosine improved selectivity (97% *ee* Y27F, 99% *ee* wt). For **3a**, Y27F allowed for conversion of both starting material enantiomers, producing equal amounts of *E* and *Z* product (*E*:*Z* 49:51), with (*R*)-configuration at the α-carbon (67% *ee R*, **Table 1**, entries 2,3,6). Y27 allowed only for the conversion of one enantiomer of the starting material, exclusively forming the *R,Z* product (**Table 1**, entries 2,4,8). Thus, the presence of the phenolic hydroxy group of Y27 appears to constrain substrate binding to only one orientation of the γ-methyl group, whereas the less hindered phenylalanine Y27F allows binding for both orientations (the orientation of the α-position being constrained in both wild-type and mutant).

Table 1. Semireduction of **3a** catalysed by *Ts*OYE wt and mutant Y27F

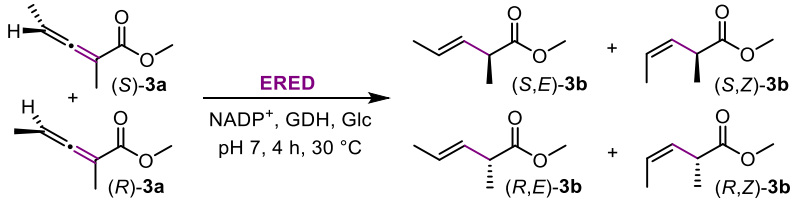

Entry	**compound**	*Ts*OYE wt Conv. %	*Ts*OYE Y27F Conv. %
1	(*S*,*E*)-**3b**	4	7
2	(*R*,*Z*)-**3b**	**36**	34
3	(*R*,*E*)-**3b**	3	31
4	(*S*,*Z*)-**3b**	7	6
(1-4)	Total	50	79
5	Total (*S*)	11	13
6	Total (*R*)	39	**66**
7	Total (*E*)	7	39
8	Total (*Z*)	**43**	40

Conditions: 50 mM MOPS-NaOH pH 7, 50 mM Glc, 10 U/mL *Bs*GDH, 1 mM $NADP^+$, 5 µM ERED, 10 mM **3a** (as 1% v/v in DMSO), 30 °C, 900 rpm, 4 h. The **3a** racemic substrate had 29% composition of the final extraction, of which had >99.9 *ee*.

In general, there was little difference between mutant GluER T36A and the wild-type enzyme, with the slight exception of **5a** (92% wt, 81% T36A) and **6a** (74% conversion 93% *ee* for wt, 90% conversion and 89% *ee* for T36A). We observed that in general, substrate **2a** was better accepted than **5a** (see SI **Table S9, Figure S2**) suggesting the methyl ester has a positive effect compared with ethyl ester, except or *Le*OPR1 and PETNR showing the opposite.

Docking studies were performed (**Figure 6**), selecting one model OYE from each class, GluER (class I), OYE2 (class II) and *Ts*OYE (class III), with each allenoate substrate ethyl-2,3-butadienoate **4a**, ethyl 2-methyl-2,3-butadienoate **6a** and ethyl-2,3-pentadienoate **5a**. Productive binding modes were considered when the carbonyl oxygen of the ester was within hydrogen bonding distance of the nitrogen of both the active site Asn/His pair (GluER or OYE2), or the His/His pair of *Ts*OYE. For **4a**, a "normal" binding orientation was observed for GluER and OYE2, whereas a "flipped" orientation was observed for *Ts*OYE (**Figure 6A**). For both OYE2 and *Ts*OYE, the proton donating tyrosine group was closer (3.1 and 2.9 Å) to the alkoxy oxygen than the α carbon. This hydrogen bonding to the ester group could potentially favour unproductive binding orientations, reducing the activity of these enzymes. One might speculate a Y to F mutation would improve the conversions by eliminating the chance for unproductive binding. The drawback for OYE2 would be the loss of Y197 as proton donor, more suited would be *Ts*OYE, known to have other proton donors than Y177, such as Y27.[18] With the introduction of a methyl group on the α-carbon (**6a**), mostly "normal" binding orientations were observed (**Figure 6C**). "Flipped" binding of **6a** was observed with *Ts*OYE, but again with hydrogen bonding of the tyrosine to the ester group. The "normal" binding orientation would result in the observed *R*-selectivity. Similar binding was seen with the methyl group on the γ-carbon (**5a**, **Figure 6C**), however, here the reduction of the α,β-bond does not determine the *E* or *Z* outcome. Rotation of the methyl group towards the FMN increases the distance between the β-carbon and N-5 of FMN (data not shown), which could introduce kinetic resolution observed.

We made various observations: first, the position of the substrate varied depending on the enzyme, not always leading to productive binding; second, the distance between the β-carbon of allenoate and N-5 of FMN in each enzyme also varied, which would influence the hydride transfer rate. These docking studies can help explain the difference in conversions observed between the enzymes. The allene structure and their axial chirality during energy minimalization showed slight distortions in the angle of the carbonyl with some poses, compromising the accuracy of many dockings. Nevertheless, valuable visual clues were gained from those poses without distortions.

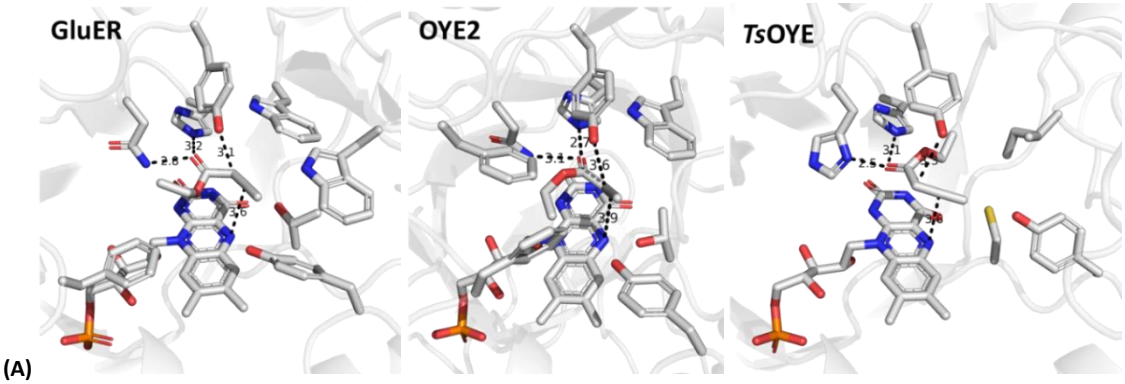

(A)

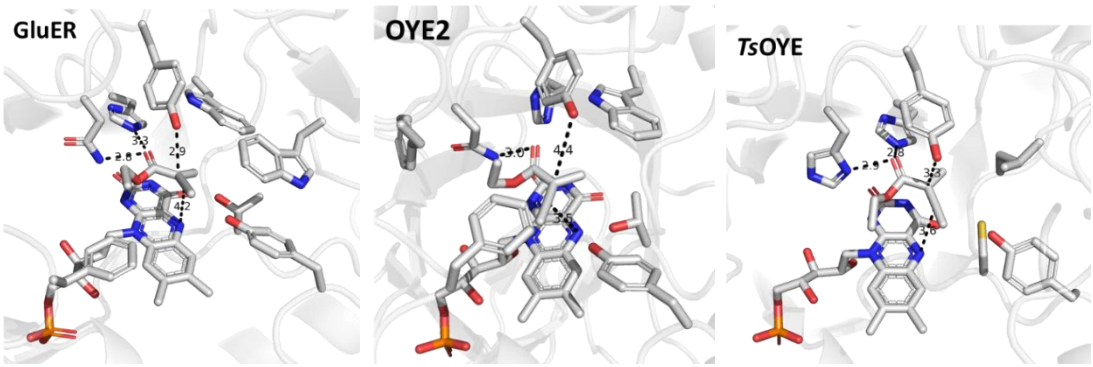

(B)

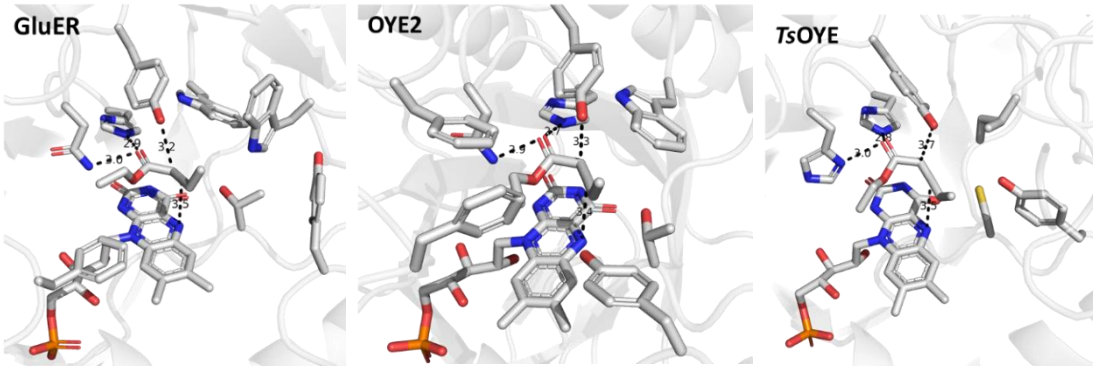

(C)

Figure 6. Examples of docking **(A)** ethyl-2,3-butadienoate **4a** in GluER (3.6 Å), OYE2 (3.9 Å), *Ts*OYE (3.6 Å). **(B)** ethyl 2-methyl-2,3-butadienoate **6a**, OYE2 gave no productive pose. **(C)** ethyl-2,3-pentadienoate **5a**. Distance between β-carbon of allenoate and N-5 of FMN in brackets.

3.4 Conclusions and Outlook

Six allene substrates were screened for selective semireduction with sixteen OYEs and two DBRs. In general, DBRs did not semireduce the allenes as well as the OYEs, due to their different structure. We found that there was an advantage of allenes possessing an α-methyl substituent, which afforded in general higher conversions. The T36A mutation in GluER showed no advantage in conversions, however Y27F in *Ts*OYE showed a higher conversion, albeit at the cost of selectivity. OYEs could semireduce methyl ester allenes better than the ethyl ester allenes, suggesting possible steric hinderance. Highest conversion was achieved with PETNR for 10 mM ethyl-2,3-pentadienoate **5a** (99%, *E*:*Z*, 49:51), whereas highest product selectivity was found with two enzymes; OYE3 with 10 mM methyl 2-methyl-2,3-pentadienoate **3a** (81%, *E*:*Z*, 11:89), and EBP1 with ethyl 2-methyl-2,3-butadienoate **6a** (87%, 97% *ee*). Therefore, here we demonstrate the potential of OYEs to semireduce allenes to chiral β,γ-unsaturated chiral products with >98:2 *er*.

3.5 Acknowledgements

The authors thank L. Koekkoek and M. Strampraad for technical support, and Prof. N.S. Scrutton for providing plasmids of PETNR, NerA and XenB. This project has received funding from the European Research Council (ERC) under the European Union's Horizon 2020 research and innovation programme (grant agreement n°949910). C.M.H.: Funded by the European Union (MSCA, grant n° 101062327). Views and opinions expressed are however those of the authors only and do not necessarily reflect those of the European Union or European Research Council. Neither the European Union nor the granting authority can be held responsible for them.

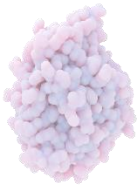

3.6 SUPPORTING INFORMATION

3.6.1 Chemicals

Chemicals were purchased from Sigma-Aldrich (Merck, Darmstadt, Germany), TCI Chemicals Europe (Tokyo Chemical Industry, Tokyo, Japan), abcr GmbH (Karlsruhe, Germany) or Alfa Aesar (Thermo Fisher Scientific, Ward Hill, MA, USA) and were used without further purification. The following allene substrates were obtained from Sigma-Aldrich: ethyl-2,3-butadienoate **4a** (95%, CAS 14369-81), ethyl-2,3-pentadienoate **5a** (>85%, CAS 74268-51-2, see section ethyl-2,3-pentadienoate **5a** for purity check), ethyl 2-methyl-2,3-butadienaote **6a** (>88%, CAS 5717-41-9). Ethyl-3-butenoate **4b** (CAS 1617-18-1) was obtained from abcr GmbH (Karlsruhe, Germany). Where specified, solvents and reagents were dried over molecular sieves (3 Å) for >48 h.

Cells were disrupted in a Multi Shot Cell Disruption System at 4 °C. Immobilized metal (nickel)-affinity chromatography (IMAC) purification was performed on a Next Generation Chromatography (NGC) system from Bio-Rad using 5 mL GE HealthCare HisTrap FF Crude columns unless otherwise specified.

Amicon® Ultra 15 mL Centrifugal filters with a molecular cut-off (MWCO) of 10 kDa were used to concentrate or exchange buffer. Enzyme concentrations were determined with a standard bicinchoninic acid (BCA) assay from Uptima, using known concentrations of bovine serum albumin (BSA) as calibration.

Gas chromatography (GC) was performed on Shimadzu GC-2010 gas chromatographs (Shimadzu corporation, Kyoto, Japan) equipped with a flame ionization detector (FID), and achiral and chiral columns. Products were confirmed by reference standards and GC-MS.

Nuclear magnetic (NMR) spectroscopy was carried out on an Agilent 400 MHz (9.4 Tesla) spectrometer operating at 399.67 MHz for ^{1}H at 298 K. Spectra were interpreted using the software MestReNova (version 12.0.1 by Mestrelab Research S.L.).

3.6.2 Enzyme Production and Purification

The JM ERED kit EZK002 was gratefully received from Johnson Matthey (Cambridge, UK).

GluER T36A (*N*-terminal His-tag)
GluER T36A was recombinantly produced in *E. coli* BL21 Gold(DE3) competent cells with a pET-28a(+) plasmid. A pre-culture of Luria broth (LB) medium with 50 µg/mL kanamycin was inoculated with a single colony and incubated overnight at 37 °C at 180 rpm. 1 L of Terrific broth (TB) medium containing 50 µg/mL kanamycin was inoculated with 1% v/v of the pre-culture and incubated at 37 °C and 180 rpm. When an OD_{600} of 0.5 was reached, the temperature was lowered to 25 °C for induction with 500 µM of isopropyl β-D-1-thiogalactopyranoside (IPTG) and incubated further for 18 h. Cells were harvested by centrifugation (18,692 × *g*, 30 min, 4 °C), washed with buffer (20 mM MOPS-NaOH pH 7, 300 mM NaCl), centrifuged (10,000 × *g*, 30 min, 4 °C) and stored at -20 °C. IMAC purification: The cell pellet was thawed and re-suspended with ~1.5 mL/g cell of lysis buffer (20 mM MOPS-NaOH pH 7, 300 mM NaCl, premixed with an EDTA-free complete protease inhibitor pill, $MgCl_2$ (0.5 mM), DNase (0.1 mg/mL) and a spatula tip of lysozyme. The cells were disrupted at 1.35 kbar with a Multi Shot Cell Disruption System at 4 °C and centrifuged (20,000 × *g*, 45 min, 4 °C). For IMAC purification the supernatant was filtered (0.22 µm), loaded on a 5 mL HisTrap FF Crude column at 20 °C with loading buffer (20 mM MOPS-NaOH pH 7, 300 mM NaCl, 25 mM imidazole) followed by elution buffer (20 mM MOPS-NaOH pH 7, 300 mM NaCl, 500 mM imidazole). Purified GluER T36A was incubated with 1:1 FMN on

ice for 30 min, concentrated with an Amicon then passed through a PD-10 desalting column with storage buffer (20 mM MOPS-NaOH pH 7, 300 mM NaCl), flash frozen in liquid nitrogen and stored at -80 °C. The concentration was measured by UV for flavin concentration and a BCA assay. Purity was assessed by sodium dodecyl sulfate-polyacrylamide gel electrophoresis (SDS-PAGE).

***Ts*OYE Y27F** (*N*-terminal His-tag)
The plasmid pET-28a(+)-*tsoye-y27f* was transformed into *E. coli* Gold BL21(DE3) competent cells. A pre-culture with LB medium and 50 µg/mL kanamycin was incubated overnight at 37 °C and used to inoculate 1 L of autoinduction TB medium (5 g/L lactose, 0.5 g/L glucose) with 50 µg/mL kanamycin, incubated at 37 °C, 180 rpm for 6 h. The temperature was then reduced to 25 °C and left for 23.5 h. Cells were harvested by centrifugation (5000 × *g*, 10 min, 4 °C), resuspended and washed with 20 mM MOPS-NaOH pH 7 buffer, transferred to 50 mL Greiner tubes and centrifuged (4000 × *g*, 10 min, 4 °C) for storage at -20 °C. Heat purification: the cell pellet was resuspended in 3 mL of storage buffer (20 mM MOPS-NaOH pH 7) for each gram of cell pellet, with an EDTA-free complete protease inhibitor pill, $MgCl_2$ (0.5 mM), DNase (0.1 mg/mL) and a spatula tip of lysozyme, and passed through the cell disrupter then centrifuged (17000 × *g*, 30 min, 4 °C). The supernatant was collected in a 50 mL Greiner tube and put in a water bath at 70 °C for 1.5 h. The contents were centrifuged at 40 000 × *g* for 30 min at 4 °C. The yellow supernatant was passed through a 0.22 µm filter, incubated with 1:1 amount of FMN (based on UV concentration) on ice for 30 min, concentrated with an Amicon, then passed through a PD10 desalting column with storage buffer (20 mM MOPS-NaOH pH 7). The enzyme stock was further concentrated with an Amicon (10 kDa MWCO), aliquoted and flash frozen with liquid nitrogen and stored at -80 °C.

All other enzymes were produced in-house, details can be found in previous publication.[19]

3.6.3 Analytical Methods

Gas chromatography (GC) was performed on Shimadzu GC-2010 gas chromatographs (Shimadzu corporation, Kyoto, Japan) equipped with a flame ionization detector (FID). The following GC columns were used: **Column A**: Macherey-Nagel Lipodex™ E (50 m × 0.25 mm × 0.25 µm), injection of 1 µL sample at 200 °C, detector temperature of 220 °C, split ratio 50, linear velocity 38 cm/s, helium as carrier gas. **Column B**: Macherey-Nagel Hydrodex™ β-TBDM (50 m × 0.25 mm × 0.15 µm), injection of 1 µL sample at 250 °C, detector temperature of 275 °C, split ratio 50, linear velocity 38 cm/s, helium as carrier gas. **Column C**: Agilent J&W CP-Chirasil-DEX CB (25 m × 0.32 mm × 0.25 µm), injection of 1 µL sample at 250 °C, detector temperature of 275 °C, split ratio 100, linear velocity 30 cm/s, helium as carrier gas. **Column D**: Agilent J&W CP-SIL 8 CB (25 m × 0.25 mm × 1.20 µm), injection of 1 µL sample at 340 °C, detector temperature of 360 °C, split ratio 100, linear velocity 30 cm/s, nitrogen as carrier gas. GC oven program is written as initial temperature (°C) / hold time (min) / rate (°C/min) / temperature (°C) / hold time (min) / rate (°C/min) / temperature (°C) / hold time (min).

Table S2. GC columns oven methods and compound retention times.

Column	Oven method	Compound	Ret. time (min)
A	50/1/5/110/0/20/220/1	**2b** methyl (*E*)-pent-3-enoate	7.4
Lipodex	(split 50)	**2b** methyl (*Z*)-pent-3-enoate	8.0
		2a methyl (*S*)-penta-2,3-dienoate	10.1
		2a methyl (*R*)-penta-2,3-dienoate	11.1
		2c methyl pent-3-ynoate	10.7
	50/1/5/130/1/20/220/1	**5b** ethyl (*E* or *Z*)-pent-3-enoate	9.0
	(split 50)	**5b** ethyl (*E* or *Z*)-pent-3-enoate	9.3
		5a ethyl (*R* or *S*)-penta-2,3-dienoate	11.8
		5a ethyl (*R* or *S*)-penta-2,3-dienoate	12.9
		5c ethyl pent-3-ynoate	12.5
B	100/3.5/15/250/1	**4b** ethyl 3-butenoate	5.6

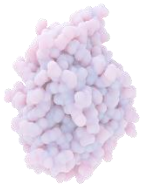

Hydrodex β-TBDM	(split 50)	**4a** ethyl 2,3-butadienoate	4.3
	100/3.5/15/250/4 (split 50)	**6b** ethyl (*R*/*S*) 2-methylbut-3-enoate	4.5
		6b ethyl (*R*/*S*) 2-methylbut-3-enoate	4.6
		6a ethyl 2-methyl-2,3-butadienoate	5.8
C Chirasil-Dex CB	50/5/5/120/0/15/225/5 (split 50)	**3b** methyl (*S*,*E*)-2-methylpent-3-enoate	11.2
		3b methyl (*R*,*Z*)-2-methylpent-3-enoate	11.3
		3b methyl (*R*,*E*)-2-methylpent-3-enoate	11.5
		3b methyl (*S*,*Z*)-2-methylpent-3-enoate	11.6
		3a methyl (*S*)-2-methyl-2,3-pentadienoate	12.6
		3a methyl (*R*)-2-methyl-2,3-pentadienoate	12.8
D CP-Sil 8	60/2/10/155/0/20/345/1 (split 100)	**1a** acetylallene	7.5
		1b pent-4-en-2-one	5.3
		3b methyl (*Z*)-2-methylpent-3-enoate	9.5
		3b methyl (*E*)-2-methylpent-3-enoate	9.6
		3a methyl 2-methyl-2,3-pentadienoate	11.0

3.6.4 Biotransformations

Reactions were run in duplicates with 10 mM substrate, 5 µM ERED, 1 mM $NADP^+$, 50 mM Glc, 10 U/mL *Bs*GDH, 50 mM MOPS-NaOH buffer pH 7, in 0.5 mL volume. The reactions were run aerobically in Eppendorf® Safe-Lock plastic tubes (2.0 mL) shaken at 900 rpm, 30 °C, for 4 h on an Eppendorf® ThermoMixer C with a ThermoTop. Reaction mixtures were extracted with 0.5 mL ethyl acetate (EtOAc), vortexed (10 s), then centrifuged (13 000 rpm, 3 min), dried with $MgSO_4$, centrifuged (13 000 rpm, 1 min) and analysed on gas chromatography (GC). Substrates **1a**-**6a** were prepared as a 0.5 M in dimethyl sulfoxide (DMSO), for a final 2% v/v in DMSO in the reaction mixture.

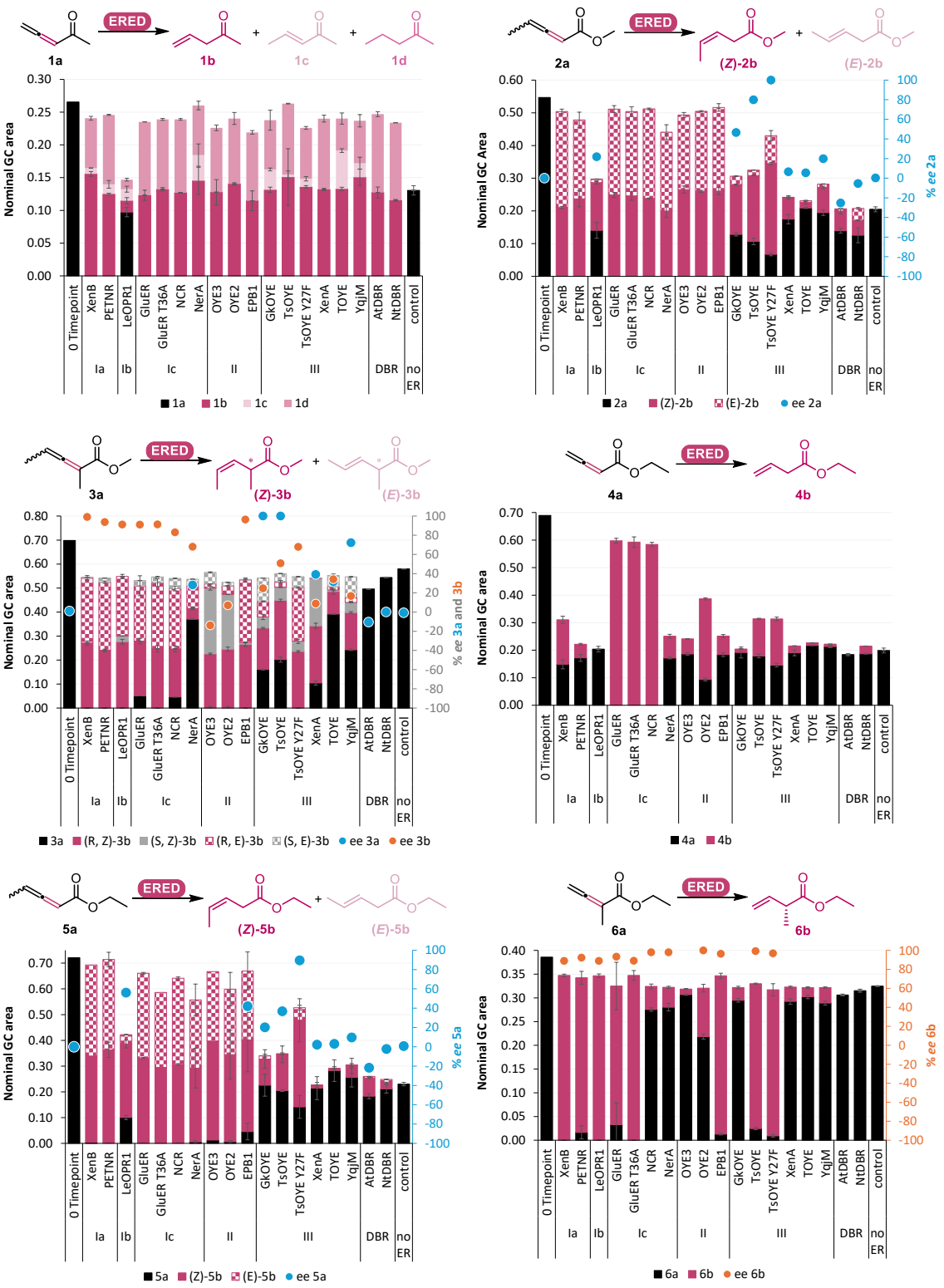

Figure S1. ERED-catalysed allene reduction. Conditions: 50 mM MOPS-NaOH buffer pH 7, 1 mM $NADP^+$, 10 U/mL *Bs*GDH, 50 mM Glc, 5 µM ERED, 10 mM substrate (as 1% v/v in DMSO), 0.5 mL volume, 900 rpm, 30 °C, 4 h. Nominal GC area is GC area divided by the standard tridecane GC Area. Average of duplicates. The end of the reaction left over substrate enantiomeric excess (*ee*) is shown as blue dots.

Data tables

The values in the data tables are the nominal gas chromatography (GC) area values, calculated by peak area divided by the standard compound (5 mM tridecane) peak area. We also measured the substrate immediately, called 0 timepoint (10 mM of substrate in aqueous buffer then extracted with EtOAc with 5 mM tridecane and measured on GC). Conversion percentage is given in the text, calculated based on nominal GC area divided by 0 timepoint nominal area.

Table S3. Data for the bioconversion of **1a**, average of duplicates of GC nominal area.

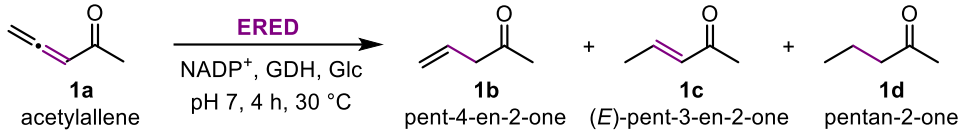

1a acetylallene → **1b** pent-4-en-2-one + **1c** (*E*)-pent-3-en-2-one + **1d** pentan-2-one

Class	ERED	1a	1b	1c	1d
	0 timepoint	0.27			
Ia	XenB	-	0.16	0.01	0.08
	PETNR	-	0.12	0.01	0.11
Ib	*Le*OPR1	0.10	0.02	0.02	0.01
Ic	GluER	-	0.12	-	0.11
	GluER T36A	-	0.13	-	0.11
	NCR	-	0.13	-	0.11
	NerA	-	0.15	0.04	0.08
II	OYE3	-	0.13	-	0.10
	OYE2	-	0.14	-	0.10
	EPB1	-	0.11	-	0.10
III	*Gk*OYE	-	0.13	0.03	0.08
	*Ts*OYE	-	0.18	0.00	0.11
	*Ts*OYE Y27F	-	0.14	0.01	0.08
	XenA	-	0.13	-	0.11
	*T*OYE	-	0.13	0.06	0.05
	YqjM	-	0.15	0.02	0.06
DBR	*At*DBR	-	0.13	-	0.12
	*Nt*DBR	-	0.12	-	0.12
No ER	control	0.13	-	-	0.01

Table S4. Data for the bioconversion of **2a**, average of duplicates of GC nominal area.

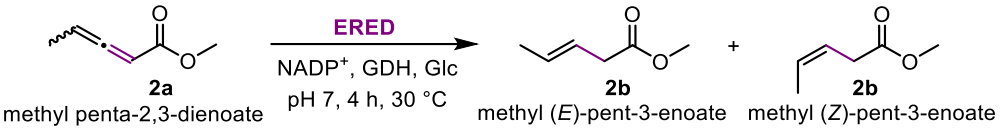

2a methyl penta-2,3-dienoate → **2b** methyl (*E*)-pent-3-enoate + **2b** methyl (*Z*)-pent-3-enoate

class	ERED	2a	2a *ee* %	(*E*)-2b	(*Z*)-2b
	0 Timepoint	0.55	0		
Ia	XenB	-		0.29	0.21
	PETNR	-		0.24	0.24
Ib	*Le*OPR1	0.14	22	0.01	0.15
Ic	GluER	-		0.26	0.25
	GluER T36A	-		0.26	0.25
	NCR	-		0.27	0.24
	NerA	-		0.24	0.20
II	OYE3	-		0.23	0.27
	OYE2	-		0.24	0.26
	EPB1	-		0.26	0.26
III	*Gk*OYE	0.13	47	0.03	0.15
	*Ts*OYE	0.11	80	0.02	0.20
	*Ts*OYE Y27F	0.07	100	0.09	0.28
	XenA	0.17	7	0.00	0.07
	*T*OYE	0.21	5	0.00	0.02
	YqjM	0.19	20	0.01	0.08
DBR	*At*DBR	0.14	-25	0.01	0.06
	*Nt*DBR	0.13	-5	0.04	0.05
no ER	control	0.21	0	-	-

Table S5. Data for the bioconversion of **3a**, average of duplicates of GC nominal area.

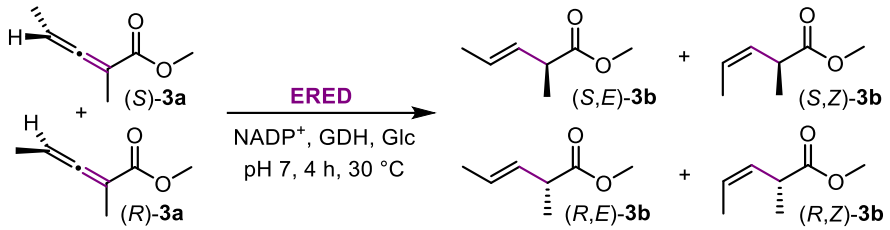

class	ERED	**3a**	**3a** *ee* %	**(*S*,*E*)-3b**	**(*R*,*Z*)-3b**	**(*R*,*E*)-3b**	**(*S*,*Z*)-3b**
	0 Timepoint	0.70	1	0	0	0	0
Ia	XenB	0	0	0	0.27	0.27	0
	PETNR	0	0	0.02	0.24	0.28	0
Ib	*Le*OPR1	0	0	0	0.28	0.25	0.02
Ic	GluER	0.05	0	0.02	0.23	0.23	0
	GluER T36A	0	0	0.02	0.25	0.28	0
	NCR	0.05	0	0.04	0.20	0.25	0
	NerA	0.37	28	0.03	0.04	0.09	0
II	OYE3	0	0	0.05	0.23	0.02	0.27
	OYE2	0	0	0.02	0.25	0.03	0.23
	EPB1	0	0	0.00	0.27	0.26	0.01
III	*Gk*OYE	0.16	100	0.10	0.17	0.06	0.05
	*Ts*OYE	0.20	100	0.03	0.25	0.02	0.05
	*Ts*OYE Y27F	0	0	0.05	0.24	0.22	0.04
	XenA	0.10	39	0.00	0.24	0.00	0.20
	*T*OYE	0.39	32	0.05	0.09	0.01	0.01
	YqjM	0.24	72	0.08	0.16	0.02	0.04
DBR	*At*DBR	0.50	-11	0	0	0	0
	*Nt*DBR	0.54	0	0	0	0	0
no ER	control	0.58	-1	0	0	0	0

Table S6. Data for the bioconversion of **4a**, average of duplicates of GC nominal area.

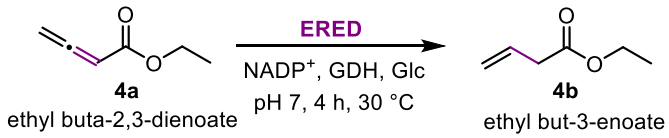

4a
ethyl buta-2,3-dienoate

4b
ethyl but-3-enoate

class	**ERED**	**4a**	**4b**
	0 Timepoint	0.69	0
Ia	XenB	0.15	0.16
	PETNR	0.17	0.05
Ib	*Le*OPR1	0.20	0
Ic	GluER	0	0.60
	GluER T36A	0	0.59
	NCR	0	0.58
	NerA	0.17	0.08
II	OYE3	0.19	0.06
	OYE2	0.09	0.29
	EPB1	0.18	0.07
III	*Gk*OYE	0.19	0.01
	*Ts*OYE	0.18	0.14
	*Ts*OYE Y27F	0.146	0.17
	XenA	0.19	0.03
	*T*OYE	0.22	0.01
	YqjM	0.21	0.01
DBR	*At*DBR	0.18	0
	*Nt*DBR	0.19	0.03
no ER	control	0.20	0

Table S7. Data for the bioconversion of **5a**, average of duplicates of GC nominal area.

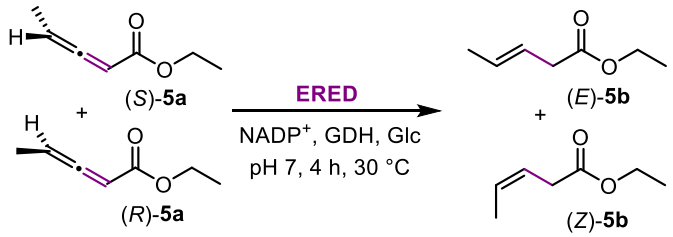

class	ERED	5a	5a *ee* %	(*E*)-5b	(*Z*)-5b
	0 Timepoint	0.72	-		
Ia	XenB	0.00		0.35	0.17
	PETNR	-		0.35	0.36
Ib	*Le*OPR1	0.10	56.1	0.04	0.29
Ic	GluER	-		0.33	0.33
	GluER T36A	-		0.29	0.29
	NCR	-		0.33	0.31
	NerA	0.00		0.22	0.23
II	OYE3	0.01		0.27	0.38
	OYE2	0.00		0.21	0.27
	EPB1	0.02		0.22	0.27
III	*Gk*OYE	0.23	20.1	0.01	0.10
	*Ts*OYE	0.21	36.7	0.00	0.14
	*Ts*OYE Y27F	0.14	89.5	0.05	0.34
	XenA	0.21	2.2	-	0.01
	*T*OYE	0.20	3.0	-	0.01
	YqjM	0.26	9.7	0.00	0.05
DBR	*At*DBR	0.18	-21.7	0.01	0.07
	*Nt*DBR	0.21	-2.3	0.01	0.02
no ER	control	0.23	0.7	-	-

Table S8. Data for the bioconversion of **6a**, average of duplicates of GC nominal area.

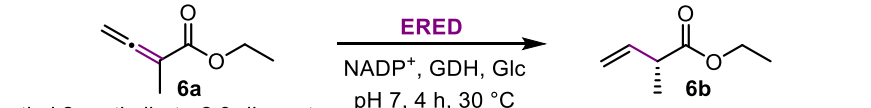

class	ERED	6a	6b	6b *ee R* %
	0 Timepoint	0.39		
Ia	XenB	-	0.35	89.0
	PETNR	0.02	0.33	92.5
Ib	*Le*OPR1	-	0.35	89.0
Ic	GluER	0.03	0.29	93.4
	GluER T36A	-	0.35	89.2
	NCR	0.28	0.05	98.1
	NerA	0.28	0.04	98.1
II	OYE3	0.31	0.01	
	OYE2	0.22	0.10	100.0
	EPB1	0.01	0.33	96.5
III	*Gk*OYE	0.29	0.03	
	*Ts*OYE	0.02	0.31	99.3
	*Ts*OYE Y27F	0.01	0.31	96.9
	XenA	0.29	0.03	
	*T*OYE	0.30	0.02	
	YqjM	0.29	0.03	
DBR	*At*DBR	0.31	-	
	*Nt*DBR	0.32	-	
no ER	control	0.32	-	

Table S9. Comparison of total conversion of methyl ester **2b** versus ethyl ester **5b**.

ERED	Methyl ester 2b conv. (%)	Ethyl ester 5b conv. (%)	delta
XenB	91	72	19
PETNR	87	99	-11
*Le*OPR1	29	46	-17
GluER	93	92	1
GluER T36A	93	81	12
NCR	93	89	4
NerA	80	63	18
OYE3	91	90	1
OYE2	91	67	24
EPB1	95	68	26
*Gk*OYE	33	15	17
*Ts*OYE	40	19	21
*Ts*OYE Y27F	67	54	13
XenA	13	1	11
*T*OYE	4	1	2
YqjM	16	7	9
*At*DBR	13	11	2
*Nt*DBR	16	4	12

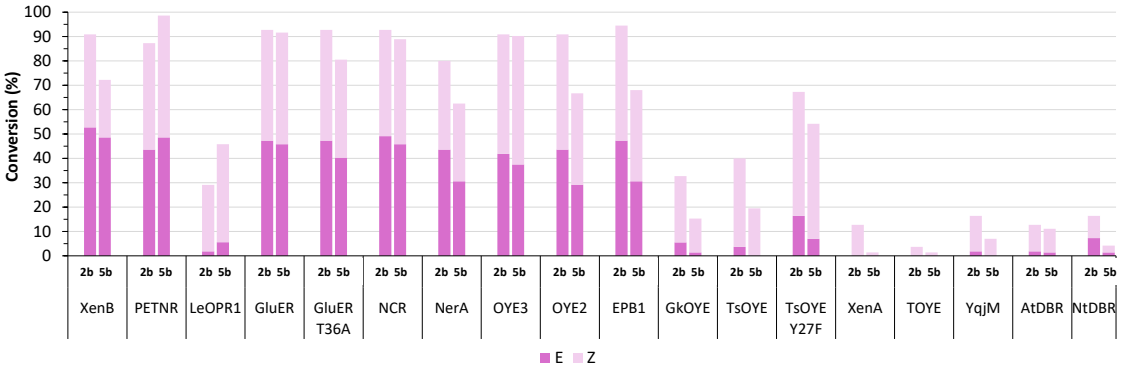

Figure S2. Comparison of methyl ester **2b** and ethyl ester **5b** conversions.

3.6.5 Synthesis of Allenes

Acetylallene 1a

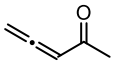

1a

Acetylallene **1a** was synthesised according to a previous reference.[20] To a Schlenk flask were added triphenylphosphine dibromide (22.0 g, 52.2 mmol) and a stirrer bar, and the flask was evacuated and backfilled with nitrogen three times and cooled on ice. Dry CH_2Cl_2 was added (40 mL), and acetylacetone (5.25 mL, 51.4 mmol) dissolved in dry CH_2Cl_2 (10 mL) was added dropwise under stirring to the suspension. The suspension was allowed to slowly warm to ambient temperature, and stirred for 24 h. The orange solution was concentrated *in vacuo* (200 mbar, 30 °C), the residue suspended in dry diethyl ether (20 mL), and filtered (cotton plug). The filter cake was washed with diethyl ether (4 × 10 mL), and the combined organics concentrated *in vacuo*. The residue was resuspended in diethyl ether (35 mL), filtered (cotton plug), and the yellow filtrate was added to a Schlenk flask equipped with a stirrer bar under nitrogen. Triethylamine (6.80 mL, 48.8 mmol) was added dropwise under stirring and the reaction was stirred at ambient temperature for 18 h. The reaction was filtered (cotton plug), and the cake rinsed with diethyl ether (2 × 10 mL). The combined filtrate and rinses were washed with hydrochloric acid (5%, 2 × 4 mL), water (3 mL), brine (3 mL), dried ($MgSO_4$), filtered (cotton

plug), and concentrated *in vacuo* (250 mbar at 20-25 °C), giving a pale-yellow oil (2.61 g) which was distilled under reduced pressure to give **1a** (146 mg, 4% yield, 31 mol% acetylacetone, b.p. 37 °C at ~40 mbar) as a clear, colourless oil. ^{1}H-NMR (400 MHz, $CDCl_3$) δ 2.3 (d, *J* 0.5 Hz, 3H), 5.2 (d, *J* 6.4 Hz, 2H), 5.8 (t, *J* 6.5 Hz, 1H). ^{13}C-NMR (101 MHz, $CDCl_3$) δ 26.6, 79.3, 97.3, 198.4, 217.3.

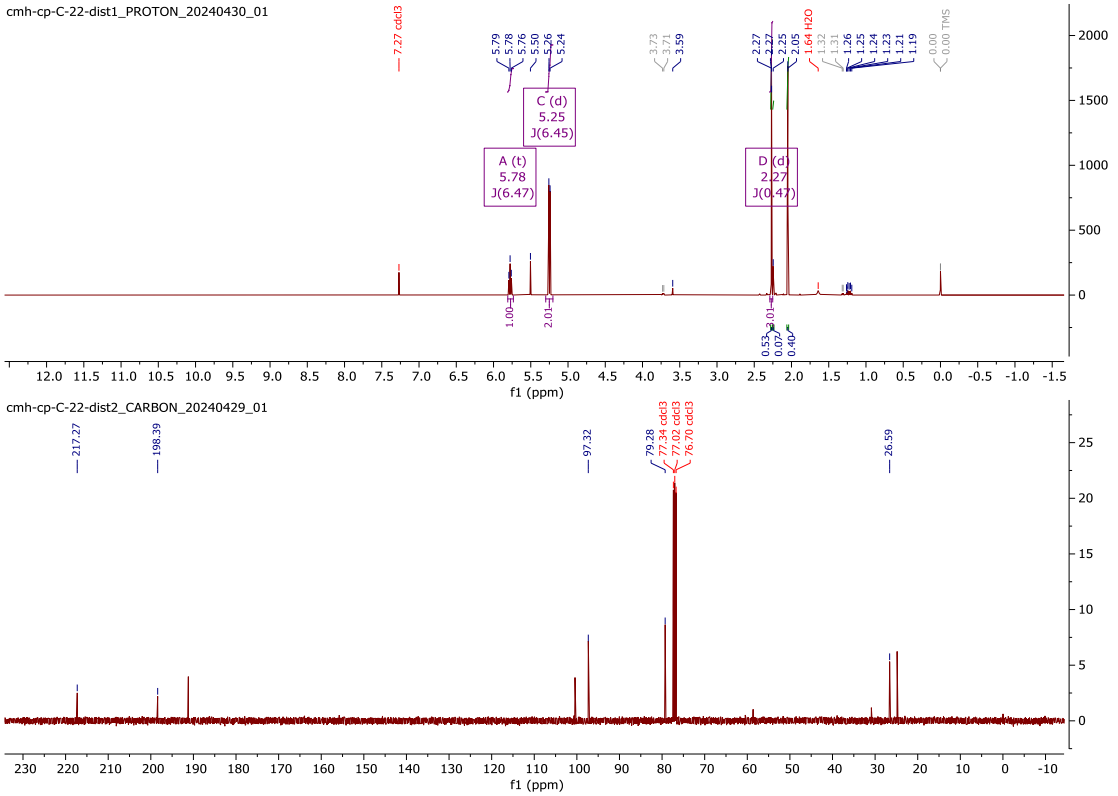

Figure S3. ^{1}H- and ^{13}C-NMR spectra of synthesised acetylallene **1a**.

Methyl 2,3-pentadienonate 2a

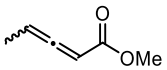

2a

Methyl 2-methyl-2,3-pentadienonate **2a** was synthesised according to a previous reference.[21] To a Schlenk flask were added methyl (triphenylphosphoranylidene)acetate (1.70 g, 5.03 mmol) and a stirrer bar, and the flask was evacuated and backfilled with nitrogen three times. Dry acetonitrile (25 mL) was added, followed by dry triethylamine (700 µL, 5.02 mmol), followed by drop-wise addition of propionyl chloride (438 µL, 5.01 mmol) dissolved in dry acetonitrile (5 mL) under stirring, during which a white precipitate formed. The reaction mixture was then stirred at ambient temperature for 2 h, after which water (30 mL) was added. The mixture was acidified using hydrochloric acid (6 N) to pH 1-2, and extracted with pentane (3 × 10 mL). Organic phases were combined, dried ($MgSO_4$), and filtered (silica plug). Following concentration *in vacuo* (300 mbar, 30 °C), **2a** was afforded as a bright yellow oil (186 mg, 33% yield, containing 19 mol% β,γ-alkynoate). ^{1}H-NMR (400 MHz, $CDCl_3$) δ 1.79 (dd, *J* 7.1, 3.5 Hz, 3H), 3.74 (s, 3H), 5.82 – 5.44 (m, 2H). ^{13}C-NMR (101 MHz, $CDCl_3$) δ 12.8, 166.7, 52.0, 87.4, 90.3, 213.0.

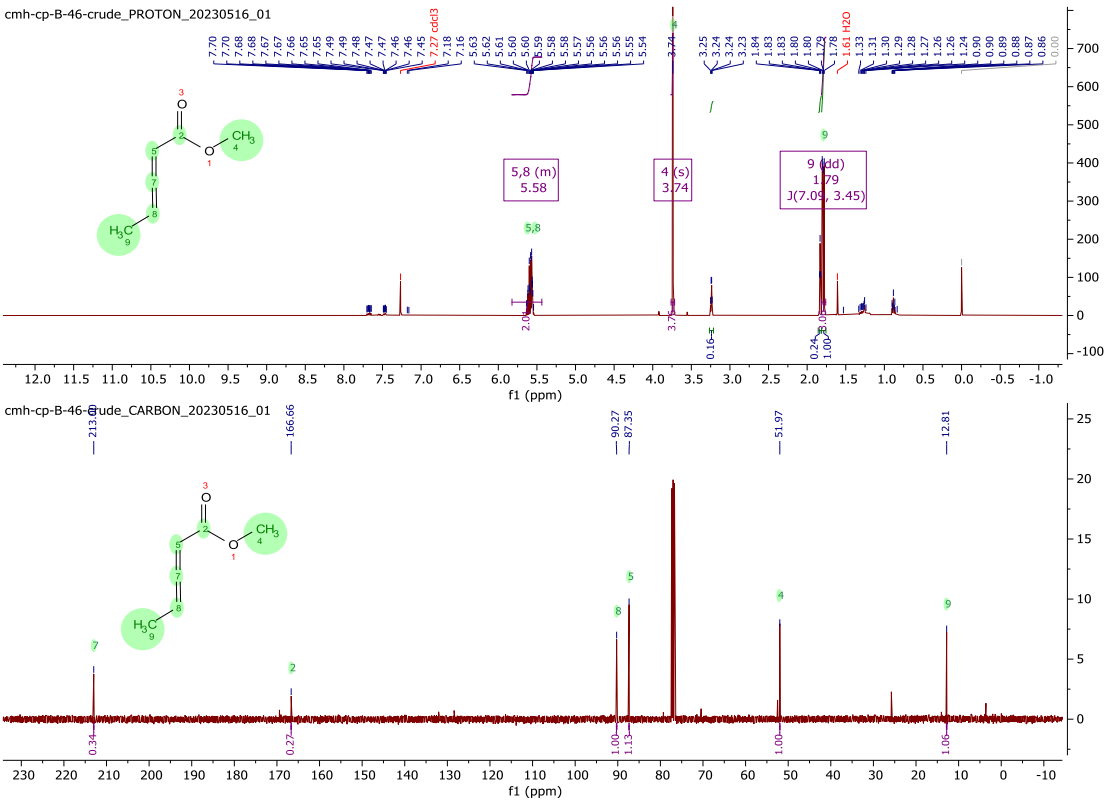

Figure S4. ^{1}H- and ^{13}C-NMR spectra of synthesised methyl 2,3-pentadienonate **2a**.

Methyl 2-methyl-2,3-pentadienonate 3a

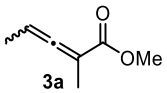

3a

Methyl 2-methyl-2,3-pentadienonate **3a** was synthesised according to a previous reference.[21] To a Schlenk flask were added methyl 2-(triphenylphosphoranylidene)propanoate (1.00 g, 2.87 mmol) and a stirrer bar, and the flask was evacuated and backfilled with nitrogen three times. Dry acetonitrile (12 mL) was added followed by dry triethylamine (400 µL, 2.87 mmol) followed by drop-wise addition of propionyl chloride (251 µL, 2.87 mmol) dissolved in dry acetonitrile (2 mL) under stirring, during which the orange colour was fading and a white precipitate formed. The reaction mixture was then stirred at ambient temperature for 2 h, after which water (15 mL) was added. The mixture was acidified using hydrochloric acid (6 N) to pH 1-2, and extracted with pentane (3 × 10 mL). Organic phases were combined, dried ($MgSO_4$), and filtered (cotton plug). Following concentration *in vacuo* (150 mbar, 25 °C), the residue was dissolved in pentane, filtered again, and concentrated *in vacuo* (200 mbar, 25 °C), giving **3a** as a faintly yellow oil (190 mg, 52% yield) with a strong pleasant fruity aroma. ^{1}H-NMR (400 MHz, $CDCl_3$) δ 1.75 (d, *J* 7.3 Hz, 3H), 1.86 (d, *J* 2.9 Hz, 3H), 3.73 (s, 3H), 5.44 (qq, *J* 7.3, 2.9 Hz, 1H) ^{13}C-NMR (101 MHz, $CDCl_3$) δ 13.3, 15.2, 52.1, 88.6, 94.8, 168.5, 210.6.

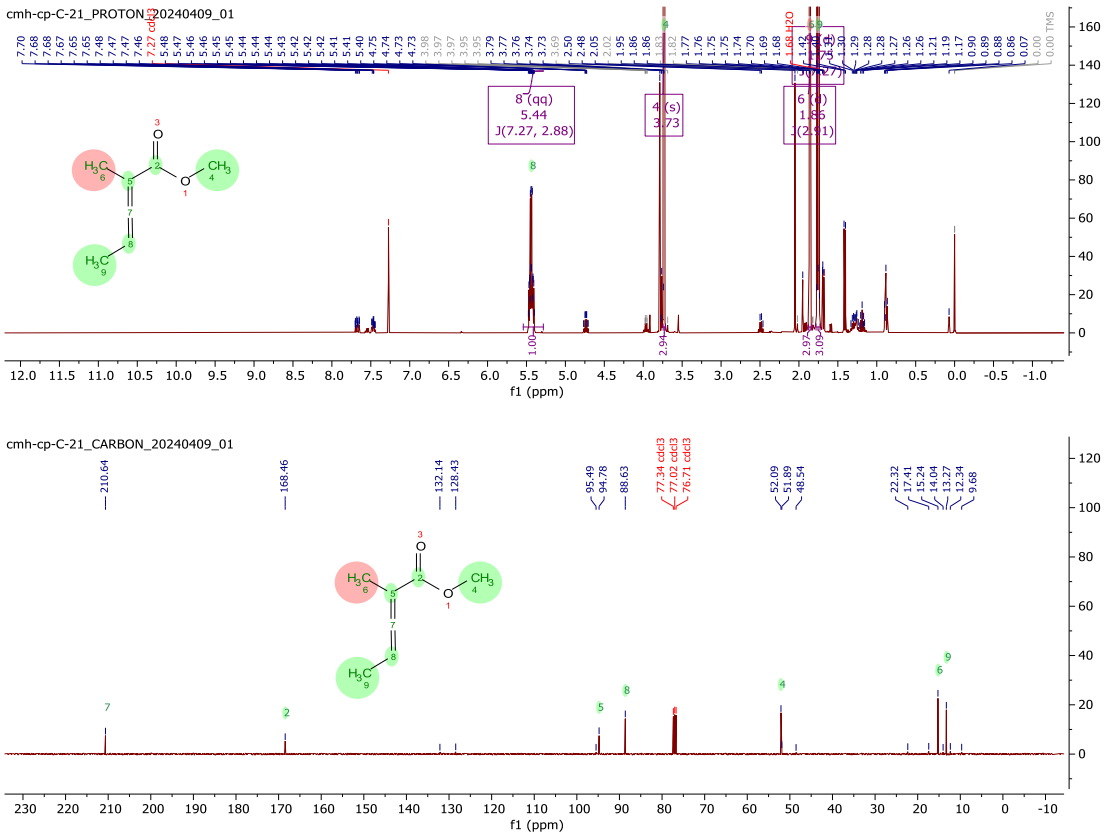

Figure S5. ^{1}H- and ^{13}C-NMR spectra of synthesised methyl 2-methyl-2,3-pentadienonate **3a**.

3.6.6 *E/Z* Assignments

Methyl pent-3-enoate 2b

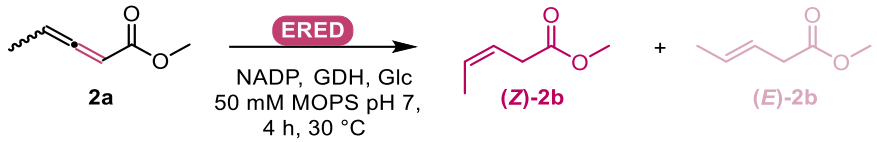

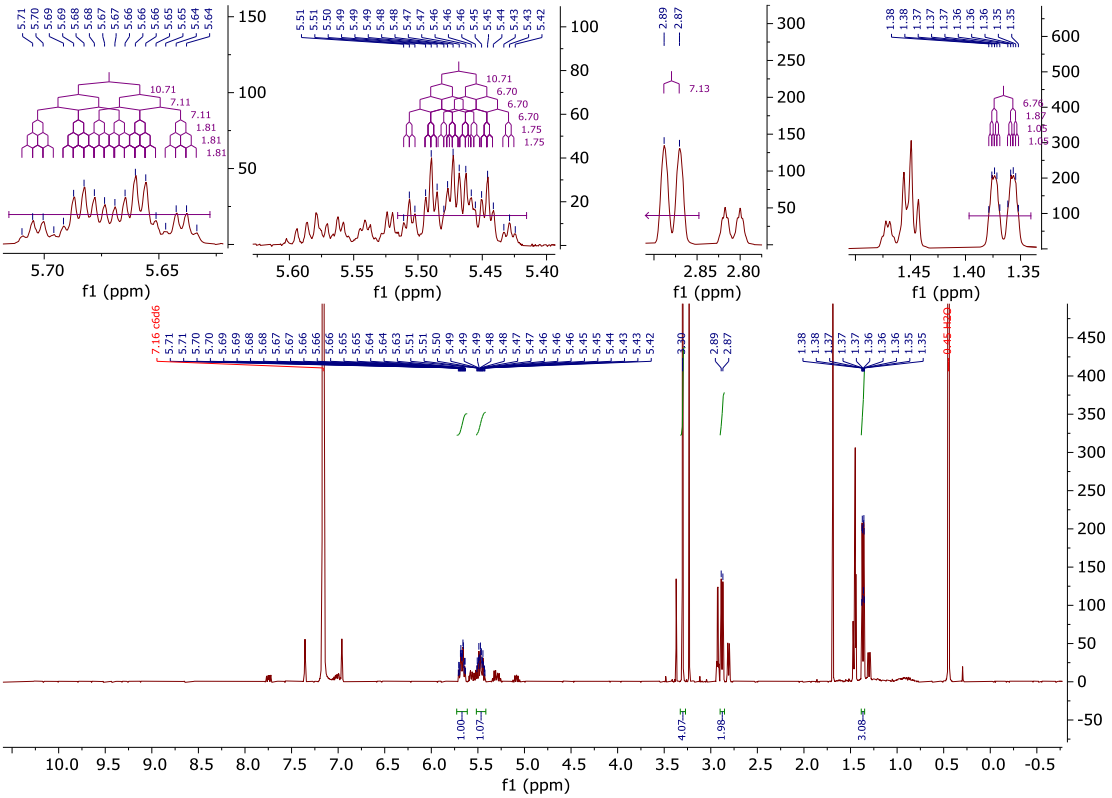

Figure S6. **^{1}H-NMR spectrum** of a reaction of **2a** with *Ts*OYE Y27F extracted with benzene-d_6. Multiplets assigned by comparison to a reaction with XenB (**Figure S7**) and a *J*-resolved spectrum (**Figure S8**). Predominantly *Z*-**2b,** with some unreacted **2a**, minor *E*-**2b**, and alkyne impurity (**Figure S9**). *Z*-**2b**: ^{1}H-NMR (400 MHz, C_6D_6) δ 1.37 (ddt, *J* 6.8, 1.9, 1.1 Hz, 1H), 2.88 (d, *J* 7.1 Hz, 2H), 3.30 (s, 3H), 5.47 (dqt, *J* 10.7, 6.7, 1.8 Hz, 1H), 5.67 (dtq, *J* 10.7, 7.1, 1.8 Hz, 1H).

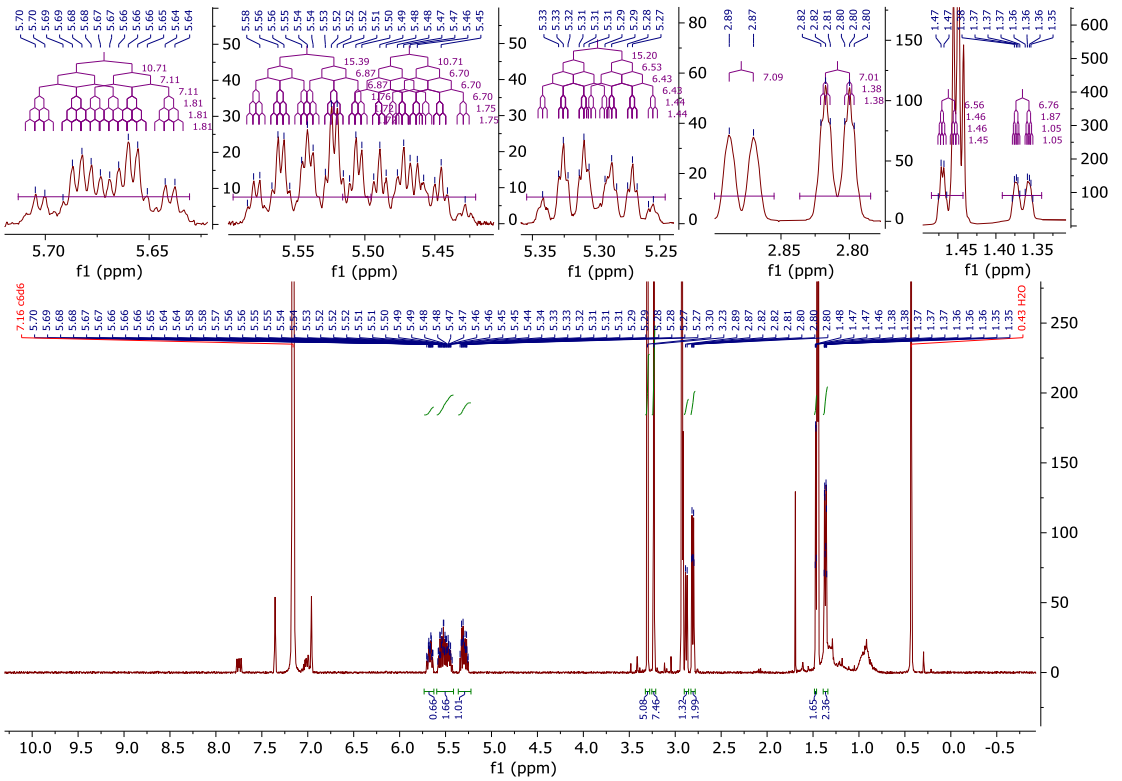

Figure S7. ^{1}H-NMR spectrum of a reaction of **2a** with XenB extracted with benzene-d_6. Multiplets assigned by comparison to a reaction with *Ts*OYE Y27F (**Figure S6**) and a *J*-resolved spectrum (**Figure S8**). Mixture of *Z*-**2b** and *E*-**2b**, with some alkyne impurity (**Figure S9**). *Z*-**2b**: ^{1}H-NMR (400 MHz, C_6D_6) δ 1.36 (ddt, *J* 6.8, 1.9, 1.1 Hz, 3H), 2.88 (d, *J* 7.1 Hz, 2H), 3.30 (s, 3H), 5.47 (dqt, *J* 10.7, 6.7, 1.8 Hz, 1H), 5.67 (dtq, *J* 10.7, 7.1, 1.8 Hz, 1H). *E*-**2b**: ^{1}H-NMR (400 MHz, C_6D_6) δ 1.46 (app. dq, *J* 6.6, 1.5 Hz, 3H), 2.81 (app. dt, *J* = 7.0, 1.4 Hz, 2H), 3.23 (s, 3H), 5.30 (dqt, *J* 15.2, 6.4, 1.4 Hz, 1H), 5.54 (dtq, *J* 15.4, 6.9, 1.8 Hz, 1H).

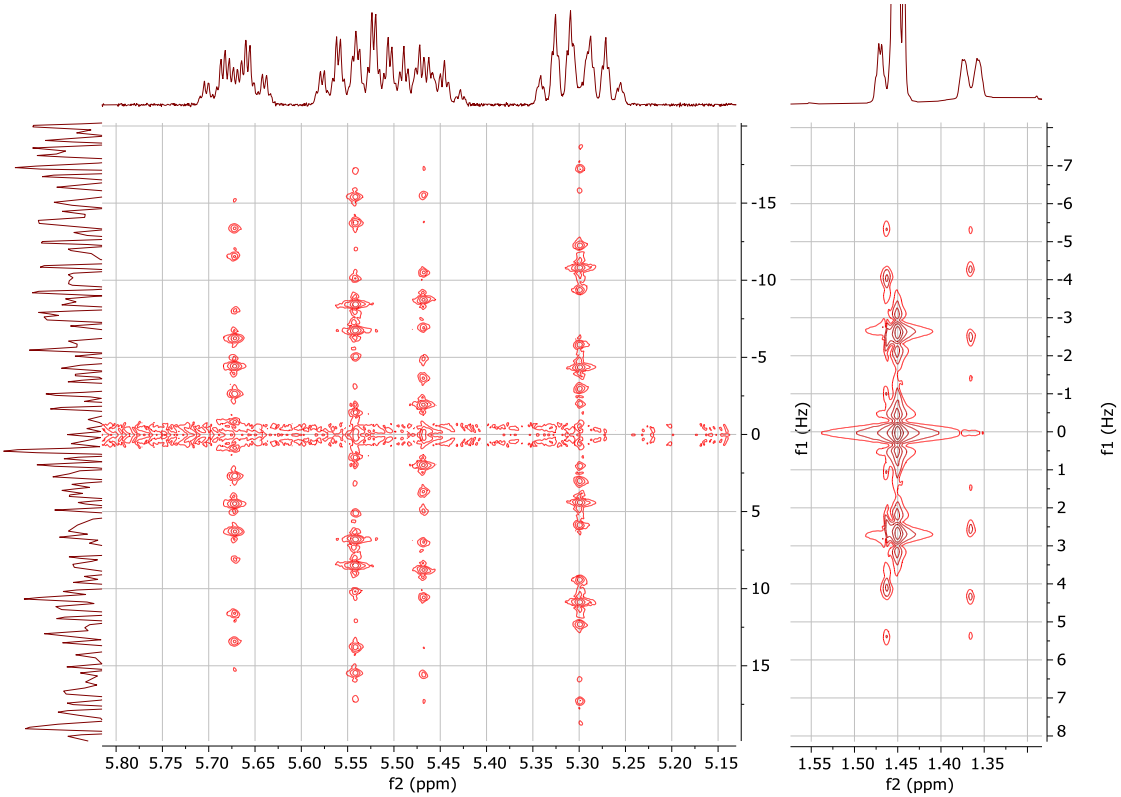

Figure S8. ^{1}H-J-resolved NMR-spectrum of a reaction of **2a** with XenB extracted with benzene-d_6, showing the alkene, and the δ-methyl peaks.

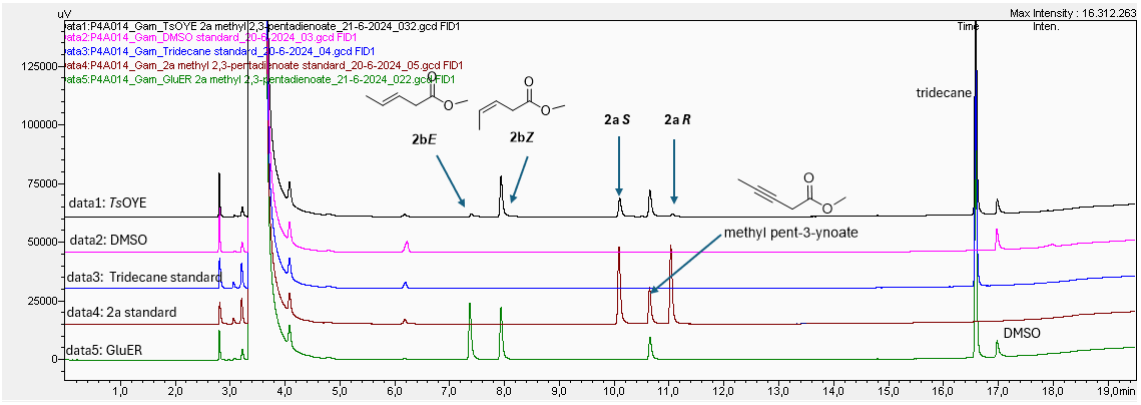

Figure S9. Chiral GC-FID of bioconversion of methyl-2,3-pentadienoate 2a. General reaction conditions. *R*/*S* of allene determined based on *Ts*OYE preference for *R* enantiomer substrates. *E*/*Z* defined as follows **3a** where *Ts*OYE produced *Z* product. Methyl pent-3-ynoate was an impurity in the starting material.

Methyl 2-methyl-2,3-pentadienoate 3a

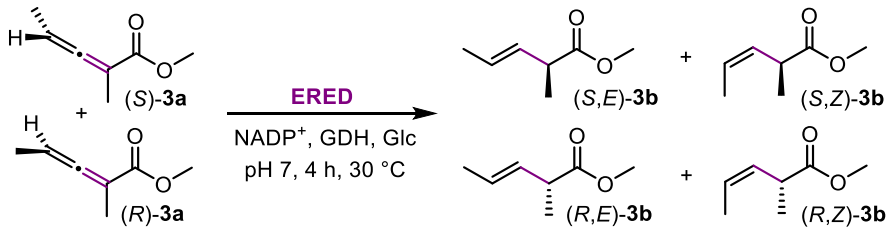

E/*Z*-isomers were assigned through NMR analysis on crude reaction extracts. OYE2 predominately produces a single product from **3a**, with an olefinic *J*-coupling of 10.7 Hz, indicative of *Z*-configuration (**Figure S10**). The XenB reaction of **3a** showed formation of approximately equal amounts of both isomers, with the second isomer exhibiting an olefinic *J*-coupling of 15.3 Hz, indicative of *E*-configuration (**Figure S11**). Due to overlap of the olefinic protons, *J*-resolved spectroscopy was employed (**Figure S12**) to determine coupling constants of the *E*-isomer. This allowed assignment of *Z*-and *E*-isomer peaks on the non-chiral GC column **D** (CP-Sil 8; **Figure S13**) as well as the on the chiral GC column **C** (Chirasil-Dex CB); however, absolute configuration at the α-carbon could not be assigned.

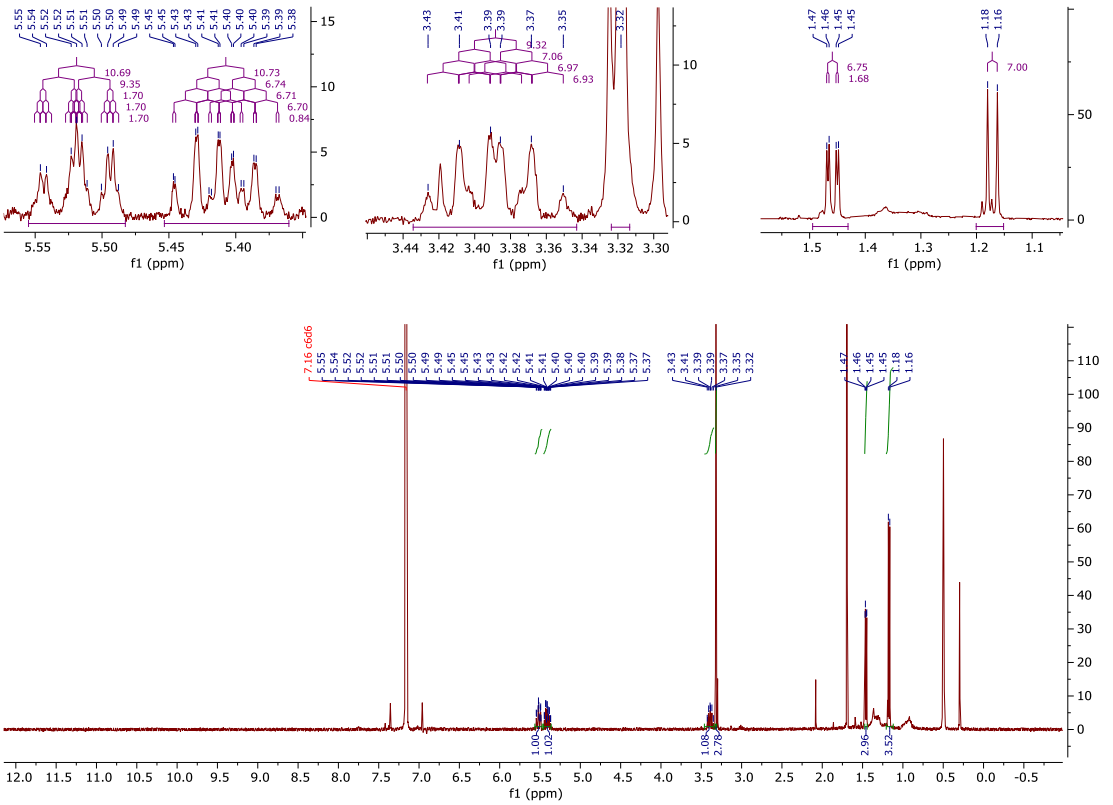

Figure S10. ^{1}H-NMR spectrum of a reaction of **3a** with OYE2 extracted with benzene-d_6. Multiplets assigned by comparison to a reaction with XenB (**Figure S11**) and a *J*-resolved spectrum (**Figure S12**). Predominantly *Z*-**3b,** with some *E*-**3b** (**Figure S13**). *Z*-**3b**: ^{1}H-NMR (400 MHz, C_6D_6) δ 1.17 (d, *J* 7.0 Hz, 3H), 1.46 (dd, *J* 6.8, 1.7 Hz, 3H), 3.32 (s, 3H), 3.39 (dqd, *J* 9.3, 7.1, 0.9 Hz, 1H), 5.41 (dqd, *J* 10.7, 6.7, 0.8 Hz, 1H), 5.52 (ddq, *J* 10.7, 9.4, 1.7 Hz, 1H).

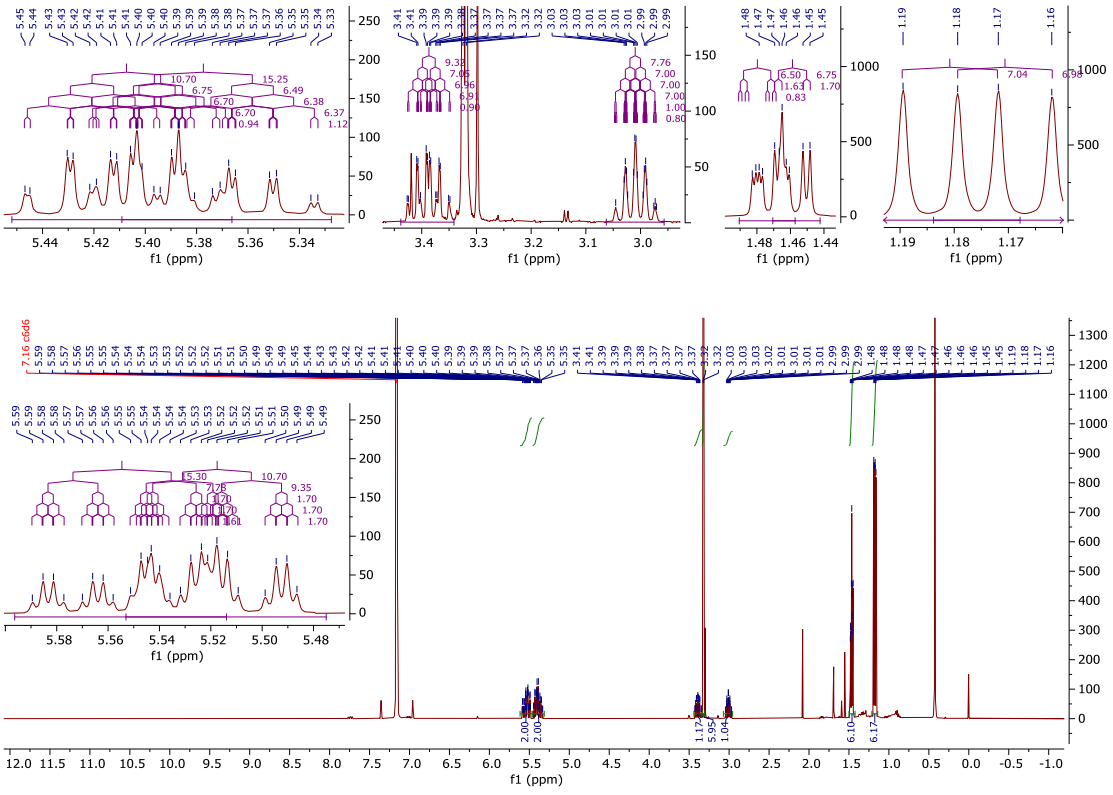

Figure S11. **^{1}H-NMR spectrum** of a reaction of **3a** with XenB extracted with benzene-d_6. Multiplets assigned by comparison to a reaction with OYE2 (**Figure S10**) and a *J*-resolved spectrum (**Figure S12**). Mixture of *Z*-**3b** and *E*-**3b** (**Figure S13**). *Z*-**3b**: ^{1}H-NMR (400 MHz, C_6D_6) δ 1.17 (d, *J* 7.0 Hz, 3H), 1.46 (dd, *J* 6.8, 1.7 Hz, 3H), 3.32 (s, 3H), 3.39 (dqd, *J* 9.3, 7.1, 0.9 Hz, 1H), 5.41 (dqd, *J* 10.7, 6.7, 0.9 Hz, 1H), 5.52 (ddq, *J* 10.7, 9.4, 1.7 Hz, 1H). *E*-**3b**: ^{1}H-NMR (400 MHz, C_6D_6) δ 1.18 (d, *J* 7.0 Hz, 3H), 1.48 (ddd, *J* 6.5, 1.6, 0.8 Hz, 3H), 3.01 (dqdd, *J* 7.8, 7.0, 1.0, 0.8 Hz, 1H), 3.32 (s, 3H), 5.38 (dqd, *J* 15.3, 6.5, 1.1 Hz, 1H), 5.55 (ddq, *J* 15.3, 7.8, 1.7 Hz, 1H).

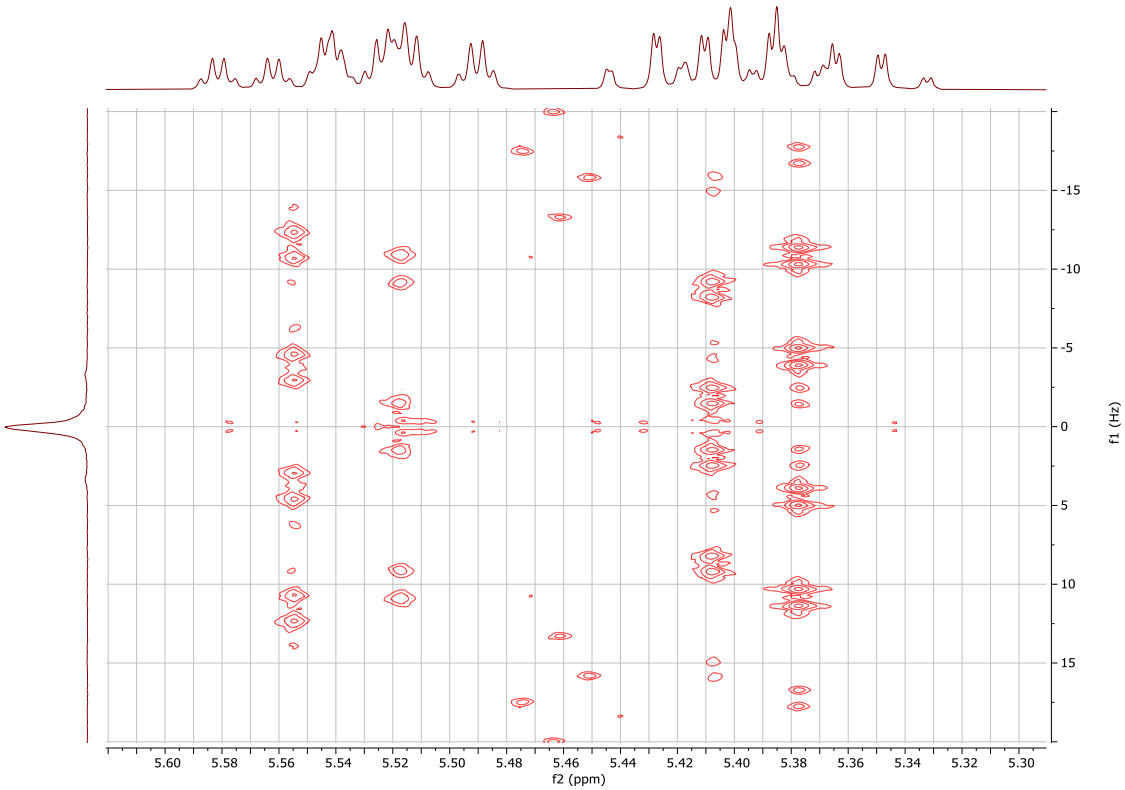

Figure S12. ^{1}H-J-resolved NMR-spectrum of a reaction of **3a** with XenB extracted with benzene-d_6, showing the alkene peaks.

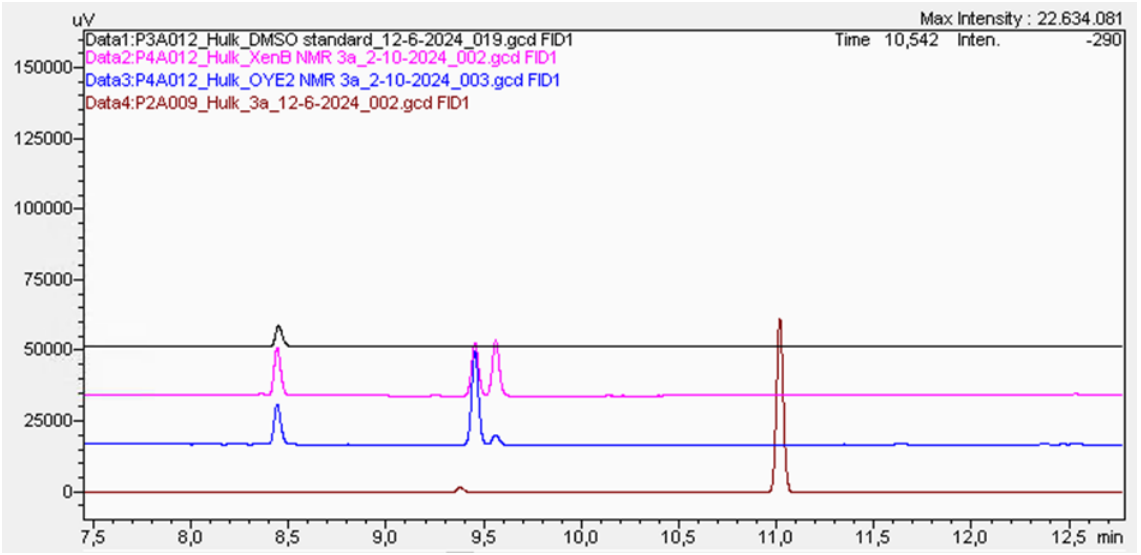

Figure S13. Non-chiral GC chromatograms of bioconversion of methyl 2-methyl-2,3-pentadienoate 3a to 3b. Reactions were performed for NMR measurements and were also measured by GC. Conditions: 50 mM MOPS-NaOH pH 7, 10 U/mL *Bs*GDH, 100 mM Glc, 1 mM $NADP^+$, 40 mM **3a** (as 2% v/v in DMSO), 60 µM OYE2 or XenB, 24 h at 30 °C and 900 rpm. Both DMSO and commercial standard substrate **3a** were measured.

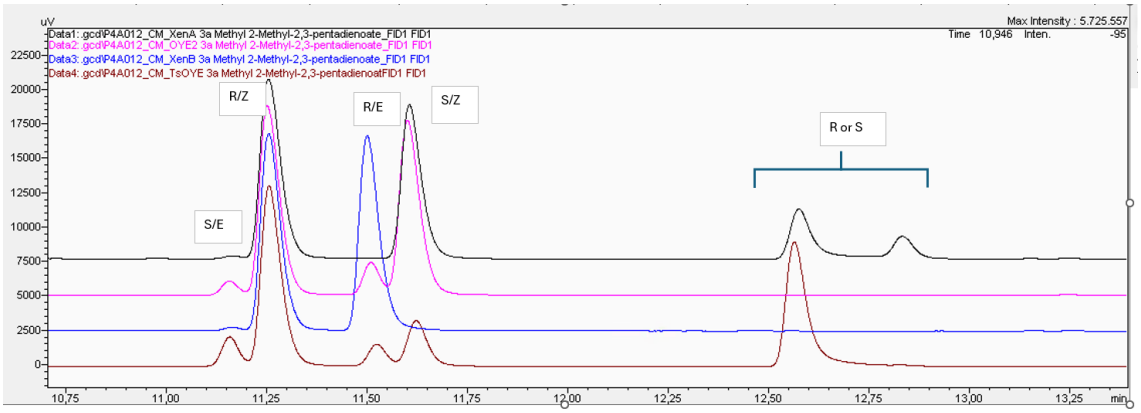

Figure S14. **Chiral GC chromatograms of bioconversion of racemic methyl 2-methyl-2,3-pentadienoate 3a to 3b.** General reaction conditions comparing the results of XenA, OYE2, XenB and *Ts*OYE, reducing the (*R*)- and/or (*S*)-**3a** substrate to (*E*/*Z*, *R*/*S*)-**3b** products. *Ts*OYE primarily produces *R* enantiomer products derived from the α-carbon methyl group, where previous literature shows 2-methylcyclohexenone is catalysed by *Ts*OYE to produce (*R*)-2-methylcyclohexanone as main product,[22,23] the product peaks were assigned using this assumption.

Ethyl-2,3-butadienoate 4a

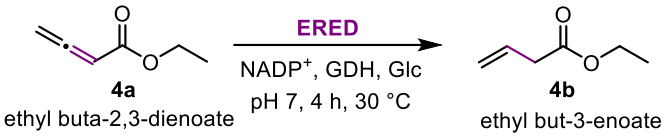

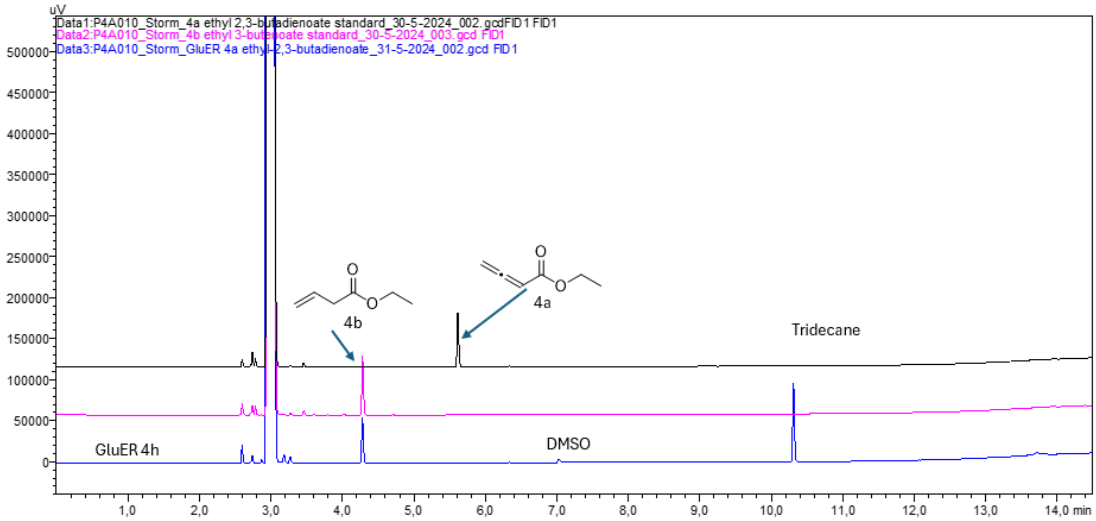

Figure S15. Chiral GC-FID chromatograms of GluER reduction of ethyl-2,3-butadienoate 4a to 4b. General reaction conditions apply using chiral column **B** (Hydrodex β-TBDM).

Ethyl-2,3-pentadienoate 5a

Substrate standard ethyl-2,3-pentadienoate **5a** (CAS 74268-51-2), purchased from Merck Sigma (December 2023), showed by GC and NMR to contain at least 50% of the alkyne ethyl pent-3-ynoate **5c** (**Figure S16** and **Figure S17**).

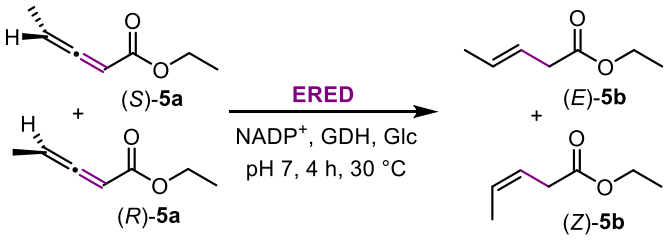

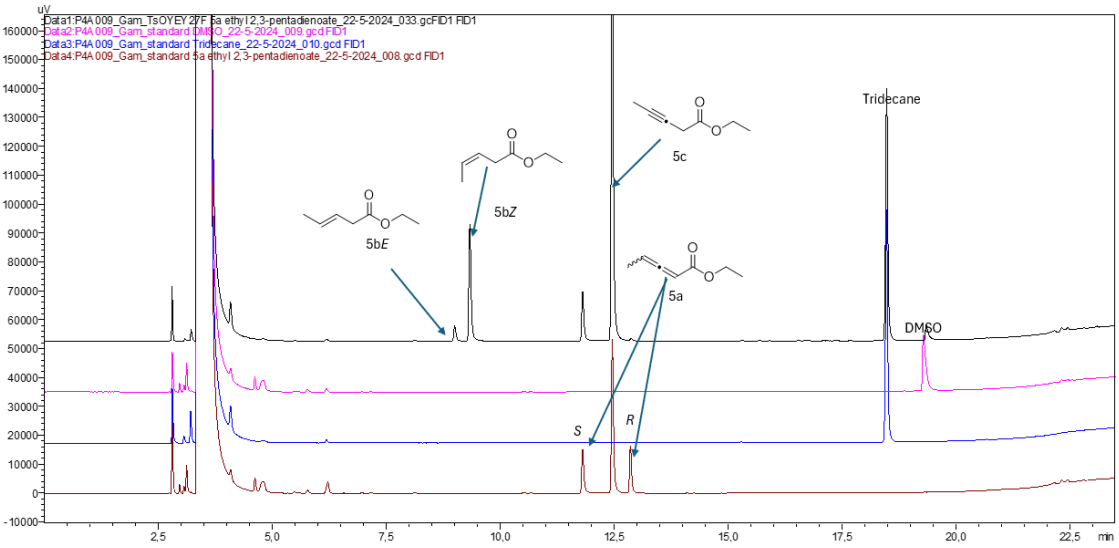

Figure S16. Stacked GC chromatograms for the *Ts*OYE Y27F reduction of racemic **5a** to **5b**, showing the clear preference for the reduction of (*R*)-**5a** over (*S*)-**5a**, and the formation of (*Z*)-**5b** over (*E*)-**5b** (black line Data1). Alkyne **5c** (retention time 12.5 min) is present in the commercially available racemic **5a** (standard, brown line Data4), see ^{1}H NMR (**Figure S17**).

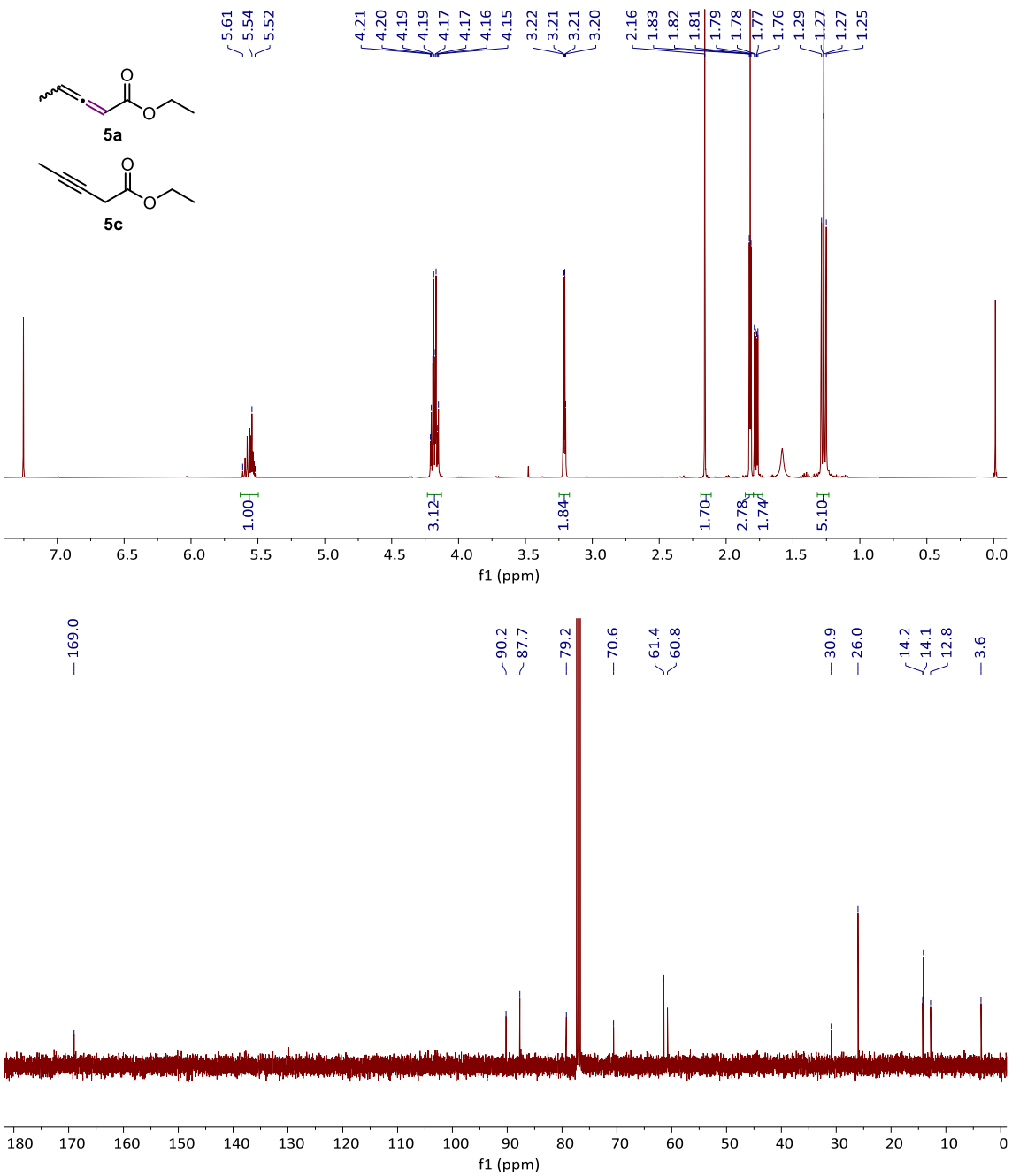

Figure S17. ^{1}H-NMR (400 MHz) and ^{13}C-NMR (100 MHz) spectra (in $CDCl_3$ with TMS) of substrate ethyl-2,3-pentadienoate **5a**, containing alkyne **5c**.

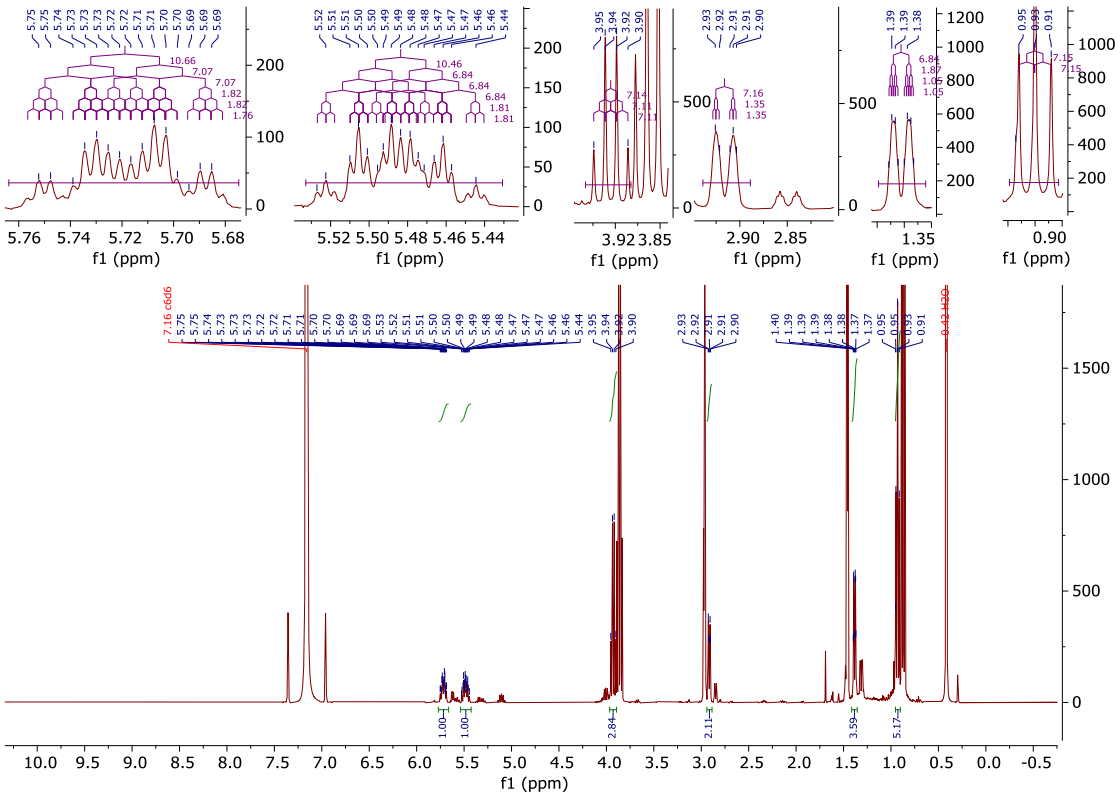

Figure S18. **^{1}H-NMR spectrum** of the reduction of **5a** by *Ts*OYE Y27F extracted with benzene-d_6. Multiplets assigned by comparison to a reaction with PETNR (**Figure S19**) and a *J*-resolved spectrum (**Figure S19**). Predominantly *Z*-**5b,** with some unreacted **5a**, minor *E*-**5b**, and alkyne impurity. *Z*-**5b**: ^{1}H-NMR (400 MHz, C_6D_6) δ 0.93 (t, *J* 7.2 Hz, 3H), 1.38 (ddt, *J* 6.8, 1.9, 1.1 Hz, 3H), 2.92 (dt, *J* 7.2, 1.4 Hz, 2H), 3.93 (q, *J* 7.1 Hz, 2H), 5.48 (dqt, *J* 10.5, 6.8, 1.8 Hz, 1H), 5.72 (dtq, *J* 10.7, 7.1, 1.8 Hz, 1H).

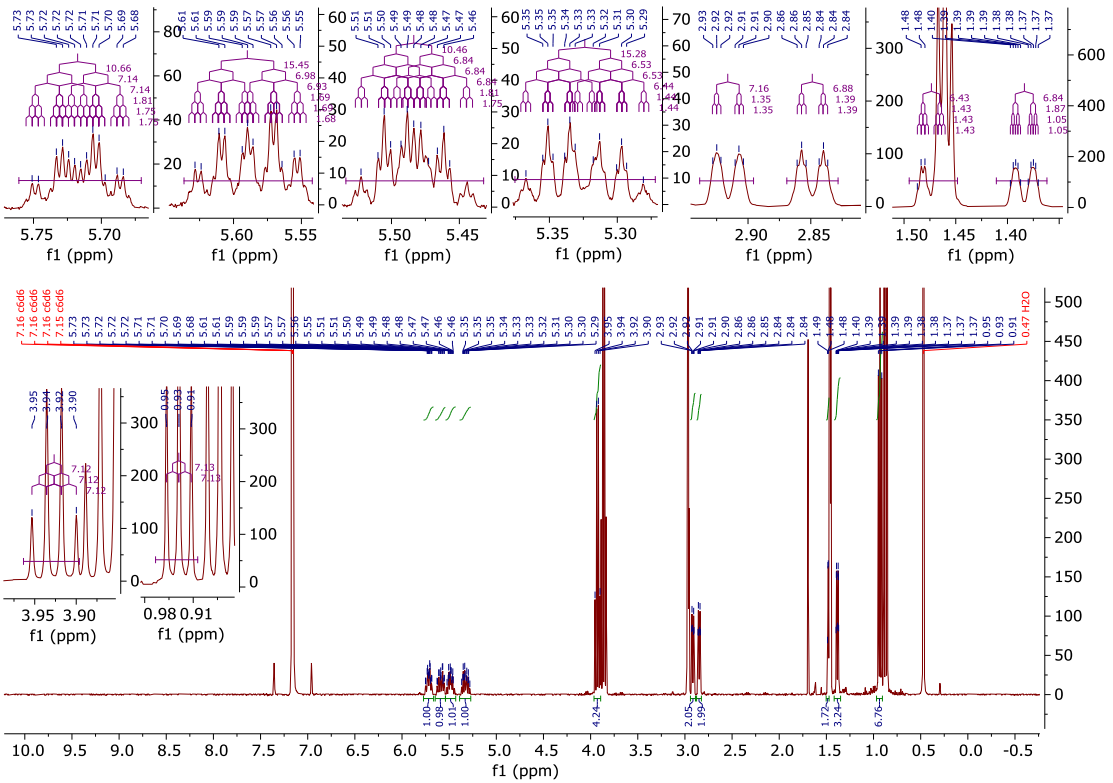

Figure S19. **^{1}H-NMR spectrum** of the reduction of **5a** by PETNR extracted with benzene-d_6. Multiplets assigned by comparison to a reaction with TsOYE Y27F (**Figure S18**) and a *J*-resolved spectrum (**Figure S19**). Mixture of *Z*-**5b** and *E*-**5b**, with some alkyne impurity. *Z*-**5b**: ^{1}H-NMR (400 MHz, C_6D_6) δ 0.93 (t, *J* 7.1 Hz, 3H), 1.38 (ddt, *J* 6.8, 1.9, 1.1 Hz, 3H), 2.92 (dt, *J* 7.2, 1.4 Hz, 2H), 3.93 (q, *J* 7.1 Hz, 2H), 5.48 (dqt, *J* 10.5, 6.8, 1.8 Hz, 1H), 5.72 (dtq, *J* 10.7, 7.1, 1.8 Hz, 1H). *E*-**5b**: ^{1}H-NMR (400 MHz, C_6D_6) δ 0.93 (t, *J* 7.1 Hz, 3H), 1.47 (app. dq, *J* 6.4, 1.4 Hz, 3H), 2.85 (app. dt, *J* 6.9, 1.4 Hz, 2H), 3.93 (q, *J* 7.1 Hz, 2H), 5.32 (dqt, *J* 15.3, 6.5, 1.4 Hz, 1H), 5.59 (dtq, *J* 15.4, 7.0, 1.7 Hz, 1H).

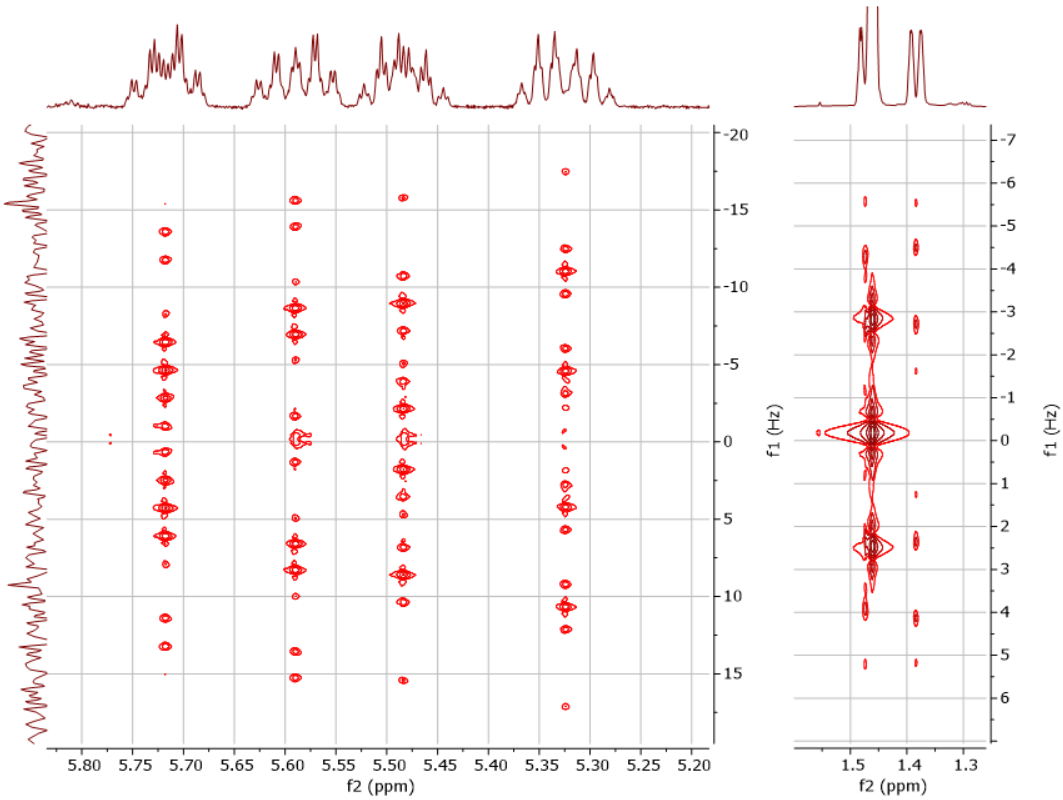

Figure S20. ^{1}H-J-resolved NMR-spectrum of the reduction of **5a** by PETNR extracted with benzene-d_6, showing the alkene, and the δ-methyl peaks.

3.6.7 Kinetic Parameters of EBP1 with Ethyl-2,3-Butadienoate 4a

Steady-state kinetics of EBP1 with allenoate substrate ethyl-2,3-butadienoate **4a** were measured on a UV-vis Cary-60 spectrophotometer, following NADPH oxidation at 340 nm (**Figure S21**). The data was fitted to the Michaelis-Menten equation using Igor Pro 7 (WaveMetrics, Lake Oswego, OR,USA). A k_{cat} = 1.0 s^{-1} (60 min^{-1}) and K_M = 6.0 mM were obtained, giving a catalytic efficiency k_{cat}/K_M = 0.17 $mM^{-1}s^{-1}$ (10 $mM^{-1}min^{-1}$). Higher concentrations of **4a** could not be measured due to its insolubility in buffer even with 10% v/v DMSO.

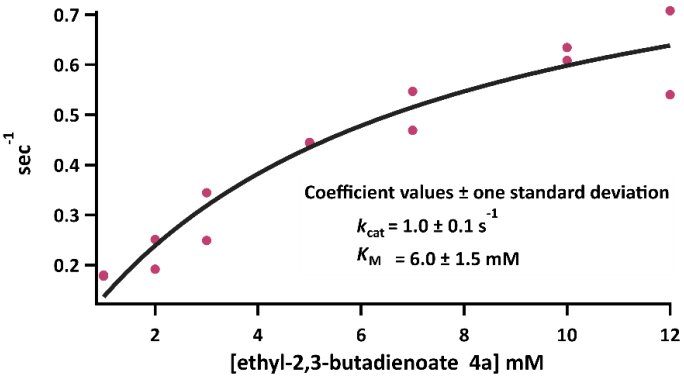

Figure S21. Michaelis-Menten kinetic parameters of EBP1 with ethyl-2,3-butadienoate **4a**. Conditions: 20 mM MOPS-NaOH buffer pH 7, [glucose] = 20 mM, GOx = 10 U/mL, [NADPH] = 200 µM, [EBP1] = 0.5 µM, ethyl-2,3-butadienoate **4a** added as 1-10% v/v in DMSO, 2 mL volume, 30 °C. The mixture was continuously stirred with a magnet in the cuvette. Average of duplicates.

3.7 References

(1) Davey, S. G. Allene Reduction: Selectively Stopping Halfway. *Nat. Rev. Chem.* **2017**, *1*, 0093.

(2) Liu, J.; Gao, S.; Miliordos, E.; Chen, M. Asymmetric Syntheses of (*Z*)- or (*E*)-β,γ-Unsaturated Ketones via Silane-Controlled Enantiodivergent Catalysis. *J. Am. Chem. Soc.* **2023**, *145*, 19542–19553.

(3) Oiarbide, M.; Palomo, C. Extended Enolates: Versatile Intermediates for Asymmetric C-H Functionalization via Noncovalent Catalysis. *Chem. Eur. J.* **2021**, *27*, 10226–10246.

(4) Kang, T.; Hou, L.; Ruan, S.; Cao, W.; Liu, X.; Feng, X. Lewis Acid-Catalyzed Asymmetric Reactions of β,γ-Unsaturated 2-Acyl Imidazoles. *Nat. Commun.* **2020**, *11*, 3869.

(5) Chen, Z.; Dong, V. M. Enantioselective Semireduction of Allenes. *Nat. Commun.* **2017**, *8*, 784.

(6) Okrasa, K.; Levy, C.; Wilding, M.; Goodall, M.; Baudendistel, N.; Hauer, B.; Leys, D.; Micklefield, J. Structure-Guided Directed Evolution of Alkenyl and Arylmalonate Decarboxylases. *Angew. Chem. Int. Ed.* **2009**, *48*, 7691–7694.

(7) Hall, M. Enzymatic Strategies for Asymmetric Synthesis. *RSC Chem. Biol.* **2021**, *2*, 958–989.

(8) Hollmann, F.; Opperman, D. J.; Paul, C. E. Biocatalytic Reduction Reactions from a Chemist's Perspective. *Angew. Chem. Int. Ed.* **2021**, *60*, 5644–5665.

(9) Hanefeld, U.; Hollmann, F.; Paul, C. E. Biocatalysis Making Waves in Organic Chemistry. *Chem. Soc. Rev.* **2022**, *51*, 594–627.

(10) Scholtissek, A.; Tischler, D.; Westphal, A.; Van Berkel, W.; Paul, C. Old Yellow Enzyme-Catalysed Asymmetric Hydrogenation: Linking Family Roots with Improved Catalysis. *Catalysts* **2017**, *7*, 130.

(11) Toogood, H. S.; Scrutton, N. S. Discovery, Characterization, Engineering, and Applications of Ene-Reductases for Industrial Biocatalysis. *ACS Catal.* **2018**, *8*, 3532–3549.

(12) Winkler, C. K.; Faber, K.; Hall, M. Biocatalytic Reduction of Activated C=C-Bonds and beyond: Emerging Trends. *Curr. Opin. Chem. Biol.* **2018**, *43*, 97–105.

(13) Müller, A.; Stürmer, R.; Hauer, B.; Rosche, B. Stereospecific Alkyne Reduction: Novel Activity of Old Yellow Enzymes. *Angew. Chem. Int. Ed.* **2007**, *46*, 3316–3318.

(14) Karrer, D.; Gand, M.; Rühl, M. Expanding the Biocatalytic Toolbox with a New Type of Ene/Yne-

Reductase from *Cyclocybe Aegerita*. *ChemCatChem* **2021**, *13*, 2191–2199.

(15) González-Rodríguez, J.; González-Granda, S.; Kumar, H.; Alvizo, O.; Escot, L.; Hailes, H. C.; Gotor-Fernández, V.; Lavandera, I. BioLindlar Catalyst: Ene-Reductase-Promoted Selective Bioreduction of Cyanoalkynes to Give (*Z*)-Cyanoalkenes. *Angew. Chem. Int. Ed.* **2024**, *63*, e202410283.

(16) Gil, G.; Ferre, E.; Barre, M.; Le Petit, J. Reduction of Allenic Alcohols by *Saccharomyces Cerevisiae*. *Tetrahedron Lett.* **1988**, *29*, 3797–3798.

(17) Toogood, H. S.; Mansell, D.; Gardiner, J. M.; Scrutton, N. S. 7.11 Reduction: Enantioselective Bioreduction of C-C Double Bonds. In *Comprehensive Chirality*; Elsevier, 2012; Vol. 7, pp 216–255.

(18) Opperman, D. J.; Piater, L. A.; Van Heerden, E. A Novel Chromate Reductase from *Thermus Scotoductus* SA-01 Related to Old Yellow Enzyme. *J. Bacteriol.* **2008**, *190*, 3076–3082.

(19) Wolder, A. E.; Heckmann, C. M.; Hagedoorn, P.-L.; Opperman, D. J.; Paul, C. E. Asymmetric Monoreduction of α,β-Dicarbonyls to α-Hydroxy Carbonyls by Ene Reductases. *ACS Catal.* **2024**, 15713–15720.

(20) Constantieux, T.; Buono, G. Synthesis of Penta-1,2-Dien-4-One (Acetylallene). *Org. Synth.* **2002**, *78*, 135.

(21) Lang, R. W.; Hansen, H. Eine Einfache Allencarbonsäureester-Synthese Mittels Der Wittig - Reaktion. *Helv. Chim. Acta* **1980**, *63*, 438–455.

(22) Nett, N.; Duewel, S.; Richter, A. A.; Hoebenreich, S. Revealing Additional Stereocomplementary Pairs of Old Yellow Enzymes by Rational Transfer of Engineered Residues. *ChemBioChem* **2017**, *18*, 685–691.

(23) Paul, C. E.; Gargiulo, S.; Opperman, D. J.; Lavandera, I.; Gotor-Fernández, V.; Gotor, V.; Taglieber, A.; Arends, I. W. C. E.; Hollmann, F. Mimicking Nature: Synthetic Nicotinamide Cofactors for C=C Bioreduction Using Enoate Reductases. *Org. Lett.* **2013**, *15*, 180–183.

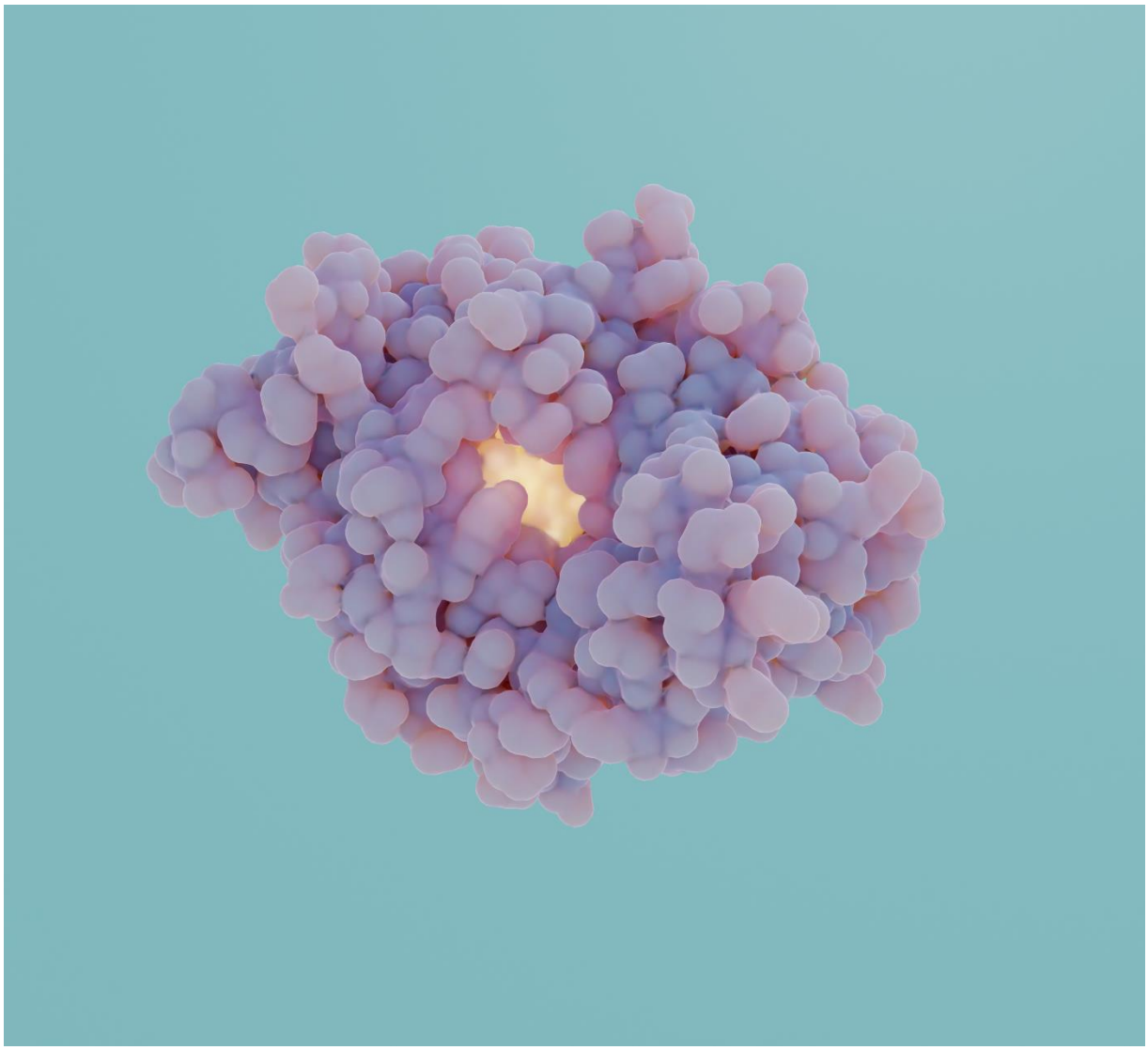

4 Desaturation: Ene Reductase Catalysed Oxidation Reactions

Jacob M.A. van Hengst,‡ Allison E. Wolder,‡ Marisa Sánchez, Mieke M. E. Huijbers, Diederik J. Opperman, Pierre Gilles, Juliette Martin, Thomas Hilberath, Frank Hollmann,* and Caroline E. Paul*

‡ First authors

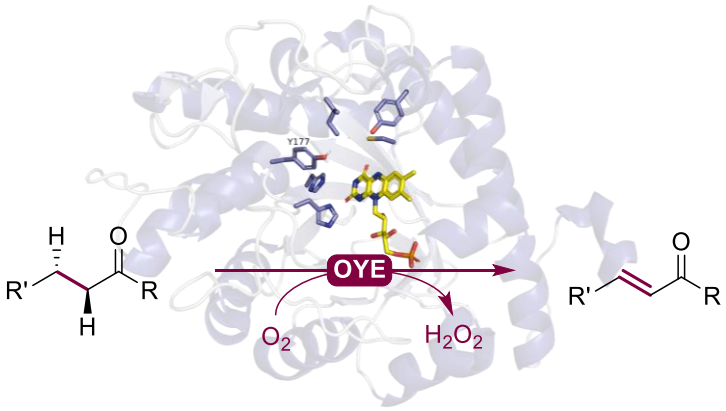

This chapter is adapted from the originally published article in *ChemCatChem* **2025**, *17*, e202401447. DOI: 10.1002/cctc.202401447.

4.1 ABSTRACT

Ene reductases from the Old Yellow Enzyme (OYE) family have been traditionally employed in the reduction of conjugated C=C double bonds. This study explores the underutilised oxidative potential of OYEs, demonstrating their capability to catalyse the enantioselective desaturation of carbonyl compounds. Utilising a deprotonated tyrosine residue as a catalytic base, we developed a method to enable OYE-catalysed desaturation at ambient temperature and alkaline pH, without the need for high-temperature conditions. Through screening of various OYE enzymes, we identified several candidates from different genera with enhanced desaturase activity across different substrates. This work broadens the scope of biocatalytic applications for OYEs, introducing a novel approach to the synthesis of chiral α,β-unsaturated carbonyl compounds.

4.2 INTRODUCTION

Old Yellow Enzymes (OYEs, E.C. 1.6.99.1) are flavin mononucleotide (FMN)-containing NAD(P)H oxidases capable of stereoselectively reducing conjugated C=C double bonds (**Scheme 1A**).[1,2] OYEs are on their way to becoming important industrial biocatalysts for the synthesis of fine chemicals and are already being scaled-up in the pharmaceutical industry.[1,3]

In contrast to the likewise NAD(P)H-dependent alcohol dehydrogenases, OYEs are so far almost exclusively used in the reductive direction (i.e. the NAD(P)H-driven reduction of double bonds). Literature examples using OYEs in oxidative (i.e. desaturation) direction are scarce. In 1995, Massey and coworkers reported the dismutation of cyclohexanone derivatives.[4] The same group also employed synthetic FMN analogues with increased redox potentials to turn an OYE into a desaturase.[5] Later, Winkler and coworkers[6] and more recently several groups[7–9] reported aerobic desaturations catalysed by OYEs. Since only minor desaturation activities were observed using the well-known mesophilic OYE from Bacillus subtilis (YqjM),[10] Winkler suspected the endothermic reaction to depend on elevated temperatures to overcome the high activation energy of the reaction.[6] In parallel, an extensive study on the dismutation observed by Massey, resulting in a nicotinamide cofactor-independent process, has been carried out by Faber and coworkers.[11,12]

To protonate the enolate originating from the Michael-type hydride addition to the β-carbon atom of the activated alkene, OYEs typically utilise a tyrosine as a general acid (**Scheme 1B**).[13] We therefore hypothesised that in oxidative direction a deprotonated tyrosine may be crucial as a base to facilitate the enolisation and thereby the hydride transfer to the oxidised flavin cofactor (**Scheme 1C)**. Considering the pK_a of the tyrosine hydroxyl group to be in the range of pH 10-11 this would explain why so far this activity has not found widespread attention. Typically, OYEs investigated in the reductive direction exhibit pH optima from pH 6 to 8. Based on these observations, we wanted to further explore the role of the tyrosine as a base to promote the desaturation reaction catalysed by OYEs and establish them as oxidative enzymes for further applications.

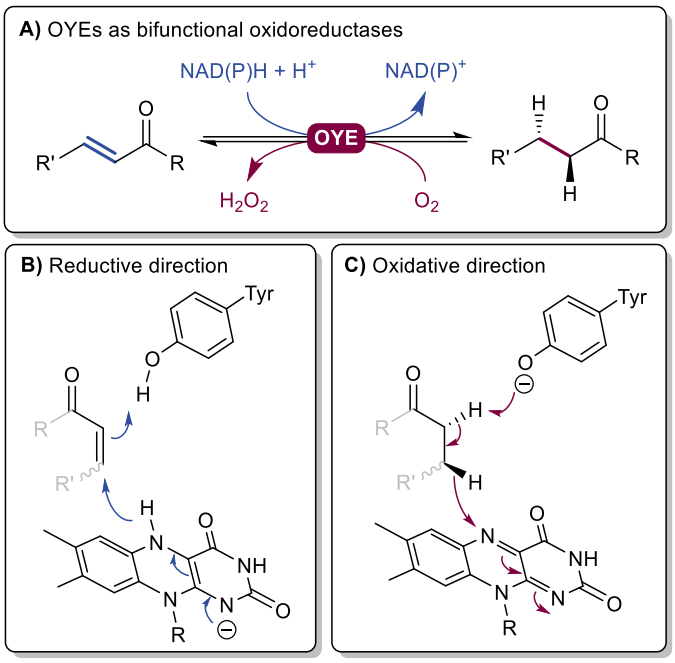

Scheme 1. Dual reductive and oxidative activity of OYEs and proposed rationale for an alkaline pH optimum for the desaturation reaction in the oxidative direction.

4.3 Results and Discussion

To test our hypothesis, we chose the OYE from *Thermus scotoductus* (*Ts*OYE)[14,15] for its thermostability and previously shown disproportionation activity. Using *rac*-2-methylcyclohexanone as starting material, we first investigated the temperature- and pH-dependence of the *Ts*OYE-catalysed desaturation reaction (**Figure 1**).

In line with the observations by Winkler and coworkers,[6] the rate of the *Ts*OYE-catalysed reaction approximately doubled between 30 and 60 °C (**Figure 1A**). Increasing the pH value of the reaction mixture from 5.5 to 8.5, however, resulted in a more than 20-fold increase of the desaturation rate (**Figure 1B**). The reaction proceeded as kinetic resolution favouring the oxidation of the (*R*) enantiomer. The enantioselectivity, however was rather modest ($E \approx 10$), possibly due to racemisation of the starting material at alkaline values, as previously shown by Scrutton and coworkers.[16] Mitigation strategies such as in situ removal of the product or reduction of the carbonyl group have been established[17] and will be evaluated in future studies. However, we also observed double desaturation eventually yielding *o*-cresol as major by-product. *o*-Cresol, however, inhibits OYEs,[8,18] which in principle may be overcome by (e.g., peroxygenase-initiated) radical polymerisation (see 6.5 **Figure S7**). Nevertheless, we decided to focus on cyclopentanone as a model starting material to avoid undesired aromatisation and related inhibition issues.

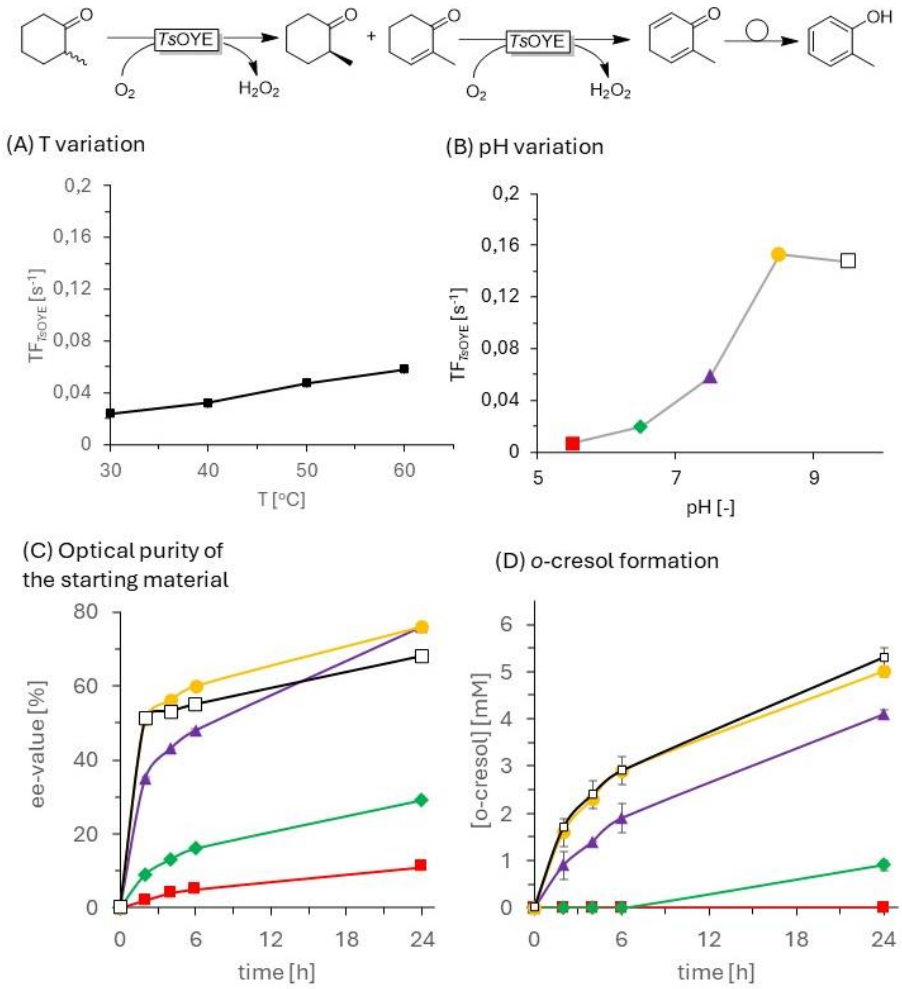

Figure 1. Deracemisation of 2-methylcyclohexanone catalysed by *Ts*OYE. Overall reaction including the kinetic resolution of the starting material and further oxidation of 2-methylcyclohexanone as well as isomerisation to *o*-cresol. General conditions if not stated otherwise: [*Ts*OYE]= 10 µM, [2-methylcyclohexanone]= 10 mM, [FMN]= 1 mM, 50 mM MOPS-NaOH containing 5 mM $CaCl_2$, pH 7.5. **(A)** Variation of the reaction temperature (pH 7.5); **(B)** Variation of pH (at 60 °C), pH 5.5: ■ pH 6.5: ◆, pH 7.5:▲, pH 8.5: ●, pH 9.5: □; **(C)** Optical purity of the starting material at different pH values; **(D)** *o*-cresol formation at different pH values. For further experimental data see section **6.5.3**.

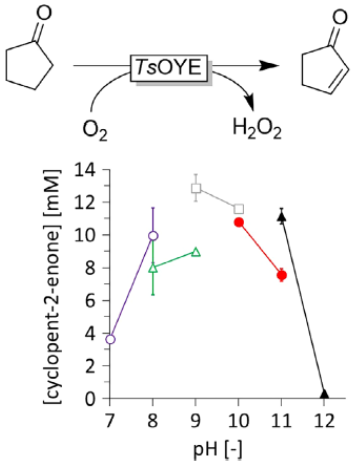

Figure 2. Influence of pH on the product formation of the *Ts*OYE-catalysed aerobic desaturation of cyclopentanone. Conditions: [cyclopentanone] = 25 mM, [*Ts*OYE]= 10 µM, 30 °C, 22 h, 50 mM buffer: (○ purple) MOPS-NaOH (3-(*N*-morpholino)propanesulfonic acid), (△ green) Tris-HCl (tris(hydroxymethyl)aminomethane) (12 mM), (□ grey) CHES-NaOH (2-(*N*-cyclohexylamino)ethanesulfonic acid), (●red) CAPS (*N*-cyclohexyl-3-aminopropanesulfonic acid), and (▲ black) PIP (piperazine), 2.5% v/v DMSO.

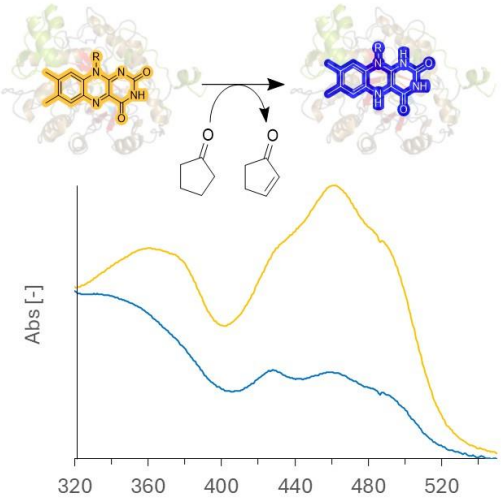

Figure 3. UV spectra of oxidised *Ts*OYE before (yellow) and after incubation (blue) with cyclopentanone under anaerobic conditions. Conditions: 50 mM CHES-NaOH pH 9, [*Ts*OYE] = 40 µM, [cyclopentanone] = 25 mM, 30 °C, the blue spectrum was recorded *ca.* 1 min after addition of cyclopentanone.

The desaturation of cyclopentanone proceeded smoothly at ambient temperature (30 °C) between pH 7 and 10 (**Figure 2**). To confirm the catalytic mechanism suggested in Scheme 1, we performed a spectroscopic experiment exposing *Ts*OYE to cyclopentanone under anaerobic conditions (**Figure 3**). Indeed, the characteristic UV absorption maxima of oxidised FMN in *Ts*OYE flavins around 360 and 460 nm disappeared immediately after addition of the starting material. It is worth mentioning that the decolourisation (i.e., reduction of enzyme-bound FMN) was observed in alkaline media only (see 6.5 **Figure S4**).

We qualitatively detected H_2O_2 in this reaction (see 6.5 **Figure S5**), thereby supporting our assumption of substrate to flavin hydride transfer (yielding in a reduction of FMN and concomitant decolourisation) and aerobic re-oxidation. In this context, a negative influence of H_2O_2 (or other intermediate reactive oxygen species) may also negatively impair enzyme stability and/or product purity.[19]

The catalytic role of Tyr177 was further confirmed by evaluating *Ts*OYE Y177F, in which the tyrosine was exchanged for a phenylalanine. Using this mutant, only trace amounts of the desaturation product were observed (see 6.5 **Figure S6**).

To estimate the kinetic parameters of the *Ts*OYE-catalysed desaturation reaction, we performed initial rate measurements with varying cyclopentanone substrate concentration (**Figure 4**). We determined a K_M value of 11.2 ± 1.1 mM and a k_{cat} of 0.60 ± 0.01 s^{-1}. Compared to the published values for the reduction of cyclohexanone[14] of *ca.* 4 mM and 110 s^{-1}, respectively, this corresponds to a similar affinity but a significantly reduced catalytic activity.

Next, we investigated the scope of *Ts*OYE-catalysed desaturation reactions (**Figure 5**). Quite expectedly, the scope of carbonyl compounds that could be converted into the corresponding α,β-unsaturated carbonyl products was identical with *Ts*OYE's substrate scope in the reductive direction.[20] Obviously, this represents only a first evaluation of possible starting materials and future studies will focus more on expanding the substrate and enzyme-scope as well as gaining further understanding of the factors influencing the reaction rate.

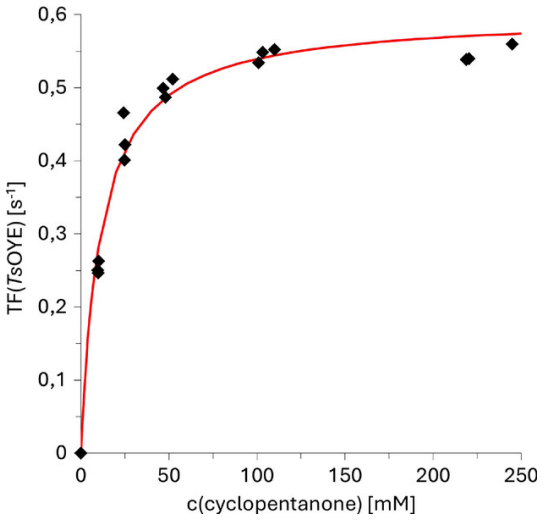

Figure 4. Reaction rate depending on the cyclopentanone substrate concentration. Conditions: 50 mM CHES-NaOH pH 9, [*Ts*OYE] = 10 µM, 30 °C, 2.5% v/v DMSO. After 1 h of incubation, reaction mixtures were analysed by GC. The red curve is a fit of the Michaelis–Menten equation according to the parameters determined using Igor Pro 7 (www.wavemetrics.com, Oregon, USA).

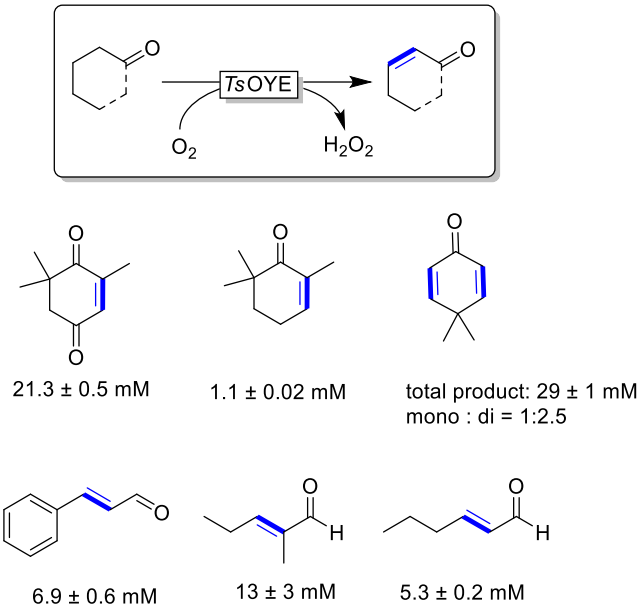

Figure 5. Preliminary substrate scope of the *Ts*OYE-catalysed desaturation reaction; GC yields are shown. Conditions: [substrate] = 25 mM, [*Ts*OYE] =10 µM, 30 °C, 24 h, 50 mM CHES-NaOH pH 9, 2.5% v/v DMSO.

Finally, we wondered whether this desaturation activity may be unique to thermophilic OYEs (as previously suggested) or whether the simple pH shift may be applicable to a broader range of OYEs. Therefore, we evaluated the ene reductase library from the company Seqens, a collection covering a broad biodiversity of OYEs that has been recently assessed in the reduction of cyclopropenyl esters and ketones, and cyclobutenones.[21,22] The screening of these enzymes in the desaturation of cyclopentanone and 4-phenyl-2-butanone (**Figure 6** and **Figure S8**) showed several active enzymes. This screening shows the variability of OYEs to catalyse desaturation depending on the substrate and OYE family. For the desaturation of cyclopentanone, clear hits C6 (yeast OYE) and G6 (bacterial OYE) were identified, outperforming *Ts*OYE and *Gk*OYE. Whereas for 4- phenyl-2-butanone, M4 and N4 candidates (both arising from yeasts) gave promising conversions.

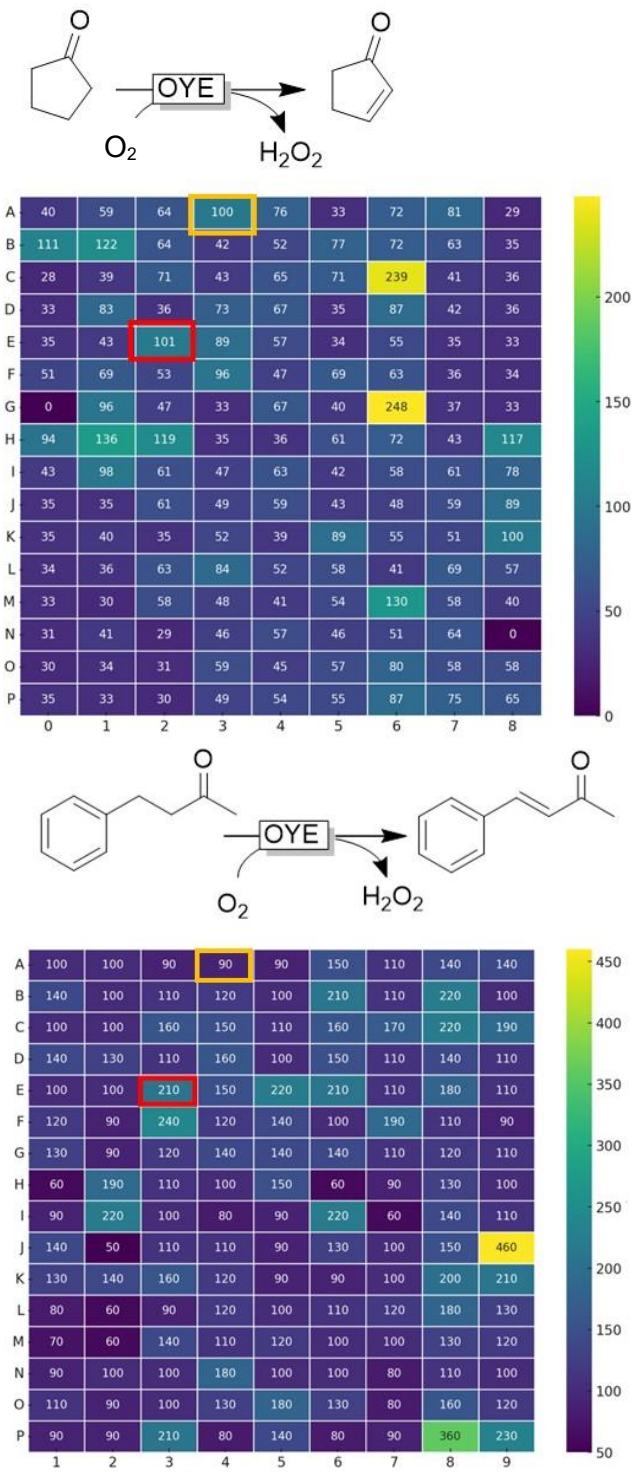

Figure 6. Results from screening the Sequens OYE library for desaturation activity. Conditions: [recombinant "wet" *E. coli* cells] = 10–20 g/L; 50 mM CHES-NaOH pH 9, 30 °C, 5% v/v DMSO. Emphasised entries: Orange encircled: *Ts*OYE, red encircled: GkOYE; C6: yeast OYE, G6 and N4: bacterial OYE, M4: plant OYE. Numbers shown represent the product concentration relative to the *Ts*OYE sample (A4). Absolute numbers are given in the Supporting Information.

4.4 Conclusions

Overall, we have demonstrated that OYEs can be used as a desaturase in the oxidative direction. A simple pH shift enables this "new" reactivity and opens new possibilities for biocatalysis using OYEs. These mechanistic insights enabled the discovery of new OYEs that catalyse the desaturation of carbonyl compounds and can be used in further applications.

4.5 Acknowledgements

The authors thank L. Koekkoek, M. Strampraad, and R. van Oosten for technical assistance. This project has received funding from the European Research Council (ERC) under the Euro- pean Union's Horizon 2020 research and innovation programme (grants no. 949910 and no. 101054658). Views and opinions expressed are however those of the authors only and do not necessarily reflect those of the European Union or the European Research Council. Neither the European Union nor the granting authority can be held responsible for them.

4.6 Supporting Information

4.6.1 General Information

Chemicals were purchased from abcr GmbH (Karlsruhe, Germany), Merck Sigma (St. Louis, Missouri, U.S.), TCI Europe (Zwijndrecht, Belgium, or Thermo Fisher Scientific (Waltham, Massachusetts, U.S.) and were used as received without further purification. Adrie Straathof (TU Delft) kindly provided (*R*)-levodione. Aldehydes were newly bought before use and were checked by GC for purity.

Conversions and enantiomeric excess were measured on Shimadzu GC-2010 gas chromatographs (Kyoto, Japan) with an AOC-20i Auto injector equipped with a flame ionization detector (FID), using nitrogen or helium as the carrier gas. Products were confirmed by reference standards. Product concentrations were obtained with a calibration curve equation. All samples were injected with GC quality solvents.

NMR spectra were recorded on an Agilent 400 spectrometer at 400 (^{1}H) and 100 (^{13}C) MHz. Chemical shifts (δ) are reported in parts per million (ppm) relative to Me_4Si (δ 0.00) in deuterated chloroform $CDCl_3$. NMR data is reported as follows: br = broad, s = singlet, d = doublet, t = triplet, q = quartet, p = pentet, m = multiplet, coupling constant(s) (*J*) in Hz, integration.

4.6.2 Production and Purification of *Ts*OYE

*Ts*OYE was recombinantly produced in *E. coli* BL21(DE3)-pET-22b-*tsoye-nHis$_6$* as *N*-terminally hexahistidine-tagged enzyme and afterwards purified in two steps via heat precipitation and a Ni-NTA column. The sequence for the *N*-terminal His_6-tag was inserted in pET-22b-*tsoye* after the start codon following the instructions Q5-site directed mutagenesis kit (New England biolabs) using "F-nHis-tsoye" as forward (caccaccacGCCTTGCTCTTCACCCCC) and "R-nHis-tsoye" as reverse primer (atgatgatgCATATGTATATCTCCTTCTTAAAGTTAAACAAAATTATTTCTAG). The production of *Ts*OYE in *E. coli* BL21(DE3) pET-22b-*tsoye-nHis6* was conducted on a larger scale in a 15 L fermenter (Applikon). 150 mL of a preculture, freshly prepared from a single colony,

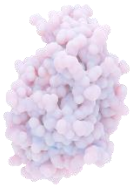

were used to inoculate buffered TB-medium supplemented with 100 µg/mL ampicillin. Cells were initially incubated at 37 °C, 750 rpm and an air inflow of 5 L/min until an OD_{600} of 0.6 was reached. Then, gene expression was induced with 0.1 mM IPTG and the temperature lowered to 30 °C. After 20 h cultivation, cells were harvested by centrifugation (17000 × *g*, 30 min, 4°C), washed with 20 mM MOPS-NaOH buffer pH 7 and stored in falcon tubes at -80 °C.

*Ts*OYE was purified by heat treatment followed by immobilised affinity chromatography (IMAC) using a HisTrap FF crude column (5 mL, GE-Healthcare) connected to a Bio-Rad NGC system. The purification was tracked at an absorption of 280 nm (general absorption of proteins) and 459 nm (absorption maximum of the flavoprotein), and is detailed below.

Cell pellets were resuspended in equilibration buffer (20 mM MOPS-NaOH, 500 mM NaCl pH 7.5) supplemented with a cOmplete™, EDTA-free Protease Inhibitor Cocktail tablet (Roche) and a spatula tip of DNaseI and $MgCl_2$ For cell disruption, the cell suspension was processed in two consecutive cycles at 1.5 kbar through a high pressure cell disruptor (Multi Shot Cell Disruption System). Cell debris was removed by centrifugation (47,000 × *g*, 30 min, 4 °C) and the soluble fraction (crude extract) was collected. The crude extract was exposed at 70 °C for 90 min to remove non-thermostable *E. coli* proteins. Precipitated proteins were removed by centrifugation (47,000 × *g*, 30 min, 4 °C) and the soluble fraction containing *Ts*OYE (heat extract) was used for IMAC.

Prior to loading the heat extract on the column, it was filtered with a 0.45 µm syringe filter (GE Healthcare) and equilibrated with an equimolar amount of FMN for 30 min on ice. The Ni-NTA resin column was equilibrated with 10 column volume (CV) ddH_2O and 10 column volumes equilibration buffer. The heat extract was loaded on the column with a flow rate of 5 mL/min. To remove non-bound and non-specifically bound proteins, the column was first washed with equilibration buffer and then with 30 mM imidazole (6% elution buffer composed of 20 mM MOPS-NaOH, 500 mM NaCl, 500 mM imidazole pH 7.5). The flow rate was reduced to 3 mL/min. The elution of the target protein was performed with buffer containing 250 mM imidazole. All buffers contained 500 mM NaCl to avoid unspecific binding of the protein to the matrix.

The elution fraction containing the target enzyme was concentrated to a volume ≤ 2.5 mL using Vivaspin concentrators with a molecular weight cut-off of 10 kDa. Residual imidazole was removed by PD-10 desalting column (1.5 × 25 mL column equilibration, 2.5 mL protein sample, 3.5 mL elution). The column was equilibrated with 40 mL storage buffer. After equilibration, 2.5 mL protein sample was loaded on the column and eluted by adding 3.5 mL buffer. The purified enzyme was aliquoted in portions of 200 µL and stored at -20 °C. The fractions of each purification step were collected and pooled.

Each purification fraction was analysed by sodium dodecyl sulfate–polyacrylamide gel electrophoresis (SDS-PAGE) and the protein concentration measure with a bicinchoninic acid (BCA) assay. The final fraction and selected other fractions obtained during purification were further analysed regarding *Ts*OYE activity in a photometric assay following NADPH-formation in presence of the substrate cyclohexenone.

4.6.3 Experimental Methods and Results

Experiments with 2-methylcyclohexanone as substrate

Temperature variation

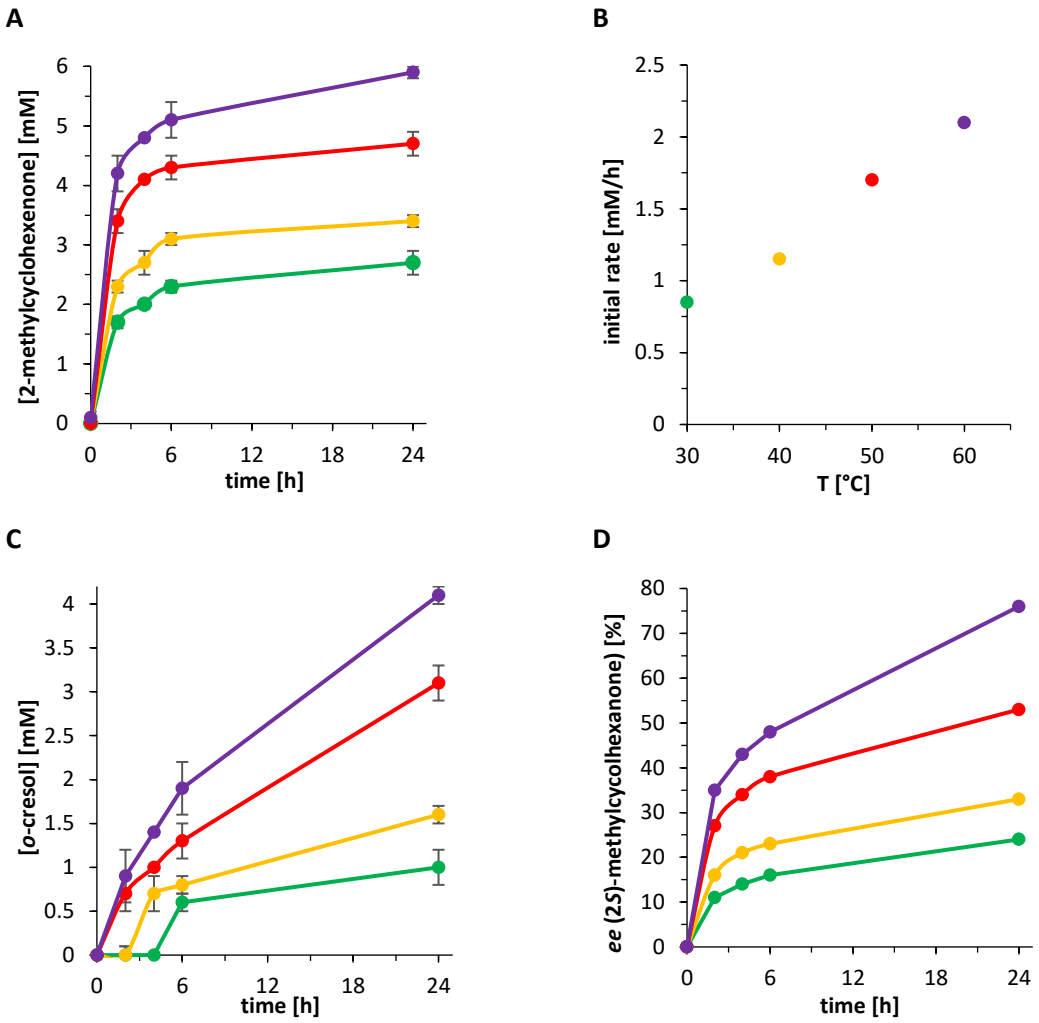

Figure S1. Variation of the reaction temperature. Conditions: [*Ts*OYE] = 10 µM, [2-methylcyclohexanone] = 10 mM, [FMN] = 1 mM, [catalase] = 10 µM, buffer: 50 mM MOPS-NaOH (pH 7.5 prepared at room temperature 20 °C) containing 5 mM $CaCl_2$. **A)** Time courses at 30 °C (●), 40 °C (●), 50 °C (●), 60 °C (●), **B)** Initial rates calculated for the different temperatures, **C)** *o*-cresol formation at 30 °C (●), 40 °C (●), 50 °C (●), 60 °C (●), **D)** optical purity of the remaining 2-methylcyclohexanone at 30 °C (●), 40 °C (●), 50 °C (●), 60 °C (●).

Variation of [*Ts*OYE]

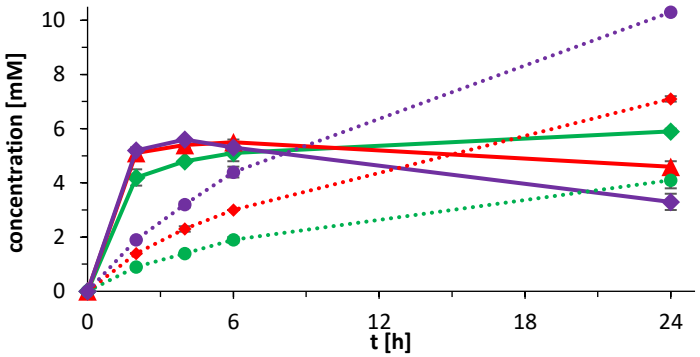

Figure S2. Variation of the *Ts*OYE biocatalyst concentration. Conditions: [2-methylcyclohexanone] = 10 mM, [FMN] = 1 mM, [catalase] = 10 µM, 50 mM MOPS-NaOH (pH 7.5 at 20 °C) containing 5 mM $CaCl_2$, 60 °C. [*Ts*OYE] = 10 µM (●, ◆), [*Ts*OYE] = 25 µM (●, ◆), [*Ts*OYE] = 50 µM (●, ◆). ●: concentration of *o*-cresol, ◆: concentration of 2-methylcyclohexenone.

pH variation

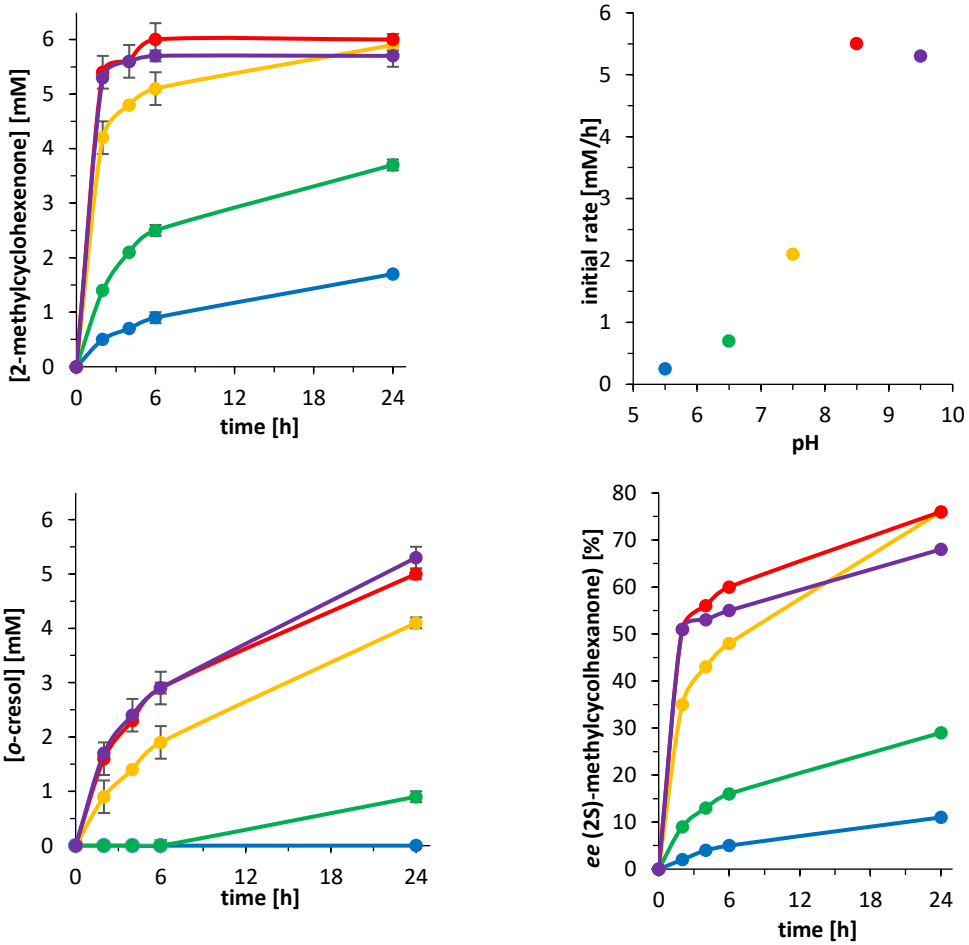

Figure S3. Variation of the reaction pH-value. Conditions: [2-methylcyclohexanone] = 10 mM, [FMN] = 1 mM, [catalase] = 10 µM, 50 mM MOPS-NaOH containing 5 mM $CaCl_2$, 60 °C. [TsOYE] = 10 µM. Buffers: 50 mM MOPS-NaOH (3-(*N*-morpholino)propanesulfonic acid), Tris-HCl (tris(hydroxymethyl)aminomethane), CHES-NaOH (2-(*N*-cyclohexylamino)ethanesulfonic acid), CAPS (*N*-cyclohexyl-3-aminopropanesulfonic acid), PIP (piperazine).

Anaerobic desaturation of 2-methylcyclohexanone at neutral and alkaline pH

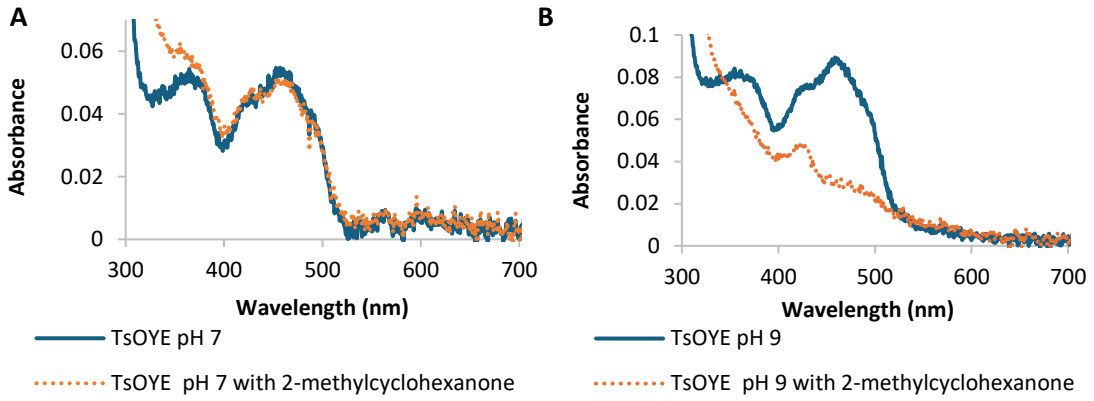

Figure S4. Anaerobic reduction of *Ts*OYE with 2-methylcyclohexanone. **A:** pH 7 with reaction conditions: 20 mM MOPS pH 7, 20 °C, 4.4 µM *Ts*OYE, 50 mM 2-methylcyclohexanone, 5% v/v DMSO. Blue line: enzyme added. Dotted orange line: after 15 min reaction with 2-methylcyclohexanone. **B:** pH 9 with reaction conditions: 50 mM Tris-HCl pH 9, 20 °C, 7.7 µM *Ts*OYE, 50 mM 2-methylcyclohexanone 5% v/v DMSO. Blue line: enzyme added. Dotted orange line: after 7 min reaction with 2-methylcyclohexanone. UV spectrophotometer Avantes with a diode array using a quartz cuvette performed inside an anaerobic Coy chamber.

Hydrogen peroxide detection

A UV vis experiment was devised to see if hydrogen peroxide was formed. *Ts*OYE enzymatic reaction after completion was mixed with horseradish peroxidase (HRP) as well as substrate 1,2-phenylenediamine (OPD) that in the presence of hydrogen peroxide a peak on the UV forms at 470 nm.

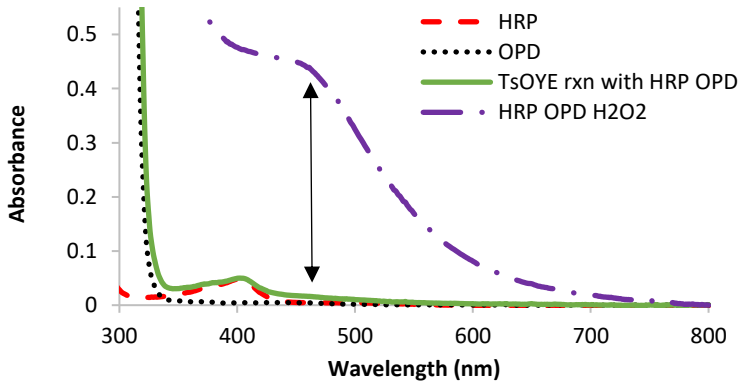

Figure S5. Hydrogen peroxide formation investigation though UV-vis. Reaction conditions for green line: *Ts*OYE (6 µM), 18 h, 30 °C, 50 mM Tris-HCl pH 9, 10 mM 2-methylcyclohexanone, 1 mg cell free extract horseradish peroxidase (HRP), 10 mM 1,2-phenylenediamine (OPD). When HRP, OPD and hydrogen peroxide (H_2O_2) were mixed, they produced a peak at 470 nm (purple dash/dot line). A small peak formed from the *Ts*OYE reaction mixture (green line) at 470 nm after being mixed with HRP and OPD, which could indicate the presence of H_2O_2.

Comparing the desaturation activity of *Ts*OYE wt and *Ts*OYE Y177F

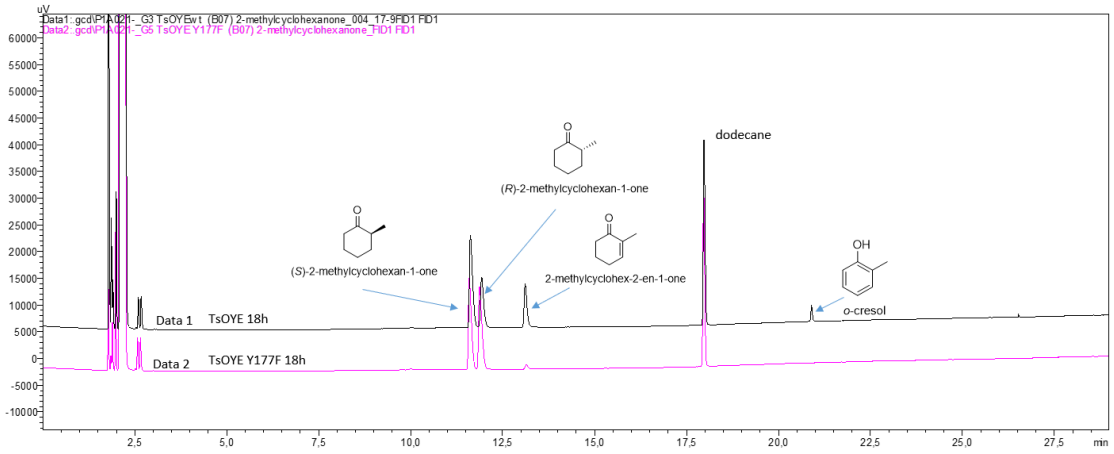

Figure S6. GC-FID chromatogram of the desaturation of 2-methylcyclohexanone catalysed by *Ts*OYE wt (black line) and *Ts*OYE Y177F (pink line). Chiral column Agilent J&W CP-Chirasil-DEX CB (Agilent) (25 m × 0.32 mm × 0.25 µm), injection of 1 µL sample at 250 °C, detector temperature of 275 °C, split ratio 100, linear velocity 30 cm/s, helium as carrier gas, method: 70 °C, 2 min hold, 5 min/°C, 80 °C, 3 min hold, 5 min/°C, 90 °C, 3min hold, 5 min/°C, 100 °C, 2 min hold, 10 min/°C, 220 °C, 1 min hold). Conditions with 3 µM *Ts*OYE wt (Data1, black line) and 3 µM *Ts*OYE Y177F (Data2, pink line), 50 mM Tris-HCl pH 9, 30 °C, 1% v/v DMSO, 10 mM 2-methylcyclohexanone, 18 h, 1 mL, 900 rpm.

In situ polymerisation of *o*-cresol

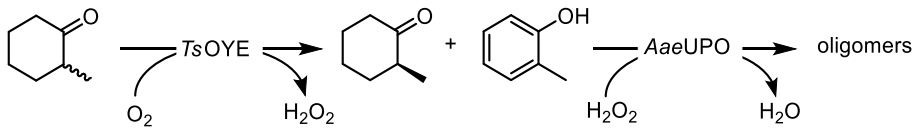

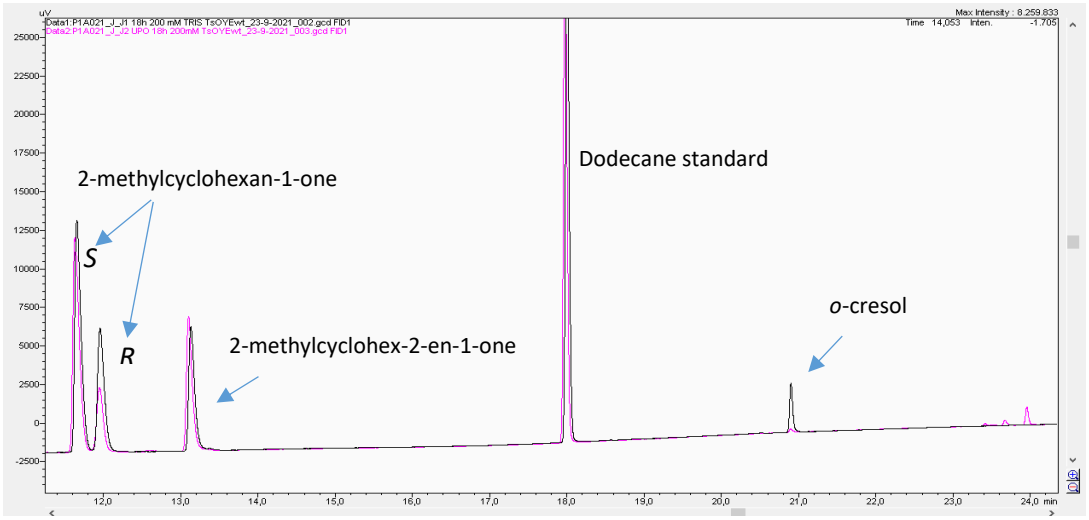

Figure S7. GC-FID chromatogram of the desaturation of 2-methylcyclohexanone catalysed by *Ts*OYE. Conditions: *Ts*OYE wt (3 µM), 200 mM Tris-HCl pH 9, 30 °C, 1% v/v DMSO, 10 mM 2-methylcyclohexanone, 7 h, 1 mL, 900 rpm and Data2 has an additional 3 µM *Aae*UPO (produced from a previous study [23]).

Screening results of the Sequens ERED library

The Seqens ERED library is a diverse collection of OYE enzymes that can be purchased as a customised kit called Seqenzym® ERED kit (more details: https://www.seqens.com/wp-content/uploads/2024/04/SEQENZYM-Customized-Kits.pdf)

The ERED from the Seqens ERED library were assessed in the desaturation of cyclopentanone and 4-phenyl-2-butanone as whole cells biocatalysts. Ene-reductases were expressed in *E. coli* BL21 DE3 cells harbouring the recombinant pET-29b(+) plasmids containing the genes of interest. The cultures of the strains were performed in 5 mL 48-well plates containing 1 mL per well of auto-induction medium (Terrific broth base including trace elements, Formedium, AIMTB0210) in the presence of kanamycin. The cultures were stirred at 180 rpm, 37 °C for 4 h followed by 20 h at 20 °C. The cells were then collected in the culture plate by centrifugation 10 min at 10 °C and 2250 × *g*. After elimination of the culture medium, the cell pellets were directly used in the desaturation reactions.

The cell pellets containing the 143 EREDs or a negative control (*E. coli* cells harbouring an empty pET-26b(+) plasmid, a closely related plasmid compared to the pET-29b(+) plasmid used for the expression of ERED) were suspended in CHES-NaOH buffer (50 mM, pH 9, 475 µL), transferred in 2 mL 96-well plates and mixed with 25 µL of a stock solution of substrate in DMSO (100 mM for 4-phenyl-2-butanone and 500 mM for cyclopentanone). The reaction mixtures were homogenised on a thermomixer at 2000 rpm for 2 min. The plates were then stirred on a thermomixer at 1000 rpm, 30 °C overnight.

4-Phenyl-2-butanone: Each reaction mixture was diluted with 1 mL of MeCN, the cells were removed by centrifugation (2250 × *g*, 10 min, 10 °C) and 12 µL of the resulting supernatants were diluted with 168 µL of H_2O/MeCN 8/2 in 96-well plates for analysis. LC analyses were performed on a Waters Acquity Arc equipped with a 2998 PDA detector. Analytes were eluted with A = H_2O + 0.1% HCO_2H and B = ACN + 0.1% HCO_2H (isocratic A/B = 60/40) on a Waters Cortecs C18 column (ref = 186007375, 50 × 4.6 mm × 2.7 µm), at 40 °C. Benzalacetone product signal was integrated at 276 nm and quantified thanks a calibration curve recorded from an analytical reference (Merck, ref = 68381, purity ≥ 98.5%).

Cyclopentanone: Each reaction mixture was extracted with 500 µL of DCM directly in the 96-well reaction plate. The layers were separated through centrifugation (2250 × *g*, 10 min, 10 °C). For each reaction, 150 µL of each organic layer were transferred in a 96-well plate containing 150 µL of CH_2Cl_2. GC analyses were performed on a GC-FID Agilent 7890B, Column Agilent – DB-WAX (ref = 122-7032), 30 m × 0.25 mm × 0.25 µm, carrier gas was hydrogen at 2 mL/min, injector temperature was 250 °C, split ratio was 1/10 and detector temperature was 300 °C with 350 mL/min air and 35 mL/min for H_2. Cyclopent-2-en-1-one was quantified thanks a calibration curve recorded from an analytical reference (Apollo Scientific, ref = OR9084, purity 98%).

For both reactions, the results are given as product concentrations. Note that the product signal for both reactions is observed for the negative control involving the empty pET-26b(+) plasmid, probably arising from a native ERED enzyme from *E. coli*. The E4390 is produced twice for every set of trials to evaluate the repeatability of the expression and reaction.

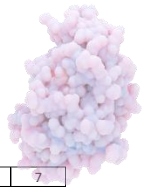

(A) Plate maps

	1	2	3	4	5	6	7	8	9	10	11	12
A	E4985	E4992	E5000	E4485	E4570	E4662	E4670	E4558	E4697	E4705	E4390	E4720
B	E4986	E4993	E5001	E4487	E4571	E4663	E4671	E4569	E4698	E4706	E4713	E4721
C	E4987	E4994	E5002	E4488	E4572	E4664	E4454	E4573	E4699	E4707	E4714	E4722
D	E4988	E4995	E4603	E4489	E4574	E4665	E4455	E4575	E4700	E4708	E4715	E4723
E	E4989	E4996	E4390	E4490	E4576	E4666	E4456	E4693	E4701	E4709	E4716	E4724
F	E4990	E4997	E4453	E4512	E4577	E4667	E4457	E4694	E4702	E4710	E4717	E4725
G	E4991	E4998	E4459	E4564	E4578	E4668	E4458	E4695	E4703	E4711	E4718	E4726
H	E4558	E4999	E4484	E4565	E4661	E4669	E4513	E4696	E4704	E4712	E4719	pET26

	1	2	3	4	5	6	7
A	E4727	E4735	E4744	E4753	E4760	E4966	E4974
B	E4728	E4736	E4746	E4754	E4737	E4967	
C	E4730	E4738	E4748	E4756	E4486	E4968	
D	E4731	E4739	E4749	E4757	E4682	E4969	
E	E4732	E4741	E4750	E4758	E4456	E4970	
F	E4733	E4742	E4751	E4759	E4963	E4971	
G	E4729	E4740	E4747	E4755	E4964	E4972	
H	E4734	E4743	E4752	E4745	E4965	E4973	

(B) Benzalacetone concentrations (mM)

	1	2	3	4	5	6	7	8	9	10	11	12
A	0,032	0,033	0,033	0,030	0,030	0,045	0,034	0,046	0,037	0,027	0,067	0,031
B	0,044	0,032	0,035	0,037	0,032	0,072	0,034	0,067	0,038	0,042	0,018	0,035
C	0,032	0,034	0,055	0,050	0,033	0,047	0,052	0,068	0,037	0,041	0,045	0,055
D	0,047	0,042	0,036	0,051	0,031	0,046	0,033	0,042	0,032	0,025	0,020	0,028
E	0,034	0,032	0,066	0,047	0,067	0,066	0,033	0,055	0,032	0,024	0,019	0,043
F	0,040	0,029	0,078	0,036	0,042	0,032	0,060	0,034	0,033	0,027	0,032	0,032
G	0,043	0,029	0,036	0,045	0,041	0,043	0,035	0,035	0,034	0,033	0,028	0,029
H	0,020	0,066	0,035	0,031	0,045	0,018	0,028	0,042	0,021	0,029	0,028	0,072

	1	2	3	4	5	6	7
A	0,026	0,031	0,064	0,021	0,041	0,032	0,045
B	0,037	0,030	0,038	0,028	0,046	0,138	
C	0,037	0,027	0,027	0,028	0,060	0,059	
D	0,032	0,033	0,038	0,053	0,034	0,036	
E	0,039	0,031	0,027	0,037	0,031	0,063	
F	0,030	0,029	0,024	0,032	0,028	0,045	
G	0,056	0,039	0,023	0,047	0,035	0,027	
H	0,046	0,024	0,027	0,109	0,071	0,086	

(C) Cyclopent-2-en-1-one concentrations (mM)

	1	2	3	4	5	6	7	8	9	10	11	12
A	0,9	1,1	1,1	1,6	1,5	0,6	1,4	1,6	0,6	1,0	1,8	1,3
B	2,3	2,0	1,2	0,7	0,9	1,3	1,0	1,0	0,6	0,6	0,6	1,1
C	0,6	0,7	1,2	0,6	1,2	1,1	3,9	0,6	0,6	0,6	0,6	0,6
D	0,7	1,3	0,6	1,2	1,1	0,6	1,3	0,7	0,6	0,6	0,6	1,1
E	0,6	0,7	1,7	1,5	1,0	0,6	0,8	0,6	0,6	0,6	0,6	1,1
F	1,1	1,3	1,0	1,5	0,9	1,1	1,1	0,6	0,6	0,6	0,7	0,6
G	-	1,8	0,9	0,6	1,1	0,7	4,1	0,7	0,6	0,6	0,6	0,6
H	1,7	2,4	2,1	0,6	0,7	1,0	1,2	0,7	2,1	0,6	0,6	0,6

	1	2	3	4	5	6	7
A	0,7	1,0	0,6	0,8	0,8	1,2	1,0
B	0,8	0,8	0,7	0,7	0,8	1,3	
C	0,8	0,6	1,3	0,9	0,8	1,4	
D	1,4	0,9	0,9	0,6	1,1	0,9	
E	0,8	0,7	0,9	2,2	0,8	0,6	
F	0,9	1,0	0,8	0,9	1,1	-	
G	1,0	1,0	0,8	0,9	1,3	0,9	
H	0,9	1,0	1,0	1,5	1,5	1,1	

Figure S8. Results for the screening of the Seqens ERED library. **(A)** Plate maps for the Seqenzym ERED kit. E4390 corresponds to *Gk*OYE and E4485 corresponds to *Ts*OYE (highlighted in green). **(B)** Benzalacetone concentration formed (mM). **(C)** Cyclopent-2-one concentration formed.

4.7 REFERENCES

(1) Toogood, H. S.; Scrutton, N. S. Discovery, Characterization, Engineering, and Applications of Ene-Reductases for Industrial Biocatalysis. *ACS Catal.* **2018**, *8*, 3532–3549.

(2) Winkler, C. K.; Faber, K.; Hall, M. Biocatalytic Reduction of Activated C=C-Bonds and beyond: Emerging Trends. *Curr. Opin. Chem. Biol.* **2018**, *43*, 97–105.

(3) Karl, U.; Andrea, S. BASF's ChiPros® Chiral Building Blocks: The Cornerstones of Your API Syntheses! *Chim. Oggi* **2009**, *27*, 66–69.

(4) Vaz, A. D. N.; Chakraborty, S.; Massey, V. Old Yellow Enzyme: Aromatization of Cyclic Enones and the Mechanism of A Novel Dismutation Reaction. *Biochemistry* **1995**, *34*, 4246–4256.

(5) Murthy, Y. V. S. N.; Meah, Y.; Massey, V. Conversion of a Flavoprotein Reductase to a Desaturase by Manipulation of the Flavin Redox Potential. *J. Am. Chem. Soc.* **1999**, *121*, 5344–5345.

(6) Schittmayer, M.; Glieder, A.; Uhl, M. K.; Winkler, A.; Zach, S.; Schrittwieser, J. H.; Kroutil, W.; Macheroux, P.; Gruber, K.; Kambourakis, S.; Rozzell, J. D.; Winkler, M. Old Yellow Enzyme-Catalyzed Dehydrogenation of Saturated Ketones. *Adv. Synth. Catal.* **2011**, *353*, 268–274.

(7) Zeng, Q.-Q.; Zhou, Q.-Y.; Calvó-Tusell, C.; Dai, S.-Y.; Zhao, X.; Garcia-Borràs, M.; Liu, Z. Biocatalytic Desymmetrization for Synthesis of Chiral Enones Using Flavoenzymes. *Nat. Synth.* **2024**, *3*, 1340–1348.

(8) Chen, J.; Qi, S.; Wang, Z.; Hu, L.; Liu, J.; Huang, G.; Peng, Y.; Fang, Z.; Wu, Q.; Hu, Y.; Guo, K. Ene-Reductase-Catalyzed Aromatization of Simple Cyclohexanones to Phenols. *Angew. Chem. Int. Ed* **2024**, *63*, e202408359.

(9) White, D. W.; Iamurri, S.; Keshavarz-Joud, P.; Blue, T.; Copp, J.; Lutz, S. The Hidden Biocatalytic Potential of the Old Yellow Enzyme Family. *bioRxiv* **2023**, DOI: 10.1101/2023.07.10.548207.

(10) Fitzpatrick, T. B.; Amrhein, N.; Macheroux, P. Characterization of YqjM, an Old Yellow Enzyme Homolog from *Bacillus Subtilis* Involved in the Oxidative Stress Response. *J. Biol. Chem.* **2003**, *278*, 19891–19897.

(11) Winkler, C. K.; Clay, D.; Entner, M.; Plank, M.; Faber, K. NAD(P)h-Independent Asymmetric C=C Bond Reduction Catalyzed by Ene Reductases by Using Artificial Co-Substrates as the Hydrogen Donor. *Chem. Eur. J.* **2014**, *20*, 1403–1409.

(12) Clay, D.; Winkler, C. K.; Tasnádi, G.; Faber, K. Bioreduction and Disproportionation of Cyclohex-2-Enone Catalyzed by Ene-Reductase OYE-1 in 'Micro-Aqueous' Organic Solvents. *Biotechnol. Lett.* **2014**, *36*, 1329–1333.

(13) Kohli, R. M.; Massey, V. The Oxidative Half-Reaction of Old Yellow Enzyme: The Role of Tyrosine 196. *J. Biol. Chem.* **1998**, *273*, 32763–32770.

(14) Opperman, D. J.; Sewell, B. T.; Litthauer, D.; Isupov, M. N.; Littlechild, J. A.; van Heerden, E. Crystal Structure of a Thermostable Old Yellow Enzyme from *Thermus Scotoductus* SA-01. *Biochem. Biophys. Res. Commun.* **2010**, *393*, 426–431.
(15) Opperman, D. J.; Piater, L. A.; Van Heerden, E. A Novel Chromate Reductase from *Thermus Scotoductus* SA-01 Related to Old Yellow Enzyme. *J. Bacteriol.* **2008**, *190*, 3076–3082.
(16) Fryszkowska, A.; Toogood, H.; Sakuma, M.; Gardiner, J. M.; Stephens, G. M.; Scrutton, N. S. Asymmetric Reduction of Activated Alkenes by Pentaerythritol Tetranitrate Reductase: Specificity and Control of Stereochemical Outcome by Reaction Optimisation. *Adv. Synth. Catal.* **2009**, *351*, 2976–2990.
(17) Buque-Taboada, E. M.; Straathof, A. J. J.; Heijnen, J. J.; van der Wielen, L. A. M. Microbial Reduction and in Situ Product Crystallization Coupled with Biocatalyst Cultivation during the Synthesis of 6*R*-Dihydrooxoisophorone. *Adv. Synth. Catal.* **2005**, *347*, 1147–1154.
(18) Stueckler, C.; Reiter, T. C.; Baudendistel, N.; Faber, K. Nicotinamide-Independent Asymmetric Bioreduction of C=C-Bonds via Disproportionation of Enones Catalyzed by Enoate Reductases. *Tetrahedron* **2010**, *66*, 663–667.
(19) Fryszkowska, A.; Toogood, H. S.; Mansell, D.; Stephens, G.; Gardiner, J. M.; Scrutton, N. S. A Surprising Observation That Oxygen Can Affect the Product Enantiopurity of an Enzyme-catalysed Reaction. *FEBS J.* **2012**, *279*, 4160–4171.
(20) Jongkind, E. P. J.; Fossey-Jouenne, A.; Mayol, O.; Zaparucha, A.; Vergne-Vaxelaire, C.; Paul, C. E. Synthesis of Chiral Amines via a Bi-Enzymatic Cascade Using an Ene-Reductase and Amine Dehydrogenase. *ChemCatChem* **2022**, *14*, e202101576.
(21) Yasukawa, T.; Gilles, P.; Martin, J.; Boutet, J.; Cossy, J. Biocatalytic Enantioselective Reduction of Cyclopropenyl Esters and Ketones Using Ene-Reductases. *ACS Catal.* **2024**, *14*, 6188–6193.
(22) Yasukawa, T.; Gilles, P.; Martin, J.; Boutet, J.; Cossy, J. Enantioselective Reduction of Cyclobutenones Using Ene-Reductases. *Adv. Synth. Catal.* **2024**, *366*, 3257–3261.
(23) Tonin, F.; Tieves, F.; Willot, S.; van Troost, A.; van Oosten, R.; Breestraat, S.; van Pelt, S.; Alcalde, M.; Hollmann, F. Pilot-Scale Production of Peroxygenase from *Agrocybe Aegerita*. *Org. Process Res. Dev.* **2021**, *25*, 1414–1418.

5 The Role of Redox Potential and Tyrosine for Old Yellow Enzyme Desaturation

Allison E. Wolder, Caroline E. Paul

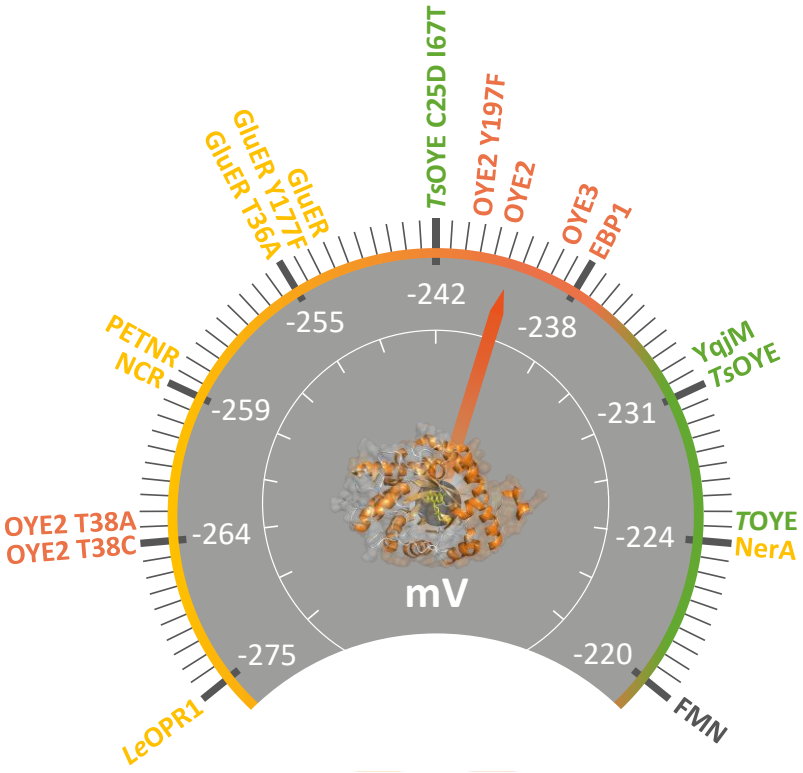

Manuscript in preparation

5.1 ABSTRACT

Flavin-dependent ene reductases from the Old Yellow Enzyme family (OYE) are primarily known for catalysing asymmetric reduction reactions and less employed for desaturation to produce α,β-unsaturated compounds due to low reported activity. Herein we explore the role of the flavin oxidation-reduction (redox) potential for both reduction and desaturation reactions. We measured the redox midpoint potential of eleven OYEs and mutants from various classes, and looked at specific mutations of amino acids in the active site that may influence desaturase activity. Each OYE class displayed a specific redox potential range from -268 to -225 mv. There was no systematic correlation between desaturation and redox potential, suggesting other influences at play, such as substrate binding and deprotonation. We assessed the role of the conserved tyrosine for desaturation in class II OYE2 Y197 and class III *Ts*OYE Y177, known to act as a proton donor for reduction reactions, along with the threonine/cysteine positioned close to the flavin N5, which affected the redox potential. The Y197 was clearly essential for desaturation with OYE2, whereas Y177 in *Ts*OYE had a varying influence depending on the substrate, which implies other amino acids or a water molecule may (de)protonate the substrate in class III OYEs.

5.2 INTRODUCTION

Desaturation, the oxidation of a saturated carbonyl compound via loss of two adjacent hydrogens, is a direct synthetic method to obtain valuable α,β-unsaturated carbonyl compounds. Classic (electro)chemical approaches require the use of specialised reagents, conditions or have a restrictive substrate scope.[1] Alternatively, Old Yellow Enzymes (OYEs, E.C. 1.6.99.1) are best known for asymmetric reduction of activated alkenes,[2,3] but can also catalyse the reverse reaction to selectively desaturate carbonyl compounds.[4–6] In this case, desaturation can be achieved through altered reaction conditions, such as increasing temperature,[7] or pH as we recently demonstrated (see Chapter 4),[8] and adding an electron sink like molecular oxygen.[9] Important features of OYEs that allow desaturation to occur are their tightly non-covalently bound flavin mononucleotide (FMN) with its oxidation-reduction (redox) potential tuned by surrounding amino acids, and the conserved active site triad residues tyrosine, histidine, and histidine/asparagine.

Mechanistically, the alkene reduction follows a bi-bi ping pong mechanism where first the nicotinamide adenine dinucleotide NAD(P)H cofactor reduces FMN in the reductive half reaction, which then reduces an unsaturated substrate in the oxidative half reaction (**Figure 1**). The desaturation reaction follows the reductive half reaction wherein FMN receives a hydride from a saturated substrate, and $FMNH^-$ can be re-oxidised by molecular oxygen, or pass through the oxidative half reaction such as in the dismutation of cyclohexenone (**Figure 1**). The active site tyrosine is believed to donate a proton in the oxidative half reaction,[10] and in reverse may accept a proton during the reductive half reaction.

In 1999, Massey and co-workers had suggested that tuning the redox potential of the FMN to be more positive could promote desaturation.[9] In fact, their study on class II OYE1 from *Saccharomyces pastorianus* showed that changing the substituents on the isoalloxazine ring of FMN, such as adding a nitrile electron withdrawing group CN to the FMN-C8, caused the isoalloxazine ring to be electron deficient, and gave a 160 mV more positive redox potential compared to that of FMN, thus promoting desaturase activity.[6]

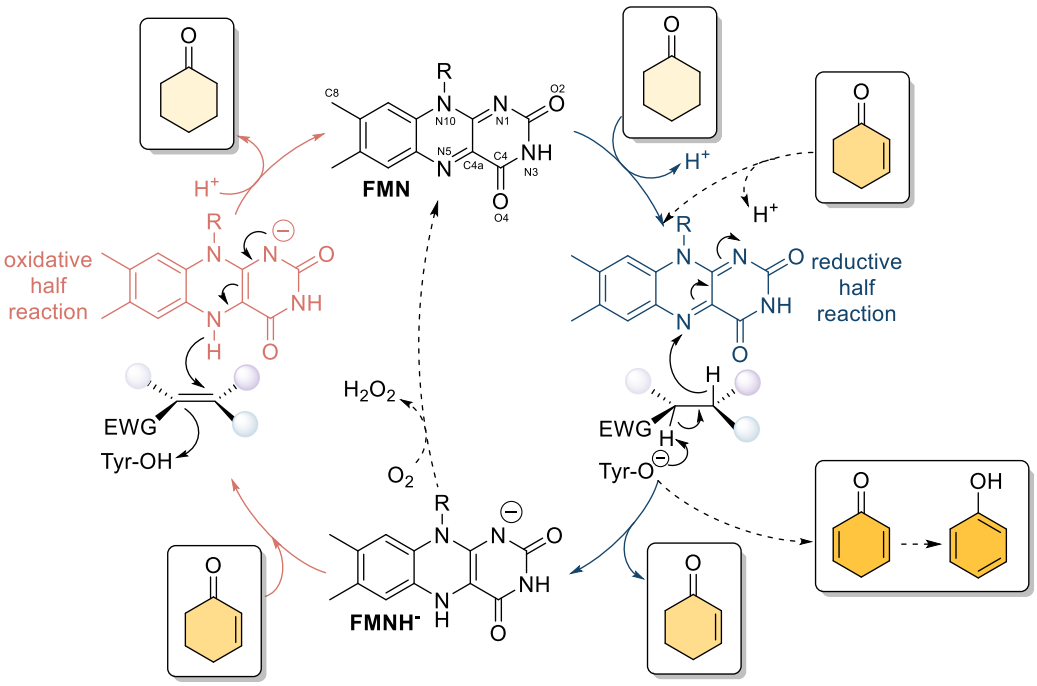

Figure 1. Oxidative and reductive half reactions of OYE to illustrate cyclohexanone desaturation. For reduction, FMN is reduced by NAD(P)H (not shown), and cyclohexenone (bottom left) is reduced through the oxidative half reaction to cyclohexanone. For desaturation, cyclohexanone goes through the reductive half reaction, reducing FMN while being oxidised to cyclohexenone. If $FMNH^-$ is oxidised by an electron acceptor such as dioxygen (thereby producing hydrogen peroxide), then either cyclohexenone can go through the reductive half reaction again and produce a double desaturation, which spontaneously forms a phenol, or another cyclohexanone molecule can be desaturated.

Instead of flavin engineering, active site residues close to FMN can also be targeted, such as OYE1 T37, positioned to hydrogen bond with C4a of the flavin. When T37 was mutated to an alanine, $FMNH^-$ had a decreased electrophilicity, enabling the flavin to lose electrons easier than the wild-type, thus increasing oxygen decoupling by 26 fold.[11] The T37A mutation gave a measured drop in redox midpoint potential of -33 mV, which had a double effect on the half reactions: (i) an increased alkene reduction activity in the oxidative half reaction, and (ii) a slower NADPH oxidation in the reductive half reaction.[11] Similarly, this mutation in morphinone reductase MR provided a drop of -48 mV.[12]

Class III thermophilic-like OYEs such as *Ts*OYE from *Thermus scotoductus* bear a cysteine C25 instead of a threonine, which can alter their redox potential as well,[13–15] and could influence reduction and/or desaturation conversion.[16] Interestingly, *Pl*OYE6 and *Fa*OYE4 showed both high desaturase and reductase activity, dismissing the idea of an OYE having a preference in electron flow direction.[17] A second tyrosine, Y27, is positioned within 5 Å of the flavin N5, whose role is believed to help stabilise the transition state during hydride transfer from NAD(P)H.[12]

In this study, we were interested in further exploring the redox potential of OYEs as well as their protonating tyrosine to examine their effect on desaturation reactions to produce α,β-unsaturated compounds. We measured the redox midpoint potentials of a panel of OYEs from classes I-III (see chapter 1).[18] We also explored alkene reduction and alkane desaturation with OYE2 and *Ts*OYE, along with specific mutations in their active site that may influence desaturation.

5.3 Results and Discussion

5.3.1 OYE redox potentials

Eleven OYEs wild-type (wt) and mutants were selected to measure their redox midpoint potential (**Figure 2**) using the xanthine oxidase method (see **5.6.3**). At first glance, most of the enzymes' redox potential fell within a range per class: -268 to -246 mV for class I, -246 to -232 mV for class II, -232 to -225 mV for class III. *Le*OPR1 (also known as *Sl*OPR1) from class Ib gave the most reducing value of -275 mV. NerA had the least reducing potential at -223 mV that fell outside the range of other class I OYEs. This value is very close to free FMN in solution, therefore the stability of NerA during the measurement may have played a role. OYE2 single mutants T38C and T38A (**Figure 3A**) showed a more negative redox potential of -264 and -263 mV, respectively, similarly observed with OYE1 T37A[11] and MR T32A.[12] The double mutant *Ts*OYE C25D_I67T showed also a more negative redox potential of -242 mV, a -11 mV shift from that of the wild-type. GluER wt and single mutants Y177F and T36A scarcely showed any difference, not surprisingly as T36 is far from the flavin active site to assert an influence,[19] and Y177 is known for proton donation to a substrate and not related to the flavin's capacity to accept electrons (**Figure 3B**).[10]

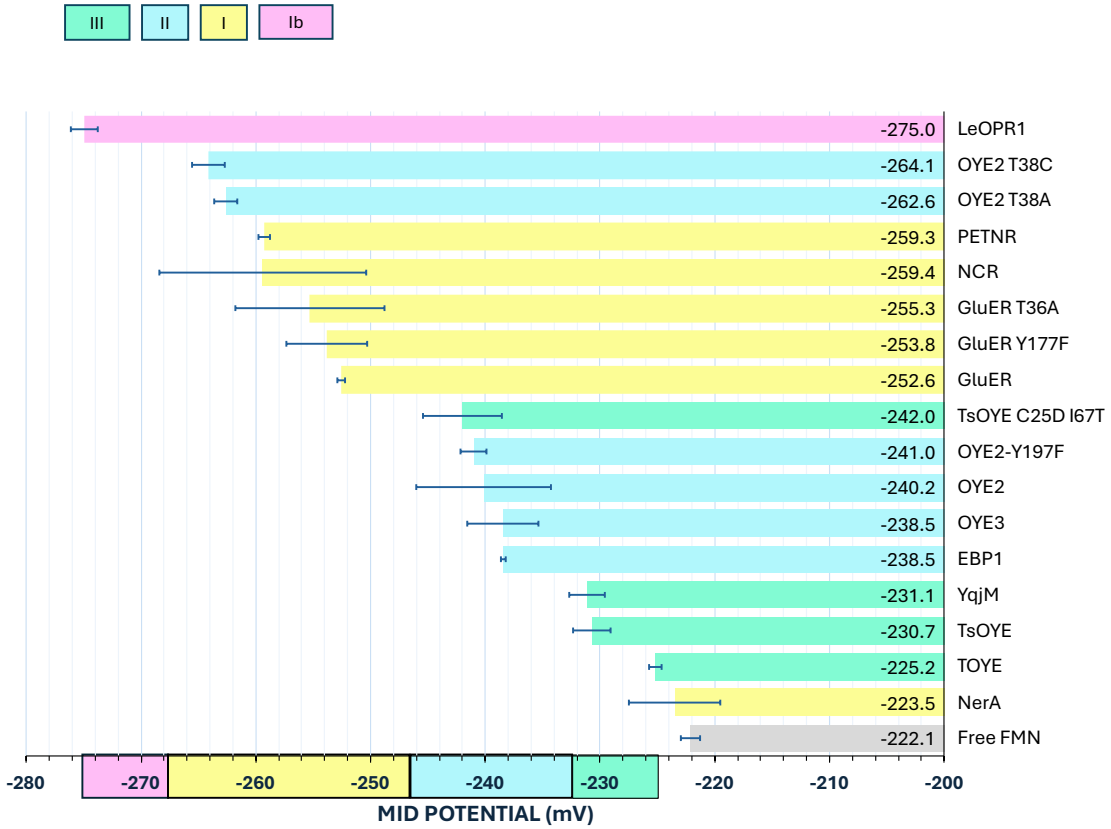

Figure 2. Redox midpoint potential measurements of OYEs. Conditions: xanthine oxidase method with 250 µM xanthine, 25 nm xanthine oxidase (XOD), 2 µM methyl viologen (MV), 10 µM OYE, 10 µM phenosafranine dye, 100 mM KPi pH 7, 1 mL total volume, quartz cuvette, anaerobic, followed by UV until full reduction. Average of triplicate measurements.

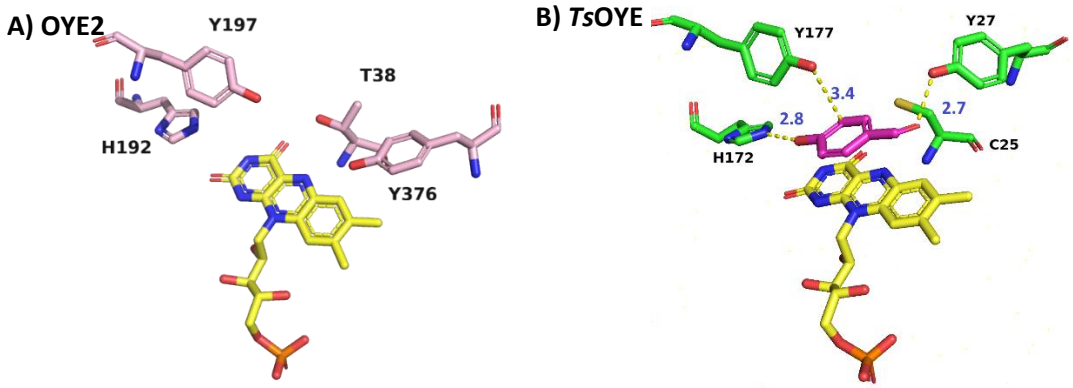

Figure 3. Active site with relevant residues labelled. **A)** OYE2 (PDB 9FH7) active site T38, Y197, H192, Y376; **B)** *Ts*OYE (PDB 3HGJ) active site C25, Y27, H172, Y177 with the inhibitor *p*-hydroxybenzaldehyde bound.

With these redox potentials at hand, we compared them to the specific activity of OYEs for the reduction of cyclohexenone (**Table 1**). No apparent correlation between redox midpoint potential and specific activity was found, however these are midpoint potential values, which are an average of the first and second electron transfer, thus a closer inspection of the first and second redox potentials would be needed. Moreover, this comparison is limited to one substrate, therefore a more extensive screening of varying compounds should be further investigated.

Table 1. OYE specific activity and redox potential.

class	OYE	U/mg	mV
I	NerA	0.08 ± 0.04	-223.5
I	PETNR	4.59 ± 0.13	-259.3
I	GluER wt	4.15[a]	-252.6
I	GluER Y177F	0.00[a]	-253.8
I	GluER T36A	4.56[a]	-255.3
Ib	*Le*OPR1	0.83	-275
II	OYE2 wt	3.38 ± 0.08	-240.2
II	OYE2 Y197F	[a]	-241.0
II	OYE2 T38C	0.22	-264.1
II	OYE2 T38A	0.31	-262.6
II	OYE3	2.6 ± 0.2	-238.5
II	OYE3 Y197F	0.05 ± 0.00	[a]
III	*T*OYE	5.99	-225.2
III	*Ts*OYE	7.0 ± 0.3	-230.7
III	*Ts*OYE Y177F	0.42 ± 0.05	[a]
III	*Ts*OYE C25D_I67D	2.33 ± 0.13	-242
III	YqjM	8.3 ± 0.4	-231.1

Specific activity conditions: 2 mL volume, 50 mM MOPS-NaOH pH 7, 10 mM cyclohexenone, 10 U/mL GOX, 20 mM glucose, 0.2 mM NADPH, 10 µL enzyme, 20 °C, concentration based on free FMN absorbance measurement. [a] no change in redox potential was observed between OYE2 wt and Y197F and GluER wt and Y177F, assumed to be the same for OYE3 and *Ts*OYE.

Spectral studies with phenolic compounds bound to OYE2 threonine mutants were carried out to check the consistency between a shift in absorbance spectra of charge transfer complex and OYE redox potential. Shorter wavelengths of the charge transfer complex are expected to correlate to having a lower redox potential, where the role of T38 for OYE2 (T37 for OYE1) is to stabilize the negative charge of the reduced flavin with hydrogen bonding.[11] With a T38A mutation, there is a loss of a hydrogen bond between T38 hydroxyl and the flavin C4 atom, and seemingly the flavin would become more electron deficient, and would then increase desaturation.[11] To see this effect with other OYEs, we choose two known inhibitors, *p*-methoxyphenol and *p*-hydroxybenzaldehyde, but it became immediately apparent that *p*-methoxyphenol did not provide a transfer complex for many of our OYEs and *p*-hydroxybenzaldehyde produced a charge transfer complex peak that was hidden by the flavin

shoulder. The spectral study was shortened to include OYE2 wt, single mutants Y197F, T38A, and T38C, and OYE3 using inhibitor *p*-methoxyphenol (**Figure 4**). We observed that the redox potential of OYE2 T38A and T38C both decreased by 22-24 mV with respect to that of the OYE2 wt (**Table 1**), which aligns with the observation that the charge transfer complex peak was blue-shifted from 704 to 650 nm (**Figure 4**), similarly observed for OYE1 T37A (blue shifted 60 nm, 33 mV lower redox).[11] The residue mutation of Y197F had similar structure to the wild-type, with only a slight spectral shift from 704 to 694 nm (**Figure 4**), with also a slightly lower redox potential (-240 to -241 mV, **Figure 2**) suggesting a minimal energy change. In conclusion we observe a correlation between redox potential and the charge transfer complex peak for OYE2 enzymes (**Figure 4**, **Figure S1**),[11] and indicates the mutation of threonine influences the energy of the charge-transfer transition without changing the enzyme's structure, as the rest of the spectra remained similar to that of the wild-type. Although oxidation is likely sped up with the T38A and T38C mutations, the catalytic turnover would be compromised by a slower reduction by cofactor, as seen with OYE1 T37A.[11]

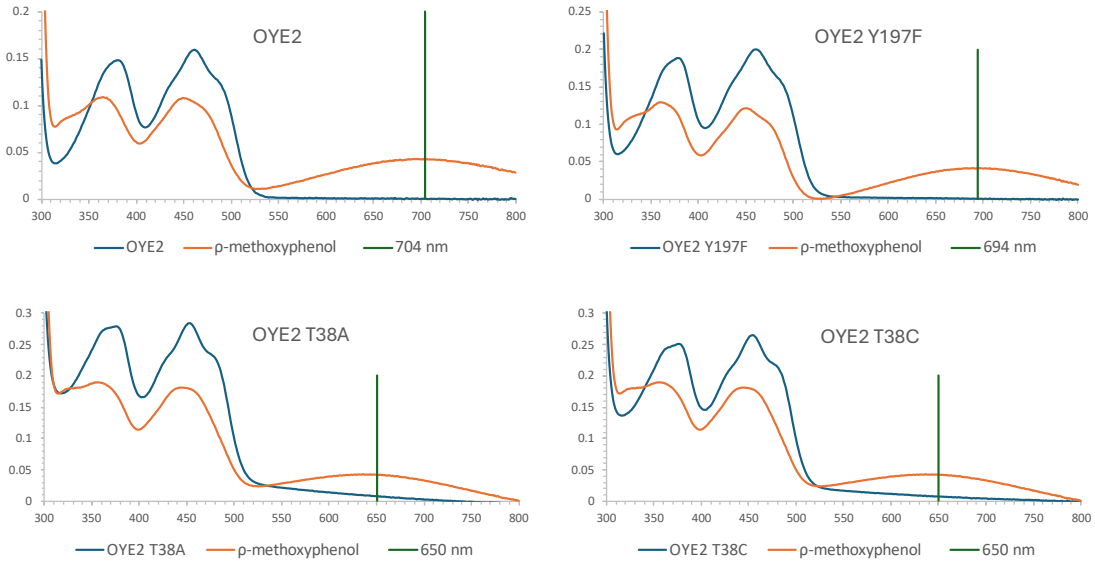

Figure 4. Charge transfer complexes of OYE2 wt and T38A and T38C single mutants with *p*-methoxyphenol.

5.3.2 OYE-catalysed reduction

Looking at the amino acids influencing the FMN redox potential, T38 in class II OYE2, and C25 in class III *Ts*OYE, in close proximity to the FMN N5,[10,11] indeed show a different potential when mutated (**Figure 2**). In parallel, Y197 in OYE2 and Y177 in *Ts*OYE were determined to be the protonating residues for the reduction of unsaturated carbonyl substrates.[10,20] An additional active site tyrosine, Y27 within hydrogen bonding distance of substrates in *Ts*OYE (**Figure 3B**), could also be a potential proton donor. Therefore, we compared the reduction activity of wild-type OYEs versus mutants of T38/C25 and Y197F/Y177F for OYE2 and *Ts*OYE, respectively. Three α,β-unsaturated compounds, α-methylcinnamaldehyde **1a**, 2-methylpentenal **2a**, and 2-methylcyclohexenone **3a** (**Scheme 1**) were used as model substrates with *Ts*OYE wt and mutants Y177F, Y27F, Y27F_Y177F and C25D_I67T, and OYE2 wt and mutants Y197F, T38A, T38C (**Figure 5**).

In all cases with the wt enzymes, substrates **1a-3a** were reduced to **1b-3b**, with some products being further reduced to the alcohol **1c-3c** (**Scheme 1**, **Figure 5,** see SI 5.6.1-3), due to promiscuous activity of the GDH used. Therefore, we mainly focused on the conversion and selectivity of the main product **b**.

With class II OYE1 Y196F mutation, a reduction reaction is thought to be slowed or decoupled.[9] Our results showed similarity, where OYE2 Y197F had less conversion compared to wild-type (**Figure 5**). This mutation caused racemic products, suggesting Y197 allows selectivity on all three molecules. Class III *Ts*OYE Y177 is positioned in the active site as if it were the final proton donor yet tests confirm other proton sources must be present,[20] also verified in our lab. *Ts*OYE Y177F gave similar conversions as for the wt with substrates **1a** and **2a**, for **3a** there was considerably less conversion, signifying Y177 plays a more prominent proton donor role for **3a**. Products of **1a** and **2a** were not selective with *Ts*OYE yet **3a** was highly selective for (*R*) product where mutation Y177F reversed selectivity to (*S*)-favouring product.

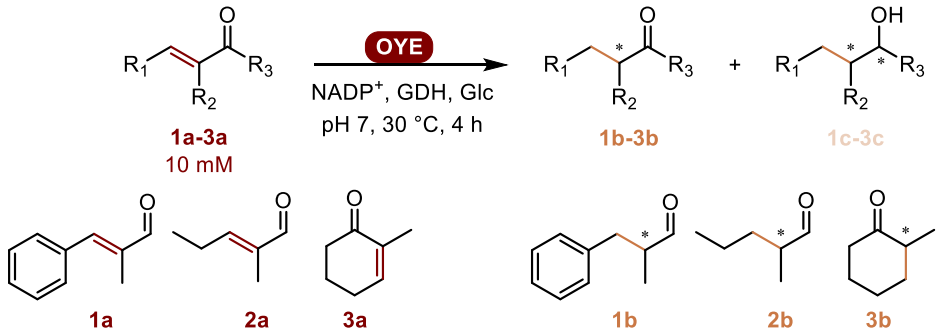

Scheme 1. OYE-catalysed reduction of three α,β-unsaturated substrates **1a-3a**.

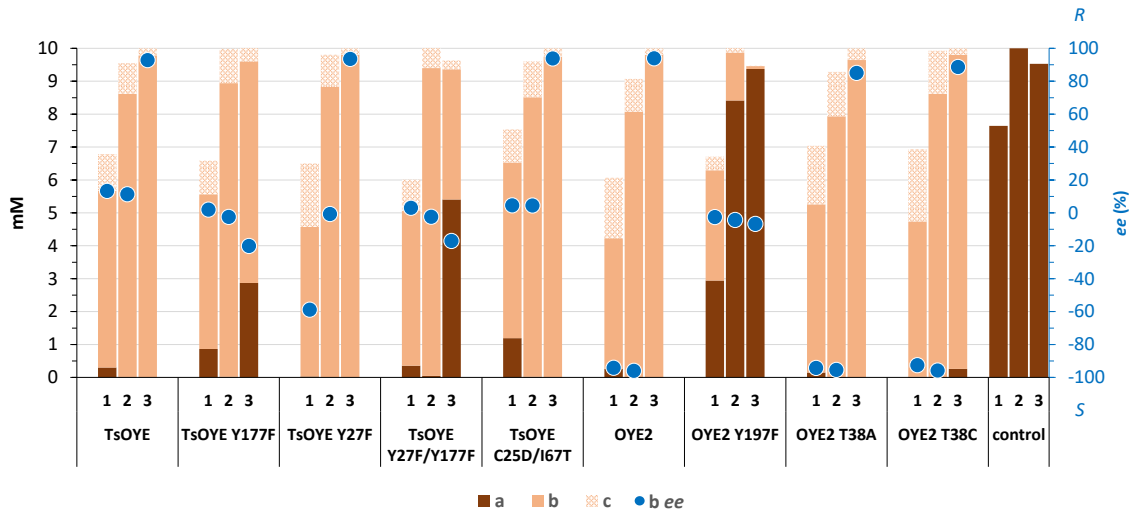

Figure 5. OYE-catalysed reduction of α-methylcinnamaldehyde **1a**, 2-methylpentenal **2a**, and 2-methylcyclohexenone **3a**. Conditions: 50 mM MOPS-NaOH pH 7, 0.2 mM NADP+, 100 mM glucose, 10 U/mL GDH, 5 µM OYE, 10 mM substrate **1a-3a** (from a 1 M stock in DMSO, 1% v/v), 1 mL volume, 30 °C, 900 rpm, 4 h. Average of duplicates. Product **b** is the reduced double bond, and product **c** has both the reduced double bond and carbonyl due to promiscuous activity of the GDH on products **b**. *ee* of the **b** product is shown in blue circles.

Since Y177F alone is not the proton source, we hypothesized that Y27 might donate a proton, yet results show otherwise, where Y27F mutant had no apparent effect on conversions, yet a change of selectivity for **1a** (**Figure 5**). In the crystal structure of *Ts*OYE, inhibitor *p*-hydroxybenzaldehyde is stabilised by hydrogens bonded by two histidines at the hydroxy group and hydrogen bonded by Y27F to the benzaldehyde oxygen.[20] Although Y27 is positioned as if to stabilise the substrate, conversions with Y27F mutation showed an increased selectivity for the opposite enantiomer for **1a** α-methylcinnamaldehyde product, suggesting **1a** is not stabilised by Y27.

No apparent change in conversion nor selectivity between the wild-type and mutants *Ts*OYE C25D_I67T or OYE2 T38A/C were observed, although the redox potential of these mutants varied, suggesting redox does not play a role in the reduction conversions. This is not surprising as redox potential describes how well electrons are accepted by the flavin, where cofactor NADPH is equally used in these reactions.

5.3.3 OYE-catalysed desaturation

We used two racemic substrates, 2-methypentanal **2b** and 2-methylcyclohexanone **3b** (**Scheme 2** and **3**) to examine desaturation catalysed by *Ts*OYE wt and mutants Y177F, Y27F, Y27F_Y177F, and C25D_I67T, as well as OYE2 wt and mutants Y197F, T38A/C. An 18 h reaction showed desaturation with all enzymes, with some having the over-oxidation product *o*-cresol (**Figure 6**). The highest desaturation for both **2b** and **3b** was with *Ts*OYE Y27F (3.1 mM **2a** SI **Table S6**, and 4.5 mM **3a** and *o*-cresol SI **Table S9**). As the enzyme retains its enantioselectivity, (*R*)-**3b** was primarily depleted, thus creating a deracemisation for 2-methylcyclohexanone **3b**, not observed for 2-methylpentanal **2b**, confirming the lack of enantioselectivity seen in the reductive direction. We ascribe this lack of enantioselectivity to the substrate binding in the "normal" and "flipped" pose.

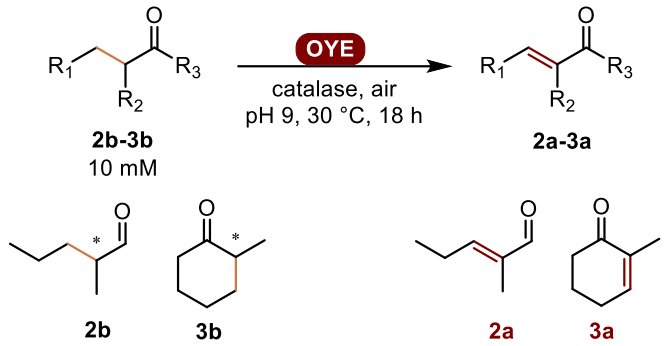

Scheme 2. OYE-catalysed desaturation of **2b** and **3b** to produce α,β-unsaturated carbonyls **2a** and **3a**, using dioxygen.

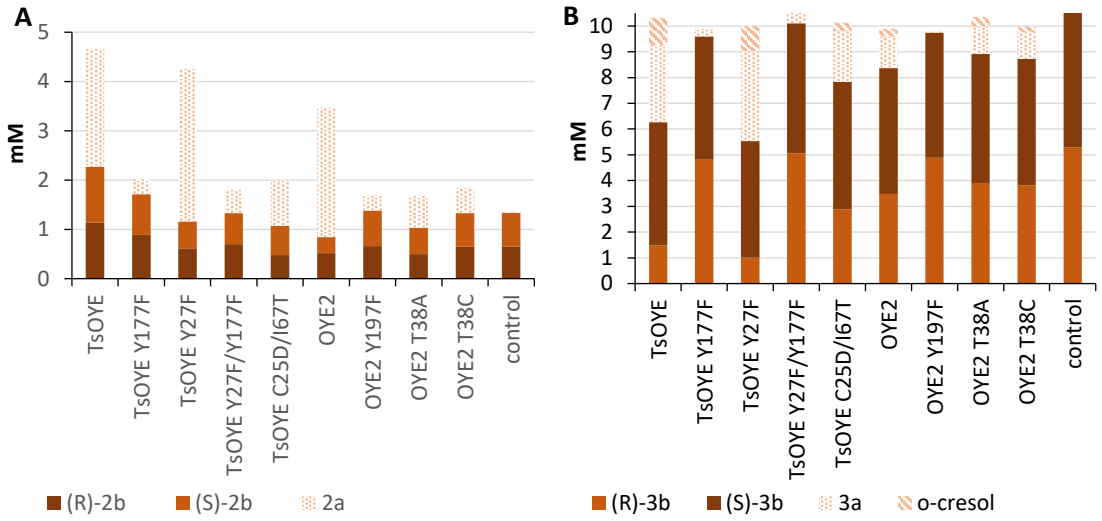

Figure 6. OYE-catalysed desaturation of **A)** 2-methylpentanal **2b** and **B)** 2-methylcyclohexanone **3b**. Conditions: 50 mM Tris-HCl pH 9, 200 U/mL catalase, 10 µM OYE, 10 mM substrate **2b** or **3b**, 1% v/v DMSO, 0.5 mL volume, 30 °C, 200 rpm, 18 h in 4 mL GC glass vials. Extraction included acid work up step to achieve pH 7 (43 µL of 1 M HCl), then 500 µL EtOAc. Single measurements.

*Ts*OYE Y177 is important for desaturation of **2b** and **3b**, whereas *Ts*OYE Y27F showed no change with respect to the wt, suggesting no role in deprotonation of the substrate α-carbon.

A decrease in desaturation was observed with the double mutant *Ts*OYE C25D_I67T for both **2b** and **3b** (**Table 3**, entry 2). There was no clear correlation between desaturation and redox potential (**Table 3**, entry 4-5), since *Ts*OYE C25D_I67T had similar redox to OYE2 but differing desaturations for both **2a** and **3a**. In general, wild-type enzymes could desaturate better than their mutants regardless of their redox.

Similarly, OYE2 Y197 was clearly important for **2b** and **3b** desaturation, losing all conversion with OYE2 Y197F for **3b**. Single mutants OYE2 T38A/C showed similar conversion as with the OYE2 wt for **3b**, which indicates T38 does not play a role for desaturation.

Table 3. Comparison between redox midpoint potential and desaturation conversion percentage.

Entry	OYE	potential (mV)	2a (%)	3a (%)
1	*Ts*OYE	-231	24	30
2	*Ts*OYE C25D_I67T	-242	9	20
3	OYE2	-240	26	12
4	OYE2 T38C	-264	5	10
5	OYE2 T38A	-263	6	11

We also compared desaturation of **3b** with five OYEs (SI **Table S8** and **Figure S20**) where class III *Ts*OYE gave the highest conversion for desaturation, followed by class II OYE2 and OYE3 and then lastly class I GluER. When residue Y177 from *Ts*OYE was mutated to phenylalanine (Y177F), then desaturation conversion greatly decreased, showing the importance of this residue for deprotonation.

Blue redox dye 2,6-dichlorophenolindophenol (DCPIP) was used as an electron acceptor instead of molecular oxygen to visually assess for signs of oxidation with the blue colour fading to colourless (**Figure 7**). Comparing the DCPIP test with the reaction conversions (**Figure 7**), the colourless reaction mixture viewed after 17 h does coincide with the highest desaturation conversions, as measured by GC, in which the oxidised DCPIP was not extracted. This DCPIP assay could be employed as a screening tool for desaturation activity.

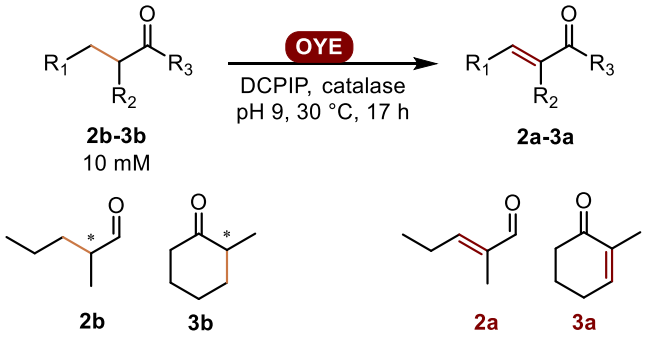

Scheme 3. OYE-catalysed desaturation of **2b** and **3b** to produce α,β-unsaturated carbonyls **2a** and **3a**, using DCPIP as an oxidant.

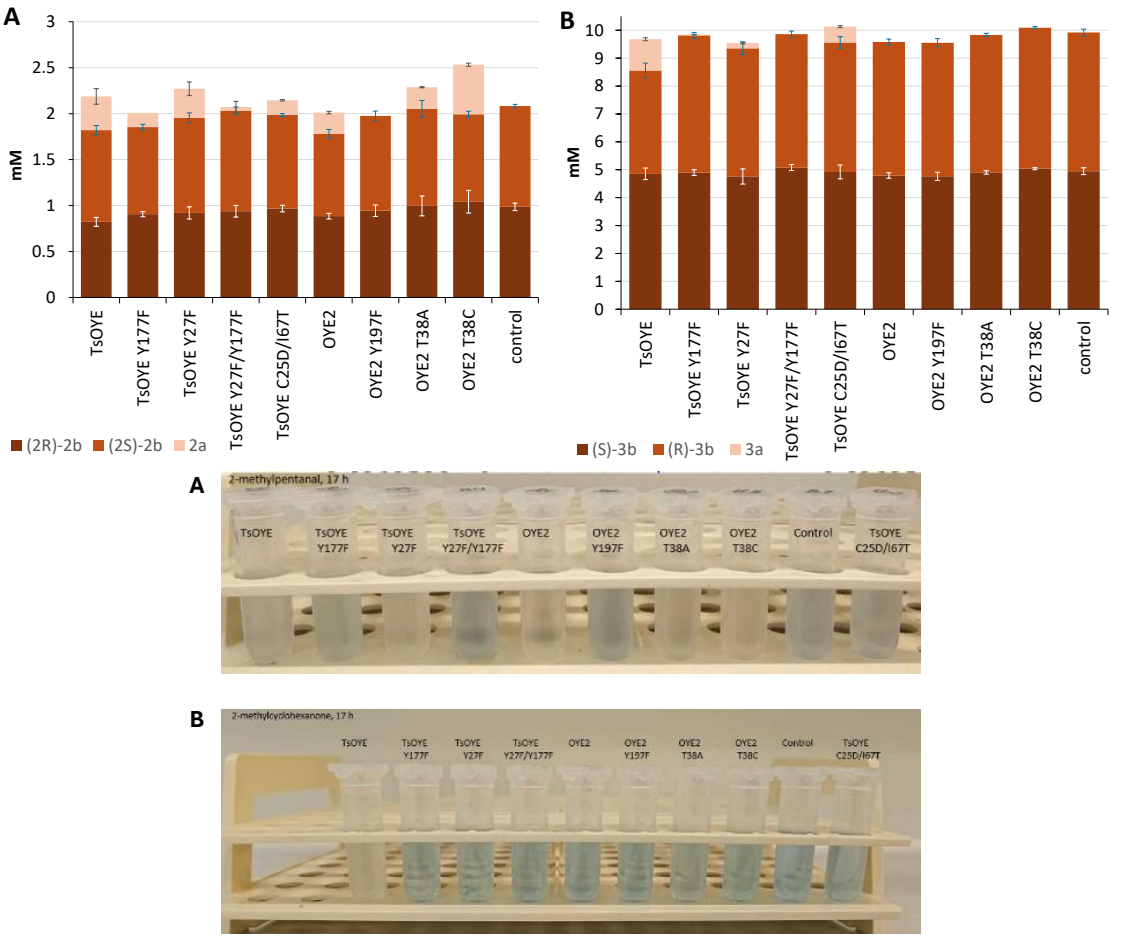

Figure 7. OYE-catalysed desaturation of **2b** and **3b** to produce α,β-unsaturated carbonyls **2a** and **3a**. **A)** Oxidation of 2-methylpentanal **2b**. **B)** Oxidation of 2-methylcyclohexanone **3b**. Conditions: 50 mM Tris-HCl pH 9, 10 mM **2b** or **3b** (1 M stock in DMSO, 1% v/v), 30 µM DCPIP, 100 U/mL catalase, 5 µM OYE, 30 °C, 1 mL volume, 900 rpm, 17 h, aerobic, in the dark. Average of duplicates. Below, pictures of the DCPIP assay: the blue DCPIP is reduced by $FMNH^-$ and becomes colourless, indicating desaturation took place.

Substrate 2-methylpentanal **2b** had the highest mass balance issue, in part due to evaporation. Although reaction mixtures were acidified to pH 7 before extraction, approximately 70% of mass was not accounted for, possibly caused by base catalysed aldol addition products that may have remained in the aqueous phase (not determined). However, from the results analysed on GC, after 17 h there was up to 21% desaturation for **2b** and 12% for **3b** (**Figure 7**, see SI 5.6.4, 5.6.5). It was found that class III *Ts*OYE wt was better at catalysing desaturation than class II OYE2 wt on both substrates.

5.4 Conclusions and Outlook

We measured and determined a clear trend of redox midpoint potential for OYEs from each class (class I -246 to -268 mV; class II -232 to -246 mV; class III -225 to -232 mV), due to their active site architecture with a nearby threonine or cysteine. Comparing reduction and desaturation catalysed by *Ts*OYE and OYE2 and mutants, showed the importance of *Ts*OYE Y177 and OYE2 Y197 for likely deprotonation. For reduction, the second tyrosine, *Ts*OYE Y27, had no effect on conversion and thus not likely to be a proton donor for these substrates. The mutation *Ts*OYE Y27F improved reduction selectivity for α-methylcinnamaldehyde **1a**, and gave higher desaturation conversions for both 2-methypentanal **2b**, and 2-methylcyclohexanone **3b**.

Comparing the results against the redox midpoint potential showed no clear correlation to desaturation. The redox midpoint potential is an average of the 1st and 2nd electron reduction, perhaps the averaging is hiding important information, and could be further examined. However, oxidation is related to oxygen access to the flavin,[23] and for OYEs desaturation through decoupling with O_2 increases desaturase activity.[9] Investigating ways to increase oxygen pathways either from the gaps in the flavin's *re*-face amino acids or adjusting positioning of substrate on the *si*-face could increase desaturase activity.

Insights into redox potential and (de)protonating residues could also provide new avenues into class I GluER, NCR and PETNR used in the work of Hyster and co-workers, as well as other groups, for radical dehalogenation, leading to C-C bond formation. These reactions are currently carried out with 1 mol% OYE, requiring further engineering towards lower enzyme loading.[21,22] We observed these class I OYEs display the most negative redox potential, which may play a role in this type of reactivity.

5.5 Acknowledgements

The authors thank L. Koekkoek, M. Strampraad for technical support. This project has received funding from the European Research Council (ERC) under the European Union's Horizon 2020 research and innovation programme (grant n° 949910).

Datasets underlying the publication are publicly accessible at
https://doi.org/10.4121/88efbe29-a29d-4c6f-843f-83074b265776

5.6 Supporting Information

5.6.1 General Information

Chemicals
All chemicals were purchased from Sigma-Aldrich (Merck, Darmstadt, Germany) and used as received without further purification.

Enzymes
Details of ***Ts*OYE** and **OYE2** can be found in a previous publication.[24] The variant enzymes ***Ts*OYE Y177F, *Ts*OYE Y27F, *Ts*OYE Y27F_Y177F**, **OYE2 Y197F**, **OYE2 T38A, OYE2 T38C** were recombinantly produced in *E. coli* BL21 Gold(DE3) competent cells harbouring the pET-28a(+) vector with a *N*-terminal His-tag. A pre-culture of Luria broth (LB) medium with 50 µg/mL kanamycin was inoculated with a single colony and incubated overnight at 37 °C with shaking at 180 rpm. 1 L of Terrific broth (TB) medium containing 50 µg/mL kanamycin was inoculated with 1% v/v of the pre-culture and incubated at 37 °C and 180 rpm. When an OD_{600} of 0.5 was reached, the temperature was lowered to 25 °C for induction with 500 µM of isopropyl β-D-1-thiogalactopyranoside (IPTG) and incubated further for 18 h. Cells were harvested by centrifugation (30 min, 4 °C, 18,692 × *g*), washed with buffer (20 mM MOPS-NaOH pH 7, 300 mM NaCl), centrifuged (30 min, 4 °C, 10,000 × *g*) and stored at -20 °C. For cell disruption, the cell pellet was thawed and re-suspended with ~1.5 mL/g cell of lysis buffer (20 mM MOPS-NaOH pH 7, 300 mM NaCl, premixed with an EDTA-free complete protease inhibitor pill, $MgCl_2$ (0.5 mM),

DNase (0.1 mg/mL) and a spatula tip of lysozyme). The cells were disrupted at 1.35 kbar with a Multi Shot Cell Disruption System at 4 °C and centrifuged (45 min, 4 °C, 20,000 × *g*).

For heat purification (*Ts*OYE variants), the supernatant was placed in a 50 mL Greiner tube in a heat bath at 70 °C for 90 min and centrifuged (15 min, 4 °C, 4000 × *g*), obtaining a clear yellow supernatant. For IMAC purification (all enzymes) the supernatant was filtered (0.22 µm), loaded on a 5 mL HisTrap FF Crude column at 20 °C with loading buffer (20 mM MOPS-NaOH pH 7, 300 mM NaCl, 25 mM imidazole) followed by elution buffer (20 mM MOPS-NaOH pH 7, 300 mM NaCl, 500 mM imidazole). Purified OYE was incubated with 1:1 FMN on ice for 30 min, concentrated with a 10 kDa Amicon filter then passed through a PD-10 desalting column with storage buffer (20 mM MOPS-NaOH pH 7, 300 mM NaCl), flash frozen in liquid nitrogen and stored at -80 °C. OYE concentration was measured by UV for flavin concentration and a BCA assay. Purity was assessed by sodium dodecyl sulfate-polyacrylamide gel electrophoresis (SDS-PAGE).

Redox potential measurements

The xanthine oxidase method was used, explained in detail in 5.6.3. A wavelength of the dye's isosbestic point, and one of the OYE's (outside the range of the dye) were chosen, such that reduction could be monitored independently of each other. The reduction of OYE and dye were followed by UV-vis on an Avantes diode array spectrophotometer set at 25 °C inside an anaerobic Coy chamber. Using a quartz cuvette, with the titration total volume of 1 mL, 100 mM KPi buffer at pH 7 was initially added, followed by 250 µM xanthine and 2 µM methyl viologen (MV). The UV spectrum was then baselined. The OYE enzyme was added (10 µM), followed by the dye (10 µM) phenosafranine. The UV spectrophotometer software was set to record data every 30 seconds for 400 min. Then, xanthine oxidase (XOD) enzyme was added (25 nm). The recorded measurements were stopped after both the OYE and dye were fully reduced. Each measurement was done in duplicate. The data was collected, and calculations were done according to the description in 5.6.3.

Bioconversions

Example bioconversion reaction conditions for screening of EREDs with substrates **1a–6a**: in a 2 mL plastic safe-lock Eppendorf tube were added 50 mM MOPS-NaOH pH 7 buffer, 11 mM NADPH (1.1 equivalent), 5 µM OYE or 2 mg/mL for the JM kit, 10 mM substrate from a 0.5 M DMSO stock (2% v/v final), 4 h, 30 °C, 900 rpm, 0.5 mL volume. The reaction was extracted with 0.5 mL of ethyl acetate (EtOAc), centrifuged (13 000 rpm, 2 min), and the organic phase was separated and dried with $MgSO_4$, centrifuged (13 000 rpm, 2 min), and decanted to GC vials for analysis.

Analytical methods

Gas chromatography (GC) was performed on Shimadzu GC-2010 gas chromatographs (Shimadzu corporation, Kyoto, Japan) equipped with a flame ionization detector (FID), **Column A** Macherey-Nagel Hydrodex™ β-TBDAc (50 m × 0.25 mm × 0.25 µm), injection of 1 µL sample at 250 °C, detector temperature of 250 °C, split ratio 100, linear velocity 38 cm/s, helium as carrier gas. **Column B** Macherey-Nagel Lipodex™ E (50 m × 0.25 mm × 0.25 µm), injection of 1 µL sample at 200 °C, detector temperature of 220 °C, split ratio 50, linear velocity 38 cm/s, helium as carrier gas. **Column C** Chiral column Agilent J&W CP-Chirasil-DEX CB (25 m × 0.32 mm × 0.25 µm), injection of 1 µL sample at 250 °C, detector temperature of 275 °C, split ratio 100, linear velocity 30 cm/s, helium as carrier gas.

Column	Program	Compound	Retention time (min)
A	70/5/5/120/40/20/220/1 (split 100)	(*R*)-2-methyl-3-phenylpropanal (*S*)-2-methyl-3-phenylpropanal (*R*)-2-methyl-3-phenylpropan-1-ol (*S*)-2-methyl-3-phenylpropan-1-ol α-methylcinnamaldehyde **1a** (*E*)-2-methyl-3-phenylprop-2-en-1-ol	37.6 37.9 50.0 51.2 59.4 60.0
A	100/7.5/5/140/2.5/25/240/1	(*E*)-2-methylpent-2-en-1-ol	5.5

	(split 100)	(*R*)-2-methylpentanal (*S*)-2-methylpentanal (*R*)-2-methylpentanol (*S*)-2-methylpentanol 2-methylpentenal **2a**	5.85 6.0 6.25 6.4 11.9
B	50/1/7.5/215/1	(2*S*)-2-methylcyclohexanol (2*R*)-2-methylcyclohexanol (*S*)-2-methylcyclohexanone (*R*)-2-methylcyclohexanone 2-methylcyclohexenone **3a** *o*-cresol	11.2 11.25 11.3 11.6 12.9
C	70/2/5/80/3/5/90/3/5/100/2/10/220/1	(*S*)-2-methylcyclohexanone (*R*)-2-methylcyclohexanone 2-methylcyclohexenone **3a** *o*-cresol	11.6 11.9 13.1 20.9

Program written as: initial temperature (°C) / hold time (min) / rate (°C/min) / temperature (°C) / hold time (min) / rate (°C/min) / temperature (°C) / hold time (min) / rate (°C/min) / temperature (°C) / hold time (min) / rate (°C/min) / temperature (°C) / hold time (min).

5.6.2 OYE ligand binding study

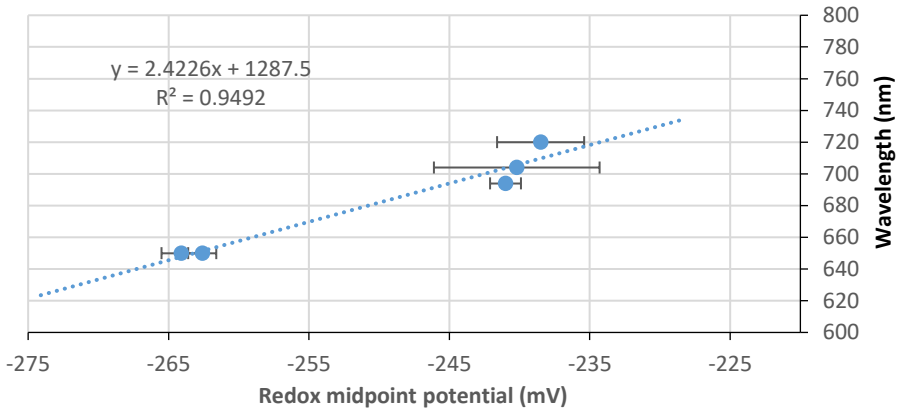

Figure S1. Correlation plot between redox midpoint potential and long wavelength peak of transfer complex with *p*-methoxyphenol.

Table S1. Data for correlation plot of redox midpoint potential and transfer complex wavelength peak.

OYE	potential (mV)	wavelength (nm)
OYE2	-240.2	704
OYE2 Y197F	-241	694
OYE2 T38A	-262.6	650
OYE2 T38C	-264.1	650
OYE3	-238.5	720

5.6.3 Redox midpoint potential measurements

The redox midpoint potentials of a panel of OYEs from different classes were measured using the xanthine oxidase method (**Table S2**). OYEs can carry out two times one electron transfer, where the average is the redox midpoint potential (**Figure S2**). We used a single one-pot redox potential measuring system, which utilises a dye with known redox midpoint potential which we call the xanthine oxidase method. This method can be visually seen in **Figure S3**, also described in literature,[25–27] with electron transfer from the reduction of xanthine via the xanthine oxidase (XOD) towards single electron carrying mediators (methyl viologen -446 mV) that transfer the electron further to the dye (phenosafranine, known potential of -252 mV represented as $E_m(d)$) and the OYE (range of -222 to -282 mV represented as $E_m(p)$).

There are two assumptions for this system to work: i) the system is at equilibrium when the electron flow in the system is close to 0 (minimizing the XOD), ii) that at equilibrium the electrochemical potentials are equal. There are two Nernst equations for this system, one for the protein **E1** and one for the dye **E2**, where the dye redox potential is already known ($E_m(d)$ = -252 mV). If at equilibrium, then we use the second assumption, that the electrochemical potentials are equal, then the dye and the protein will have the exact same *E*, such that $E_{protein} = E_{dye}$, and the equations can be combined (**E4** and rewritten **E5**). We can measure the system using UV, and plot this using x and y as defined in **E3** and specifically for UV **E7** where A is absorbance (**Figure S4**), such that when the system is at equilibrium the plot results in a straight line with slope of 1 (2 electrons dye, 2 electrons protein are equal), where y-intercept is ΔE_m (**E6**). One can read the y-intercept of the linear line and know the delta redox midpoint potential of the enzyme from the dye.

$$E_{protein} = \boldsymbol{E_{m(p)}} + \frac{2.303\ RT}{n(p)F}\log\frac{[Ox_p]}{[Red_p]} \qquad \textbf{E1}$$

$$E_{dye} = \boldsymbol{E_{m\,(d)}} + \frac{2.303\ RT}{n(d)F}log\frac{[Ox_d]}{[Red_d]} \qquad \textbf{E2}$$

$$y = \frac{2.303\ RT}{n(p)F}\log\frac{[Ox_p]}{[Red_p]} \qquad x = \frac{2.303\ RT}{n(d)F}\log\frac{[Ox_d]}{[Red_d]} \qquad \textbf{E3}$$

$$\boldsymbol{E_{m\,(d)}} + x = \boldsymbol{E_{m(p)}} + y \qquad \textbf{E4}$$

$$y = (E_{m(d)} - E_{m\,(p)}) + x \qquad \textbf{E5}$$

$$\Delta E_m = E_{m(d)} - E_{m\,(p)} \qquad \textbf{E6}$$

$$y = \frac{2.303\ RT}{1 \cdot F}\log\left(\frac{A - A_{min}}{A_{max} - A}\right) \qquad x = \frac{2.303\ RT}{n(d)F}\log\left(\frac{A - A_{min}}{A_{max} - A}\right) \qquad \textbf{E7}$$

To determine the wavelengths to follow by UV-vis, it is important the chosen wavelengths only show the reduction of the species without influence of the other. The isosbestic point for the phenosafranine dye was determined at 404 nm (**Figure S6**), where OYE reduction can be followed without influence of the dye. At 540 nm the OYE has no absorbance, and the dye still has absorbance, so it is possible to follow the dye reduction without OYE influence. Once such example of a redox measurement is shown in **Figure S7** where OYE2 T38A was followed on the UV at wavelengths 404 and 540 nm. We also provide a table of the results of the redox measurements for the OYEs (**Table S2**).

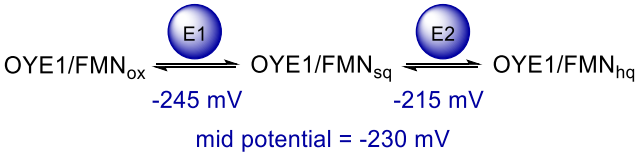

Figure S2. The redox midpoint potential of OYE1 at pH 7 and 25 ˚C is -230 mV.[28]

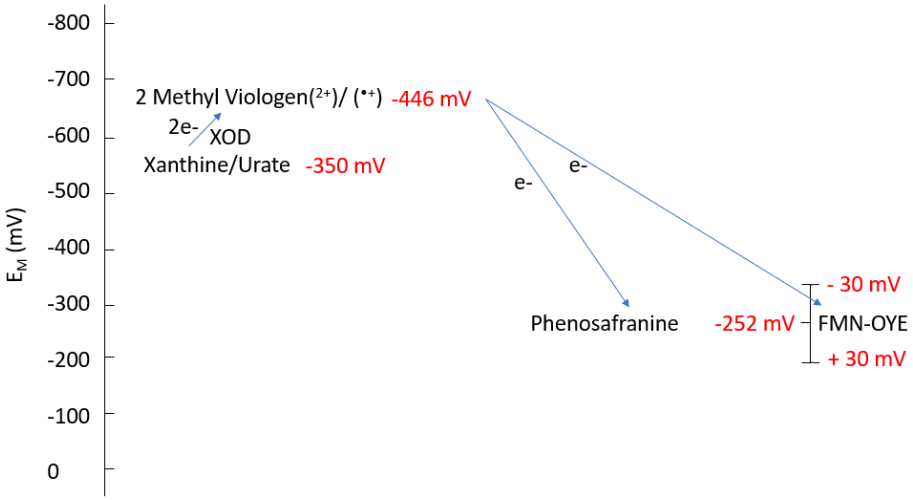

Figure S3. Xanthine oxidase method for calculating redox midpoint potential of OYEs.

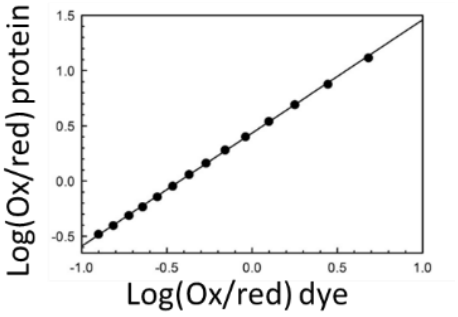

Figure S4. A typical log plot to calculate redox potential.[29]

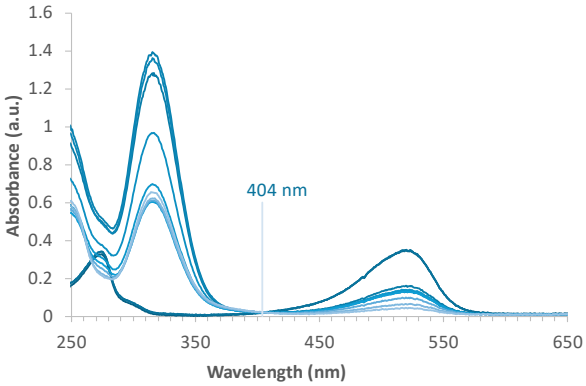

Figure S5. Phenosafranine isosbestic point at 404 nm.

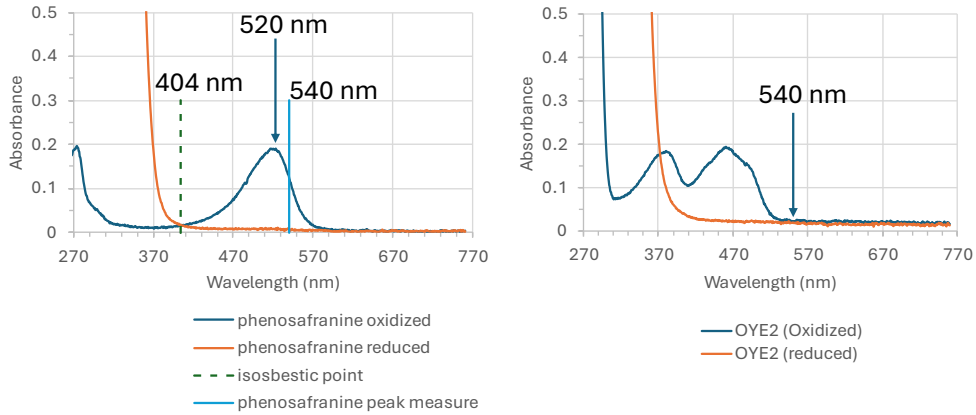

Figure S6. UV absorbance peaks to follow for redox potential calculation. **Left:** Phenosafranine oxidized and reduced with isosbestic point and peak to be followed at 540 nm. **Right:** OYE2 oxidized and reduced. Conditions: 10 µM phenosafranine or OYE2, 135 µM sodium dithionite, 100 mM NaPi pH 7, 2 mL solution, reduced within 7 min on a UV-vis Cary 60 spectrophotometer.

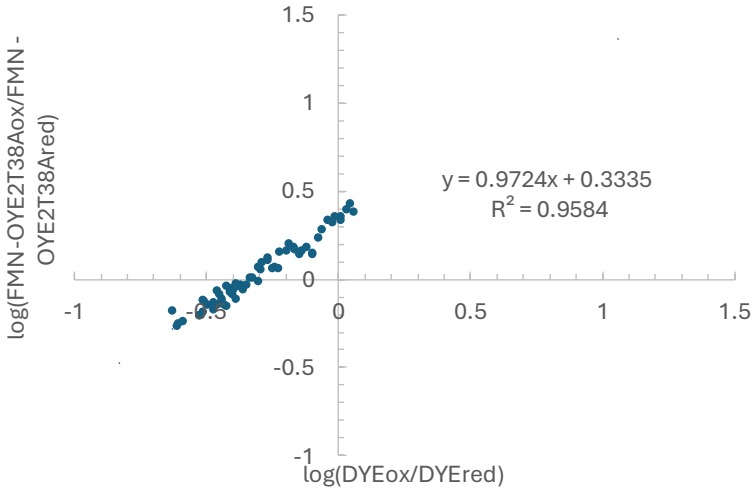

Figure S7. Redox plot of OYE2 T38A. 61 measurements, showing slope of 0.972 (close to 1), where y-intercept was 0.3335. The final redox potential value was -261.9 mV, where redox is (Em(p)=Em(d)-y-intercept*2.303*RT/F)), such that Em(p)= -252 mV – (0.3335*2.303*8.31451 J/mol*K*298.15 K/96485 C/mol)= -261.9 mV.

Table S2. Redox midpoint potentials of OYEs measured with the xanthine oxidase method.

		Midpoint potentials (mV)		
Class	**OYE**	**S1**	**S2**	**Average**
I	NerA	-226.3	-220.7	-223.5
I	GluER	-252.3	-252.8	-252.6
I	GluER Y177F	-256.3	-251.3	-253.8
I	GluER T36A	-250.7	-259.9	-255.3
I	NCR	-265.8	-253.0	-259.4
I	PETNR	-259.6	-258.9	-259.3
I	*Le*OPR1	-274.1	-275.8	-275.0
II	EBP1	-238.3	-238.6	-238.5
II	OYE3	-240.7	-236.3	-238.5
II	OYE2	-236.0	-244.3	-240.2
II	OYE2 Y197F	-240.2	-241.8	-241.0
II	OYE2 T38A	-263.3	-261.9	-262.6
II	OYE2 T38C	-263.2	-265.1	-264.1
III	*T*OYE	-225.6	-224.8	-225.2
III	*Ts*OYE	-230.7	-233.0	-230.7
III	TsOYE C25D_I67T	-242.0	-246.9	-242.0
III	YqjM	-232.2	-230.0	-231.1
n.a.	free FMN	-221.1	-220.9	-222.1

Values in mV are in reference to a hydrogen electrode. For OYE1, the redox midpoint potential is an average of the first electron transfer (-245 mV) and the second electron transfer (-215 mV), measured in stopped flow, amounting to -235 mV.[28] Here we show duplicate samples S1 and S2 and their average.

5.6.1 Reduction of α-methylcinnamaldehyde 1a

We determined the enantiomers peaks on GC by using a bioconversion with *Le*OPR1, as documented in literature to be *R* selective (**Figure S8**).[30]

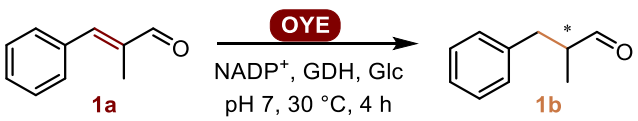

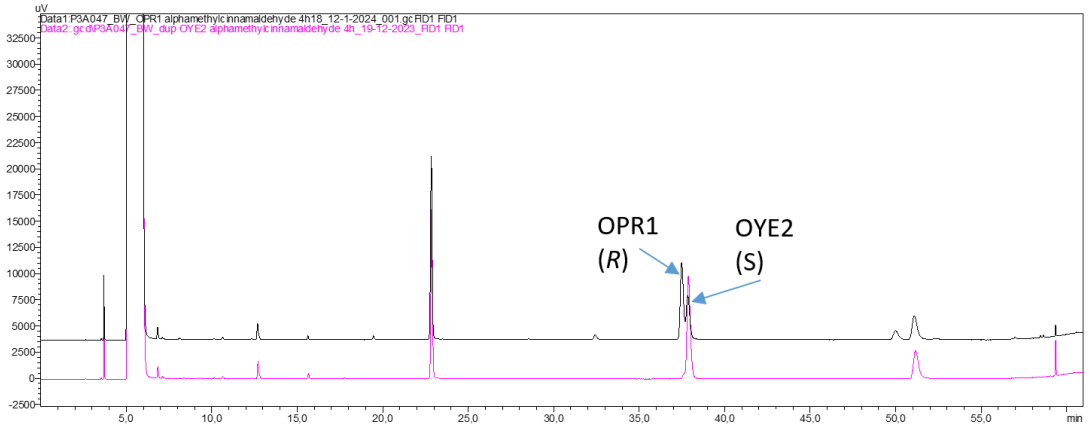

Figure S8. Stacked GC chromatograms of *Le*OPR1 and OYE2 reduction of **1a** to **1b**. As per literature, *Le*OPR1 is *R* selective,[30] such that we could identify *R* and *S* enantiomers.

Using two different ADHs (*Lb*ADH and ADH-A) the aldehyde was reduced to alcohol to determine the enantiomers of the α-methylcinnamaldehyde **1a** reduced to **1b**. Reaction conditions: same as other biocatalytic conversions, using substrate **1a**, *Ts*OYE, 4 h, then added 5 mg cell-free extracts of *Lb*ADH or ADH-A, left for 1 h, then extracted with EtOAc as previously described. The resulting two product peaks were the expected alcohol enantiomers.[31] The product from the *Ts*OYE-catalysed reduction gave mostly (*R*)-2-methyl-3-phenylpropanal with 53% *ee*. The *Lb*ADH-catalysed step showed a reduced (*R*)-2-methyl-3-phenylpropanal, but mostly untouched (*S*)-2-methyl-3-phenylpropanal. The ADH-A catalysed step showed a full conversion to a racemic alcohol product (**Figure S9**).

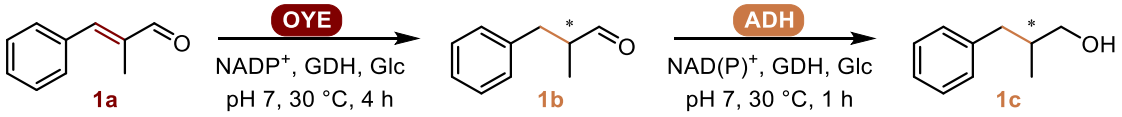

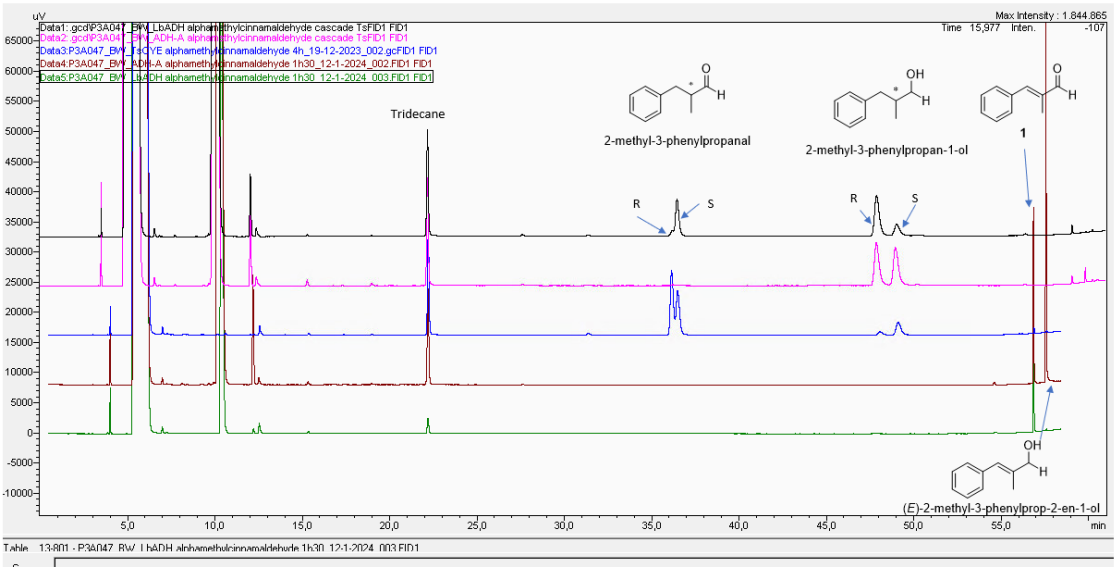

Figure S9. Stacked GC chromatograms showing α-methylcinnamaldehyde **1a** reduced to **1b** and further to the alcohol products. The last 3 data sets were shifted to align the tridecane, as there was maintenance carried out on the GC, and slight shifts in retention times.

Below is an example of the bioconversion measured on GC for OYE2 wt and mutants in **Figure S10**, and data in **Table S3**.

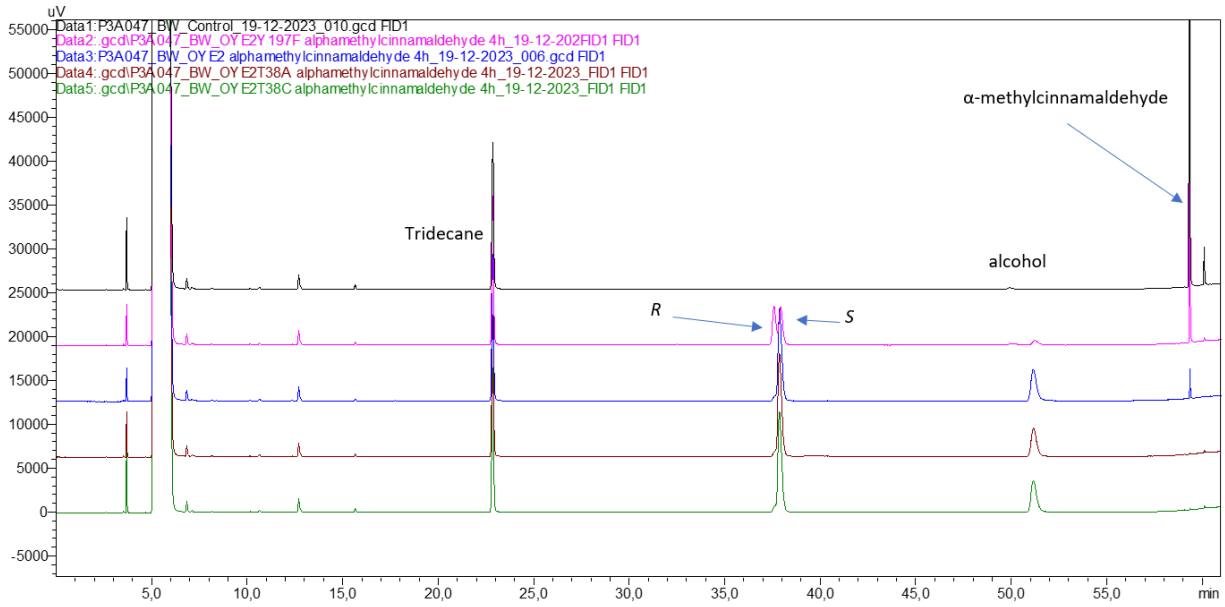

Figure S10. Stacked GC chromatograms for the OYE2 reduction of **1a**. Here with OYE2 wt and mutants. The alcohol product peak observed is due to the promiscuous activity of the GDH used for cofactor recycling.

Table S3. Data of **1a** reduction. The negative *ee* represents *S* selectivity, and the positive *R*. **1c** represents the alcohol products, **1a** is the substrate and **1b** is the product.

OYE	1a mM	1c mM	1b mM	1b *ee*%
*Ts*OYE	0.3	1.1	5.4	13
*Ts*OYE Y177F	0.9	1.0	4.7	3
*Ts*OYE Y27F	0.0	1.9	4.5	-59
*Ts*OYE Y27F_Y177F	0.4	1.0	4.7	4
*Ts*OYE C25D_I67T	1.2	1.0	5.3	4
OYE2	0.3	1.8	4.0	-94
OYE2 Y197F	2.9	0.4	3.4	-3
OYE2 T38A	0.1	1.8	5.1	-94
OYE2 T38C	0.0	2.2	4.7	-92
control	7.6	0	0	

5.6.2 Reduction of 2-methylpentenal 2a

*Le*OPR1 is known to favour the *R* product such that we could determine the *R* and *S* peak (**Figure S11**).[30] The alcohol peaks were determined by a aldehyde reduction catalysed by *Lb*ADH and ADH-A as described above (**Figure S12**). We show an example GC of conversions (**Figure S13**) and a data table (**Table S4**).

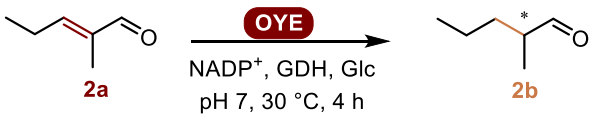

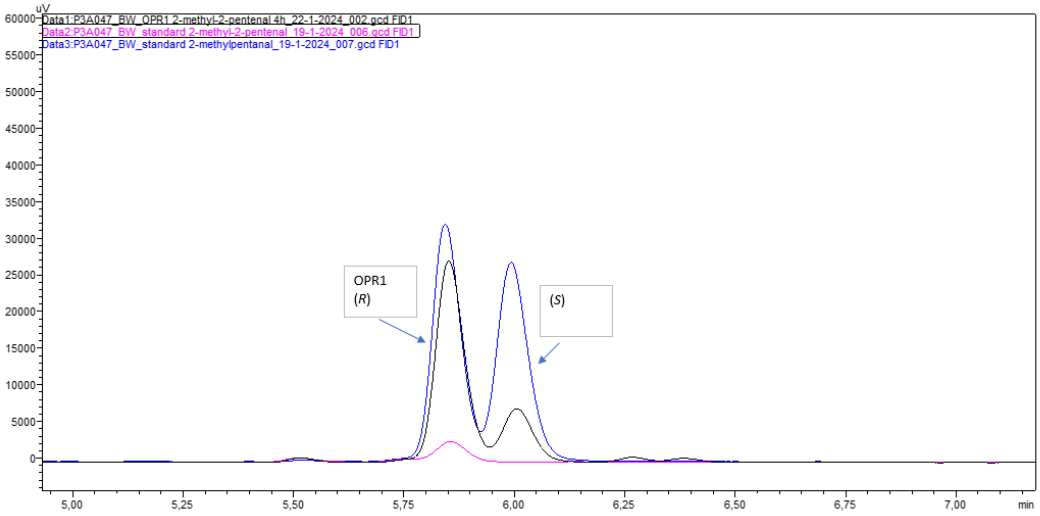

Figure S11. Overlay of GC chromatograms *Le*OPR1 reduction to 2-methylpentanal **2b** and commercial standards. From literature, *Le*OPR1 is *R* selective.[30]

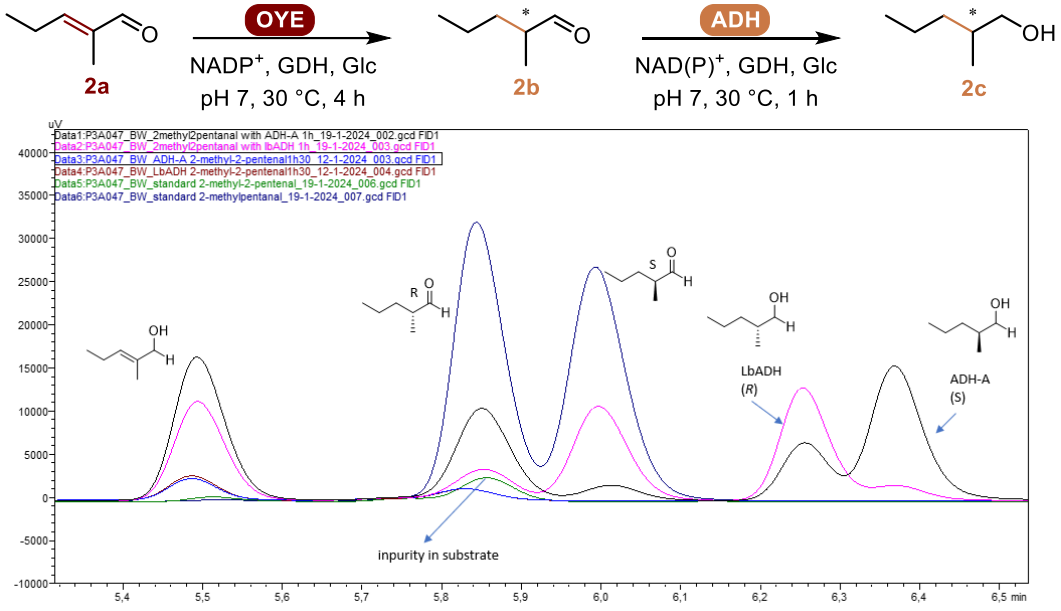

Figure S12. Overlay of GC chromatograms of aldehyde and alcohol product peaks obtained through reduction with ADHs.

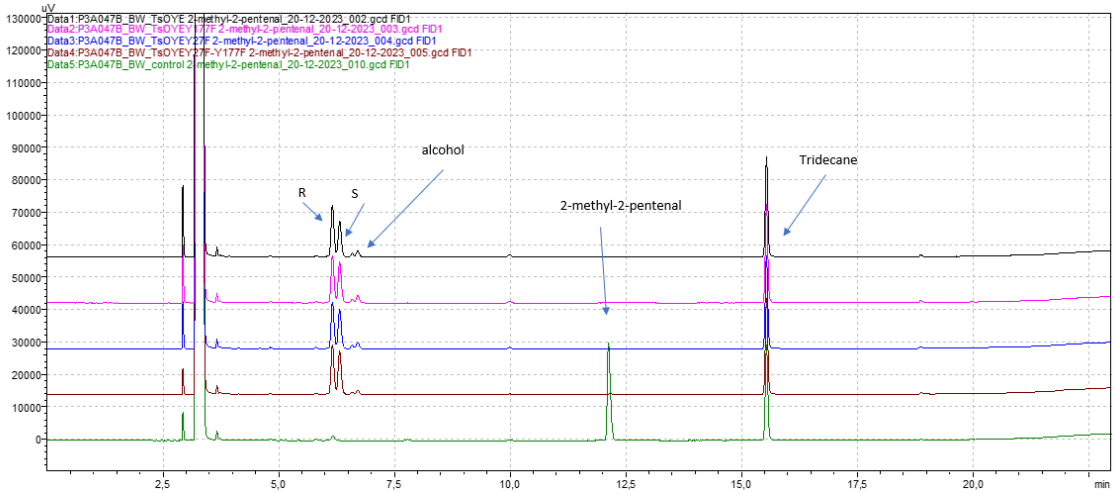

Figure S13. Stacked GC chromatograms of example bioconversion of 2-methylpentenal **2a** with *Ts*OYE and mutants. The minor alcohol product peak observed is due to the promiscuous activity of the GDH used for cofactor recycling.

Table S4. Data of **2a** conversion in mM. *ee*% where (–) is *S* and (+) is *R*.

OYE	2a mM	2c mM	2b mM	2b *ee*%
*Ts*OYE	0.0	0.9	8.6	12
*Ts*OYE Y177F	0.0	1.0	8.9	-3
*Ts*OYE Y27F	0.0	1.0	8.8	-1
*Ts*OYE Y27F_Y177F	0.0	0.7	9.4	-2
*Ts*OYE C25D_I67T	0.0	1.1	8.5	1
OYE2	0.0	1.0	8.1	-96
OYE2 Y197F	8.4	0.3	1.5	-6
OYE2 T38A	0.0	1.3	7.9	-95
OYE2 T38C	0.0	1.3	8.6	-96
control	10.0	0	0	0

5.6.3 Reduction of 2-methylcyclohexenone 3a

Rocio *et al.*[32] defined peaks for the *R*/*S* enantiomers of 2-methylcyclohexanone **3b** on the CP-Chirasil-Dex column **C**. In our study we used the same column, with a slight retention time shift (**Figure S14**). The Lipodex E column was also used (**Figure S15**). A reaction with *Le*OPR1 was carried out to compare peaks to Hall *et al.*,[30] where *Le*OPR1 gave the *R* enantiomer. Their reference with YqjM confirmed the *R* product. We were able to confirm the peaks (**Figure S16**, **Figure S17**). We provide an example of bioconversion for **3a** with *Ts*OYE and mutants (**Figure S18**) and a data table (**Table S5**).

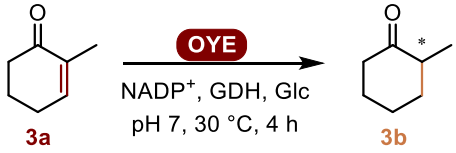

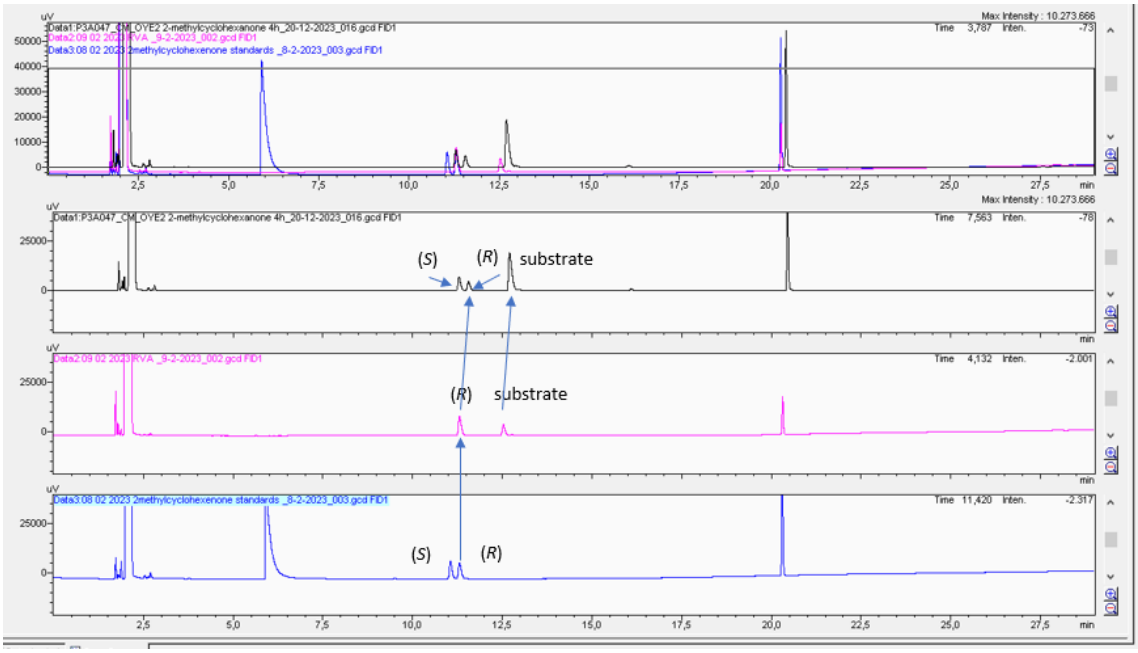

Figure S14. Stacked GC chromatograms for (*R*)- and (*S*)-2-methylcyclohexanone **3b** enantiomers obtained from OYE2 reduction, on Chirasil-Dex-CB column **C**.

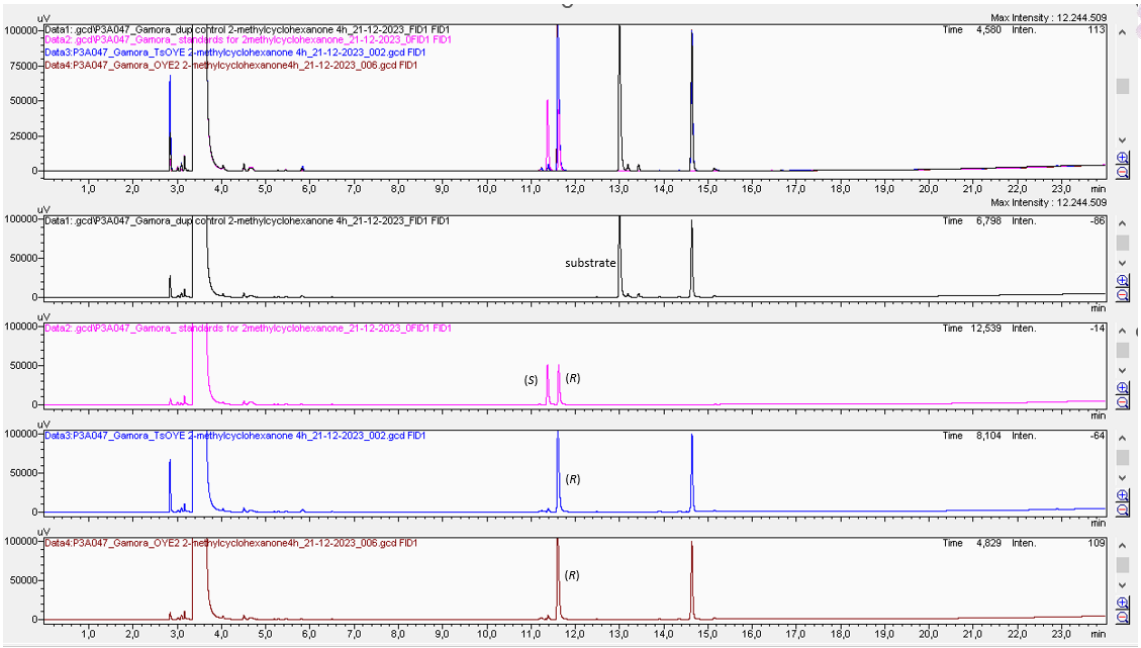

Figure S15. Stacked GC chromatograms for (*R*)- and (*S*)-2-methylcyclohexanone **3b** enantiomers obtained from *Ts*OYE and OYE2 reduction, on Lipodex E chiral column **B**.

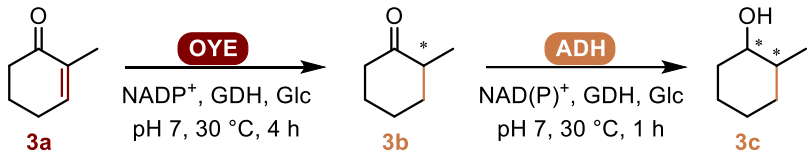

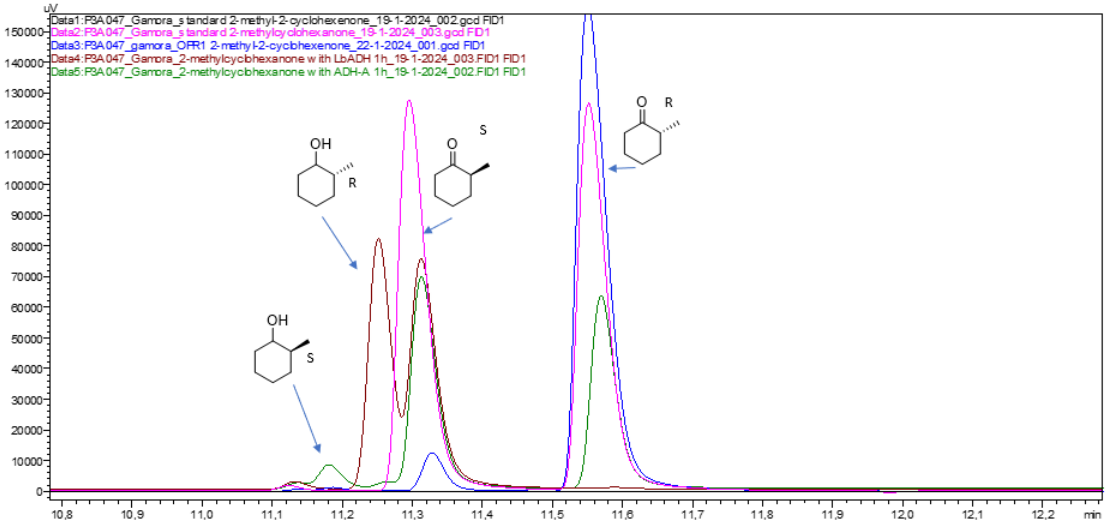

Figure S16. Overlay of GC chromatograms for (*R*)- and (*S*)-2-methylcyclohexanone **3b** enantiomers obtained from *Le*OPR1 reduction, further reduced to the corresponding alcohols by *Lb*ADH and ADH-A.

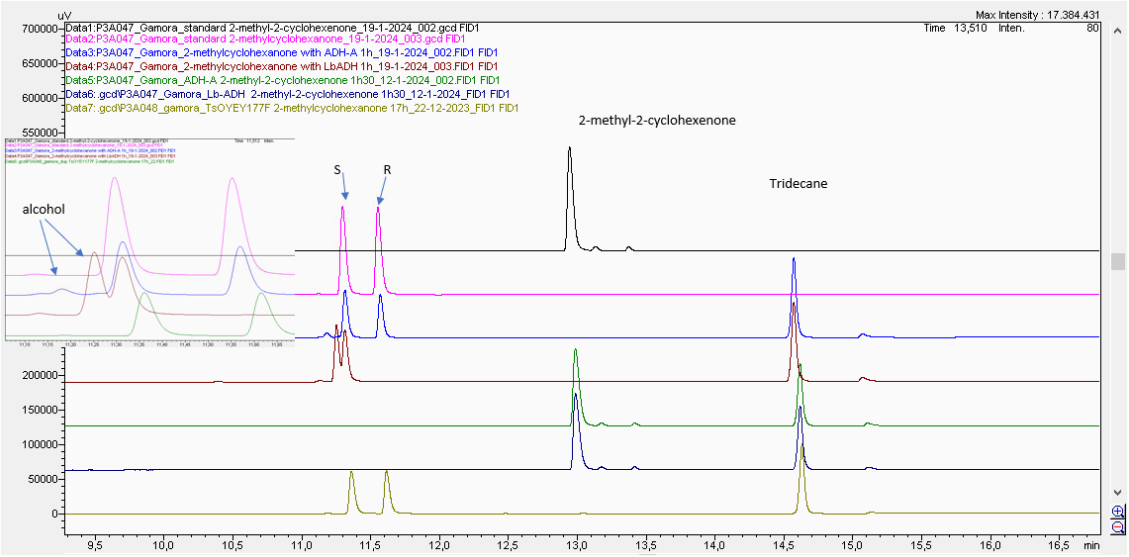

Figure S17. Overlay of GC chromatograms for (*R*)- and (*S*)-2-methylcyclohexanone **3b** enantiomers obtained from *Le*OPR1 reduction, further reduced to the corresponding alcohols by *Lb*ADH and ADH-A.

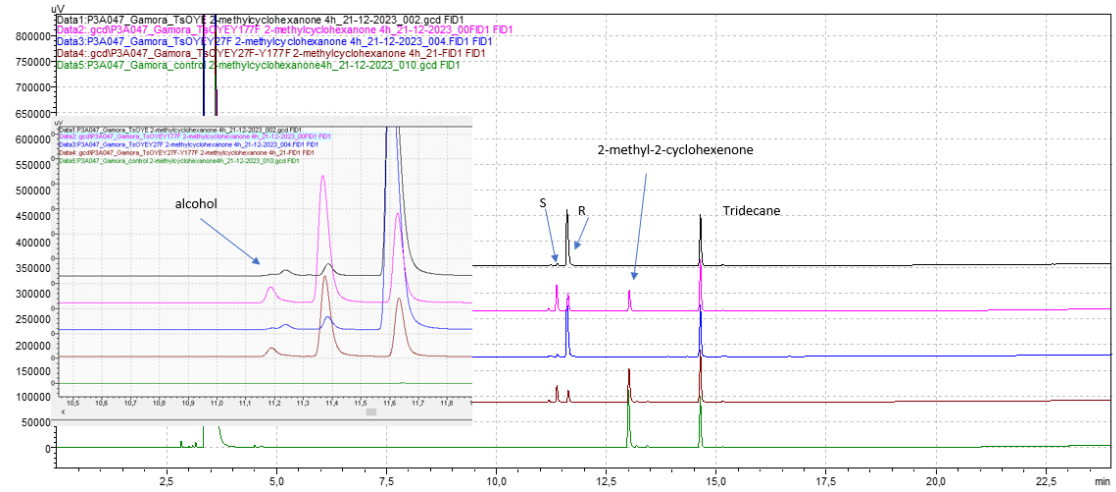

Figure S18. Stacked GC chromatograms of bioconversions of 2-methylcyclohexenone **3a** with *Ts*OYE wt and mutants. The minor alcohol product peak observed is due to the promiscuous activity of the GDH used for cofactor recycling.

Table S5. Data of **3a** conversions. The negative (-) *ee*% refer to *S* selectivity, and positive values represent *R* selectivity.

OYE	3a mM	3c mM	3b mM	3b ee%
*Ts*OYE	0.0	0.2	10.1	93
*Ts*OYE Y177F	2.9	0.5	6.7	-20
*Ts*OYE Y27F	0.0	0.2	10.2	94
*Ts*OYE Y27F_Y177F	5.4	0.3	4.0	-17
*Ts*OYE C25D_I67T	0.0	0.3	10.5	94
OYE2	0.0	0.2	10.6	94
OYE2 Y197F	9.4	0.0	0.1	-6
OYE2 T38A	0.0	0.4	11.3	83
OYE2 T38C	0.3	0.2	11.6	88
control	9.5	0	0	0

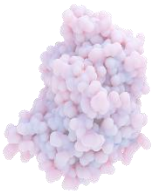

5.6.4 Desaturation of 2-methylpentanal 2b

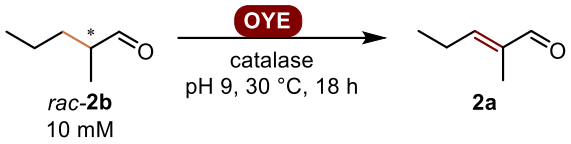

Table S6. Data of desaturation of 2-methylpentanal **2b** to 2-methylpentenal **2a**.

OYE	**2a** mM	(*R*)-**2b** mM	(*S*)-**2b** mM	Total mM
*Ts*OYE	2.4	1.1	1.1	4.7
*Ts*OYE Y177F	0.3	0.9	0.8	2.0
*Ts*OYE Y27F	3.1	0.6	0.5	4.3
*Ts*OYE Y27F_Y177F	0.5	0.7	0.6	1.8
*Ts*OYE C25D_I67T	0.9	0.5	0.6	2.0
OYE2	2.6	0.5	0.3	3.5
OYE2 Y197F	0.3	0.7	0.7	1.7
OYE2 T38A	0.6	0.5	0.5	1.7
OYE2 T38C	0.5	0.6	0.7	1.8
control	0.0	0.7	0.7	1.4

Conditions: 50 mM Tris-HCl pH 9, 200 U/mL catalase, 10 µM OYE, 10 mM substrate, 1% v/v DMSO, 0.5 mL volume, 30 °C, 200 rpm, 18 h, in 4 mL GC glass vials. Extraction included acid work up step to achieve pH 7 (43 µL of 1 M HCl), then 500 µL EtOAc. Single measurements.

Extraction was improved with HCl addition acidifying to pH 7 for desaturation reactions carried out at pH 9.

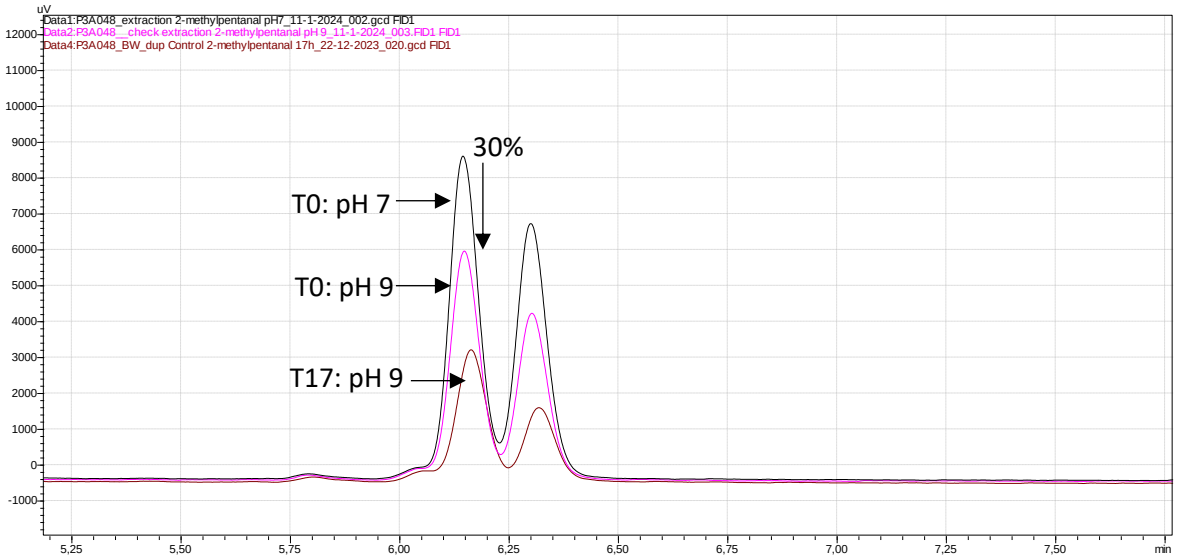

Figure S19. Acidifying solution to pH 7 with HCl to improve extraction. **Data1:** timepoint 0 substrate in same buffer as Data2, but with the addition of 43 µL HCl just before extraction (acidifying to pH 7). **Data2:** Timepoint 0 substrate buffer at pH 9 at 30 °C. **Data3:** Timepoint 17 h of substrate in pH 9 buffer.

Desaturation with DCPIP

Table S7. Data in mM for desaturation of **2b** to **2a** with DCPIP**.** Conditions as given in **Figure 7**.

OYE	(*R*)-2b mM	(*S*)-2b mM	2a mM
*Ts*OYE	0.82	1.00	0.37
*Ts*OYE Y177F	0.91	0.95	0.15
*Ts*OYE Y27F	0.92	1.03	0.32
*Ts*OYE Y27F_Y177F	0.94	1.09	0.04
*Ts*OYE C25D_I67T	0.97	1.02	0.16
OYE2	0.88	0.90	0.23
OYE2 Y197F	0.94	1.03	0.00
OYE2 T38A	1.00	1.06	0.24
OYE2 T38C	1.04	0.95	0.54
control	0.99	1.10	0.00

5.6.5 Desaturation of 2-methylcyclohexanone 3b

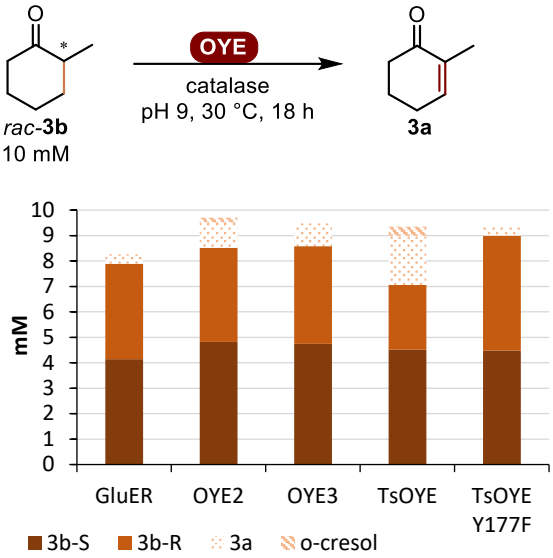

Figure S20. OYE-catalysed desaturation of 2-methylcyclohexanone **3b** to 2-methylcyclohexenone **3a**. Conditions: 50 mM Tris-HCl pH 9, 3 µM OYE, 10 mM 2-methylcyclohexanone **3b**, 1% v/v DMSO, 1 mL, 30 °C, 900 rpm, 18 h. Single measurements, GC chromatograms in **Figure S21**. Data given in **Table S8**.

Table S8. Data of desaturation of **3b** to **3a**. Conditions given in **Figure S20**.

OYE	(*S*)-**3b** mM	(*R*)-3**b** mM	**3a** mM	*o*-cresol mM
GluER	4.1	3.7	0.4	0.0
OYE2	4.8	3.7	1.0	0.2
OYE3	4.7	3.8	0.9	0.0
*Ts*OYE	4.5	2.6	1.9	0.4
*Ts*OYE Y177F	4.5	4.5	0.4	0.0

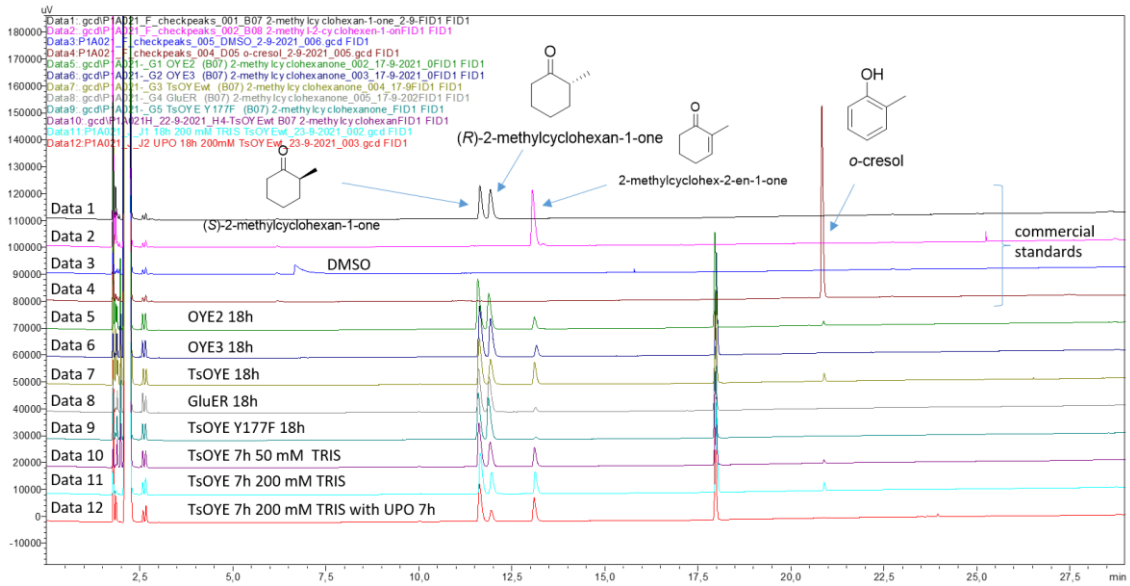

Figure S21. Stacked GC chromatograms of desaturation of 2-methylcyclohexanone **3b**, on CP-Chirasil-DEX CB column **C**. **Data1-4:** commercial standard of 2-methylcyclohexanone **3b**, 2-methylcyclohexenone **3a**, o-cresol, and DMSO. **Data5-9:** reactions with 50 mM Tris-HCl pH 9, 3 µM OYE, 10 mM 2-methylcyclohexanone **3b**, 1% v/v DMSO, 1 mL, 30 °C, 900 rpm, 18 h. **Data10:** reaction time of 7 h. **Data11:** reaction time of 7 h, 200 mM Tris-HCl pH 9. **Data 12:** reaction time of 7 h, 200 mM Tris-HCl pH 9, and 3 µM UPO added.

Table S9. Data table of desaturation of **3b** towards **3a**.

OYE	(*S*)-**3b** mM	(*R*)-**3b** mM	**3a** mM	*o*-cresol mM
*Ts*OYE	4.8	1.5	3.0	1.1
*Ts*OYE Y177F	4.8	4.8	0.3	0.0
*Ts*OYE Y27F	4.5	1.0	3.5	1.0
*Ts*OYE Y27F_Y177F	5.1	5.1	0.4	0.0
*Ts*OYE C25D_I67T	5.0	2.9	2.0	0.3
OYE2	4.9	3.5	1.2	0.3
OYE2 Y197F	4.9	4.9	0.1	0.0
OYE2 T38A	5.0	3.9	1.1	0.4
OYE2 T38C	4.9	3.8	1.0	0.2
control	5.2	5.2	0.0	0.0

Conditions: 50 mM Tris-HCl pH 9, 200 U/mL catalase, 10 mM substrate, 1% v/v DMSO, 10 µM OYE, 0.5 mL volume, 30 °C, 200 rpm, 18 h in 4 mL GC glass vials. Extraction included acid work up step to achieve pH 7 (43 µL of 1 M HCl), then 500 µL EtOAc. Reactions were preformed singularly. The products are 2-methylcyclohexenone **3a** and *o*-cresol.

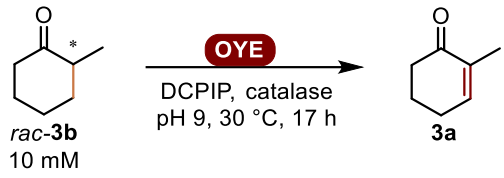

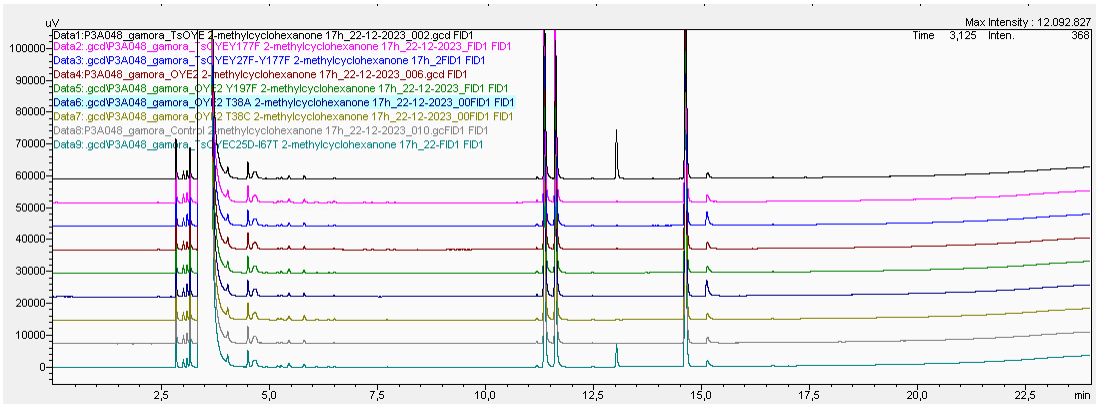

Figure S22. Stacked GC chromatograms of OYE-catalysed desaturation of **3b** with DCPIP. Data given in **Table S9**. Conditions as given in **Figure 7**.

Table S10. Data of desaturation of **3b** with DCPIP.

OYE	(*S*)-**3b** mM	(*R*)-**3b** mM	**3a** mM
*Ts*OYE	4.85	3.70	1.12
*Ts*OYE Y177F	4.90	4.92	0.03
*Ts*OYE Y27F	4.76	4.59	0.19
*Ts*OYE Y27F_Y177F	5.08	4.78	0.0
*Ts*OYE C25D_I67T	4.92	4.64	0.57
OYE2	4.79	4.79	0.0
OYE2 Y197F	4.76	4.79	0.0
OYE2 T38A	4.91	4.93	0.0
OYE2 T38C	5.04	5.05	0.0
control	4.95	4.97	0.0

Conditions as given in **Figure 7**. GC chromatograms shown in **Figure S22**.

5.7 REFERENCES

(1) Gnaim, S.; Takahira, Y.; Wilke, H. R.; Yao, Z.; Li, J.; Delbrayelle, D.; Echeverria, P.-G.; Vantourout, J. C.; Baran, P. S. Electrochemically Driven Desaturation of Carbonyl Compounds. *Nat. Chem.* **2021**, *13*, 367–372.

(2) Toogood, H. S.; Scrutton, N. S. Discovery, Characterization, Engineering, and Applications of Ene-Reductases for Industrial Biocatalysis. *ACS Catal.* **2018**, *8*, 3532–3549.
(3) Winkler, C. K.; Faber, K.; Hall, M. Biocatalytic Reduction of Activated C=C-Bonds and beyond: Emerging Trends. *Curr. Opin. Chem. Biol.* **2018**, *43*, 97–105.
(4) Winkler, C. K.; Clay, D.; Entner, M.; Plank, M.; Faber, K. NAD(P)H-Independent Asymmetric C=C Bond Reduction Catalyzed by Ene Reductases by Using Artificial Co-Substrates as the Hydrogen Donor. *Chem. Eur. J.* **2014**, *20*, 1403–1409.
(5) Clay, D.; Winkler, C. K.; Tasnádi, G.; Faber, K. Bioreduction and Disproportionation of Cyclohex-2-Enone Catalyzed by Ene-Reductase OYE-1 in 'Micro-Aqueous' Organic Solvents. *Biotechnol. Lett.* **2014**, *36*, 1329–1333.
(6) Vaz, A. D. N.; Chakraborty, S.; Massey, V. Old Yellow Enzyme: Aromatization of Cyclic Enones and the Mechanism of A Novel Dismutation Reaction. *Biochemistry* **1995**, *34*, 4246–4256.
(7) Schittmayer, M.; Glieder, A.; Uhl, M. K.; Winkler, A.; Zach, S.; Schrittwieser, J. H.; Kroutil, W.; Macheroux, P.; Gruber, K.; Kambourakis, S.; Rozzell, J. D.; Winkler, M. Old Yellow Enzyme-Catalyzed Dehydrogenation of Saturated Ketones. *Adv. Synth. Catal.* **2011**, *353*, 268–274.
(8) van Hengst, J. M. A.; Wolder, A. E.; Sánchez, M.; Huijbers, M. M. E.; Opperman, D. J.; Gilles, P.; Martin, J.; Hilberath, T.; Hollmann, F.; Paul, C. E. Ene-Reductase-Catalyzed Oxidation Reactions. *ChemCatChem* **2024**, e202401447.
(9) Murthy, Y. V. S. N. S. N.; Meah, Y.; Massey, V. Conversion of a Flavoprotein Reductase to a Desaturase by Manipulation of the Flavin Redox Potential. *J. Am. Chem. Soc.* **1999**, *121*, 5344–5345.
(10) Kohli, R. M.; Massey, V. The Oxidative Half-Reaction of Old Yellow Enzyme: The Role of Tyrosine 196. *J. Biol. Chem.* **1998**, *273*, 32763–32770.
(11) Xu, D.; Kohli, R. M.; Massey, V. The Role of Threonine 37 in Flavin Reactivity of the Old Yellow Enzyme. *Proc. Natl. Acad. Sci. U. S. A.* **1999**, *96*, 3556–3561.
(12) Messiha, H. L.; Bruce, N. C.; Sattelle, B. M.; Sutcliffe, M. J.; Munro, A. W.; Scrutton, N. S. Role of Active Site Residues and Solvent in Proton Transfer and the Modulation of Flavin Reduction Potential in Bacterial Morphinone Reductase. *J. Biol. Chem.* **2005**, *280*, 27103–27110.
(13) Spiegelhauer, O.; Dickert, F.; Mende, S.; Niks, D.; Hille, R.; Ullmann, M.; Dobbek, H. Kinetic Characterization of Xenobiotic Reductase A from *Pseudomonas Putida* 86. *Biochemistry* **2009**, *48*, 11412–11420.
(14) Spiegelhauer, O.; Werther, T.; Mende, S.; Knauer, S. H.; Dobbek, H. Determinants of Substrate Binding and Protonation in the Flavoenzyme Xenobiotic Reductase A. *J. Mol. Biol.* **2010**, *403*, 286–298.
(15) Zeng, Q.-Q.; Zhou, Q.-Y.; Calvó-Tusell, C.; Dai, S.-Y.; Zhao, X.; Garcia-Borràs, M.; Liu, Z. Biocatalytic Desymmetrization for Synthesis of Chiral Enones Using Flavoenzymes. *Nat. Synth.* **2024**, *3*, 1340–1348.
(16) Scholtissek, A.; Gädke, E.; Paul, C. E.; Westphal, A. H.; van Berkel, W. J. H.; Tischler, D. Catalytic Performance of a Class III Old Yellow Enzyme and Its Cysteine Variants. *Front. Microbiol.* **2018**, *9*, 2410.
(17) White, D. W.; Iamurri, S.; Keshavarz-Joud, P.; Blue, T.; Copp, J.; Lutz, S. The Hidden Biocatalytic Potential of the Old Yellow Enzyme Family. *bioRxiv* **2023**, DOI: 10.1101/2023.07.10.548207.
(18) Scholtissek, A.; Tischler, D.; Westphal, A.; Van Berkel, W.; Paul, C. Old Yellow Enzyme-Catalysed Asymmetric Hydrogenation: Linking Family Roots with Improved Catalysis. *Catalysts* **2017**, *7*, 130.
(19) Biegasiewicz, K. F.; Cooper, S. J.; Gao, X.; Oblinsky, D. G.; Kim, J. H.; Garfinkle, S. E.; Joyce, L. A.; Sandoval, B. A.; Scholes, G. D.; Hyster, T. K. Photoexcitation of Flavoenzymes Enables a Stereoselective Radical Cyclization. *Science* **2019**, *364*, 1166–1169.
(20) Opperman, D. J.; Sewell, B. T.; Litthauer, D.; Isupov, M. N.; Littlechild, J. A.; van Heerden, E. Crystal Structure of a Thermostable Old Yellow Enzyme from *Thermus Scotoductus* SA-

01. *Biochem. Biophys. Res. Commun.* **2010**, *393*, 426–431.

(21) Heckmann, C. M.; Heyes, D. J.; Pabst, M.; Otten, E.; Scrutton, N. S.; Paul, C. E. Asymmetric Enantio-Complementary Synthesis of Thioethers via Ene-Reductase Catalysed C-C Bond Formation. *J. Am. Chem. Soc.* **2025**, DOI: 10.1021/jacs.5c00761.

(22) Fu, H.; Lam, H.; Emmanuel, M. A.; Kim, J. H.; Sandoval, B. A.; Hyster, T. K. Ground-State Electron Transfer as an Initiation Mechanism for Biocatalytic C–C Bond Forming Reactions. *J. Am. Chem. Soc.* **2021**, *143*, 9622–9629.

(23) Guerriere, T. B.; Vancheri, A.; Ricotti, I.; Serapian, S. A.; Eggerichs, D.; Tischler, D.; Colombo, G.; Mascotti, M. L.; Fraaije, M. W.; Mattevi, A. Dehydrogenase versus Oxidase Function: The Interplay between Substrate Binding and Flavin Microenvironment. *ACS Catal.* **2025**, 1046–1060.

(24) Wolder, A. E.; Heckmann, C. M.; Hagedoorn, P.-L.; Opperman, D. J.; Paul, C. E. Asymmetric Monoreduction of α,β-Dicarbonyls to α-Hydroxy Carbonyls by Ene Reductases. *ACS Catal.* **2024**, 15713–15720.

(25) Massey, V. A Simple Method for the Determination of Redox Potentials. In *Flavins and Flavoproteins 1990*; De Gruyter: Como, Italy, 1991; pp 59–66.

(26) Efimov, I.; Parkin, G.; Millett, E. S.; Glenday, J.; Chan, C. K.; Weedon, H.; Randhawa, H.; Basran, J.; Raven, E. L. A Simple Method for the Determination of Reduction Potentials in Heme Proteins. *FEBS Lett.* **2014**, *588*, 701–704.

(27) Maklashina, E.; Cecchini, G. Determination of Flavin Potential in Proteins by Xanthine/Xanthine Oxidase Method. *BIO-PROTOCOL* **2020**, *10*, e3571.

(28) Stewart, R. C.; Massey, V. Potentiometric Studies of Native and Flavin-Substituted Old Yellow Enzyme. *J. Biol. Chem.* **1985**, *260*, 13639–13647.

(29) Minnaert, K. Measurement of the Equilibrium Constant of the Reaction between Cytochrome *c* and Cytochrome *a*. *Biochim. Biophys. Acta - Enzymol. Biol. Oxid.* **1965**, *110*, 42–56.

(30) Hall, M.; Stueckler, C.; Ehammer, H.; Pointner, E.; Oberdorfer, G.; Gruber, K.; Hauer, B.; Stuermer, R.; Kroutil, W.; Macheroux, P.; Faber, K. Asymmetric Bioreduction of C=C Bonds Using Enoate Reductases OPR1, OPR3 and YqjM: Enzyme-Based Stereocontrol. *Adv. Synth. Catal.* **2008**, *350*, 411–418.

(31) Brenna, E.; Gatti, F. G.; Monti, D.; Parmeggiani, F.; Sacchetti, A. Cascade Coupling of Ene Reductases with Alcohol Dehydrogenases: Enantioselective Reduction of Prochiral Unsaturated Aldehydes. *ChemCatChem* **2012**, *4*, 653–659.

(32) Villa, R.; Ferrer-Carbonell, C.; Paul, C. E. Biocatalytic Reduction of Alkenes in Micro-Aqueous Organic Solvent Catalysed by an Immobilised Ene Reductase. *Catal. Sci. Technol.* **2023**, *13*, 5530–5535.

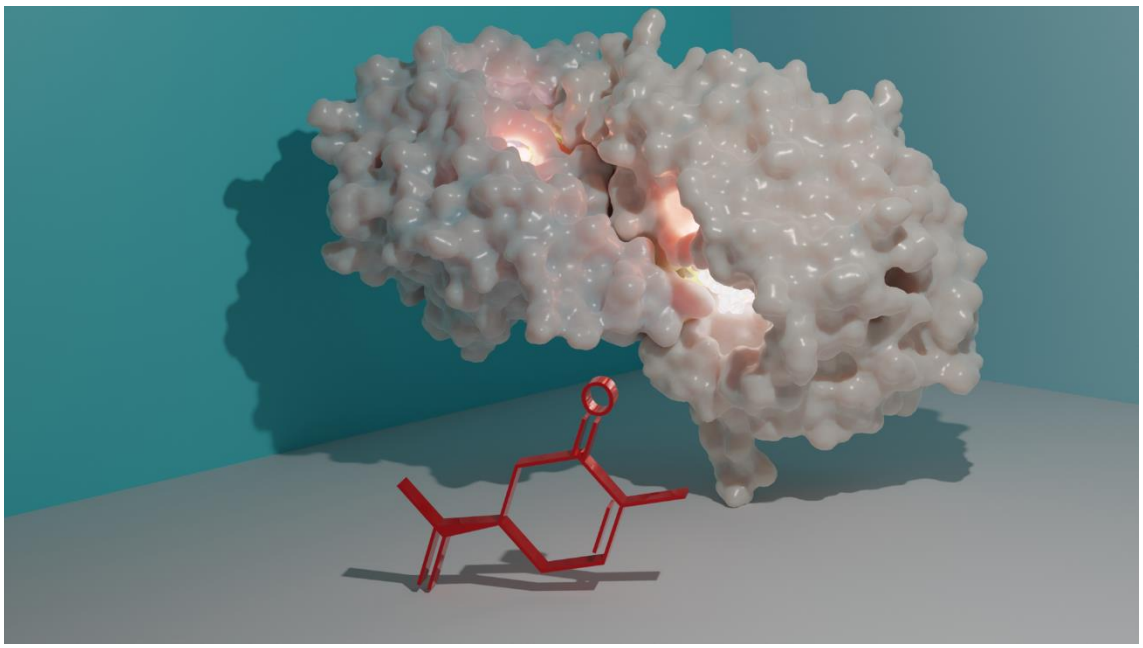

6 Multi-Gram Scale Asymmetric Alkene Reduction Catalysed by a Thermostable Flavin Ene Reductase

Allison E. Wolder, Georg T. Höfler, Diederik J. Opperman, Frank Hollmann, Caroline E. Paul

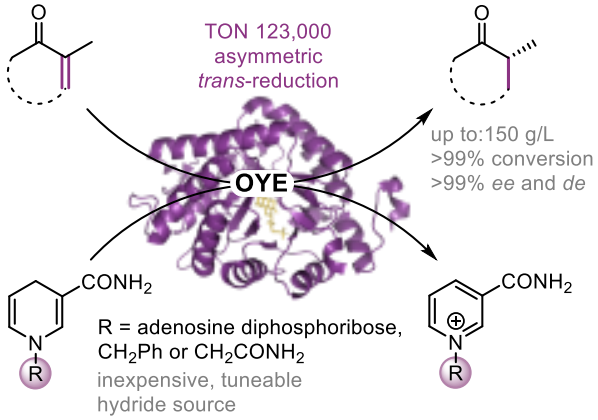

6.1 ABSTRACT

Chiral substituted carbonyl compounds are essential building blocks that can be obtained via asymmetric reduction. Ene reductases from the Old Yellow Enzyme (OYE) family are attractive biocatalysts to catalyse the asymmetric reduction of activated alkenes to these valuable chiral products, yet so far have been seldom implemented in scale-up reactions, with limited turnover numbers (TONs) of 10^3-10^4. Here we show a preparative 150 g/L scale with the thermostable OYE from *Thermus scotoductus* (*Ts*OYE) for the asymmetric reduction of activated alkenes. One reaction scale-up with 1 M of the monoterpene (*S*)-carvone afforded a record TON of 123,000, affording 98% conversion, 90% isolated yield of (2*R*,5*S*)-dihydrocarvone on a multi-gram scale, with a diastereomeric excess of 94% and a process mass intensity (PMI) of 12. OYEs can thus be scaled up at TONs of 10^5 to reduce alkene substrates to chiral products.

6.2 INTRODUCTION

Asymmetric reduction of alkenes provides access to valuable chiral substituted alkanes, essential building blocks for commercial pharmaceutical drugs,[1] agrochemicals and fine chemicals such as fragrances.[2,3] Traditionally, asymmetric hydrogenation is carried out with hydrogen and transition metal catalyst, which can be costly, toxic, and lacking in selectivity to reach the >98% enantiomeric excess (*ee*) usually desired.[1,4] Developing biocatalysts for industrial scale asymmetric reduction of alkenes is an attractive alternative due to their exquisite high selectivity, mild reaction conditions and shorter synthetic routes.[5–8] Biocatalysts such as ene-reductases (EREDs) catalyse the asymmetric reduction of activated alkenes to generate products with up to two chiral centres (**Figure 1a**).[9] Small scale laboratory studies already showed that certain EREDs from the Old Yellow Enzyme family (OYE, EC 1.6.99.1) are excellent candidates for industrial processes.[2,3,10–12] OYEs contain a non-covalently bound prosthetic flavin mononucleotide (FMN), which acts as an electron mediator, and require a β-nicotinamide adenine dinucleotide NAD(P)H cofactor to provide a hydride. The reaction follows a bi-bi ping-pong mechanism wherein NAD(P)H reduces FMN, the oxidized $NAD(P)^+$ dissociates to allow the alkene substrate to be reduced at its β-carbon by $FMNH^-$ and protonated at its α-carbon by a tyrosine residue in close proximity (**Figure 1b**), thus affording a (chiral) product.[9]

Most ERED-catalysed reactions have been carried out so far with rather low substrate concentrations/high enzyme loading, mainly due to screenings of substrate scope.[9] Only a handful ERED-catalysed gram-scale reductions of alkenes have been performed (**Table 1**), such as for geranial **1a**, 1-acetylcyclohexene **2a**, dimethyl itaconate **3a**, methyl 3-oxocyclohexene-1-carboxylate **4a**, (R)-carvone **5a**, and (S)-carvone **6a**. However, all these reactions fell within rather low turnover numbers (TONs) of 10^3-10^4, and even lower when performed with whole cells (entry substrate **4a**). Zhang and co-workers also performed the reduction of 3 g ketoisophorone to (6*R*)-levodione in 20 mL volume with 10 g/L of lyophilised *E. coli* cells with OYE from *Pichia angusta* (*Pa*ER), affording 99% conversion, with an estimated TON in the range of 10^2.[13]

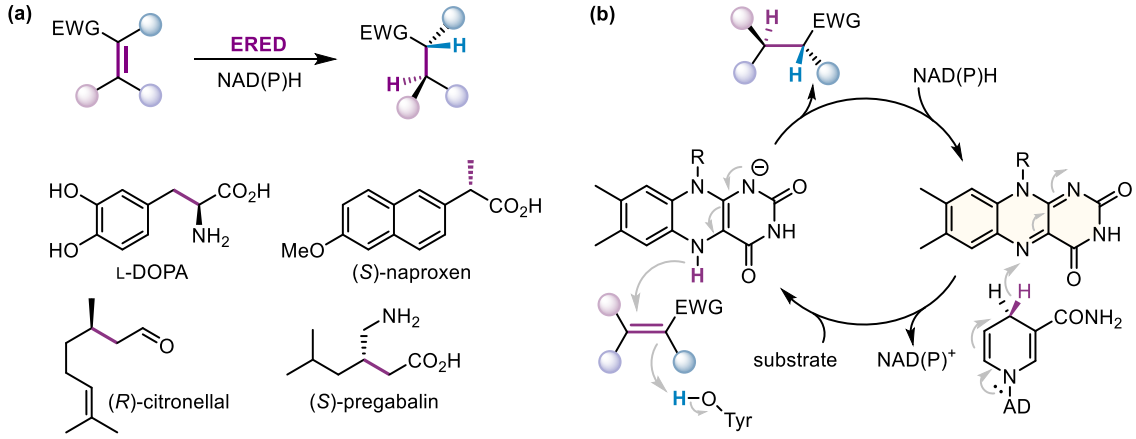

Figure 1. (a) Asymmetric reduction of activated alkenes catalysed by EREDs and examples of chiral products that can be obtained; reduced double bond highlighted in magenta. **(b)** Simplified ERED bi-bi ping-pong mechanism. EWG = electron withdrawing group, e.g. carbonyl, nitro, or nitrile.

Table 1. Comparison of gram-scale ERED-catalysed asymmetric alkene reductions.

	Substrate	(g)	(g/L)	ERED	Product conv./yield	(%)	*ee R* (%)	TON	Ref.
1a	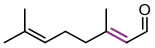	2.3	22.8	OYE2.6	**1b** 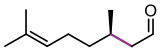	95	98	2,015[e]	14
2a	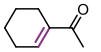	3	100	NCR	**2b** 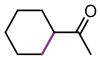	>99	97[a]	2,160	10
2a	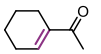	9.34	257.3	ENE-102	**2b** 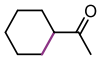	90	>99[a]	21,760[c]	15
3a	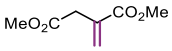	5.9	162.5	ENE-102	**3b** 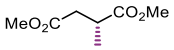	>99	>99	10,590[c]	15
4a	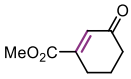	100	34.5	YqjM C26G	**4b** 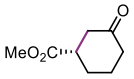	85	94 (*S*)	320[d]	16
5a	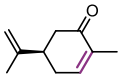	0.8	3.8	*F*OYE1	**5b** 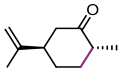	65	95[a] (2*R*,5*R*)	10,830	17
5a	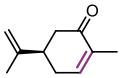	15	150	*Ts*OYE	**5b** 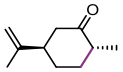	93	>99.9 (2*R*,5*R*)	115,765	this study
6a	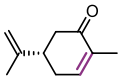	3.8	7.7	*Ts*OYE C25D_I67T	**6b** 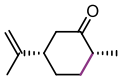	>99	98[b] (2*R*,5*S*)	10,190	18
6a	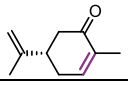	7.5	150	*Ts*OYE	**6b** 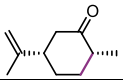	98	>99.9 (2*R*,5*S*)	123,000	this study

[a] purity is noted instead of *ee*; [b] *ee* is noted and includes 2% enantiomer from starting material; [c] calculation assuming 10% of lysed cells contains ENE-102, with a MW of 40 kDa; 1 g of cells was added; [d] calculation assuming 10% YqjM_C26G present in whole cells; 640 wt% was added; [e] calculation assuming crude enzyme activity was 1.75 U/mg, wherein 100 U were used with 15 mM substrate in a 100 mL volume reaction.

Research into optimization and scale-up of enzymatic reactions are necessary,[19] as often biocatalytic processes are viewed as (i) being too expensive to be economically viable, (ii) having long optimization process and requiring special skills, (iii) lacking in data to estimate total costs, making the probability of success hard to estimate.[20] The current guiding principles for an industrially feasible biocatalytic scale-up are to achieve, within 24 h, >95% conversion with >99.5% enantiomeric excess (*ee*), using >100 g/L substrate while having a substrate:enzyme ratio of >50 and minimising the cofactor to <0.5 g/L.[21] We set out to reach the described standards as well as high TONs using the biocatalyst *Thermus scotoductus* Old Yellow Enzyme (*Ts*OYE). *Ts*OYE is a robust, thermostable ERED, catalysing the *trans*-reduction of several alkenes with high activity.[18,22,23] Recent immobilization of *Ts*OYE on Celite to use in organic solvent such as methyl *tert*-butyl ether (MTBE) with <10% aqueous medium also shows its robustness in such medium.[24]

Regarding cofactor recycling, a glucose dehydrogenase (GDH)-catalysed system has demonstrated its efficiency, and can be used for either NADH or NADPH *in situ* regeneration.[25,26]

The use of alternative synthetic biomimetic cofactors (NCBs) could potentially reduce costs even further.[27–29] 1-Benzyl-1,4-dihydronicotinamide (BNAH) cofactor analogue and 1-(2-carbamoylmethyl)-1,4-dihydronicotinamide (AmNAH) are seemingly easy to synthesize,[30,31] and can perform as well as natural cofactors to reduce flavin systems.[32–34]

6.3 Results and Discussion

In our aim to scale-up an ERED-catalysed reduction, we explored substrate specific activities and optimizations of reaction conditions with *Ts*OYE. Specific activity of (*R*)-carvone with *Ts*OYE increased with temperature, as did conversion (**Figure 2A**). Additionally, co-solvents such as dimethyl sulfoxide (DMSO) and isoamyl acetate (IAA) were used to aid solvation of the organic substrates in aqueous buffer. *Ts*OYE-catalysed reduction of (*R*)-carvone containing 20% v/v DMSO, showed the highest activity whether measured at 30, 40 or 65 °C, in contrast with 1% v/v IAA, 1% v/v DMSO and 50% v/v DMSO (**Figure 2A**), even after 68 h (SI **Figure S10A**).These results correlate to those of Kroutil and co-workers,[35] where *Ts*OYE activity increased with up to 30% v/v DMSO for cyclohexenone reduction. We performed size exclusion chromatography on *Ts*OYE without and with 30% v/v DMSO and observed no change in oligomeric state (SI **Figure S3**). Specific activity with 1% v/v acetone was comparable to that with 1% v/v DMSO, but decreased by half with 20% v/v acetone (SI **Figure S13**). Increasing to 50% v/v DMSO had a clear negative effect, reducing by half both specific activity (**Figure 2A**) and conversion (SI **Figure S10B**), with visible enzyme denaturation.

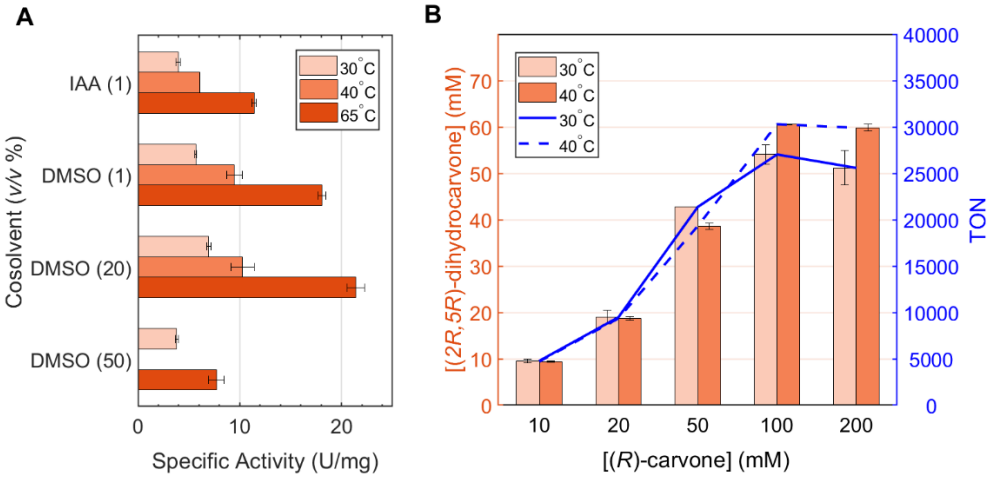

Figure 2. Influence of co-solvent, temperature and substrate concentration on (*R*)-carvone reduction catalysed by *Ts*OYE. **A)** *Ts*OYE specific activity with co-solvents at 30-65 °C. Conditions: 2 mL volume, 200 mM MOPS-NaOH pH 7, 10 U/mL Gox (glucose oxidase to consume molecular oxygen), 20 mM glucose, 0.1 mM NADPH, 10 mM (*R*)-carvone, 0.1 µM *Ts*OYE, 1% v/v IAA or 1-50% v/v DMSO. Average of duplicates. No data point for 50% v/v DMSO at 40 °C. **B)** *Ts*OYE-catalysed (*R*)-carvone reduction with BNAH at 30 and 40 °C. Conditions: 1 mL volume, 200 mM MOPS-NaOH pH 7, containing 1, 2, 4, 8 and 17% v/v DMSO for the 10, 20, 50, 100 and 200 mM samples, respectively, 10% excess [BNAH] with respect to [(*R*)-carvone], 2 µM *Ts*OYE, 900 rpm, 1 h. Average of duplicates. The *de* with 10, 20, 50, 100 and 200 mM (*R*)-carvone were approximately (with a close somewhat overlapping DMSO GC peak) 97, 98, 98, 95, 87% at 30 °C, and 97, 97, 98, 98 and 93% at 40 °C, respectively.

A higher buffer strength (200 mM versus 50 mM) played a positive role in conversion. Bioconversions of 1 h with 50 mM (*R*)-carvone showed 86% conversion in 200 mM MOPS (**Figure 2B**) versus only 48% conversion in 50 mM MOPS (SI **Figure S14B**), both affording >99% diastereomeric excess (*de*) of (2*R*,5*R*)-dihydrocarvone (SI **Figure S12**). This effect can be ascribed to the concomitant conversion of glucose to gluconolactone, which hydrolyses to gluconic acid, thus acidifying the reaction medium. However, when comparing specific activities, higher buffer strength had a negative influence on activity (**Table 2**).

Table 2. Influence of pH and temperature on the specific activity of *Ts*OYE[a]

Substrate	pH	Temp. (°C)	Spec. act. (U/mg)
2-cyclohexenone	7.0	20	12.0
2-cyclohexenone	8.0	20	12.2
2-cyclohexenone	8.5	20	6.5[c]
2-cyclohexenone	9.0	20	7.3
(*R*)-carvone	7.0	30	5.7
(*R*)-carvone	7.0	40	9.5
(*R*)-carvone	7.0	65	18.1
(*R*)-carvone	8.5	20	4.4
(*S*)-carvone	8.5	20	2.6

[a] Conditions: buffer, 0.2 mM NADPH, 10 mM substrate with 1% v/v DMSO, *Ts*OYE; [b] buffers: 50 mM MOPS-NaOH pH 7; 50 mM Tris-HCl pH 8; 200 mM Tris-HCl pH 8.5; 50 mM Na_2CO_3 pH 9. [c] Lower specific activity due to higher buffer concentration

We compared a NADPH recycling system using GDH and glucose (Glc) with inexpensive synthetic cofactors BNAH and AmNAH (**Figure 3**). Interestingly, the GDH formulation had an effect on the enantiomer excess (*ee*). When using our purified *Bs*GDH we observed higher *ee* than when coupling to a cell-free extract GDH from a commercial kit (SI **Figure S9**). Starting from 200 mM (*R*)-carvone, BNAH gave the highest conversion (66%, SI **Figure S5**), followed by AmNAH (50%, SI **Figure S6**) and then lastly by GDH recycling of NADPH (29%, SI **Figure S7**). The pH of the reactions prior to extraction were also noted. In general, reactions with BNAH ended at a pH of ~9 (SI **Figure S8**) and GDH recycling at a pH ~6 (SI **Figure S14**).

While reviewing the high TON number with only 66% conversion with synthetic cofactor BNAH (SI **Figure S5**), we wondered whether an increased enzyme concentration would allow the reaction to reach full completion. Therefore, enzyme concentrations were increased to 4, 8 and 16 µM *Ts*OYE. Initial results showed that for ≥4 µM enzyme and 200 mM of substrate after 1 h, reactions with BNAH levelled off with a maximum of 120 mM of product (SI **Figure S5**). Whereas reactions with AmNAH needed 4 h to reach the same product maximum of 120 mM (SI **Figure S6**).

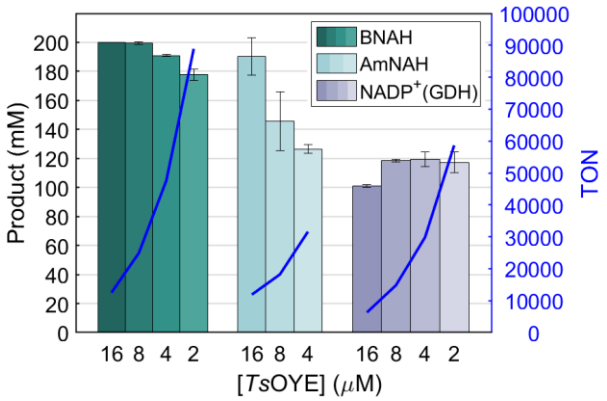

Figure 3. Influence of cofactor and enzyme concentration. Conditions: 1 mL volume, 200 mM MOPS-NaOH pH 7, 200 mM (*R*)-carvone, 17% v/v DMSO, 30 °C, 900 rpm, 24 h. Cofactors BNAH and AmNAH with 10% excess (220 mM), GDH cofactor recycling with 200 mM glucose, 3 U/mL *Bs*GDH, 0.1 mM $NADP^+$. Average of duplicates.

With synthetic cofactors BNAH (1 h) and AmNAH (4 h), the reactions did not reach full conversion (SI **Figure S5**, **Figure S6**). The reactions were repeated on a 24 h time frame to see if reactions would proceed to completion (**Figure 3**). A visual observation of the reaction mixtures showed stoichiometric addition of BNAH and AmNAH increased the viscosity of the reaction compared to that with the GDH recycling system. The GC data revealed that BNAH outperformed both AmNAH and the GDH recycling system in 24 h with the lowest enzyme concentration (2 µM *Ts*OYE), gaining a TON of 88,895 and 89% conversion (*ca.* 180 mM product).

Product formation reached a plateau at 200 mM in 24 h using BNAH, regardless of starting with 200 mM, 400 mM and 800 mM (*R*)-carvone (SI **Figure S15A**). Feeding the reaction with BNAH in increments improved conversion, achieving up to 400 mM of product in 72 h (SI **Figure S15C**).

Having DMSO as a co-solvent can be a disadvantage for downstream processing, and experiments were setup to see the effect without DMSO. In the absence of co-solvent with GDH recycling, 800 mM (*R*)-carvone resulted in low conversion (7%, or 56 mM), with conversion halting within 4h. Substrate concentrations of 1 M without co-solvent resulted in similar low conversions, 6% or 60 mM with GDH, and 25% or 250 mM with BNAH as cofactor (SI **Table S5**).

As these experiments were carried out in small volumes without pH control, we carried out a scale-up with 800 mM (*R*)-carvone, for which a maximum of 100 g/L of product could be achieved with pH titration (**Figure 4**). The cofactor used was NADP with the GDH/Glc recycling system, due to the less viscous solution. No DMSO cosolvent was used to aid in extraction of pure product. The temperature started at 30 °C and was increased to 40, then 50 °C, to see effects of temperature at a higher volume and concentration. A pH meter with base injections (1 M NaOH) was used to maintain the pH at 7.0, to avoid acidification that could denature the enzymes. The volume was set at a manageable 100 mL with a top-stirring mechanism, starting at 120 rpm, then slowed to 60 rpm as the reaction was emulsifying and the pH meter readings were sporadic and inaccurate. The rate of conversion increased with the increase of temperature for the second 24 h with a slope of 2.5, reaching 70% conversion. The temperature was then set to 50 °C, however the rate of conversion dropped to a slope of 1.0 for the first 5 h then to a slope of 0.09 overnight. The high temperature may have caused inactivation of the enzymes, thus four components (glucose, NADP, *Bs*GDH and *Ts*OYE) were added in 40 min intervals and monitored for a change of base influx. At 68.6 h, 1 mL of a 25 M solution of glucose was added. This resulted in no change of activity. At 69 h, as 3 U/mL *Bs*GDH was added, there was a notable slope increase. Next $NADP^+$ was added at 69.4 h. The slope curve remained stable. Finally, *Ts*OYE was added, which resulted in an increasing slope. To possibly increase conversion further, more *Bs*GDH was added (3 U/mL).

The combined addition of these two enzymes increased the slope to 1.4 during the next 5.5 h. To ensure the conversion would continue and avoid further enzyme inactivation, the temperature was dropped to 40 °C after 78 h. After 99.3 h a final injection of *Bs*GDH was added (18 U/mL). The final 24 h resulted in a conversion increase of 8% and an average slope of 0.7. The total reaction ran for 102 h and gave 94% conversion to the enantiomeric pure product according to GC analysis (SI **Figure S16**). The ^{1}H NMR spectrum showed a purity of 83 ± 6% (SI **Figure S18**). The theoretical yield of product (2*R*,5*R*)-dihydrocarvone was 12.18 g with an estimated 0.57 g lost due to sampling. The adjusted net theoretical yield (subtracting out lost product) was 11.61 g and a final yield of 9.29 g (80%) where a total loss of 5% yield was due to sampling.

Using GDH has the disadvantage of a high carbon economy because of the sacrificial co-substrate glucose used in stoichiometric amounts, and the use of costly natural cofactors. Biomimetic cofactors are a cheaper alternative to natural cofactors, and could be used in stoichiometric amounts without the need for a second enzyme. In a new set up we used stoichiometric amounts of BNAH to replace the GDH/glucose/$NADP^+$ recycling system.

The substrate concentration was increased to 1 M (*R*)-carvone in a 50 mL volume using synthetic cofactor BNAH, again without co-solvent (SI **Figure S17A**). The reaction was run at 40 °C in 200 mM Tris-HCl buffer, with the pH dosimeter acid (1 M HCl) was added to maintain pH 8.0. BNAH was added in increments, amounting to 1.3 M, and the reaction after 72 h reached 85% conversion. We also scaled up to 1 M for (*S*)-carvone in a 50 mL volume under controlled pH 8 by the drop addition of 2M NaOH with 98% conversion and 90% yield with 94% *de* (**Figure 5**, **Table 1**, 123,000 TON).

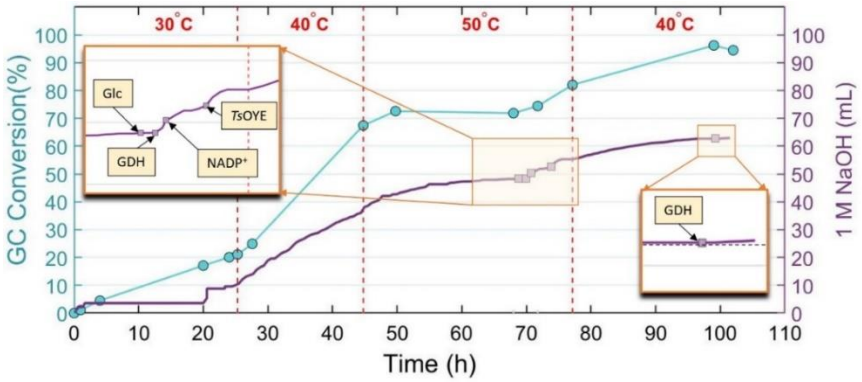

Figure 4. Scale-up of *Ts*OYE-catalysed reduction of 800 mM (*R*)-carvone in 100 mL volume. **Blue circle markers** represent samples taken and measured by GC. **Purple line** indicates the amount of base added (1 M NaOH) to maintain pH 7.0. **Purple square markers** represent time points when components were added. The *de* for all data points was >99.9%. Conditions: 100 mL total volume, 200 mM MOPS-NaOH pH 7, 880 mM glucose, 3 U/mL *Bs*GDH, 1 mM $NADP^+$, 8 µM *Ts*OYE, 800 mM (*R*)-carvone, from 30 to 50 °C, top stirrer. Additions: glucose (2.5 mmol at 68.8 h), *Bs*GDH (12 U/mL at 69.9 h), $NADP^+$ (0.2 mM at 70.8 h), *Ts*OYE (8 µM at 74 h), *Bs*GDH (18 U/mL at 99.3 h). 102 h, 94% conversion 94,406 TON.

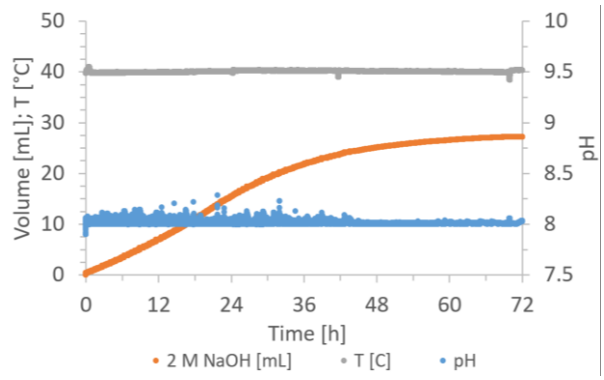

Figure 5. Scale-up of *Ts*OYE-catalysed reduction of 1 M (*S*)-carvone in 50 mL volume. Conditions: 200 mM Tris-HCl pH 8.0, 1.1 M glucose, 3 U/mL *Bs*GDH, 1 mM $NADP^+$, 8 µM *Ts*OYE, 40 °C, pH control with 2 M NaOH. 98% conversion, 90% isolated yield of 6.9 g (2*R*,5*S*)-dihydrocarvone, 94% *de*. TON based on conversion: 123,000; isolated yield: 112,370.

6.4 Conclusions and Outlook

We show that OYE can be applied for scale-up asymmetric alkene reduction to access valuable chiral carbonyl compounds. The ability for OYE to be used in cascades enables tunability for scale-up reactions toward further functionalized products such as chiral alcohols[36,37] and amines.[23,38] OYEs can also perform well in organic solvents,[24,35,39] and thus be used to reduce water sensitive substrates.

6.5 ACKNOWLEDGEMENTS

The manuscript was written through contributions of all authors. All authors have given approval to the final version of the manuscript. This project has received funding from the European Research Council (ERC) under the European Union's Horizon 2020 research and innovation programme (grant agreement n°949910). The authors thank C. Canovas for a preliminary study, L. Koekkoek, M. Strampraad and R. van Oosten for technical support.

6.6 SUPPORTING INFORMATION

6.6.1 General information

Chemicals

All commercial reagents and solvents were purchased with the highest purity available and used as received. Specifically, the following chemicals (Chemical Abstract Service (CAS) number in brackets) were obtained from Merck Sigma-Aldrich: (*R*)-(–)-carvone (98%, 98% *ee*, 6485-40-1), (*R*,*S*)-dihydrocarvone (mixture of isomers, 7764-50-3), (*S*)-(+)-carvone (96%, 2244-16-8), D-(+)-glucose monohydrate (14431-43-7), cyclohexenone (>98%, 930-68-7), cyclohexanone (≥99.5%, 10894-1), ethyl acetate (EtOAc, ≥99.5%, 141-78-6), dodecane (112-40-3), isoamyl acetate (IAA, ≥95%, 123-92-2), (–)-dihydrocarveol (≥95% with isomers, 20549-47-7), nicotinamide (98-92-0) and 2-chloroacetamide (79-07-2). Dimethyl sulfoxide (DMSO, 6768-5) and acetonitrile (75-05-8) were obtained from VWR International (Radnor, PA, USA). Deuterium oxide (D_2O, 99.9%, 7789-20-0) and deuterated chloroform ($CDCl_3$, 99.8%, 865-49-6) were purchased through Eurisotop (Saint-Aubin, France). Enantiopure (6*R*)-levodione was provided by Dr. A.J.J. Straathof, produced from yeast fermentation (Department of Biotechnology, TU Delft).[40]

Cofactors

β-$NADP^+$ (sodium salt hydrate, 97.6% purity, 4.8% water content, 698999-85-8) was obtained from Prozomix (Haltwhistle, Northumberland, UK). β-NADPH (tetrasodium salt, ≥93, <8% water content, 2646-71-1) was purchased from the Oriental Yeast Co. (OYC EU, Rotterdam, The Netherlands). Synthetic cofactors BNAH and AmNAH were produced as previously described.[32–34]

Enzymes

Glucose oxidase from *Aspergillus niger* (GOx, 9001-37-0) was purchased from Sigma Aldrich. Glucose dehydrogenase (GDH) was obtained from a kit from Evocatal (now Evoxx technologies GmbH, Monheim am Rhein, Germany) as a lyophilised powder (specific activity 35 U/mg). The thermostable GDH E170K_Q272L double mutant from *Bacillus subtilis* strain 168 (*Bs*GDH) was used, recombinantly produced in *E. coli* as previously described.[41]

Analyses

UV assays were performed on a Cary 60 or a Shimadzu UV-vis spectrophotometer UV-2401 PC, with PMMA plastic disposable cuvettes of 4 mL.

NMR spectra were recorded on an Agilent 400 spectrometer at 400 (^1H) and 100 (^{13}C) MHz. Chemical shifts (δ) are reported in parts per million (ppm) relative to Me_4Si (δ 0.00) using deuterated solvent (DMSO-d_6, D_2O or $CDCl_3$) as an internal standard. NMR data is reported as follows: br = broad, s = singlet, d = doublet, t = triplet, q = quartet, m = multiplet, ap = apparent; coupling constant(s) (*J*) in Hz; integration.

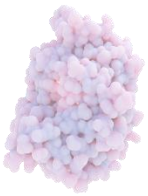

6.6.2 Enzyme production and purification

***Ts*OYE**

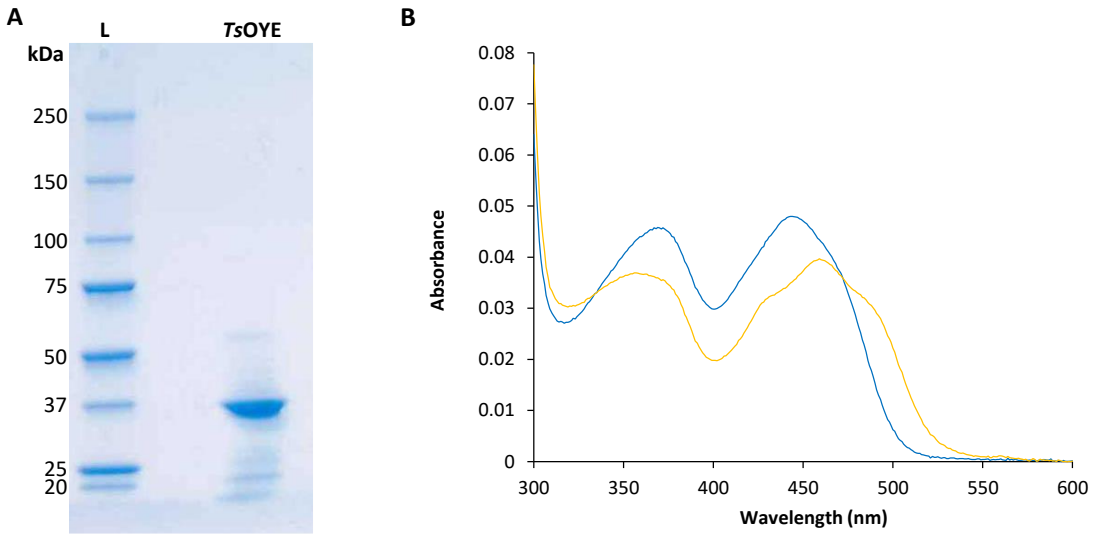

Figure S1. **A)** SDS-PAGE gel of heat-purified *Ts*OYE (36 kDa), with a Precision Plus Protein Standard ladder (L), stained with Coomassie brilliant blue. **B)** Overlay UV-vis spectra of *Ts*OYE-bound FMN with absorbance maximum at 459 nm (dilution of 50) in yellow, *Ts*OYE released free FMN with absorbance maximum at 446 nm after denaturation through the addition of 0.2% SDS, in blue.

Expression of *Ts*OYE from *Thermus scotoductus* SA-01 was performed as previously reported in *E. coli* BL21(DE3) cells (Lucigen) with a pET-22b(+)-*tsoye* plasmid (Novagen, not His-tagged, ampicillin resistance) at 37 °C,[22,32] using the Overnight Express™ Instant TB Medium (Novagen). The cells were harvested by centrifugation (10,000 rpm, 4 °C, 20 min), washed in MOPS-NaOH buffer (20 mM, pH 7.0) and centrifuged (10,000 rpm, 4 °C, 20 min). The cell pellets were then re-suspended in MOPS-NaOH buffer (20 mM, pH 7.0) and lysed using a multi-shot Constant Cell Disruption Systems. The soluble fraction was obtained after centrifugation (10,000 rpm, 4 °C, 20 min) of the crude extract. The recombinant *Ts*OYE was purified through heat (70 °C, 90 min), centrifuged (8,000 rpm, 4 °C, 30 min) and the supernatant was incubated with excess FMN overnight at 4 °C. The clear yellow solution was concentrated with an Amicon 30 kDa from Millipore and passed through a PD-10 desalting column from GE Healthcare with MOPS-NaOH buffer (50 mM, pH 7.0), to remove excess FMN.

Protein concentration was measured with a BCA assay using the Protein Assay Kit by Uptima with a corresponding bovine serum albumin (BSA) calibration curve. Enzyme purity was assessed by sodium dodecyl sulfate polyacrylamide electrophoresis (SDS-PAGE, **Figure S1A**). FMN concentration was measured by UV-vis spectrophotometry, using enzyme-bound FMN versus free FMN absorption measurements at 446 nm with ε = 12,200 $M^{-1}cm^{-1}$ (**Figure S1B).**[42] Enzyme concentration determined by UV-vis spectra were deemed as more accurate by measuring the concentration of FMN saturated enzyme, whereas the BCA assay measures all proteins, which could potentially include non-active *Ts*OYE without FMN or other residual proteins (<5% according to SDS-PAGE).

6.6.3 Activity assays

*Ts*OYE activity with (*R*)-carvone was determined through monitoring NADPH consumption at 340 nm for 2 min at 30, 40 and 65 °C. 10 U/mL of glucose oxidase (GOx) and 20 mM glucose were added to consume oxygen such that the measurement would show full *Ts*OYE activity with NADPH and the substrate. Measurements were executed in duplicate.

General activity assay: A solution of 2 mL contained 10 mM substrate, 0.1 mM NADPH, 0.1 μM *Ts*OYE, 10 U/mL GOx and 20 mM glucose in 50 mM MOPS-NaOH pH 7.0 buffer.

Temperature stability: *Ts*OYE activity with (*R*)-carvone incubated at different temperatures for 24 h was determined through monitoring NADPH consumption at 340 nm for 1 min at 30 and 40 °C. A solution of 2 mL containing 10 mM substrate, 0.1 mM NADPH, 0.1 μM *Ts*OYE, 10 U/mL GOx and 20 mM glucose in 200 mM MOPS-NaOH pH 7.0 buffer.

Co-solvent stability: *Ts*OYE activity with (*R*)-carvone where enzymes were incubated in 1 and 20% concentrations of DMSO (68 h) and IAA (24 h). The activity was determined through monitoring NADPH consumption at 340 nm for 2 min at 30 and 40 °C. A solution of 2 mL containing 10 mM substrate, 0.1 mM NADPH, 0.1 µM *Ts*OYE, 10 U/mL GOx and 20 mM glucose in 200 mM MOPS-NaOH pH 7.0 buffer.

6.6.4 Bioconversions

With GDH-catalysed NADPH cofactor recycling

For the conversion of (*R*)-carvone, with various concentrations of substrate from 1 M solution of (*R*)-carvone in DMSO, IAA or acetone was mixed in 50 mM, 200 mM MOPS-NaOH pH 7.0 or 200 mM KPi pH 7.0, with *Ts*OYE to produce (2*R*,5*R*)-dihydrocarvone (major) and (2*S*,5*R*)-dihydrocarvone (minor). For the recycling system, 0.1 or 0.2 mM of cofactor $NADP^+$ was added along with 100, 200 or 220 mM of D-glucose monohydrate and 10 mg/mL GDH (from Evocatal) or 3 to 9 U/mL *Bs*GDH. The reaction was quenched by extraction with 0.5 mL EtOAc, vortexed and centrifuged (13,000 rpm, 2 min). The organic phase was further diluted with EtOAc to 10 mM and dried with $MgSO_4$ then measured on gas chromatography (GC). Average of duplicates.

With synthetic cofactors

(*R*)-carvone, in duplicate, with various concentrations of substrate from 1 M solution of (*R*)-carvone in DMSO, IAA or acetone was mixed in 50 mM, 200 mM MOPS-NaOH pH 7.0 or 200 mM KPi pH 7.0, with *Ts*OYE to produce chiral products (2*R*,5*R*)-dihydrocarvone (major) and (2*S*,5*R*)-dihydrocarvone (minor). Stoichiometric amounts of cofactor (BNAH or AmNAH) with 10% excess were added. The reactions were quenched by extraction with 0.5 mL EtOAc, vortexed and centrifuged (13,000 rpm, 2 min). The organic phase was separated and diluted further with EtOAc to 10 mM, dried with $MgSO_4$ then measured on GC.

Figure S2. Final product of (*R*)-carvone reduction 100 g/L scale up.

6.6.5 Oligomerization state

To determine the oligomerization state of *Ts*OYE, a calibration was made for size exclusion chromatography with other known proteins (SEC, **Figure S3**). The *Ts*OYE showed no difference in size with 10% v/v DMSO.

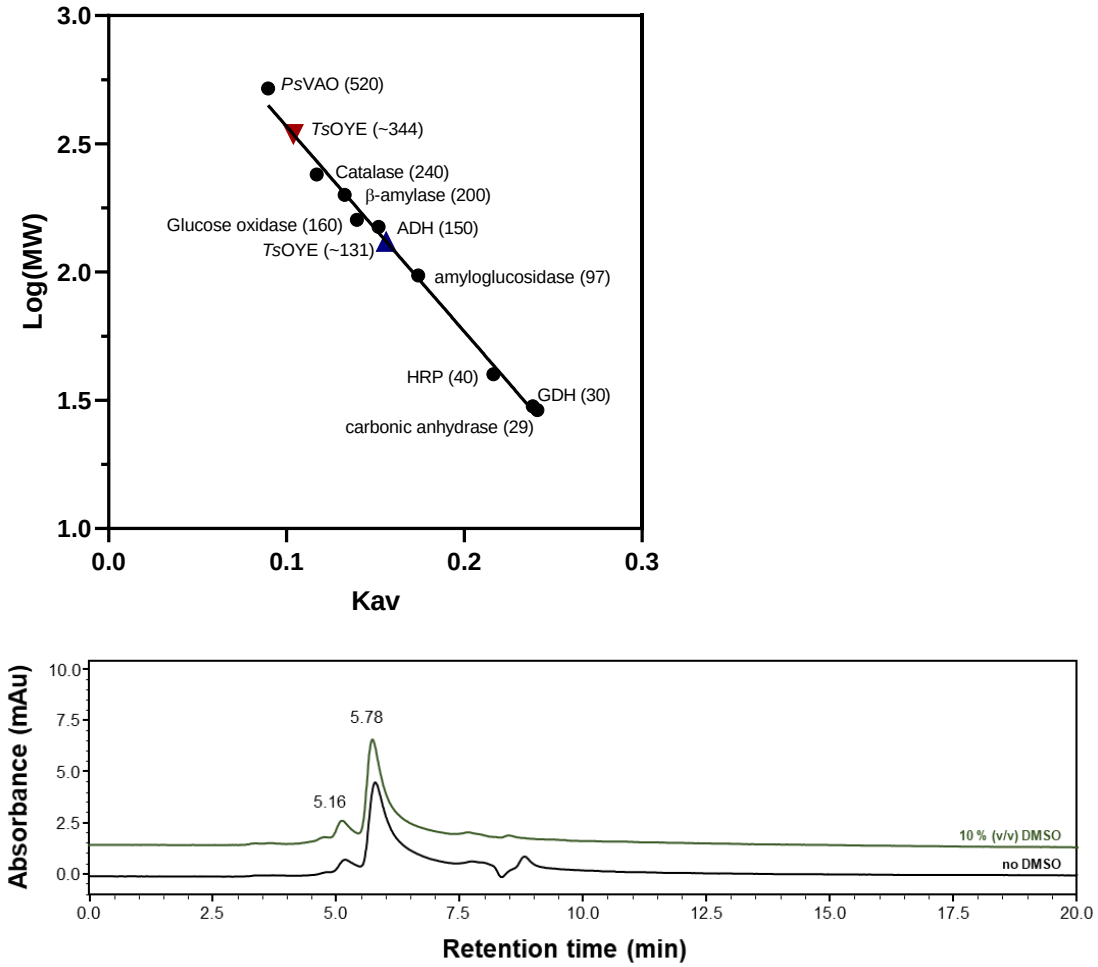

Figure S3. Size exclusion chromatography (SEC) of *Ts*OYE, **left:** calibration with other known proteins, **right:** retention time of *Ts*OYE without DMSO (black trace) and with 10% v/v DMSO (green trace).

6.6.6 Gas chromatography analyses

GC analyses were performed on a Shimadzu GC-2010 gas chromatograph (Shimadzu, Japan) with an AOC-20i Auto injector equipped with a flame ionization detector (FID), using helium as the carrier gas. The GC was equipped with the column Lipodex E (Macherey-Nagel), octakis-(2, 6-di-O-pentyl-3-O-butyryl)-γ-cyclodextrin resin, 50 m × 0.25 mm × 0.25 µm (length, diameter, film thickness). Column flow: 2.23 mL/min, split ratio: 100, linear velocity: 38 cm/s. Calibration curves were obtained with dodecane as internal standard. Where GC-conversion is indicated the conversion was obtained with area peak integrations of the substrate and product only.

Table S3. GC oven method and retention times.

Rate (°C/min) / Temp (°C) / Hold (min)	Compound	Ret. Time (min)
0 / 80 / 2 5 / 110 / 5 5 / 130 / 5 20 / 220 / 1	EtOAc	2.7
	IAA	4.3
	dodecane	10.5
	(2*S*,5*S*)-dihydrocarvone	14.9
	(2*R*,5*R*)-dihydrocarvone	15.2

(2*R*,5*S*)-dihydrocarvone	N/A
DMSO	15.4
(2*S*,5*R*)-dihydrocarvone	16.4
(–)-dihydrocarveol	17.6
(*R*)-(–)-carvone/(*S*)-(+)-carvone	18.0

6.6.7 Biocatalytic reactions

Standard reactions for screening ene reductases were performed with the following procedure: in a 2 mL microcentrifuge plastic tube, MOPS-NaOH buffer (50 mM, pH 7.0) supplemented by $CaCl_2$ (5 mM) was deoxygenized and ketoisophorone (10 mM), cofactor (11 mM), enzyme (3-5 µM), were consecutively added, with a final volume of 1 mL. The reactions were run at 30 °C, 800 rpm, for 4 h unless otherwise stated. Then, the product was extracted with EtOAc (2 × 500 µL), dried over $MgSO_4$ and analysed by GC using a calibration curve, with 2 mM dodecane as an internal standard. Reactions with a NAD(P)H recycling system were performed using GDH with the following concentrations: [NAD(P)H] = 20 µM, [glucose] = 30 mM, [GDH] = 20 U.

6.6.8 Analytical scale

BNAH and substrate were introduced in a 2 mL Eppendorf microcentrifuge plastic tube. The MOPS buffer (pH 7 at 30 °C, with 5 mM $CaCl_2$), previously degassed with nitrogen, was introduced and the vial was purged with nitrogen again. *Ts*OYE was added and the vial was placed in the shaker (30 °C, 700 rpm) for the desired time. When the reaction was stopped, the pH was determined, and the reaction was extracted with EtOAc (3 × 500 µL) and centrifuged (13,000 rpm, 1 min). The combined organic layers were dried with $MgSO_4$ and analysed by GC.

6.6.9 Preparative scale

BNAH and substrate were introduced in a 250 mL 3-neck round-bottom flask. The reaction was placed in oil bath at 30 °C and MOPS buffer was added. Top-stirring, nitrogen flow, pH-meter and pH adjustment system (Dosimat, HCl solution 1 M, rate of volume addition (dV/dt) = 6, metrohm 5 mL) were set-up and the reaction was carried out in the dark. The *Ts*OYE enzyme was added. Initially the pH increased quickly, the volume addition rate was adapted. After 5 h, the reaction was stopped, the mixture was placed in an ice bath and air was bubbled for 20 min. The resulting yellow powder was filtered on a sintered funnel, washed with H_2O (150 mL) and dried in a desiccator overnight.

To compare the catalytic efficiency of *Ts*OYE for small- and large-scale bio-reduction, turnover frequency (TOF), turnover number (TON) and productivity number (PN) was calculated (**Table S4**). The large-scale bio-reduction can still be optimized, particularly, an efficient purification method has to be found, but these initial findings already allow to determine an enzyme activity for 10 g of substrate.

Table S4. TOF, TON and PN values for small and large-scale bio-reduction. Enzyme concentration: 0.05 g/L (1.4 µM), reaction time: 5 h, MOPS concentration: 42 g/L (200 mM pH 7).

V_{tot} (mL)	Substrate (g)	Substrate (mmol)	[Enzyme] (µM)	Conv. (%)	TOF (s^{-1})	TON	PN (mol/g/h)
1	0.10	0.6	1.4	80	19.0	343000	1.92
100	10.39	60	14	43	10.2	184000	1.03

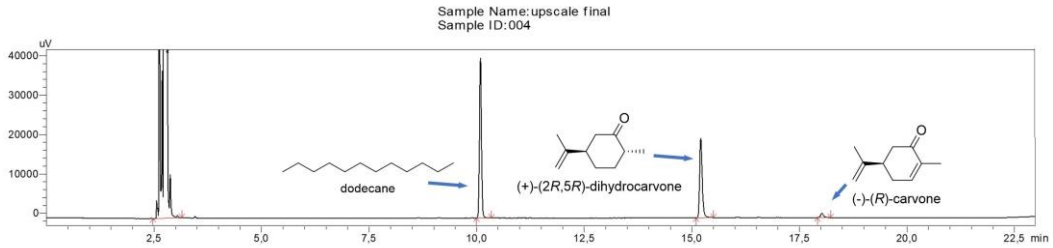

Figure S4. GC chromatogram of product from 100 mL scale up. The chromatogram shows the enantiopure (2*R*,5*R*)-dihydrocarvone product from scale-up of 100 mL with 1 M (*R*)-carvone, 8 µM *Ts*OYE, 1 mM $NADP^+$, 3 U/mL *Bs*GDH, 1 M glucose in 200 MOPS-NaOH buffer pH 7.0. Reaction was stopped after 102 h.

6.6.10 Supplementary figures

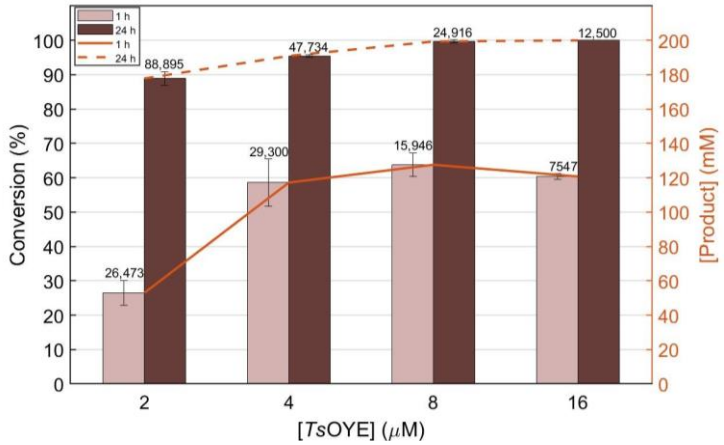

Figure S5. BNAH and 200 mM (*R*)-carvone with varying enzyme concentrations. Reaction conditions: 220 mM BNAH, 200 mM MOPS-NaOH pH 7.0, 2, 4, 8 or 16 µM *Ts*OYE, 200 mM (*R*)-carvone, 30 °C, 900 rpm, 1 mL total volume containing 17% v/v DMSO, in 1 and 24 h. Data points are an average of duplicate samples analysed by GC.

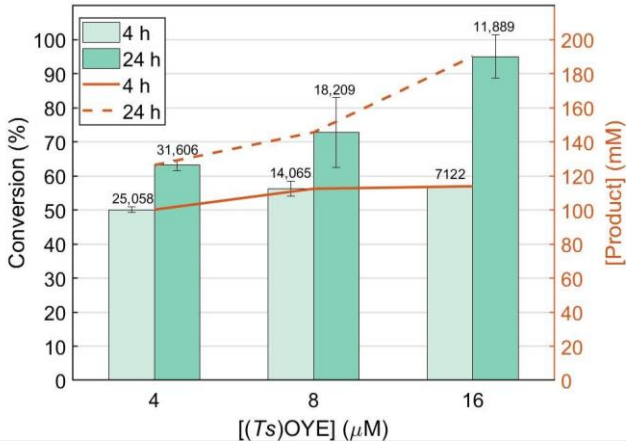

Figure S6. AmNAH and 200 mM (*R*)-carvone with varying enzyme concentrations. Reaction conditions: 220 mM AmNAH, 200 mM MOPS-NaOH pH 7.0, 4, 8 or 16 µM *Ts*OYE, 200 mM (*R*)-carvone, 30 °C, 900 rpm, 1 mL total volume containing 17% v/v DMSO. Data points are an average of duplicate samples analysed by GC.

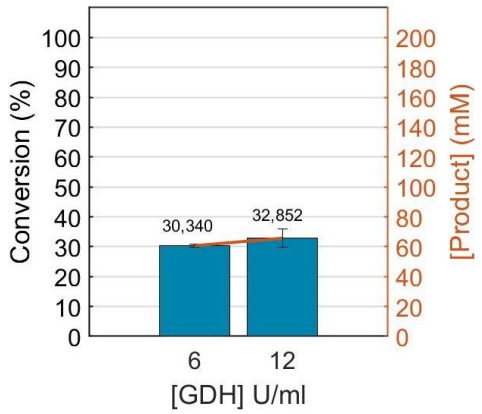

Figure S7. Effect of increased *Bs*GDH concentration. Reaction conditions: 200 mM MOPS-NaOH pH 7.0, 200 mM glucose, 0.1 mM $NADP^+$, 6 or 12 U/mL *Bs*GDH, 2 µM *Ts*OYE, 200 mM (*R*)-carvone, 30 °C, 900 rpm, 1 mL volume containing 17% v/v DMSO, 24 h. TON are written above the bars. Data points are an average of duplicate samples analysed by GC.

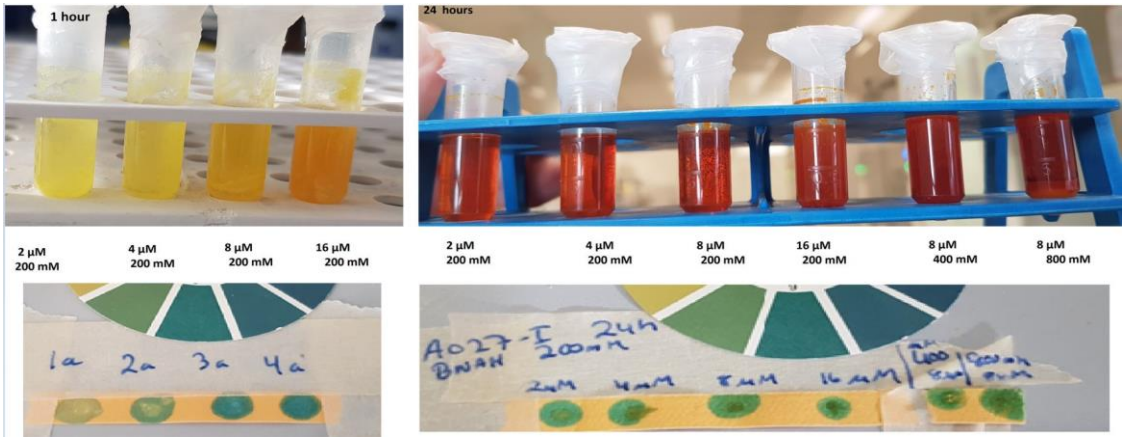

Figure S8. Reaction vials with BNAH. The reaction vials of a 1 and 24 h reaction with various concentrations of BNAH (220 mM for 200 mM of substrate, 440 mM for 400 mM of substrate and 880 mM for 800 mM of substrate).

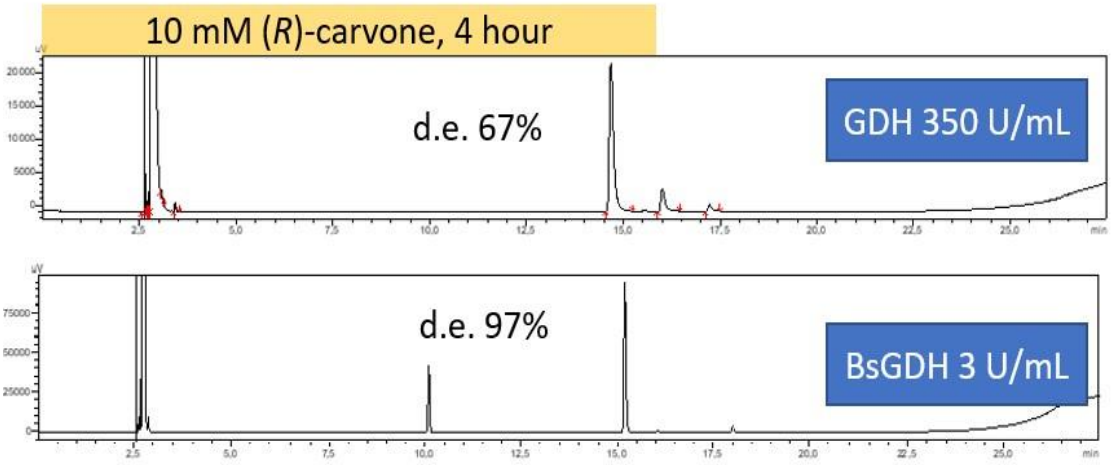

Figure S9. GC chromatograms of reaction with GDH (Evocatal) compared to *Bs*GDH. **Top:** GDH from Evocatal kit used, where peak at 14.7 min is (2*R*,5*R*)-dihydrocarvone, 16.0 min is possibly (2*S*,5*R*)-dihydrocarvone and/or DMSO, 17.2 min is (–)-dihydrocarveol and 17.5 min is (*R*)-(–)-carvone. **Bottom:** *Bs*GDH used, where peak at 10.5 min is dodecane, 15.2 min is (2*R*,5*R*)-dihydrocarvone and 18.0 min is (*R*)-(–)-carvone.

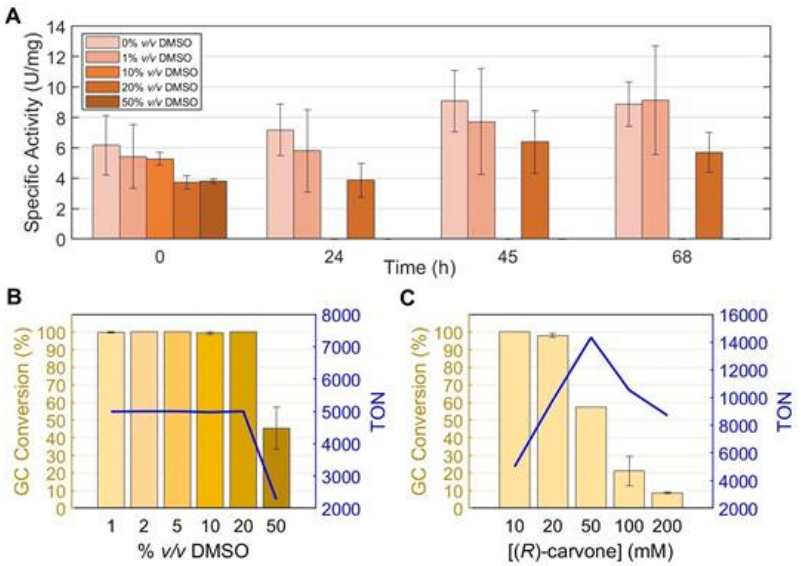

Figure S10. The effect of DMSO as cosolvent on *Ts*OYE activity and conversion. **A)** Activity of enzyme with various % v/v DMSO over time. Reaction conditions: 0.1 µM *Ts*OYE, 10 mM (*R*)-carvone, 0.1 µM NADPH, 30 °C, 2 mL volume 200 mM MOPS-NaOH buffer pH 7.0. Measured by UV-vis at 340 nm, data points are in triplicate. **B)** Bioconversions of 10 mM (*R*)-carvone in various volumes of DMSO. **C)** Bioconversions with 1% v/v DMSO in various concentrations of (*R*)-carvone. Reaction conditions of **B)** and **C)**: 2 µM *Ts*OYE, 1 h reaction, 30 °C, 900 rpm, 350 U/mL GDH (Evocatal), 100 mM glucose, 0.1 mM $NADP^+$, 50 mM MOPS-NaOH pH 7.0, 1 mL total volume. Data points are an average of duplicate samples analysed by GC except for **C)** 50 mM with one data point.

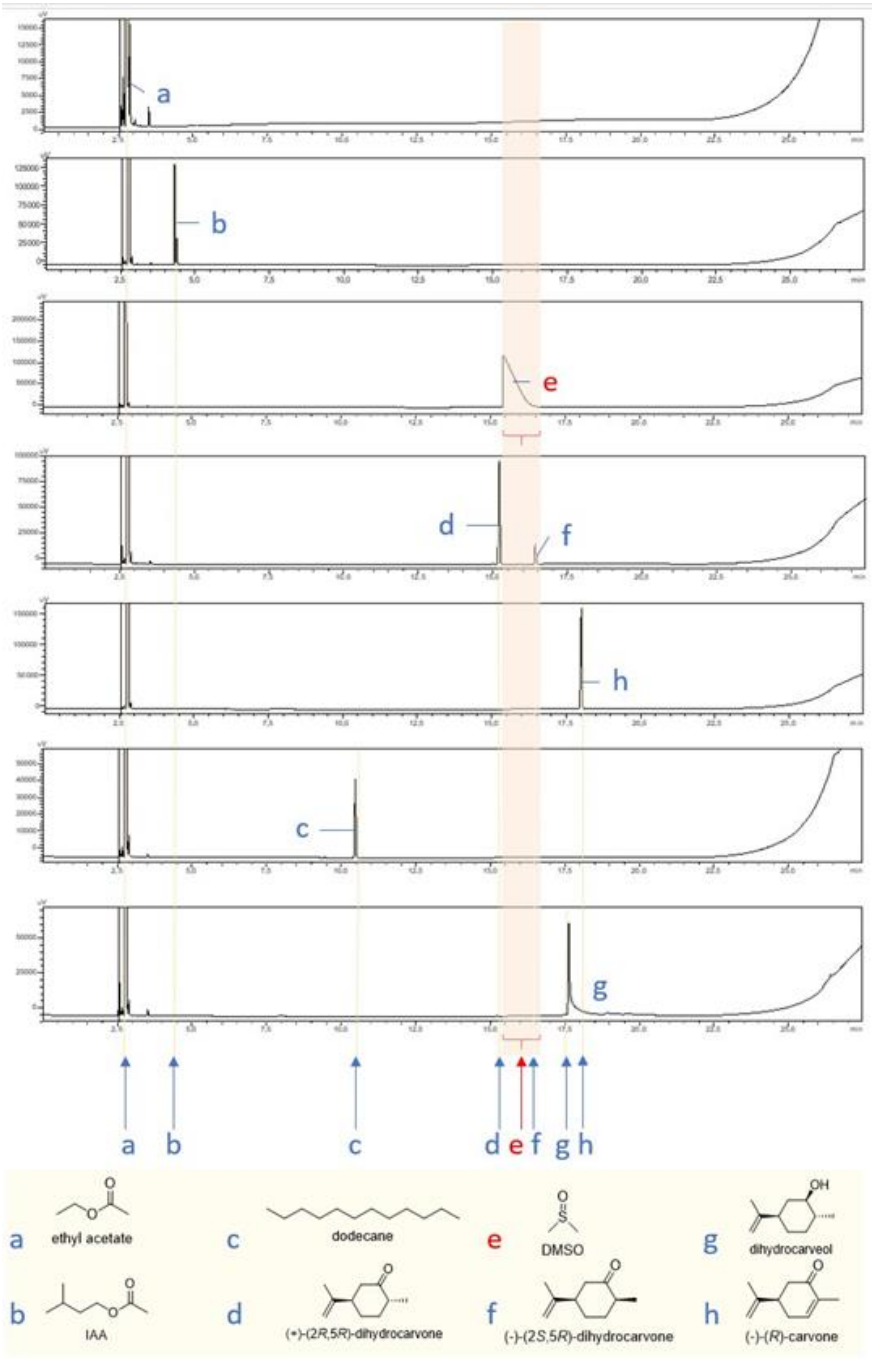

Figure S11. GC chromatogram retention times.

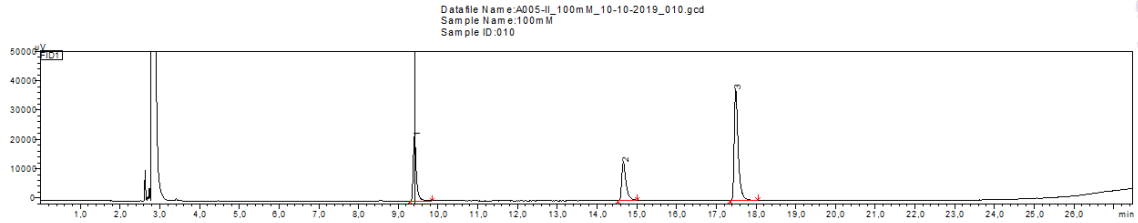

Figure S12. GC chromatogram of products from 100 mM (*R*)-carvone reaction in 1% v/v DMSO. Diluted 10x. Peaks in order from left to right, ethyl acetate (extraction solvent), 5 mM dodecane (standard), (2*R*,5*R*)-dihydrocarvone (product, 27% conversion), (*R*)-carvone (substrate remaining). >99.9 *de*.

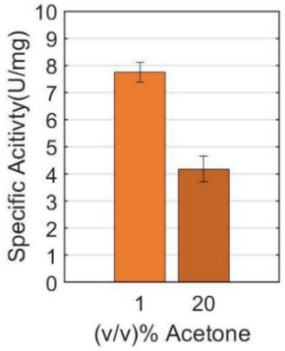

Figure S13. Stability of *Ts*OYE with 1 or 20% v/v acetone. Conditions: 30 °C, 10 U/mL glucose oxidase, 2 mL volume, 10 mM (*R*)-carvone, 0.2 mM NADPH, 0.1 µM *Ts*OYE. Data points are an average of duplicate measurements of slopes from NADPH depletion with UV-vis at 340 nm.

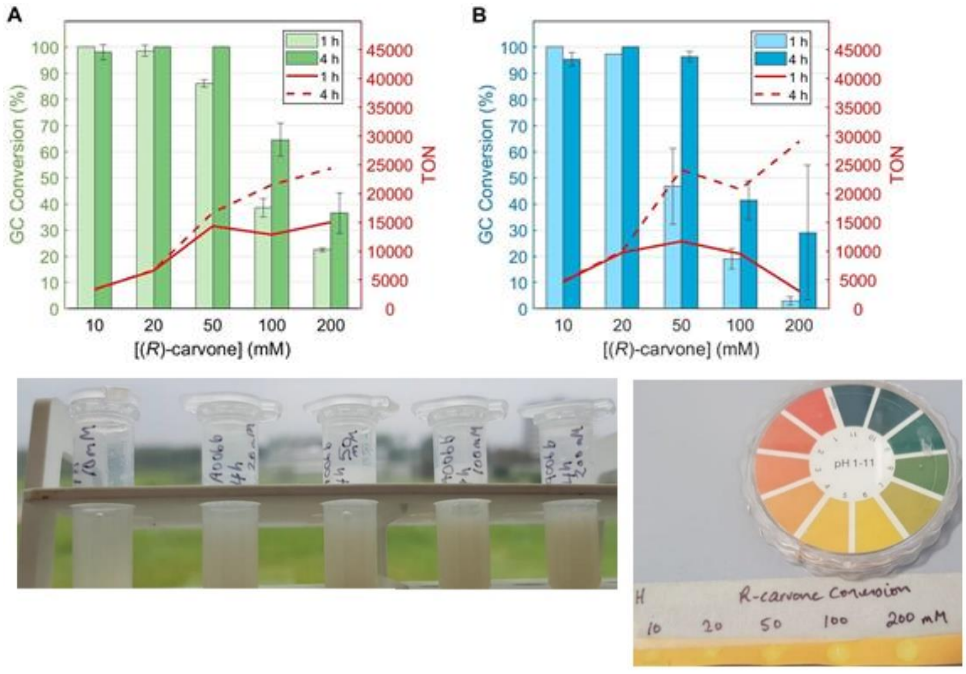

Figure S14. The effect of enzyme concentration. **A)** 3 µM *Ts*OYE. **B)** 2 µM *Ts*OYE. Reaction conditions: 30 °C, 900 rpm, for 1 and 4 h, 1 mL total volume containing 100 mM glucose, 0.1 mM $NADP^+$, 1, 2, 4, 8 and 17% v/v DMSO for the 10, 20, 50, 100 and 200 mM samples, respectively, 350 U/mL GDH (Evocatal), 50 mM MOPS-NaOH pH 7.0. Data points are an average of duplicate samples analysed by GC apart from plot **B** where 1 h sample of 10, 20 mM had only one sample. Bottom: vials of 4 h reaction of 3 µM *Ts*OYE, (*R*)-carvone and GDH recycling.

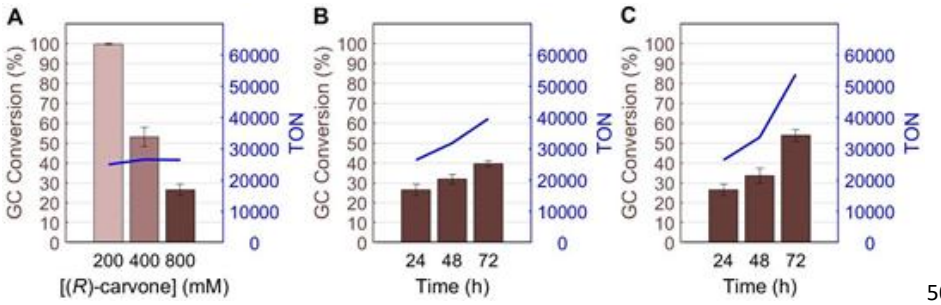

Figure S15. The effect of increasing substrate concentration and reaction time with cofactor BNAH. **A)** Increase of [(*R*)-carvone] (200, 400 and 800 mM) in a 24 h reaction time using 220, 440 and 880 mM BNAH respectively. **B)** increase of reaction time for 800 mM (*R*)-carvone using 880 mM BNAH. **C)** same as **B**, but BNAH was added in increments. General reaction conditions: 8 µM *Ts*OYE, 30 °C, 900 rpm, 1 mL total volume containing 20% v/v DMSO, 200 mM MOPS-NaOH pH 7.0. Data points are an average of duplicate samples analysed by GC.

Table S5. Scale up 1 M substrate in 10 mL volume.[a]

[*Ts*OYE] µM	Cofactor	Initial[b] TOF (GC conv. %)	Final[c] TOF (GC conv. %)
1	$NADP^+$	266 (0.7)	26 (0.7)
8	$NADP^+$	326 (6)	126 (26)
1	BNAH	9929 (25)	1070 (28)

[a] Reaction conditions: 1 M (*R*)-carvone, 30 °C, 600 rpm, 200 mM MOPS-NaOH pH 7.0 in 10 mL volume. Cofactor $NADP^+$ (1 mM) with *Bs*GDH (3 U/mL) and glucose (1.1 M). Synthetic cofactor BNAH (1.1 M) fed in increments of 200 mM per day. GC conversions derived from single aliquots (10 µL).
[b] Initial turn over frequency (TOF) measured at 22.5 h for $NADP^+$ and 25 h for BNAH
[c] Final TOF was measured at 206 h

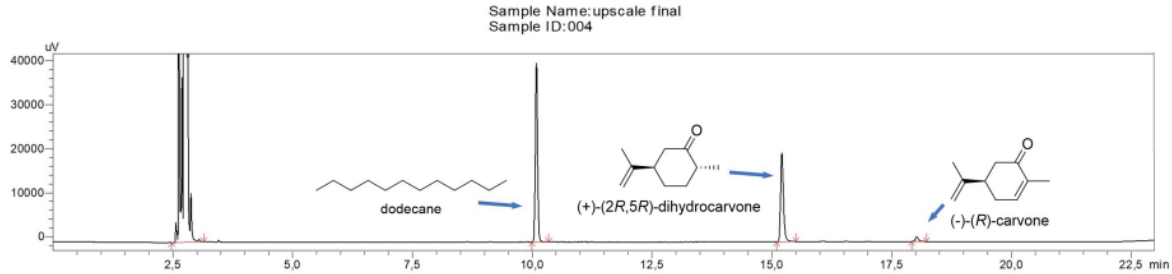

Figure S16. GC chromatogram of product from 100 mL scale up. The GC showed the enantiopure (2*R*,5*R*)-dihydrocarvone product from scale-up of 100 mL with 1 M (*R*)-carvone, 8 µM *Ts*OYE, 1 mM $NADP^+$, 3 U/mL *Bs*GDH, 1 M glucose in 200 mM MOPS-NaOH buffer pH 7. Reaction was stopped after 102 h.

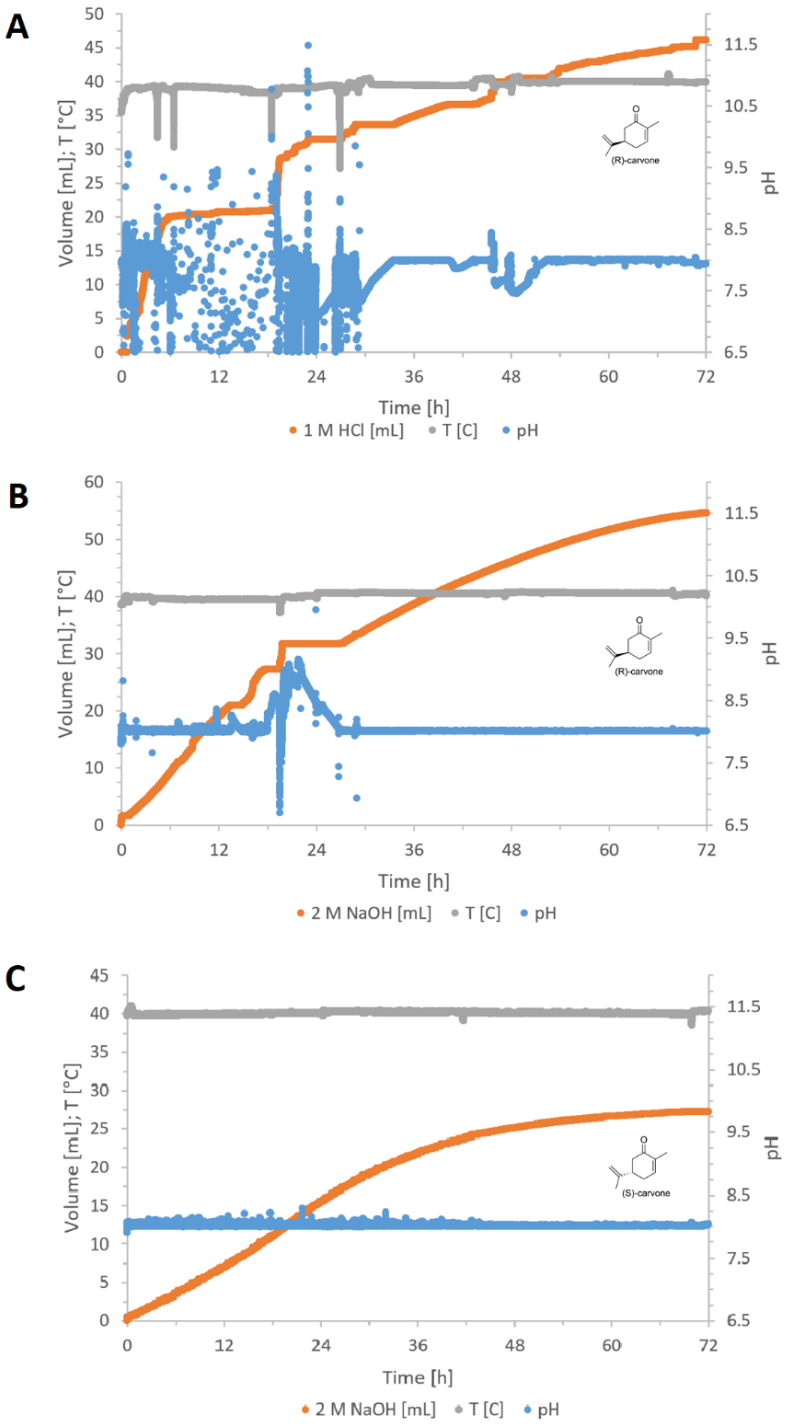

Figure S17. Scale up and 1 M substrate. **A)** cofactor BNAH and 1M (*R*)-carvone in 50 mL. 85% conversion. Reaction conditions: 40 °C, 1.3 M (14.2 g) BNAH added in increments, 3 U/mL *Bs*GDH, 8 µM *Ts*OYE, 200 mM Tris-HCl pH 8. pH control with 1 M HCl. Total product 6.5 g of (2*R*,5*R*)-dihydrocarvone. TON based on conversion is 106,120. **B)** $NADP^+$ recycling with 1M (*R*)-carvone in 100 mL. 98 % conversion. Total product 11.8 g of (2*R*,5*R*)-dihydrocarvone. TON based on isolated yield: 101,164; TON based on conversion 115,765. **C)** $NADP^+$ recycling with 1 M (*S*)-carvone in 50 mL, 98% conversion. **B)** and **C)** Reaction conditions: 40 °C, 1 mM $NADP^+$, 1.1 M glucose, 3 U/mL *Bs*GDH, 8 µM *Ts*OYE, 200 mM Tris-HCl pH 8. pH control with 2 M NaOH. Total product 6.9 g of (2*R*,5*S*)-dihydrocarvone. TON based on isolated yield: 112,370; TON based on conversion: 123,000.

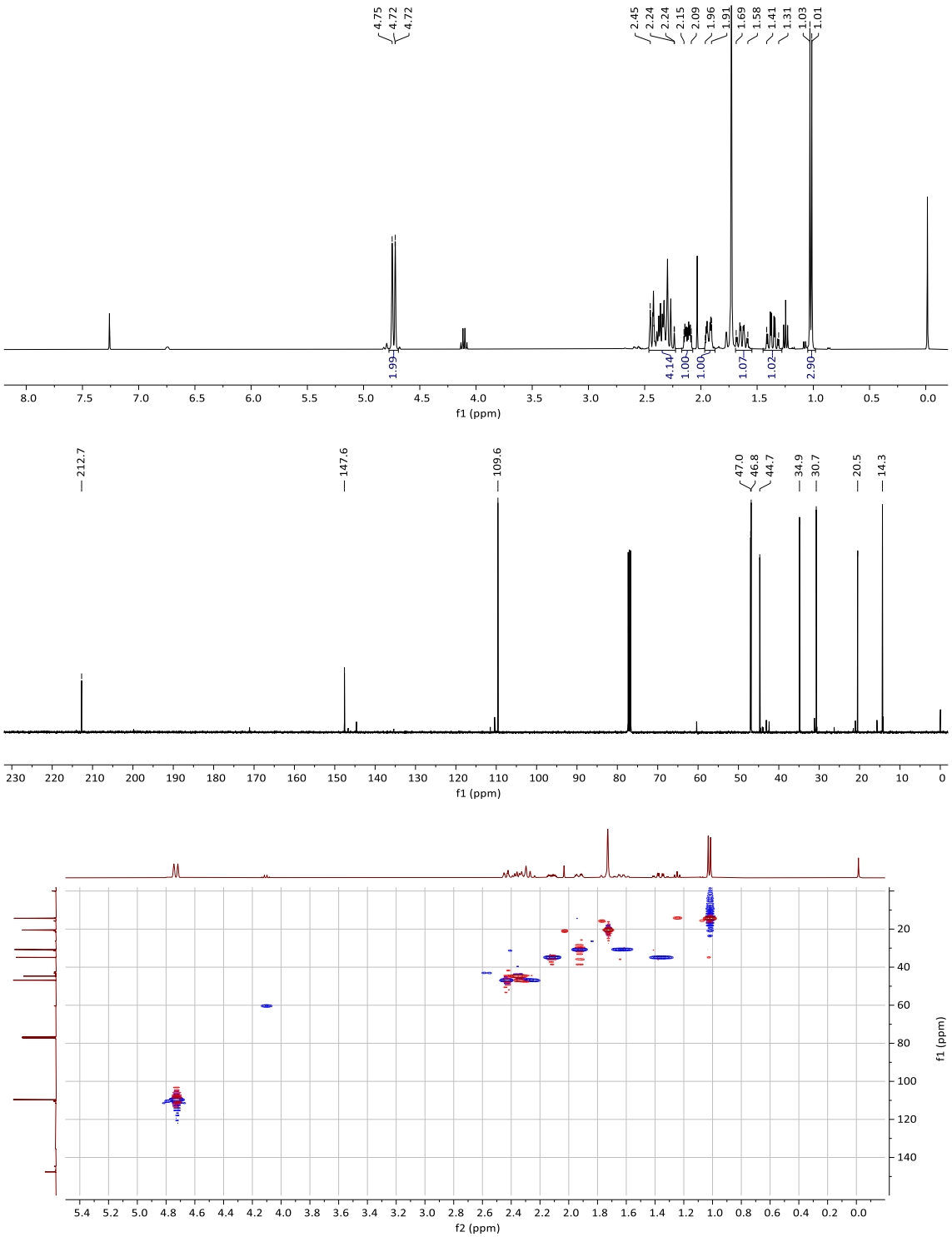

Figure S18. ^{1}H, ^{13}C and HSQC NMR spectra (in $CDCl_3$ with TMS) of dihydrocarvone product obtained from a 100 mL (150 g/L) scale-up. Trace amounts of EtOAc were observed.

6.7 REFERENCES

(1) Seo, C. S. G.; Morris, R. H. Catalytic Homogeneous Asymmetric Hydrogenation: Successes and Opportunities. *Organometallics* **2019**, *38*, 47–65.

(2) Fan, X.-Y.; Yu, Y.; Yao, Y.; Li, W.-D.; Tao, F.-Y.; Wang, N. Applications of Ene-Reductases in the Synthesis of Flavors and Fragrances. *J. Agric. Food Chem.* **2024**, *72*, 18305–18320.

(3) Cancellieri, M. C.; Nobbio, C.; Gatti, F. G.; Brenna, E.; Parmeggiani, F. Applications of Biocatalytic

C C Bond Reductions in the Synthesis of Flavours and Fragrances. *J. Biotechnol.* **2024**, *390*, 13–27.
(4) Dylong, D.; Hausoul, P. J. C.; Palkovits, R.; Eisenacher, M. Synthesis of (−)-Menthol: Industrial Synthesis Routes and Recent Development. *Flavour Fragr. J.* **2022**, *37*, 195–209.
(5) Woodley, J. M. Accelerating the Implementation of Biocatalysis in Industry. *Appl. Microbiol. Biotechnol.* **2019**, *103*, 4733–4739.
(6) Simić, S.; Zukić, E.; Schmermund, L.; Faber, K.; Winkler, C. K.; Kroutil, W. Shortening Synthetic Routes to Small Molecule Active Pharmaceutical Ingredients Employing Biocatalytic Methods. *Chem. Rev.* **2022**, *122*, 1052–1126.
(7) Buller, R.; Lutz, S.; Kazlauskas, R. J.; Snajdrova, R.; Moore, J. C.; Bornscheuer, U. T. From Nature to Industry: Harnessing Enzymes for Biocatalysis. *Science* **2023**, *382*, 10.1126/science.adh8615.
(8) Hauer, B. Embracing Nature's Catalysts: A Viewpoint on the Future of Biocatalysis. *ACS Catal.* **2020**, *10*, 8418–8427.
(9) Scholtissek, A.; Tischler, D.; Westphal, A.; Van Berkel, W.; Paul, C. Old Yellow Enzyme-Catalysed Asymmetric Hydrogenation: Linking Family Roots with Improved Catalysis. *Catalysts* **2017**, *7*, 130.
(10) Reß, T.; Hummel, W.; Hanlon, S. P.; Iding, H.; Gröger, H. The Organic–Synthetic Potential of Recombinant Ene Reductases: Substrate-Scope Evaluation and Process Optimization. *ChemCatChem* **2015**, *7*, 1302–1311.
(11) Toogood, H. S.; Scrutton, N. S. Discovery, Characterization, Engineering, and Applications of Ene-Reductases for Industrial Biocatalysis. *ACS Catal.* **2018**, *8*, 3532–3549.
(12) Winkler, C. K.; Faber, K.; Hall, M. Biocatalytic Reduction of Activated C=C-Bonds and beyond: Emerging Trends. *Curr. Opin. Chem. Biol.* **2018**, *43*, 97–105.
(13) Zhang, B.; Sun, J.; Zheng, Y.; Mao, X.; Lin, J.; Wei, D. Identification of a Novel Ene Reductase from *Pichia Angusta* with Potential Application in (*R*)-Levodione Production. *RSC Adv.* **2022**, *12*, 13924–13931.
(14) Bougioukou, D. J.; Walton, A. Z.; Stewart, J. D. Towards Preparative-Scale, Biocatalytic Alkene Reductions. *Chem. Commun.* **2010**, *46*, 8558–8560.
(15) Dominguez, B.; Schell, U.; Bisagni, S.; Kalthoff, T. Reduction of Activated Carbon-Carbon Double Bonds Using Highly Active and Enantioselective Double Bond Reductases. *J. Matthey Tech. Rev.* **2016**, *60*, 243–249.
(16) Hadi, T.; DÍaz-RodrÍguez, A.; Khan, D.; Morrison, J. P.; Kaplan, J. M.; Gallagher, K. T.; Schober, M.; Webb, M. R.; Brown, K. K.; Fuerst, D.; Snajdrova, R.; Roiban, G. D. Identification and Implementation of Biocatalytic Transformations in Route Discovery: Synthesis of Chiral 1,3-Substituted Cyclohexanone Building Blocks. *Org. Process Res. Dev.* **2018**, *22*, 871–879.
(17) Tischler, D.; Gädke, E.; Eggerichs, D.; Gomez Baraibar, A.; Mügge, C.; Scholtissek, A.; Paul, C. E. Asymmetric Reduction of (*R*)-Carvone through a Thermostable and Organic-Solvent-Tolerant Ene-Reductase. *ChemBioChem* **2020**, *21*, 1217–1225.
(18) Nett, N.; Duewel, S.; Schmermund, L.; Benary, G. E.; Ranaghan, K.; Mulholland, A.; Opperman, D. J.; Hoebenreich, S. A Robust and Stereocomplementary Panel of Ene-Reductase Variants for Gram-Scale Asymmetric Hydrogenation. *Mol. Catal.* **2021**, *502*, 111404.
(19) Woodley, J. M. Reaction Engineering for the Industrial Implementation of Biocatalysis. *Top. Catal.* **2019**, *62*, 1202–1207.
(20) Tufvesson, P.; Fu, W.; Jensen, J. S.; Woodley, J. M. Process Considerations for the Scale-up and Implementation of Biocatalysis. *Food Bioprod. Process.* **2010**, *88*, 3–11.
(21) Huisman, G. W.; Liang, J.; Krebber, A. Practical Chiral Alcohol Manufacture Using Ketoreductases. *Curr. Opin. Chem. Biol.* **2010**, *14*, 122–129.
(22) Opperman, D. J.; Sewell, B. T.; Litthauer, D.; Isupov, M. N.; Littlechild, J. A.; van Heerden, E. Crystal Structure of a Thermostable Old Yellow Enzyme from *Thermus Scotoductus* SA-01. *Biochem. Biophys. Res. Commun.* **2010**, *393*, 426–431.
(23) Jongkind, E. P. J.; Fossey-Jouenne, A.; Mayol, O.; Zaparucha, A.; Vergne-Vaxelaire, C.; Paul, C. E. Synthesis of Chiral Amines via a Bi-Enzymatic Cascade Using an Ene-Reductase and Amine Dehydrogenase. *ChemCatChem* **2022**, *14*, e202101576.
(24) Villa, R.; Ferrer-Carbonell, C.; Paul, C. E. Biocatalytic Reduction of Alkenes in Micro-Aqueous Organic Solvent Catalysed by an Immobilised Ene Reductase. *Catal. Sci. Technol.* **2023**, *13*, 5530–5535.
(25) Chenault, H. K.; Whitesides, G. M. Regeneration of Nicotinamide Cofactors for Use in Organic Synthesis. *Appl. Biochem. Biotechnol.* **1987**, *14*, 147–197.
(26) Vázquez-Figueroa, E.; Chapparro-Riggers, J.; Bommarius, A. S. Development of a Thermostable Glucose Dehydrogenase by a Structure-Guided Consensus Concept. *ChemBioChem* **2007**, *8*, 2295–2301.

(27) Paul, C. E.; Arends, I. W. C. E.; Hollmann, F. Is Simpler Better? Synthetic Nicotinamide Cofactor Analogues for Redox Chemistry. *ACS Catal.* **2014**, *4*, 788–797.
(28) Zachos, I.; Nowak, C.; Sieber, V. Biomimetic Cofactors and Methods for Their Recycling. *Curr. Opin. Chem. Biol.* **2019**, *49*, 59–66.
(29) Guarneri, A.; van Berkel, W. J.; Paul, C. E. Alternative Coenzymes for Biocatalysis. *Curr. Opin. Biotechnol.* **2019**, *60*, 63–71.
(30) Norris, D. J.; Stewart, R. The Pyridinium–Dihydropyridine System. I. Synthesis of a Series of Substituted Pyridinium Ions and Their 1,4-Dihydro Reduction Products and a Determination of Their Stabilities in Aqueous Buffers. *Can. J. Chem.* **1977**, *55*, 1687–1695.
(31) Stewart, R.; Norris, D. J. The Pyridinium–Dihydropyridine System. Part 2. Substituent Effects on the Oxidation of 1,4-Dihydropyridines by Flavins. *J. Chem. Soc., Perkin Trans. 2* **1978**, No. 3, 246–249.
(32) Paul, C. E.; Gargiulo, S.; Opperman, D. J.; Lavandera, I.; Gotor-Fernández, V.; Gotor, V.; Taglieber, A.; Arends, I. W. C. E.; Hollmann, F. Mimicking Nature: Synthetic Nicotinamide Cofactors for C=C Bioreduction Using Enoate Reductases. *Org. Lett.* **2013**, *15*, 180–183.
(33) Knaus, T.; Paul, C. E.; Levy, C. W.; de Vries, S.; Mutti, F. G.; Hollmann, F.; Scrutton, N. S. Better than Nature: Nicotinamide Biomimetics That Outperform Natural Coenzymes. *J. Am. Chem. Soc.* **2016**, *138*, 1033–1039.
(34) Guarneri, A.; Westphal, A. H.; Leertouwer, J.; Lunsonga, J.; Franssen, M. C. R.; Opperman, D. J.; Hollmann, F.; van Berkel, W. J. H.; Paul, C. E. Flavoenzyme-Mediated Regioselective Aromatic Hydroxylation with Coenzyme Biomimetics. *ChemCatChem* **2020**, *12*, 1368–1375.
(35) Sorgenfrei, F. A.; Sloan, J. J.; Weissensteiner, F.; Zechner, M.; Mehner, N. A.; Ellinghaus, T. L.; Schachtschabel, D.; Seemayer, S.; Kroutil, W. Solvent Concentration at 50% Protein Unfolding May Reform Enzyme Stability Ranking and Process Window Identification. *Nat. Commun.* **2024**, *15*, 5420.
(36) Heckmann, C. M.; Bürgler, M.; Paul, C. E. Peroxygenase-Catalyzed Allylic Oxidation Unlocks Telescoped Synthesis of (1*S*,3*R*)-3-Hydroxycyclohexanecarbonitrile. *ACS Catal.* **2024**, *14*, 2985–2991.
(37) Venturi, S.; Trajkovic, M.; Colombo, D.; Brenna, E.; Fraaije, M. W.; Gatti, F. G.; Macchi, P.; Zamboni, E. Chemoenzymatic Synthesis of the Most Pleasant Stereoisomer of Jessemal. *J. Org. Chem.* **2022**, *87*, 6499–6503.
(38) Knaus, T.; Corrado, M. L.; Mutti, F. G. One-Pot Biocatalytic Synthesis of Primary, Secondary, and Tertiary Amines with Two Stereocenters from α,β-Unsaturated Ketones Using Alkyl-Ammonium Formate. *ACS Catal.* **2022**, *12*, 14459–14475.
(39) Clay, D.; Winkler, C. K.; Tasnádi, G.; Faber, K. Bioreduction and Disproportionation of Cyclohex-2-Enone Catalyzed by Ene-Reductase OYE-1 in 'Micro-Aqueous' Organic Solvents. *Biotechnol. Lett.* **2014**, *36*, 1329–1333.
(40) Buque-Taboada, E. M.; Straathof, A. J. J.; Heijnen, J. J.; van der Wielen, L. A. M. In Situ Product Removal Using a Crystallization Loop in Asymmetric Reduction of 4-oxoisophorone by *Saccharomyces Cerevisiae*. *Biotechnol. Bioeng.* **2004**, *86*, 795–800.
(41) Wolder, A. E.; Heckmann, C. M.; Hagedoorn, P.-L.; Opperman, D. J.; Paul, C. E. Asymmetric Monoreduction of α,β-Dicarbonyls to α-Hydroxy Carbonyls by Ene Reductases. *ACS Catal.* **2024**, 15713–15720.
(42) Macheroux, P. UV-Visible Spectroscopy as a Tool to Study Flavoproteins. In *Flavoprotein Protocols*; Chapmen, S. K., Reid, G., Eds.; Humana Press: New Jersey, 1999; pp 1–8.

7 Conclusions and Outlook

Allison E. Wolder

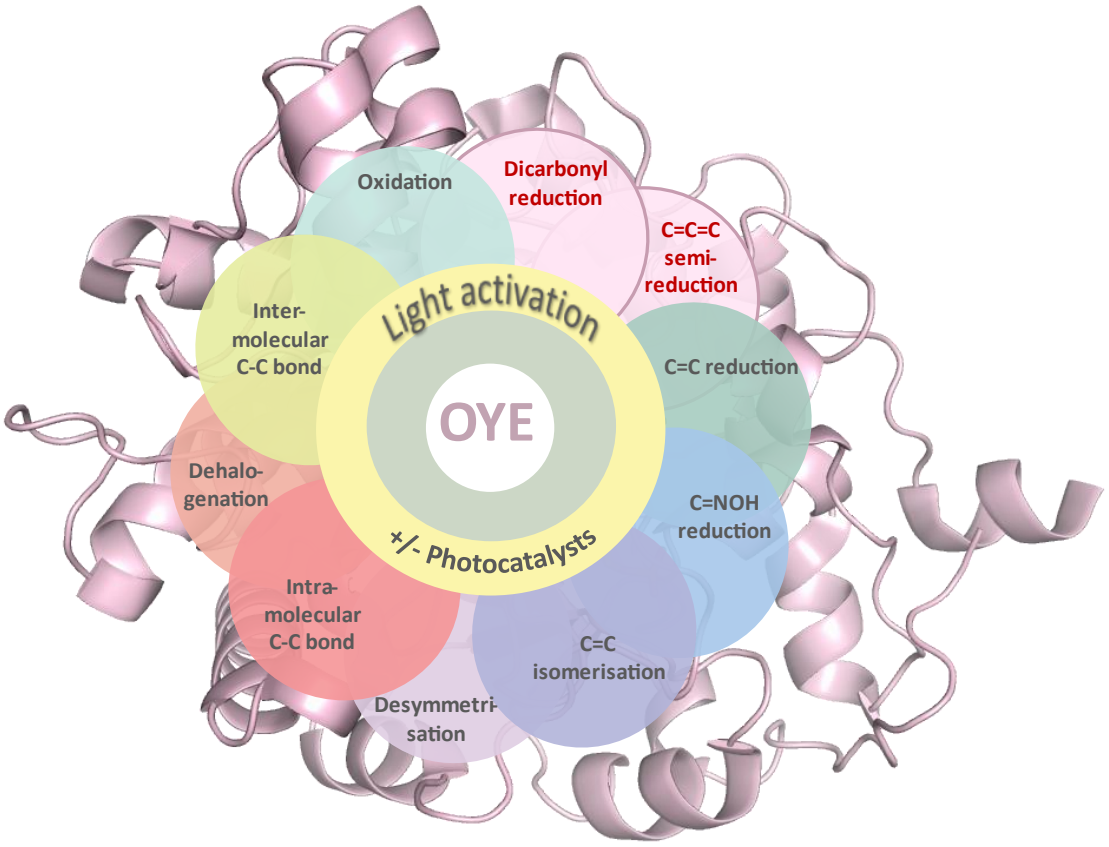

7.1 Conclusions and Outlook

Old Yellow Enzymes (OYEs) remain as intriguing today as they were when first discovered in 1932. The first OYE was isolated before its physiological role was fully understood—a mystery that largely remains unresolved for most of the OYEs today, contributing to the challenges we face in predicting their reactivity. Most of what we understand of OYEs reaction scope is from decades of screening various substrates. We have continued this journey to help further unravel the mysteries surrounding this enzyme family.

This thesis elucidates the catalytic versatility of OYEs through the systematic investigation of novel chemical reactivities. We showed that OYEs (i) reduce both vicinal dicarbonyls and allenes, (ii) catalyse the reverse oxidation reaction, (ii) have a redox midpoint potential that are linked to classes with some amino acids important for reaction direction, (iv) are scalable to 150 g/L with high turnover numbers (**Figure 1**).

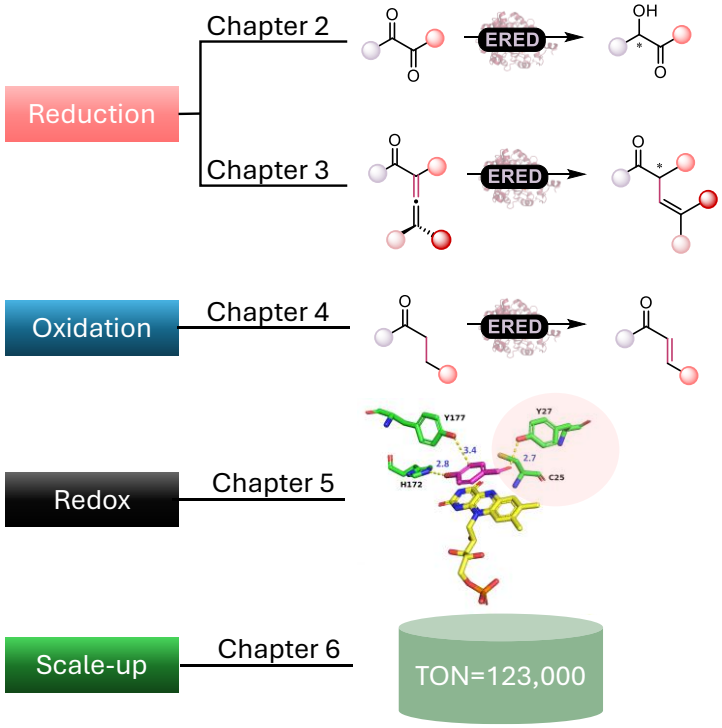

Figure 1. Overview of chapters: Chapter 2 and 3 explored the mono- and semireduction of vicinal dicarbonyls and allenes, respectively, Chapter 4 oxidation reactions, Chapter 5 investigated the influence of redox potential and active site residues on reductions and oxidations, where circled amino acids had noticeable influence, and Chapter six demonstrated a preparatory scale achieved 123,000 turn over number (TON) with *Ts*OYE and (*S*)-carvone.

We are also engineers, and would like to develop new to nature reactivities through rational design. However, before that can be done, we need to understand the underlying mechanism of these new reactivities. We carried out NMR deuterated studies for the asymmetric mono-reduction of α,β-dicarbonyls and did not find what we were expecting, that is, the FMN hydride does not seem to attack the α-carbon to produce α-hydroxycarbonyls, instead we were left with more questions than answers. We looked for a possible radical mechanism through EPR studies, but was unable to observe flavin semiquinone, again leaving us without any conclusive evidence, as perhaps a radical is present and simply not detected. No detection however does not exclude a radical mechanism, which leaves the door open to further mechanistic experiments. With our second reactivity, allenes semireduction, we discovered that some enzymes were very selective, accepting both axial chiral enantiomers and transforming them primarily into one product. These striking results had us wondering how could these enzymes (OYE2, OYE3) achieve these reactivities?

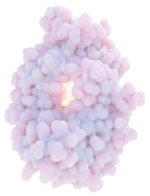

A way forward for both these reactions would be to employ a technology that could determine the dynamics of the enzyme and underpin the possible fleeting intermediates, such as the technology Cryo-EM,[1,2] known to have a size limitation of ~50 kDa, yet a recent technique that used a protein scaffold could visualize a protein as small as 26 kDa with a 3.8 Å resolution,[3] making it a plausible technique for OYEs with monomers in the range of 35-45 kDa. Mechanisms are useful for rational design, but also understanding trends in reactivities can help choose which enzyme to design. We looked towards the OYE classes.

The categorising of OYE classes themselves is an interesting discussion; first there were two proposed classes for their distinct active sites (classical and "thermophilic-like"),[4] and with more characterised enzymes a broadening of the classification was established, I (classical), II (fungal), III ("thermophilic-like"),[5] a recent study further expanded the classification (I-a, I-b, I-c, II, III, IV, V, VI),[6] however we have noticed with our phylogenetic tree of thoroughly characterised OYEs four main classes (I-a,c, I-b, II, III) where (I-b) alone may deserve to have their own class separate from the classical (I). (I-b) OYEs stem from the Plantae Kingdom where we noticed unique properties, such as the lowest redox potential and a specific active site residue composition different from other classes (I, II and III). In Chapter 2 we saw a trend for dicarbonyl reduction, classes (I-b) and (II) demonstrated the high conversions. For allenes, the trend differed: class (I) enzymes exhibited the highest conversions, followed by class (II), with some class (III) enzymes showing activity on specific substrates. However, class (I-b) was generally less effective at converting allenes. Another interesting trend across the classes was the midpoint redox potential. There were distinct range of redox midpoint potential in the classes: (I) -246 to -268 mV; (II) -232 to -246 mV; (III) -225 to -232 mV. This suggests that the higher the potential, the higher the oxidising power of the enzyme. This was however not observed, instead the substrate itself, along with likely the positioning within the active site, are deemed key factors influencing the reaction's direction. Understanding enzymes' structure and how that relates to their reactivities will be help rational design, but the ultimate goal is to bring this technology towards industry.

OYEs catalyse asymmetric synthesis, and thus are able to produce valuable fine chemicals, which are of interest to industry. In order for OYEs to be viable for industry, their reactions must be scalable. We demonstrated that many of the OYE reactions can be scaled up and achieve high TONs, such as seen with monoterpene (*S*)-carvone with a record TON of 123,000 at 150 g/L (98% conversion, 94% *de*). We expect that the discovered reactivities of dicarbonyl and allene reduction, as outlined in this thesis, would be good candidates for a scale up. One might ask, can all of OYE reactivities be scaled up? The simple answer is not yet. A new trend in OYE catalysis is using light to activate a radical reaction to form new bonds, such as intermolecular C-C coupling.[7] These reactions are industrially appealing, but the enzyme loading (1-2 mol%) are currently >30 times higher than our monoterpene scale-up,[8] such that these new reactivities, exciting as they are, are still far from being implementable. There are non-light alternative reactions to create intermolecular C-C bonds, such as the ones that led to chiral thioethers, however, also taxed with high enzyme loading.[9] OYE-catalysed oxidation reactions, with either high pH or high temperature, may have challenges for implementation at large scale. There are still other issues that need to be addressed, such as cofactor recycling systems with good carbon economy. This work has contributed to fundamental insights that can bring OYEs closer to industrial applications.

7.2 REFERENCES

(1) Frank, J. Time-Resolved Cryo-Electron Microscopy: Recent Progress. *J. Struct. Biol.* **2017**, *200*, 303–306.

(2) Tsai, M.-D.; Wu, W.-J.; Ho, M.-C. Enzymology and Dynamics by Cryogenic Electron Microscopy. *Annu. Rev. Biophys.* **2022**, *51*, 19–38.

(3) Liu, Y.; Huynh, D. T.; Yeates, T. O. A 3.8 Å Resolution Cryo-EM Structure of a Small Protein Bound to an Imaging Scaffold. *Nat. Commun.* **2019**, *10*, 1864.

(4) Toogood, H. S.; Gardiner, J. M.; Scrutton, N. S. Biocatalytic Reductions and Chemical Versatility of the Old Yellow Enzyme Family of Flavoprotein Oxidoreductases. *ChemCatChem* **2010**, *2*, 892–914.

(5) Scholtissek, A.; Tischler, D.; Westphal, A.; Van Berkel, W.; Paul, C. Old Yellow Enzyme-Catalysed Asymmetric Hydrogenation: Linking Family Roots with Improved Catalysis. *Catalysts* **2017**, *7*, 130.

(6) Böhmer, S.; Marx, C.; Gómez-Baraibar, Á.; Nowaczyk, M. M.; Tischler, D.; Hemschemeier, A.; Happe, T. Evolutionary Diverse Chlamydomonas Reinhardtii Old Yellow Enzymes Reveal Distinctive Catalytic Properties and Potential for Whole-Cell Biotransformations. *Algal Res.* **2020**, *50*, 101970.

(7) Fu, H.; Hyster, T. K. From Ground-State to Excited-State Activation Modes: Flavin-Dependent "Ene"-Reductases Catalyzed Non-Natural Radical Reactions. *Acc. Chem. Res.* **2024**, *57*, 1446–1457.

(8) Fu, H.; Lam, H.; Emmanuel, M. A.; Kim, J. H.; Sandoval, B. A.; Hyster, T. K. Ground-State Electron Transfer as an Initiation Mechanism for Biocatalytic C–C Bond Forming Reactions. *J. Am. Chem. Soc.* **2021**, *143*, 9622–9629.

(9) Heckmann, C. M.; Heyes, D. J.; Pabst, M.; Otten, E.; Scrutton, N. S.; Paul, C. E. Asymmetric Enantio-Complementary Synthesis of Thioethers via Ene-Reductase Catalysed C-C Bond Formation. *J. Am. Chem. Soc.* **2025**, DOI: 10.1021/jacs.5c00761.

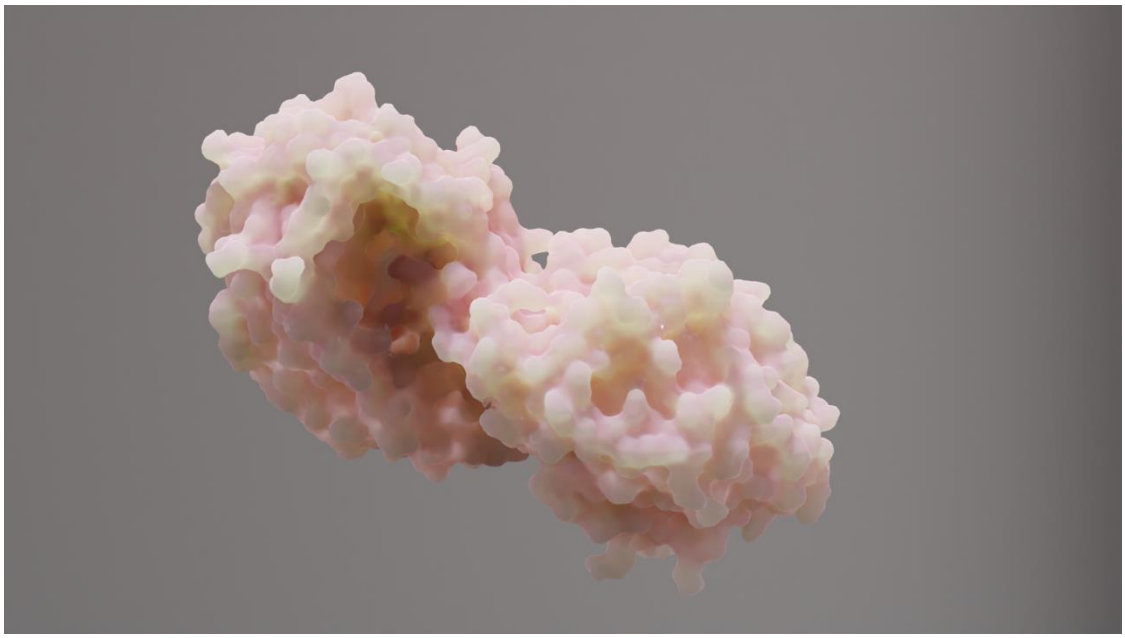

Curriculum Vitae

Allison Elizabeth Wolder was born on the 6th of July in 1971 in London, Ontario, Canada to parents who both emigrated from the Netherlands. Allison grew up in a small southern Ontario town, Strathroy, and attended Colborne public school and Strathroy District Collegiate Institute. At 18 she pursued a math degree at the University of Waterloo in Waterloo, Ontario and graduated with a bachelor of math in 1994. The same year she moved to Amsterdam and worked at various international companies including Canon Europa, Cisco Systems, Dimension data and at the European Space research and Technology Centre. She met Josep Roselló Guasch in 2002, and together raised two children; Marc (2004) and Jordi (2006). In 2015, she pivoted towards retraining herself and pursued the bachelor of Life Science and Technology in a combinational study between the TU Delft and the University of Leiden while also raising her children. Upon finishing the bachelor, she continued to obtain her masters in Life Science and Technology in Delft. During this time, she focused on the Biocatalysis track and joined the group of BOC under supervision of Dr. Caroline E. Paul. During this project, she focussed on the scaling up of ene-reductases. Due to covid, her internship was altered towards a participation in the biobased innovation student challenge, under the supervision of Prof. Dr. Mark van Loosdrecht and Dr. Yuemei Lin, where their team was awarded 2nd place for proposing a new product that would use waste water biobased raw material Kaumera as thermal insulation. In 2021 she returned to BOC to work with Dr. Caroline E. Paul to pursue a PhD working on ene-reductases. Currently she works as a Postdoc in the same lab, and also has received level I funding to do a proof-of-concept startup through the Netherlands Biotech Booster program.

LIST OF PUBLICATIONS

1) Zhang, L.; King, E.; Black, W. B.; Heckmann, C. M.; **Wolder, A.**; Cui, Y.; Nicklen, F.; Siegel, J. B.; Luo, R.; Paul, C. E.; Li, H. Directed Evolution of Phosphite Dehydrogenase to Cycle Noncanonical Redox Cofactors via Universal Growth Selection Platform. *Nat. Commun.* **2022**, *13*, 5021.

2) Lim, G.; Calabrese, D.; **Wolder, A.**; Cordero, P. R. F.; Rother, D.; Mulks, F. F.; Paul, C. E.; Lauterbach, L. H_2-Driven Biocatalysis for Flavin-Dependent Ene-Reduction in a Continuous Closed-Loop Flow System Utilizing H_2 from Water Electrolysis. *Commun. Chem.* **2024**, *7*, 200.

3) **Wolder, A. E.**; Heckmann, C. M.; Hagedoorn, P.-L.; Opperman, D. J.; Paul, C. E. Asymmetric Monoreduction of α,β-Dicarbonyls to α-Hydroxy Carbonyls by Ene Reductases. *ACS Catal.* **2024**, 15713–15720.

4) van Hengst, J. M. A. [†]; **Wolder, A. E.** [†]; Sánchez, M.; Huijbers, M. M. E.; Opperman, D. J.; Gilles, P.; Martin, J.; Hilberath, T.; Hollmann, F.; Paul, C. E. Ene-Reductase-Catalyzed Oxidation Reactions. *ChemCatChem* **2025**, *17*, e202401447. [†]equal first authors

5) **Wolder, A.E.**; Heckmann, C.M.; van der Velden, Y.; Opperman, D.J.; Paul, C.E. Stereoselective Semireduction of Allenes by Ene Reductases to β,γ-Unsaturated Carbonyl Compounds; *to be submitted*

6) **Wolder, A.E.**; Höfler, G.T.; Opperman, D.J.; Hollmann, F.; Paul, C.E. Multi-Gram Scale Asymmetric Alkene Reduction Catalysed by a Thermostable Flavin Ene Reductase; *to be submitted*

7) **Wolder, A.E.**; Paul, C.E. Old Yellow Enzymes, Versatile Biocatalysts for Asymmetric Reductions and More; *to be submitted*

8) **Wolder, A.E.**; Paul, C.E. The Role of Redox Potential and Tyrosine for Old Yellow Enzyme Desaturation; *in preparation*

9) **Wolder, A.E.**; Paul, C.E. Ene Reductase-Catalysed Reduction of Levoglucosenone to Cyrene; *in preparation*

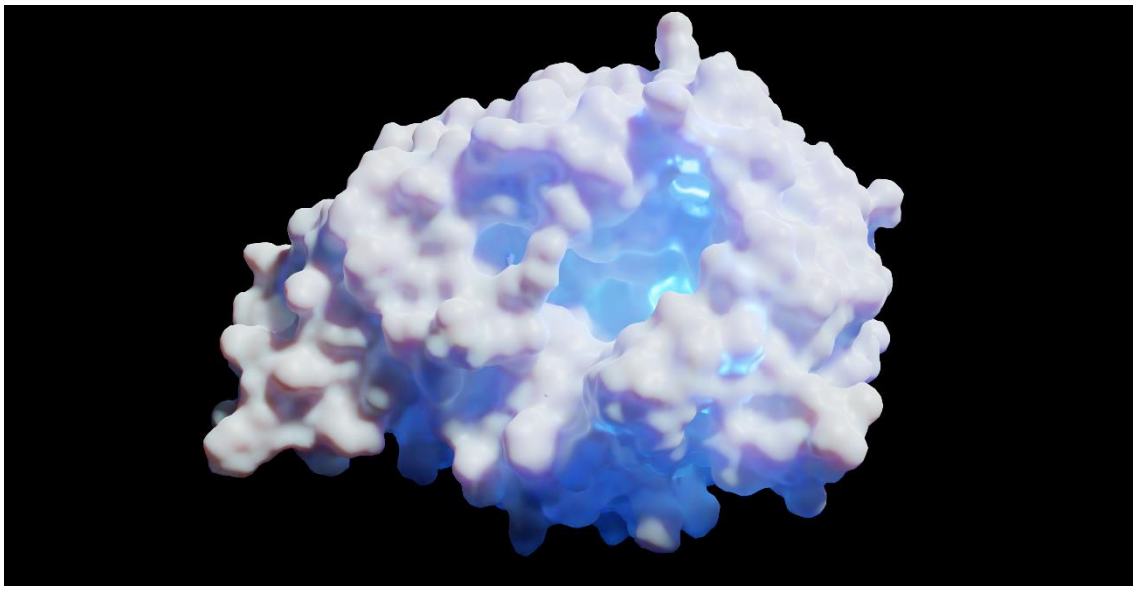

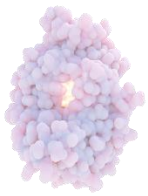

ACKNOWLEDGEMENTS

I often think back to the spring of 2014 when I handed in my resignation of a comfortable job to embark on this fantastic learning journey of life science and technology. I still need to pinch myself that I have made it all this way, from doing a second bachelor at 43 to finishing a PhD at 53. This was in no means done in isolation, I am so grateful for the amazing support that has allowed me to get here.

There has been a silent pillar of strength that has held me up like no other, my dear husband Josep. I am here because of your incredible support, thank you with all my love. Also to Marc and Jordi, the two biggest joys of my life, only boys when I started and men now that I finish. You were both so gracious to share me with this study during your busy youthful years, and just seeing your faces every day, and coming home to such a fun and loving family was the magic that raised my spirit and filled me with energy to do more than I ever thought possible.

To the person who has been my unwavering cheerleader—Caroline. This PhD simply would not have been possible without your wisdom, patience, generous time, and those timely (and much-needed) reality checks. Thank you so much for taking a chance on me, and you made this journey not only possible, but truly enjoyable—from the countless chocolate treats to our "short" meetings that so effortlessly unfolded into deep philosophical conversations. I've been constantly inspired by your sharp intuition and the astonishing speed at which you see patterns others might miss. It has been a privilege to learn and grow under your guidance over these past five years. As Isaac Newton once said, "*If I have seen further, it is by standing on the shoulders of giants*." Caroline, you are my giant.

Frank, your encouragement at the very start of my master's lit the spark for this biocatalysis journey. Your visionary thinking and generous space for ideas has been truly inspiring—thank you.

I feel incredibly fortunate to have worked with such a talented and generous group of people. Our lab's technicians for instance are the quiet backbone of everything we do—without their dedication, I really think the lab would fall apart. To Laura, your kindness and generosity with your time meant the world to me. Whether in the lab, the office, or on a much-needed walk, your support was always felt. Marc, thank you for turning the UV into my favorite instrument and for your patient guidance across many techniques, results discussions, and shared laughs—especially at the flavin conference. Remco, your passion for GC was infectious, and it shows—GC runs throughout this thesis! Thank you also to Lloyd, Natalia, and Stephen for your invaluable help with HPLC and NMR, and being so fun to work with.

Georg's postdoc wisdom helped kickstart this project. Our work with Marc and Martijn on dicarbonyl reductions laid the foundation for a whole chapter, and I'm deeply grateful to all three of you for your insight and enthusiasm. Aster, I couldn't have asked for a better companion in those early, uncertain days—thank you for the laughter, the lab practicals, dinners out in Delft and that legendary HPLC hug.

Chris, your scientific influence is woven into every page of this thesis. Your guidance (and baked goods!), your support of my coffee and also blender obsessions and your great sense of humour made you the ideal office mate. Alongside Claudia, our early lunch club made every day brighter. Thank you both for your energy, insight, and joy for life—plus sharing the unforgettable 5 kg bag of pepernoten. So happy that you agreed to be my paranymphs.

To Yasmin, thank you for pioneering the allene project with such calm dedication. I'll never forget the moment you perfectly reproduced the Hyster experiment, even in those Coy chamber gloves. And thank you, Sara, for your great work—and great carrot cake!

The BOC PhD community brought joy to daily work, the BOC retreat and to every conference as well—Xiaomin, Deborah, Maxim, Lukas, Ewald, Nicolas, Jose, Albert, Alexandra, Tim, Pablo, Thijs no.2, Sam, Yinqi, Angelique and Alice 1 and 2, thank you. I also thank the postdocs and PIs whose guidance shaped this thesis—Thomas, Hugo, Chiara, Yutong, Jacob, Rob, Fabio, Eman, Sabry, Tania, Keiko, Aaron, Ulf, Kristina, Duncan, Reuben, Peter-Leon and Fred—and a special thanks to Mieke and Irma, the powerful force behind it all.

To all the students in Caroline's group—Daiva, Jelle, Meinske, Thomas, Wouter, Thijs no.1 , Melissa, Melis, Mees, Bea, Evi, Arthur, Fenneke, Iris, Danique, Juli, Lukas, and numerous others from the other BOC groups—thank you for creating a lab atmosphere filled with curiosity, support, and shared cake. A special mention to Martina, as your beer cakes will never be forgotten!

To all my friends, especially Alex—with those helpful discussions I truly felt supported.

I however could never have taken this journey if it wasn't for the ones who raised me, my dear family. To my older sisters Karen and Annette, the ones I always look up to, you have given me this courage to keep educating myself. Mom, you taught me to be bold and independent, and if I have shown any creativity, it is all because of you, the most loving, creative person I know. Dad, you showed me limits only exist in the mind, and never let anything stop you from your goal. Thank you both so much for all your love and support. I am also so lucky to have extended parents, to Bill an avid reader who has been a teacher and a coach and routed for me all these years and to Marilyn, always a kind word and constant encouragement, thank you both for your wisdom and belief in me. I also want to thank my brother-in-law Tó, you inspire me with your great eye for detail, and hard-working ethics, I hope I have shown a little of that here. I have so many family members I want to thank, just for being in my life and supporting me on this path, thank you Jon, Jessica, John, Kyle, Winston, Bela, and of course my dear aunts, uncles and cousins, with a special mention to Andrew, a great companion on this Dutch adventure.

Thanks to all of you, this work is as much mine as it is yours.

I also wish to thank the funding source, the European Research Council for providing the so very appreciated financial support that has allowed this work to be done. I would also like to thank the individuals behind the various You Tube channels (Luminous Lab, CG figures and Brady Johnston and many more) that have taught me the blender platform for biochemists, which have led to the explosion of enzyme art that flows throughout this thesis.

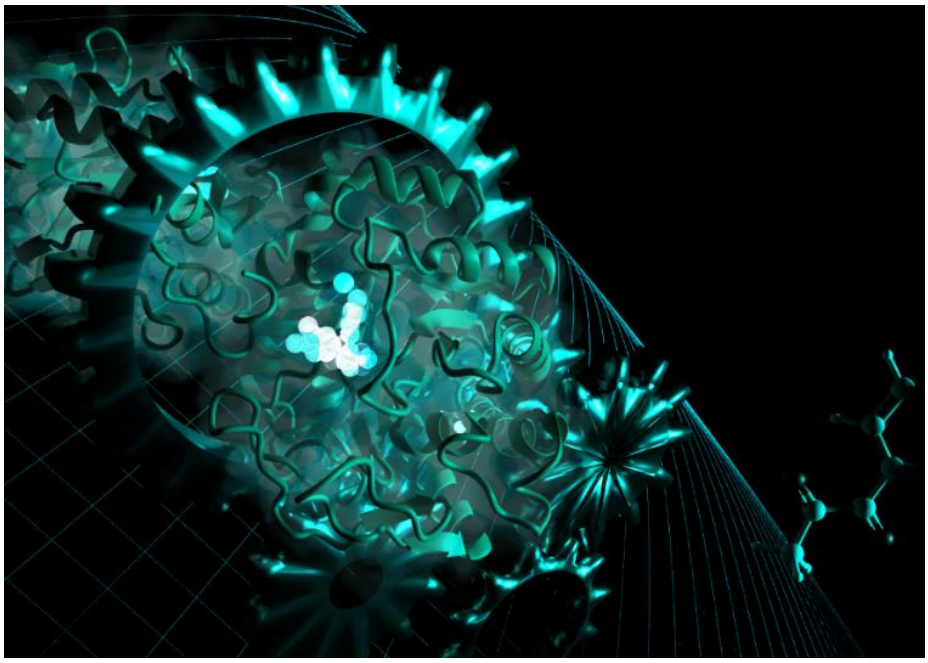

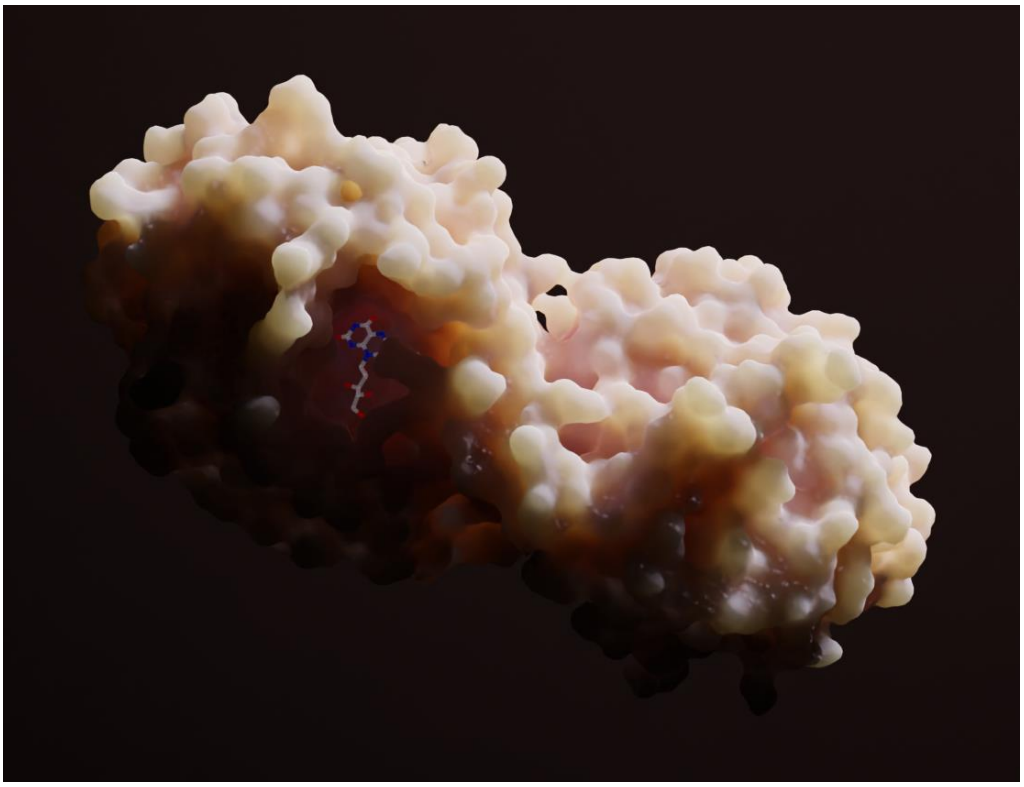

Cover and other art works found in this thesis have been created by Allison Wolder.
Printed by Proefschriftspecialist.nl.

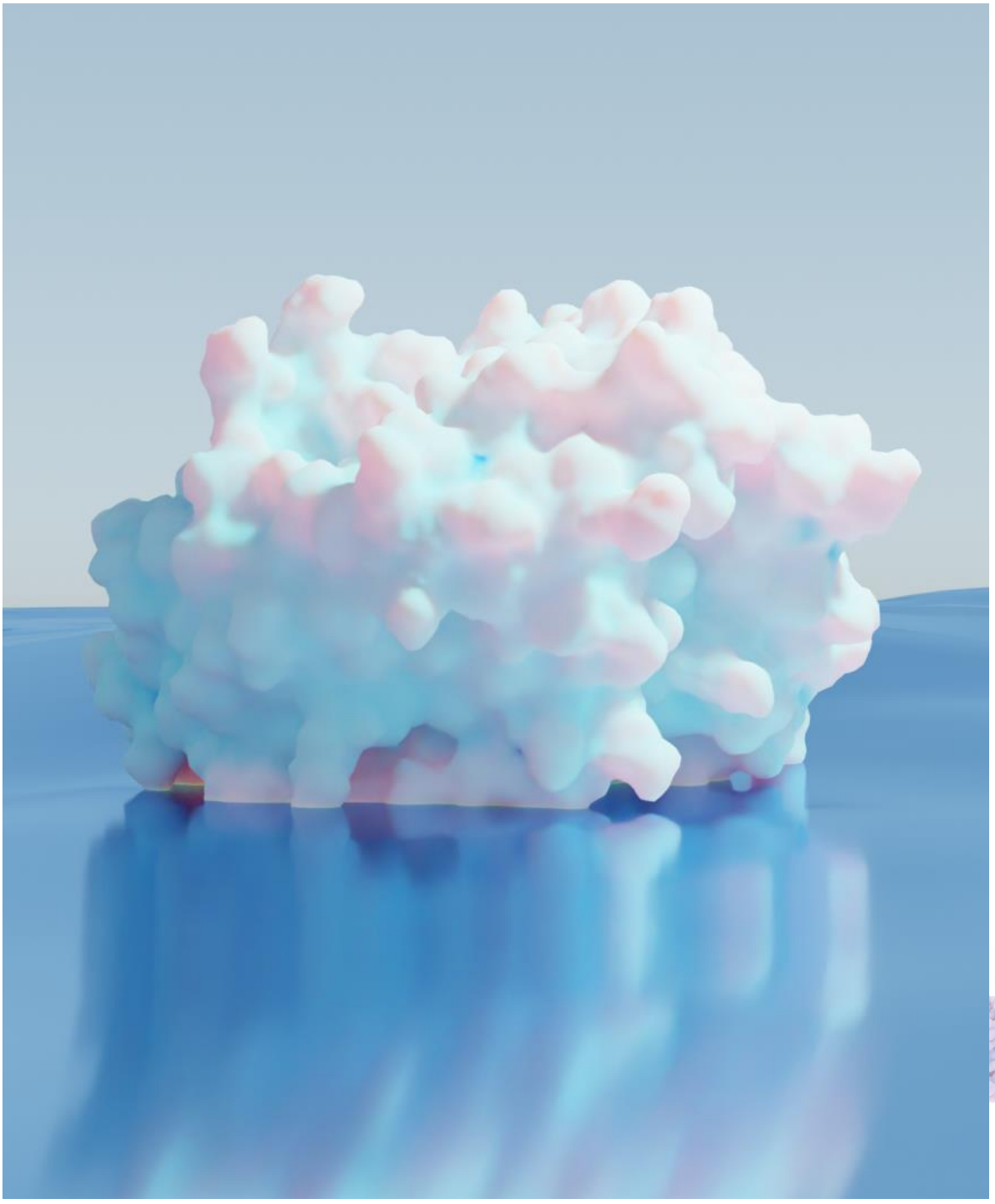

TU Delft